New Applications of Electrochemistry in Organic and Peptide Chemistry

KATIE FRANCESCA DOWELL

New Applications of Electrochemistry in Organic and Peptide Chemistry

A Thesis Presented for the Degree of Doctor of Philosophy

Department of Chemistry

Durham University, Ustinov College

Katie Dowell

Supervised by Professor Steven Cobb

2024

Declaration and Statement of Copyright

Abstract

Peptide therapeutics are an attractive alternative to both small molecule drugs and biologics, as their size and complexity enables them to hit unique targets like Protein-Protein Interactions (PPIs) effectively. However, the current development of peptide therapeutics is hindered by inherent weaknesses within this class of molecule *e.g.*, poor bioavailability, cell permeability, and solubility. The incorporation of unnatural amino acids into peptides has been used to modify their physicochemical properties and improve their 'drug-likeness'.

Synthetic electrochemistry is a versatile tool that is rapidly emerging as a 'green' alternative to more traditional synthetic techniques due to its atom efficiency and selectivity. The application of electrochemistry to modify amino acids is the primary research aim of this thesis. Electrochemical methods have been explored in the selective fluorination of a range of amino acids, and the compatibility of synthetic electrochemical procedures with various amino-protecting groups has been evaluated. Successful fluorination of a Boc-protected amino acid derivative was achieved in a yield of 34%. Chlorination has also been explored, resulting in the development of an electrochemical chlorination method that uses dichloromethane (DCM) as a chlorinating reagent under mild conditions. Successful chlorination of a range of electron rich molecules including the amino acid tryptophan (in a 55% yield) was achieved.

Electrochemical modification of amino acid substrates using transition metal catalysts was also investigated. Nickel catalysis was used to facilitate coupling of alkyl bromides with aryl bromides, generating novel arylated amino acids in varying yields. Pd-catalysed electrochemical oxidation was also explored, resulting in successful acetoxylation of a valine-derived substrate with a methoxyiminoacetic acid (MIA) directing group in a 35% yield.

Electrochemical oxidative coupling of tyrosine was investigated, and a dityrosine derivative was successfully synthesized with a 20% yield. In addition, the coupling conditions were successfully applied to a tyrosine-containing dipeptide. A Shono-type oxidation reaction of proline derivatives mediated by Selectfluor was also developed giving ready access to 5-oxoproline derivatives.

In summary, investigation into the electrochemical modification of several amino acid substrates was undertaken, resulting in synthesis of several unnatural amino acids. New insights into electrosynthetic transformations across a broad range of reaction classes were gained.

Acknowledgements

I would first like to thank my supervisor, Professor Steven Cobb for his support and guidance throughout the course of my postgraduate studies. I would also like to thank Dr Will Brittain for all his help in the lab. Additionally, I would like to thank all Cobb group members past and present (Carissa, Yazmin, Hirunika, Diana, Izzy, Eleanor, Libbi, Hannah, and Naomi) for their help and friendship, along with everyone else in Lab 115. I would like to thank the MoSMed CDT for funding this project. Finally, I would like to thank my friends and family for their encouragement and support.

Abbreviations

ACE	Angiotensin-converting enzyme
AHF	Anhydrous hydrogen fluoride
BBB	Blood-brain barrier
BDD	Boron-doped diamond (electrode)
BnBr	Benzyl bromide
Boc	*tert*-butyloxycarbonyl
COSY	Correlation spectroscopy
CPP	Cell-penetrating peptide
CV	Cyclic voltammetry
CYP	Cytochrome P450
DCC	*N,N'*-dicyclohexylcarbodiimide
DCM	Dichloromethane
DIPEA	*N,N*-Diisopropylethylamine
DMAP	4-Dimethylaminopyridine
DNP	Dinitrophenyl
ESI	Electrospray ionisation
EtOAc	Ethyl acetate
GHIH	Growth hormone-inhibiting hormone
GLP-1R	Glucagon-like peptide-1 receptor
GnRH	Gonadotropin-releasing hormone
GPCR	G protein-coupled receptor
HEWL	Hen egg white lysosome
HFIP	Hexafluoroisopropanol
HOMO	Highest occupied molecular orbital
Keto-ABNO	9-Azabicyclo[3,3,1]nonan-3-one-9-oxyl
KHMDS	Potassium hexamethyldisilazide
LCMS	Liquid chromatography-mass spectrometry
LDA	Lithium diisopropylamide
MeCN	Acetonitrile
MeOH	Methanol
MTBS	*N*-methyl-*N,N,N*-tributylammonium methylsulfate
NaOMe	Sodium methoxide

NMR	Nuclear magnetic resonance
PEG	Polyethylene glycol
Phth	Phthalimide
RVC	Reticulated vitreous carbon (electrode)
SCE	Saturated calomel electrode
SET	Single electron transfer
SPPS	Solid phase peptide synthesis
TEA	Triethylamine
TEMPO	(2,2,6,6-Tetramethylpiperidin-1-yl)oxyl
THF	Tetrahydrofuran
TIPS	Triisopropylsilyl
TIPSCl	Triisopropylsilyl chloride
TLC	Thin-layer chromatography

Table of Contents

Chapter 1: Introduction

1.1 Peptide Therapeutics

1.1.1 Overview of Peptide Drugs

In recent years, the field of peptide drug discovery has garnered an increasing amount of interest, with over 60 peptide drugs now approved for clinical use, and around 150 in clinical development.[1] Peptides are an intriguing prospect for medicinal chemists due to the fact that they occupy a unique chemical space; they are larger than the more traditional small molecule drug candidates, but smaller than biologics (*e.g.*, antibodies). Often now the long-established small molecule approach is eschewed in favour of peptide drug discovery, the latter of which offers many advantages including higher specificity and lower toxicity. Peptides are often found naturally as biological messengers in many signalling pathways within the body and it is estimated that over 7000 peptides have been identified as natural products.[2] Therefore, peptides and their analogues are ideal agonists for peptidic receptors, possessing a higher potency and selectivity than small molecules.

Peptides were first recognised as potentially viable drug candidates in 1921, when the peptide hormone insulin was isolated from dog pancreas by Banting and Best. Insulin proved immensely successful in treating human diabetic patients.[3] Early forays into peptide drug discovery mostly centred around the isolation of peptide natural products for use in replacement therapies, as the field was limited by current synthesis and sequencing techniques.[4,5] In the 1950s, Frederick Sanger successfully determined the amino acid sequence of insulin by analysing the products of the partial hydrolysis of its dinitrophenyl (DNP) derivative using paper chromatography.[6,7] This breakthrough provided indisputable evidence that peptides and proteins possess an exact and unvarying sequence of amino acids.

Around this time, chemical synthesis of peptides had also advanced to the point where assembly of a short defined amino acid sequence became feasible, thanks to the efforts of those such as Fischer[8], Bergmann[9], and Harington and Mead[10] throughout the early 20th century. The first chemical synthesis of a polypeptide hormone was reported by du Vigneaud in 1953 after the successful isolation of synthetic oxytocin (**1**)[11], a neuropeptide featuring a cyclic structure composed of nine amino acids (**Figure 1.1**). This synthesis was swiftly followed by that of synthetic vasopressin (**2**)[12], another cyclic nonapeptide with a similar

structure to oxytocin. Both compounds operate by binding to tissue-specific G protein-coupled receptors (GPCRs) and were approved for therapeutic use with various medical conditions.[13]

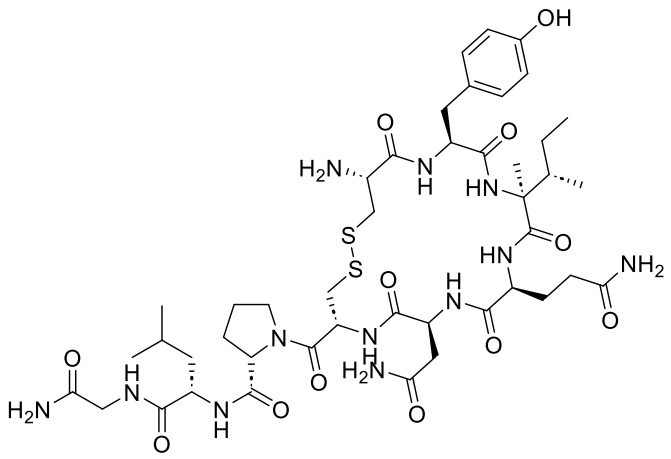

1

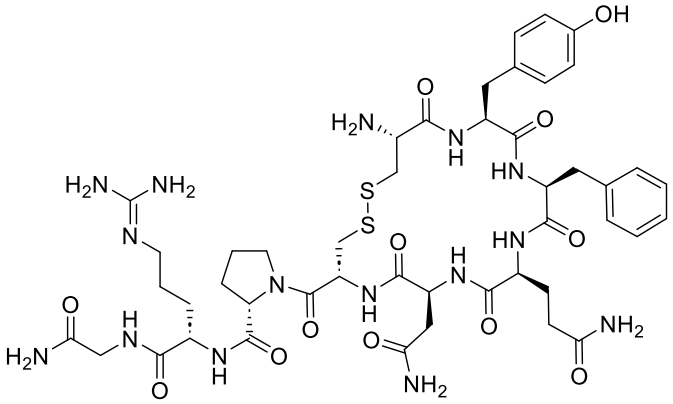

2

Figure 1.1: The structures of oxytocin (**1**) and vasopressin (**2**), the first peptide hormones chemically synthesised.

The field of peptide synthesis experienced a surge in activity in the late 1950s-60s, with the discovery of coupling agents such as *N,N'*-dicyclohexylcarbodiimide (DCC)[14], the introduction of the *tert*-butyloxycarbonyl (Boc) protecting group[15], and the rising prevalence of column chromatographic methods. Perhaps the most significant milestone of peptide synthesis was the development of solid phase peptide synthesis (SPPS)[16], pioneered by Merrifield in 1963. The arrival of this method revolutionised peptide chemistry, enabling the facile construction of much longer defined amino acid sequences without a diminished yield.

After the successful development of SPPS, there was a steady supply of peptide drugs to the market. Many drugs at this time were based upon existing peptide hormones, as these are the natural ligands of many GPCRs and as such are highly potent and selective. An example of

such a drug is the nonapeptide leuprolide (**3**)[17] (**Figure 1.2**), which is an analogue of gonadotropin-releasing hormone (GnRH) and as such binds strongly to the GnRH receptor, reducing gonadotropin production. The peptide drug octreotide (**6**) is an example of an agonist based on the structure of a peptide hormone;[18] octreotide is based on somatostatin, the growth hormone-inhibiting hormone (GHIH). It is used to treat various tumours and conditions caused by excess growth hormone (*i.e.*, gigantism or acromegaly).

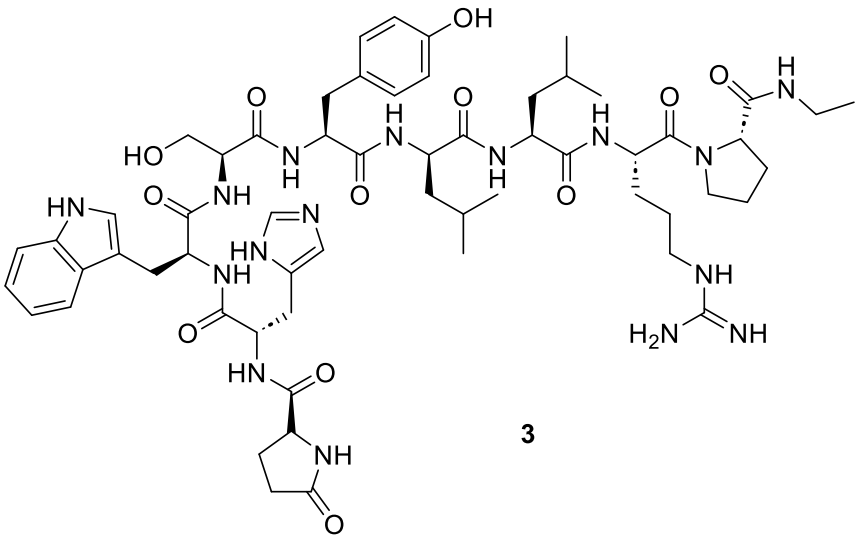

3

Figure 1.2: The structure of the peptide drug leuprolide (**3**), an analogue of the gonadotropin-releasing hormone (GnRH).

Thousands of years of selection pressure means that peptide natural products have a high affinity for their targets. Given the rich diversity and ubiquity of peptides in the natural world, there was mounting interest in mining such sources for drug discovery, particularly peptides from venomous creatures or the largely uncharted marine peptides. Captopril (**4**) (**Figure 1.3**) was the first angiotensin-converting enzyme (ACE) inhibitor to be developed as a treatment for various cardiac conditions and is an analogue of a peptide found in the venom of the Brazilian viper.[19] Another example is Exenatide, an antidiabetic drug based on the structure of a 39 amino acid peptide isolated from the saliva of the Gila monster, which works by binding to the glucagon-like peptide-1 receptor (GLP-1R).[20]

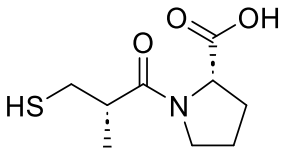

4

Figure 1.3: The chemical structure of captopril (**4**), an ACE inhibitor based on the structure of venom peptides isolated from *Bothrops jararaca.*

Research into peptide drugs was limited until the early 2000s, as the issues that hamper peptide therapeutic development became fully realised. Many peptides have poor oral bioavailability and are readily hydrolysed by proteases in the digestive tract, which means peptide therapeutics must typically be administered parenterally. In addition, peptides are often limited to extracellular targets such as cell surface GPCRs, as they are frequently large and thus cannot easily pass through cell membranes. A rare example of an early peptide drug which targets intracellular structures and can be taken orally is cyclosporine (**5**), a peptide natural product derived from the fungus *Tolypocladium inflatum*, which is now widely prescribed as an immunosuppressant.[21] Cyclosporine is somewhat anomalous in this respect; it has a unique cyclic structure featuring N-methylation and a rare instance of a naturally formed D-amino acid, which permits it to cross cell membranes (**Figure 1.4**).

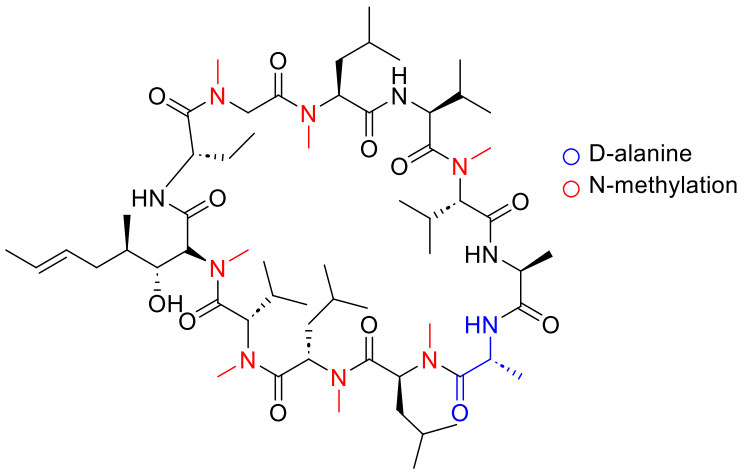

5

Figure 1.4: The chemical structure of cyclosporine (**5**), a cyclic peptide capable of crossing cell membranes.

Post-2000, advances in areas such as X-ray crystallography, combinatorial chemistry, and SPPS optimization heralded a resurgence in peptide therapeutics. The development of high-

throughput screening and phage display technologies[22] have enabled identification of novel peptide leads against a wide range of molecular targets. Progress in chemical modification strategies means that peptide therapeutics are no longer limited to extracellular receptor targets, with peptidomimetic drugs employing non-natural amino acids,[23] backbone modification[24] and bioconjugation[25] being developed to combat poor cell permeability.

Currently there is still extensive research into the field of peptide therapeutics, particularly into developing new methods of delivery and cell permeability. One area under investigation is cell-penetrating peptides (CPPs): short peptides featuring positively charged residues, which are capable of crossing cell membranes.[26] Incorporation of these into bioactive compounds would allow routine targeting of intracellular structures. Another delivery method being explored is the use of nanocarriers to transport therapeutic peptides across the blood-brain barrier (BBB).[27] An emerging trend amongst current peptide drugs is multifunctional peptides, *e.g.*, the drug candidate dopastatin, which is an agonist of both somatostatin and dopamine.[1] Peptide vaccines are another therapeutic area which is rapidly developing, with lots of potential for success.[28]

1.1.2 Issues surrounding the development of peptide therapeutics

Peptides are polymeric molecules consisting of between 2 and 50 amino acids linked by amide bonds, and often possess a secondary structure. Their large size and fixed spatial configuration means that they are much more capable of catering to larger target protein binding sites, which are often fairly flat. Small molecule drugs have difficulties in binding to such surfaces because they cannot achieve the correct shape; they are not large enough to bind to the main site, instead preferring to bind to small pockets or grooves in the target surface. Hence, small molecules are often more effective antagonists than agonists. Alternatively, peptide drugs are mostly agonists. They are usually incredibly specific and potent because their secondary structure enables efficient binding. Peptide drugs therefore fill a niche which other drugs cannot. In addition, their inherent specificity means that peptides are less likely to interact adversely with other drugs or inhibit CYP enzymes, unlike some small molecule drugs. Peptide drugs are also relatively safe; they are unlikely to bind to additional unwanted targets and are unlikely to accumulate in tissues due to short half-lives.[29]

Despite the myriad of advantages, peptide drugs are associated with certain drawbacks that have previously made them a less attractive target than small molecules.

Poor oral bioavailability

The vast majority of peptide drugs require parenteral administration because their size and structure prohibit them from evading digestive proteases and crossing the intestinal epithelium. Parenteral injection is not ideal because it is less convenient, causes issues regarding patient compliance, and requires a sterile environment. These concerns are negligible when a drug requires short-term administration, but become impractical when a drug must be taken daily, as is often the case.

There are numerous physicochemical barriers that a peptide molecule must traverse in order to reach systemic circulation. The first obstacle is the stomach, which produces a large amount of the protease pepsin and has a low pH of between 1 and 2. These conditions make peptide degradation incredibly favourable and limit protein absorption in the stomach. Proteolytic enzymes are also present in the small intestine; two of the major proteases include trypsin and chymotrypsin. The small intestine possesses a physical barrier: the intestinal mucus layer, which protects the intestinal epithelium from pathogens and other foreign bodies (**Figure 1.5**). Mucin fibres are linked together to form a macromolecular structure which controls diffusion of molecules towards the epithelium. This means that larger peptides are often excluded due to their size. Much of the mucosal layer is glycosylated, providing it with a net negative charge. Hydrophobic interactions can occur between drug molecules and mucin molecules at non-glycosylated sections of the mucin backbone and associated lipids, hence, peptides with a higher number of hydrophobic residues often have poorer diffusion rates.[30]

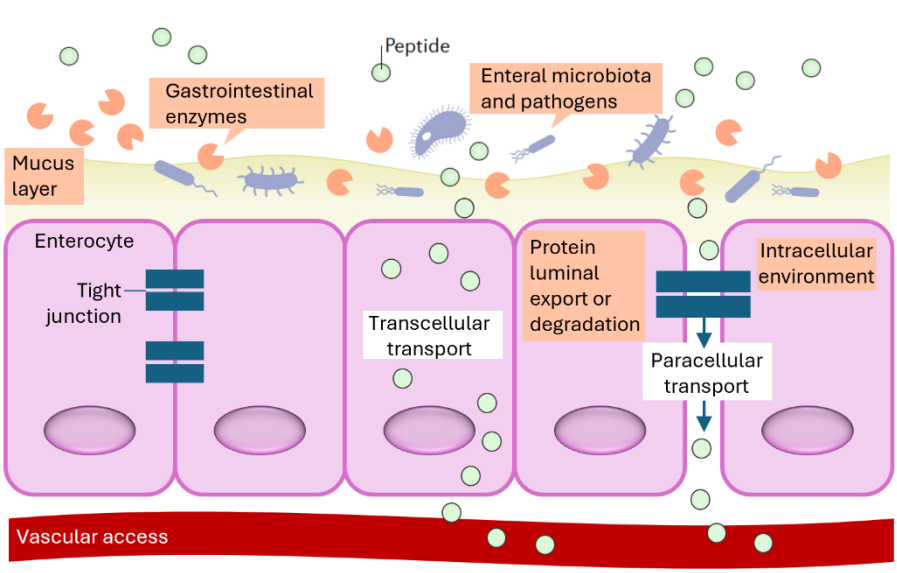

Figure 1.5: A diagram outlining the physicochemical barriers that orally administered peptide drugs will encounter. Figure modified from Drucker.[31]

The intestinal epithelium is the final barrier in the gastrointestinal tract, consisting of a single layer of cells. Molecules can cross this barrier *via* two routes: the transcellular route or the paracellular route (**Figure 1.5**). The paracellular route involves passing through water-filled channels between cells; this is difficult due to the presence of tight junctions which exclude large molecules. However, this route is attractive due to the absence of proteolytic enzymes. The transcellular route involves passing through cells, which means peptides must cross the phospholipid bilayer. This can be done by passive diffusion for lipid-soluble molecules, or carrier-mediated transport. Peptides are often too large and hydrophilic to cross this membrane and may also encounter lysosomal activity within the cells.

Even if a peptide is successful in overcoming these physicochemical barriers, it may still be degraded before it can reach the tissues. Despite the odds stacked against them, a few peptide drugs have succeeded in this endeavour, *i.e.*, cyclosporine (**5**); however, this is not the case for the vast majority of peptide drugs. There is therefore a need for strategies to modify peptide structures in order to improve their oral bioavailability.

Short plasma half-life

Numerous approaches have been trialled to combat short plasma half-life; for example, in the design of the drug octreotide (**6**), based on somatostatin. Somatostatin itself has a half-life of only a few minutes, but its synthetic analogue octreotide (**6**) has a half-life of a couple of hours. The structure of octreotide is much smaller than that of somatostatin, and some of the L-amino acids were exchanged for D-amino acids (**Figure 1.6**). Whilst D-amino acid substitution risks lowering drug potency due to alteration of the secondary structure, it can often improve proteolytic stability.[32] This is because most peptides found in nature are composed of L-amino acids. Proteolytic enzymes are chiral, so they bind efficiently to peptides with L-amino acids, but less efficiently to peptides with D-amino acids. Other strategies to improve plasma half-life include cyclisation,[33] co-administration with protease inhibitors,[34] or PEGylation.[35]

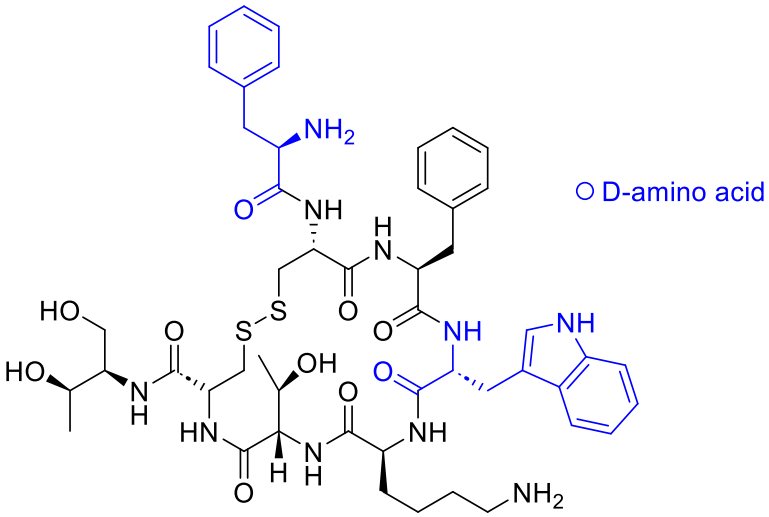

6

Figure 1.6: The chemical structure of octreotide (**6**), a peptide drug based on the structure of the growth hormone-inhibiting hormone (GHIH) somatostatin.

Poor cell permeability

Many peptides are incapable of crossing the phospholipid bilayer due to their large size and hydrophobicity. Peptides that are capable of crossing the cell membrane are likely to differ in transportation mechanism.

The first cell-penetrating peptide sequence discovered was that of the transactivating transcriptional activator (TAT) protein in HIV-1.[36] It is thought that this is because TAT contains many arginine residues, giving it a net positive charge, which allows interaction with the negatively charged bilayer.

Another example of a drug that can enter cells is cyclosporine (**5**) (**Figure 1.4**), a peptide which can be referred to as a molecular chameleon. Due to extensive intramolecular H-bonding, cyclosporine can alter its shape depending on the media it is in. In aqueous media, the lipophilic N-methylated backbone contracts so that the polar functional groups face outwards. In non-polar media, the lipophilic moves to the outside, shielding the inner polar functional groups.[37] Cyclosporine (**5**) is therefore able to pass through cell membranes *via* passive diffusion.

Poor solubility and tendency to aggregate

Aggregation is the association of peptide molecules with other peptide molecules, causing formation of large aggregates. Aggregates may be amorphous, or alternatively the formation of structured amyloid fibrils may occur. These structures can be stabilised by interactions such as van der waals forces and π-π stacking, or by bonds between peptide molecules (*e.g.*,

hydrogen bonds).[38] Peptide aggregation is often driven by the hydrophobic effect, in which hydrophobic residues accrue at the centre of the aggregate structure, so that they are prevented from having contact with aqueous media. Aggregation is a problem for peptide therapeutics because it renders the drug molecules useless and prevents them from reaching the tissues.

Solubility is another issue faced by peptide therapeutics; drugs are often large and hydrophobic, and thus poorly soluble. Poor solubility means that a higher dose is required to achieve therapeutic plasma levels, and the likelihood of aggregation is increased. Replacement of hydrophobic residues with polar or charged residues is often effective in increasing peptide solubility, though this may have an adverse effect on potency. Another method for improving solubility is PEGylation: the conjugation of the peptide with polymer chains of polyethylene glycol (PEG). This aids solubilisation because the PEG polymer contains several ether moieties so is hydrophilic.[39] However, again there is a risk of altering the biological properties of the peptide.

Table 1.1 summarises the advantages and disadvantages of peptides drug candidates when compared to small molecules.

Small molecule drugs	Peptide drugs
Lower selectivity	Higher selectivity
Lower potency	High potency
Higher toxicity	Lower toxicity
Broad range of targets	Broad range of targets
High oral bioavailability and metabolic stability	Poor oral bioavailability and easily metabolised
High membrane permeability	Poor membrane permeability

Table 1.1: A table summarising the advantages and disadvantages of therapeutic peptides when compared to small molecule drugs.

1.2 Halogenated amino acids

1.2.1 Modification of peptides through incorporation of halogenated amino acids

When designing a peptide drug, there are clearly many intrinsic weaknesses that must be mitigated. One way of doing this is by incorporating non-natural amino acids into a target peptide sequence in order to modify its physicochemical properties. The inclusion of novel amino acids lends stability and protection from proteolysis to the peptide molecule, whilst

preserving its biological activity. Peptides with unnatural amino acids are examples of peptidomimetics: molecules designed so that they mimic the structure and properties of a natural peptide. Many methods for modification of natural amino acids exist: one of the most effective ways of alteration is to introduce halogenated groups into the molecule

Bromine-containing amino acids

The majority of bromine-containing peptide natural products are found in marine organisms, due to a higher abundance of bromide salts in the ocean. Brominated natural products are formed mostly by post-translational modification; bromoamino acids are not generally observed in nature.[40]

The addition of a bromine atom to a molecule can improve membrane permeability, because it can increase the overall lipophilicity due to its large size. This effect was observed by Gentry *et al.*,[41] when comparing the blood-brain barrier (BBB) permeability of a novel enkephalin analogue (DPLPE-Phe) to its bromo- and chloro-substituted derivatives. Halogenation of the enkephalin (DPLPE-Phe) was achieved by inclusion of a modified phenylalanine residue in the peptide structure. The halogenated DPLPE-Phe derivatives displayed an enhanced ability to pass through an *in vitro* BBB (**Figure 1.7**).

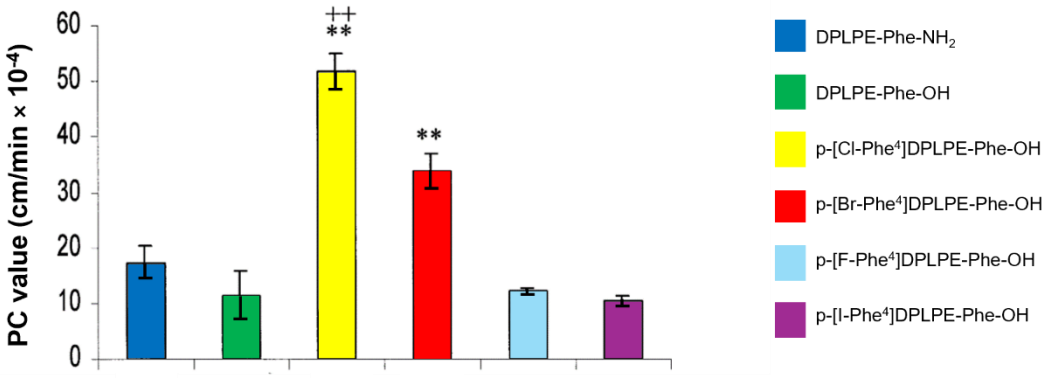

Figure 1.7: A graph displaying the mean permeability coefficient (PC) of a range of DPLPE-Phe analogues. The brominated analogue (p-[Br-Phe[4]]DPLPE-Phe-OH) and the chlorinated analogue (p-[Cl-Phe[4]]DPLPE-Phe-OH) show a significantly higher PC value than the parent compound (DPLPE-Phe-OH). Figure modified from Gentry *et al.*[41]

Bromine substitution may also influence the binding affinity of a peptide; this is illustrated in work by Jia *et al.*,[42] in which the antimicrobial peptide (AMP) Jelleine-I was evaluated alongside its halogenated derivatives (F-J-I, Cl-J-I, Br-J-I, and I-J-I), to examine the effect of halogenation on antimicrobial activity and proteolytic stability amongst other factors. The halogenated Jelleine-I derivatives were synthesised through incorporation of halo-

phenylalanine into the peptide sequence (P**F**KLSLHL-NH_2). The authors observed an increase in the antimicrobial activity for all halogenated analogues, (**Figure 1.8**) and an increase in proteolytic stability for the bromo- and fluoro-analogues.

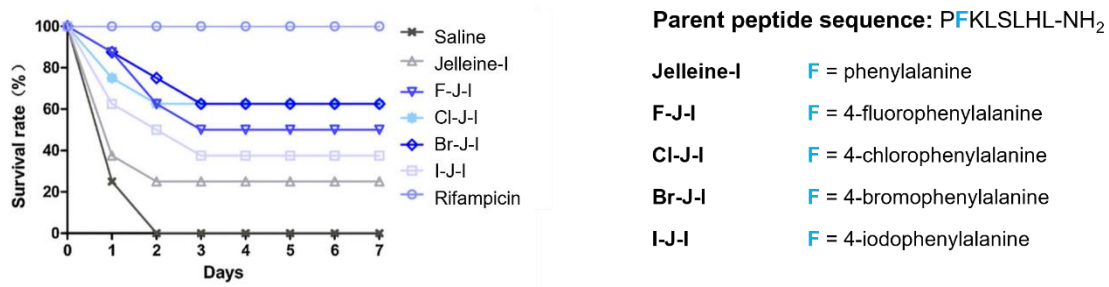

Figure 1.8: Graph displaying the *in vivo* antimicrobial efficacy of halogenated Jelleine-I derivatives in a mouse model infected with *E.coli*.[42] Saline and rifampicin were used as negative and positive controls, respectively. All halogenated derivatives displayed an increased antimicrobial efficacy over the parent Jelleine-I. Figure modified from Jia *et al.*[42]

Chlorine-containing amino acids

Chlorine is the most represented halogen in pharmaceutical products, with over 233 chlorine-containing FDA-approved drugs on the market, comprised of 167 unique small molecules (**Figure 1.9**).[43]

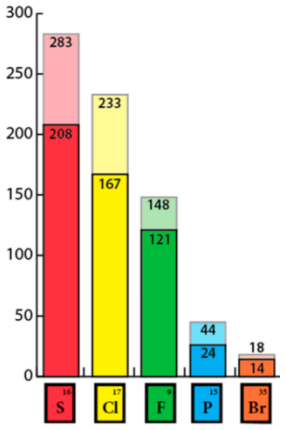

Figure 1.9: Chart displaying the frequency with which elements (excluding C, H, O, and N) are featured in small molecule FDA-approved drugs as of 2014. Figure modified from Smith *et al.*[43]

This is due to the prevalence of chlorine-containing natural products amongst terrestrial organisms, and the ability of chlorine to strike a balance between being able to form halogen bonds but being small enough to not significantly disrupt the molecular structure. The introduction of chlorine into peptides can increase lipophilicity,[44] membrane permeation,[41] and

metabolic stability.[45] An example of the varied effects chlorine addition can impart can be seen in the glyco-peptide drug vancomycin (**7**). Vancomycin (**7**) is an antibiotic glycopeptide drug which is produced naturally by the soil bacterium *Amycolatopsis orientalis*,[46] and features two aryl chloride moieties (**Figure 1.10**).

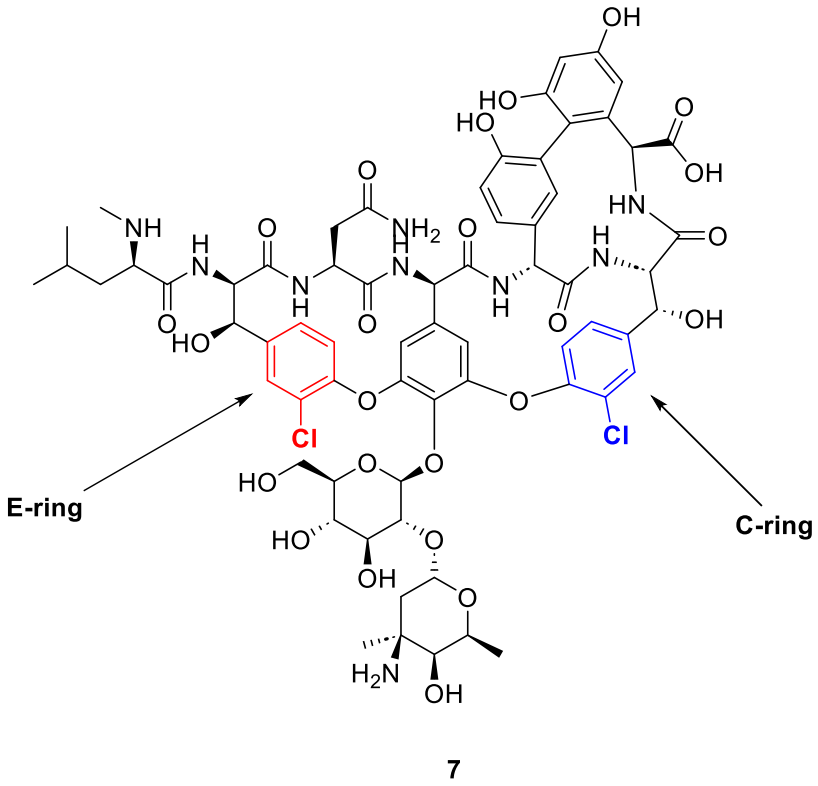

7

Figure 1.10: The structure of the antibiotic vancomycin (**7**), a naturally occurring glycopeptide with two aryl chloride groups. The E-ring chloride is marked in **red** and the C-ring chloride is marked in **blue.**

Vancomycin (**7**) disrupts bacterial cell wall biosynthesis by binding to the peptidoglycan precursor D-Ala-D-Ala.[47] Both of the chloride substituents in vancomycin (**7**) possess a different role in the binding affinity of the drug. The C-ring chloride helps to define the shape of the hydrophobic binding pocket, thereby increasing the binding affinity of the drug.[48] The E-ring chloride, whilst not directly involved in target binding due to its location outside of the pocket, may stabilise the dimeric form of the drug by engaging in a hydrophobic interaction with the other half of the dimer.[49] Both chlorine substituents reduce the mobility of the aryl rings, and both have been shown to be important for drug efficacy.[50]

Fluorine-containing amino acids

Fluorine is an outlier among the halogens due to its small size and high electronegativity. As a result, it has a very low polarizability and forms incredibly strong and short bonds with carbon

(1.35 Å). Its small size means that fluorine is an approximate bioisotere for hydrogen, hence substitution of hydrogen with a fluorine atom can significantly alter the properties of a molecule whilst preserving its conformational structure.[51–53] As a result, fluorine has been incorporated extensively into many pharmaceutical products with around 20% of marketed pharmaceuticals containing at least one fluorine atom.[54]

Many studies have been dedicated to exploring the effects of incorporating fluorinated amino acids into peptide sequences.[55–57] An example of how fluorination can impact peptide properties is outlined in work by Meng *et al.*, in which certain residues in the peptide hormone GLP-1 were replaced with hexafluoroleucines (**8**) to create multiple fluorinated GLP-1 analogues (**Figure 1.11**).[58] The authors found that the hexafluoroleucine additions conferred proteolytic resistance to the GLP-1 analogues, whilst mostly retaining the efficacy of the parent peptide.

GLP-1	NH_2-HAEGTFTSDVSSYLEGQAAKEFIAWLVKGR-$CONH_2$
F8	NH_2-H**L**EGTFTSDVSSYLEGQAAKEFIAWLVKGR-$CONH_2$
F9	NH_2-HA**L**GTFTSDVSSYLEGQAAKEFIAWLVKGR-$CONH_2$
F89	NH_2-H**LL**GTFTSDVSSYLEGQAAKEFIAWLVKGR-$CONH_2$
F10	NH_2-HAE**L**TFTSDVSSYLEGQAAKEFIAWLVKGR-$CONH_2$
F28	NH_2-HAEGTFTSDVSSYLEGQAAKE**L**IAWLVKGR-$CONH_2$
F29	NH_2-HAEGTFTSDVSSYLEGQAAKEF**L**AWLVKGR-$CONH_2$
F32	NH_2-HAEGTFTSDVSSYLEGQAAKEFIAW**L**VKGR-$CONH_2$

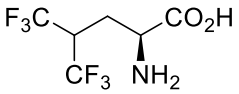

L (**8**)

Figure 1.11: L-R; A table displaying the sequences of the fluorinated GLP-1 analogues synthesised by Meng *et al.*,[58] **L** = hexafluoroleucine residue; the structure of 5,5,5′,5′,5′,5′-2S-hexafluoroleucine (**8**) is also shown.

Iodine-containing amino acids

Iodine atoms have the largest radius of the halogens (140 pm), and therefore have a higher polarizability. As such, they are able to participate in halogen bonding most efficiently. Iodinated amino acids are uncommon in nature, but diiodotyrosine is a prominent example of a stable iodo-amino acid which is essential for thyroid function (present in the thyroid hormones T3 and T4). Iodination of a peptide sequence may induce an increased propensity for self-assembly, as demonstrated by Bertolani *et al.*[59] In this study, an amyloidogenic fragment was compared against an iodinated analogue, and the latter was shown to form hydrogels at a much lower concentration than the wild-type peptide fragment (2.5 mM versus 75 mM for the parent peptide).

Additionally, iodine atom substitution has been shown to facilitate transport through the plasma membrane. Jakka *et al.* reported that the replacement of a tyrosine residue in a green fluorescent protein (GFP) with 3-iodo-tyrosine caused cell uptake of the protein to increase 6-fold (**Figure 1.12**).[60]

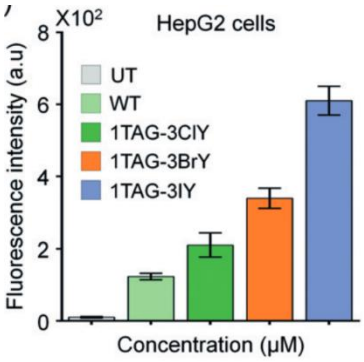

Figure 1.12: A graph displaying the fluorescence intensity of HepG2 cells after 90 minutes of treatment with the wild type (WT) GFP and its halogenated analogues (1TAG-3ClY, 1TAG-3BrY, and 1TAG-3IY). A much higher fluorescence intensity was measured for the iodinated analogue (1TAG-3IY), indicating that addition of an iodine atom facilitates membrane transport. Figure modified from Jakka *et al.*[60]

1.2.2 Traditional methods for halogenation of proteinogenic amino acids

There is a considerable amount of literature detailing the many syntheses of unnatural amino acids featuring at least one halogen atom.[40,61–63] In general, these can be divided into three categories: *de novo* synthesis from halogenated substrates, modification of a non-proteinogenic intermediate, or direct halogenation of a natural amino acid. Here, given the aims of the thesis, the focus will be on reviewing methods associated with direct halogenation.

A straightforward method of direct halogenation which has been used for many decades involves the application of elemental halogens, *i.e.*, Cl_2, Br_2, F_2, and I_2.[64] Aromatic amino acids (*i.e.*, phenylalanine, tyrosine etc.) can be converted into their corresponding aryl halide *via* electrophilic aromatic substitution. An example of the electrophilic chlorination of tyrosine (**9**) with Cl_2 is shown in **Scheme 1.1**.[65]

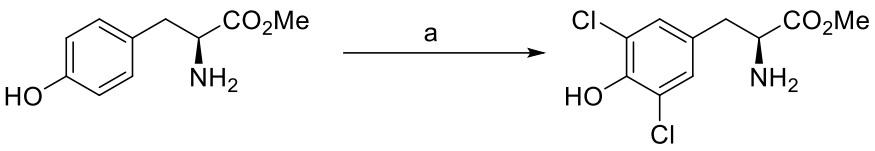

Scheme 1.1: Conversion of *L*-tyrosine (**9**) to 3,5-dichloro-*L*-tyrosine (**10**);[65] reagents and conditions: a) Cl_2, AcOH, strong heating.

Despite being an atom-economic and environmentally friendly method of halogenation, a drawback to using elemental halogens is that they are very reactive and difficult to handle, particularly fluorine. F_2 gas is extremely toxic and corrosive, and as such is typically used as a mixture with nitrogen (10% F_2 in N_2).[66]. An additional flaw of these reagents is their inherent lack of selectivity.[67]

In order to mitigate some of the disadvantages of elemental halogens, reagents have been developed that can deliver halogens in a safe and controlled manner. One of the largest classes of such is N-halo reagents, examples of which are shown in **Figure 1.13**.

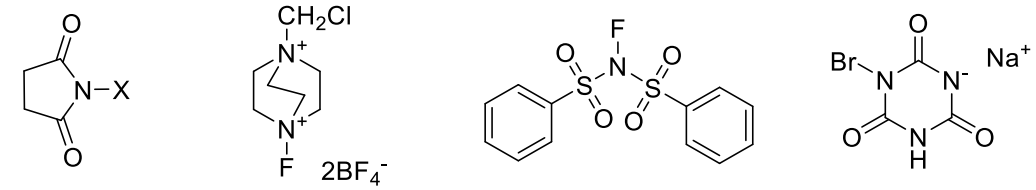

11 **12** **13** **14**

X = Br, Cl, I

Figure 1.13: Selected examples of common N-halo reagents used for halogenating amino acids; (L-R) N-halosuccinimide (**11**), Selectfluor™ (F-TEDA) (**12**), N-fluorobenzenesulfonimide (NFSI) (**13**), bromoisocyanuric acid sodium salt (**14**).

The N-halosuccinimides (NBS, NCS, and NIS) have been widely used for synthesising halogenated amino acids due to their stability and effectiveness. The N-X bond has a large dipole moment due to the electron-withdrawing nature of the N-succinimide fragment; NXS reagents are therefore an excellent source of halogen radicals or cations for electrophilic halogenation. They are capable of halogenating a range of amino acid functionalities, including hydroxyl groups,[68] aromatics,[69] and unactivated sp^3 carbons.[70]

Similarly to the N-succinimide reagents, N-F reagents like Selectfluor (**12**) and NSFI (**13**) facilitate electrophilic fluorination by pairing a fluorine atom with an electron withdrawing fragment. This induces a partial positive charge on the fluorine atom (δ^+), promoting lysis of the N-F bond. However, there has been extensive debate as to whether electrophilic

fluorination with N-F reagents proceeds via a radical (SET) or S_N2 pathway due to the difficulty of breaking the N-F bond heterolytically and forming F^+.[71] The reaction in **Scheme 1.2** demonstrates an example of how N-F reagents have been used to fluorinate amino acid derivatives.

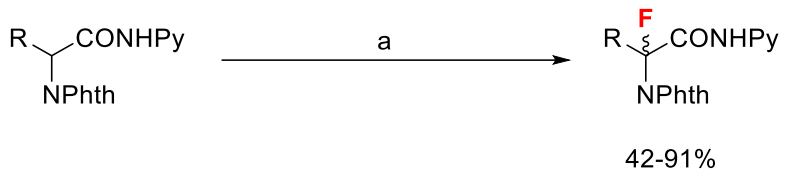

Scheme 1.2 α-fluorination of amino acid derivatives using Selectfluor (**12**) to produce α-quaternary amino acids, R = alkyl, aryl;[72] reagents and conditions: a) $Cu(OAc)_2$ (40 mol%), Selectfluor, (*R*)-3-hydroxy quinuclidine (20 mol%), $AgCO_3$, MeCN, 115°C, Ar, 8 h, 42-91%.

Another class of reagents frequently used for amino acid halogenation is those containing S-X bonds; examples of these are shown in **Figure 1.14**.

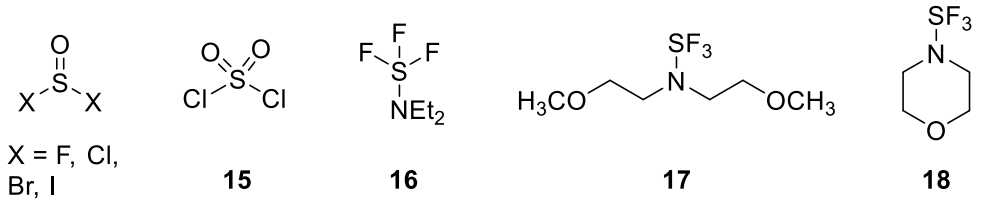

Figure 1.14: A selection of halogenating reagents containing a S-X bond: (L-R) thionyl halide (X = F, Cl, Br, I), sulfuryl chloride (**15**), diethylaminosulfur trifluoride (DAST) (**16**), Deoxo-fluor (**17**), Morpho-DAST (**18**).

Of the thionyl halides, thionyl chloride is the most commonly used reagent, although thionyl bromide is occasionally employed. Along with sulfuryl chloride (**15**), these two reagents are strongly acidic so are often overlooked in favour of the N-halosuccinimides; however, sulfuryl chloride has been used to chlorinate valine and alanine derivatives (**19, 20**) at the β-position (**Scheme 1.3**).[73]

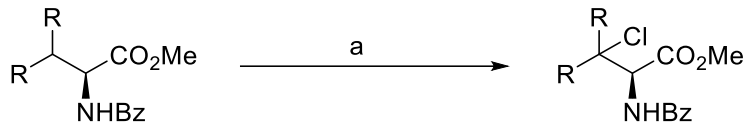

19 R = H
20 R = Me

21 R = H
22 R = Me

Scheme 1.3: β-chlorination of amino acid derivatives (**19**, **20**);[73] reagents and conditions: a) sulfuryl chloride, benzoyl peroxide (cat.), benzene, N_2, reflux, 1h, 92% (**22**), 36% (**21**).

The dialkylaminosulfur trifluorides are effective fluorinating agents, typically used for deoxofluorination of hydroxyl and carbonyl groups. DAST (**16**) in particular has found widespread use for this kind of fluorination.[74] However, the use of DAST is significantly limited by its liability to explode when heated to high temperatures.[75] Consequently a number of safer DAST derivatives were developed, including Deoxo-fluor (**17**), morpho-DAST (**18**), and Xtalfluor. Morpho-DAST has been successfully used to synthesise fluorinated proline derivatives (**Scheme 1.4**).[76]

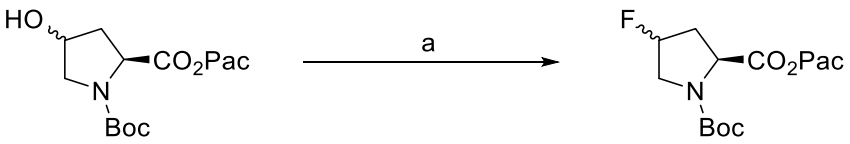

23 **24**

Scheme 1.4: Conversion of a 4-hydroxyproline derivative (**23**) to a 4-fluoroproline derivative (**24**);[76] reagents and conditions: a) morpho-DAST (**18**), DCM, -78 °C, N_2, 48 h, 94%.

An alternative approach to the chemical methods outlined above is to use halogenases to effect enzymatic halogenation. Halogenases can be divided into three categories by their mode of action: electrophilic halogenation, radical halogenation, and nucleophilic halogenation enzymes.[77] The earliest discovered electrophilic halogenases were haloperoxidases, followed later by flavin-dependent halogenases (FDH). An example of enzymes which perform radical halogenation are non-heme iron α-ketoglutarate-dependent halogenases. Nucleophilic halogenases are typically fluorinases, of which there are few, due to the scarcity of fluoride ions in the natural world and their high heat of hydration. [78]

An example of how enzymes can be used to halogenate amino acids is shown below in **Scheme 1.5**. In this study, the reductase/halogenase pair RebF and RebH was used to convert *L*-tryptophan (**25**) into 7-chloro- or 7-bromo-*L*-tryptophan.[79]

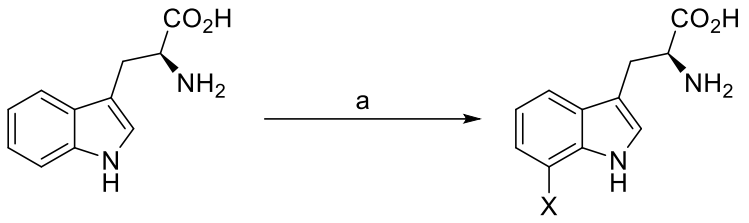

25

Scheme 1.5: Enzymatic conversion of *L*-tryptophan (**25**) into its 7-halo derivative (X = Br, Cl); a) *L*-tryptophan (2 mM), FAD (20 μM), NADH (50 mM), RebH (30 μM), RebF (120 μM), NaX (50 mM), incubated with agitation, 24 h.

Other notable reagents for amino acid halogenation include PCl_5,[80] trimethylsilyl halides,[81] and the classic combination of triphenylphosphine (PPh_3) and carbon tetrahalides used in the Appel reaction (**Scheme 1.6**).

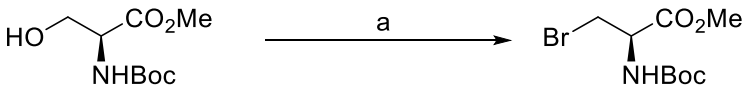

26 **27**

Scheme 1.6: An example of how the Appel reaction can be used to convert a derivative of *L*-serine (**26**) into a bromoalanine derivative (**27**);[82] reagents and conditions: a) CBr_4, PPh_3, DCM, 0 °C, 3 h, N_2, 73%.

The Appel reaction proceeds *via* a phosphonium halide intermediate generated from the reaction of CX_4 with PPh_3, and is used for converting alcohols into alkyl halides. A disadvantage of this reaction is the large amount of triphenylphosphine oxide generated as waste, and the toxicity of the CX_4 starting material in the case of carbon tetrachloride.

Many of the techniques for halogenating amino acids described above have significant issues surrounding their safety, toxicity, waste production, or ease of use. Hence, there is a need to develop methods of amino acid and peptide halogenation which do not suffer from the drawbacks associated with traditional chemical methods.

Fluorinated amino acids

Fluorine has been extensively incorporated into many pharmaceutical products because it modifies the properties of molecules in unique ways without drastically altering the steric effects.[51–53] The addition of fluorine will often change the pKa of neighbouring groups and the

hydrophobicity of the molecule. Naturally occurring organofluorine compounds are very rare; many strategies for the incorporation of fluorine into organic molecules have been developed.

Fluorine is a small atom with very high electronegativity, which forms an incredibly strong and short bond with carbon. When introduced to drug molecules, C-F bonds may slow down the metabolic process due to their strength and resistance to degradation. For example, the addition of a *para* fluorine substituent to an aromatic ring helps to prevent metabolic hydroxylation of a drug by CYP450 enzymes. The drug ezetimibe (**29**) was based upon the structure of compound **28**, a potent cholesterol absorption inhibitor (**Figure 1.15**). However, compound **28** was found to be prone to metabolic breakdown by CYP450 enzymes, so fluorine was introduced into the molecule to block the sites susceptible to metabolic attack.[83]

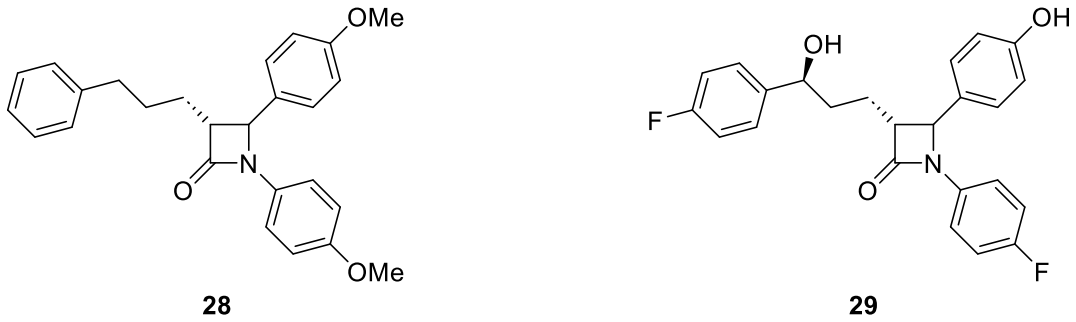

Figure 1.15: The structures of lead compound **28** and the cholesterol adsorption inhibitor ezetimibe (**29**). Fluorine atoms are used to prevent hydroxylation of the phenyl ring and dealkylation of the aryl ether.

The replacement of hydrogen atoms or methyl groups with single fluorine substituents or trifluoromethyl groups also increases the lipophilicity of a molecule,[84] as fluorine has a very low polarizability and is more lipophilic than hydrogen. This is important for drug molecules because they must be sufficiently lipophilic in order to pass through cell membranes *via* passive diffusion.

Hence, the synthesis of novel fluorinated amino acids as building blocks for target peptide sequences has been well studied. Many strategies for incorporating fluorine into canonical amino acids have been developed; **Figure 1.16** shows a small selection of the variety of fluorinated amino acids now within synthetic reach.[62]

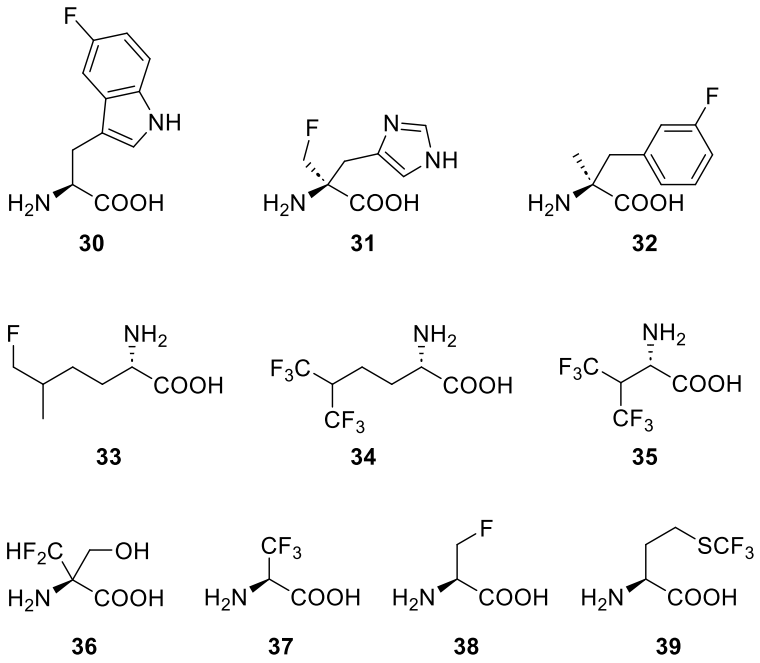

Figure 1.16: Examples of novel fluorinated amino acids that have been synthesised chemically.

There are many ways in which fluorinated amino acids can be synthesised; some synthetic routes use the natural amino acids as substrates, others require an asymmetric approach with non-amino acid reagents. **Scheme 1.7** shows examples of synthetic routes towards fluorinated amino acids. Route **1** involves the formation of an α-chloro ether from ethyl trifluoropyruvate (**40**), which then undergoes reductive dehalogenation to give a very reactive Michael acceptor (**41**). This compound reacts with $(Bu_3Sn)_2CuLi$ to form an organostannane (**42**), which can then undergo a Pd/Cu catalysed coupling reaction followed by conversion to a β-fluoro-α-keto acid (**44**). This is then converted to β-fluorophenylalanine (**45**).[85]

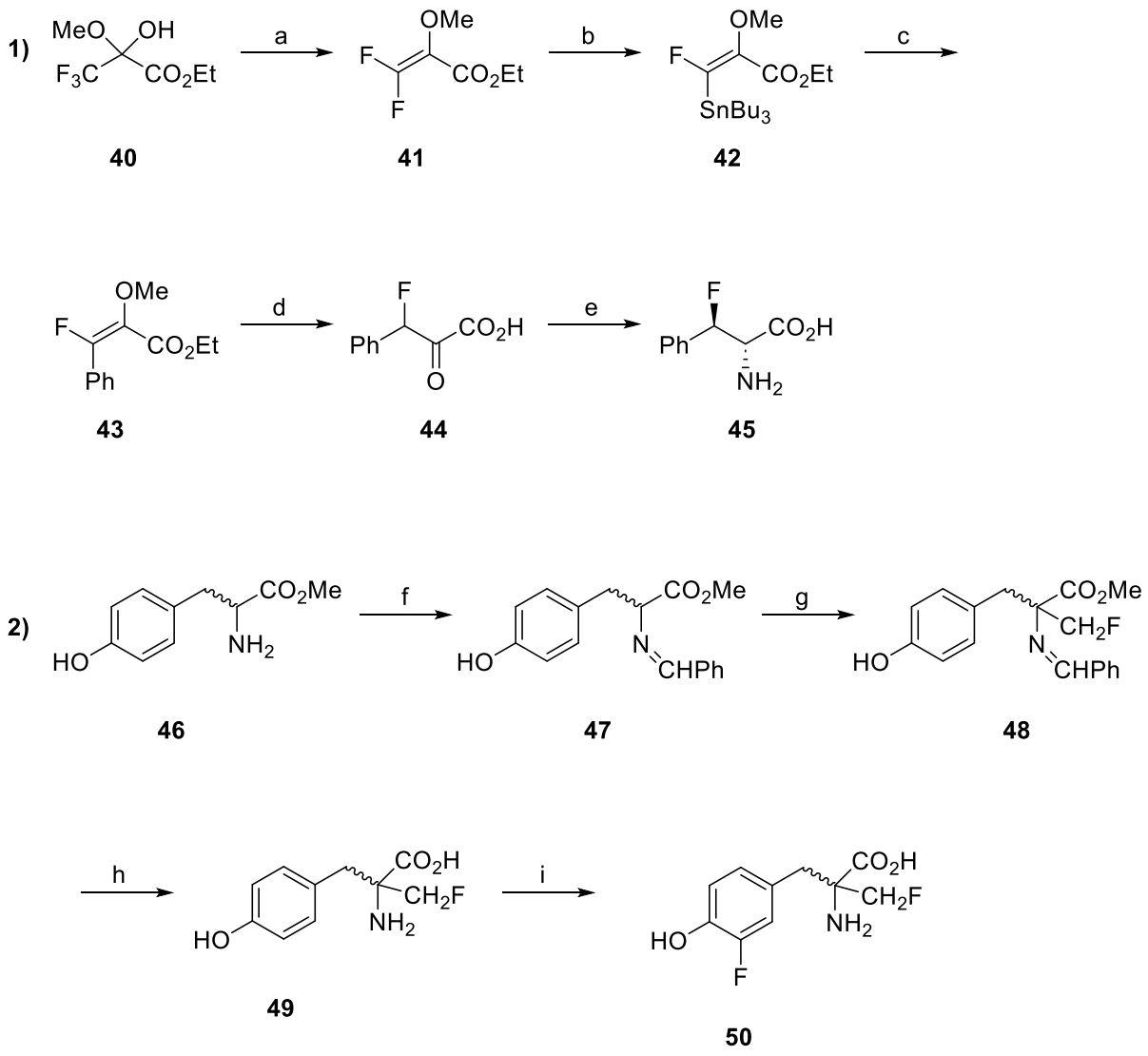

Scheme 1.7: Examples of syntheses of novel fluorinated amino acids. **1)** a) $SOCl_2$, pyridine, Zn, DMF, 75%; b) $(Bu_3Sn)_2CuLi$, 81%; c) CuI, $Pd(PPh_3)_4$, C_6H_5I, 95%; d) Me_3SiI, 75%; e) $NaBH_4$, NH_3, 40%; **2)** f) NEt_3, PhCHO, 97%; g) LDA, CH_2ClF, 25%; h) HCl, HBr, 80%; i) AcOF, TFA, 35%.

Route **2** involves the protection of tyrosine methyl ester (**46**) with benzaldehyde, followed by treatment with LDA and fluorochloromethane to furnish an α-fluoromethyl derivative (**48**). This is then deprotected, and AcOF is used to directly fluorinate the aromatic ring at the 3-position.[86]

Whilst a vast number of fluorinated amino acids have been synthesised, none have yet been incorporated into a successful peptide drug, although non-peptide drugs incorporating a novel fluorinated amino acid have been developed, *e.g.*, the HCV NS3/4A inhibitor Voxilaprevir, which contains a novel difluorinated amino acid with a cyclopropane ring (**51**) (**Figure 1.17**).[87]

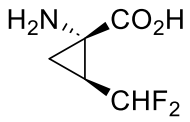

51

Figure 1.17: The novel fluorinated amino acid **51** used in the synthesis of Voxilaprevir.

1.3 Introduction to Electrochemistry

The use of electrochemistry as a synthetic tool has attracted an increasing amount of interest in recent years, as the trend towards more sustainable synthetic pathways continues. Electrochemistry is considered a very 'green' and atom-efficient alternative to the more traditional use of harsh chemical oxidants and reductants to effect transformations, as it uses electrons as both a reactant and energy source.

The most basic example of an electrochemical cell consists of an anode and a cathode connected to a power supply and submerged in an electrolyte solution (**Figure 1.18**).

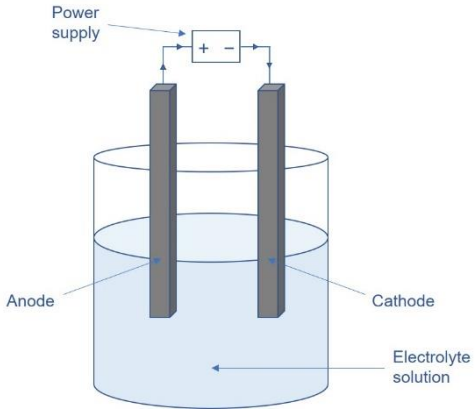

Figure 1.18: Diagram of a basic electrochemical cell containing an anode and a cathode connected to a power supply in an electrolyte solution.

When a substrate is dissolved in the electrolyte solution and a current is passed through the system, electrons can flow from the anode to the cathode *via* the power supply. This allows oxidation to occur at the anode, and reduction at the cathode. Oxidation and reduction must occur in tandem, but usually only one process is of synthetic interest. The electrode at which the reaction of interest is happening is referred to as the working electrode, and the other electrode is referred to as the counter electrode. During electrochemical reactions single electron transfer (SET) occurs between the solid electrode surface and the substrate in

solution, often creating a radical species. Electrochemical reactions are therefore heterogeneous processes.

When a current is passed through the system, a potential difference is created. If this potential is larger than the oxidation or reduction potential of the substrate, oxidation or reduction will occur. Redox potentials of substrates can be measured against a reference compound using cyclic voltammetry (CV). If the redox potential is known, it is possible to enhance the selectivity of an electrochemical reaction by controlling the electrochemical potential so that it remains just above the redox potential of the substrates. This type of reaction is called a potentiostatic reaction and requires a third electrode (reference electrode) to measure the potential difference between the cathode and anode. Alternatively, the current of the reaction can be controlled; this is referred to as a galvanostatic reaction. Whilst galvanostatic reactions are less selective, they are more commonly used due to ease of setup.[88]

1.3.1 Overview of electrochemical techniques

Electro-organic synthesis is an extremely broad field of research; this section will highlight a few well-studied techniques used in electrosynthesis.

Indirect electrolysis

Indirect electrolysis involves the use of a redox mediator: a redox active species that is capable of initiating the desired reaction in its active form. The redox mediator undergoes SET at the electrode surface to form a radical species which will then cause oxidation or reduction of the substrate, essentially acting as an electron shuttle (**Figure 1.19**).[89]

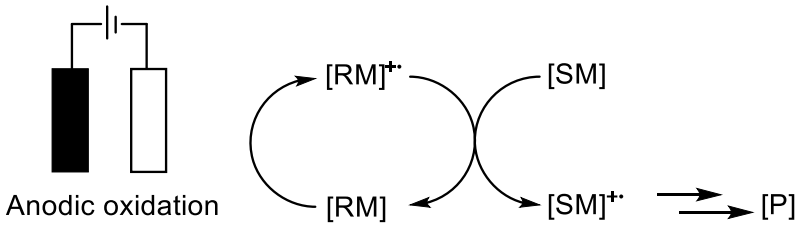

Figure 1.19: Diagram to show interaction of redox mediator (RM) with electrode and starting material (SM) to form product (P).

Redox mediators are chosen because they can act as an shuttle between the electrode surface and the substrate. Instead of a heterogeneous electron transfer process between the electrode surface and the substrate, a homogeneous reaction between the activated mediator

species and the substrate in solution is permitted. Often heterogeneous electrochemical processes can have associated kinetic issues, due to the necessity for substrate diffusion from bulk solution to the electrode surface. Additional energy is required for adsorption, desorption, and charge transfer processes. Therefore, the use of a redox mediator to enable a homogenous process circumvents these kinetic obstacles, permitting the reaction to be carried out at a lower potential.[90]

The 'cation pool' method [91]

Often electrochemical reactions feature oxidation of a substrate to a radical cation, which is then trapped by a nucleophile to yield the product. However, such nucleophiles can also be prone to anodic oxidation, which limits the success of these types of reactions. The cation pool method involves generation of carbocations *via* anodic oxidation at low temperatures (-78 °C) in solvents such as DCM. No nucleophiles are present in the reaction mixture at this stage, and the reaction is carried out in a divided cell so that the newly generated carbocations are not reduced at the cathode. In the next step, the carbocations are introduced to nucleophiles to allow product formation. This method is advantageous for controlling and facilitating electrochemical reactions that would be otherwise impossible

Paired electrolysis

In an electrochemical reaction, when one species is oxidised at the anode, another species must be reduced at the cathode and *vice versa*. Usually only one of these processes is of synthetic interest. However, in paired electrolysis both the oxidation and the reduction reactions are of interest. This increases the overall energy efficiency of the process.

A prominent example of a paired electrolysis reaction in industry is the chlor-alkali process, which uses sodium chloride to produce chlorine and sodium hydroxide, both desired products.

$$2Cl^- \rightarrow 2e^- + Cl_2 \qquad \textbf{[Eq. 1]}$$

$$2H_2O + 2e^- \rightarrow H_2 + OH^- \qquad \textbf{[Eq. 2]}$$

$$2NaCl + 2H_2O \rightarrow Cl_2 + H_2 + 2NaOH \qquad \textbf{[Eq. 3]}$$

Chlorine gas is produced at the anode (**Eq. 1**), whilst sodium hydroxide is produced at the cathode (**Eq. 3**).

Cyclic voltammetry

Cyclic voltammetry (CV) is an analytical tool used in electrochemistry to investigate the oxidation and reduction processes of molecules and record their redox potentials.[92] A voltammogram is produced that shows the change in current as the potential is swept from positive potential to negative potential, and then back to positive potential (**Figure 1.20**). Cyclic voltammetry experiments often include ferrocene/ferrocenium (Fc/Fc^+) as a reference, as it has a very predictable trace. Ferrocene is added after the substrate scan.

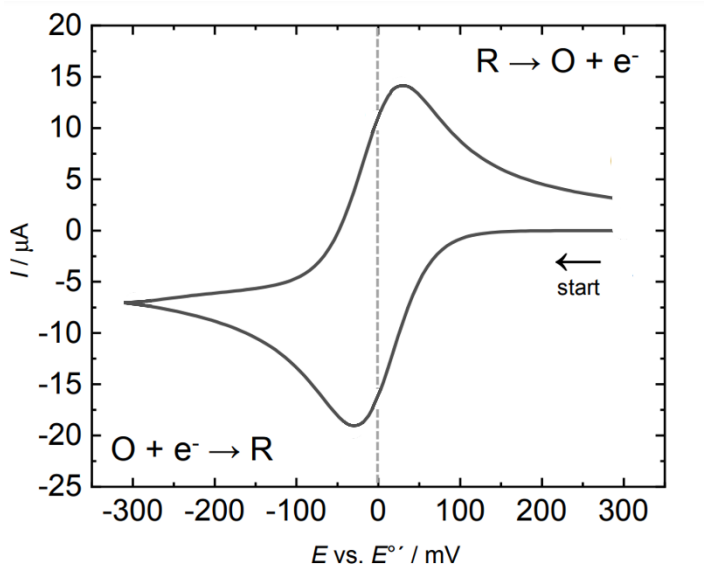

Figure 1.20: Diagram of a cyclic voltammogram displaying the typical peak shape for a reversible redox event. Figure modified from Yamada *et al.*[93]

Peaks are seen in a cyclic voltammogram, which indicate that a redox event is occurring, and pinpoints the potential at which the event takes place. As a substance undergoes SET at the electrode surface, a spike in current occurs. As more of the substance is oxidised or reduced, its concentration in the area around the electrode decreases. Therefore, the measured current will also decrease.[94] It is possible to determine redox potentials from a cyclic voltammogram when using a reference compound (e.g., ferrocene), which can aid reaction design.

1.3.2 Advantages and disadvantages of electrosynthesis

Advantages

Electrosynthesis is viewed as an environmentally friendly method compared to traditional oxidation/reduction reactions, in which large quantities of harmful oxidants or reductants are

required. Many chemical reactions produce a large amount of toxic waste as a result of this, so techniques with metal-free and oxidant-free conditions are increasingly favoured. An example of how an electrochemical reaction can provide a cleaner alternative to a chemical reaction is electrochemical C-H amination (**Scheme 1.8**).[95]

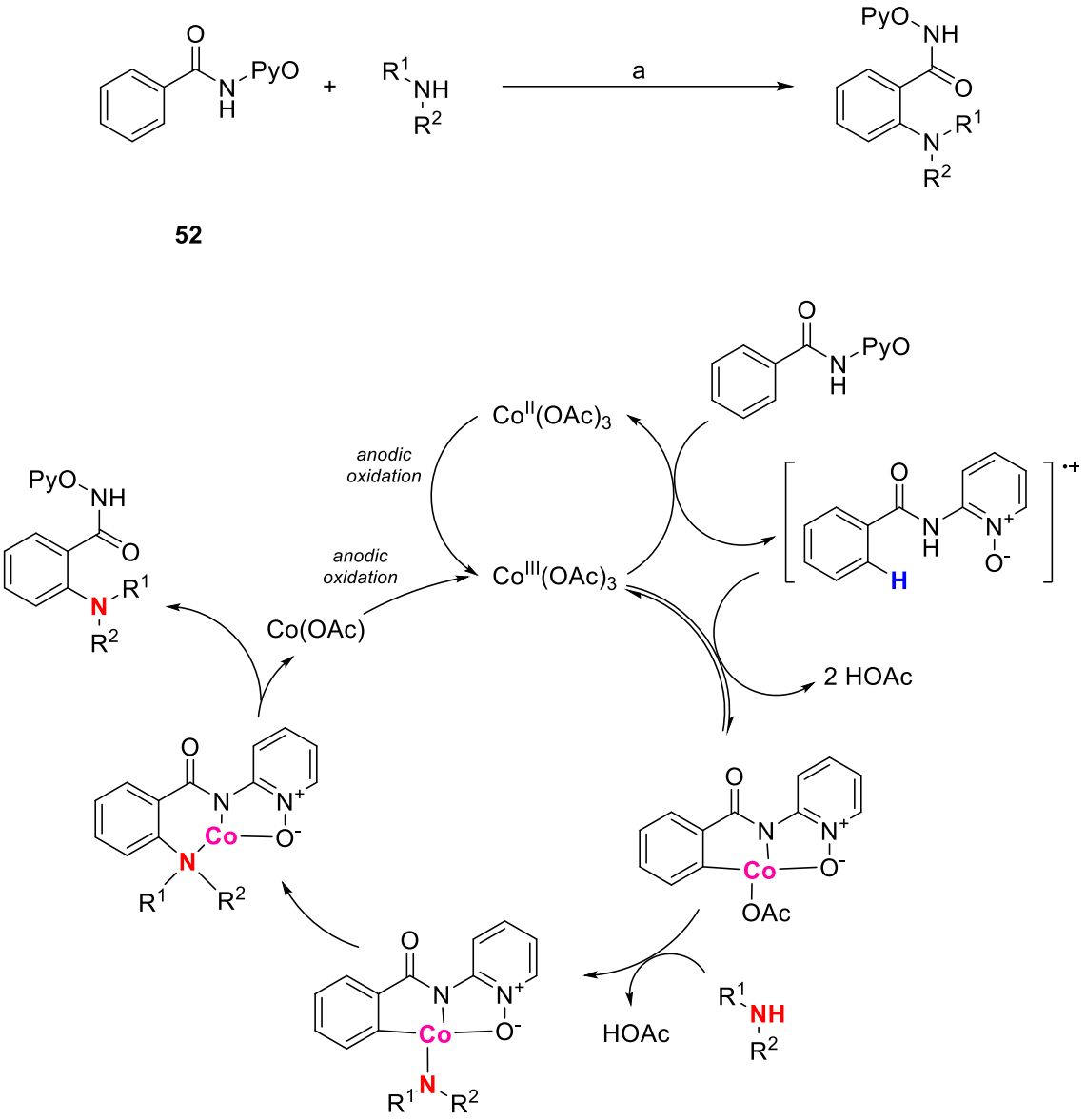

Scheme 1.8: Electrochemical C-H amination reaction using renewable solvent and substoichiometric copper acetate catalyst; R^1, R^2 = alkyl;[95] reagents and conditions: a) $Co(OAc)_2.4H_2O$ (10 mol%), KOAc, nBu_4NPF_6, GVL, 24 h, 40 °C, RVC (+) Pt (-), 51-83%. The mechanism for this reaction proposed by Sauermann *et al.* is also shown above.

Non-electrochemical amination reactions of this type often require high temperatures and super-stoichiometric amounts of chemical oxidants, whereas the electrochemical process only requires a small amount of copper acetate, which is continually recycled by anodic oxidation throughout the course of the reaction.

The ability to use milder conditions also means that electro-organic reactions often have a higher tolerance for functional groups and protecting groups. This is beneficial for reactions which use complex molecules as substrates or for late-stage functionalisation of larger molecules. The high tolerance for functional groups characteristic of electrochemical reactions is also caused by their inherent selectivity. Different functional groups have different oxidation potentials, which means that it is possible to selectively oxidise or reduce certain parts of a molecule under potentiostatic conditions. An example is one of the key steps in the synthesis of alliacol A, shown in **Scheme 1.9**.[96]

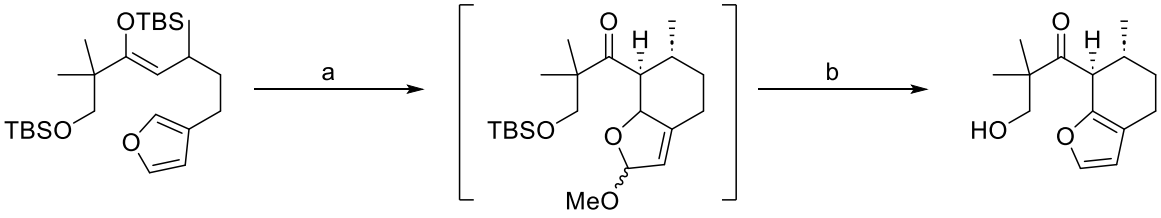

53 **54** **55**

Scheme 1.9: A key step in the synthesis of alliacol A;[96] reagents and conditions a) (+) RVC (-) C, 0.4 M $LiClO_4$, MeOH/DCM (1:4), 2,6-lutidine, rt, 15-20 mA, 2.2 F/mol; then b) TsOH, 4.5 h, RT, 88%.

Both the enoxysilane and furan functional groups in **53** are able to be oxidised, but in this reaction the enoxysilane is oxidised first in the presence of the furan, causing cyclisation. This is because the enoxysilane functional group has a lower oxidation potential than the furan (0.9 and 1.3 V, respectively). Therefore, the enoxysilane is oxidised first.

Additionally, electrochemical reactions can be scaled up with relative ease, hence the number of industrial processes featuring electrochemical reactions. This is because the technique is well suited to automation; reactions can be easily stopped by switching off the electricity and the current or potential can be monitored. The development of electrochemical flow reactors allows reactions to be run continuously. Automated equipment also means that electrochemical reactions can be highly controlled, and conditions are contained to the cell.

Disadvantages

A specialised electrochemical reactor set-up is required, which carries an associated cost. Electrochemistry can be performed in basic cells, but often the desired reaction requires specific electrode material, solvent, electrolyte and cell design, all of which can increase the cost of running the reaction.

The necessity of using an electrolyte increases the amount of waste produced by electrochemical reactions. Certain electrolytes (*e.g.* tetraalkylammonium salts) may also

complicate purification post-reaction as they are not able to be easily removed with an aqueous work-up. The range of solvents that can be used in electrochemical reactions is also limited; the solvent must be sufficiently polar to dissolve the electrolyte.

1.3.3 Electrochemistry in organic synthesis

The field of electrochemistry has been well-studied ever since the invention of the first electrical battery in the form of the Volta Pile in 1800. Synthetic organic electrochemistry began to pick up steam in the 1830s after Faraday observed the conversion of acetate anions to CO_2 and ethane *via* anodic oxidation.[97] Other significant contributions to the field by Faraday include the discovery of the laws of electrolysis, and the coinage of modern electrochemical terms such as 'electrode', 'anode', and 'cathode' in collaboration with Whewell.[98]

One of the earliest electro-organic reactions discovered was the Kolbe electrolysis, described by the same in 1848.[99] Inspired by Faraday's work, Kolbe discovered that valeric acid could be transformed into *n*-octane by electrolysis in an aqueous solution. The general reaction scheme for the Kolbe electrolysis is given below in **Scheme 1.10**.

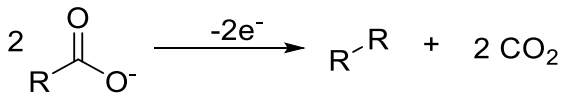

Scheme 1.10: General scheme for the Kolbe electrolysis for coupling carboxylic acids.

Electrochemical decarboxylation leaves an alkyl radical as an intermediate; subsequent combination with a second alkyl radical causes formation of a new C-C bond. The Kolbe electrolysis is still widely used in modern synthetic electrochemistry for its ease of access to alkyl radicals;[100] mixed-Kolbe reactions have also since been developed, in which the reagents are two different carboxylic acids (**Scheme 1.11**).

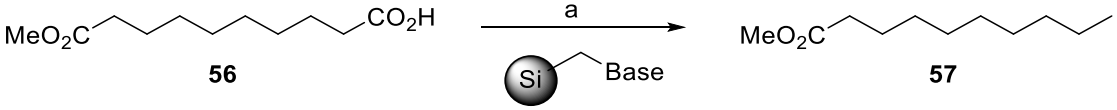

Scheme 1.11: Example of a mixed Kolbe electrolysis reaction which uses a solid-supported base;[101] reagents and conditions: a) (+) Pt (-) Pt, CH_3CO_2H, MeOH/MeCN, 100 mA/cm^2, 52%.

Research into electrosynthesis continued into the early 20th century; notable achievements included the development of the Tafel rearrangement in 1907, an example of a cathodic reduction reaction.[102] The Tafel rearrangement allows synthesis of hydrocarbons *via* rearrangement of substituted acetoacetic esters in an alcoholic sulfuric acid solution, using a lead cathode (**Scheme 1.12**).

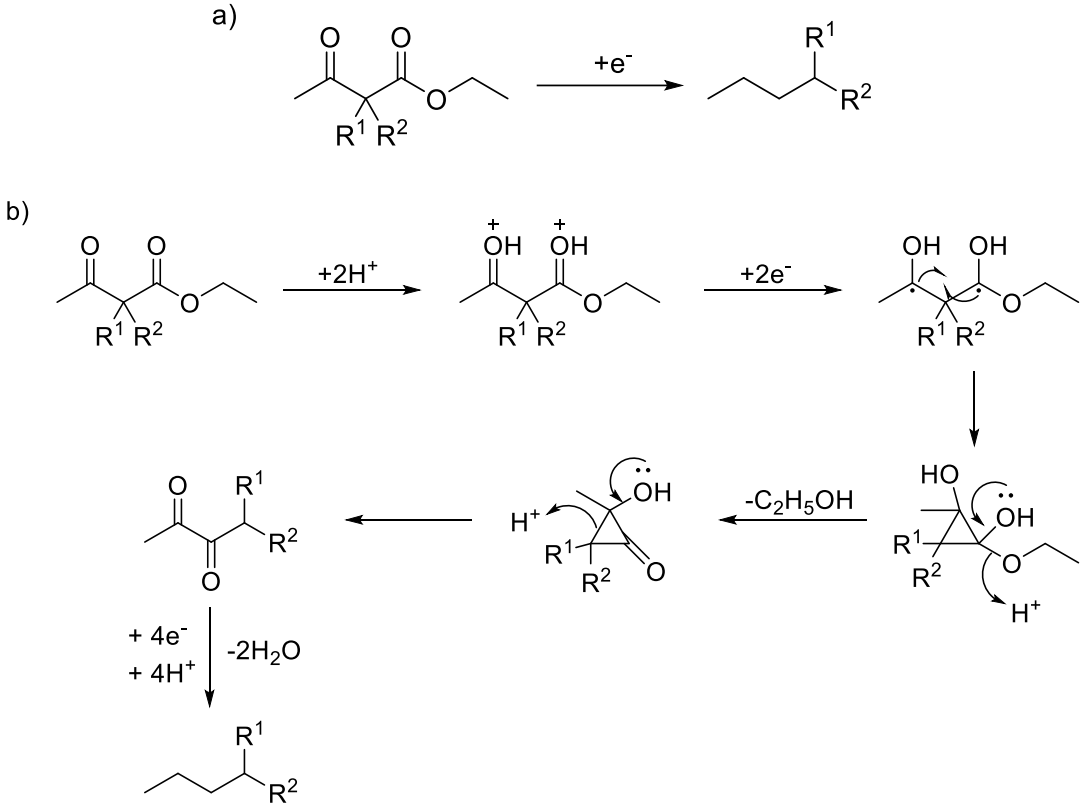

Scheme 1.12: a) General scheme for the Tafel rearrangement of substituted acetoacetic acid esters; b) the Tafel rearrangement mechanism.

Synthetic electrochemistry was widely researched throughout the 20th century, and was adopted frequently by industry, as the technique lends itself well to scale-up. One of the first electro-organic processes developed by industry was the cathodic reduction of glucose to form sorbitol and mannitol in 1937.[103] A later example of a successful industrial electrochemical process is the Monsanto adiponitrile process, developed in the 1960s. This process involves the hydrodimerization of two acrylonitrile (**58**) molecules using a lead cathode and a lead-silver anode to form adiponitrile (**59**), which is an important precursor to Nylon-6,6 (**Scheme 1.13**).[104]

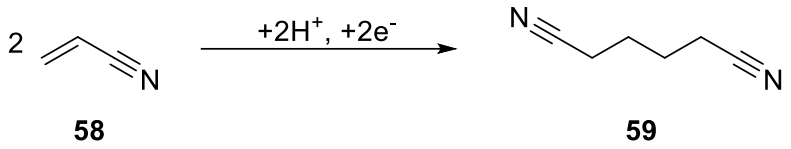

58 **59**

Scheme 1.13: General scheme describing the Monsanto adiponitrile process.

In the mid-20th century, electro-organic chemistry was bolstered by the discovery of several advances in electroanalytical tools and electrochemical engineering. The development of polarography and voltammetry enabled the analysis of several organic compounds and measurement of their electrochemical potentials. The development of the potentiostat allowed potentiostatic electrochemical reactions to be carried out, which afforded higher specificity to electro-organic reactions.

Notable advances in electrosynthesis in the latter half of the century include the Shono oxidation (**Scheme 1.14**) and the introduction of electroauxiliaries. The Shono oxidation features a two-electron anodic oxidation of carbamates (*e.g.*, **60**) or alkyl amides to form an *N*-carbamoyl iminium ion (**61**), which can then be trapped by a nucleophile.[105]

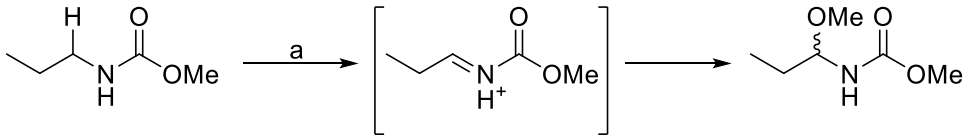

60 **61** **62**

Scheme 1.14: The Shono oxidation of methyl *N*-propylcarbamate (**60**);[105] reagents and conditions: a) (+) C (-) C, 500 mA, MeOH, Et_4NOTs, rt, 2 F/mol, undivided cell, 62%

A recent example of a Shono-type oxidation was published by Liu *et al.* in 2024 (**Scheme 1.15**).[106] This reaction uses anodic oxidation to generate an amidyl radical, which is captured by the nearby carboxylic acid moiety to form lactones. The principles of the Shono oxidation have been expanded to include imidate and imine substrates,[107] phosphoramides,[108] and sulfinamides.[109]

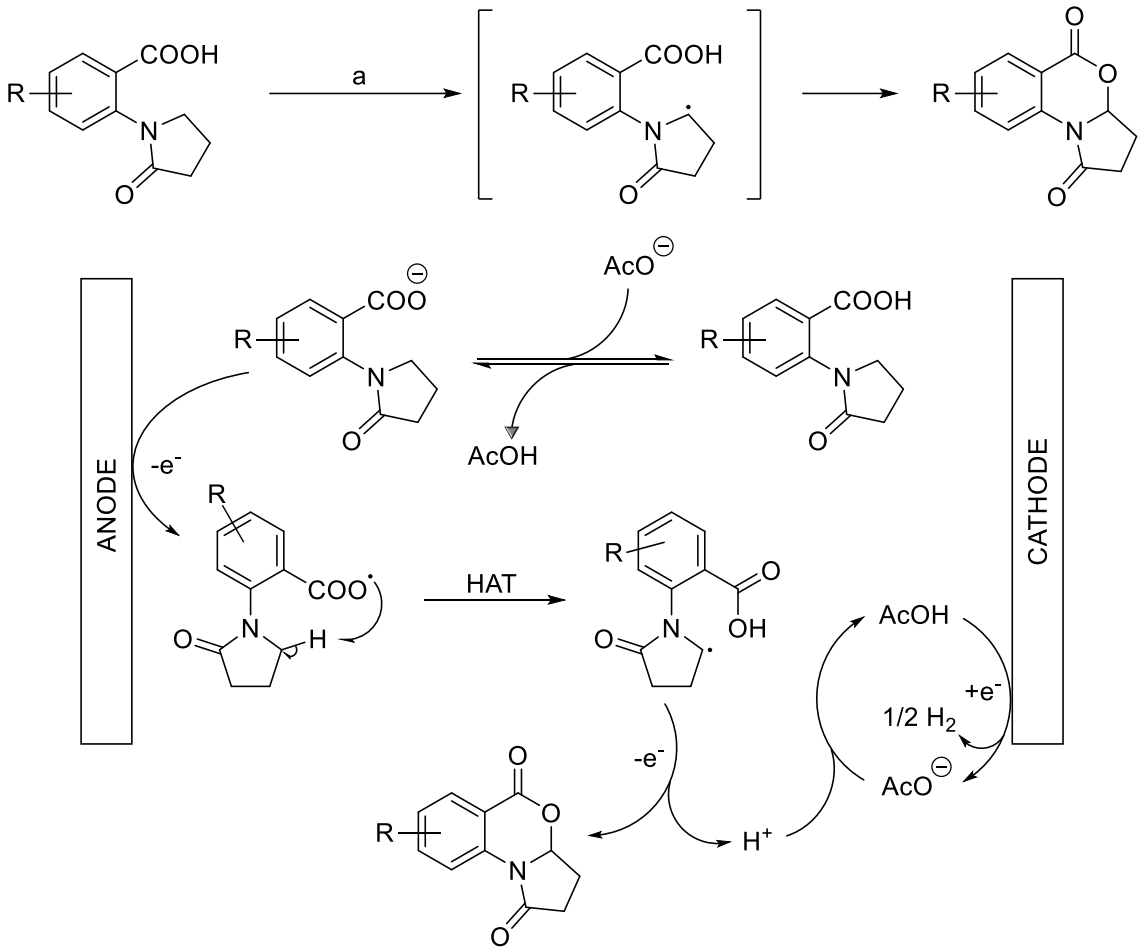

Scheme 1.15: Electrochemical lactonization using functionalised benzoic acid derivatives *via* a Shono-type mechanism, R = various;[106] reagents and conditions: Et_4NBF_4, MeCN/AcOH (11:1), C (+) C (-), 2.5 V, 6 h, undivided cell, 13-97%. The reaction mechanism proposed by Liu *et al.* is also shown.

An electroauxiliary is a particular functional group that when added to a substrate, facilitates an electrochemical reaction by altering the substrate's redox potential. Electroauxiliaries are often organosilicon or organotin moieties, *e.g.*, $Si(CH_3)_3$. This is because the σ(C-Si) bonding orbital has a higher energy than the C-H and C-C σ bonding orbitals. When the electroauxiliaries are present in a molecule with a double bond or a heteroatom, the σ(C-Si) bonding orbital can overlap well with the π orbitals or non-bonding p orbitals respectively. This raises the energy of the HOMO, meaning that electron transfer is favoured. Therefore, the redox potential will be lower.[110]

Scheme 1.16 shows an example of how an electroauxiliary can lower redox potential.[110] There are two double bonds in the substrate molecule (**63**), yet only one is next to the silicon electroauxiliary. This double bond is selectively oxidised in the presence of the other.

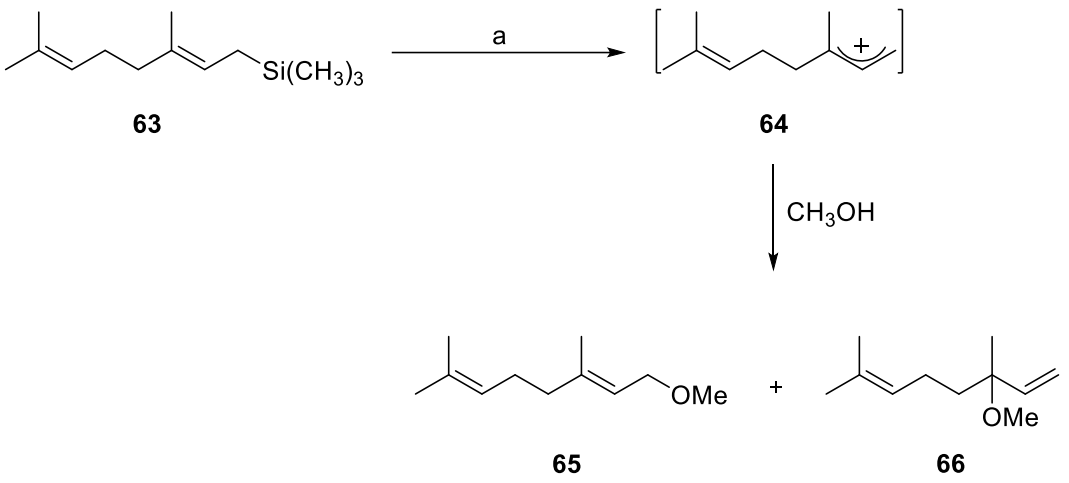

63 **64** **65** **66**

Scheme 1.16: Selective anodic oxidation of geranyltrimethylsilane (**63**);[110] reagents and conditions: a) C (+) C (-), 0.2 M Et_4NOTs/MeOH, 2.1 F/mol, 10 mA, 69% (68:32 **65:66**).

1.4 Electrochemistry applications in amino acid and peptide science

1.4.1 Electrochemical modification of amino acids

Electrochemical experiments using amino acids as substrates have been performed as early as the 1920s, when it was discovered that electrooxidation of glycine produced ammonia, formaldehyde, and CO_2, and that the expected Kolbe electrolysis did not take place.[111] Early research mostly focussed on investigating the products of electrochemical degradation of amino acids. In 1951, Weedon *et al.* reported an electrochemical method for the alkoxylation of amino acids (**Scheme 1.17**).[112]

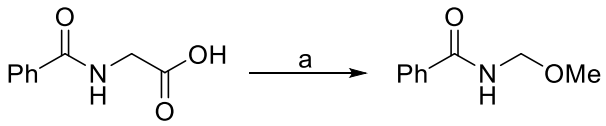

67 **68**

Scheme 1.17: Electrochemical alkoxylation of hippuric acid (**67**) to *N*-methoxymethyl benzamide (**68**);[112] reagents and conditions: a) (+) Pt (-) Pt, MeOH, 100-200 mA, 61%.

Theoretically, electrochemical methods could be beneficial for the modification of amino acids. Electro-organic synthesis can be a mild and functional group-tolerant technique. This would be very appropriate for reactions with amino acids, which inherently feature sensitive acid and amine groups. However, electrochemical reactions involving amino acid modification have

been relatively unexplored. In 1980, Brabec and Mornstein found that of the proteinogenic amino acids, only tyrosine, tryptophan, histidine, cystine, cysteine, and methionine were susceptible to anodic oxidation.[113] A couple of examples of more recent amino acid modification protocols are shown below.

Tyrosine

Selective tagging of tyrosine residues using phenothiazine derivatives has been achieved using an electrochemical method (**Scheme 1.18**).[114] In this reaction, the phenothiazine molecule (**70**) undergoes anodic oxidation to form an N-centred radical, which can then attack the *ortho* position on the tyrosine molecule (**69**).

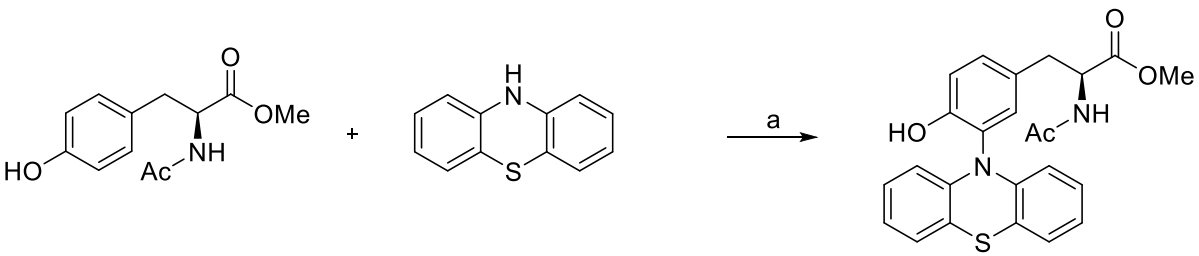

69 **70** **71**

Scheme 1.18: Electrochemical reaction of protected tyrosine (**69**) with a phenothiazine derivative (**70**);[114] reagents and conditions: a) (+) C (-) Ni, 10mA, CH_3CN/PBS, rt, N_2, 2.3 F/mol, 85%.

Studies have also utilised the *ortho* position on tyrosine (**9**) to conjugate it to other molecules, *e.g.*, phenylurazoles (**72**) (**Scheme 1.19**).[115]

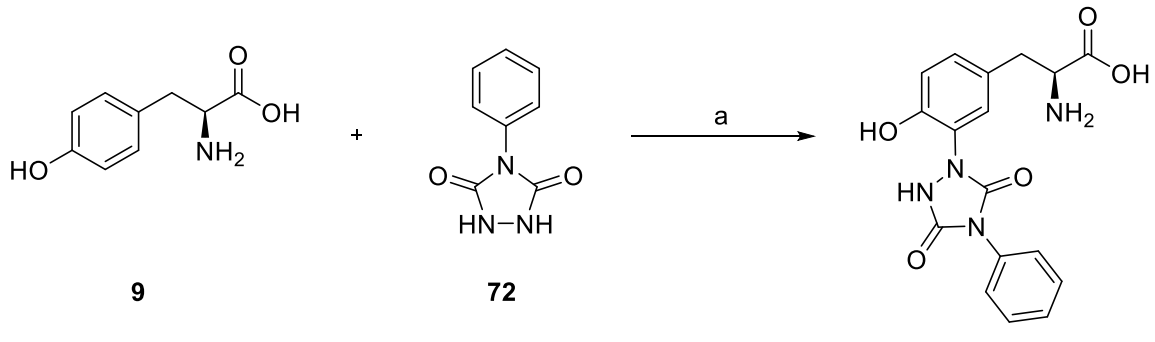

9 **72** **73**

Scheme 1.19: Conjugation of tyrosine (**9**) to phenylurazole (**72**) *via* anodic oxidation;[115] reagents and conditions: a) (+) C (-) Pt, SCE, PB, 0.36 V vs. SCE, 2 F/mol, N_2, 96%.

Tryptophan

Tryptophan residues have been subjected to bioconjugation with the molecule keto-ABNO (**74**) (**Scheme 1.20**).[116] The mechanism for this reaction is thought to occur *via* an oxoammonium cation generated by anodic oxidation of keto-ABNO (**74**), which then acts as an electrophile on reaction with the tryptophan residue.

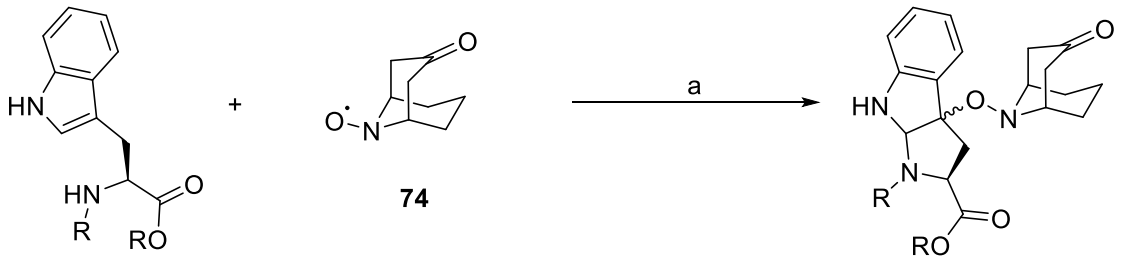

Scheme 1.20: Conjugation of tryptophan residues with keto-ABNO (**74**); R = peptide;[116] reagents and conditions: a) keto-ABNO (1 equiv), 4-oxo-TEMPO (0.2 equiv), CH_3CN-H_2O (1:1), 50 mM TBAP, (+) graphite (-) Pt, 0.9-1.2 V, 1-3 F/mol, 27-97%.

Serine

Nickel(II) Schiff base derivatives of serine (**75**) have been subjected to electrochemical reaction with NaBr to form the nickel(II) bromo-glycine derivative (**76**).[117] The reaction is stereoselective, as only one diastereoisomer of the brominated product is formed. This is due to the chiral nature of the Ni^{II} Schiff base. The Ni^{II} Schiff base essentially acts as a chiral auxiliary, as the amino acid product can then be isolated from the Ni^{II} derivative (**Scheme 1.21**).

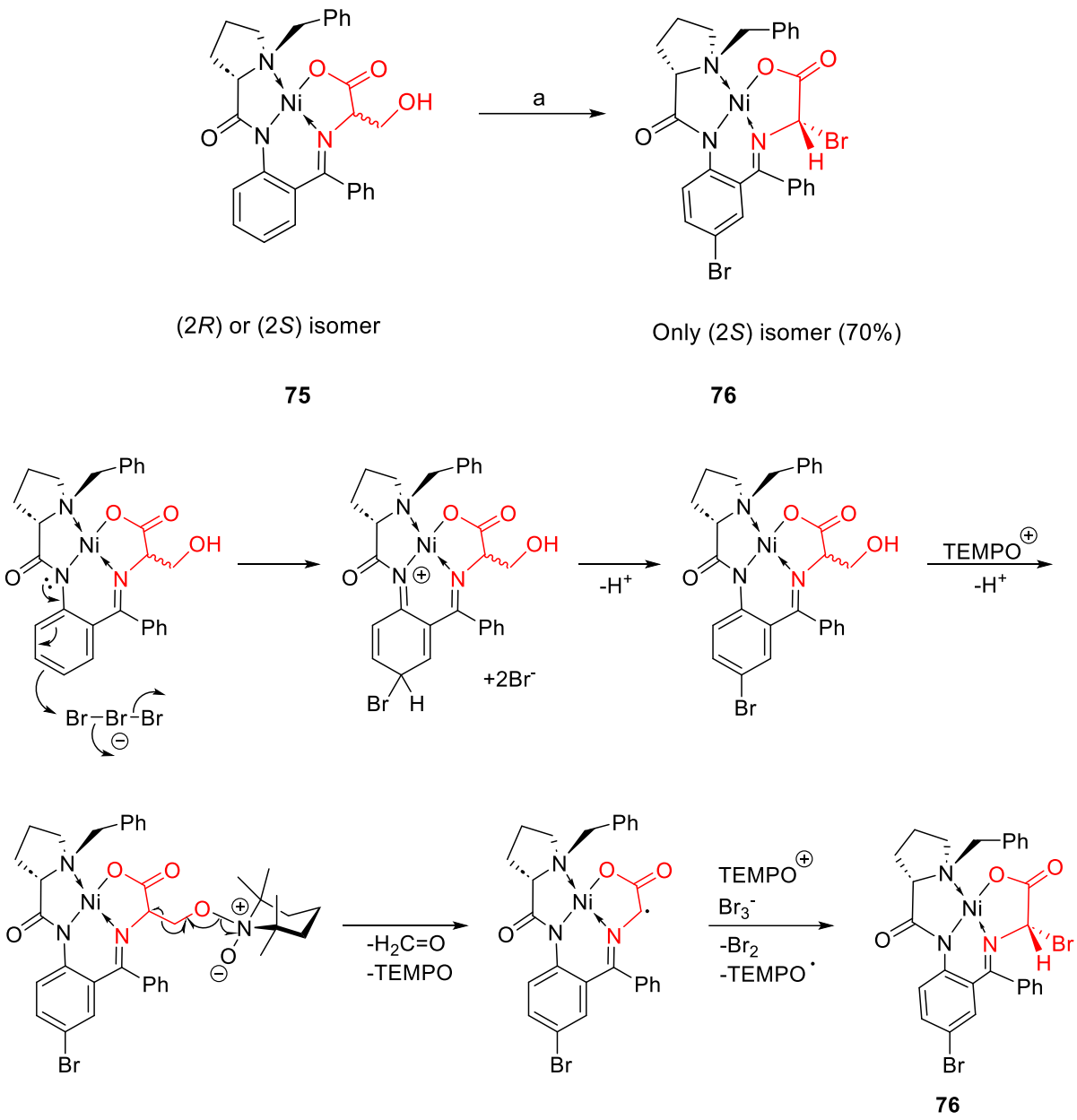

Scheme 1.21: Stereoselective anodic oxidation of a Ni^{II} serine derivative (**75**) to form a bromo-glycine derivative (**76**);[117] reagents and conditions a) C (+) C (-), NaBr, $NaHCO_3$, TEMPO, H_2O/DCM, 20 mA/cm^2, 2 F/mol, 70%. An illustration of the mechanism suggested by Levitskiy *et al.* is also provided.

Other examples of amino acid halogenation using traditional or electrochemical means will be discussed further in **Chapter 2**.

1.4.2 Electrochemical modification of peptides

Studies exploring the electrochemical modification of peptides have been carried out since the early 1960s, when Iwasaki successfully subjected the cyclic polypeptide rufomycin A to

selective electrooxidation.[118] Rufocmycin (**77**) is an antibiotic peptide isolated from a *Streptomyces* strain featuring a 3-nitrotyrosyl alanine linkage (**Scheme 1.22**). This linkage was successfully oxidised and cleaved in the presence of a tryptophan residue; organic methods up until this point had cleaved both tyrosyl and tryptophyl peptide bonds indiscriminately. Despite this early success, studies in the area of electrochemical peptide modification have been few and far between, with only a handful of publications on the subject.

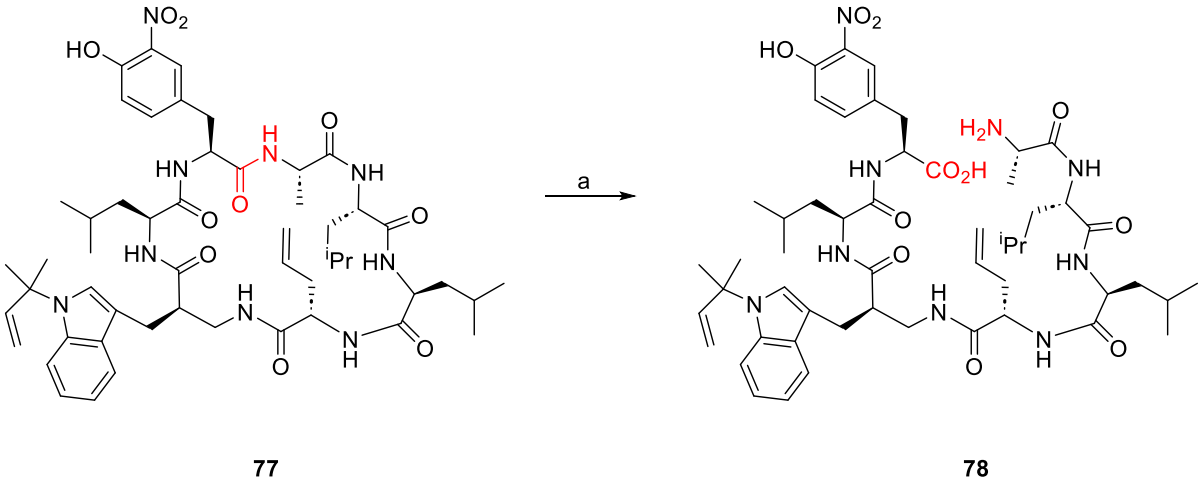

77 **78**

Scheme 1.22: The selective electrochemical cleavage of the 3-nitrotyrosyl-alanine linkage in the peptide Rufomycin A (**77**), an antibiotic isolated from *Streptomyces atratus*;[118] reagents and conditions: a) EtOH/ AcOH/H_2O/Dowex 50W X4, 100 V, Pt (+) Pt (-), 6 h, divided cell (acrylamide gel bridge).

Cyclisation

Early attempts to cyclise peptides or peptide isoteres utilised the Kolbe electrolysis to oxidatively couple two intramolecular carboxylic acid groups together, creating a C-C bond linkage (**Scheme 1.23**).[119]

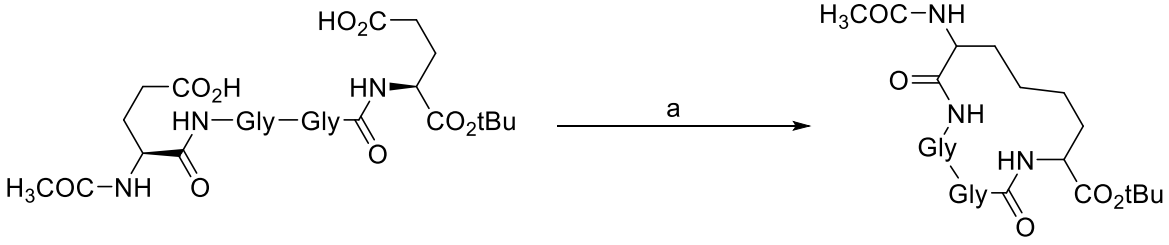

79 **80**

Scheme 1.23: Example of cyclisation of a Glu-Gly-Gly-Glu tetrapeptide (**79**) *via* oxidative Kolbe electrolysis;[119] reagents and conditions: a) (+) Pt (-) Pt, Na, NaOMe, MeOH/pyridine (3:1), 2.8 V, 2 h, 76%.

Anodic oxidation of amide groups has also been proven to facilitate cyclisation. **Scheme 1.24** shows how this technique has been used to create highly constrained bicyclic structures from dipeptides.[120] The reaction is highly diastereoselective, creating a new chiral centre at the ether.

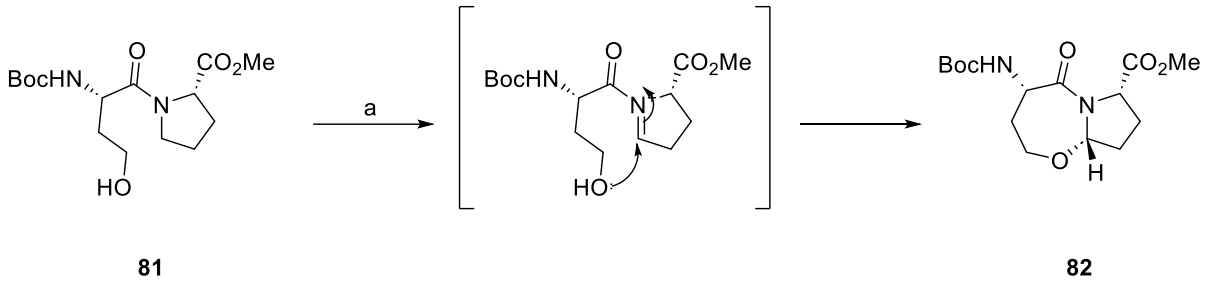

Scheme 1.24: Electrochemical cyclisation of the dipeptide Boc-L-homoserine-L-proline-OMe (**81**) to form a 1-aza-6-oxa-2-oxobicyclo[5.3.0]decane ring (**82**);[120] reagents and conditions: a) (+) Pt (-) Pt, 1 M Bu_4NBF_4 in MeCN/*i*-PrOH (95:5), 6.9 mA/cm^2, 3.8 F/mol, 48%

Nitration and Iodination

Selective nitration of tyrosine residues *via* electrooxidation was observed in globular proteins such as hen egg white lysozyme (HEWL) (**Scheme 1.25**).[121]

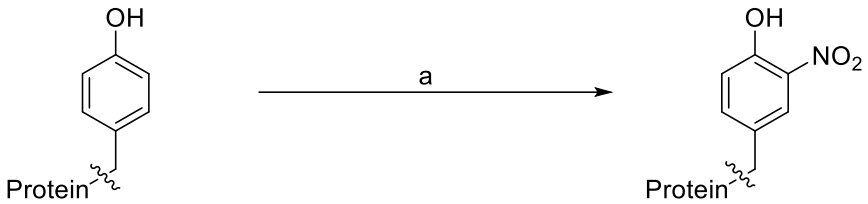

Scheme 1.25: Electrooxidation of Tyr residues in HEWL to form nitrated Tyr residues;[121] reagents and conditions: a) (+) Pt (-) Pt (Ref) SCE, 0.85 V, 50 mM sodium nitrite, 50 mM sodium tetraborate, 15 min, 33%

In this reaction, sodium nitrite provides a source of NO_2^- ions, which are oxidised to produce $NO_2^{\cdot}$ radicals. The radical will then nitrate the tyrosine residue at the 3-position. In a similar way to the above reaction, selective electrochemical iodination of proteins has also been explored. However, iodide ions were used in place of nitrite ions to electrochemically iodate the tyrosine residues present in horse heart myoglobin.[122] Non-selective electrochemical iodination has also been explored as a method of radiolabelling peptides and proteins.[123]

Methoxylation

A method for regioselective anodic methoxylation of dipeptides at the α-position has been reported, using NaCl as a mediator (**Scheme 1.26**).[124]

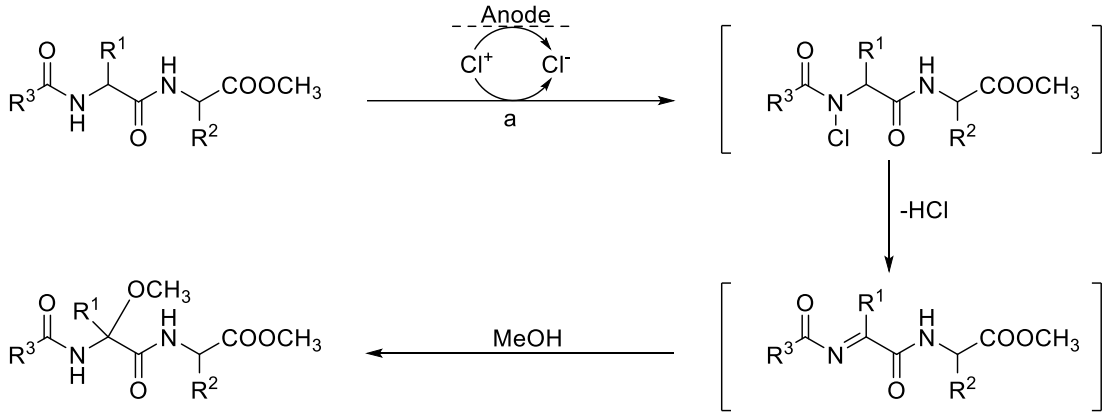

Scheme 1.26: General scheme for anodic methoxylation of dipeptides in the presence of chloride ions;[124] reagents and conditions: a) (+) Pt (-) Pt, MeOH, 0.2 M $LiClO_4$, NaCl, 200 mA, 3 F/mol, 6-69%

In this reaction, chloride ions undergo a 2-electron oxidation at the anode to produce chlorine cations, which replace the proton on one of the nitrogens. Subsequent loss of HCl leads to an imino- compound, which can react with methanol to form the methoxylated product (**Scheme 1.26**).

An excellent review of more recent developments in the field of electrochemical modification of peptides and proteins was published in 2021 by the Malins group.[125] This review outlines the current status of electrochemical peptide modification, and discusses how the technique has been used for a number of applications, including peptide synthesis,[126] C-terminal modification,[127] and disulfide bond formation.[128] Another informative review which focussed on residue-specific electrochemical peptide modification was published by Sarkar in 2024.[129]

1.5 Project Aims

The aim of this research is to explore methods of synthesising novel amino acids, which could then be built into peptides. The effect of the incorporation of these novel amino acids into peptides on peptide structure and function can then be assessed. Often the inclusion of novel amino acids can improve a peptide's 'drug-like' properties and can help mitigate some of the inherent weaknesses of peptide drugs. This research will focus on two areas of interest:

synthesis of fluorinated amino acids and the use of electrochemistry to modify amino acids and peptides.

Novel fluorinated amino acids are a desirable target because the addition of fluorine often has a significant effect on a compound's chemical and physical properties; in particular it can improve metabolic stability, which is a common obstacle faced by peptide drugs. This research will focus on identifying ways of modifying canonical amino acids by adding fluorine-containing groups.

The second half of this research will focus on modification of amino acid substrates using electrochemistry. The use of electrochemistry is an attractive prospect because it is often a highly specific technique which uses relatively mild conditions. It is therefore potentially suitable for late-stage modification of peptides, or for selective tagging of specific amino acid residues on a larger peptide.

1.6 References

1 J. L. Lau and M. K. Dunn, *Bioorg. Med. Chem.*, 2018, **26**, 2700–2707.
2 K. Fosgerau and T. Hoffmann, *Drug Discov. Today*, 2015, **20**, 122–128.
3 F. G. Banting, C. H. Best, J. B. Collip, W. R. Campbell and A. A. Fletcher, *Can. Med. Assoc. J.*, 1922, **12**, 141–6.
4 D. J. Craik and M. W. Kan, *Expert Opin. Drug Discov.*, 2021, **16**, 1399–1402.
5 L. Wang, N. Wang, W. Zhang, X. Cheng, Z. Yan, G. Shao, X. Wang, R. Wang and C. Fu, *Signal Transduct. Target Ther.*, 2022, 7.
6 F. Sanger, *Biochem. J.*, 1945, **39**, 507–15.
7 F. Sanger and H. Tuppy, *Biochem. J.*, 1951, **49**, 463–81.
8 E. Fischer and E. Fourneau, *Ber. Dtsch. Chem. Ges.*, 1901, **34**, 2868–2877.
9 M. Bergmann and L. Zervas, *Ber. Dtsch. Chem. Ges.*, 1932, **65**, 1192–1201.
10 C. R. Harington and T. H. Mead, *Biochem. J.*, 1935, **29**, 1602–11.
11 V. du Vigneaud, C. Ressler, J. M. Swan, C. W. Roberts and P. G. Katsoyannis, *J. Am. Chem. Soc*, 1954, **76**, 3115–3121.
12 V. du Vigneaud, D. T. Gish and P. G. Katsoyannis, *J. Am. Chem. Soc*, 1954, **76**, 4751–4752.
13 M. Cottet, L. Albizu, S. Perkovska, F. Jean-Alphonse, R. Rahmeh, H. Orcel, C. Méjean, S. Granier, C. Mendre, B. Mouillac and T. Durroux, *Curr. Opin. Pharmacol.*, 2010, 10, 59–66.
14 J. C. Sheehan and G. P. Hess, *J. Am. Chem. Soc*, 1955, **77**, 1067–1068.
15 F. C. McKay and N. F. Albertson, *J. Am. Chem. Soc*, 1957, **79**, 4686–4690.
16 R. B. Merrifield, *J. Am. Chem. Soc*, 1963, **85**, 2149–2154.
17 A. C. Wilson, S. Vadakkadath Meethal, R. L. Bowen and C. S. Atwood, *Expert Opin. Investig. Drugs*, 2007, **16**, 1851–1863.
18 W. Bauer, U. Briner, W. Doepfner, R. Haller, R. Huguenin, P. Marbach, T. J. Petcher and J. Pless, *Life Sci.*, 1982, **31**, 1133–1140.
19 M. Ondetti and D. Cushman, US Patent, 4046889A, 1977.
20 J.-P. Raufman, *Regul. Pept.*, 1996, **61**, 1–18.

21 R. Y. Calne, S. Thiru, P. Mcmaster, G. N. Craddock, D. J. G. White, D. B. Evans, D. C. Dunn, B. D. Pentlow and K. Rolles, *The Lancet*, 1978, **312**, 1323–1327.
22 R. Derda, S. K. Y. Tang, S. C. Li, S. Ng, W. Matochko and M. R. Jafari, *Molecules*, 2011, **16**, 1776–1803.
23 Y. Ding, J. P. Ting, J. Liu, S. Al-Azzam, P. Pandya and S. Afshar, *Amino Acids*, 2020, **52**, 1207–1226.
24 J. Shi, T. Sun and M. Yang, *Org. Chem. Front.*, 2024, **11**, 1623–1640.
25 S. B. Yang, N. Banik, B. Han, D. N. Lee and J. Park, *Pharmaceutics*, 2022, **14**, 1378.
26 D. M. Copolovici, K. Langel, E. Eriste and Ü. Langel, *ACS Nano*, 2014, 8, 1972–1994.
27 A. Lalatsa, A. G. Schatzlein and I. F. Uchegbu, *Mol. Pharm.*, 2014, 11, 1081–1093.
28 W. Li, M. D. Joshi, S. Singhania, K. H. Ramsey and A. K. Murthy, *Vaccines (Basel)*, 2014, **2**, 515–536.
29 M. S. Mitra, S. DeMarco, B. Holub, L. Thiruneelakantapillai and E. A. Thackaberry, *Regul. Toxicol. Pharmacol.*, 2020, **117**, 104766.
30 M. Boegh, M. García-Díaz, A. Müllertz and H. M. Nielsen, *Eur. J. Pharm. Biopharm.*, 2015, **95**, 136–143.
31 D. J. Drucker, *Nat. Rev. Drug Discov.*, 2020, **19**, 277–289.
32 S. Y. Hong, J. E. Oh and K.-H. Lee, *Biochem. Pharmacol.*, 1999, **58**, 1775–1780.
33 B. Khatri, V. R. Nuthakki and J. Chatterjee, *Methods Mol. Biol.,* 2019, **2001**, 17– 40.
34 A. Bernkop-Schnürch, *J. Contr. Release*, 1998, **52**, 1–16.
35 S. Jevševar, M. Kunstelj and V. G. Porekar, *Biotechnol. J.*, 2010, **5**, 113–128.
36 A. D. Frankel and C. O. Pabo, *Cell*, 1988, **55**, 1189–1193.
37 C. A. Lipinski, *Adv. Drug Deliv. Rev.*, 2016, 101, 34–41.
38 K. L. Zapadka, F. J. Becher, A. L. Gomes dos Santos and S. E. Jackson, *Interface Focus*, 2017, 7.
39 Y. Li, K. A. Clark and Z. Tan, *Chin. Chem. Lett.*, 2018, **29**, 1074–1078.
40 S. Bittner, R. Scherzer and E. Harlev, *Amino Acids*, 2007, 33, 19–42.
41 C. L. Gentry, R. D. Egleton, T. Gillespie, T. J. Abbruscato, H. B. Bechowski, V. J. Hruby and T. P. Davis, *Peptides (N.Y.)*, 1999, **20**, 1229–1238.
42 F. Jia, Y. Zhang, J. Wang, J. Peng, P. Zhao, L. Zhang, H. Yao, J. Ni and K. Wang, *Peptides (N.Y.)*, 2019, **112**, 56–66.
43 B. R. Smith, C. M. Eastman and J. T. Njardarson, *J. Med. Chem.*, 2014, 57, 9764–9773.
44 P. Jeschke, *Pest Manag. Sci.*, 2010, 66, 10–27.
45 K. Naumann, *Pest Manag. Sci.*, 2000, 56, 3–21.
46 R. S. Griffith, *J. Antimicrob. Chemother.*, 1984, **14**, 1–5.
47 E. Mühlberg, F. Umstätter, C. Kleist, C. Domhan, W. Mier and P. Uhl, *Can. J. Microbiol.*, 2020, **66**, 11–16.
48 J. R. Pinchman and D. L. Boger, *Bioorg. Med. Chem. Lett.*, 2013, **23**, 4817–4819.
49 U. Gerhard, J. P. Mackay, R. A. Maplestone and D. H. Williams, *J. Am. Chem. Soc*, 1993, **115**, 232–237.
50 C. M. Harris, R. Kannan, H. Kopecka and T. M. Harris, *J. Am. Chem. Soc*, 1985, **107**, 6652–6658.
51 E. P. Gillis, K. J. Eastman, M. D. Hill, D. J. Donnelly and N. A. Meanwell, *J. Med. Chem.*, 2015, **58**, 8315–8359.
52 J. Han, A. M. Remete, L. S. Dobson, L. Kiss, K. Izawa, H. Moriwaki, V. A. Soloshonok and D. O'Hagan, *J. Fluor. Chem.*, 2020, 239.
53 S. Purser, P. R. Moore, S. Swallow and V. Gouverneur, *Chem. Soc. Rev.*, 2008, **37**, 320–330.
54 M. Inoue, Y. Sumii and N. Shibata, *ACS Omega*, 2020, **5**, 10633–10640.
55 S. Huhmann and B. Koksch, *Eur. J. Org. Chem.*, 2018, **2018**, 3667–3679.

56 A. A. Berger, J. S. Völler, N. Budisa and B. Koksch, *Acc. Chem. Res.*, 2017, **50**, 2093–2103.
57 J. N. Sloand, M. A. Miller and S. H. Medina, *Peptide Science*, 2021, **113**, e21484.
58 H. Meng, S. T. Krishnaji, M. Beinborn and K. Kumar, *J. Med. Chem.*, 2008, **51**, 7303–7307.
59 A. Bertolani, L. Pirrie, L. Stefan, N. Houbenov, J. S. Haataja, L. Catalano, G. Terraneo, G. Giancane, L. Valli, R. Milani, O. Ikkala, G. Resnati and P. Metrangolo, *Nat. Commun.*, 2015, **6**, 7574.
60 S. R. Jakka, V. Govindaraj and G. Mugesh, *Angewandte Chemie*, 2019, **131**, 7795–7799.
61 M. Strickland and C. L. Willis, in *Amino Acids, Peptides and Proteins in Organic Chemistry*, Wiley, 2009, pp. 441–471.
62 W. D. G. Brittain, C. M. Lloyd and S. L. Cobb, *J. Fluor. Chem.*, 2020, **239**, 109630.
63 M. Zhou, Z. Feng and X. Zhang, *Chem. Commun.*, 2023, **59**, 1434–1448.
64 I. Saikia, A. J. Borah and P. Phukan, *Chem. Rev.*, 2016, 116, 6837–7042.
65 R. Zeynek, *Hoppe Seylers Z Physiol. Chem.*, 1921, **114**, 275–285.
66 D. Znidar, D. Dallinger and C. O. Kappe, *ACS Chem. Health Safe.*, 2022, 29, 165–174.
67 P. Bovonsombat, P. Khanthapura, M. M. Krause and J. Leykajarakul, *Tetrahedron Lett.*, 2008, **49**, 7008–7011.
68 V. Kraehmer and D. Rehder, *Dalton Transactions*, 2012, **41**, 5225–5234.
69 R. Jain, B. Avramovitch and L. A. Cohen, *Tetrahedron*, 1998, **54**, 3235–3242.
70 C. J. Easton, C. A. Hutton, W. T. Eng and E. R. T. Tiekink, *Tetrahedron Lett.*, 1990, **31**, 7059–7062.
71 T. Umemoto, Y. Yang and G. B. Hammond, *Beilstein J. Org. Chem.*, 2021, **17**, 1752–1813.
72 Q. Wei, Y. Ma, L. Li, Q. Liu, Z. Liu and G. Liu, *Org. Lett.*, 2018, **20**, 7100–7103.
73 N. J. Bowman, M. P. Hay, S. G. Love and C. J. Easton, *J. Chem. Soc. Perkin 1*, 1988, 259.
74 L. Demange, A. Ménez and C. Dugave, *Tetrahedron Lett.*, 1998, **39**, 1169–1172.
75 P. A. Messina, K. C. Mange and W. J. Middleton, *J. Fluor. Chem.*, 1989, **42**, 137–143.
76 M. Doi, Y. Nishi, N. Kiritoshi, T. Iwata, M. Nago, H. Nakano, S. Uchiyama, T. Nakazawa, T. Wakamiya and Y. Kobayashi, *Tetrahedron*, 2002, **58**, 8453–8459.
77 C. Crowe, S. Molyneux, S. V. Sharma, Y. Zhang, D. S. Gkotsi, H. Connaris and R. J. M. Goss, *Chem. Soc. Rev.*, 2021, 50, 9443–9481.
78 D. O'Hagan and H. Deng, *Chem. Rev.*, 2015, 115, 634–649.
79 E. Yeh, S. Garneau and C. T. Walsh, *Proc. Natl. Acad. Sci.*, 2005, **102**, 3960–3965.
80 J. L. Wood and L. Van Middlesworth, *J. Biol. Chem.*, 1949, **179**, 529–533.
81 D. Choi and H. Kohn, *Tetrahedron Lett.*, 1995, **36**, 7011–7014.
82 H. Dong, J. Li, H. Liu, S. Lu, J. Wu, Y. Zhang, Y. Yin, Y. Zhao and C. Wu, *J. Am. Chem. Soc*, 2022, **144**, 5116–5125.
83 J. W. Clader, *J. Med. Chem.*, 2004, 47, 1–9.
84 A. A. Berger, J. S. Völler, N. Budisa and B. Koksch, *Acc. Chem. Res.*, 2017, **50**, 2093–2103.
85 G. Shi, Z. Zhao and X. Zhang, *J. Org. Chem.*, 1995, **60**, 6608–6611.
86 O. T. De Jesus, D. Murali, R. Kitchen, T. R. Oakes and R. J. Nickles, *J. Fluor. Chem.*, 1993, **65**, 73–77.
87 N. A. Meanwell, *J. Med. Chem.*, 2018, 61, 5822–5880.
88 M. Rafiee, M. N. Mayer, B. T. Punchihewa, and M. R. Mumau, *J. Org. Chem.,* 2021, 86, **22**, 15866–15874
89 R. Francke and R. D. Little, *Chem. Soc. Rev.*, 2014, 43, 2492–2521.

90 W. Shao, B. Lu, J. Cao, J. Zhang, H. Cao, F. Zhang, and C. Zhang, *Chem. Asian. J.* 2023, **18**, e202201093
91 J. I. Yoshida and S. Suga, *Chem. Eur. J.*, 2002, **8**, 2650–2658.
92 N. Elgrishi, K. J. Rountree, B. D. McCarthy, E. S. Rountree, T. T. Eisenhart and J. L. Dempsey, *J. Chem. Educ.*, 2018, **95**, 197–206.
93 H. Yamada, K. Yoshii, M. Asahi, M. Chiku and Y. Kitazumi, *Electrochemistry*, 2022, **90**, 22–66082.
94 M. Rafiee, D. J. Abrams, L. Cardinale, Z. Goss, A. Romero-Arenas and S. S. Stahl, *Chem. Soc. Rev.*, 2024, 53, 566–585.
95 N. Sauermann, R. Mei and L. Ackermann, *Angew. Chem.*, 2018, **130**, 5184–5188.
96 J. Mihelcic and K. D. Moeller, *J. Am. Chem. Soc*, 2003, **125**, 36–37.
97 M. Faraday, *Philos. Trans. R. Soc. Lond.*, 1834, **124**, 77–122.
98 R. Oesper and M. Speter, *Sci. Mon.*, 1937, **45**, 535–546.
99 H. Kolbe, *Justus Liebigs Ann. Chem.*, 1848, **64**, 339–341.
100 N. Sbei, S. Aslam and N. Ahmed, *React. Chem. Eng.*, 2021, 6, 1342–1366.
101 H. Kurihara, T. Tajima and T. Fuchigami, *Electrochemistry*, 2006, **74**, 615–617.
102 J. Tafel and H. Hahl, *Ber. Dtsch. Chem. Ges.*, 1907, **40**, 3312–3318.
103 M. T. Sanders and R. A. Hales, *J. Electrochem. Soc.*, 1949, **96**, 241.
104 D. S. P. Cardoso, B. Šljukić, D. M. F. Santos and C. A. C. Sequeira, *Org. Process Res. Dev.*, 2017, 21, 1213–1226.
105 T. Shono, H. Hamaguchi and Y. Matsumura, *J. Am. Chem. Soc*, 1975, **97**, 4264–4268.
106 C. Liu, Y. Liu, S. Yang, B. Zheng and Y. Zhang, *Org. Lett.*, 2024, **26**, 1936–1940.
107 D. Baba and T. Fuchigami, *Tetrahedron Lett.*, 2003, **44**, 3133–3136.
108 E. Sierecki, S. Turcaud, T. Martens and J. Royer, *Synthesis (Stuttg)*, 2006, **2006**, 3199–3208.
109 S. Turcaud, T. Martens, E. Sierecki, J. Pérard-Viret and J. Royer, *Tetrahedron Lett.*, 2005, **46**, 5131–5134.
110 J. Yoshida and K. Nishiwaki, *J. Chem. Soc., Dalton Transactions*, 1998, 2589–2596.
111 Fr. Fichter and M. Schmid, *Helv. Chim. Acta.*, 1920, **3**, 704–714.
112 R. P. Linstead, B. R. Shephard and B. C. L. Weedon, *J. Chem. Soc. (Resumed)*, 1951, 2854.
113 V. Brabec and V. Mornstein, *Biophys. Chem.*, 1980, **12**, 159–165.
114 C. Song, K. Liu, Z. Wang, B. Ding, S. Wang, Y. Weng, C. W. Chiang and A. Lei, *Chem. Sci.*, 2019, **10**, 7982–7987.
115 D. Alvarez-Dorta, C. Thobie-Gautier, M. Croyal, M. Bouzelha, M. Mével, D. Deniaud, M. Boujtita and S. G. Gouin, *J. Am. Chem. Soc*, 2018, **140**, 17120–17126.
116 E. Toyama, K. Maruyama, T. Sugai, M. Kondo, S. Masaoka, T. Saitoh, K. Oisaki and M. Kanai, *ChemRxix*, 2019, preprint, DOI: 10.26434/chemrxiv.7795484.v1.
117 O. A. Levitskiy, O. I. Aglamazova, Y. K. Grishin, K. A. Paseshnichenko and T. V. Magdesieva, *ChemElectroChem*, 2020, **7**, 3361–3367.
118 H. Iwasaki and B. Witkop, *J. Am. Chem. Soc*, 1964, **86**, 4698–4708.
119 A. Joran, US Patent, 5364851A, 1994.
120 F. Cornille, U. Slomczynska, M. L. Smythe, D. D. Beusen, K. D. Moeller and G. R. Marshall, *J. Am. Chem. Soc*, 1995, **117**, 909–917.
121 D. Matters, H. J. Cooper, L. McDonnell, J. Iniesta, J. Heptinstall, P. Derrick, D. Walton and I. Peterson, *Anal. Biochem.*, 2006, **356**, 171–181.
122 J. Iniesta, H. J. Cooper, A. G. Marshall, J. Heptinstall, D. J. Walton and I. R. Peterson, *Arch. Biochem. Biophys.*, 2008, **474**, 1–7.
123 R. A. Rosenberg, S. A. Muzaffar, J. N. M. Heersche, D. Jez and T. M. Murray, *Anal. Biochem.*, 1983, **128**, 331–341.

124 A. Papadopoulos, J. Heyer, K. Ginzel and E. Steckhan, *Chem. Ber.*, 1989, **122**, 2159–2164.
125 A. S. MacKay, R. J. Payne and L. R. Malins, *J. Am. Chem. Soc*, 2022, **144**, 23–41.
126 S. Nagahara, Y. Okada, Y. Kitano and K. Chiba, *Chem. Sci.*, 2021, **12**, 12911–12917.
127 Y. Lin and L. R. Malins, *Chem. Sci.*, 2020, **11**, 10752–10758.
128 S. Kitada, M. Takahashi, Y. Yamaguchi, Y. Okada and K. Chiba, *Org. Lett.*, 2012, **14**, 5960–5963.
129 A. Bandyopadhyay, P. Biswas, S. K. Kundu and R. Sarkar, *Org. Biomol. Chem.*, 2023, 22, 1085–1101.

Chapter 2: Electrochemical halogenation of amino acids

2.1 Overview

Halogenated biomolecules are not uncommon in the natural world; over 5000 organohalogens have been discovered and isolated from various organisms.[1] In many of these molecules, the halogen atoms play a critical role in preserving their activity and function. The larger size and hydrophobicity of the heavier halogens (Cl, Br, I) permit formation of halogen bonds,[2] whilst the electronegativity and smaller size of fluorine can increase lipophilicity and prevent metabolic degradation.[3]

The incorporation of halogenated amino acids into peptides can have a significant impact on the parent peptide's physical and physicochemical properties.[4] Additionally, installation of a halogen atom into a peptide may also be useful as a labelling method,[5] or as a way to incorporate a reactive handle for further modifications, *e.g.*, Pd-catalysed cross-coupling.[6] Exploration into finding novel methods of synthesising halogenated amino acids is therefore of interest to those working in both the chemical-biology and medicinal chemistry communities.

2.2 Chapter aims

Peptide therapeutics are an attractive prospect for medicinal chemists due to their high specificity and efficacy (**See Section 1.1.1**). However, natural peptides often have a myriad of drawbacks for clinical development, including poor cell permeability and bioavailability.[7] These drawbacks can be mitigated by incorporating unnatural amino acids into peptide sequences, or by performing residue-specific modification on a peptide.

Electro-organic synthesis is a technique that has quickly risen in popularity in recent years. It is considered to be a 'green' and atom-economic technique, with a high capacity for specificity.[8] It is therefore well suited to modification of amino acids and peptides, which often have multiple functional groups.

The primary aims of this chapter are:

- To investigate whether an electrochemical fluorination procedure for unactivated sp^3 carbons could be expanded to a number of amino acids with tertiary centres
- To explore the compatibility of the above procedure with a range of amine protecting groups
- To investigate the electrochemical fluorination of proline

- To develop a novel electrochemical chlorination method

2.3 Electrochemical fluorination

2.3.1 Introduction

Whilst the emergence of electro-organic synthesis as a popular mainstream tool has been a relatively recent phenomenon, electrochemical fluorination has had a longer history due to its early adoption by industry. This was due to the commercialisation of the Simons process, an early electrochemical fluorination method developed in the late 1930s for perfluorination of organic molecules. Despite its earlier invention, this work was not published until ten years later, [9] due to the secrecy surrounding the Manhattan project and associated research. The Simons process uses anhydrous hydrogen fluoride (AHF) as the fluorine source and nickel electrodes to effect the electrochemical transformation.

Throughout the latter half of the 20th century, electrochemical fluorination continued to garner interest from a small number of research groups, despite the challenges that the approach presented. Early electrochemical fluorination methods required careful selection of electrodes (*e.g.*, platinum or nickel), to avoid heavy corrosion by HF. Additionally, high oxidation potentials were required due to the disparity between the rate of substrate cation formation and the rate of fluorination. This meant that often competitive polymerisation processes were observed instead of the desired selective fluorination.[10]

Until the 1970s, selective electrochemical fluorination was beyond reach due to the necessity of the nickel anode/AHF electrolyte pairing, which precludes the formation of partially fluorinated products.[11] Around this time, a novel electrolyte composition was developed by Knunyants *et al.* which revitalised the field: triethylamine-HF dissolved in acetonitrile was used with platinum electrodes to selectively fluorinate naphthalene (**83**)(**Scheme 2.1**).[12]

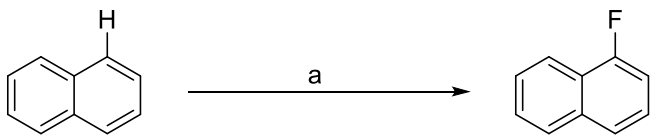

83 **84**

Scheme 2.1: Conversion of naphthalene (**83**) to a variety of fluorinated derivatives including 1-fluoronapthalene (**84**). A degree of selectivity was observed, as 2-fluoronapthalene was not formed, nor were any perfluorinated products; reagents and conditions: a) triethylamine HF (1.2 M) in MeCN, Pt anode, 1.8 V (relative to NCE), 1.6 F/mol, 27%.

From this point, fluorination systems of the type $Et_3N.nHF$[13] or $Et_4NF.nHF$[14] (and later Olah's reagent, pyridine.HF)[15] in acetonitrile (MeCN) were regularly employed in electrochemical reactions. An example of an electrochemical fluorination reaction using a base-HF complex as the source of fluorine is shown below in **Scheme 2.2**.[16] Chen *et al.* used $Et_3N.5HF$ to cleave and fluorinate cyclic ketones (*e.g.*, **85**) *via* a fluoroacyl fluoride intermediate.

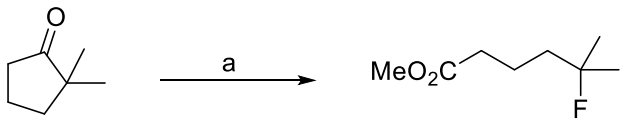

85 **86**

Scheme 2.2: Electrochemical fluorination and α-cleavage of cyclic ketones;[16] reagents and conditions: a) anhydrous $Et_3N.5HF$, 0°C, 2-2.4 V, pulse electrolysis (2 s), Pt (+) Pt (-), 91%.

Reactions that employ base/HF complexes as dual electrolyte/fluorine sources are examples of nucleophilic fluorination, as F^- ions are generated. The reaction of substrates with nucleophilic fluorinating reagents proceeds through a radical cation due to the very high discharge potential of the fluoride ions generated.

In later years electrochemical fluorination reactions using $R_xN.nHF$ or $R_xNF.nHF$ have been performed neat,[17] as these reagents can act as ionic liquids. This technique circumvents issues accompanying the use of these reagents as a solution in MeCN, because it reduces anode passivation caused by MeCN, and increases the concentration of fluoride ions in solution.[18]

For many years, the use of base/HF complexes has dominated the field of electrochemical fluorination, despite their toxicity. However, recently a number of procedures employing alternative fluorine sources have been published, *e.g.*, using metal fluorides. In 2019, Noël *et al.* illustrated how potassium fluoride (KF) could be used to electrochemically synthesise sulfonyl fluorides from thiols or disulfides.[19] In 2023 Hintz *et al.* used caesium fluoride (CsF) in conjunction with a copper catalyst to fluorinate a range of C(sp^3)-H bonds (**Scheme 2.3**).[20]

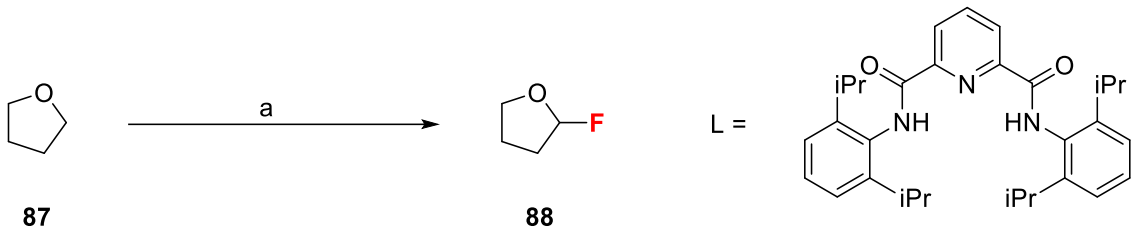

87 88

Scheme 2.3: Copper-catalysed electrochemical C(sp^3)-H fluorination using CsF as the fluoride source;[20] reagents and conditions: a) $LCu^{II}MeCN$ (2 mol%), CsF, C_6F_6, collidine, $TBAClO_4$ (20 mol%), TFA collidinium, propylene carbonate/MeCN (1:1), RVC (+) Pt (-), 3.3 V.

Lam *et al.* have demonstrated how fluorine-containing salts such as collidinium tetrafluoroborate can also be used as fluorine sources (**Scheme 2.4**).[21] Tetrafluoroborate salts are often used as a supporting electrolyte in various electrochemical reactions; this method obviates the need for additional electrolyte.

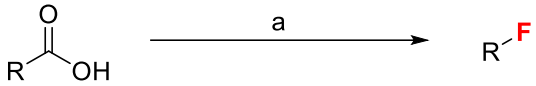

Scheme 2.4: Electrochemical decarboxylative fluorination to form tertiary alkyl fluorides using tetrafluoroborate salts, R = tertiary alkyl; reagents and conditions: a) collidinium BF_4, collidine, DCM, C (+) C (-), 15 mA, 4 F/mol, 12-61%.

Electrophilic sources of fluorine such as Selectfluor (**12**) (**Figure 1.13**) have also been used in electrochemical fluorination reactions. Selectfluor is a particularly intriguing reagent as it can have multiple functions: as a fluorine source, oxidising agent, or electrolyte. In 2023, Holt *et al.* found that Selectfluor can act as a coordinated hydrogen atom abstraction agent *via* its radical dication, resulting in directed fluorination of steroidal substrates (**Scheme 2.5**).[22]

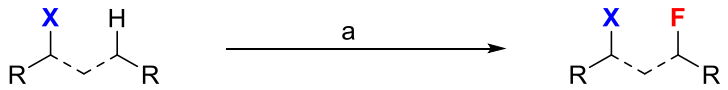

Scheme 2.5: Selectfluor-enabled directed electrochemical fluorination, **X** = directing group *e.g.* enone, lactam, alcohol, ester etc., R = steroid based substrates; reagents and conditions: a) Selectfluor (**12**)(25 mol%), MeCN, RVC (+) RVC (-), 3 mA, 3 F/mol, 23-89%.

Whilst a few studies which use Selectfluor have been published recently, including Holt's directed fluorination (**Scheme 2.5**), the use of electrophilic fluorinating reagents for electrochemical reactions only really gained traction after Baran and coworkers published their seminal paper on electrochemical C(sp^3)-H fluorination in 2019 (**Scheme 2.6**).[23]

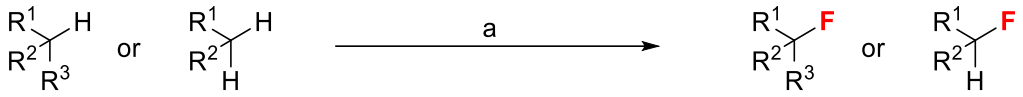

Scheme 2.6: Selective electrochemical fluorination of unactivated sp^3 carbons, R = alkyl; reagents and conditions: a) Selectfluor (**12**), $NaNO_3$ (20 mol%), MeCN, RVC (+) RVC (-), alternating polarity (2 min), 3 mA, 0.25-3 F/mol, 25-83%.

In this reaction, Selectfluor is used as a source of electrophilic fluorine, the electrolyte, and as a redox mediator. A redox mediator is a species which is capable of being oxidised at the anode to produce a reactive intermediate which can subsequently oxidise the substrate via homogenous electron transfer. This process is illustrated in the proposed mechanism (**Scheme 2.1**). Redox mediators ideally will have a lower oxidation potential, which means that substrates which are difficult to oxidise, *i.e.*, those with unactivated C(sp^3)-H bonds, can be indirectly oxidised at lower potentials.

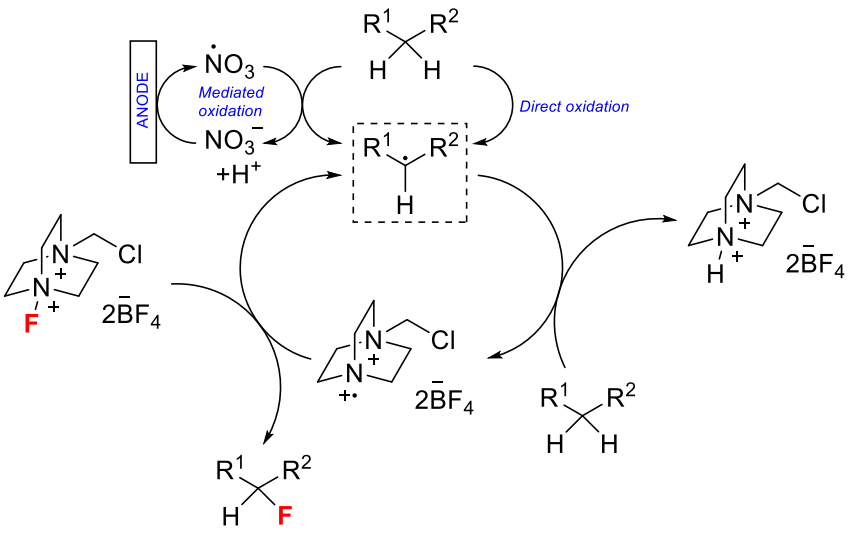

Figure 2.1: Mechanism for electrochemical fluorination using Selectfluor proposed by Baran *et al.*[23]

Sodium nitrate also participates in the reaction as an activator; it can undergo anodic oxidation to form NO_3 radicals, which are able to abstract protons from substrates. This process is similar to Selectfluor's role as a mediator, but is more supplementary than essential.

The electrochemical fluorination of a range of substrates with secondary or tertiary unactivated carbon centres was executed, including derivatives of the amino acids valine (**89**) and leucine (**90**) (**Figure 2.2**).

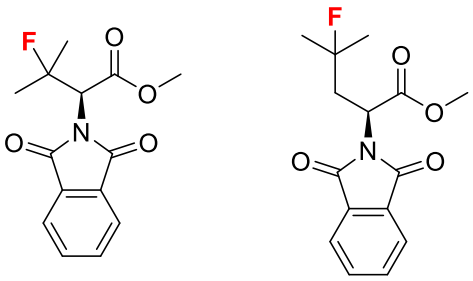

89 **90**

Figure 2.2: Structures of the fluorinated amino acids with tertiary centres synthesised by Baran's electrochemical method; (L-R) *N*-phthaloyl-3-fluoro-*L*-valine methyl ester (**89**), and *N*-phthaloyl-4-fluoro-*L*-leucine methyl ester (**90**).

2.3.2 Results and Discussion – Electrochemical fluorination of tertiary centres

Due to the apparent selectivity of Baran's fluorination technique and its compatibility with amino acids, the primary aim of our foray into electrochemical fluorination was to replicate some of Baran's results and investigate whether the scope of this reaction could be expanded to include other amino acids with tertiary centres, *e.g.*, methyl proline (**94**) or isoleucine (**93**) (**Figure 2.3**).

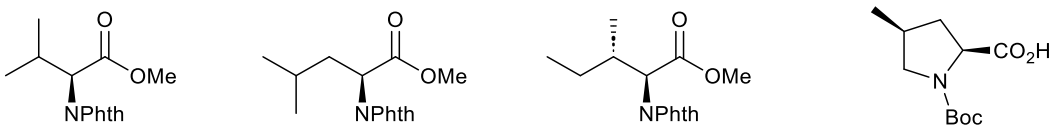

91 **92** **93** **94**

Figure 2.3: Intended substrates for electrochemical fluorination; *N*-Phth-Val-OMe (**91**), *N*-Phth-Leu-OMe (**92**), *N*-Phth-Ile-OMe (**93**), *cis*-4-methyl proline (**94**).

Of the four intended substrates for electrochemical fluorination, the three *N*-phthaloyl amino acids (**91-93**) required synthesis, whereas *cis*-4-methyl proline (**94**) is commercially available. An initial attempt to synthesise *N*-phthaloyl valine methyl ester (**91**) *via* the direct reaction of H-Val-OMe (**95**) with phthalic anhydride (**96**) failed. This is probably due to the choice of toluene as a solvent, which makes the removal of water during the reaction more difficult (**Scheme 2.6**).

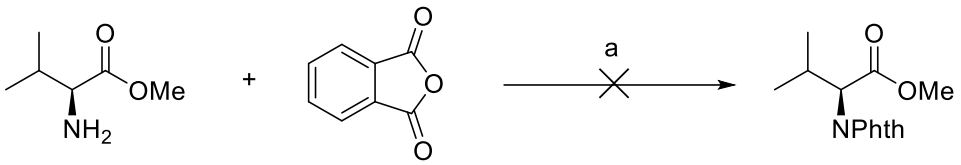

95 **96** **91**

Scheme 2.6: The attempted reaction of H-Val-OMe (**95**) with phthalic anhydride (**96**); reagents and conditions: a) 0.1 equiv. TEA, toluene, reflux (Dean-Stark apparatus), 24 h.

This reaction was repeated, instead heating H-Val-OMe (**95**) and phthalic anhydride (**96**) together neat at 170 °C under reduced pressure. These conditions successfully delivered the desired product (**91**), albeit in a poor yield of 22%.

Due to the diminished yield, an alternative approach was taken; *L*-valine (**97**) was instead reacted with phthalic anhydride (**96**) to form *N*-phthaloyl valine (**98**). This was then converted to the methyl ester derivative in a subsequent step (**Scheme 2.7**).

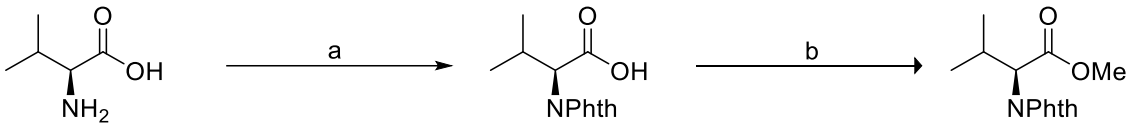

97 **98** **91**

Scheme 2.7: Reaction of *L*-valine (**97**) with phthalic anhydride (**96**) followed by esterification using thionyl chloride; reagents and conditions: a) phthalic anhydride, 170 °C, vacuum, 3h, 99%; b) $SOCl_2$ (0°C), MeOH, 24 h, rt, 72%

This method was successful, with the initial reaction with phthalic anhydride furnishing the product in a quantitative yield. *N*-phthaloyl leucine methyl ester (**92**) and *N*-phthaloyl isoleucine methyl ester (**93**) were therefore synthesised in the same manner (yield over two steps: 79% and 77%, respectively).

The synthesised *N*-phthaloyl amino acid substrates were then subjected to electrochemical fluorination using Baran's conditions. The fluorination of *N*-Phth-Val-OMe (**91**) is shown in **Scheme 2.8**. An initial attempt at this reaction resulted in ~5% conversion to the fluorinated product (**89**). This conversion yield was established from examination of the crude ^{1}H NMR spectrum. The presence of the desired product (**89**) was confirmed by comparison of the ^{1}H- and ^{19}F NMR chemical shifts to literature values.[23]

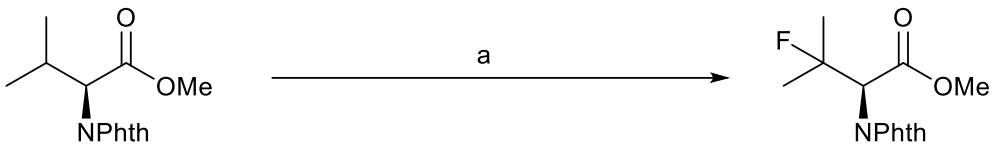

91 **89**

Scheme 2.8: Electrochemical fluorination of *N*-Phth-Val-OMe (**91**) to form the 3-fluoro derivative (**89**), using conditions described by Baran *et al.*; reagents and conditions: a) (+) RVC (-) RVC, Selectfluor (3 equiv.), $NaNO_3$, anhydrous MeCN, 3 mA/cm^2, 2 F/mol, 5% (^{1}H NMR conversion yield).

However, when the substrate mixture was degassed for 30 minutes prior to reaction, the conversion observed by ^{1}H NMR spectroscopy rose to 60%. Purification of this product mixture proved difficult due to the similar Rf values of the product and the starting material. In an attempt to push the reaction to completion, the total charge was increased from 2 F/mol to 3 F/mol. Total charge refers to the moles of electrons passed through the reaction mixture; *i.e.*, 2 F/mol means two moles of electrons applied for every mole of substrate. This resulted in complete conversion to the desired 3-fluoro product (**89**), negating the need for further purification. The isolated yield for this reaction was 71%, which is comparable to Baran's reported yield (66%).

N-Phth-Leu-OMe (**92**) was then subjected to electrochemical fluorination using the improved conditions used for the valine derivative (**Scheme 2.9**).

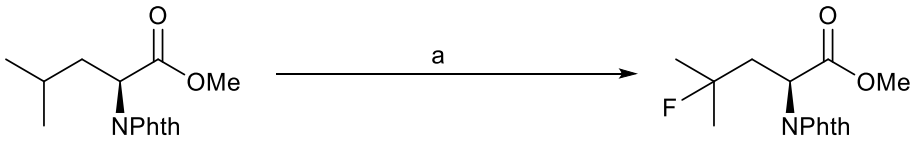

92 **90**

Scheme 2.9: Electrochemical fluorination of *N*-Phth-Leu-OMe (**92**) to form the 4-fluoro derivative (**90**); reagents and conditions: a) (+) RVC (-) RVC, Selectfluor (3 equiv.), $NaNO_3$, anhydrous MeCN, 3 mA/cm^2, 3 F/mol, 45%.

The desired 4-fluoro product (**90**) was isolated using column chromatography in a 45% yield. The remaining material recovered from this reaction was confirmed to be starting material by TLC and ^{1}H NMR spectroscopy.

The same electrochemical fluorination procedure was then applied to *N*-Phth-Ile-OMe (**93**). Unlike the valine and leucine substrates, the potential products from the fluorination of isoleucine were less certain. In the case of isoleucine, the fluorine atom could potentially add to one of two places; the tertiary β-position (**99**) or the secondary γ-position (**100**) (**Scheme**

2.10). Fluorination at either of these positions could lead to formation of diastereomers due to the creation of a chiral centre.

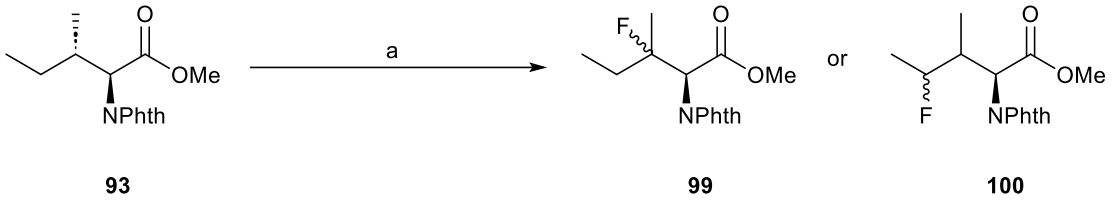

93 **99** **100**

Scheme 2.10: Electrochemical fluorination of *N*-Phth-Ile-OMe (**93**) showing the potential products which could arise (**99**,**100**); reagents and conditions: a) (+) RVC (-) RVC, Selectfluor (3 equiv.), $NaNO_3$, anhydrous MeCN, 3 mA/cm^2, 3 F/mol.

^{19}F NMR spectroscopic analysis of the crude mixture from the reaction confirmed that fluorination had taken place, though not in a selective manner as four fluorine multiplets were present (**Figure 2.4**). This is likely due to fluorination taking place at both the tertiary and secondary centres in equal measure, resulting in generation of two sets of diastereomers (**Figure 2.5**).

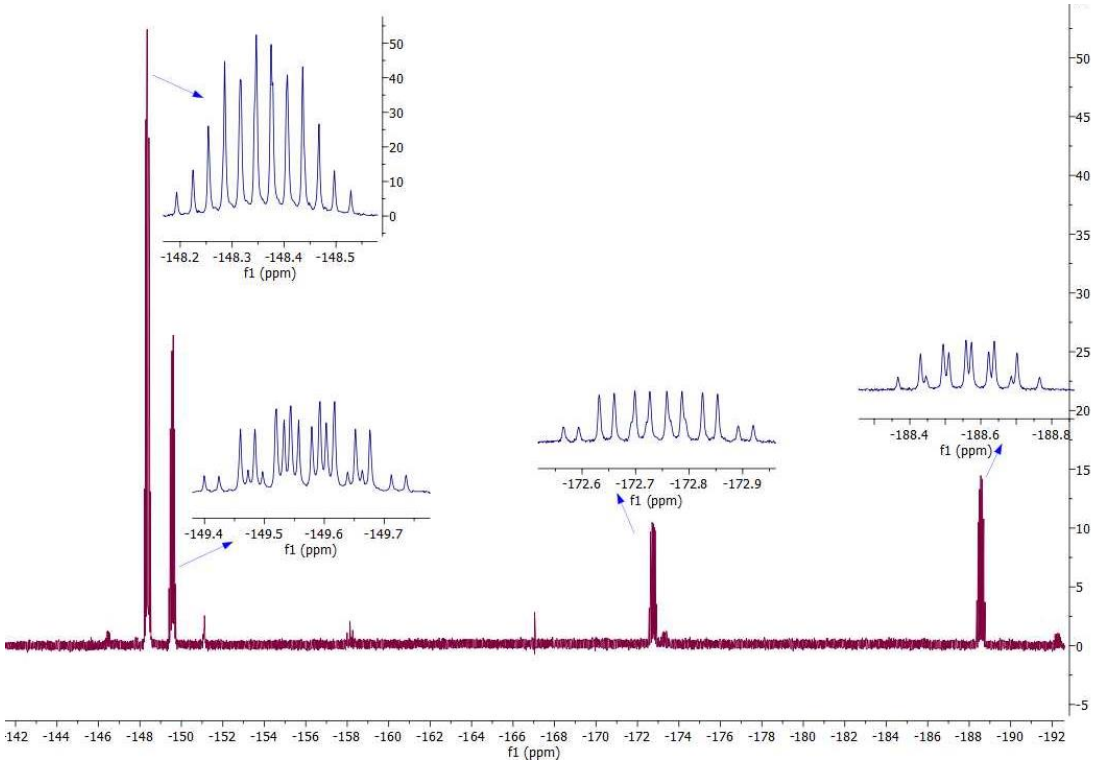

Figure 2.4: ^{19}F NMR spectrum (376 MHz, $CDCl_3$) of the isoleucine product mixture post-fluorination, featuring four multiplets at -148.4, -149.6, -172.7, and -188.6 ppm.

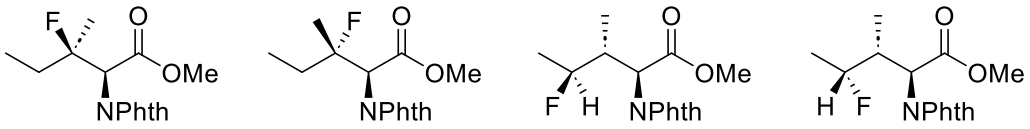

99a **99b** **100a** **100b**

Figure 2.5: Possible diastereomeric products formed from electrochemical fluorination at both the secondary and tertiary positions.

Chromatographic separation of the products (**99-100**) proved difficult due to their diastereomeric nature. Comparison of the ^{1}H NMR spectrum of the starting material (**93**) with that of the product fractions suggested that fluorination had taken place. Shifting of the α-proton doublet peak was observed in some of the fractions, and the peaks due to the CH_2 and CH_3 groups had an increased *J*-value, which indicated coupling to fluorine atoms. Two extra α-proton peaks were observed in some fractions, which lends support to the idea that both β-fluorinated isoleucine and γ-fluorinated isoleucine are present in the product mixture. Only one of the diastereomers displayed in **Figure 2.5** was isolated cleanly by means of preparative TLC. Analysis of the ^{1}H NMR spectrum suggested that this product was **99a** or **99b**, as the resonance associated with the β-H was missing when compared to the ^{1}H NMR spectrum of the starting material.

Electrochemical fluorination of *N*-Boc 4-methyl proline (**94**) was attempted using the reaction conditions displayed in **Scheme 2.11**. It was expected that *N*-Boc 4-methyl proline (**94**) would be fluorinated at the 4-position (**Scheme 2.11**).

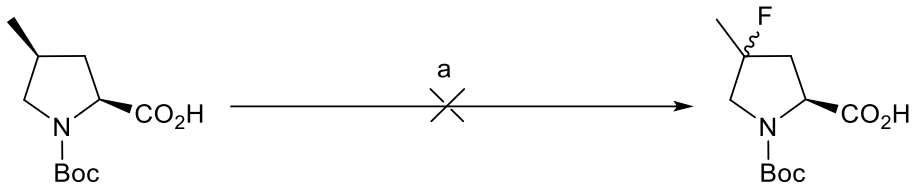

94 **101**

Scheme 2.11: Attempted fluorination of *N*-Boc 4-methyl proline (**94**); reagents and conditions: a) (+) RVC (-) RVC, Selectfluor (3 equiv.), $NaNO_3$, anhydrous MeCN, 3 mA/cm^2, 3 F/mol

The ^{19}F NMR spectrum of the crude reaction mixture contained a single doublet (-75.6 ppm, *J* = 6.4). This suggested that the substrate had not been fluorinated at the tertiary 4-position (**101**), as fluorination at this site would have given rise to a fluorine signal with a more complex splitting pattern. It is possible that fluorination had occurred at either the 3- or 5-positions (**Figure 2.6**). However, formation of either **102** or **103** is unlikely, as in both cases a more

complex ^{19}F NMR signal than a doublet would be expected due to coupling with protons on adjacent carbons. Additionally, multiple fluorine peaks would be expected in the ^{19}F NMR spectra of both cases (**102, 103**) due to the generation of diastereomers.

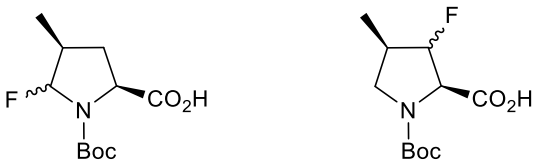

102 **103**

Figure 2.6: Possible structures of electrochemical fluorination products of 4-methylproline (**94**); 4-methyl-5-fluoroproline (**102**), 4-methyl-3-fluoroproline (**103**).

The major product from this reaction was isolated and ^{1}H NMR spectroscopic analysis confirmed that it was not starting material. However, after this was left in an NMR tube for 3 weeks, the doublet in the ^{19}F NMR spectrum vanished. This could potentially be due to the product being unstable and eliminating fluorine to produce an alkene, or that the fluorine peak originally seen was due to trace amounts of a fluorinated substance rather than a fluorinated major product. This reaction was repeated once more but the resulting product mixture did not appear to contain fluorine.

Each time this reaction was performed, the proton NMR spectrum of the major product remained the same (**Figure 2.7**). The spectrum does not match the starting material (**94**) or Selectfluor (**12**); there is also no Boc group peak visible. The four main peaks (3.8-4.6 ppm) integrate in a ratio of 2:3:3:2, and a COSY spectrum confirmed that only the two multiplets are correlated to each other. Whilst the pattern of the peaks suggests a Selectfluor-derived substance, the integration values do not corroborate this. The peaks are however in the correct region for alkene protons (4.00-4.60 ppm). It is not clear exactly what the structure of this product is.

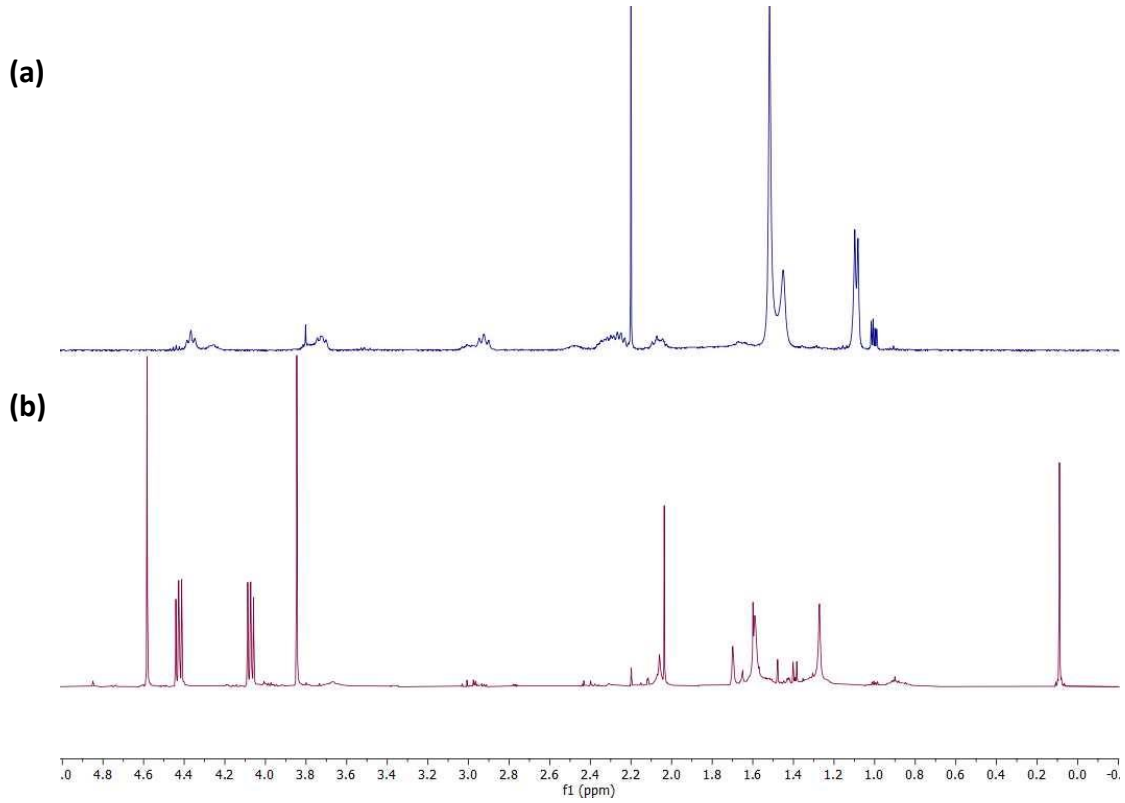

Figure 2.7: ^{1}H NMR spectra (400 MHz, $CDCl_3$) of 4-methylproline (**94**) (**a**) and the unknown product of the attempted fluorination of 4-methylproline using Selectfluor (**b**).

The results of these experiments suggest that the electrochemical fluorination reaction is perhaps not as selective as it appears to be with the amino acids valine and leucine.

A secondary aim of this project was to investigate the impact of replacing the phthalimide group with alternative protecting groups, which may be more compatible with peptide synthesis. Whilst the phthalimide group is very effective at masking the nucleophilicity of the amine group so that it may not interfere with the reaction,[24] it is not a practical choice due to the harsh conditions required for its installation and removal.

Three alternative protecting group systems were initially proposed: *N*(Boc)$_2$, *N*(Bn)$_2$, and *N*(Boc)(Me) (**Figure 2.8**). Valine methyl ester was selected as a model substrate due to its proven compatibility with electrochemical fluorination and its formation of a single fluorinated product. A phthalimide group removes both protons on an amine group, so two protecting groups were used in each of the molecules shown in **Figure 2.8** to ensure both NH protons were removed. *N,N'*-(Boc)(Me)-Val-OMe (**106**) is commercially available, but the *N*-(Boc)$_2$ and *N*-(Bn)$_2$ derivatives required synthesis.

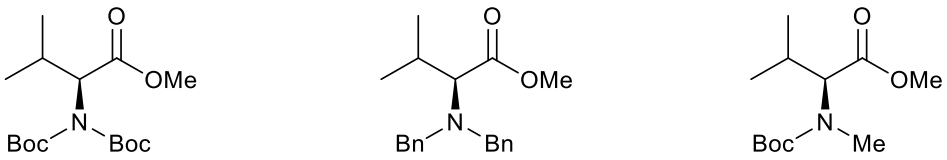

104 **105** **106**

Figure 2.8: Structures of valine derivatives with alternative amine protecting groups: *N*-(Boc)$_2$-Val-OMe (**104**), *N*-(Bn)$_2$-Val-OMe (**105**), *N,N'*-(Boc)(Me)-Val-OMe (**106**).

N-(Bn)$_2$-Val-OMe (**105**) was synthesised *via* reaction of *L*-valine methyl ester (**95**) with three equivalents of benzyl bromide (**Scheme 2.12**). A significant amount of the mono-benzylated derivative (**107**) was also isolated from this reaction, hence the reduced yield (46%) of the desired dibenzyl product.

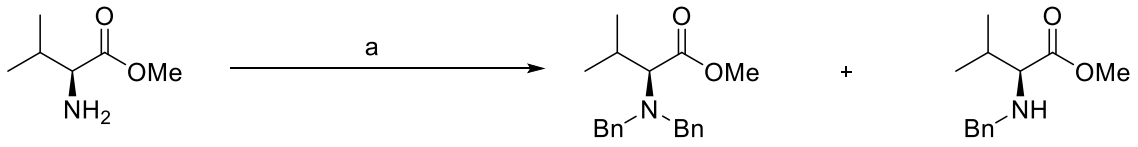

95 **105** **107**

Scheme 2.12: The dibenzylation of H-Val-OMe (**95**) by reaction with benzyl bromide; reagents and conditions: a) BnBr (3 equiv.), K_2CO_3 (3.15 equiv.), EtOH, reflux, 3h, 46%.

In order to synthesise *N*-(Boc)$_2$-Val-OMe (**104**) from the commercially available *N*-Boc-Val-OMe (**108**), a number of conditions were attempted (**Table 2.1**). A standard Boc protection procedure using DMAP as the base failed to yield any product, which is likely due to the higher pKa of the -NHBoc group compared to an -NH_2 group. The reaction was therefore repeated using NaH instead, due to its higher pKa (~35). However, this reaction was also unsuccessful. Using KHMDS as the base instead successfully generated the desired product, though the yield was very low (27%) (**Scheme 2.13**).

Entry	Reaction conditions	Yield[a] (%)
1	Boc_2O (1.5 equiv.), DMAP (1 equiv.), MeCN, 24h, rt	n/a
2	Boc_2O (1.1 equiv.), NaH (1.1 equiv.), DMAP (0.1 equiv.), MeCN, 24 h, rt	n/a
3	KHMDS (THF) (0.93 equiv.), Boc_2O (2 equiv.), THF, -78 °C, N_2, 20 h	27

Table 2.1: Reaction conditions attempted for the synthesis of N-(Boc)$_2$-Val-OMe (**104**) from N-Boc-Val-OMe (**108**); a = isolated yield of desired DiBoc product (**104**).

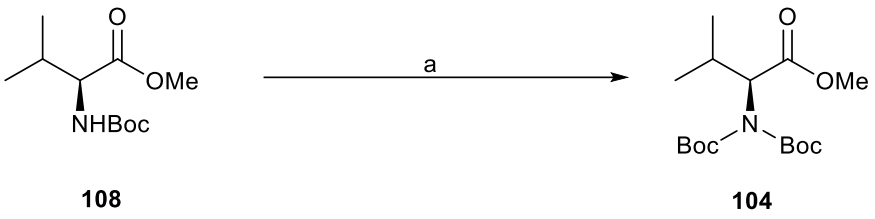

108 **104**

Scheme 2.13: The synthesis of *N*-(Boc)$_2$-Val-OMe (**104**) from *N*-Boc-Val-OMe (**108**); reagents and conditions: a) KHMDS (THF) (0.93 equiv.), Boc_2O (2 equiv.), THF, -78 °C, N_2, 20 h, 27%

With the three protected valine derivatives in hand, each was then subjected to electrochemical fluorination. Fluorination of *N*-(Bn)$_2$-Val-OMe (**105**) was initially attempted, but the desired product (**109**) was not obtained (**Scheme 2.14**).

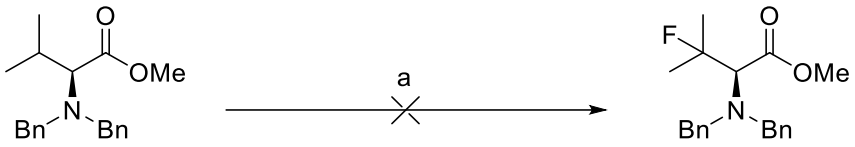

105 **109**

Scheme 2.14: Attempted fluorination of *N,N*-dibenzyl valine methyl ester (**105**); reagents and conditions: a) (+) RVC (-) RVC, Selectfluor (3 equiv.), $NaNO_3$, anhydrous MeCN, 3 mA/cm^2, 3 F/mol.

^{1}H and ^{19}F NMR spectral analysis of the crude reaction mixture revealed that multiple products were present, but no starting material was observed. The ^{19}F NMR spectrum presented a major doublet peak at -76 ppm (J = 6.8), and a minor singlet peak at 18 ppm, which suggested that the molecule had not been fluorinated at the β-position as expected, but perhaps at either the benzyl or α-position. However, when this reaction was repeated twice more, only the singlet peak at 18 ppm was present in the crude ^{19}F NMR spectra.

When chromatographic separation was attempted with this reaction, benzaldehyde (**110**) was observed in one of the fractions. This suggests that the substrate underwent some sort of debenzylation/oxidation reaction instead of the desired fluorination (**Scheme 2.15**). The presence of benzaldehyde may also account for the singlet peak at 18 ppm observed in the ^{19}F NMR spectrum, as Selectfluor has been known to convert benzaldehyde derivatives into benzoyl fluoride derivatives.[25] Benzoyl fluoride (**111**) gives rise to a singlet peak at 18 ppm in its ^{19}F NMR trace.[26]

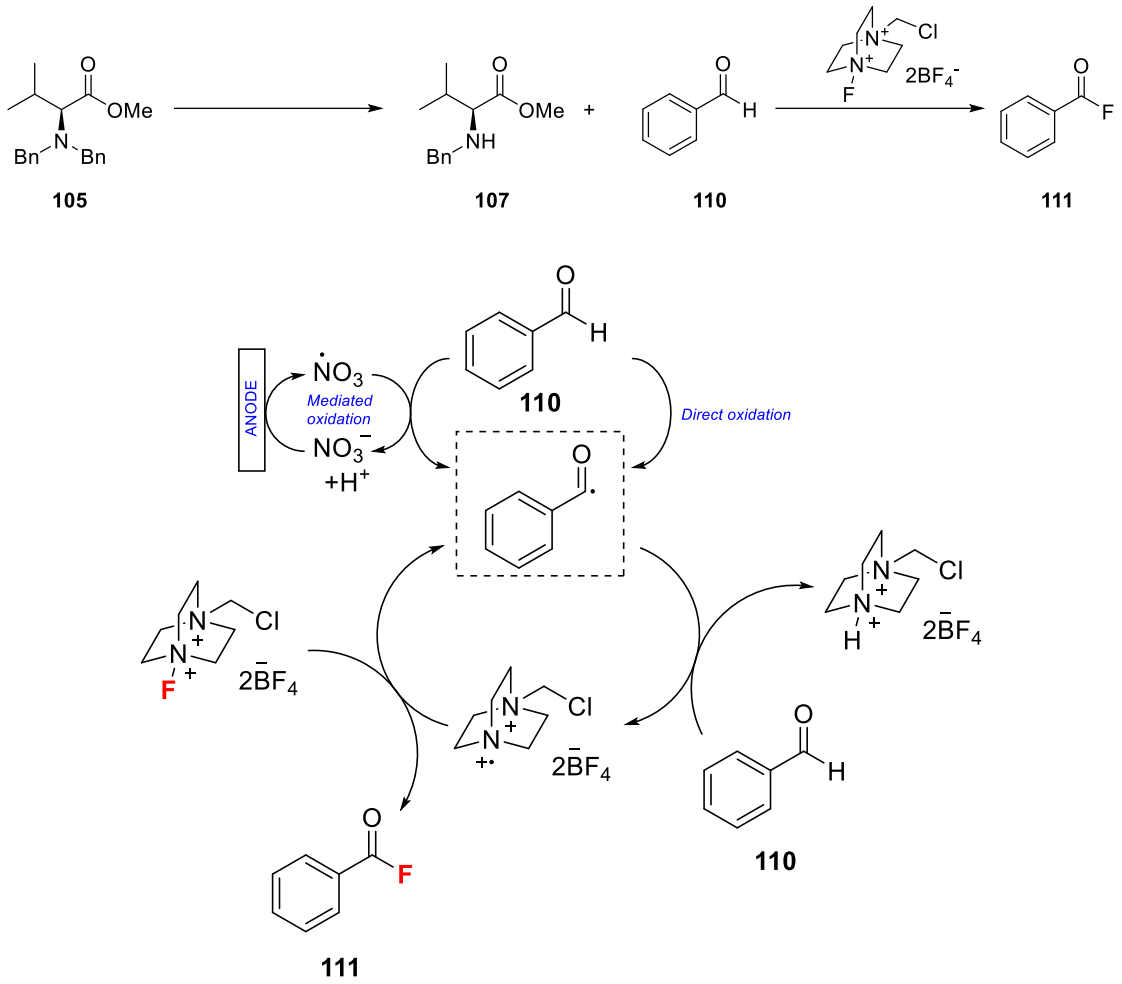

Scheme 2.15: Proposed transformation of **105** to form the mono-benzylated derivative (**107**) and benzaldehyde (**110**), and possible subsequent formation of benzoyl fluoride (**111**) effected by Selectfluor (**12**). A mechanism for the formation of benzoyl fluoride (**111**) from benzaldehyde (**110**) under electrochemical conditions is also proposed.

Another product from the reaction shown in **Scheme 2.15** was observed by NMR spectroscopy. The ^{1}H NMR spectrum of this fraction consists of three triplets, each of which correspond to three quartets (**Figure 2.9**). This suggests the presence of a CH_2-CH_3 fragment and possibly points to a Selectfluor degradation product; however, the integration values of each triplet-quartet pair are not consistent with this. The first two peak pairs integrate with a 1:1 ratio, and the third peak pair integrates with a ratio of 2:1 (t:q). The identity of this substance is unknown.

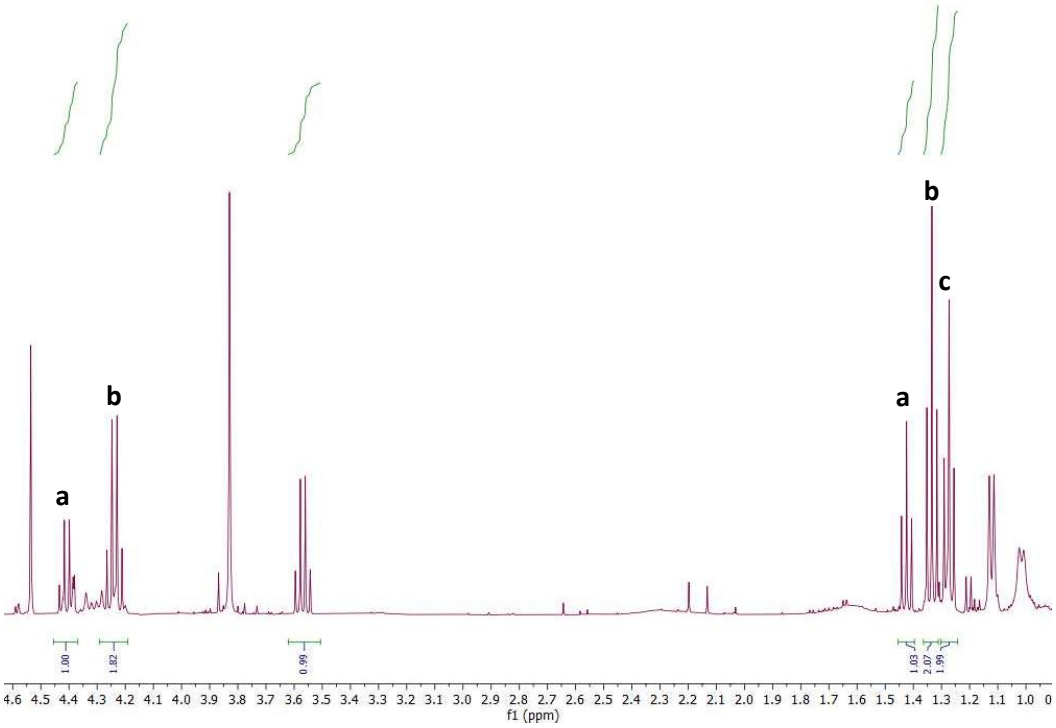

Figure 2.9: ^{1}H NMR spectrum (400 MHz, $CDCl_3$) of fraction 1 of attempted dibenzyl fluorination reaction. Triplets and quartets are labelled with letters **a**, **b**, and **c** to indicate protons which correlate to each other in the COSY spectrum.

A second fraction taken from this reaction (**Scheme 2.14**) contained a mixture of three valine-derived products (**Figure 2.10**). One of the products matches the spectrum of mono-benzylated valine methyl ester (**107**), which supports the theory that benzaldehyde is formed as a result of benzyl group loss. All three products in this mixture appear to have an α-proton (doublet), a β-proton (multiplet), and a methyl ester peak (singlet). All also appear to have the CH_2 benzylic protons present as an AB spin system with roofing, indicating that the two protons are diastereotopic. This is due to the proximity of the methylene protons to the chiral centre in the molecule. This kind of splitting is not visible in the spectrum of the starting material, so it is likely that all three are mono-benzylated derivatives.

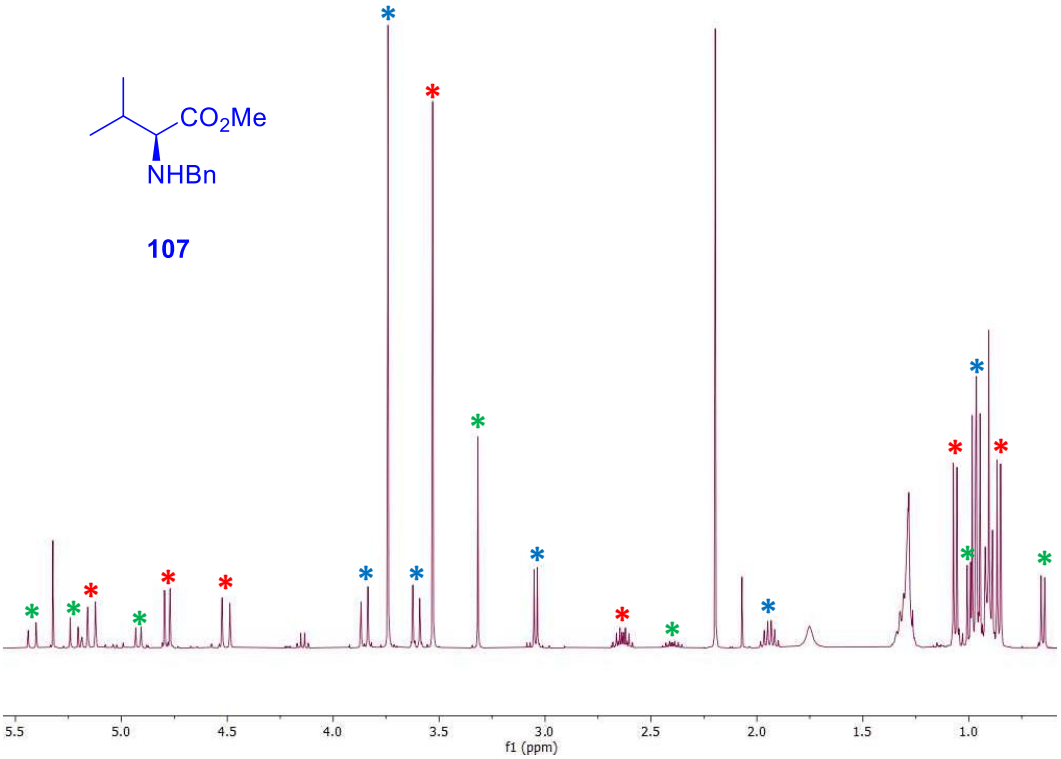

Figure 2.10: ^{1}H NMR spectrum (400 MHz, $CDCl_3$) of fraction 2 from dibenzyl fluorination reaction; each of the three compounds are labelled with a different coloured star (***). The mono-benzylated valine (**107**) is represented by the blue stars (*)

Re-examination of the ^{1}H NMR spectrum from the first attempt at this reaction revealed that the same mixture of products was also formed in this case. It is not clear why a doublet was observed at -76 ppm in the ^{19}F NMR spectrum. Possibly fluorination could have taken place at one of the benzylic positions, before loss of the benzyl group and oxidation to form benzoyl fluoride.

The reaction shown in **Scheme 2.14** was then performed without Selectfluor, but otherwise under the same conditions displayed in **Scheme 2.14** (with the addition of $^{n}Bu_4NBr$ as electrolyte) (**Scheme 2.16**). The product mixture contained primarily starting material (**105**), with trace amounts of benzaldehyde (**110**).

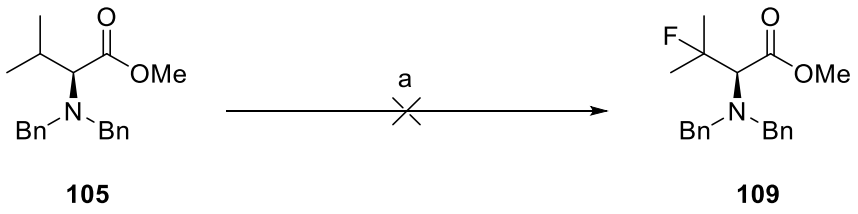

105 **109**

Scheme 2.16: Trial reaction of *N,N*-dibenzyl valine methyl ester (**105**) under electrochemical conditions; reagents and conditions: a) (+) RVC (-) RVC, $^{n}Bu_4NBr$ (3 equiv.), $NaNO_3$, anhydrous MeCN, 3 mA/cm^2, 3 F/mol.

Ultimately, this investigation shows that dibenzyl protecting groups are clearly not a good substitute for phthalimide protecting groups in the attempted electrochemical fluorination of valine.

Electrochemical fluorination of *N*-Boc-*N'*-Me-Val-OMe (**106**) was then attempted using the same conditions as shown in **Scheme 2.14**. ^{1}H and ^{19}F NMR spectral analysis of the crude product mixture revealed that it was mostly starting material, with only a singlet at -75 ppm observed in the ^{19}F NMR spectrum. Therefore, the mixture was abandoned. The N-Boc, N-Me protecting group combination appears to be a poor substitute for the phthalimide protecting group in regard to electrochemical fluorination.

N-$(Boc)_2$-Val-OMe (**104**) was then subjected to electrochemical fluorination. The anticipated reaction is shown below in **Scheme 2.17**.

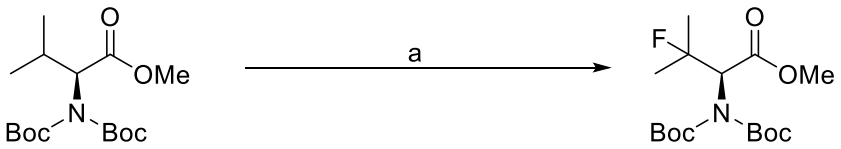

104 **112**

Scheme 2.17: Anticipated reaction for the electrochemical fluorination of *N*-$(Boc)_2$ valine methyl ester (**104**); reagents and conditions: a) (+) RVC (-) RVC, Selectfluor (3 equiv.), $NaNO_3$, anhydrous MeCN, 3 mA/cm^2, 3 F/mol.

On examination of the ^{1}H and ^{19}F NMR spectra of the crude reaction mixture, it was clear that two compounds were present. The ^{1}H NMR spectrum contained two sets of α-proton and methyl ester peaks, but no peaks for β-protons, indicating that fluorination at the β-position had occurred. The ^{19}F NMR spectrum contained two multiplets, suggesting that two β-fluorinated compounds had indeed been formed. The most likely explanation for this is that a Boc group has been lost at some point in the reaction, resulting in an $N(Boc)_2$ fluorinated product (**112**) and a NH(Boc) fluorinated product (**113**) (**Scheme 2.18**).

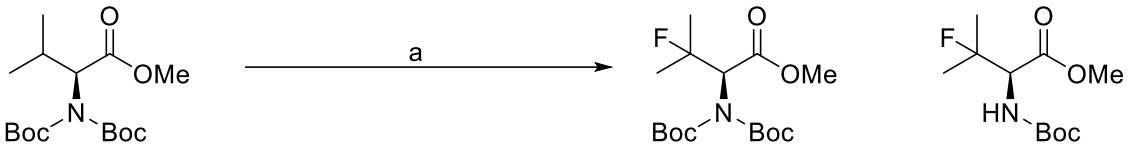

104 **112** **113**

Minor **Major**

Scheme 2.18: Electrochemical fluorination of *N*-(Boc)$_2$-Val-OMe (**104**) to produce *N*-Boc-(3-fluoro)-Val-OMe (**113**) as the major product (34%) and *N*-(Boc)$_2$-(3-fluoro)-Val-OMe (**112**) as the minor product (mixed, 80% pure by ^{1}H NMR); reagents and conditions: a) (+) RVC (-) RVC, Selectfluor (3 equiv.), $NaNO_3$, anhydrous MeCN, 3 mA/cm^2, 3 F/mol.

The major fluorinated product was isolated in a 34% yield, and the minor compound was partially isolated (~80% pure). ^{1}H NMR spectral analysis revealed that the minor product was fluorinated N(Boc)$_2$ protected valine (**112**) and the major product was indeed fluorinated NHBoc-protected valine (**113**) (**Scheme 2.18**).

It is unclear whether loss of the Boc protecting group occurs before or after fluorination, and whether this occurs due to the oxidative conditions or due to interaction with Selectfluor. Additional non-fluorinated products were not observed in the product mixture, which suggests that Boc deprotection occurs post-fluorination.

A similar reaction without Selectfluor was performed, instead using ^{n}Bu$_4$NBr as a substitute electrolyte. Mostly starting material was produced, with only trace amounts of Boc-Val-OMe (**108**) being observed. This suggests that either Boc loss is triggered by initial fluorination, or it occurs as a result of oxidative action by Selectfluor.

Due to the successful fluorination of *N*-(Boc)$_2$-Val-OMe (**104**), it was thought that perhaps a single Boc group may be sufficient for protection of the amine. Using a single Boc group would be much preferable than either the DiBoc or phthalimide groups, as it can be easily installed and removed in quantitative yields. Therefore, Boc-Val-OMe (**108**) was subjected to electrochemical fluorination as shown in **Scheme 2.19**.

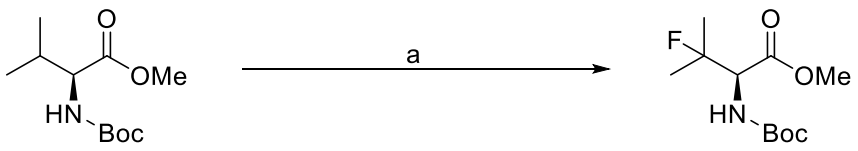

108 **113**

Scheme 2.19: Electrochemical fluorination of Boc-Val-OMe (**108**) to produce *N*-Boc-(3-fluoro)-Val-OMe (**113**); reagents and conditions: a) (+) RVC (-) RVC, Selectfluor (3 equiv.), $NaNO_3$, anhydrous MeCN, 3 mA/cm^2, 3 F/mol, 34%

This reaction successfully produced the desired product (**113**) in 34% yield. Whilst this yield is lower than that of the *N*-Phth-Val-OMe (**91**) substrate, the benefits of being able to use a simple Boc protecting group may outweigh this.

2.3.3 Results and Discussion - Attempted fluorination of hemioxalates

In 2019, an iridium-catalysed photochemical deoxofluorination procedure was published by MacMillan *et al.*[27] (**Scheme 2.20**). The mechanism for this reaction involved generation of alkyl radicals, which are subsequently fluorinated with Selectfluor.

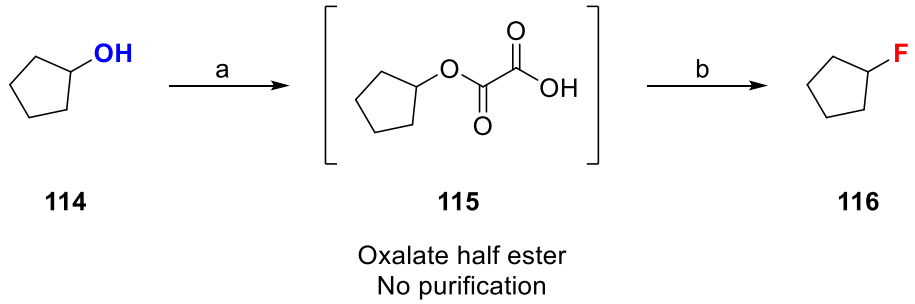

Scheme 2.20: Photochemical Ir-catalysed conversion of alcohols to fluoroalkanes *via* an activated hemioxalate intermediate;[27] reagents and conditions: a) oxalyl chloride, Et_2O, 0 °C, 1-18 h, then H_2O, 1 h, 93% b) $Ir[F(Me)ppy]_2(dtbbpy)PF_6$ (1 mol%), Na_2HPO_4, Selectfluor (2.25 equiv), acetone/H_2O (4:1), LEDs, 2 h, 84%.

It was thought that a similar transformation may be achieved under electrochemical conditions without a catalyst, which could circumvent the requirement for the expensive iridium photocatalyst. A proline derivative was included in the substrate scope of the aforementioned paper, and the procedure could also potentially be expanded to other alcoholic amino acids *e.g.*, serine, homoserine.

Therefore, Boc-Hyp-OMe (**117**) was converted to its hemioxalate derivative (**118**) using oxalyl chloride (**Scheme 2.21**).

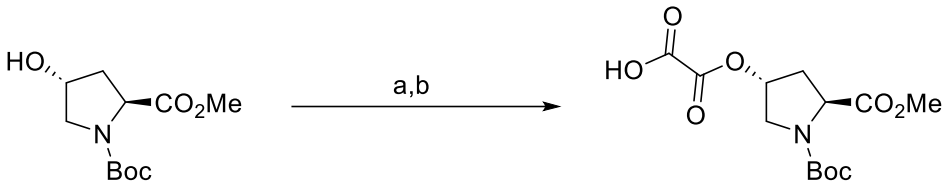

117 **118**

Scheme 2.21: Conversion of Boc-Hyp-OMe (**117**) to its hemioxalate derivative (**118**); reagents and conditions: a) Oxalyl chloride, 0°C, anhydrous Et_2O, N_2, 18 h; b) H_2O, 0°C, 1 h, 84%.

The desired product (**118**) was isolated as a mixture of rotamers (84%). The hemioxalate was then reacted with Selectfluor using similar conditions to the photochemical procedure. The attempted transformation is shown in **Scheme 2.22**.

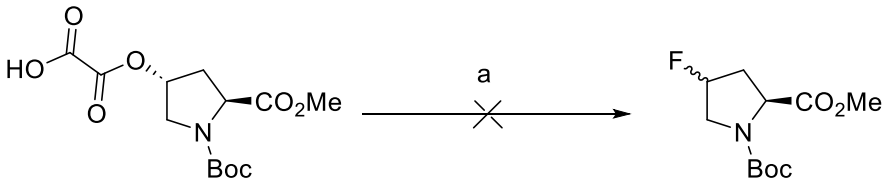

118 **119**

Scheme 2.22: Attempted deoxofluorination of a proline hemioxalate derivative (**118**); a) various conditions, outlined below in **Table 2.2**.

Entry	Reaction conditions	Yield of 119[b] (%)
1	Selectfluor (2 eq.), $NaNO_3$, MeCN/H_2O (9:1), 2 F/mol, 5 mA, graphite electrodes	n/a
2	**Entry 1**, but with anhydrous MeCN and a N_2 atmosphere	n/a
3	**Entry 2**, but with K_2HPO_4 (2 equiv.) and glassy carbon electrodes	n/a
4	**Entry 2** but with RVC electrodes and 3 equiv. Selectfluor	n/a

Table 2.2: The sets of conditions attempted for the deoxofluorination reaction shown in **Scheme 2.22**; b = isolated yield of desired product (**119**).

The inclusion of water in the reaction conditions (**Table 2.2, Entry 1**) appeared to cause conversion to a pyroglutamic acid derivative (**Figure 2.11**).

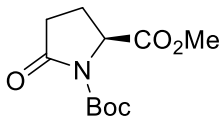

120

Figure 2.11: A pyroglutamic acid derivative (**120**) produced in the electrochemical reaction of hemioxalate proline (**118**) with Selectfluor.

This effect had been previously observed when Boc-Pro-OMe (**121**) was reacted with Selectfluor under similar conditions (See **Chapter 4**, **Section 4.4**). A plausible explanation is that the hemioxalate moiety did indeed cleave under the oxidative conditions to generate an alkyl radical, which then abstracted a proton from a water molecule. The generation of the carbonyl bond at the 5-position appears to occur whenever a protecting group creates an amide or carbamate bond with the amine, as discussed in **Section 4.4**.

Therefore, the reaction was then reattempted using anhydrous MeCN. This generated a reaction mixture which gave rise to a number of fluorine multiplets in the R_3CF region of the ^{19}F NMR trace (**Figure 2.12**).

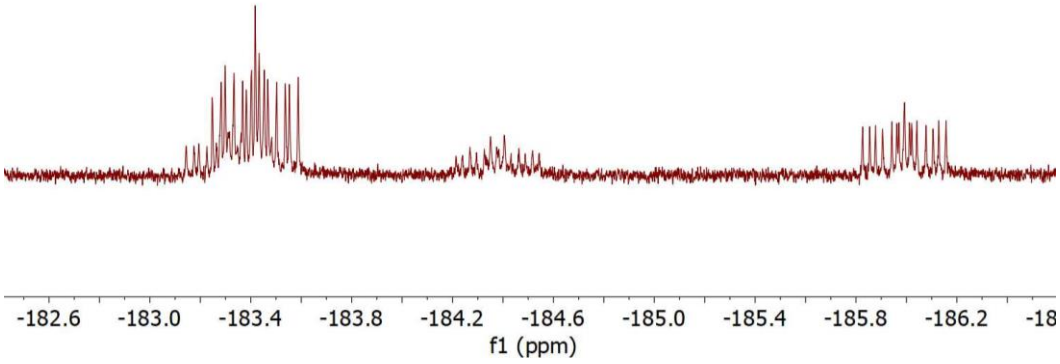

Figure 2.12: ^{19}F NMR spectrum (376 MHz, $CDCl_3$) of the crude reaction mixture from **Table 2.2, Entry 2.**

Unfortunately, no identifiable product could be isolated.. A couple of variations on these conditions were tried (**Table 2.2, Entries 3 and 4**), but both of these failed to produce any peaks in the fluorine NMR. It was thought that the Boc protecting group may be interfering in the reaction, so a benzyl-protected proline hemioxalate derivative (**124**) was synthesised (**Scheme 2.23**).

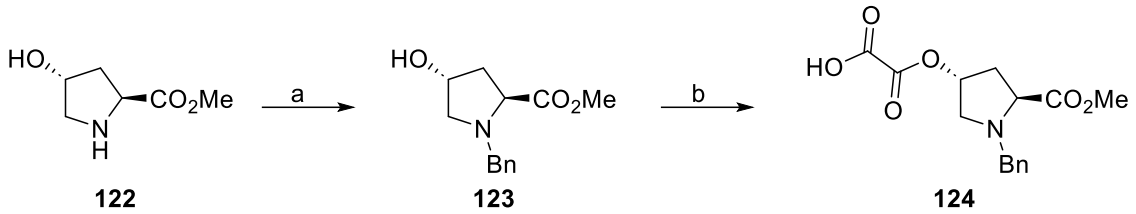

122 **123** **124**

Scheme 2.23: Synthesis of Bn-Pro(Ox)-OMe (**124**) from Boc-Hyp-OMe (**122**); reagents and conditions: a) BnBr, DIPEA, toluene, 110°C, 6 h, 58%; b) oxalyl chloride, anhydrous Et_2O, 0 °C, 20 h, then H_2O added, 0°C, 1 h, 51%.

Benzylation of hydroxyproline methyl ester (**122**) proceeded smoothly, but an initial attempt at formation of the corresponding hemioxalate (**124**) instead produced a dimeric compound (**125**) (**Figure 2.13**). This is probably due to early termination of the reaction (after ~ 45 mins) after excessive bubbling and solid formation was observed. It is also possible that not enough oxalyl chloride was added.

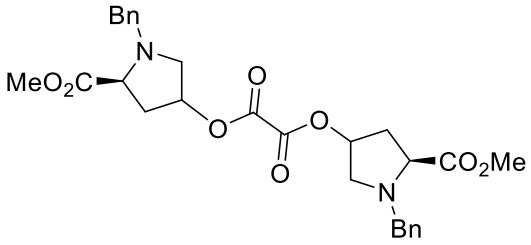

125

Figure 2.13: Dimeric product (**125**) inadvertently formed instead of the desired proline hemioxalate derivative (**124**).

A second attempt at this reaction gave rise to the desired product (**124**) in a 51% yield (**Scheme 2.23**). Whilst the dimeric product was unwanted, it was thought that it may perhaps have some use as an additional substrate to try. A few sets of conditions were attempted to replicate the accidental synthesis of this dimer (**125**) (**Table 2.3**).

Entry	Reaction conditions	Yield of 125[a] (%)
1	Oxalyl chloride (0.5 eq.), in dry Et_2O for 1 h, then 1 h with H_2O	n/a
2	Oxalyl chloride (0.5 eq.) in dry Et_2O for 12 h, then reflux for 3 h	n/a
3	Oxalyl chloride (0.5 eq.) in dry Et_2O/pyridine, reflux for 3 h	62%

Table 2.3: Sets of reaction conditions attempted when trying to convert Bn-Hyp-OMe (**123**) to **125**; a = isolated yield of the desired dimeric product (**125**).

Eventually the dimer (**125**) was synthesised successfully in a 62% yield using a pyridine/diethyl ether solvent and heating at reflux for 3 hours. This was then reacted with Selectfluor using the conditions shown in **Scheme 2.24**.

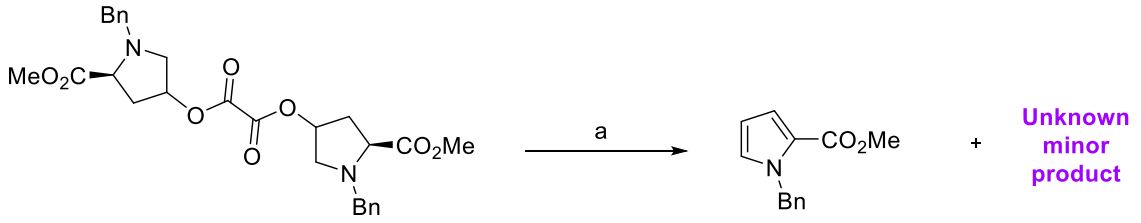

125 **126**

Scheme 2.24: Reaction of compound **125** with Selectfluor to produce a pyrrole derivative (**126**) as the major product and an unknown compound as the minor product; reagents and conditions: a) Selectfluor, K_2HPO_4, MeCN/H_2O (9:1), 5 mA, 2 F/mol, RVC electrodes, N_2, alt. polarity every 2 mins.

This reaction changed colour from a pale yellow to a deep purple within 15 mins. The major product was a pyrrole derivative (**126**), which was confirmed by comparison of ^{1}H NMR spectra to literature values.[28] The transformation of proline to pyrrole had been observed in previous reactions with proline substrates (see **Chapter 4, Section 4.4**) The minor product was an intensely purple-coloured compound, which appeared to also be some form of pyrrolic compound, with a ^{1}H NMR shift in the alkene/aromatic region (δ = 6.25 ppm). However, this product could not be identified.

Given the known propensity of *N*-benzyl proline derivatives to convert to pyrroles under oxidative conditions (see **Chapter 4, Section 4.4**), it was hypothesised that this transformation takes place first, with subsequent partial conversion to the purple compound (**Scheme 2.25**).

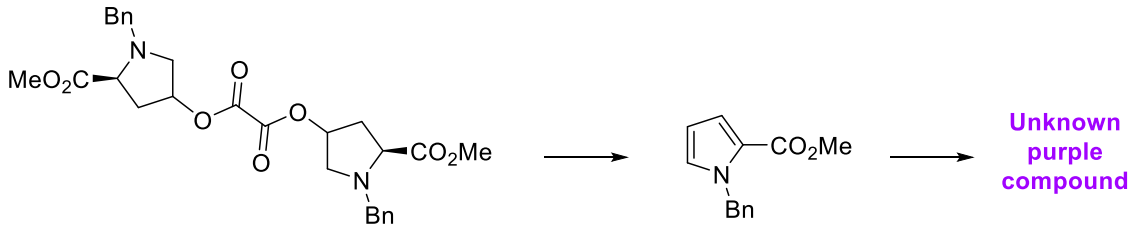

125 **126**

Scheme 2.25: Proposed route for generation of unknown purple compound. Dimer **125** is initially converted to pyrrole **126**, which then undergoes further modification to produce the unknown purple compound.

This theory was investigated by subjecting *N*-benzyl pyrrole carboxylate methyl ester (**126**) to the same conditions (**Scheme 2.26**).

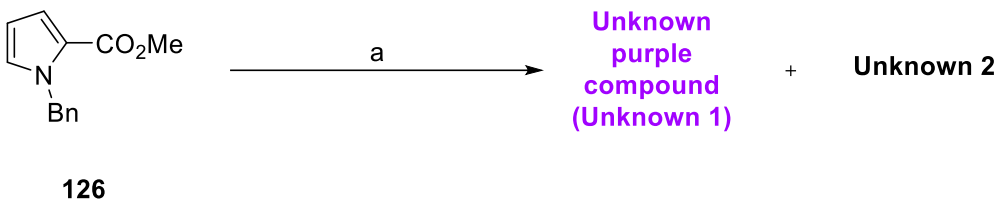

126

Scheme 2.26: Reaction of *N*-benzylpyrrole carboxylate methyl ester (**126**) with Selectfluor; reagents and conditions: a) Selectfluor, K_2HPO_4, MeCN/H_2O (4:1), N_2, 5 mA, 2 F/mol.

As expected, the reaction quickly turned purple. Preparative TLC was used to isolate the purple compound (**Unknown 1**), along with another unidentified compound (**Unknown 2**).

When **Unknown 2** was submitted for high-field NMR studies, it appeared that the original compound isolated had been transformed over time to another with a similar structure (**Figure 2.14**).

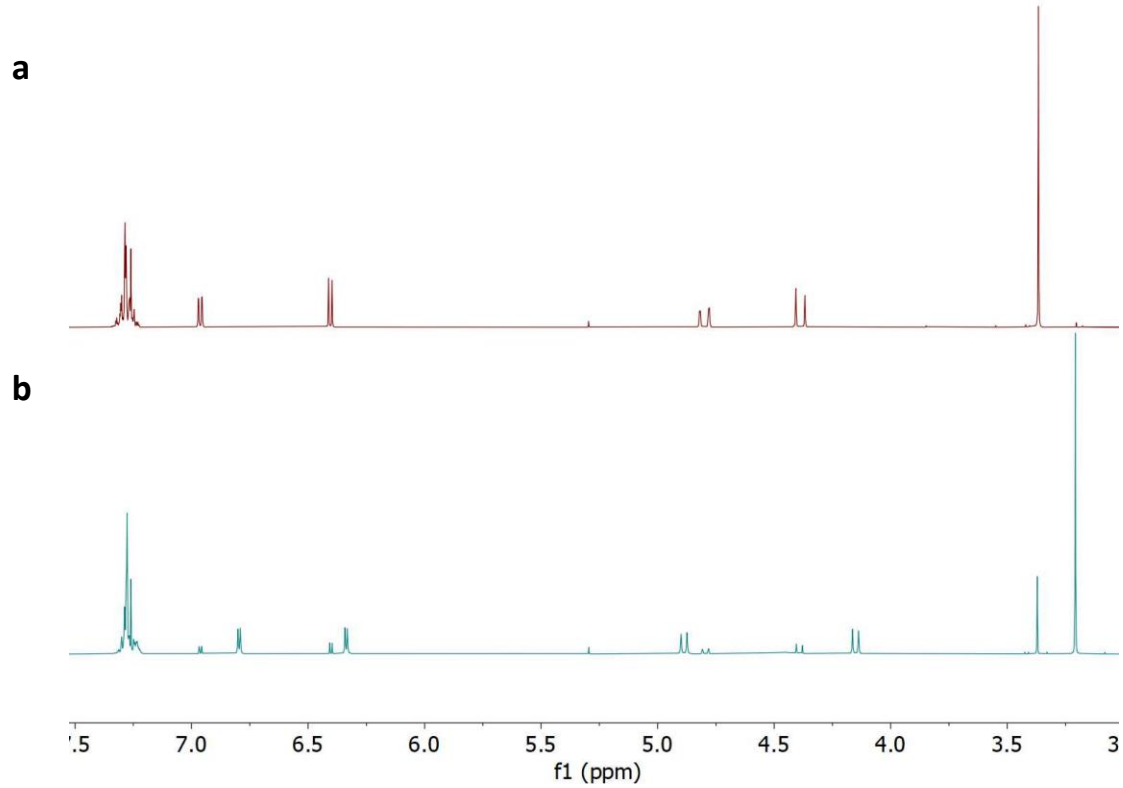

Figure 2.14: The initial ^{1}H NMR spectrum (400 MHz, $CDCl_3$) of **Unknown 2** (a), stacked with the high-field proton NMR spectrum (600 MHz, $CDCl_3$) which was recorded 3 days later (b). Integration of **Unknown 2** spectrum (a): 5:1:1:1:1:3.

When full conversion of **Unknown 2** to this secondary product had taken place, the compound was crystallised. X-Ray crystallography revealed that the secondary product featured an enone moiety and an additional hydroxyl group on the α-carbon (**127**) (**Figure 2.15** and **Scheme 2.27**).

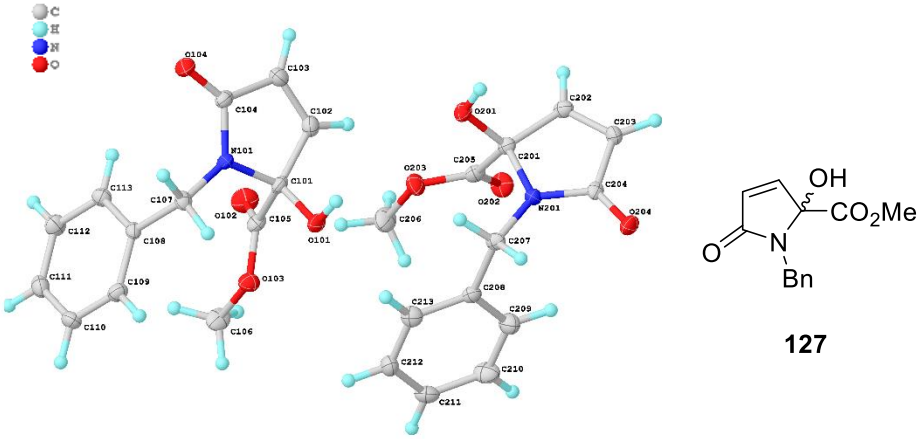

Figure 2.15: X-Ray molecular structure of the secondary product (**127**) formed from **Unknown 2**. The molecule is now chiral; the asymmetric unit possesses one molecule of each isomer (*R* and *S*). Crystal structure reported with a 50% thermal ellipsoid probability.

Scheme 2.27: A scheme displaying the origins of each unknown compound discussed in this section for clarity.

When comparing the HSQC and HMBC NMR spectra of the original **Unknown 2** and **127**, there was one major difference. The ^{13}C NMR signals corresponding to C-2, C-3, and C-6 in **Unknown 2** were all doublets. Aside from minor shifts in the rest of the signals, the ^{1}H and ^{13}C NMR spectra of **127** and **Unknown 2** were very similar, and the carbonyl on C-5 was still intact (δ = 169.6 ppm). This indicates that the substituent on C-3 is not a hydroxyl group, but

a fluorine atom (**Figure 2.16**). The LCMS data for this compound mixture also supports this conclusion (*m/z* 250, $[M+H]^+$ for **128** = 250). The ^{19}F NMR spectrum for **Unknown 2** (**128**) features a single peak at δ -141.1 ppm, suggesting that the fluorine atom is indeed situated on a sp^3 carbon.

127 **128**

Unknown 2

Figure 2.16: Proposed structures of **Unknown 2** (**128**) and its secondary product **127**. ^1H- and ^{13}C NMR spectral analysis for **128** revealed that C-3, C-2, and C-6 were all doublets.

Proline derivatives with a fluorine substituent at the α-carbon are known to be highly unstable (see **Chapter 4, Section 4.4**). It is probable that the α-fluorinated **128** was similarly unstable, and slowly transformed into the α-hydroxylated **127** upon exposure to air.

It is likely that the purple compound **Unknown 1** has a similar structure to fluorinated enone **128** and α-hydroxylated enone **127**. The ^1H NMR spectrum of **Unknown 1** is shown in **Figure 2.17**.

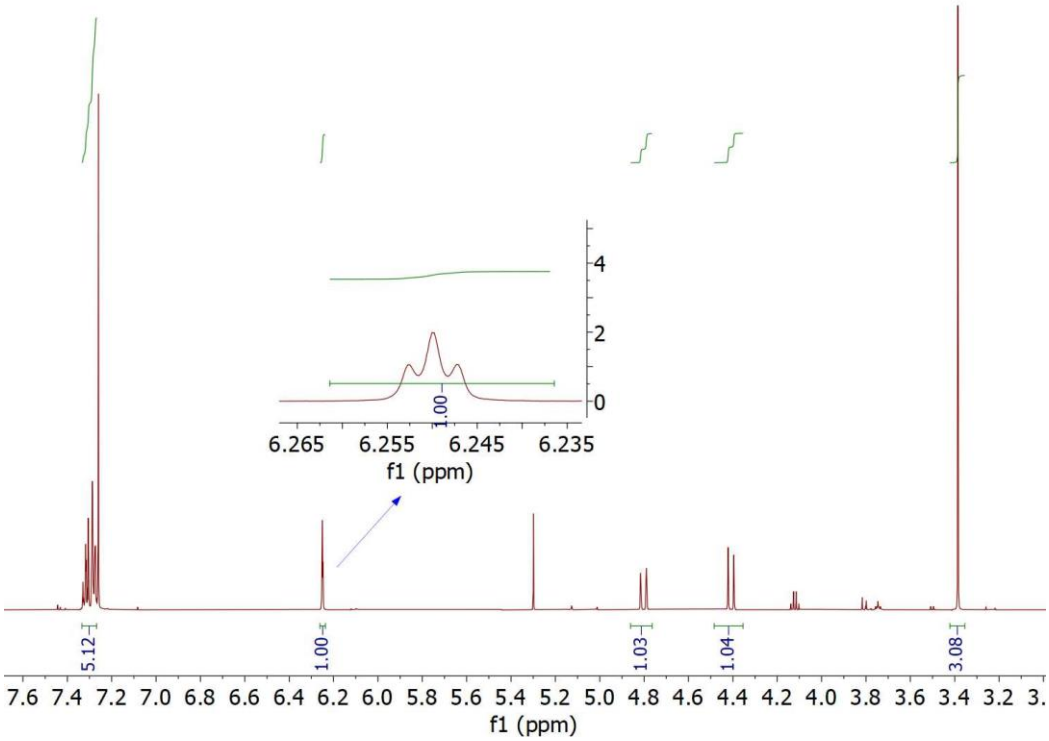

Figure 2.17: The ^{1}H NMR spectrum (600 MHz, $CDCl_3$) of **Unknown 1**, a compound isolated from the reaction shown in **Scheme 2.26**.

Aside from the peaks due to the benzyl and methyl ester protecting groups, the ^{1}H NMR spectrum for **Unknown 1** has only a single triplet peak, which is in the alkene region. The HSQC spectrum indicates that the proton causing this peak (δ = 6.25 ppm) is attached to a carbon which gives a signal (dd) at 113 ppm. The fact that this resonance shows coupling indicates the presence of fluorine. Additionally, the chemical shift at 113 ppm has a fairly low frequency than would be expected for an alkene carbon; this supports the possible presence of a fluorine atom, as an adjacent C-F bond can shift peaks to a lower frequency in a ^{13}C NMR spectrum.

Analysis of the HMBC spectrum revealed that a carbonyl group was again present adjacent to the nitrogen, which prohibits a pyrrolic structure. The alkene CH (δ = 6.25) was correlated with two doublets (δ = 97.07, 154.27). The carbon peak of the methyl ester (C=O) was also split into a doublet. This could indicate that two fluorine atoms are present in the molecule (**129**) (**Figure 2.18**). The two doublets at 97 and 154 ppm are consistent with shifts associated with fluorinated pyrrolic structures.[29]

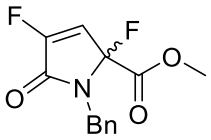

129

Figure 2.18: Proposed structure for the identity of **Unknown 1** (**129**) based on ^{1}H- and ^{13}C NMR spectral analysis

The LCMS recorded for **Unknown 1** supports this theory (*m/z* = 268, $[M+H]^+$ for **129** = 268). Analysis of the ^{19}F NMR spectrum revealed that two fluorine peaks were indeed present (δ = -130.5 (t, J = 2.0) and -142.8 ppm). The peak at -130 ppm is likely to be due to the fluorine on C-4, and the peak at -142 ppm will be due to the fluorine on C-2.

Whilst the synthesis and isolation of the above fluorinated enones was interesting, it was still unclear why the use of a benzyl protecting group on a proline substrate causes conversion to a pyrrole derivative and loss of the C-4 substituent. This outcome takes place when the substrate is Bn-Pro-OMe (**130**) or the oxalate dimer (**125**). To evaluate what occurs during reaction with Selectfluor when the substrate is Bn-Hyp-OMe (**123**), the reaction shown in **Scheme 2.28** was attempted using a number of conditions (**Table 2.4**).

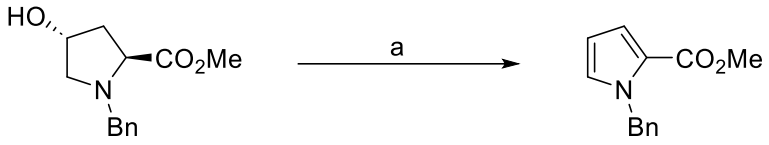

123 **126**

Scheme 2.28: Reaction of Bn-Hyp-OMe (**123**) with Selectfluor to form *N*-benzyl pyrrole carboxylate methyl ester (**126**); a) various conditions, displayed below in **Table 2.4**.

Entry	Reaction conditions (a, Scheme 2.28)	Yield[b]
1	Selectfluor, K_2HPO_4, MeCN/H_2O (4:1), 5 mA, 2 F/mol, N_2, RVC electrodes, alt. polarity 2 mins.	100
2	See **entry 2**, but with acetone instead of MeCN	100

Table 2.4: Reaction conditions for the transformation of Bn-Hyp-OMe (**123**) to form *N*-benzyl pyrrole carboxylate methyl ester (**126**); b = % conversion to pyrrole **126** as observed by ^{1}H NMR spectroscopy.

Both reaction conditions gave rise to the expected pyrrole (**126**). **Entry 1** (**Table 2.4**) produced solely pyrrole, but peaks were observed in the ^{19}F NMR spectrum which were attributed to minor fluorinated impurities. Exchanging the solvent for acetone (**Table 2.4, Entry 2**) still led

to the pyrrole being formed as the major product, but the ^{1}H NMR spectrum of the crude reaction mixture revealed that both fluorinated enone **128** and α-hydroxylated enone **127** were present in minor amounts.

The reactions shown above in **Scheme 2.28** were repeated, this time with the *N*-benzyl proline hemioxalate (**124**) (**Scheme 2.29**).

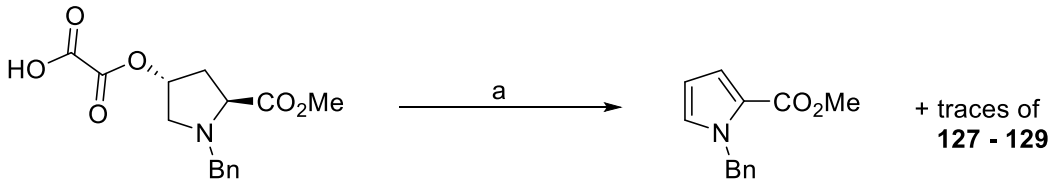

124 **126**

Scheme 2.29: Reaction of *N*-benzyl proline hemioxalate (**124**) with Selectfluor; a) **Entry 1** and **Entry 2** from **Table 2.4**.

The reaction was run first in acetone then in acetonitrile. Both reactions resulted in generation of a mixture of difluorinated enone **129**, fluorinated enone **128**, and α-hydroxylated enone **127**, in addition to the pyrrole. The reaction in acetone had a product ratio of 1 : 4.3 : 2.5 : 8.5 (**129** : **128** : **127** : **126**), and the reaction in acetonitrile had a product ratio of 1 : 0 : 1.9 : 1.8 (**129** : **128** : **127** : **126**). These ratios were determined by comparing the integrals of known product peaks in the ^{1}H NMR spectra of the crude reaction mixture.

When Bn-Hyp-OMe (**123**) was reacted with sodium triflinate instead of Selectfluor, the major product was a trifluoromethyl-substituted pyrrole derivative (**Scheme 2.30**). This was determined by examination of the ^{1}H- and ^{19}F NMR spectra of the crude reaction mixture alongside LCMS data.

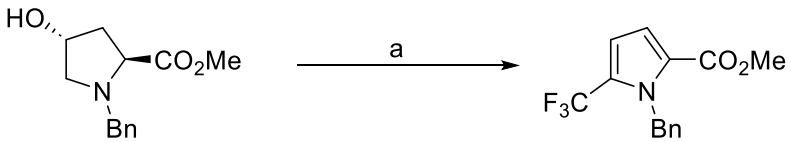

123 **131**

Scheme 2.30: The conversion of Bn-Hyp-OMe (**123**) to a 2-trifluoromethyl pyrrolic derivative (**131**); reagents and conditions: a) sodium triflinate, K_2HPO_4, MeCN/H_2O (4:1), 5 mA, 2 F/mol, N_2, RVC electrodes, alt. polarity 2 mins.

A probable explanation for this transformation is that the pyrrole is formed initially, which subsequently reacts with sodium triflinate. This result suggests that conversion to the pyrrole is not exclusive to reaction with Selectfluor, and that the pyrrole is not formed via elimination of fluorine substituents.

Caesium oxalates have also been known to form alkyl radicals under oxidative conditions.[30,31] Therefore, Bn-Hyp-OMe (**123**) was converted to a caesium oxalate derivative (**133**) via an ethyl hemioxalate intermediate (**132**) (**Scheme 2.31**).

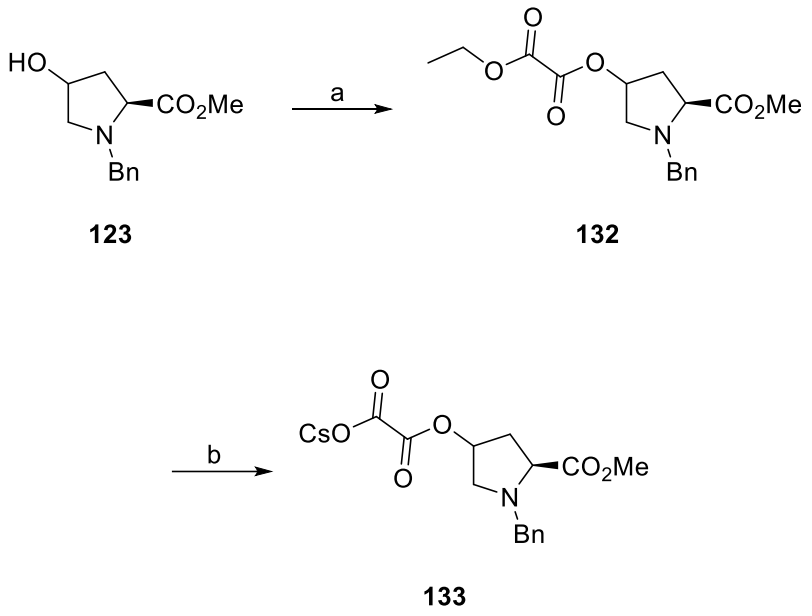

123 **132** **133**

Scheme 2.31: Conversion of Bn-Hyp-OMe (**123**) to **133** *via* **132**; reagents and conditions: a) ethyl chloroxoacetate, Et_3N, DMAP (cat.), anhydrous DCM, 0 °C, 1 h, 59%; b) CsOH (1 M, aq.), THF, 50 mins, vigorous stirring, rt.

Both the ethyl hemioxalate (**132**) and the caesium oxalate (**133**) were then reacted with Selectfluor in the electrochemical cell using the same conditions as **Table 2.4, Entry 1** (**Scheme 2.32**). In both cases these particular substrates resulted exclusively in formation of the pyrrole (**126**).

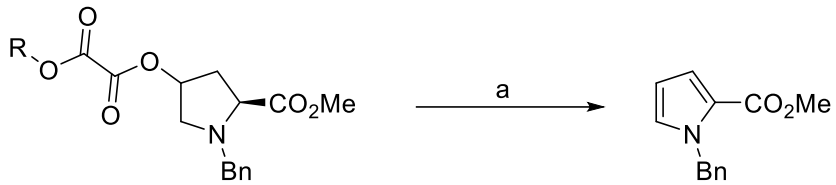

R = Et **132**
R = Cs **133**

126

Scheme 2.32: Electrochemical reaction of ethyl hemioxalate **132** and caesium hemioxalate **133** with Selectfluor, resulting in formation of pyrrole **126** in both cases; reagents and conditions: a) Selectfluor, K_2HPO_4, MeCN/H_2O (4:1), 5 mA, 2 F/mol, N_2, RVC electrodes, alt. polarity 2 mins.

A tetrafluoropyridyl derivative[32] of Bn-Hyp-OMe (**134**) was then synthesised to assess the influence of this group against pyrrole formation (**Scheme 2.33**).

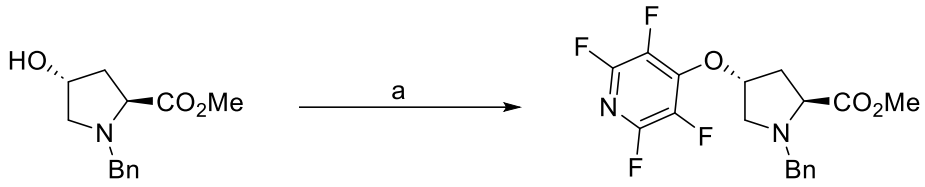

123 **134**

Scheme 2.33: Conversion of Bn-Hyp-OMe (**123**) to Bn-Hyp(TFP)-OMe (**134**); reagents and conditions: a) pentafluoropyridine, K_2CO_3, MeCN, 20 h, rt, 45%.

When the *N*-benzyl proline-TFP derivative (**134**) was subjected to reaction with Selectfluor, the four enone products (**126 - 129**) were produced in the ratio 1 : 2.4 : 5.8 : 5.5 (**129** : **128** : **127** : **126**) (**Figure 2.19**).

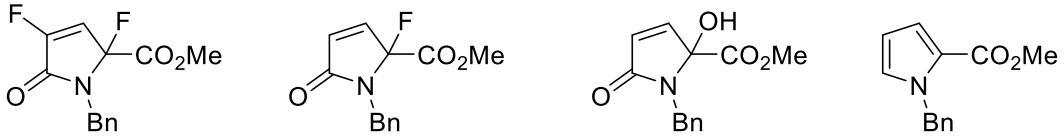

129 **128** **127** **126**

Figure 2.19: Four enone or pyrrolic products (**129, 128, 127, 126**) obtained from the reaction of Bn-Hyp(TFP)-OMe (**134**) with Selectfluor in the ratio 1 : 2.4 : 5.8 : 5.5 (**129** : **128** : **127** : **126**). This ratio was determined by comparison of the integrals of known product shifts in the ^{1}H NMR spectra of the crude product mixture.

Given the outcomes of the aforementioned experiments, it appears that no matter which group is present at C-4, elimination and pyrrole formation will take place under oxidative conditions if the protecting group employed is a benzyl group.

To evaluate the effect of leaving the proline -NH group unprotected, hydroxyproline methyl ester hydrochloride was subjected to the standard electrochemical fluorination conditions (**Scheme 2.34**).

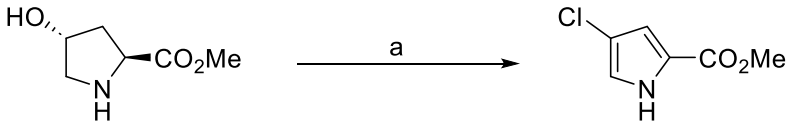

122 **135**

Scheme 2.34: Reaction of H-Hyp-OMe•HCl (**122**) with Selectfluor to produce a 4-chloro derivative (**135**); reagents and conditions: a) Selectfluor, K_2HPO_4, MeCN/H_2O (4:1), N_2, 5 mA, 2 F/mol, 57%.

The major product of this reaction was revealed by X-Ray crystallography to be 4-chloro-2-methylpyrrole carboxylate (**135**) (**Figure 2.20**).

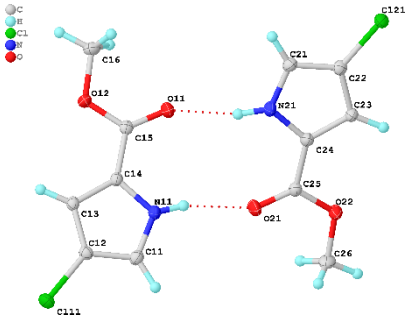

Figure 2.20: The X-Ray molecular structure of 4-chloro-2-methylpyrrole carboxylate (**135**). Molecular structure reported with a 50% thermal ellipsoid probability.

A plausible route to this product could be initial conversion to pyrrole **136**, followed by chlorination caused by the substrate being a hydrochloride salt (**Scheme 2.35**).

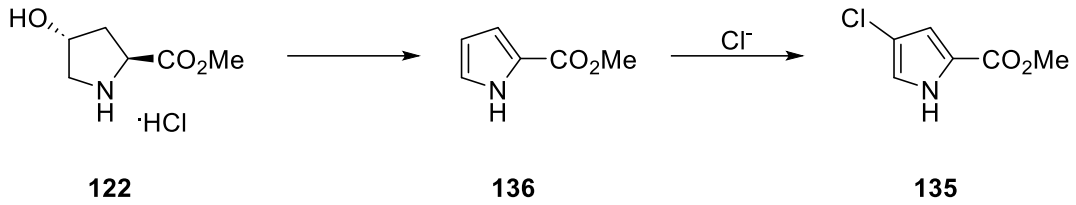

122 **136** **135**

Scheme 2.35: Plausible route towards generation of 4-chloropyrrole derivative **135** *via* pyrrole **136**.

Chloride ions in the solution may be converted to chlorine radicals or Cl_2, which could substitute onto the electron-rich pyrrole (**136**). This transformation suggests that proline-pyrrole conversion is not a unique function of the benzyl protecting group.

The pyrrole derivative of proline (**136**) was then reacted with Selectfluor to assess whether similar structures to the *N*-benzyl fluorinated cyclic lactams (**128, 129**) could be formed (**Scheme 2.36**). The reaction quickly turned pink when under electrolysis.

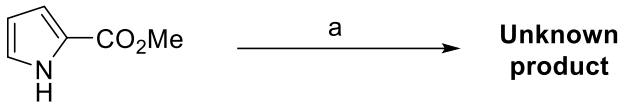

136

Scheme 2.36: Reaction of methyl-2-pyrrole carboxylate (**136**) with Selectfluor resulting in partial conversion to an unknown product; reagents and conditions: a) Selectfluor, K_2HPO_4, MeCN/H_2O (4:1), N_2, 5 mA, 2 F/mol, 5% (^{1}H NMR conversion yield)

^{1}H NMR spectral analysis of the crude reaction mixture revealed that it mostly consisted of starting material, with trace amounts of an unknown product (~ 5% conversion). There was also a signal in the ^{19}F NMR spectrum (δ -113.19, dd, J = 3.0, J' = 2.0), which was attributed to the minor product formed. The reaction was repeated without the nitrogen atmosphere, which resulted in an increased formation of the minor product. The same fluorine signal was present. The ^{1}H NMR spectrum of the product isolated compared to the starting material is shown in **Figure 2.21**.

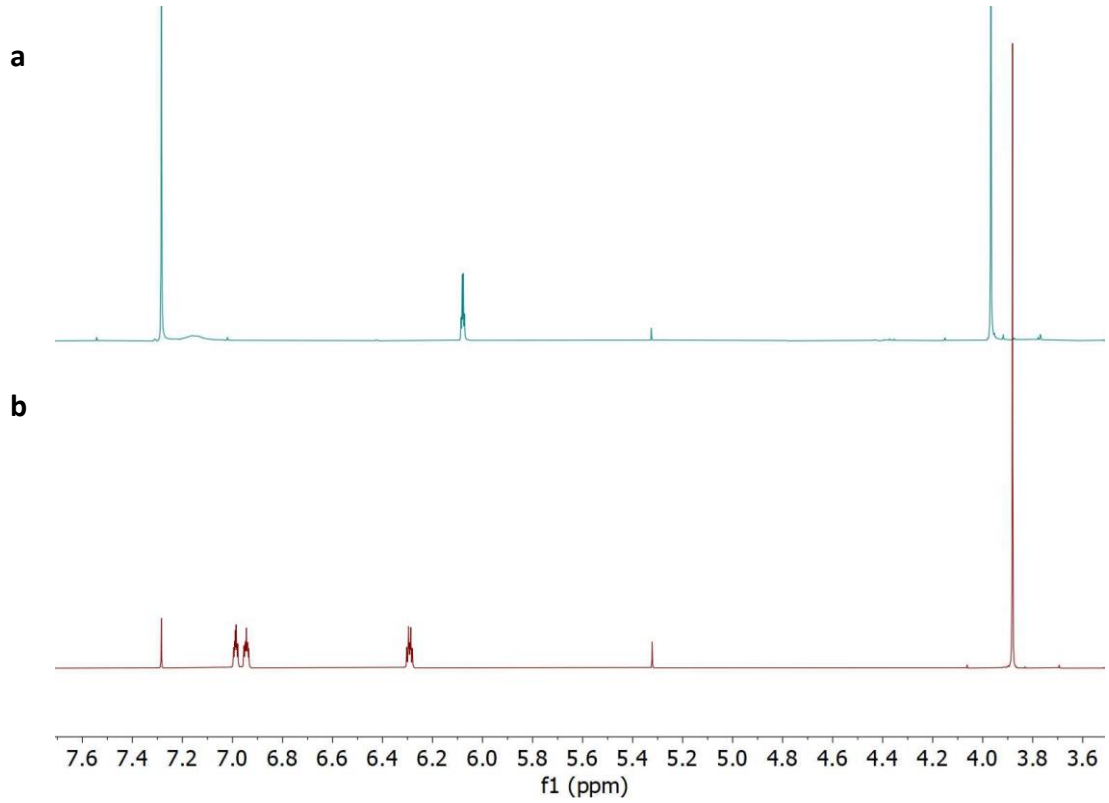

Figure 2.21: ^{1}H NMR spectrum (600 MHz, $CDCl_3$) of the unknown product (a) compared to the ^{1}H NMR spectrum (400 MHz, $CDCl_3$) of the starting material (**136**) (b). The unknown product was isolated from the reaction of 2-methylpyrrole carboxylate (**136**) with Selectfluor.

The major difference in the ^{1}H NMR spectra of the starting material and product (**Figure 2.21**) is that there are three resonances in the ^{1}H NMR spectrum of the starting material, but only a single proton resonance in the product spectrum. This resonance is in the alkene region. Based on the characterisation of the *N*-benzyl fluorolactams (**128, 129**), it is likely that the product of the reaction displayed in **Scheme 2.36** has a similar structure. The proposed structure is shown in **Figure 2.22**.

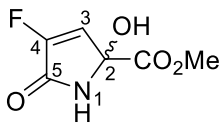

137

Figure 2.22: Proposed structure for the minor product from the reaction described in **Scheme 2.36**.

Analysis of the ^{13}C NMR spectrum of **137** revealed that the majority of the peaks were split into doublets or triplets, which is consistent with fluorinated molecules (**Figure 2.23**). Two

peaks in the C=O region were present (δ = 165.8 (t) and 159.3 ppm), which confirms the presence of a ketone at the 5-position. A triplet resonance at 140.4 ppm is in the alkene region and correlates to the peak at 6.05 ppm in the ^{1}H NMR spectrum (**Figure 2.21**), which again supports the structural assignment given in **Figure 2.22**. The ^{13}C NMR spectrum also contains a triplet peak at 112.5 ppm (*J* = 251.5). Given the large *J* coupling and large shift to a lower frequency from the alkene region, it is likely that this carbon is directly attached to a fluorine atom.

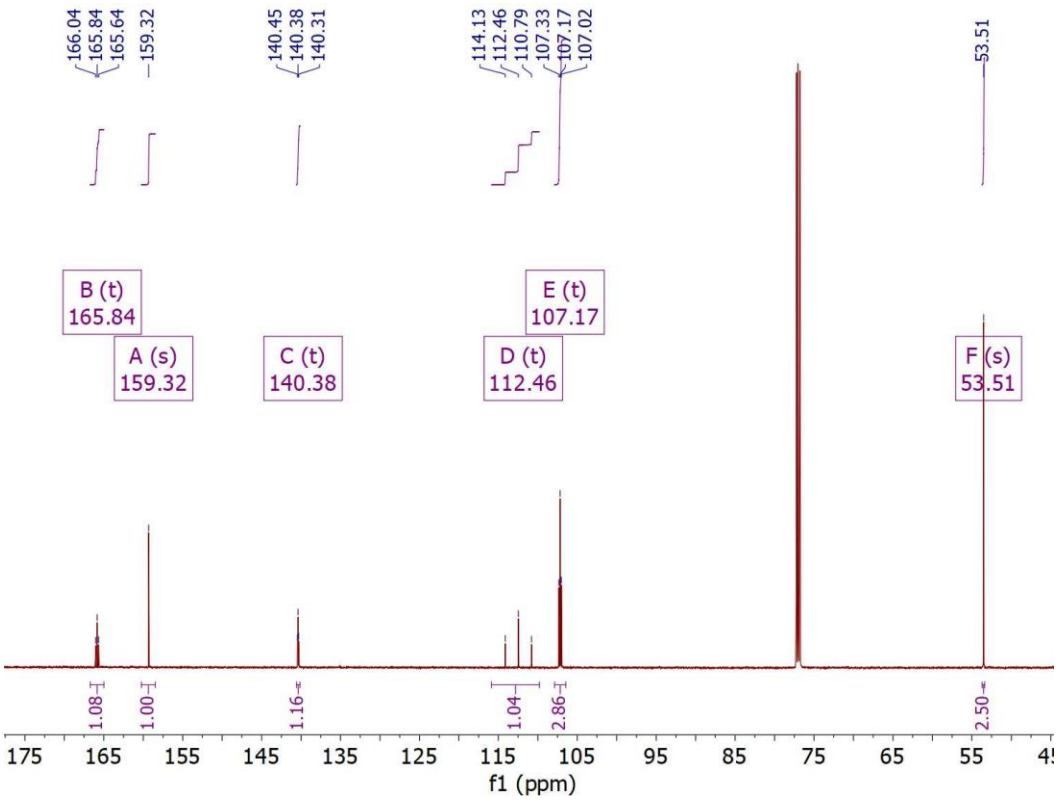

Figure 2.23: ^{13}C NMR spectrum (151 MHz, $CDCl_3$) for fluoropyrrole **137**.

However, the HRMS mass obtained for compound **137** was $[M-H]^-$ = 176 instead of the expected 174.

Interestingly, when the reaction of **136** with Selectfluor was performed without electrolysis (0.3 mmol scale), ^{1}H NMR spectral analysis of the crude reaction mixture revealed that full conversion to the fluorinated product (**137**) had taken place, and hence no further purification was necessary (**Scheme 2.37**). However, the yield was very low (9%).

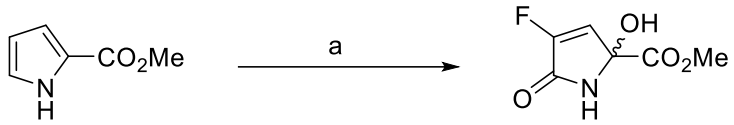

136 **137**

Scheme 2.37: Reaction of pyrrole **136** with Selectfluor and K_2HPO_4 without electrolysis resulting in isolation of a fluorinated product (**137**); reagents and conditions: a) Selectfluor, K_2HPO_4, MeCN/H_2O (4:1), 20 h, rt, 9%.

When this reaction was performed on a larger scale (1.9 mmol), the yield of **137** was again low (7%). Whilst there did not appear to be any other products present post-workup (determined through ^{1}H NMR analysis of the crude product), TLC analysis of the aqueous layer during work-up revealed the presence of a baseline spot. The aqueous layer was re-extracted and subjected to purification using silica gel chromatography, and two additional products were isolated (**Figure 2.24**).

Product 1	**Product 2**
$[M+H]^+$ = 176	$[M+H]^+$ = 157
^{19}F NMR: δ = -135.5 ppm	No fluorine
^{1}H NMR: One alkene peak	^{1}H NMR: Two alkene peaks

Figure 2.24: A summary of preliminary data collected regarding the two additional products obtained from the large scale version of the reaction displayed in **Scheme 2.37**.

Product 1 was thought to be similar to the structure of fluorolactam **137**, as it has the same mass ($[M+H]^+$ = 176), and a single alkene proton peak in the ^{1}H NMR spectrum (t, δ = 6.28 ppm). However, the fluorine signal was much more deshielded (δ = -135.5 ppm), suggesting that the fluorine atom is situated on an sp^3 carbon rather than an alkene carbon. The structure for this product is therefore proposed below in **Figure 2.25**.

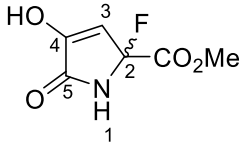

Product 1
138

Figure 2.25: Proposed structure for **Product 1** (**138**) isolated from the reaction displayed in **Scheme 2.37**.

Furthermore, examination of the ^{13}C NMR spectrum of the compound **138** revealed that the peak for C-4 was at an unusually high chemical shift for an alkene (δ = 153.6 ppm). This is consistent with the structure proposed in **Figure 2.25**, as it is likely that the enol functionality causes a shift downfield for the peak at C-4.

The second product isolated from the reaction shown in **Scheme 2.37** (**Product 2**) does not have any fluorine (as evidenced by the lack of any signals in the ^{19}F NMR spectrum). The LCMS ($[M+H]^+$ = 157) indicates that the product structure features an enone moiety and a hydroxyl substituent at the α-C (**Figure 2.26**).

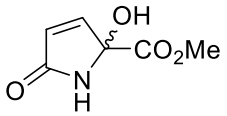

Product 2
139

Figure 2.26: Proposed structure for **Product 2** (**139**) isolated from the reaction displayed in **Scheme 2.37**.

The ^1H NMR spectrum of **Product 2** supports this assignment, as it contains two proton signals in the alkene region (δ = 6.93 and 6.17 ppm), which are correlated to each other (confirmed by COSY). The ^{13}C NMR spectrum consists of two peaks in the C=O region (δ = 172.3 and 170.0 ppm) and two in the alkene region (δ = 146.9 and 128.6 ppm).

A summary of the reaction which produced all three products discussed above is shown in **Scheme 2.38**.

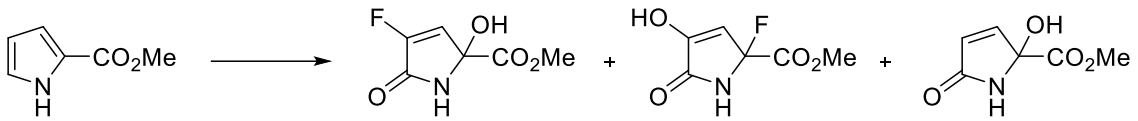

136 **137** **138** **139**

Scheme 2.38: Summary scheme of the reaction between methyl-2-pyrrole carboxylate (**136**) and Selectfluor to produce three enone derivatives: **137** (7%), **138** (4%), and **139** (12%)

Whilst the original goal of electrochemical decarboxylative fluorination of amino-acid derived hemioxalates was not achieved, this work furthered our insight into the unusual behaviours of

proline under electrochemical conditions. In addition, a range of novel proline derived fluorinated enones were isolated and characterised.

In 2023, the Lam group successfully achieved deoxyfluorination of hemioxalates under electrochemical conditions (**Scheme 2.39**).[33] The authors used collidinium tetrafluoroborate as a fluorinating agent in favour of Selectfluor.

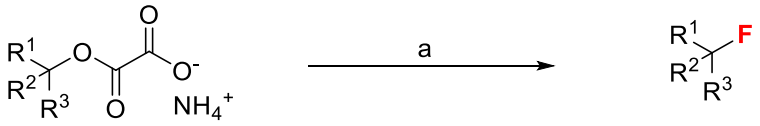

Scheme 2.39: Electrochemical fluorination of activated alcohols using collidinium tetrafluoroborate as fluorinating reagent and electrolyte to generate a range of tertiary alkyl fluorides;[33] reagents and conditions: a) collidinium tetrafluoroborate (5 eq.), 3Å mol. sieves, DCM (10 mL), 10 mA, 5 F/mol, alt. pol. 2 mins, C (+) C (-), undivided cell, 12-70%.

The majority of the substrates fluorinated in the Lam paper were tertiary hemioxalates, though examples of secondary and primary substrates were also included.

2.4 Electrochemical trifluoromethylation

2.4.1 Introduction

Introducing fluorine into bioactive molecules can often be difficult to accomplish directly. An alternative approach is to instead incorporate a trifluoromethyl group; trifluoromethylating agents are often easier and safer to use in comparison to fluorinating reagents. Several commercial drugs possess the -CF_3 moiety (**Figure 2.27**). Of all fluoro-pharmaceuticals currently on the market, 19.2% feature trifluoromethyl groups.[34]

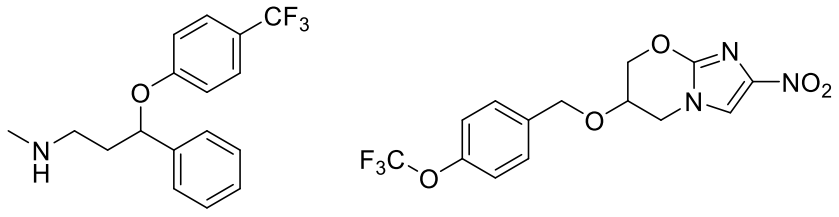

140 **141**

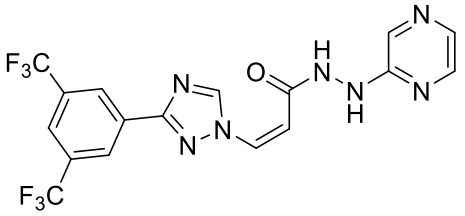

142

Figure 2.27: Examples of drugs containing trifluoromethyl moieties; the antidepressant fluoxetine (**140**), the antitubercular drug pretomanid (**141**), and the anticancer drug selinexor (**142**)

Similarly to monofluorination, trifluoromethylation reactions can proceed *via* electrophilic, nucleophilic, or radical routes (involving CF_3^+, CF_3^-, $\bullet CF_3$, respectively). Electrochemical trifluoromethylation reactions will most often proceed *via* a radical pathway. A handful of the most common trifluoromethylating reagents are displayed in **Figure 2.28**. These reagents are frequently employed for trifluoromethylation reactions using both electrochemical and traditional chemical methods.

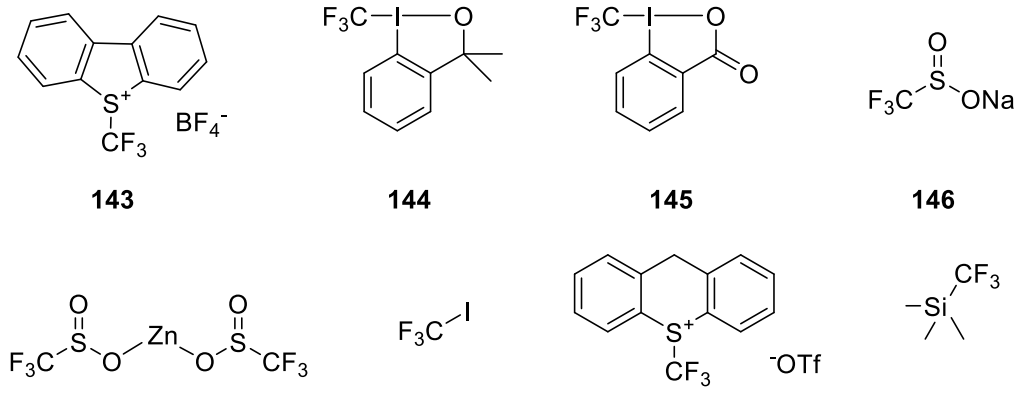

143 **144** **145** **146**

147 **148** **149** **150**

Figure 2.28: Examples of commonly used trifluoromethylating reagents; (L-R) Umemoto's reagent (**143**), Togni's reagent I (**144**), Togni's reagent II (**145**), Langlois' reagent (sodium triflinate) (**146**), zinc trifluoromethylsulfinate (Baran's reagent) (**147**), trifluoroiodomethane (**148**), Ritter's reagent (**149**), $TMSCF_3$ (**150**).

Previous research into electrochemical trifluoromethylation has mainly focussed on the trifluoromethylation of unsaturated or aromatic compounds *via* anodic oxidation. An example of this is shown in **Scheme 2.40**.

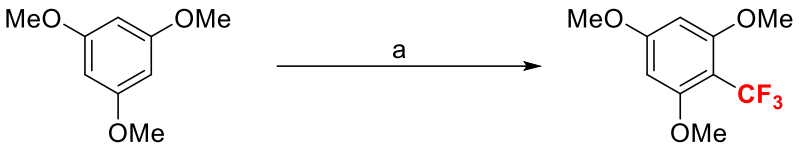

151 **152**

Scheme 2.40: Electrochemical oxidative trifluoromethylation of aromatic compounds by Lei and Gao and coworkers;[35] reagents and conditions: a) sodium triflinate, $^{n}Bu_4NBF_4$, $MeCN/H_2O$ (10:1), C (+) Fe (-), 10 mA, 5 h, undivided cell, 90%.

Often reactions with aromatic molecules require careful selection of substrates due to the reactivity of the $\bullet CF_3$ radical and thus the potential for multiple substitutions.

Electrochemical trifluoromethylation of alkenes is useful for creating C_{alkyl}-CF_3 bonds and can provide the opportunity to introduce two functional groups into a molecule. Lin *et al.* demonstrated that the use of sodium triflinate in conjunction with $MgCl_2$ could facilitate the heterodifunctionalisation of alkenes (**Scheme 2.41**).[36]

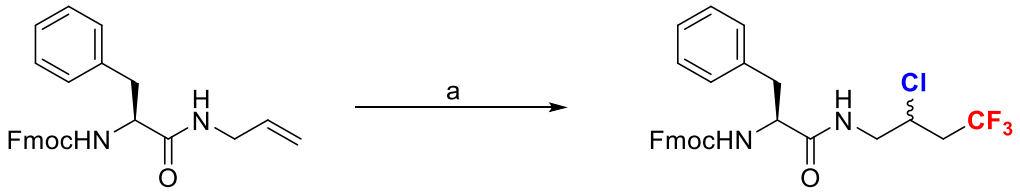

153 **154**

Scheme 2.41: Electrochemical chloro-trifluoromethylation of alkenes; reagents and conditions:[36] a) Langlois' reagent, $MgCl_2$, $Mn(OAc)_2$ (10 mol%), $LiClO_4$ (0.1 M), MeCN/TFA (10:1), C(+) Pt (-), 15 mA, 4 h, 46%, dr = 1:1.

Due to the readiness with which alkenes react, electrochemical trifluoromethylation has also found a niche in the promotion of cascade cyclisation reactions. These types of reactions involve initial reaction of an alkene with a trifluoromethylating reagent, leaving a radical on the adjacent carbon. This radical can then react with another part of the molecule, *i.e.*, an aromatic ring. An example is shown in **Scheme 2.42**.

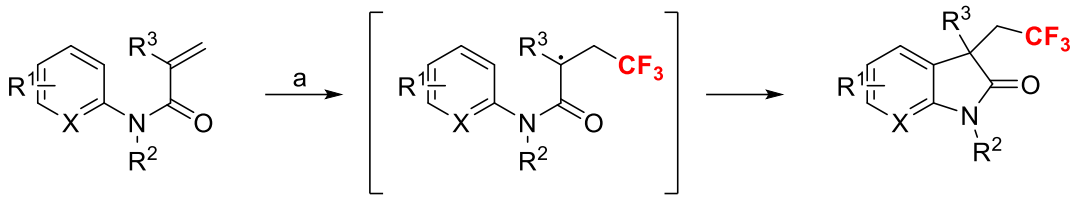

Scheme 2.42: Electrochemical trifluoromethylation/ring-closing of *N*-substituted acrylamides via a carbon-centred radical transition state, demonstrated by Ackermann *et al.*;[37] reagents and conditions: a) sodium triflinate, Et_4NClO_4, MeCN/H_2O (2:1), 4 mA, RVC (+) Pt (-), 16 h, 40-77%.

However, electrochemical trifluoromethylation of sp^3 carbons has remained unexplored, largely due to the difficulty of combining an unactivated carbon centre with the transient $\bullet CF_3$ radical. Very recently, Ding *et al.* published a study detailing how the trifluoromethylation of sp^3 carbons could be achieved using an electrochemical multicomponent cascade reaction (**Scheme 2.43**).[38]

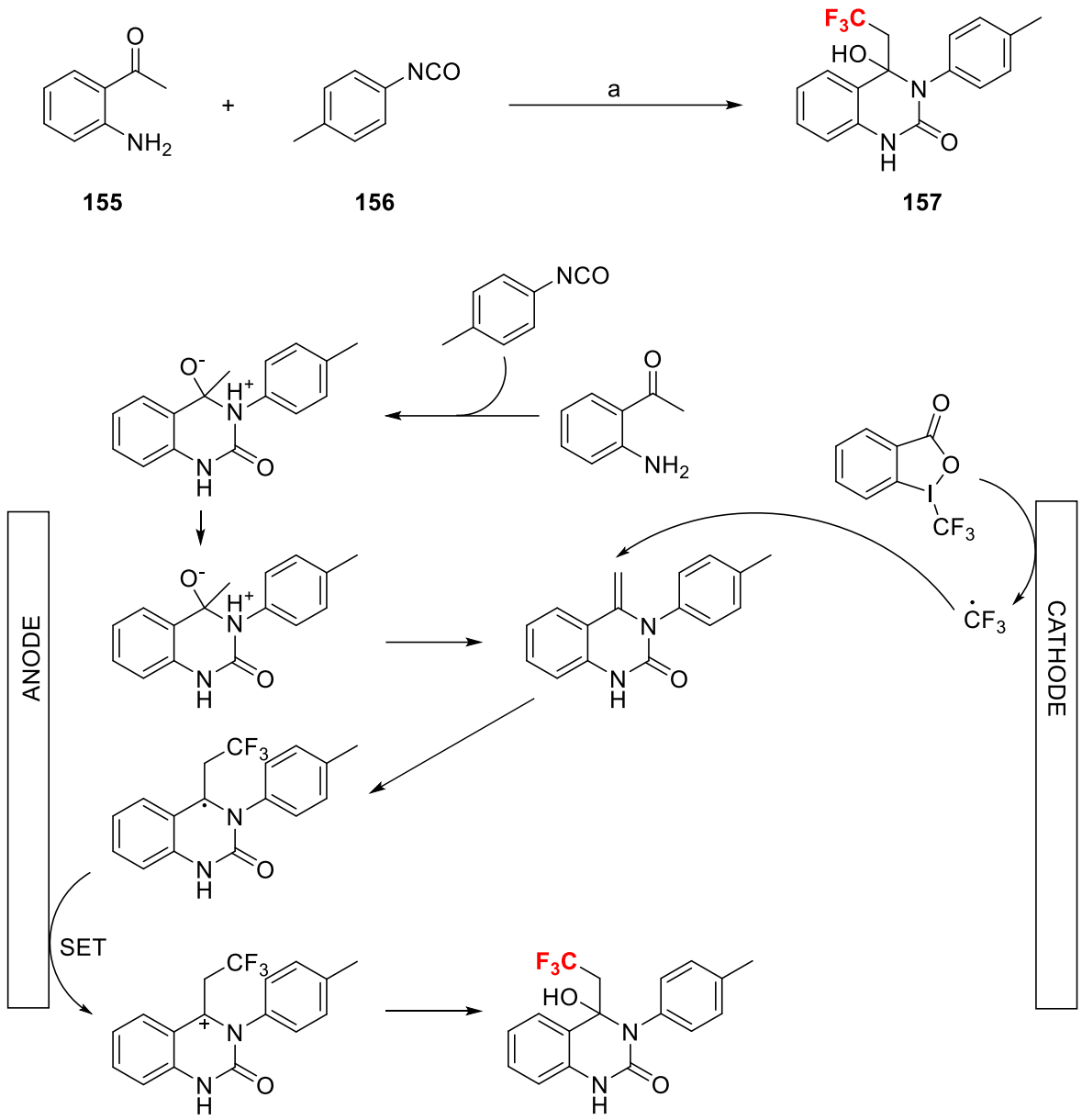

Scheme 2.43: Electrochemical cascade trifluoromethylation of sp^3 carbons;[38] reagents and conditions: a) Togni II, Bu_4NBF_4, THF/H_2O (5:1), C (+) Ni (-), 3 mA, 50 °C, 3 h, 71%. The mechanism proposed by Ding *et al.* is also provided.

2.4.2 Results and Discussion – Trifluoromethylation of amino acid derivatives

Inspired by Baran's electrochemical fluorination (see **Section 2.3.2**), we decided to investigate whether the replacement of Selectfluor with a number of trifluoromethylating agents would be effective in adding a CF_3 group to unactivated sp^3 carbons. An example of the desired transformation is shown below in **Scheme 2.44**.

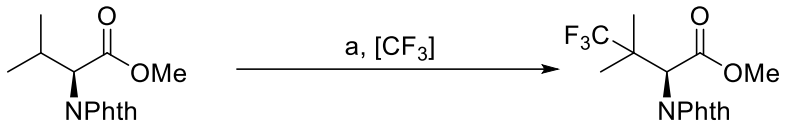

91 **158**

Scheme 2.44: Desired transformation of *N*-Phth-Val-OMe (**91**) to form the β-trifluoromethylated derivative (**158**); reagents and conditions: a) (+) RVC (-) RVC, [CF_3] (3 equiv.), $NaNO_3$, anhydrous MeCN, 3 mA/cm^2, 3 F/mol.

N-Phth-Val-OMe (**91**) was selected as a trial substrate in order to mimic the fluorination conditions as closely as possible. The conditions attempted are displayed in **Table 2.5**.

Entry	Reaction conditions	Yield of 158 (%)
1	Sodium triflinate (**146**), (a)	n/a
2	Umemoto's reagent (**143**), (a)	n/a
3	Togni's reagent (I) (**144**), ^{t}Bu$_4$NBr, (a)	n/a
4	Sodium triflinate (**146**), (+) Pt (-) Pt, $NaNO_3$, MeCN, $MnBr_2.4H_2O$, AcOH (2 equiv.), 10 mA, 2 F/mol.	n/a
5	Ritter's reagent (**149**), (a)	n/a

Table 2.5: Various reaction conditions trialled when attempting to trifluoromethylate a valine derivative, deviation from (a) detailed in **Scheme 2.44**.

None of the reaction conditions in **Table 2.5** were found to successfully generate the desired product (**158**). After the initial failure of sodium triflinate (**Table 2.5, Entry 1**), it was thought that electrophilic trifluoromethylating reagents such as Umemoto's and Togni's reagents may work better. Whilst the use of Umemoto's reagent did elicit a number of singlet peaks in the ^{19}F NMR spectrum of the crude product mixture, and a peak in the MS with the correct product mass, no trifluoromethylated product was isolated (**Table 2.5, Entry 2**). The reaction with Togni's reagent returned only starting material (**Table 2.5, Entry 3**).

As displayed in Entry 4 (**Table 2.5**), a reaction incorporating a redox mediator was then set up, in an attempt to regulate the concentration of CF_3 radicals and facilitate substrate oxidation. $MnBr_2$ has been used in conjunction with sodium triflinate to trifluoromethylate sp^2 carbons,[39] so this was selected as the redox mediator. Whilst a number of singlet resonances (-63.0, -61.1, and -16.7 ppm) were observed in the ^{19}F NMR spectrum of the crude product mixture, these were attributed to minor fluorinated impurities present. The only change observed was partial deprotection of the methyl ester.

Ritter's reagent (**149**) was synthesised according to the procedure by Ritter *et al.*[40] (**Scheme 2.45**).

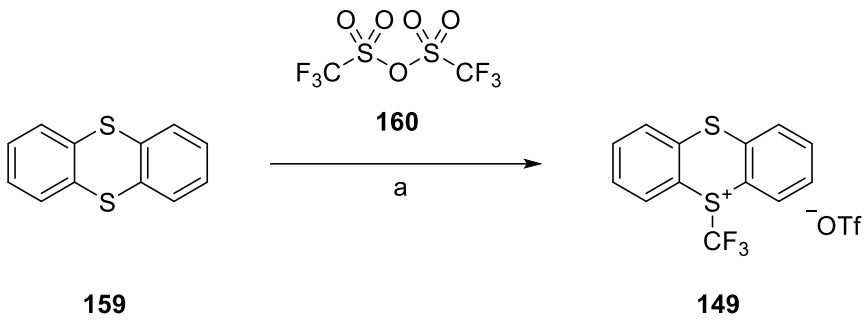

Scheme 2.45: The synthesis of Ritter's reagent (**149**) from thianthrene (**159**) and triflic anhydride (**160**); Reagents and conditions: a) DCM, 35°C, 22 h, 57%

This reagent was chosen due to its ability to react as $^{+}CF_3$, $\bullet CF_3$, or $^{-}CF_3$. Unfortunately, no product was observed when it was reacted with *N*-Phth-Val-OMe (**91**) (**Table 2.5, Entry 5**). Evidently, trifluoromethylation of unactivated sp^3 centres is much harder than sp^3 fluorination. This endeavour was therefore abandoned.

After the trifluoromethylation of sp^3 centres in amino acids like valine proved difficult, attention was instead turned to sp^2 centres in amino acids. The electron-rich indole scaffold of tryptophan derivatives should respond well to electrochemical oxidation and subsequent nucleophilic attack by a trifluoromethylating reagent; tryptophan was therefore chosen as a target for electrochemical trifluoromethylation.

Sodium triflinate was selected as the trifluoromethylating reagent, alongside conditions which have been reported for the trifluoromethylation of quinolinones, which are similarly electron-rich.[41] A phthalimide protecting group was initially selected for this reaction, to ensure any reactivity of the amine group was completely nullified. This was synthesised using conditions displayed in **Scheme 2.46**.

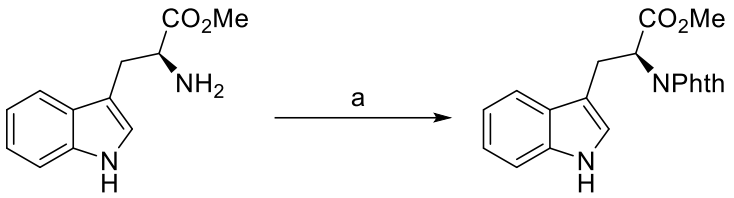

161 **162**

Scheme 2.46: Phthalimide protection of *L*-tryptophan methyl ester (**161**); reagents and conditions: a) phthalic anhydride, Et_3N, toluene, reflux, 12 h, 67%.

This substrate was then subjected to electrochemical trifluoromethylation. **Scheme 2.47** shows the desired trifluoromethylation reaction, and **Table 2.6** displays the conditions attempted to effect this transformation.

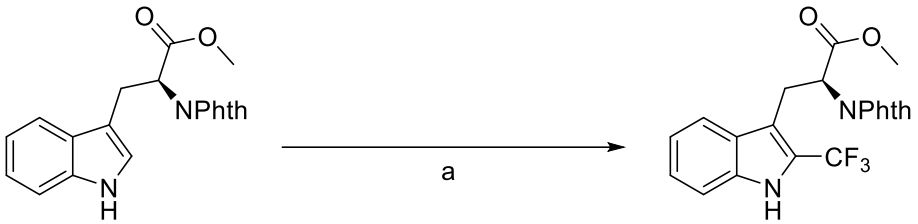

162 **163**

Scheme 2.47: The conversion of *N*-Phth-Trp-OMe (**162**) to its trifluoromethylated derivative (**163**); reagents and conditions: a) Sodium triflinate (2 equiv.), 0.2 M Bu_4NPF_6, DMSO, 10 mA, 6 h.

Entry	Deviation from a) (Scheme 2.47)	Yield of 163[b] /%
1	None	0[c]
2	5 mA, 3 F/mol, 1.7 equiv. [CF_3]	35
3	5 mA, 3 F/mol, 1.4 equiv.[CF_3]	26
4	HFIP, 5 mA, 3 F/mol, 1.5 equiv.[CF_3]	0
5	5 mA, 2 F/mol, 2 equiv. [CF_3]	23
6	*N*-Boc-Trp-OMe (**164**), same as **Entry 2**	23

Table 2.6: The various conditions attempted during the investigation into tryptophan trifluoromethylation; b = isolated yield, c = di-trifluoromethylated products observed rather than the desired mono-trifluoromethylated derivative.

A higher current of 10 mA (**Table 2.6**, **Entry 1**) appeared to cause a greater degree of over-substitution of CF_3, resulting in di-trifluoromethylated derivatives. Whilst lowering of the current to 5 mA enabled isolation of the desired mono-trifluoromethylated product (**163**),

ditrifluoromethylated products were still observed (**Table 2.6, Entries 2, 3, and 5**). The presence of ditrifluoromethylated products was confirmed through ^{1}H- and ^{19}F NMR analysis of an additional product isolated. The ^{19}F NMR spectrum featured two singlet peaks (δ -57.7, -57.9 ppm) and the ^{1}H NMR spectrum possessed one less peak in the aromatic region, indicating that the second CF_3 substituent is situated somewhere on the benzene ring.

The number of equivalents of sodium triflinate also seemed to have a significant effect upon the yield of the reaction (**Table 2.6, Entries 2, 3, and 5**). This is understandable given tryptophan's apparent propensity for double substitution.

Interestingly, the replacement of the DMSO with HFIP halted the reaction. HFIP is a popular electrochemical solvent as it can stabilise radicals and has a broad solvent window. The inhibitory effect of HFIP on this reaction may be due to its tendency to aggregate and form H-bonds, which may cause a steric clash with the large phthalimide group. Many products with high masses were observed in the LCMS so it is possible that HFIP was directly adding to the substrate. The reaction of HFIP with indole substrates under electrochemical conditions has been published previously by Mo *et al.* (**Scheme 2.48**).[42]

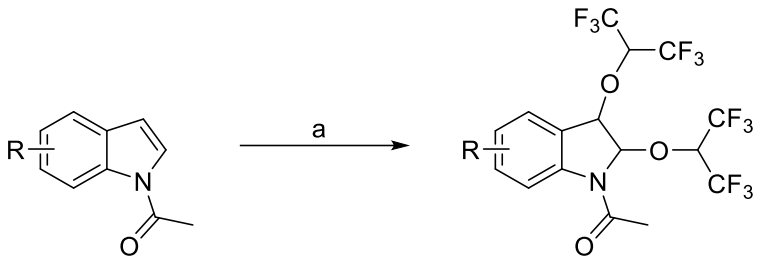

Scheme 2.48: Electrochemical reaction of *N*-acetylindoles with HFIP;[42] Reagents and conditions: a) nBu$_4$NPF$_6$, K$_2$CO$_3$, HFIP/CH$_2$Cl$_2$ (4:3, 7 mL), RVC (+) Pt (-), rt, 6 h

The use of a Boc-protected substrate (**164**) instead of a phthalimide-protected substrate resulted in a reduced yield of the desired product (**Table 2.6, Entry 6**).

Due to the necessity of synthesising the *N*-Phth protected substrate, it was thought that a commercially available model substrate like 3-methyl indole (**165**) could be used to optimise the trifluoromethylation more efficiently. However, when this reaction was attempted, an unexpected tricyclic dimeric product (**166**) was obtained instead of the desired trifluoromethylated product (**Scheme 2.49**).

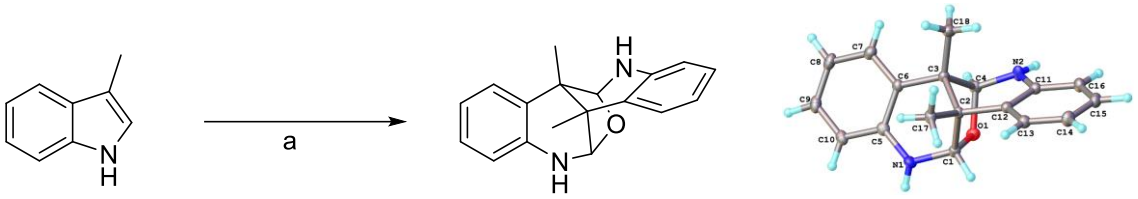

Scheme 2.49: Conversion of 3-methyl indole (**165**) to polycyclic dimer (**166**), the structure of which was confirmed by X-Ray crystallography. Molecular structure reported with 50% thermal ellipsoid probability. reagents and conditions: a) sodium triflinate, 0.2M Bu_4NPF_6, DMSO, 5 mA, 3 F/mol, graphite electrodes.

This structure has been previously reported in the literature,[43] but further research into these kinds of structures from indole substrates was scarce. Discussion of further studies into electrochemical oxidation of indoles can be found in **Chapter 4**.

2.5 Electrochemical chlorination

2.5.1 Introduction

In recent years a number of electrochemical chlorination procedures have been developed, due to the issues associated with traditional chlorination reagents. Elemental chlorine is toxic and difficult to handle, whilst use of NCS is not particularly atom economic. Using electro-organic synthesis methods enables milder chlorinating reagents to be employed.[44]

In an early breakthrough for electrochemical chlorination, Kakiuchi *et al.* developed a method for regioselective chlorination of aromatic molecules using HCl (**Scheme 2.50**).[45]

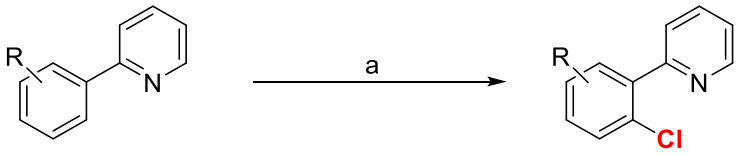

Scheme 2.50: Pd-catalysed electrochemical chlorination of aromatic molecules, assisted by a pyridyl directing group. R = 2-CH_3, 3-CH_3, 3-OCF_3, 3-CF_3, 3-CO_2CH_3;[45] reagents and conditions: a) $PdCl_2$ (10 mol %), H-type divided cell: anodic chamber (DMF, 10 mL) and cathodic chamber (HCl, 2 M, 10 mL), Pt (+) Pt (-), 90°C, 20 mA, 87-93%.

The use of simple HCl as the chlorinating reagent facilitated purification of the products, and reduced the amount of organic waste typically produced in analogous reactions.

In later years, metal chlorides have also been used as cheap and safe alternative chlorinating reagents under electrochemical conditions.[46] In 2019, Chen *et al.* demonstrated how LiCl could be used to chlorinate arenes (**Scheme 2.51**).[47]

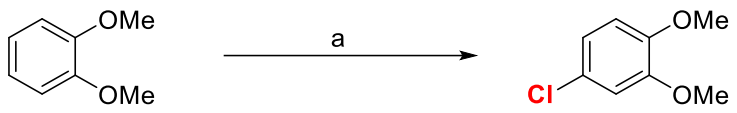

167 **168**

Scheme 2.51: Electrochemical chlorination of arenes using LiCl and a hydrogen bond network system;[47] reagents and conditions: a) LiCl, AcOH/HFIP (1:1), Pt (+) Pt (-), 3 V, 8 h, undivided cell, 80%.

The authors proposed that the reaction proceeds *via* anodic oxidation of substrates and chloride ions to generate radical cations and •Cl, which combine to give the product. Cationic polymerisation is reduced by utilising a AcOH/HFIP solvent, which stabilises the substrate through H-bonding interactions.

In 2021 Morrill *et al.* described how metal chlorides (*e.g.*, $MgCl_2$) could also be used to chlorinate alkenes in a *Z*-selective manner (**Scheme 2.52**).[48] This reaction exploits the steric hindrance between the chloro-substituent and the tosyl group to selectively form *Z*-isomers.

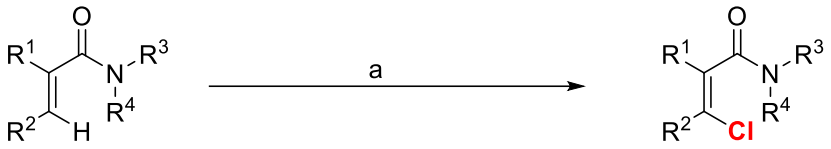

Scheme 2.52: Electrochemical chlorination of acrylamides to selectively form the *Z*-isomer;[48] reagents and conditions: a) $MgCl_2$, MeCN/AcOH (7:1), C (+) Pt (-), 10 mA, 2.5 F/mol, N_2, 2 h, undivided cell, 34-92%.

2.5.2 Results and Discussion – Electrochemical chlorination

Electrochemical chlorination is still an emerging topic of research, with a majority of papers on the subject having been published post-2019. Our interest in electrochemical chlorination was sparked due to a serendipitous discovery whilst attempting to dimerise indole compounds (See **Chapter 4, Section 4.5**) (**Scheme 2.53**). When 3-methylindole carboxylate (**169**) was reacted under electrochemical conditions, a minute amount of a then-unknown compound was isolated instead of the desired dimer.

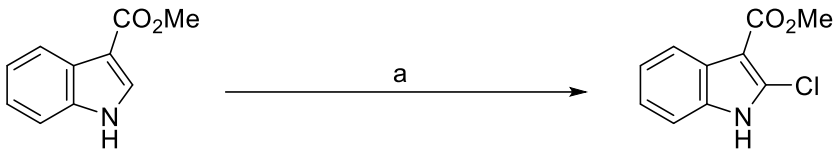

169 **170**

Scheme 2.53: The attempted dimerization of 3-methylindole carboxylate (**169**), resulting in the isolation of a 2-chloro derivative (**170**) in 3% yield; reagents and conditions: a) DMSO, Bu_4NPF_6 (0.22 M), C (+) C (-), 5 mA, 3 F/mol, 3%.

The identity of this unknown product was confirmed to be 2-chloro-3-methylindole carboxylate (**170**) after a crystal structure was obtained (**Figure 2.29**).

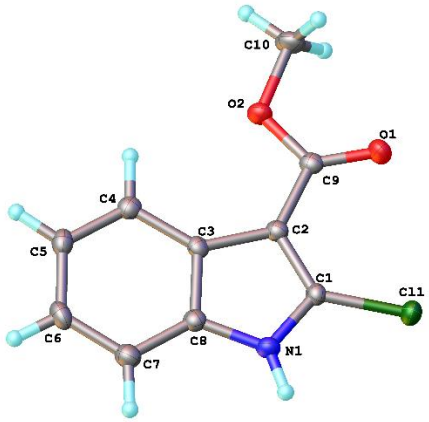

Figure 2.29: Molecular structure obtained for the product of the reaction shown in **Scheme 2.53**; 2-chloro-3-methylindole carboxylate (**170**). Molecular structure reported with a 50% thermal ellipsoid probability.

This result was initially confusing, due to the absence of any chlorinating reagents in the reaction. The cause of this transformation was postulated to be trace amounts of dichloromethane (DCM) present in the reaction mixture, either due to contamination or due to contact during the aqueous work up.

This hypothesis was confirmed when the reaction was run with DCM present in the reaction mixture (DMSO/DCM 10:1), which resulted in a 24% yield of the desired 2-chloro derivative (**170**). DCM is not typically used as a chlorinating agent due to its perceived unreactivity; indeed, it is often used as an inert solvent in electrochemical reactions. Due to this intriguing result, the reaction was then optimised using 3-methylindole carboxylate (**169**) as a model compound (**Table 2.7**).

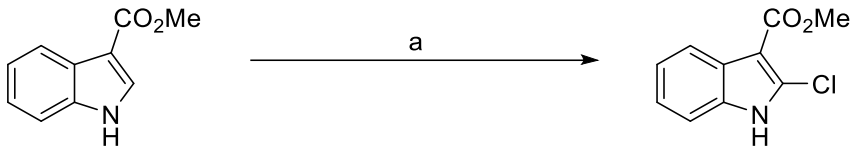

Entry	Variation from standard conditions (a)	Yield /%
1	None	24[c]
2	No DCM	0
3	10 mA	18[b]
4	30% DCM	15[b]
5	6 F/mol	35[b]
6	MeCN instead of DMSO	0
7	0.11 M Bu_4NPF_6	49[b]
8	Bu_4NBF_4	39[b]
9	$CHCl_3$, 0.11 M Bu_4NPF_6	58[b]
10	0.11 M Bu_4NBF_4, 6 F/mol	79[b], 69[c]
11	DCE, **10**	76[b]
12	$CHCl_3$, **10**	75[c]
13	No electrical current	0
14	10 mol% $MnBr_2$	0
15	15% DCM	20[b]
16	0.06 M Bu_4NPF_6	49[b]
17	RVC electrodes	5[b]

Table 2.7: Optimisation of reaction conditions; a = standard reaction conditions: undivided cell, graphite electrodes, 10% v/v DCM/DMSO (4 mL), Bu_4NPF_6 (0.22 M), 0.3 mmol substrate, 5 mA, 3 F/mol. b = conversion determined by ^1H NMR (%), c = isolated yield (%).

Reports of solvents being used as chlorinating agents under electrochemical conditions are not unheard of; in 2019, Liang *et al.* published a hetero/aryl chlorination procedure using dichloroethane (DCE) (**Scheme 2.54**).[49] A couple of years later, Waldvogel *et al.* also

employed DCE for the vicinal dichlorination of alkenes.[50] Tetrachloromethane (CCl_4) has also been used for electrochemical chlorination.[51]

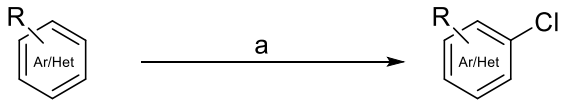

Scheme 2.54: Electrochemical dichlorination of hetero/aryl compounds using DCE *via* generation of HCl and vinyl chloride;[49] reagents and conditions: a) DCE, $^{n}Bu_4NOH$ (37% in MeOH), C (+) Pt (-), 10 mA, 60°C, undivided cell, 3-20 h, 31-97%.

There have been some recent reports of chlorination reactions using DCM, *e.g.*, Liu and Fang outlined their method for electrochemical chlorination of 8-aminoquinoline amides in 2021.[52] This work appears to be the first account of an electrochemical chlorination procedure which uses DCM. However, the versatility of this method is hampered by a limited substrate scope and the requirement for a transition metal catalyst and high current (100 mA). DCM has also been used to effect oxydichlorination of alkynes.[53]

During our optimisation studies of the chlorination of 3-methylindole carboxylate (**Table 2.7**), a number of observations were noted. Firstly, no reaction took place when no electric current was applied, and only starting material was recovered (**Table 2.7, Entry 13**). The same outcome was also observed when no DCM was added to the reaction mixture (**Table 2.7, Entry 2**). This confirms that both of these conditions are necessary for successful chlorination.

Additionally, the replacement of DMSO with MeCN prohibited the reaction (**Table 2.7, Entry 6**). This was surprising, as MeCN is very commonly used in electrochemical reactions due to its wide solvent window and high dielectric constant. This could indicate that DMSO is playing a role in the reaction mechanism. DMSO and other sulfoxides have been known to promote chlorination of electron-rich aromatic molecules.[54,55] Due to the weak nucleophilicity of DMSO, it is capable of stabilising chlorine species through either the sulfur or oxygen centre.[56]

When DCE or chloroform ($CHCl_3$) were used in place of DCM, the chlorination proceeded efficiently with comparative yields (**Table 2.7, Entries 11 and 12**). This was expected, due to the similarity of the three solvents and the prior work published.[49, 50]

When RVC electrodes were used instead of graphite electrodes, the yield of chlorinated product was reduced (**Table 2.7, Entry 17**). The higher surface area of the RVC electrodes will decrease the charge density, consequently lowering the potential.[57] This reaction may require a higher potential in order to proceed, which could explain the lowered yield with RVC electrodes. Additionally, halving the concentration of electrolyte improved the yield (**Table 2.7,**

Entry 7) Given that reducing the electrolyte concentration will increase the potential, this supports the theory that lower potentials disfavour the reaction.

$MnBr_2$ was added to a trial reaction because it has previously been used as a redox mediator (**Table 2.7, Entry 14**).[58] Redox mediators can lower the potential required to oxidise or reduce a species by facilitating indirect oxidation/reduction. Given that this reaction appears to require a high potential, it was though that a redox mediator might improve the yield. However, the addition of a catalytic amount of $MnBr_2$ inhibited the reaction completely, suggesting that the Mn^{2+} ion was indeed being oxidised preferentially to Mn^{3+}, but SET between the Mn^{3+} ion and the substrate/active chlorine source was not able to take place.

Exchanging the Bu_4NPF_6 electrolyte for Bu_4NBF_4 had a positive impact on the yield, as did increasing the total charge to 6 F/mol (**Table 2.7, Entries 8 and 10**). 10% DCM in DMSO was found to be the ideal solvent composition (**Table 2.7, Entry 4 and 15**). The conditions shown in **Entry 10** (**Table 2.7**) were determined to be optimal for chlorination. These conditions were then applied to a number of different substrates, with varying levels of success (**Table 2.8**).

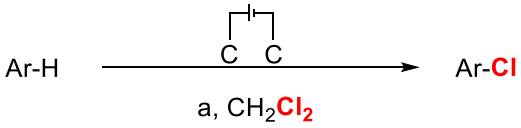

Entry	Substrate	Product	Yield/%
1	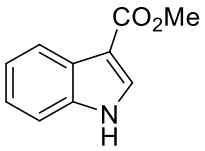 **169**	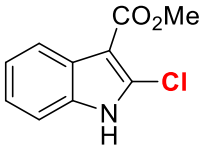 **170**	69
2	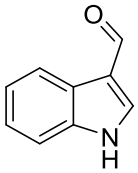 **171**	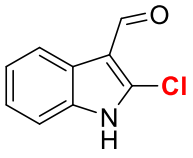 **172**	11

3	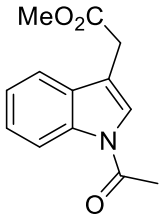 **173**	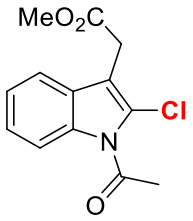 **174**	19
4	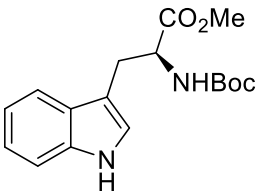 **164**	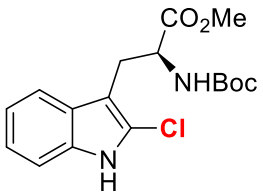 **175**	55
5	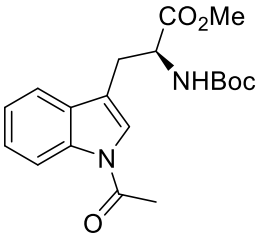 **176**	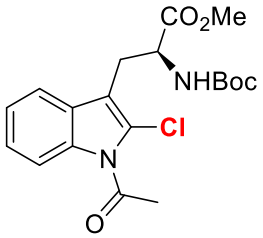 **177**	41
5	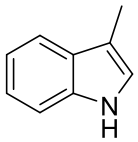 **165**	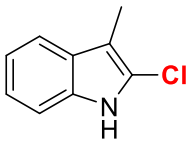 **178**	8
6	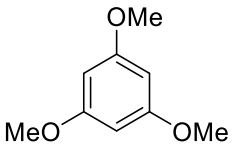 **151**	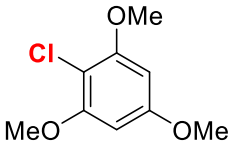 **179**	39[b]
7	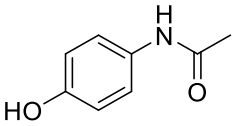 **180**	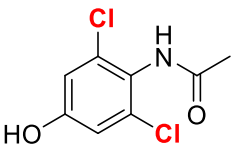 **181**	41

8	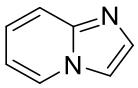 **182**	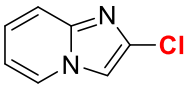 **183**	84
9	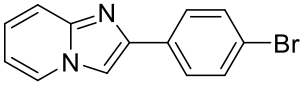 **184**	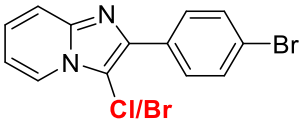 **185** (Cl), **186** (Br)	c
10	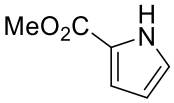 **136**	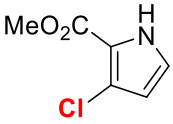 **187**	45
11	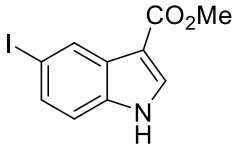 **188**	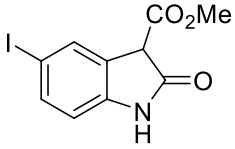 **189**	18
12	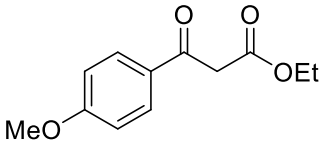 **190**	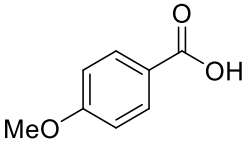 **191**	
13	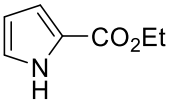 **192**	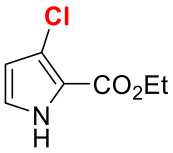 **193**	38[d]
14	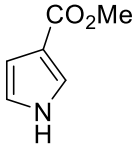 **194**	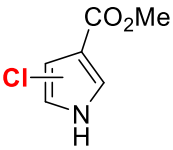	e

Table 2.8: Scope of the reaction; reagents and conditions: a) 0.3 mmol substrate, 10% v/v DCM/DMSO (4 mL), Bu_4NBF_4 (0.11 M), C (+) C (-), 5 mA, 6 F/mol, undivided cell, isolated yields; b = dichlorinated product also observed; c = X-Ray crystallography revealed a mixed Cl/Br substituent in 0.6:0.4 ratio; d = conversion yield (as observed by ^{1}H NMR spectroscopy); e = mixture of two structural isomers formed.

The majority of the substrates that were successfully chlorinated were electron-rich, suggesting that the reaction proceeds *via* anodic oxidation of the substrates. Pleasingly, Boc-Trp-OMe (**164**) was chlorinated in a 55% yield to selectively produce the 2-chloro derivative (**175**) (**Table 2.8, Entry 4**). Chlorine-substituted tryptophans have been used for a number of different applications. Becker *et al.* have reported the direct assembly of 2-chlorotryptophans into chondramide derivatives, as the chlorine substituent was found to impart increased cytotoxicity against tumour cell lines.[59] A number of other groups have used chlorotryptophans as intermediates; for Pd-catalysed coupling, [60] for the creation of spirocyclic natural products, [61], and for blocking unwanted sites during total synthesis.[62]

Often electrochemical transformations of amino acid substrates require robust protecting groups that are incompatible with subsequent peptide synthesis *e.g.*, a phthalimide group, but the chlorination of the Boc-protected tryptophan proceeded smoothly. However, the total charge for this substrate was reduced from 6 F/mol to 3 F/mol due to over-oxidation at 6 F/mol. An attempt to chlorinate Phth-Trp-OMe (**162**) was unsuccessful, which could be due to the electron-withdrawing phthalimide group diminishing the electron density of the C-2 position. *N*-Acetyl tryptophan methyl ester (**176**) was also successfully chlorinated, albeit in a slightly reduced yield than the Boc derivative (**Table 2.8, Entry 5**). A crystal structure was obtained for this compound (**177**) (Figure **2.30**).

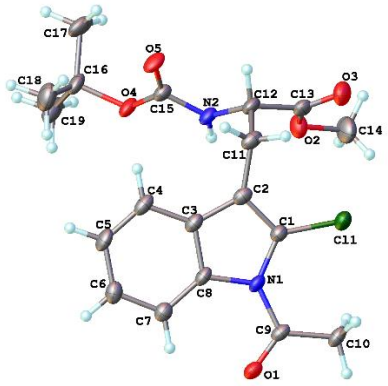

Figure 2.30: Molecular structure obtained for *N*-Acetyl-2-chlorotryptophan methyl ester (**177**). The molecule is in (*S*)-C12 configuration. Molecular structure reported with a 50% thermal ellipsoid probability.

Dichlorination was observed with 1,3,5-trimethoxybenzene (**151**) (**Table 2.8, Entry 6**) and 4-acetamidophenol (**180**) (**Table 2.8, Entry 7**). The reaction of 1,3,5-trimethoxybenzene (**151**) resulted in a fairly equal mix of the mono-chlorinated (**179**) and di-chlorinated derivative, which is likely due to its increased electron density and the equal viability of the three available substitution positions (2,4,6). However, an attempt to chlorinate 1,3-diethoxybenzene (**218**)

was unsuccessful. 4-Acetamidophenol (**180**) reacted to exclusively form the dichlorinated derivative (**181**), which has been noted in previous reports of electrochemical chlorination.[49]

Interestingly, when the 5-iodo derivative of 3-methylindole carboxylate (**188**) was reacted under the chlorination conditions, an oxindole (**189**) was formed instead (**Table 2.8, Entry 11**). Similar effects were also observed in **Chapter 4, Section 4.5**, when attempting to dimerise *N*-Phth-Trp-OMe (**162**) and 3-ethylindole carboxylate (**195**). The generation of an oxindole is feasible, as the chlorination conditions do not exclude water or air. However, this transformation demonstrates that the addition of a weakly electron-withdrawing iodo substituent distant from the C-2 position can have a great effect on the reactivity of the substrate.

Other interesting reactions observed during investigation of the substrate scope included the accidental cleavage of ethyl 3-(4-methoxyphenyl)-3-oxopropanoate (**190**) to produce 4-methoxybenzoic acid (**191**) (**Scheme 2.55**) (**Table 2.8, Entry 12**). Such a transformation has been observed before by Zeng *et al.* [63] during an attempted reaction of the same substrate which proceeded via a brominated intermediate. It is therefore likely that an α-chlorodicarbonyl derivative may have been formed, which has then reacted in a similar fashion.

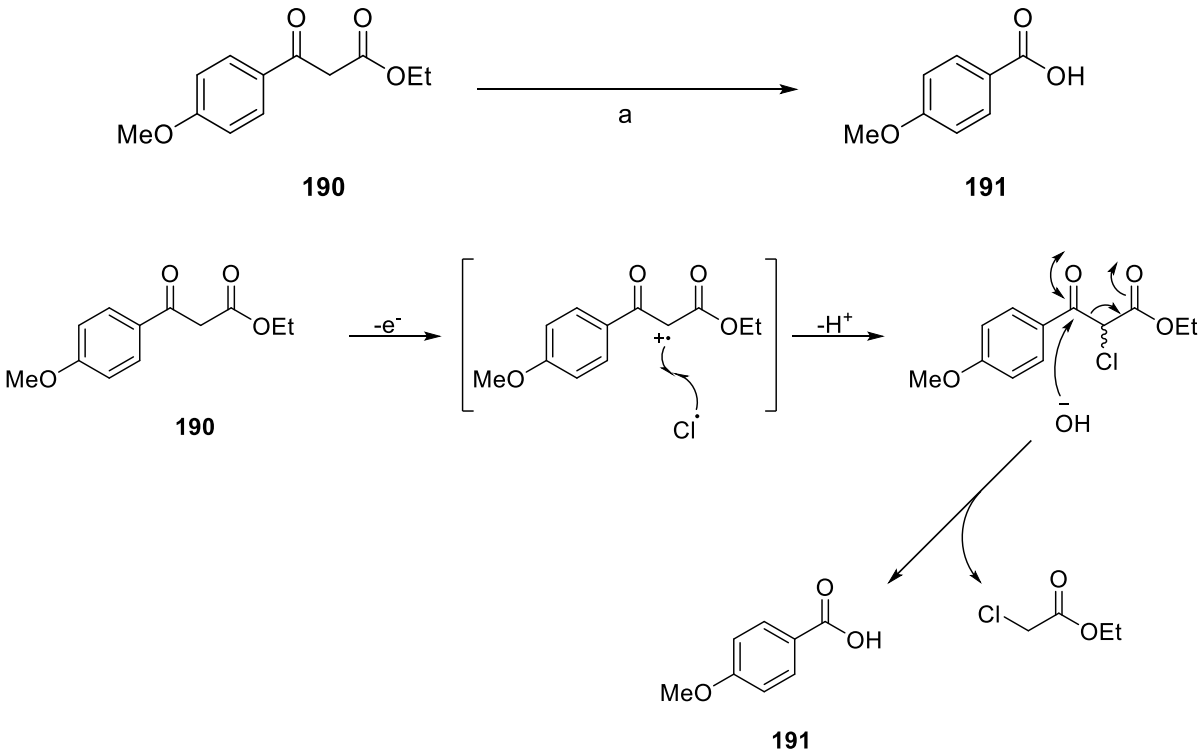

Scheme 2.55: Reaction of ethyl 3-(4-methoxyphenyl)-3-oxopropanoate (**190**) to form 4-methoxybenzoic acid (**191**); reagents and conditions: a) 0.3 mmol substrate, 10% v/v DCM/DMSO (4 mL), Bu_4NBF_4 (0.11 M), C (+) C (-), 5 mA, 6 F/mol, undivided cell, 41%. A mechanism for this

transformation is also proposed, illustrating how the product may be formed *via* an α-chlorodicarbonyl derivative.

Another unexpected result occurred during the reaction of 2-(4-bromophenyl)imidazo[1,2-a]pyridine (**184**) under the chlorination conditions (**Table 2.8, Entry 9**). Although the substrate appeared to have been chlorinated upon first inspection, the ^{1}H NMR and LCMS data did not quite match what was expected. The product was recrystallised, resulting in a mixture of two substances (**185**, **186**) (**Figure 2.31**). The C-Cl bond length was very long with unusually low thermal displacement parameters, so it was considered to be a Cl/Br mixed atom in 0.6/0.4 ratio.

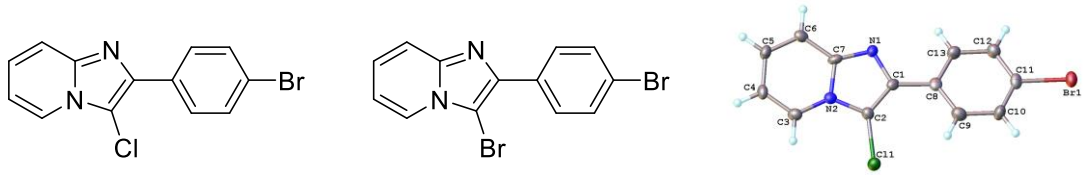

185 **186**

Figure 2.31: The product mixture (**185**, **186**) of the attempted chlorination of 2-(4-Bromophenyl)imidazo[1,2-a]pyridine (**184**), and the molecular structure obtained from recrystallisation of this mixture.

A reaction without DCM was performed to probe the unexpected bromine migration (**Scheme 2.56**). At first glance, the dibrominated product (**186**) appeared to have been formed as the major product. However, comparison of the ^{1}H NMR spectra of this product with literature data suggested that another product may be present (**Figure 2.32**). The second product was thought to be due to a mono-brominated product with the bromine at C-2 rather than at C-11 (**196**). This was confirmed by comparison of the ^{1}H NMR spectrum to literature data (**Figure 2.32**).[64]

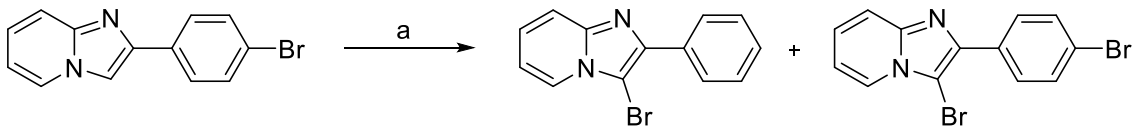

184 **196** **186**

Scheme 2.56: Reaction of 2-(4-Bromophenyl)imidazo[1,2-a]pyridine (**184**) under electrochemical conditions to produce mono-bromo **196** and di-bromo **186**; reagents and conditions: a) 0.3 mmol substrate, DMSO (4 mL), Bu_4NBF_4 (0.11 M), C (+) C (-), 5 mA, 6 F/mol, undivided cell.

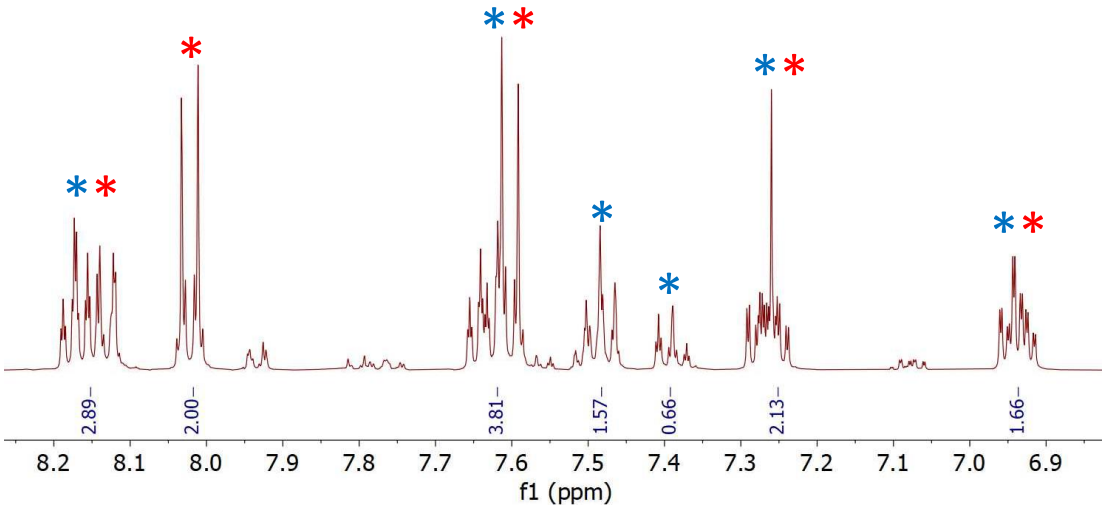

Figure 2.32: ^{1}H NMR spectrum of the brominated products from **Scheme 2.56**. The red (*) stars represents peaks caused by dibrominated **186** (structure displayed in red). The blue (*) stars represent peaks caused by mono-brominated **196** (structure displayed in blue). Peak assignment was determined by comparisons to literature data. The two products appear to be present in a 1:0.8 ratio (**186** : **196**).

The presence of both products indicate that bromine migration does indeed take place with this particular substrate under electrochemical conditions. Therefore, it is unlikely that the migration is a side effect of the chlorination. Given the lack of a bromine source present, it is likely that the additional bromine originates from the substrate itself. The identity of the dibrominated product **186** was confirmed when an X-Ray molecular structure was obtained (**Figure 2.33**).

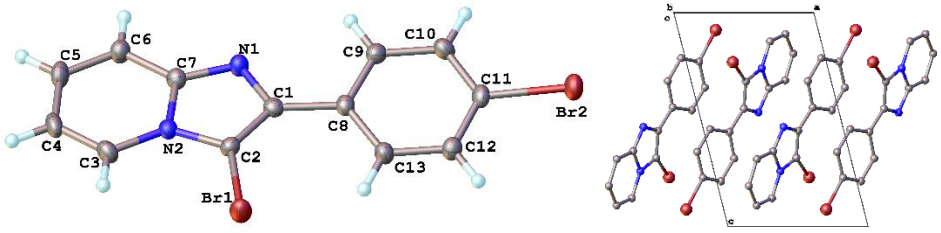

Figure 2.33: Molecular structure obtained after the reaction of 2-(4-Bromophenyl)imidazo[1,2-a]pyridine (**184**) with DCM excluded. Molecules in the crystal are arranged in anti-parallel stacks along the a-axis.

After the accidental synthesis of methyl-4-chloropyrrole carboxylate (**135**) from H-Hyp-OMe •HCl (**122**) described in **Section 2.3.3**, it was thought that pyrroles may be sufficiently electron

dense to undergo electrochemical chlorination with DCM. The reaction of methyl-2-pyrrole carboxylate (**136**) with DCM did indeed furnish a chloro-substituted product in a 45% yield. However, this product was determined to be the 3-chloro substituted derivative (**187**) after comparison with the 4-chloro pyrrole (**135**) and examination of its COSY spectrum.

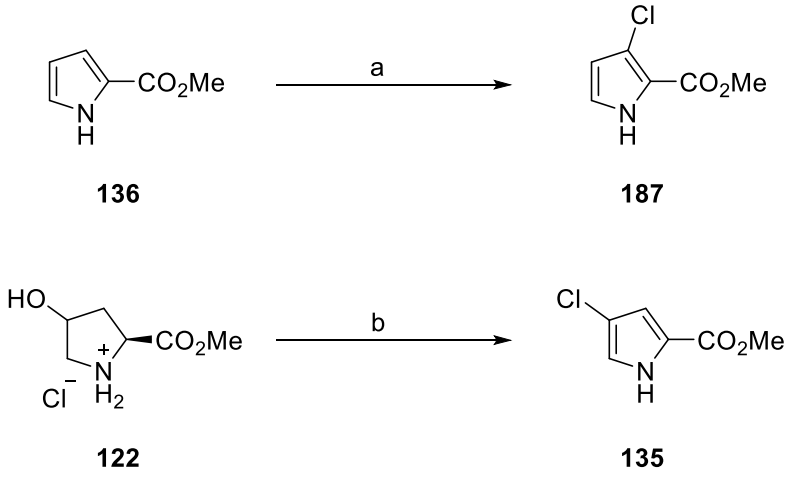

Scheme 2.57: A scheme displaying the electrochemical syntheses of chloropyrroles using two different methods; reagents and conditions: a) 10% v/v DCM/DMSO (4 mL), Bu_4NBF_4 (0.11 M), C (+) C (-), 5 mA, 6 F/mol, undivided cell, 45%; b) Selectfluor, K_2HPO_4, MeCN/H_2O (4:1), N_2, 5 mA, 2 F/mol, 57%.

The generation of different structural isomers using the two methods shown in **Scheme 2.57** could suggest that the two chlorination events proceed via different mechanisms, *i.e.*, in the case of the hydroxyproline substrate, a 4-chloroproline derivative could be formed prior to the subsequent oxidation to the pyrrole.

Ethyl pyrrole-2-carboxylate (**192**) was also subjected to electrochemical chlorination (**Table 2.8**, **Entry 13**). Whilst the 3-chloro-2-ethylpyrrole carboxylate product (**193**) was not isolated, a ^{1}H NMR spectrum of the crude reaction mixture revealed that conversion to the desired product had taken place (38% conversion by ^{1}H NMR).

When 3-methylpyrrole carboxylate (**194**) was reacted with DCM under the electrochemical conditions (**Table 2.8**, **Entry 14**), conversion to two chlorinated products was observed (**Scheme 2.58**). This was confirmed by LCMS analysis; the mass spectrum featured two peaks with the same mass ($[M+H]^+$, *m/z* = 160). These two products were isolated as a mixture. ^{1}H NMR analysis confirmed that one of the chlorinated products was the 2-chloro derivative (**197**), which has been made before.[65] The other compound is likely to be either the 4- or 5-chloro derivatives (**198, 199**). The 2-chloro derivative (**197**) and its structural isomer (**198** or **199**) were produced in a ratio of 43:57 (determined by ^{1}H NMR spectral analysis).

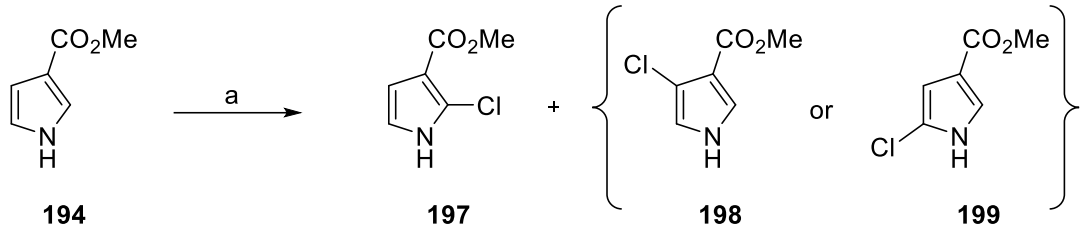

Scheme 2.58: Electrochemical chlorination of 3-methylpyrrole carboxylate (**194**) to form 2-chloro-3-methylpyrrole carboxylate (**197**) and a second chlorinated derivative (**198** or **199**); reagents and conditions: a) 10% v/v DCM/DMSO (4 mL), Bu_4NBF_4 (0.11 M), C (+) C (-), 5 mA, 6 F/mol, undivided cell.

An attempt to chlorinate *N*-Boc methyl pyrrole carboxylate (**200**) failed to deliver any chlorinated product (**Scheme 2.59**). This is likely due to the added Boc group tempering the electron density of the pyrrole ring and thus lowering its reactivity.

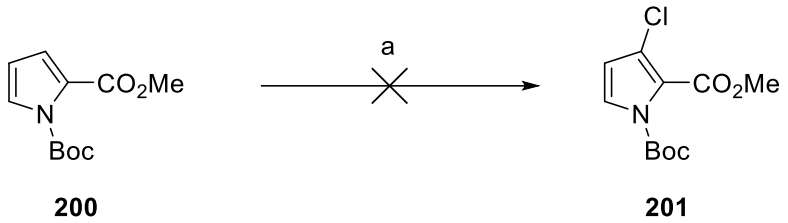

Scheme 2.59: Unsuccessful attempted chlorination of *N*-Boc-2-methylpyrrole carboxylate (**200**) to form the corresponding chloropyrrole (**201**); reagents and conditions: a) 10% v/v DCM/DMSO (4 mL), Bu_4NBF_4 (0.11 M), C (+) C (-), 5 mA, 6 F/mol, undivided cell.

To investigate whether the electrochemical chlorination could be applied to larger peptide-based natural products, the 2,5,-diketopiperazine brevianamide F (**206**) was synthesised using a literature procedure,[66] and subjected to electrochemical chlorination. The synthesis of **206** is shown in **Scheme 2.60**.

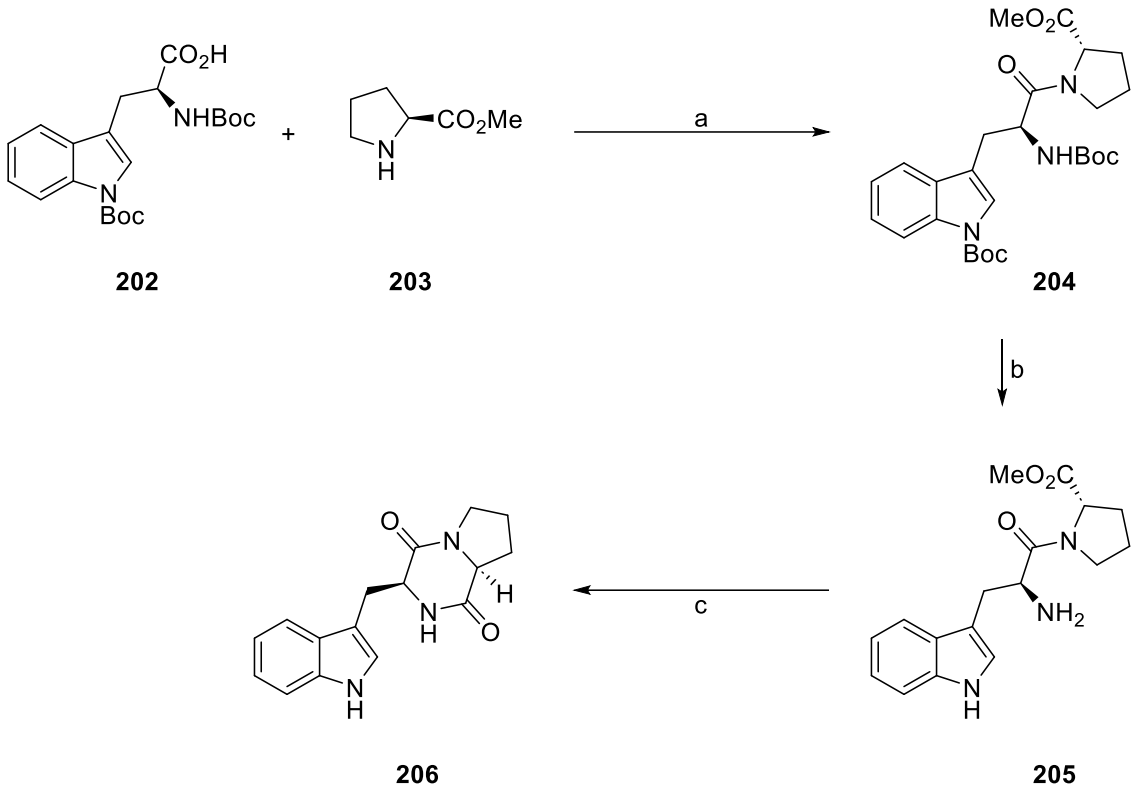

Scheme 2.60: Synthesis of the diketopiperazine (DKP) natural product brevianamide F (**206**); reagents and conditions: a) EDC•HCl, HOBt, Et_3N, DCM, 0 °C, then 20 h RT; b) TFA, DCM, 1 h; c) NH_4OH, MeOH, 0 °C, then 20 h RT, 28% (yield across 3 steps).

Brevianamide F (**206**) was then reacted under the standard electrochemical chlorination conditions (**Scheme 2.61**).

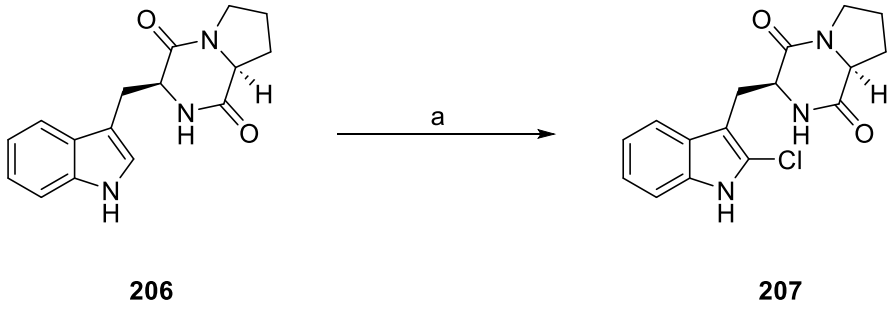

Scheme 2.61: Electrochemical chlorination of the DKP natural product brevianamide F (**206**) to produce the corresponding chlorinated derivative (**207**); reagents and conditions: a) 10% v/v DCM/DMSO (4 mL), Bu_4NBF_4 (0.11 M), C (+) C (-), 5 mA, 3 F/mol, undivided cell.

Analysis of the product mixture by LCMS revealed that the correct peak (*m/z* 318) was present in the spectrum, along with the starting material, and peaks corresponding to products with a higher mass (*m/z* 368). However, when purification of this compound using silica gel chromatography (0-10% MeOH in DCM) was attempted, the remaining electrolyte co-eluted

with the product due to the high polarity of the compound. An attempt to use filtration through a silica plug to remove the electrolyte largely failed. Purification of the crude mixture using preparative TLC was then undertaken, using a MeOH/toluene/DCM eluent (1:4:5).

Using preparative TLC, a fraction which was not the starting material was isolated. ^{1}H NMR spectroscopic analysis of this fraction suggested that the substance in this fraction was structurally similar to the brevianamide F starting material (**206**), but with one less peak in the aromatic region. A comparison of the ^{1}H NMR spectra of starting material (**206**) and product is displayed below in **Figure 2.34**.

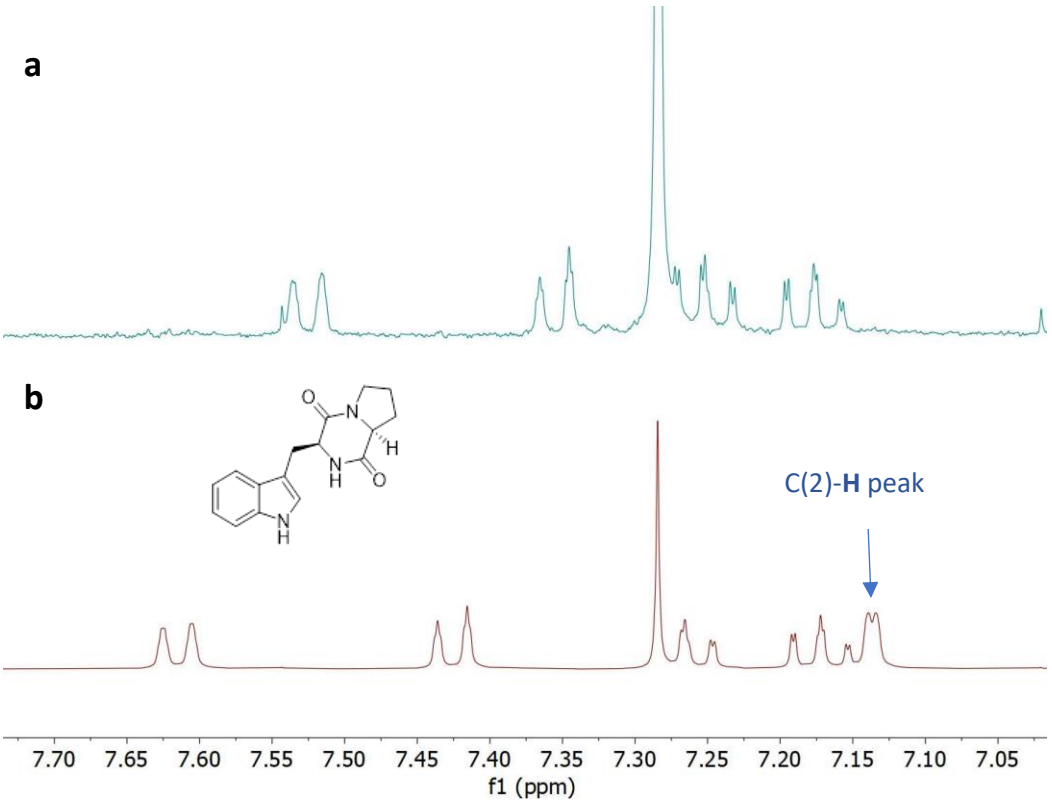

Figure 2.34: Comparison of the aromatic regions of the ^{1}H NMR spectra of brevianamide F (**206**) (b) and its chlorinated derivative (**207**) (a). The proton signal at δ = 7.14 ppm has vanished, indicating chlorination at C-2. ^{1}H NMR spectra recorded at 400 MHz in $CDCl_3$.

This implies that chlorination has taken place at the 2-position. This was confirmed by LCMS (*m/z* = 317.9). Unfortunately, the chlorinated brevianamide F derivative **207** could not be fully isolated, as there was still some electrolyte present (as determined by ^{1}H NMR spectroscopic analysis).

In order to probe the mechanism of the chlorination reaction, radical trapping experiments were carried out using the radical scavenger 2,6-di-*tert*-butyl-4-methylphenol (BHT) (**208**). Four equivalents of BHT were added to a chlorination reaction which used 3-methylindole

carboxylate (**169**) as the substrate. As a result, the yield of chlorinated product dropped significantly to 18%, indicating that the reaction proceeds *via* a radical mechanism. Additionally, a BHT-substrate adduct (**209**) was observed in the HRMS (**Figure 2.35**), which suggests that a carbon-centred radical is generated on the substrate prior to chlorination.

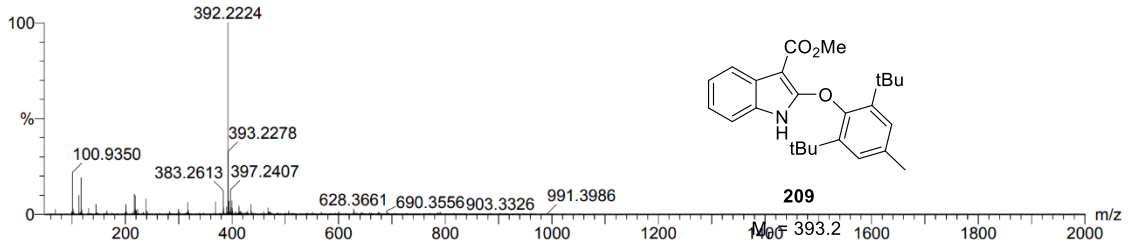

Figure 2.35: ESI-HRMS spectrum showing the $[M-H]^-$ BHT-substrate adduct ion (**209**), *m/z* = 392. The molecular structure and mass of the BHT-substrate adduct (**209**) are also displayed.

Despite the successful chlorination of the handful of molecules detailed in **Table 2.8**, many more substrates failed to undergo chlorination under these conditions. The structures of the substrates with which chlorination was unsuccessfully attempted are shown in **Figure 2.36**.

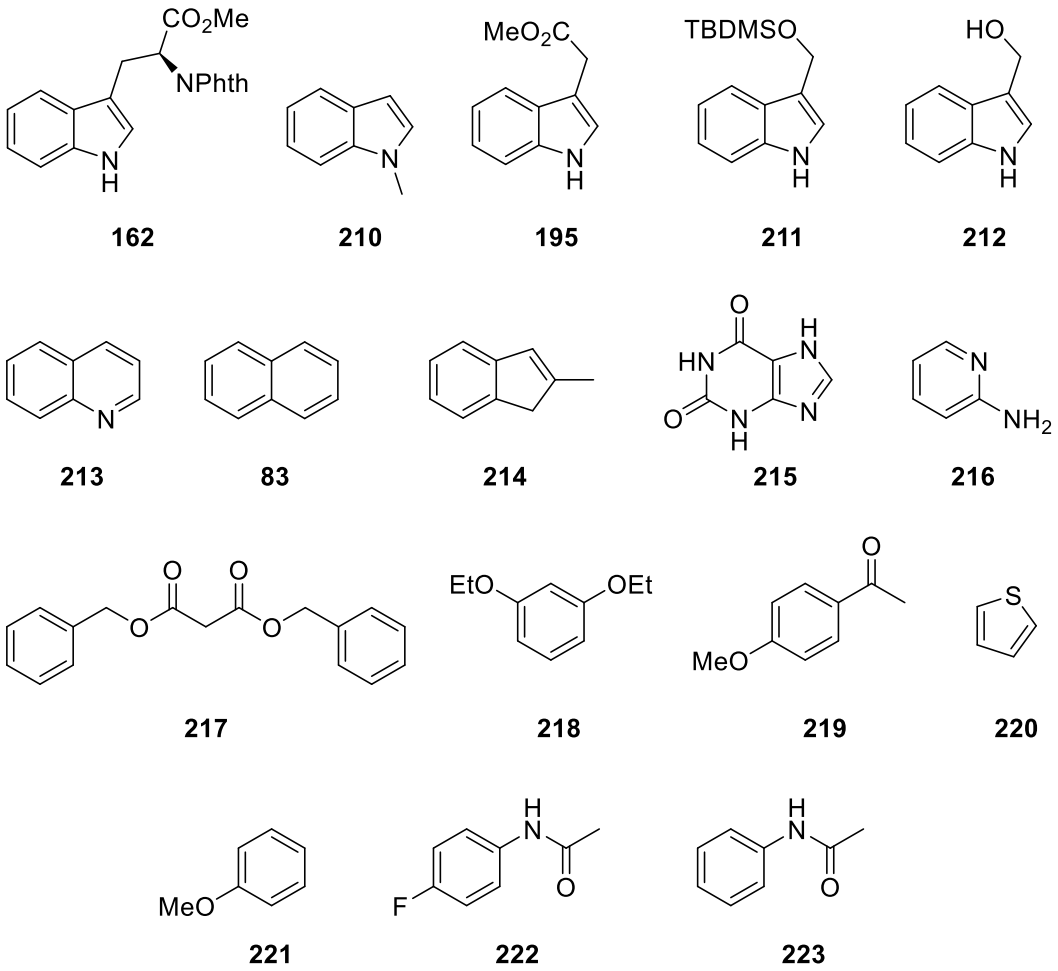

Figure 2.36: Molecules which failed to undergo electrochemical chlorination using DCM (conditions displayed in **Scheme 2.8**.

Some of the above substrates returned only starting material post-reaction, *e.g.*, **213**, **83**, and **218**. Other substrates failed to undergo chlorination due to degradation of the starting material or formation of multiple undesired products, *e.g.*, **210**, **216**, and **2.11**. Some of the substrates, *e.g.*, **215** and **223** produced traces of a chlorinated product (as determined by LCMS) but the product could not be isolated.

The likeliest explanation for the failure of the above substrates (**Figure 2.36**) is that they either do not have enough electron density to readily undergo oxidation at the anode, or are sterically hindered by bulky groups.

To summarise, a novel electrochemical technique for the chlorination of hetero/aromatics was developed, using DCM as the chlorinating reagent. **Scheme 2.62** displays a comparison of our method with traditional chlorination procedures alongside electrochemical chlorination procedures which have been previously published.

1. Classical approaches for chlorination of arenes and heteroaromatics:

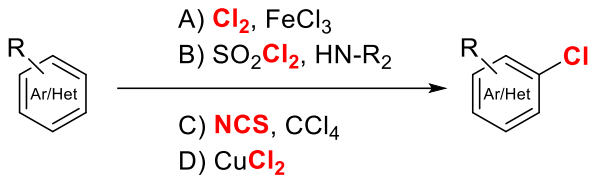

2. Previous electrochemical chlorination reactions:

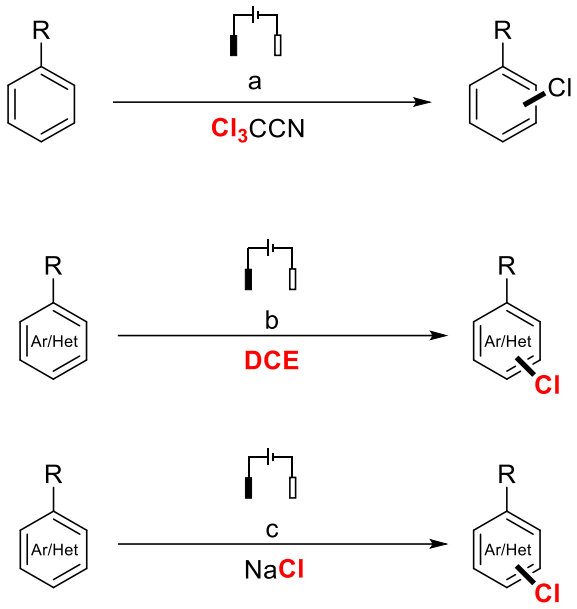

3. This work:

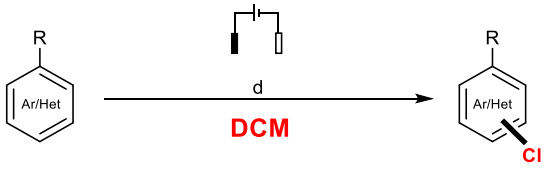

Scheme 2.62: Previous classical and electrochemical strategies for chlorination; a) Cl_3CCN, Et_4NCl, CH_3CN (5 mL), graphite felt as anode and cathode, undivided cell, 20 mA/cm^3, 2h, 23 °C;[67] b) n-Bu_4NOH (37% MeOH solution), graphite anode, Pt-plate cathode, 10 mA, DCE, 60-88 °C, undivided cell;[49] c) carbon rod anode, platinum plate cathode, 12 mA, 2.0 equiv. NaCl, 5% v/v H_2O in DMF, 80 °C, N_2, 5.2 F/mol;[45] d) Graphite electrodes, 10% v/v DCM in DMSO, 0.11M Bu_4NBF_4, 4 mL, 0.3 mmol substrate, 5 m/A, 6 F/mol.

2.6 Chapter summary

This chapter detailed attempts to introduce halogen substituents into amino acid substrates under electrochemical conditions. The first section of the chapter focussed on exploration of the electrochemical fluorination reaction published by the Baran group. Efforts to expand this reaction to other amino acids with a tertiary centre were largely unsuccessful. However,

following investigation of the compatibility of various amine protecting groups with the electrochemical fluorination reaction, it was found that the reaction was successful when using a simple Boc group (**Scheme 2.63**).

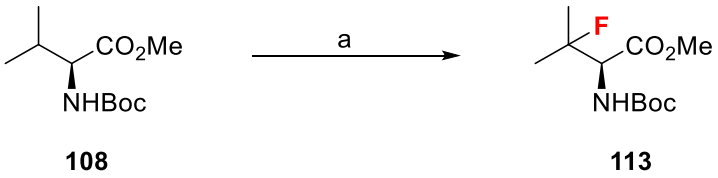

108 **113**

Scheme 2.63: Electrochemical fluorination of Boc-Val-OMe (**108**) to produce the corresponding fluorinated derivative **113**; reagents and conditions: (+) RVC (-) RVC, Selectfluor (3 equiv.), $NaNO_3$, anhydrous MeCN, 3 mA/cm^2, 3 F/mol, 34%.

Attempts to introduce fluorine into amino acid substrates *via* hemioxalate derivatives were unsuccessful. However, during the course of this investigation an unusual fluorination of pyrrole derivatives was observed, resulting in isolation of a number of fluorinated enones (**Scheme 2.64**).

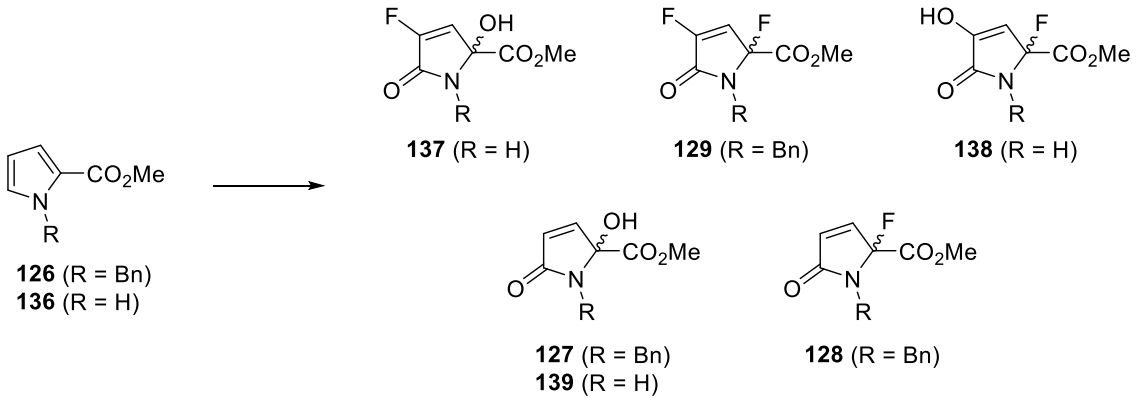

Scheme 2.64: Fluorination of proline-derived pyrroles (**126** and **136**) using Selectfluor, resulting in generation of several fluorinated enones (**128, 129, 137, 138**); Reagents and conditions: various, see **Section 2.3.3.**

Trifluoromethylation of amino acid substrates was also explored, resulting in isolation of a trifluoromethyl-substituted tryptophan derivative (**Scheme 2.65**).

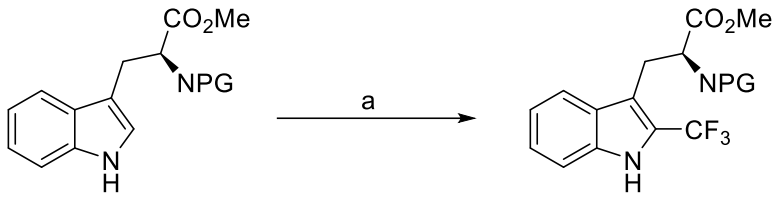

164 (PG = Boc)
162 (PG = Phth)

224 (PG = Boc)
163 (PG = Phth)

Scheme 2.65: Electrochemical trifluoromethylation of derivatives of *L*-tryptophan (**164, 162**) using sodium triflinate; reagents and conditions: a) sodium triflinate (1.7 equiv.), 0.2 M Bu_4NPF_6, DMSO, 5 mA, 3 F/mol, 35% **163**, 23% **224**.

In the final section of this chapter, a novel electrochemical method using dichloromethane as the chlorine source was developed and explored. This protocol was applied to a range of electron-rich aromatic molecules (**Scheme 2.66**). Tryptophan was among the substrates which were successfully chlorinated, providing access to a 2-chlorotryptophan (**175**) in a single step.

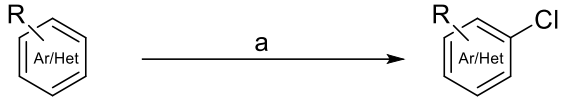

Scheme 2.66: Electrochemical chlorination of electron-rich substrates using DCM; reagents and conditions: a) 0.3 mmol substrate, 10% v/v DCM/DMSO (4 mL), Bu_4NBF_4 (0.11 M), C (+) C (-), 5 mA, 6 F/mol, undivided cell

2.7 References

1 G. W. Gribble, *Environ. Chem.*, 2015, 12, 396–405.
2 R. Wilcken, M. O. Zimmermann, A. Lange, A. C. Joerger and F. M. Boeckler, *J. Med. Chem.*, 2013, 56, 1363–1388.
3 P. Shah and A. D. Westwell, *J. Enzyme Inhib. Med. Chem.*, 2007, 22, 527–540.
4 J. Li, L. Zhou, Z. Han, L. Wu, J. Zhang, W. Zhu and Z. Xu, *J. Med. Chem.*, 2024, **67**, 4782–4792.
5 L. Lang, W. Li, H.-M. Jia, D.-C. Fang, S. Zhang, X. Sun, L. Zhu, Y. Ma, B. Shen, D. O. Kiesewetter, G. Niu and X. Chen, *Theranostics*, 2011, **1**, 341–353.
6 S. Dachwitz, D. H. Duwe, Y. H. Wang, H. Gruß, Y. Hannappel, T. Hellweg and N. Sewald, *Chem. Eur. J.*, 2020, **26**, 16357–16364.
7 G. Rossino, E. Marchese, G. Galli, F. Verde, M. Finizio, M. Serra, P. Linciano and S. Collina, *Molecules*, 2023, 28.
8 D. Pollok and S. R. Waldvogel, *Chem. Sci.*, 2020, 11, 12386–12400.
9 J. H. Simons, *J. Electrochem. Soc.*, 1949, **95**, 47.
10 M. Noel, V. Suryanarayanan and S. Chellammal, *J. Fluor. Chem.*, 1997, **83**, 31–40.
11 I. N. Rozhkov, *Russ. Chem. Rev.*, 1976, **45**, 615–629.

12 I. L. Knunyants, I. N. Rozhkov, A. V. Bukhtiarov, M. M. Gol'din and R. V. Kudryavtsev, *Bull. Acad. Sci. USSR Div. Chem. Sci.*, 1970, **19**, 1155–1155.
13 T. Brigaud and E. Laurent, *Tetrahedron Lett.*, 1990, **31**, 2287–2290.
14 A. Bensadat, G. Bodennec, E. Laurent and R. Tardivel, *Tetrahedron Lett.*, 1977, **18**, 3799–3802.
15 S. M. Lee, J. M. Roseman, C. Blair Zartman, E. P. Morrison, S. J. Harrison, C. A. Stankiewicz and W. J. Middleton, *J. Fluor. Chem.*, 1996, **77**, 65–70.
16 S.-Q. Chen, T. Hatakeyama, T. Fukuhara, S. Hara and N. Yoneda, *Electrochim. Acta*, 1997, **42**, 1951–1960.
17 K. Momota, K. Mukai, K. Kato and M. Morita, *Electrochim. Acta*, 1998, **43**, 2503–2514.
18 T. Fuchigami and T. Tajima, *J. Fluor. Chem.*, 2005, **126**, 181–187.
19 G. Laudadio, A. D. A. Bartolomeu, L. M. H. M. Verwijlen, Y. Cao, K. T. De Oliveira and T. Noël, *J. Am. Chem. Soc*, 2019, **141**, 11832–11836.
20 H. Hintz, J. Bower, J. Tang, M. LaLama, C. Sevov and S. Zhang, *Chem. Cat.*, 2023, **3**, 100491.
21 M. C. Leech, D. Nagornîi, J. M. Walsh, C. Kiaku, D. L. Poole, J. Mason, I. C. A. Goodall, P. Devo and K. Lam, *Org. Lett.*, 2023, **25**, 1353–1358.
22 E. Holt, M. Wang, S. A. Harry, C. He, Y. Wang, N. Henriquez, M. R. Xiang, A. Zhu, F. Ghorbani and T. Lectka, *J. Org. Chem.*, 2023, **88**, 2557–2560.
23 Y. Takahira, M. Chen, Y. Kawamata, P. Mykhailiuk, H. Nakamura, B. K. Peters, S. H. Reisberg, C. Li, L. Chen, T. Hoshikawa, T. Shibuguchi and P. S. Baran, *Synlett*, 2019, **30**, 1178–1182.
24 Z. Chen, Q. Cai, Y. T. Boni, W. Liu, J. Fu and H. M. L. Davies, *Org. Lett.*, 2023, **25**, 3995–3999.
25 P. T. Nyffeler, S. G. Durón, M. D. Burkart, S. P. Vincent and C. H. Wong, *Angew. Chem. Int. Ed.*, 2004, **44**, 192–212.
26 S. B. Munoz, H. Dang, X. Ispizua-Rodriguez, T. Mathew and G. K. S. Prakash, *Org. Lett.*, 2019, **21**, 1659–1663.
27 M. González-Esguevillas, J. Miró, J. L. Jeffrey and D. W. C. MacMillan, *Tetrahedron*, 2019, **75**, 4222–4227.
28 S. Liu and C. C. Tzschucke, *Eur. J. Org. Chem.*, 2016, **2016**, 3509–3513.
29 B. M. Kim, Q. Z. San, L. R. Bhatt, S. K. Kim and K. Y. Chai, *Bull. Korean Chem. Soc.*, 2010, **31**, 31–34.
30 É. Vincent and J. Brioche, *Eur. J. Org. Chem.*, 2021, **2021**, 2421–2430.
31 J. Y. Su, D. C. Grünenfelder, K. Takeuchi and S. E. Reisman, *Org. Lett.*, 2018, **20**, 4912–4916.
32 W. D. G. Brittain and S. L. Cobb, *Org. Biomol. Chem.*, 2019, **17**, 2110–2115.
33 C. Kiaku, D. Martinage, Y. Sicim, M. C. Leech, J. M. Walsh, D. L. Poole, J. Mason, I. C. A. Goodall, P. Devo and K. Lam, *Org. Lett.*, 2024, **26**, 2697–2701.
34 M. Inoue, Y. Sumii and N. Shibata, *ACS Omega*, 2020, **5**, 10633–10640.
35 Y. Deng, F. Lu, S. You, T. Xia, Y. Zheng, C. Lu, G. Yang, Z. Chen, M. Gao and A. Lei, *Chin. J. Chem.*, 2019, **37**, 817–820.
36 K. Y. Ye, G. Pombar, N. Fu, G. S. Sauer, I. Keresztes and S. Lin, *J. Am. Chem. Soc*, 2018, **140**, 2438–2441.
37 Z. Ruan, Z. Huang, Z. Xu, G. Mo, X. Tian, X. Y. Yu and L. Ackermann, *Org. Lett.*, 2019, **21**, 1237–1240.
38 Y. Ding, H. Zhang, D. Lou, W. Huang, Y. Shi, H. Luo, C. Zhang and Y. Xie, *Org. Chem. Front.*, 2024, **11**, 1662–1667.
39 Z. Zhang, L. Zhang, Y. Cao, F. Li, G. Bai, G. Liu, Y. Yang and F. Mo, *Org. Lett.*, 2019, **21**, 762–766.
40 H. Jia, A. P. Häring, F. Berger, L. Zhang and T. Ritter, *J. Am. Chem. Soc*, 2021, **143**, 7623–7628.

41 C. Xu, Y. Liu, H. Liu, J. Ma, X. He, H. Wu, Y. Li, Z. Sun and W. Chu, *Tetrahedron Lett.*, 2020, **61**, 152226.
42 Z. Y. Mo, X. Y. Wang, Y. Z. Zhang, L. Yang, H. T. Tang and Y. M. Pan, *Org. Biomol. Chem.*, 2020, **18**, 3832–3837.
43 K.-Q. Ling, T. Ren, J. D. Protasiewicz and L. M. Sayre, *Tetrahedron Lett.*, 2002, **43**, 6903–6905.
44 M. R. Scheide, C. R. Nicoleti, G. M. Martins and A. L. Braga, *Org. Biomol. Chem.*, 2021, 19, 2578–2602.
45 F. Kakiuchi, T. Kochi, H. Mutsutani, N. Kobayashi, S. Urano, M. Sato, S. Nishiyama and T. Tanabe, *J. Am. Chem. Soc*, 2009, **131**, 11310–11311.
46 Y. Yuan, A. Yao, Y. Zheng, M. Gao, Z. Zhou, J. Qiao, J. Hu, B. Ye, J. Zhao, H. Wen and A. Lei, *iScience*, 2019, **12**, 293–303.
47 B. Chen, Y. Yang, Y. Yang, S. Liu, Q. Chen, X. Zeng and B. Xu, *ChemElectroChem*, 2019, **6**, 3726–3730.
48 J. Harnedy, M. D. Hareram, G. J. Tizzard, S. J. Coles and L. C. Morrill, *Chem. Commun*, 2021, **57**, 12643.
49 Y. Liang, F. Lin, Y. Adeli, R. Jin and N. Jiao, *Angew. Chem.*, 2019, **131**, 4614–4618.
50 X. Dong, J. L. Roeckl, S. R. Waldvogel and B. Morandi, *Science*, 2021, **371**, 507–514.
51 Z. Zhou, Y. Yuan, Y. Cao, J. Qiao, A. Yao, J. Zhao, W. Zuo, W. Chen and A. Lei, *Chin. J. Chem.*, 2019, **37**, 611–615.
52 X. Lin, C. Zeng, C. Liu, Z. Fang and K. Guo, *Org. Biomol. Chem.*, 2021, **19**, 1352–1357.
53 X. Meng, Y. Zhang, J. Luo, F. Wang, X. Cao and S. Huang, *Org. Lett.*, 2020, **22**, 1169–1174.
54 Y. Z. Ji, H. J. Li, Y. R. Wang, Z. Y. Zhang and Y. C. Wu, *Adv. Synth. Catal.*, 2020, **362**, 1039–1045.
55 S. Song, X. Li, J. Wei, W. Wang, Y. Zhang, L. Ai, Y. Zhu, X. Shi, X. Zhang and N. Jiao, *Nat. Catal.*, 2020, **3**, 107–115.
56 Z. W. Qu, H. Zhu and S. Grimme, *ChemCatChem*, 2021, **13**, 207–211.
57 D. M. Heard and A. J. J. Lennox, *Angew. Chem. Int. Ed.*, 2020, **59**, 18866–18884.
58 M. Liu, Z. X. Luo, T. Li, D. C. Xiong and X. S. Ye, *J. Org. Chem.*, 2021, **86**, 16187–16194.
59 D. Becker and U. Kazmaier, *Eur. J. Org. Chem.*, 2015, **2015**, 2591–2602.
60 H. Gruß and N. Sewald, *Chem. Eur. J.*, 2020, 26, 5328–5340.
61 F. Y. Miyake, K. Yakushijin and D. A. Horne, *Angew. Chem. Int. Ed.*, 2004, **43**, 5357–5360.
62 R. P. Loach, O. S. Fenton and M. Movassaghi, *J. Am. Chem. Soc*, 2016, **138**, 1057–1064.
63 L. S. Kang, M. H. Luo, C. M. Lam, L. M. Hu, R. D. Little and C. C. Zeng, *Green Chem.*, 2016, **18**, 3767–3774.
64 P. P. Sen, V. J. Roy, S. R. Roy, *J. Org. Chem.*, 2022, **87**, 9551–9564
65 L. G. Zepeda, M. Rojas-Gardida, M. S. Morales-Rios and P. Joseph-Nathan, *Tetrahedron*, 1989, **45**, 6439–6448.
66 H. Song, J. Song, L. Yan, W. He, P. Wang, Y. Xu, H. Wei and W. Xie, *Tetrahedron Lett.*, 2021, **85**, 153486.
67 F. Liu, N. Wu, and X. Cheng, *Org. Lett.*, 2021, **23**, 3015−3020.

Chapter 3: Transition metal-catalysed electrochemical modification of amino acids

3.1 Overview

3.1.1 Traditional methods for amino acid modification *via* transition metal catalysis

The field of synthetic organic chemistry has relied on transition metal (TM) catalysis for many years due to the elevated efficiency and efficacy of such processes. TM catalysts are capable of existing in multiple oxidation states, which facilitates the generation of high-energy intermediates and novel products. Many groups have successfully applied TM-catalysed procedures towards the synthesis of novel amino acids.[1,2] An example of this is displayed in **Scheme 3.1**. Song *et al.* used a rhodium catalyst to effect C-H activation and annulation of lysine-derived substrates, affording a range of amino acids containing a tricyclic fluorophore moiety.[3]

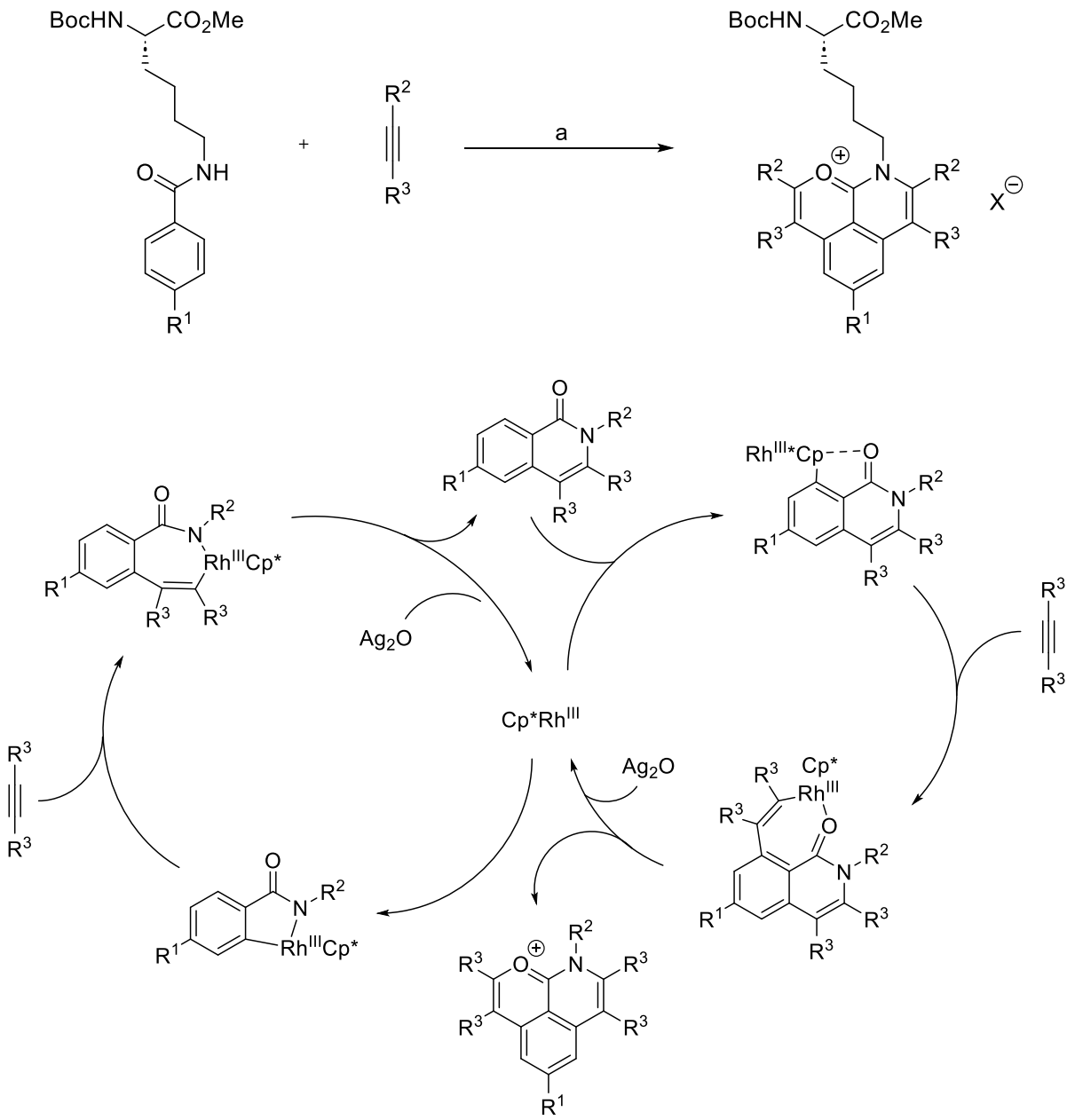

Scheme 3.1: Rhodium-catalysed double C-H activation/annulation of lysine-derived substrates to generate fluorescent unnatural amino acids. This reaction was extended to include late-stage modification of peptides containing a lysine-derived residue;[3] reagents and conditions: a)$[RhCl_2Cp^*]_2$ (5 mol %), $AgSbF_6$ (20 mol %), Ag_2O (2.0 equiv.), $NaSbF_6$ (1.5 equiv.), DCE, 120 °C, 24 h, 41-97%. The mechanism for this reaction proposed by Song *et al.* is also displayed.

The C-H activation procedure developed by Song *et al.*[3] was also successfully applied to peptides, highlighting how the use of a TM catalyst can ensure a high specificity when used in the context of late-stage functionalization.

In particular, TM catalysts are useful for modification of sp^3 carbons and C(sp^3)-H activation due to their ability to form a metallacycle, often aided by directing groups or the use of specific ligands. An example of TM-catalysed modification of sp^3 centres within the context of amino acids was published by Zhu and coworkers (**Scheme 3.2**).[4]

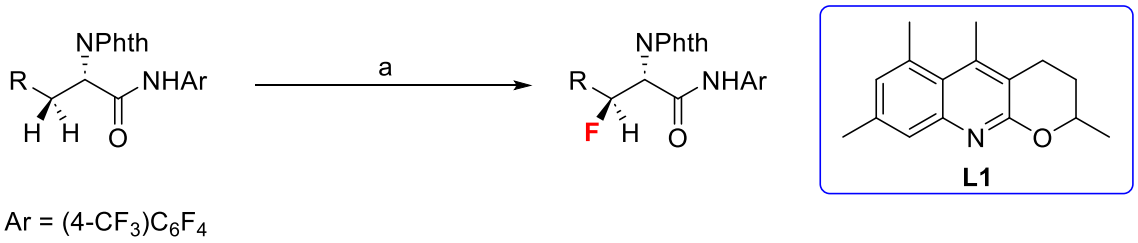

Scheme 3.2: Pd-catalysed stereoselective β-fluorination of sp^3 carbons in various amino acids, assisted by a quinoline-derived ligand (**L1**);[4] reagents and conditions: a) Selectfluor, $Pd(TFA)_2$ (10 mol%), **L1** (10 mol%), Ag_2CO_3, 1,4- dioxane, 115 °C, air, 15 h, 25-79%.

In this study a palladium catalyst was used in conjunction with Selectfluor to fluorinate the β-position on a number of phthalimide-protected amino acids. The selectivity of this reaction was attributed to the favourable formation of a five-membered palladacycle through coordination of the Pd centre to the amide nitrogen, and to the use of a quinoline-based ligand (**L1**).

Another benefit to using TM catalysis for amino acid modification is that it integrates well with other mild synthetic techniques such as photochemistry and electrochemistry. For example, Ashley *et al.* demonstrate how an iridium photocatalyst can be used to facilitate alkylation of a triflyl-protected lysine derivative under photochemical conditions (**Scheme 3.3**).[5]

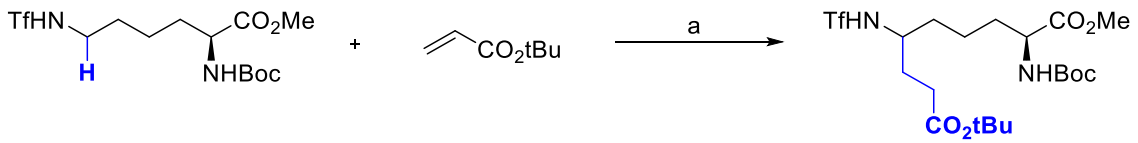

225 **226** **227**

Scheme 3.3: Photochemical sp^3 alkylation of triflimide-protected lysine (**225**) using an iridium photocatalyst;[5] reagents and conditions: a) quinuclidine, $[Ir(dF\text{-}CF_3\text{-}ppy)_2(dtbbpy)PF_6]$ (2 mol%), DMF, 34 W blue LED, 40 °C, 16 h, 58%.

The merging of photochemistry and TM catalysis enables the alkylation reaction to occur under very mild conditions, which is well-suited to amino acid and peptide substrates.

3.1.2 Previous methods for transition metal-catalysed electrosynthesis

While TM catalysis is ubiquitous in organic synthesis, there are several drawbacks. Stoichiometric amounts of toxic redox reagents are often required, which can cause

the generation of unwanted byproducts and lower the overall atom economy of the reaction process. The formation of byproducts and used-up redox reagents can then cause issues with purification. Additionally, such reactions can have a limited catalyst turnover and often necessitate harsh conditions.

The fusion of TM-catalysis with electro-organic synthesis has emerged as a popular alternative to traditional TM-catalysed reactions in recent years, and as such has been the subject of several excellent reviews.[6–10] The underlying principle of electrochemically-assisted TM-catalysed reactions is that instead of using stoichiometric amounts of an external oxidant or reductant, the electrical current provides the impetus for redox events (**Scheme 3.4**).

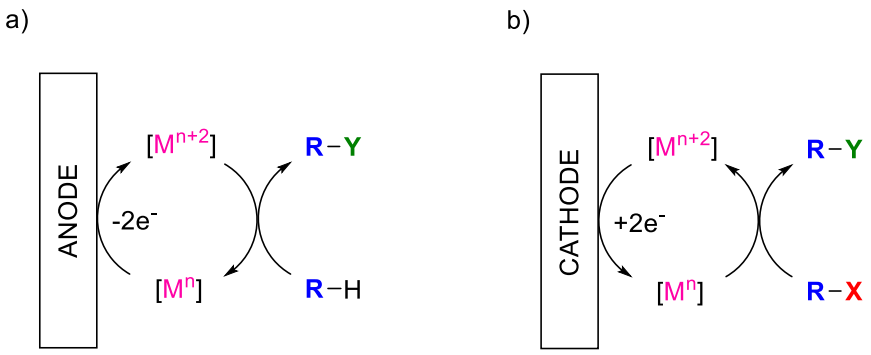

Scheme 3.4: Two possible routes for transition metal catalysed electrochemical reactions. Route a) anodic oxidation; route b) cathodic reduction

In this sense, the TM catalyst is essentially acting as a redox mediator. TM catalysts are appealing choices for redox mediators as their reactivity has been well-studied, and appropriate ligand selection can modulate their redox potential.

There are many mutual benefits to the union of electrosynthesis and TM-catalysis. When a reaction is under electrochemical control, it is possible to ‘dial in’ the exact redox potential necessary for oxidation or reduction. Therefore, very mild conditions are sufficient for catalyst activation. The lack of external redox reagents improves the atom economy and efficiency of the reaction whilst reducing byproduct generation. Additionally, the use of TM catalysts permits electrochemical reactions to be run at a lower potential, and thus limits any unwanted side reactions associated with high redox potentials.

3.2 Chapter Aims

The integration of transition metal catalysis with electro-organic synthesis is mutually beneficial. Using an electric current as a driving force permits TM-catalysed reactions to be run at lower temperatures, and provides a 'greener' alternative to toxic redox reagents.

Whilst the field of TM-catalysed electrosynthesis has proliferated in recent years, examples of applications involving amino acid substrates remain scarce. Therefore, the overall aim of this chapter was to find ways of modifying amino acids using TM-catalysed electrosynthesis. Of particular interest was the prospect of using TM-catalysed electrochemistry to modify sp^3 carbons.

The primary aims of this chapter are as follows:

- Explore methods of coupling aryl halides with activated amino acid substrates (*e.g.*, serine, threonine, and proline) using electrochemical Ni catalysis.
- Investigate Ni-catalysed electrochemical *S*-arylation reactions of cysteine-derived substrates.
- Explore Pd-catalysed electrochemical acetoxylation using valine and leucine derived substrates.

3.3 Nickel-catalysed electrochemical arylation of amino acids

3.3.1 Previous methods for Ni-catalysis of electrochemical reactions

Nickel catalysts have been widely used in organic synthesis for a range of transformations. Nickel is fairly inexpensive when compared to popular alternatives such as palladium. It is also capable of existing in multiple stable oxidation states, and in both high-spin and low-spin configurations. Nickel forms the weakest metal-carbon bonds compared to the other group 10 metals (Pt, Pd), meaning that organonickel species are highly reactive.[11] Nickel catalysts are therefore highly useful, particularly in radical processes.

The ultimate aim of many TM-catalysed coupling reactions is to form C-C bonds. Ni catalysts have been used to cross-couple electrophiles with carbon nucleophiles, *e.g.* in Negishi reactions (**Scheme 3.5**).[12]

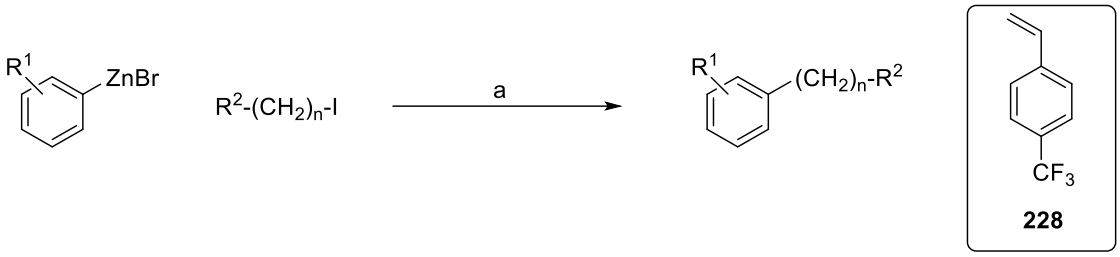

Scheme 3.5: Negishi-type coupling of arylzinc bromide with primary alkyl iodides, catalysed by $Ni(acac)_2$ in the presence of CF_3-styrene (**228**);[13] reagents and conditions: a) $Ni(acac)_2$ (10 mol%), THF-NMP (2:1), 4-(trifluoromethyl)styrene (**228**), 2-5 h, -15 °C, 71-80%.

However, the necessity of pre-forming organometallic reagents can limit the utility of such a reaction. Reductive cross-coupling can be a good alternative, in which two electrophiles are coupled using a nickel catalyst under reductive conditions. There are a number of methods that can be used to create reductive conditions, one of which can be an electrical current (**Scheme 3.6**).

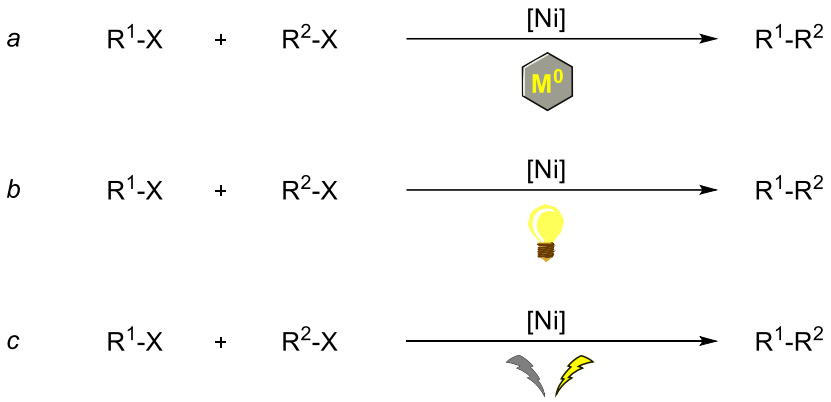

Scheme 3.6: Different ways in which Ni-catalysed reductive cross-coupling can be accomplished; a) Use of metal powders such as Zn or Mn as the reductant; b) Use of photochemistry in conjunction with nickel catalysis; c) Ni-catalysed cathodic reduction to achieve cross-coupling of electrophiles.

Since 2000, a number of groups have sought to merge electrosynthesis with nickel catalysis. An example from the Condon group is shown below, in which aryl bromides were reacted with activated olefins to generate the corresponding 1,4-addition products (**Scheme 3.7**).[14] In this reaction, the Ni^{II} catalyst undergoes cathodic reduction to generate an active Ni^0 species. The Ni^0 species then inserts into the aryl bromide substrate *via* oxidative addition. The resulting organonickel intermediate is then able to participate in conjugate addition with the activated olefin.

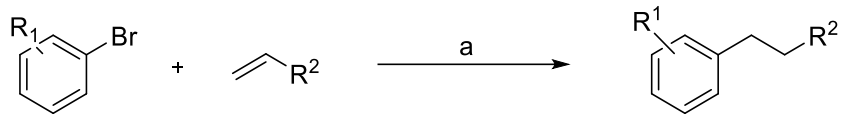

Scheme 3.7: Electroreductive Ni-catalysed conjugate addition of aryl bromides to activated olefins to form 1,4-addition products, Condon *et al.*;[14] reagents and conditions: a) $NiBr_2 \cdot 3H_2O$ (10 mol%), DMF/pyridine (9:1), 70 °C, 0.3 A/dm^2

Another example of how cathodic reduction and Ni-catalysis can be combined is shown in **Scheme 3.8**. This reaction involves generation of Ni^I as the reactive species instead of Ni^0. Lian *et al.* achieved reductive decarboxylative coupling of *N*-hydroxypthalimide esters with quinoxalinones (*e.g.*, **229**), resulting in the generation of a range of novel 3-alkylated quinoxalinone compounds.[15]

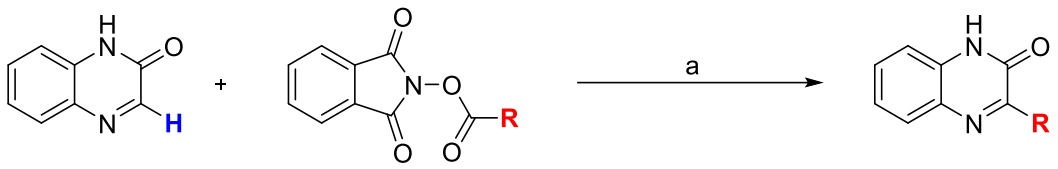

229

Scheme 3.8: Ni-catalysed decarboxylative coupling of *N*-hydroxyphthalimide esters with quinoxalinone (**229**) under electrochemical conditions;[15] reagents and conditions: a) $LiClO_4$, $NiCl_2.6H_2O$ (20 mol%), dtbbpy (20 mol%), Et_3N, anhydrous DMA (4 mL), graphite felt (+), Ni foam (-), undivided cell, 8 mA, 60 °C, 3 h, Ar, 35-91%.

The authors propose that the initial step in this transformation is the reduction of Ni^{II} to Ni^I at the cathode. The active Ni^I species then participates in single electron transfer (SET) with the *N*-hydroxyphthalimide ester, generating an alkyl radical. This alkyl radical may then add to the quinoxaline substrate (**229**), forming the desired product.

3.3.2 Electrochemical Ni-catalysis to form C-C bonds in the synthesis of novel amino acids

Relatively few groups have used electrochemical Ni-catalysis to target amino acid modification. It is often difficult to successfully apply general synthetic procedures to amino acids without a diminished yield due to the presence of both the amine and acid functionalities, which typically must be protected. An example of a protocol that has been successfully applied to a protected phenylalanine derivative (**230**) is shown in **Scheme 3.9**. Luo *et al.* used

electrochemical Ni-catalysis to couple aryl or alkenyl halides with benzyl trifluoroborates (**231**).[16] One such reaction resulted in the formation of the phenylalanine derivative **232**.

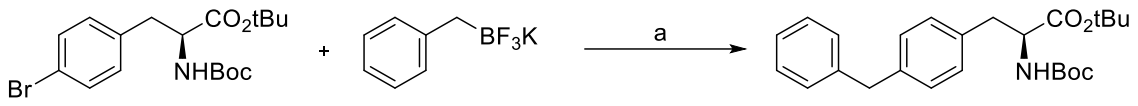

230 **231** **232**

Scheme 3.9: Electrochemical Ni-catalysed coupling of a 4-(bromo)phenylalanine derivative (**230**) with benzyl trifluoroborate (**231**) to afford unnatural amino acid **232**;[16] reagents and conditions: a) $NiCl_2$·glyme (10 mol%), dtbbpy ligand (15 mol%), K_2CO_3, $LiClO_4$ (0.2 M), DMF (5 mL), RVC electrode, 3 mA, Ar, rt, 20–36 h, 83%.

In this work the authors suggest that the Ni^{II} is initially reduced to Ni^{I} at the cathode, followed by insertion into the organic halide. At the same time, the trifluoroborate (**231**) is oxidised at the anode, generating a carbon-centred radical and BF_3. The radical is captured by the nickel species, and subsequent reductive elimination forms the desired product (**232**).

In a similar fashion, the Zhang group have also used phenylalanine-derived substrates to synthesise a novel amino acid.[17] Zhang *et al.* successfully applied their procedure for coupling α-chloroamides with alkenyl triflates to a phenylalanine-derived chloroamide (**233**) (**Scheme 3.10**).

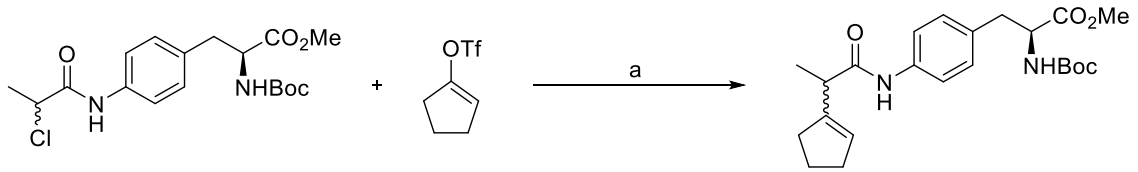

233 **234** **235**

Scheme 3.10: Electrochemical Ni-catalysed coupling of an α-chloroamide phenylalanine derivative (**233**) and alkenyl triflate **234** to produce novel amino acid derivative **235**;[17] reagents and conditions: a) $NiBr_2$·dme (10 mol%), bpy (15 mol%), NaI (0.04 M), DMF (3 mL), Fe (+), Ni foam (-), 10 mA, rt, 2.5 h, 88%.

This reaction proceeds *via* initial reduction of Ni^{II} to Ni^{I}, which can then undergo oxidative addition with the alkenyl triflate (**234**). Generation of an alkyl radical from the α-chloroamide (**233**) and subsequent reductive elimination affords the desired product (**235**).

Very recently, Baran and coworkers have published an electrochemical Ni-catalysed protocol for the synthesis of unnatural amino acids (**Scheme 3.11**).[18] This procedure utilises *N*-

hydroxyphthalimide esters derived from glutamic or aspartic acid as one of the electrophilic coupling partners. Aryl halides are used as the other electrophilic coupling partner, resulting in the synthesis of a range of phenylalanine- and homophenylalanine-derived novel amino acids. Whilst the yields obtained from these reactions were fairly poor, the paper illustrates how their one-step procedure vastly improves on existing multi-step synthetic routes. It also showcases how electrochemical Ni catalysis can be used to quickly generate a diverse library of unnatural amino acids from accessible starting materials.

Scheme 3.11: Electrochemical Ni-catalysed synthesis of unnatural amino acids using *N*-hydroxyphthalimide esters derived from glutamate or aspartate precursors;[18] reagents and conditions: a) $NiCl_2 \cdot 6H_2O$ (30 mol%), bpy (30 mol%), $AgNO_3$ (0.75 equiv.), NMP, rt, 12 mA, 5-7 F/mol, Mg (+) RVC (-), <10-61%.

3.3.3 Results and discussion

In 2021, the Li group published an excellent paper describing the electrochemical dehydroxylative coupling of alcohols and aryl halides (**Scheme 3.12**).[19] It was thought that this reaction could potentially be performed with amino acid substrates, *e.g.*, Thr, Ser, Hyp, Hse.

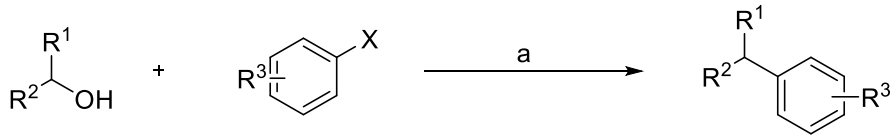

Scheme 3.12: Electrochemical Ni-catalysed dehydroxylative cross coupling of alcohols and aryl halides to create $C(sp^3)$-$C(sp^2)$ bonds;[19] reagents and conditions: a) $NiBr_2$ (10 mol%), dtbbpy (20 mol%), PPh_3 (3 or 7 equiv.), DIPEA (1.2 equiv.), LiBr (1 equiv.), NMP, 4 mA, C (+) Ni (-), 14 h, rt, 40-95%.

This reaction works by initial cathodic reduction of the Ni^{II} compound to an active Ni^0 species. This can then react with the aryl halide *via* oxidative addition to form an organonickel complex. At the same time, the alcohol substrate is converted to an alkyl bromide using an Appel-type reaction with PPh_3 and LiBr. Loss of the bromine atom from the alkyl bromide generates an alkyl radical, which can react with the organonickel complex; subsequent reductive elimination furnishes the desired cross-coupled product (**Scheme 3.13**).

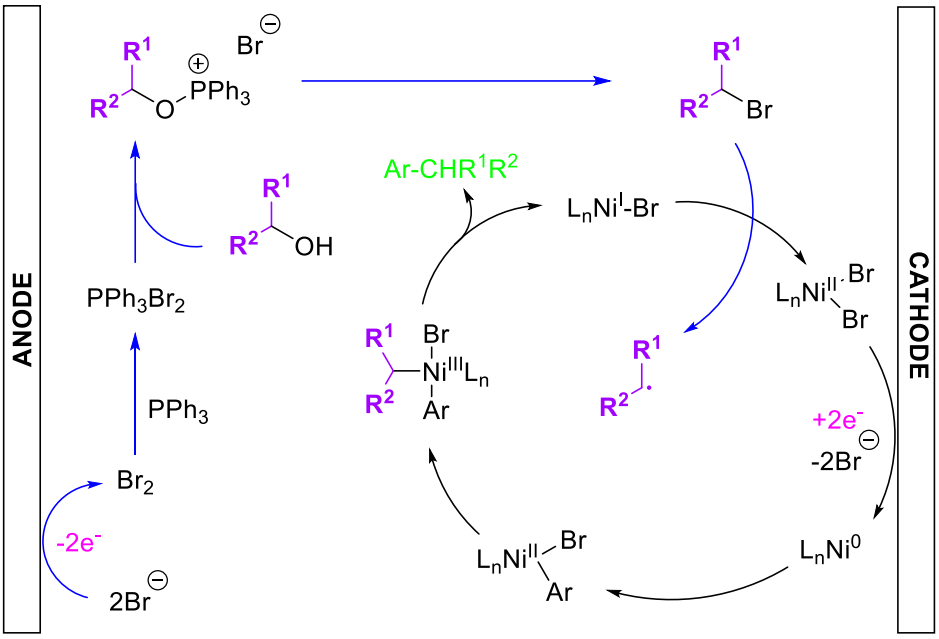

Scheme 3.13: Mechanistic scheme proposed by Li *et al.* for the electrochemical Ni-catalysed coupling of alcohols and aryl halides.[19]

To assess whether the reaction displayed in **Scheme 3.12** could be applied to amino acids with a hydroxyl moiety, trial reactions with threonine (**236**), homoserine (**239**), and 4-hydroxyproline derivatives (**117**) were performed (**Scheme 3.14**).

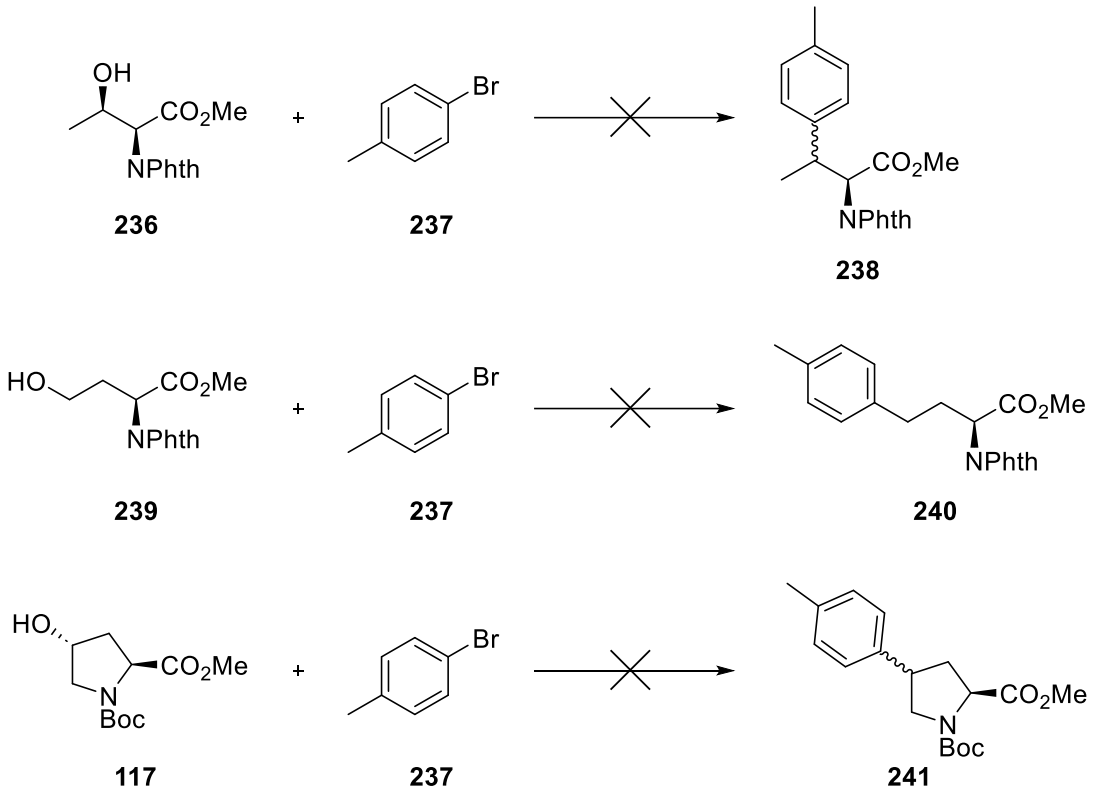

Scheme 3.14: Attempted reactions of hydroxyl-containing amino acids (**236, 239, 117**) with 4-bromotoluene (**237**) using an electrochemical method developed by Li *et al.*;[19] reagents and conditions: a) $NiBr_2$ (10 mol%), dtbbpy (20 mol%), PPh_3 (3 equiv.), DIPEA (1.2 equiv.), LiBr (1 equiv.), NMP, 4 mA, C (+) Ni (-), 14 h, rt.

None of the reactions attempted were found to generate the desired product (as determined by LCMS). All reactions appeared to form a complex product mixture with no remaining starting material. Any attempts to purify and investigate these mixtures were hampered by the necessity of using multiple equivalents of PPh_3 (thus producing multiple equivalents of OPP-h_3), and the use of NMP as the reaction solvent. Therefore, attention was turned towards alternate methods of Ni-catalysed electrochemical amino acid modification.

In 2021, MacMillan *et al.* published a procedure for synthesizing unnatural amino acids *via* Ni- and Ir- catalysed photochemical arylation of serine derivatives.[20] The general scheme for these reactions is shown below in **Scheme 3.15**.

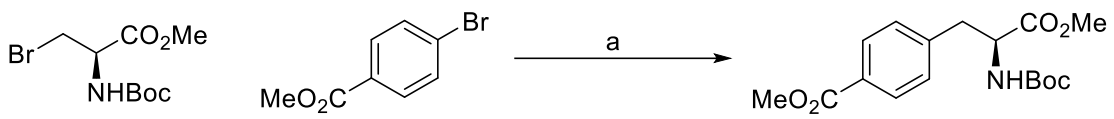

27 **242** **243**

Scheme 3.15 The photochemical arylation of Boc-Ala(Br)-OMe (**27**) published by MacMillan *et al.*;[20] reagents and conditions: a) [Ir(dF(CF$_3$)ppy)$_2$(dtbbpy)] (1 mol %), NiCl$_2$·dtbbpy (5 mol %), (TMS)$_3$SiH (1 equiv.), Na$_2$CO$_3$ (0.1 M), DME, 34 W blue LED, 4 h, 79%.

This reaction was thought to proceed via initial photoexcitation of the iridium photocatalyst, which can generate a bromine radical from a bromide anion. This radical can then abstract a hydrogen atom from the super silane (**244**). The resulting silyl radical (**245**) can react with the bromoalanine (**27**) to yield an alkyl radical (**246**), which is then capable of undergoing Ni-catalysed coupling with the aryl bromide (**Scheme 3.16**).

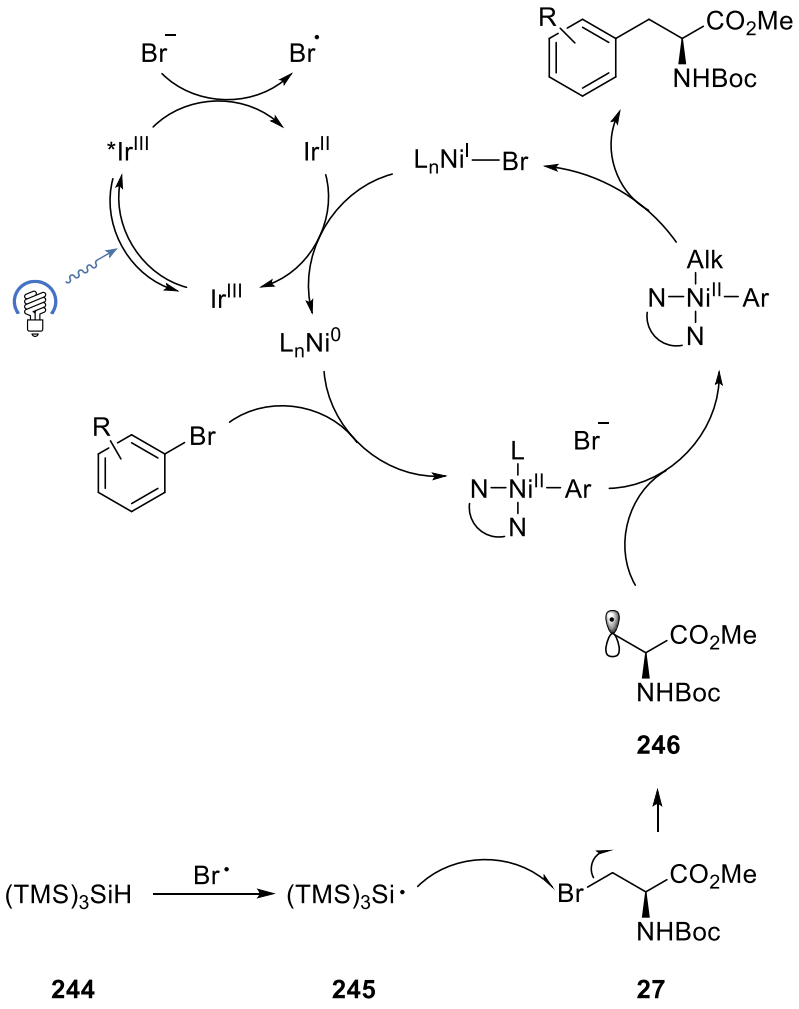

Scheme 3.16: Mechanism proposed by MacMillan *et al.* for the metallaphotoredox arylation of a bromoalanine derivative (**27**).[20]

It was envisaged that the generation of an alkyl radical from bromoalanine derivatives may be achieved under electrochemical conditions, which would circumvent the need for an expensive iridium photocatalyst and stoichiometric amounts of super silane (**244**). Additionally, the arylation procedure could be expanded to other amino acids from which a bromo-derivative could be easily accessed; *e.g.*, proline, threonine, and homoserine.

Therefore, Boc-Ala(Br)-OMe (**27**) was synthesised using an Appel reaction from Boc-Ser-OMe (**Scheme 3.17**).

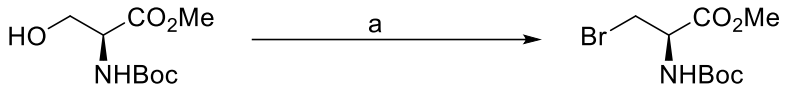

26 **27**

Scheme 3.17: Appel bromination of Boc-Ser-OMe (**26**) to form Boc-Ala(Br)-OMe (**27**); reagents and conditions: a) NBS, PPh_3, THF, 0 °C, 20 h, 63%

An initial attempt to electrochemically arylate the protected bromoalanine derivative (**27**) is shown in **Scheme 3.18**. 4-bromobenzotrifluoride (**247**) was selected as the aryl bromide coupling partner so that ^{19}F NMR spectroscopy could be used as a rapid indicator of reaction success.

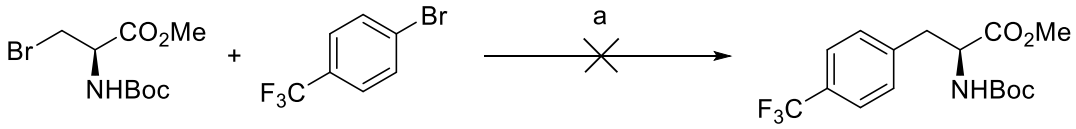

27 **247** **248**

Scheme 3.18: Attempted formation of Boc-Phe(4-trifluoromethyl)-OMe (**248**); reagents and conditions: $NiCl_2$•glyme (5 mol%), 4,4'-di-tertbutyl-2,2'-bipyridine (dtbbpy)(5 mol%), Na_2CO_3 (2 equiv.), anhydrous DME (3 mL), Ar, 5 mA, graphite anode, Ni foam cathode, 10 h.

The first set of conditions trialled were kept as close to those in the photochemical procedure, omitting the iridium photocatalyst, LED light, and super silane (tris(trimethylsilyl)silane). The active $NiCl_2$•dtbbpy catalyst was prepared prior to its addition to the main reaction mixture by dissolving the $NiCl_2$•glyme and dtbbpy together in DME and sonicating until a green suspension was formed.

However, the Na_2CO_3 base was not soluble enough in the DME to permit a current to pass through the reaction mixture. LiBr and tetrabutylammonium bromide both failed to dissolve in DME. Lithium iodide appeared to be sparingly soluble in DME, so it was added to the reaction

mixture to act as an electrolyte. This somewhat improved the conductivity of the solution, although the voltage was still high (~10 V). However, this reaction was ultimately unsuccessful; the only product isolated from the reaction was an acrylate derivative (**249**) (**Figure 3.1**). The identity of this product was determined by comparison of its ^{1}H NMR spectrum to previously published data,[21] and further confirmed by LCMS analysis.

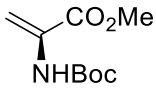

249

Figure 3.1: Acrylate product (**249**) derived from elimination of Boc-Ala(Br)-OMe (**27**)

It was suspected that LiBr may be a better electrolyte. Therefore, the reaction displayed in **Scheme 3.18** was repeated using 3 equiv. of LiBr in addition to 0.5 mL of DMA to aid the dissolution of the electrolyte. Whilst no product was observed from this reaction, the DMA was found to be very effective at dissolving the LiBr. As a result, another reaction was set up using DMA as the solvent (**Table 3.1**, **Entry 1**).

Using this set up the formation of the desired product (**248**) was observed in trace quantities, as determined by LCMS of the crude reaction mixture. Several other alkene derived products were also observed, as displayed in Entry 1 (**Table 3.1**). The presence of the unsaturated derivative **250** was inferred from the examination of LCMS and ^{19}F NMR spectroscopic data. The identities of the mono-bromo **251** and the dibromo **252** were revealed by comparison of ^{1}H NMR spectra to published data, in conjunction with LCMS data. The major product from this reaction was confirmed to be the unsaturated dibromo- derivative (**252**) after a crystal structure was obtained (**Figure 3.2**).

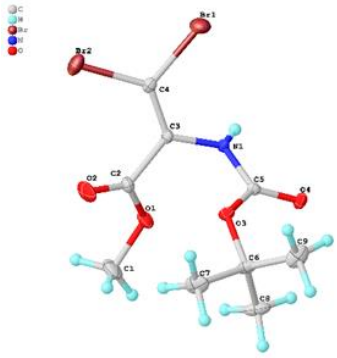

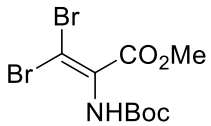

252

Figure 3.2: Molecular structure obtained for the major product (**252**) from **Table 3.1, Entry 1**.

A possible explanation for the generation of these alkene-derived products is that the acrylate product (**249**) was formed initially, which subsequently reacted with free bromine species or aryl bromide to form the molecules shown in **Entry 1** (**Table 3.1**) (**Scheme 3.19**).

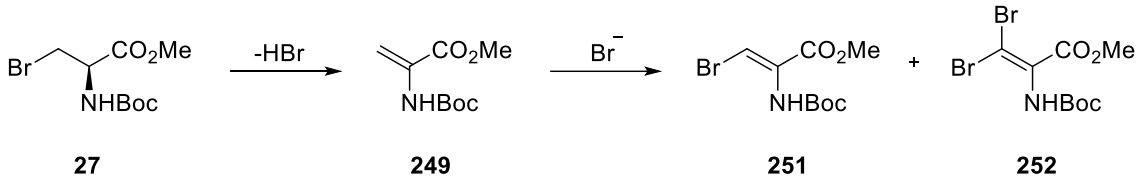

27 **249** **251** **252**

Scheme 3.19: Possible transformation of β-bromoalanine **27** into unsaturated products (**251, 252**) via formation of acrylate **249**.

It was thought that the inorganic base (Na_2CO_3) might be hindering the reaction due to its inability to dissolve in the DMA. Therefore, the reaction was repeated using DIPEA *in lieu* of the Na_2CO_3 (**Table 3.1**, **Entry 2**). This reaction was successful in that the desired product was observed by examination of the ^{1}H NMR and ^{19}F NMR spectra. However, the product and starting material could only be isolated as an inseparable mixture, and the acrylate (**249**) remained the major product of the reaction. Whilst not isolated, biaryl **253** also appeared to be present in the reaction mixture; this was evidenced by a comparison of ^{1}H and ^{19}F NMR spectra to published data.[22]

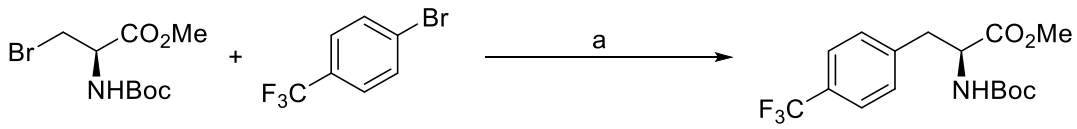

27 **247** **248**

Reagents and conditions: a) $NiCl_2$•dtbbpy (10 mol%), LiBr (X M), Na_2CO_3, anhydrous DMA, 4 mL, Ar, 3 mA, C (+) Ni (-), rt, 10 h.

Entry	Deviation from above (a)	Products observed	Yield[b]
1	None	+ trace amount of desired product	NI

		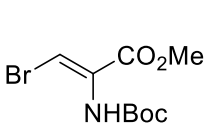 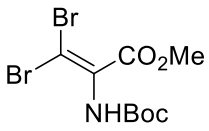 **251** **252** 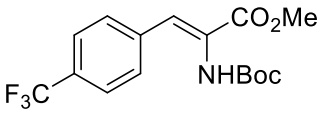 **250**	
2	DIPEA instead of Na_2CO_3	Mixed product and starting material isolated 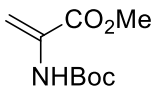 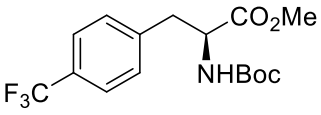 **249** **248** 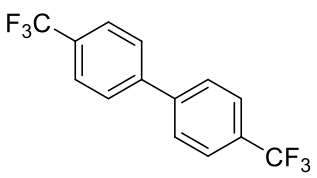 **253**	NI
3	See **Entry 2** but with 1.5 mA	See Entry 2	NI
4	See **Entry 2** but with Boc-Ala(I)-OMe (**260**) as the substrate	Trace product in MS. Single alkene spot on TLC	NI
5	See **Entry 2** but with 4-iodobenzotrifluoride (**261**) as the aryl coupling partner	See Entry 2	NI
6	**Entry 2** but with an additional 2 equiv. pyridine	Mixture of biaryl + alkene + bialkane + product. No starting material	12
7	4 equiv. of DIPEA	Biaryl + alkene + product. No starting material	19
8	See **Entry 2** but with a drop of pyridine added	See **Entry 7**	14
9	See **Entry 2** but with threonine	Trace product observed but mainly Boc-Thr-OMe (**255**) produced.	NI

	oxalate as the substrate 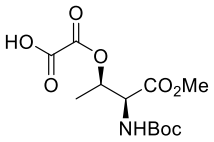 **254**	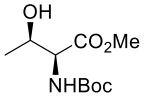 **255**	
10	10 equiv. DIPEA	See **Entry 7**	11
11	See **Entry 7** but with Boc-Thr(Br)-OMe (**258**) as the substrate 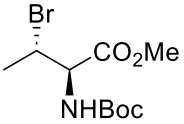 **258**	Boc-Thr-OMe, both *E/Z* isomers and both product diastereomers observed 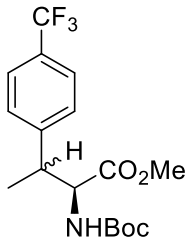 **256** 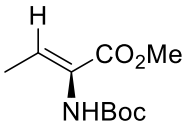 ***Z*-257** 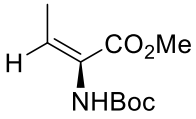 ***E*-257** 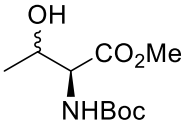 **255**	NI
12	See **Entry 7** but with Boc-Pro(Br)-OMe 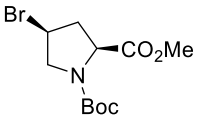 **259**	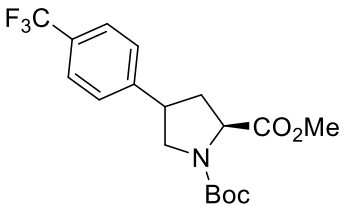 **263** No alkene was produced. Product and starting material are inseparable.	36[c]

Table 3.1: Various conditions explored for the Ni-catalysed coupling of serine-derived alkyl bromides and aryl bromides. The presence of any products observed was confirmed using TLC, LCMS, NMR, or X-ray crystallography; b = isolated yield, c = conversion yield as observed by ^{1}H NMR; NI = not isolated.

Several variations of the conditions described in **Entry 2** (**Table 3.1**) were attempted. The current was reduced to 1.5 mA (**Table 3.1, Entry 3**), which did not have a significant impact on the product mixture composition.

It was thought that perhaps an iodoalanine derivative (**260**) may make a better coupling partner for this reaction, as alkyl iodides are known to be more reactive.[23] Iodine atoms are much larger, and their electron density is more diffuse; the C-I bond is therefore much weaker than the C-Br bond and thus more easily broken. Boc-Ala(I)-OMe (**260**) was synthesized from Boc-Ser-OMe (**26**) using Appel reaction conditions (**Scheme 3.20**).

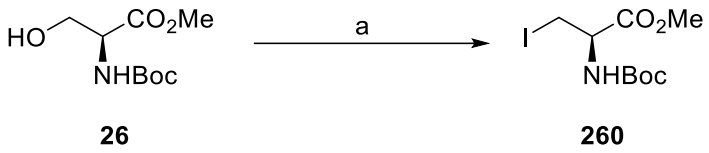

26 **260**

Scheme 3.20: Conversion of Boc-serine methyl ester (**26**) to Boc-iodoalanine methyl ester (**260**) using an Appel reaction; reagents and conditions: a) I_2, PPh_3, imidazole, DCM, 16 h, 75%.

Unfortunately, when the alkyl iodide substrate (**260**) underwent the coupling reaction (**Table 3.1, Entry 4**), only trace amounts of the desired product were observed by LCMS, with the major product being the acrylate (**249**). It is possible that the alkene-forming reaction is dominant under these conditions, so the increased reactivity of the alkyl iodide causes increased alkene formation. This is to the detriment of the alkyl-aryl coupling reaction, and thus reduced product formation is observed.

A reaction with 4-iodobenzotrifluoride (**261**) instead of the 4-bromo- derivative (**247**) was also attempted (**Table 3.1, Entry 5**); however, this substitution did not alter the product composition when compared to **Table 3.1, Entry 2**.

At this point it became clear that this reaction could not be properly optimised until the issue of unwanted alkene formation was resolved. This could potentially be due to either an E2 elimination mechanism or a β-hydride elimination mechanism (**Figure 3.3**).

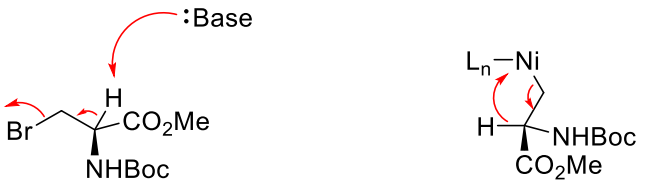

E2 Elimination **β-H Elimination**

Figure 3.3: An illustration of two possible elimination mechanisms that may be responsible for acrylate formation; (L-R) E2 elimination and β-hydride elimination.

It was thought that a weaker and more nucleophilic base like pyridine may reduce alkene formation. Pyridine has a much lower pKa than DIPEA (5.23 and 10.8 respectively), which could disfavour an E2 elimination reaction. Additionally, pyridine may act as a ligand to the nickel centre, which could help prevent β-H elimination by increasing steric hindrance. Pyridine has also been used as an additive in catalytic quantities (10 mol%) by Weix *et al.* to improve the yields of alkyl halide/aryl halide coupling reactions.[24] Therefore, a reaction was run with two equivalents of pyridine in addition to two equivalents of DIPEA (**Table 3.1**, **Entry 6**). For the first time, the desired product (**248**) was isolated in a 12% yield, along with the usual biaryl (**253**) and alkene (**249**) products. A bialkane product (**262**) was also observed (**Figure 3.4**), generated from the homocoupling of two alkyl substrates. The identity of this product was established through a comparison of the ^{1}H NMR spectra obtained to published data.[25] LCMS and TLC analysis of the crude product mixture confirmed that no starting material remained.

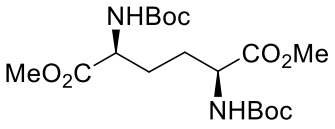

262

Figure 3.4: The structure of the bialkane formed (**262**) from the Ni-catalysed coupling of two β-bromoalanine molecules. This compound was not fully isolated.

It was unclear whether the lack of remaining starting material was due to the addition of pyridine or the fact that there were 4 equivalents of base in the reaction. A later reaction with pyridine only (See **Table 3.5, Entry 8**) revealed that the latter was likely correct. This was confirmed when 4 equivalents of DIPEA were used in the reaction (**Table 3.1**, **Entry 7**). All of the starting material was consumed, and the usual products (alkene (**249**), biaryl (**253**), Boc-Phe(4-CF_3)-OMe (**248**)) were generated. The desired product (**248**) was isolated in a 19% yield. A further reaction using 10 equivalents of DIPEA (**Table 3.1**, **Entry 10**) resulted in a lowered yield of the product **248** (11%).

Interestingly, the formation of bialkane (**262**) was not observed when pyridine was not included in the reaction. Indeed, when a reaction was run with a drop of pyridine added to two equivalents of DIPEA (**Table 3.1**, **Entry 8**), the bialkane **262** was again formed alongside the desired product (**248**) (14% yield). It is possible that pyridine is able to act as a ligand and coordinate to the nickel centre. This may increase the rate of the coupling reaction, but due to the disparity in reactivities of the alkyl and aryl bromide, biaryl **253** is formed first, leaving less aryl bromide to react with the alkyl bromide. The alkyl bromide is therefore forced to react itself, generating bialkane **262**.

Given that oxalates have been known to form alkyl radicals under oxidative conditions (See **Chapter 2, Section 2.3.3**), a reaction was attempted using threonine oxalate (**254**) as the substrate (**Table 3.1, Entry 9**). Whilst trace amounts of the desired product were observed using LCMS, the major product from this reaction was Boc-Thr-OMe (**255**). This was confirmed by examination of the ^{1}H NMR spectrum. Therefore, no further reactions with this substrate were undertaken.

To investigate the impact of employing a secondary haloalkane as a substrate compared to a primary haloalkane, a reaction was attempted using a threonine-derived substrate (**258**) (**Table 3.1, Entry 11**).

Inspection of the resultant product mixture revealed the presence of Boc-Thr-OMe (**255**), both *E/Z* isomers (**257**) (**Figure 3.5**), and both product diastereomers (**256**) (**Figure 3.5**). The *E/Z* isomers (**257**) were isolated as a mixture; their identity was confirmed by LCMS and by comparison of the ^{1}H NMR spectrum to published data.[26] The product (**256**) was isolated as a mixture alongside a minor amount of *Z*-isomer **257** (confirmed by LCMS). **256** was assumed to be diastereomeric due to two peaks in the ^{19}F NMR spectrum, and two methyl ester peaks in the ^{1}H NMR spectrum.

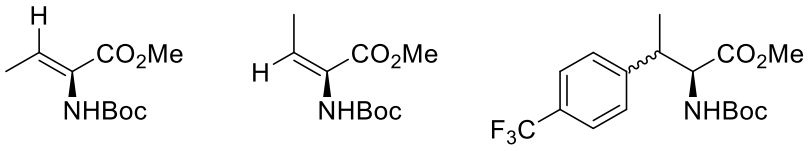

***Z*-257** ***E*-257** **256**

Figure 3.5: Structures of the products observed from **Entry 11** (**Table 3.1**). (L-R); *Z*-isomer **257**, *E*-isomer **257**, the diastereomers of the desired -Phe product (**256**).

The *E/Z* isomers (**257**) appeared to have been produced in roughly equivalent proportions. The Appel reaction is an S_N2 reaction, so the alkyl bromide produced from this transformation (**258**) should be a single enantiomer. Therefore, the ensuing elimination is unlikely to be due to β-H elimination or E2 elimination, as both of these mechanisms are stereoselective. It may be inferred that the elimination step occurs *via* either an E1 or E1cB mechanism.

To investigate whether elimination will occur when the acidic α-H is not directly adjacent to the C-Br moiety, a bromo-proline derivative (**259**) was synthesised from Boc-Hyp-OMe (**117**). This substrate was then reacted under the electrochemical coupling conditions (**Table 3.1**, **Entry 12**). The desired product **263** was formed as an inseparable mixture with the remaining starting

material (36% conversion to **263** by ^{1}H NMR). However, no alkene was observed, confirming that the elimination only takes place with β-bromo-substituted amino acids.

To investigate whether or not the alkene was being formed in part due to β-hydride elimination, a range of bulky ligands (**Figure 3.6**) were screened as alternatives to dtbbpy (**264**), using the conditions from **Table 3.1**, **Entry 7**. Bulky ligands have been known to inhibit β-H elimination as they increase the steric bulk around the metal centre. The substrate cannot therefore assume the configuration necessary for β-H elimination.[27]

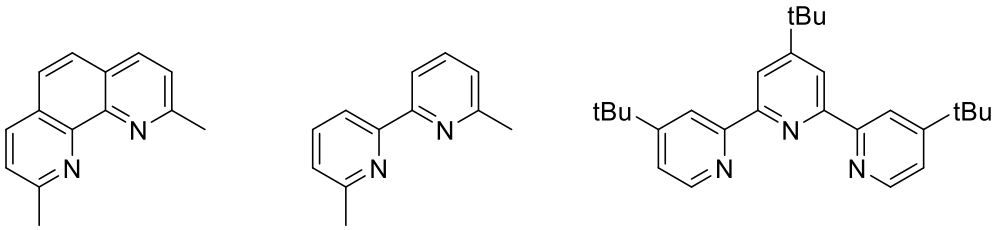

265 **266** **267**

Figure 3.6: Alternative bulky ligands screened; (L-R) 2,9-dimethyl-1,10-phenanthroline (neocuproine) (**265**), 6,6'-dimethyl-2,2'-bipyridine (**266**), 4,4′,4″-tri-tert-Butyl-2,2′:6′,2″-terpyridine (**267**).

The active NiL_n catalyst was formed in the same way as for the dtbbpy ligand (*i.e.*, stirring $NiCl_2$•glyme with the ligand in DMA for 1 h prior to use). Unfortunately, none of these ligands elicited any significant change in the product composition. When the neocuproine ligand (**265**) was used, the alkene **249** was the major product and there was still starting material present in the reaction (determined by LCMS). The dimethyl bipyridine ligand (**266**) produced the same outcome.

The terpyridine ligand (**267**) also gave rise to the alkene **249** as the major product, alongside the desired product (**248**), bialkane (**262**), and 4-(trifluoromethyl)phenol (**268**) as a mixture (assessed by LCMS, ^{1}H- and ^{19}F NMR). All three ligands displayed in **Figure 3.6** afforded alkene **249** as the major product with little change in the product composition, which lends support to the idea that alkene production is not due to a β-H elimination mechanism. Interestingly, when the terpyridyl ligand (**267**) was used in a reaction with 4-bromoproline (**259**), only starting material was observed by LCMS.

The coupling reaction was then attempted in a divided cell, to investigate whether unwanted oxidation of the active Ni catalyst at the anode may be having a deleterious effect on the reaction yield. Therefore, a reaction was performed with the substrates and catalyst in the cathodic chamber only (**Figure 3.7**).

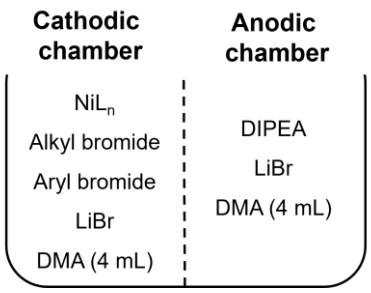

Figure 3.7: Diagram showing the components of the Ni-catalysed coupling reaction in the divided cell; both chambers require electrolyte and DMA solvent, the chambers are separated by a frit which prevents movement of substrates but permits conductivity.

On a 0.15 mmol scale (10% catalyst loading), the product (**248**) was isolated in a 25% yield. On a 0.3 mmol scale (5% catalyst loading), the yield of **248** remained the same (25%). Given this result, it would appear that the divided cell was somewhat effective at boosting the yield of the coupling reaction. This could be due to less anodic oxidation of the catalyst, but could also be due to the base (DIPEA) being restricted to the anodic chamber. It is unclear which species is acting as the base within the cathodic chamber. Tertiary amines have been used as sacrificial reductants in a similar procedure,[28] so it is possible that the DIPEA is acting in a similar manner.

The tetrafluoropyridyl group has been known to act as a leaving group.[29] A tetrafluoropyridyl-protected serine derivative (**269**) was therefore synthesised to assess its suitability as a coupling partner (**Scheme 3.21**).

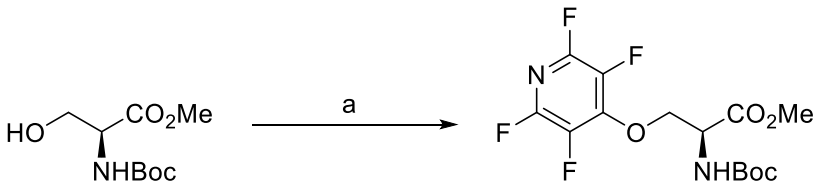

26 **269**

Scheme 3.21: The reaction of Boc-Ser-OMe (**26**) with pentafluoropyridine to produce Boc-Ser(*O*-TFP)-OMe (**269**); reagents and conditions: a) pentafluoropyridine, K_2CO_3, MeCN, 20 h, 51%.

When this was reacted under the Ni-catalysed electrochemical coupling conditions, an unexpected product (**270**) was isolated alongside the usual alkene (**249**) and remaining starting material (**269**) (**Scheme 3.22**).

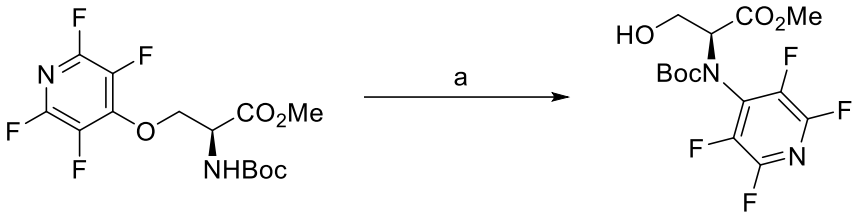

269 **270**

Scheme 3.22: Transformation of Boc-Ser(*O*-TFP)-OMe (**269**) into Boc-Ser(*N*-TFP)-OMe (**270**) under electrochemical conditions; reagents and conditions: a) $NiCl_2$•dtbbpy (10 mol%), 4-bromobenzotrifluoride, LiBr, DIPEA, anhydrous DMA, 4 mL, Ar, 3 mA, C (+) Ni (-), rt, 10 h.

The tetrafluoropyridyl group appeared to have migrated from the oxygen to the nitrogen. A comparison of the ^{1}H- and ^{19}F NMR spectra of the starting material **269** and the product **270** revealed slightly shifted proton peaks and broadened fluorine peaks (**Figure 3.8**). LCMS analysis confirmed that the mass of the starting material and the product were the same.

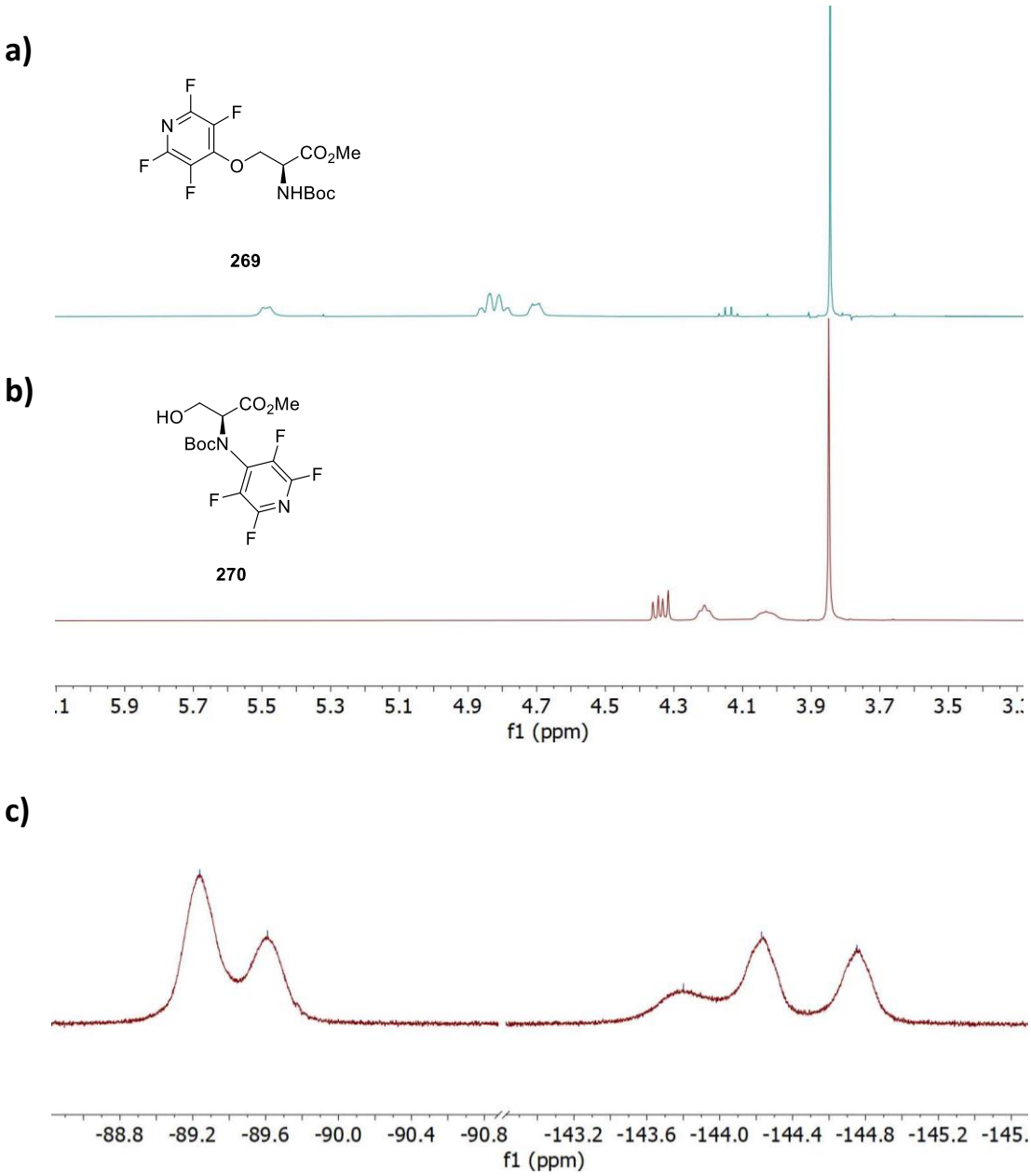

Figure 3.8: A comparison of the ^{1}H NMR spectrum (400 MHz, $CDCl_3$) of the starting material Boc-Ser(*O*-TFP)-OMe (**269**) (a), stacked with the ^{1}H NMR spectrum (400 MHz, $CDCl_3$) of the product (**270**) (b). The ^{19}F NMR spectrum (376 MHz, $CDCl_3$) of the product (**270**) is also displayed (c), illustrating the broadening of the fluorine peaks.

When the reaction displayed in **Scheme 3.22** was run again without any aryl bromide, the yield of the *N*-TFP product (**270**) was 33%. This transformation was thought to be due to a Smiles rearrangement, in which an aryl substituent migrates intramolecularly between two heteroatoms. Electrochemical Smiles rearrangements have been previously reported;[30] an example of such is shown below in **Scheme 3.23**.

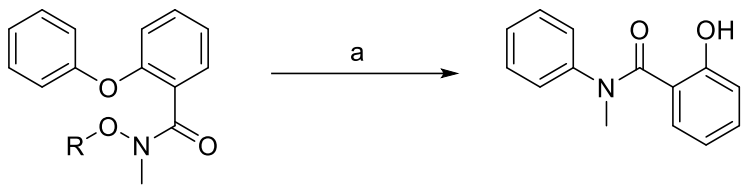

271

Scheme 3.23: Electrochemical Smiles rearrangement reported by Chang *et al.*[30]; reagents and conditions: a) NH_4Cl (0.25 M), DMSO (4 mL), undivided cell, 50 °C, Pt plate electrodes (1 cm^2), 10.0 mA, 3 h (5.6 F/mol), 50-86%.

To investigate whether the yield of this reaction could be improved, a reaction with H-Ser(*O*-TFP)-OMe (**272**) was attempted (**Scheme 3.24**). The idea behind this was that the free amine may be more nucleophilic, and therefore react more readily in a nucleophilic aromatic substitution reaction.

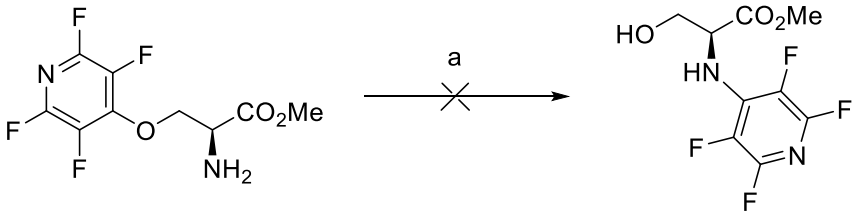

272 **273**

Figure 3.24: Attempted reaction of H-Ser(*O*-TFP)-OMe (**272**) to form TFP-Ser-OMe (**273**) under electrochemical conditions; reagents and conditions: a) $NiCl_2$•glyme, dtbbpy, DIPEA, DMA, 3 mA, 10 h, N_2, C (+) Ni (-)

However, this reaction was unsuccessful, yielding only the starting material (**272**) and the corresponding alkene (**274**) as determined by LCMS. This could be because the mechanism is a radical process, rather than a nucleophilic aromatic substitution. Therefore, the key radical intermediate may be an amidyl radical (**275**) (**Figure 3.9**), which is stabilised by the presence of protecting groups such as Boc.

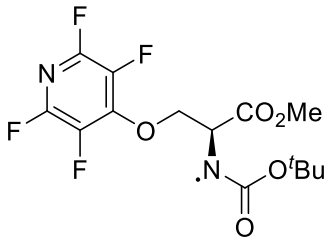

275

Figure 3.9: Possible amidyl radical intermediate (**275**) in the Ni-catalysed Smiles rearrangement of Boc-Ser(*O*-TFP)-OMe (**269**).

A reaction using a TFP cysteine derivative (**277**) was also performed. This substrate was synthesised in a similar manner to the serine derivative (**Scheme 3.25**).

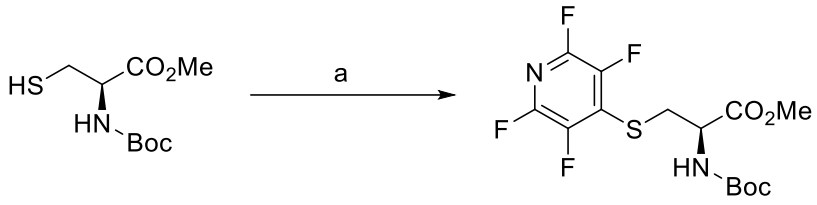

276 **277**

Scheme 3.25: Tetrafluoropyridyl protection of Boc-Cys-OMe (**276**); reagents and conditions: a) pentafluoropyridine, Et_3N, anhydrous THF, 0 °C, N_2, 20 mins, 78%.

When this substrate (**277**) was reacted under the electrochemical conditions, only starting material (**277**) and alkene (**249**) were produced (confirmed by LCMS and TLC). To try and make the TFP group a better-leaving group, a sulfone derivative (**279**) was synthesised (**Scheme 3.26**).

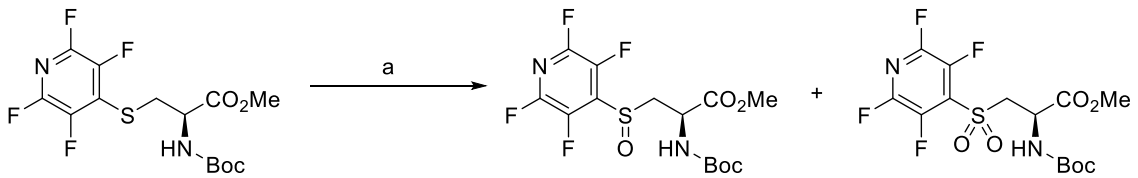

276 **278** **279**

Scheme 3.26: Oxidation of Boc-Cys(*S*-TFP)-OMe (**276**) to form a sulfoxide (**278**) and sulfone derivative (**279**); reagents and conditions: a) H_2O_2, ammonium molybdate tetrahydrate, EtOH, sealed tube, 3 h, 70 °C, 27% (**278**) and 36% (**279**). *Note* – this reaction can also be done at ambient temperature in an RBF, stirring for 3 days.

A sealed tube reaction using H_2O_2 as the oxidant resulted in a mixture of alkene **249**, a sulfoxide derivative (**278**), and a sulfone derivative (**279**). The sulfone and sulfoxide derivatives were isolated and characterised. Molecular structures were obtained for both compounds (**278, 279**) (**Figure 3.10**).

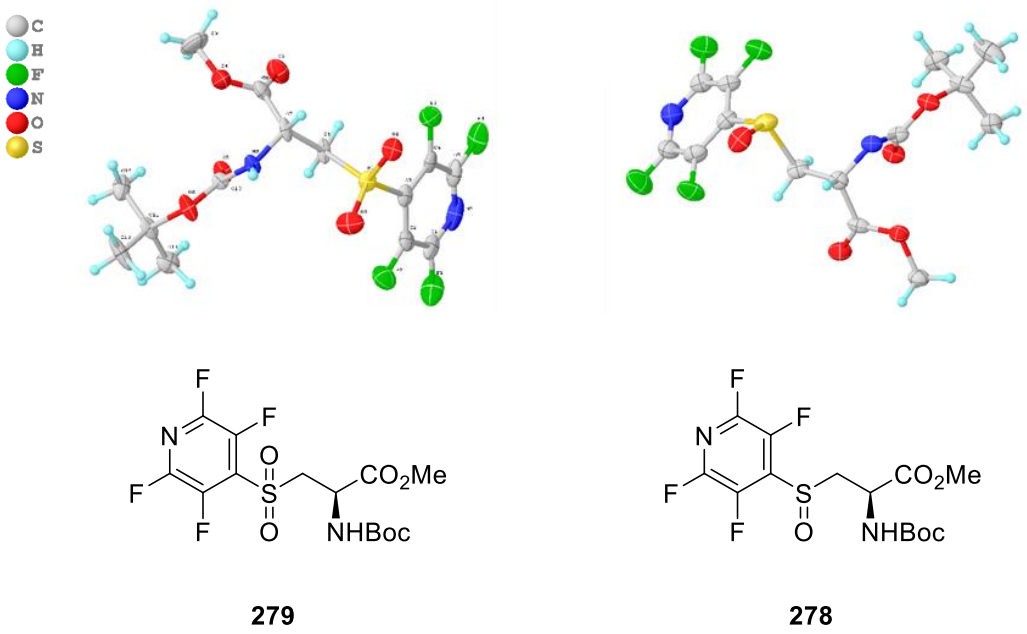

Figure 3.10: Molecular structures for the TFP-sulfone (**279**), (left), and TFP-sulfoxide (**278**), (right). Molecular structures reported with a 50% thermal ellipsoid probability.

Both the sulfoxide (**278**) and sulfone (**279**) were then subjected to the electrochemical coupling conditions (**Scheme 3.27**). Investigation of the product mixture of the sulfone (**279**) reaction revealed that the major product was alkene **249** (determined by comparison to existing samples with TLC). Whilst there did appear to be traces of other compounds present, these could not be identified. The reaction with sulfoxide **278** produced small amounts of sulfide **277** and sulfide **280**, in addition to alkene **249**. The presence of these products was confirmed by LCMS analysis and comparison of crude ^{1}H- and ^{19}F NMR spectra to published data.

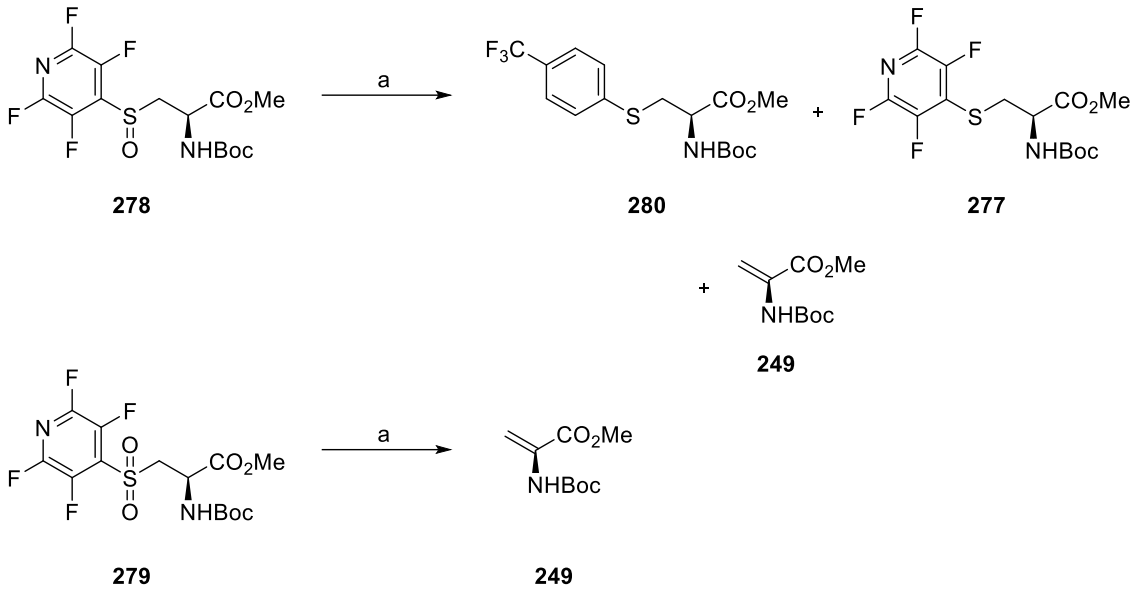

Scheme 3.27: Ni-catalysed electrochemical reaction of sulfone **279** and sulfoxide **278**; reagents and conditions: a) $Ni(bpy)_3Br_2$ (10 mol%), DMA (3 mL), DIPEA, $^nBu_4NBr$, 4 mA, 10 h, RVC (+) Ni foam (-).

The generation of the two sulfide products (**277** and **280**) suggests that the sulfoxide **278** is susceptible to oxidation at the cathode. Due to a lack of evidence of any Smiles product formation, no further reactions were undertaken to this end. Attention was returned to attempts to arylation of bromoalanine derivatives. It was thought that changing the amine-protecting group may modulate the acidity of the α-H, and thus influence the tendency towards elimination. A number of protecting groups were initially tried; these are displayed in **Table 3.2**.

Entry	Protecting group	Substrate	Products[a]
1	Fmoc	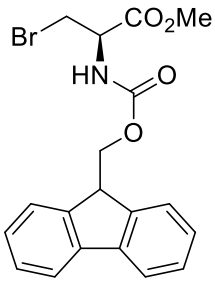 **281**	Alkene and starting material
2	Trityl	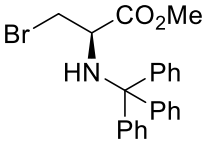 **282**	Starting material only
3	Dibenzyl	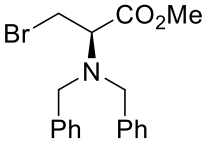 **283**	No alkene, starting material + product stereoisomers

Table 3.2: Bromoalanine derivatives with different amine protecting groups used as substrates in the Ni-calalysed coupling, alongside the corresponding coupling products; a = determined using TLC, LCMS, ^{1}H- and ^{19}F NMR analysis

Initially, a Fmoc-protected bromoalanine substrate (**281**) was trialled (**Table 3.2**, **Entry 1**). It was thought that the bulkiness of the group may influence elimination by hindering access to the α-H. However, the sole product from this reaction was the related alkene (**284**), along with leftover starting material. Similarly to the Boc group, the Fmoc group is a carbamate; it is probable that carbamate protecting groups are too electron-withdrawing to prevent the unwanted elimination. The NHBoc moiety may pull electron density from the α-C, making the α-H more acidic and facilitating elimination. This may point to an E1cB mechanism rather than E1; an electron withdrawing group would better stabilise a carbanion (**Scheme 3.28**).

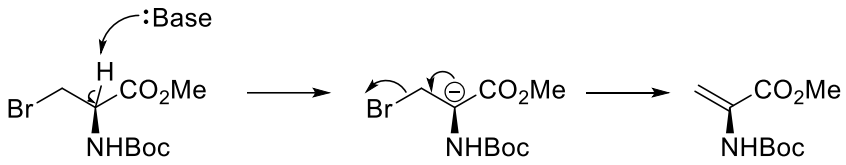

27 **249**

Scheme 3.28: Elimination of alkyl bromides via an E1cB mechanism.

Subsequently, the decision was made to try a non-carbamate trityl protecting group (**Table 3.2**, **Entry 2**). When the trityl-protected β-bromoalanine (**282**) was subjected to the coupling conditions, only starting material was recovered from the reaction mixture. This result indicated that elimination could be halted by careful selection of the protecting group. The lack of product formation could be attributed to the bulkiness of the trityl group preventing access to the reaction centre.

Given the subjective success of the trityl group, it was thought that a similar, smaller aromatic protecting group may improve the reaction yield: *i.e.*, a benzyl group. An attempt to synthesise *N*-Bn-Ser-OMe (**286**) resulted in the formation of both it and the over reacted dibenzyl derivative (**287**) (**Scheme 3.29**).

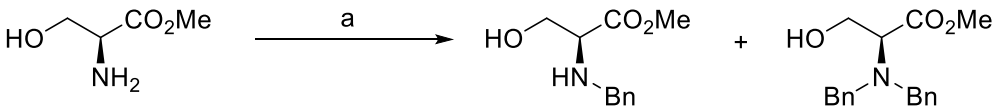

285 **286** **287**

Scheme 3.29: Benzylation of serine methyl ester (**285**) to produce mono-benzylated (**286**) and di-benzylated derivative (**287**); reagents and conditions: a) BnBr, K_2CO_3, MeCN, rt, 20 h, 35% (**286**), 20% (**287**).

Both mono-benzylated (**286**) and di-benzylated serine (**287**) derivatives were subjected to bromination using an Appel reaction, but only the di-benzyl serine reaction was successful. When *N*-$(Bn)_2$-Ala(Br)-OMe (**283**) was reacted with an aryl bromide under the usual Ni-catalysed coupling conditions (**Table 3.2**, **Entry 3**), no alkene was produced (determined using LCMS and ^{1}H NMR). Generation of the desired product (**288**) was confirmed by ^{1}H- and ^{19}F NMR spectroscopic analysis but it was difficult to establish a conversion yield because the product appeared to exist as stereoisomers, possibly rotameric. This is probably due to a steric clash between the di-benzyl protecting groups and the Ar-CF_3 moiety.

Notably, leftover 4-bromobenzotrifluoride (**247**) was observed post-reaction when the dibenzyl substrate (**283**) was used, indicating that the rate of the reaction between alkyl and aryl bromide was rapid enough to compete with the rate of the biaryl formation reaction.

The relative success of the di-benzyl protecting group led to renewed efforts to synthesise *N*-Bn-Ala(Br)-OMe (**289**), which proved difficult. This could be due to the possible formation of an aziridine (**290**) (**Scheme 3.30**). A benzyl protecting group is relatively electron-donating so the lone pair on the nitrogen is more available. The nitrogen will therefore more readily participate in an intramolecular nucleophilic substitution reaction. Aziridine formation has been observed previously by Seebach *et al.* during reactions of Bn-Ser-OMe (**286**) with CBr_4.[31]

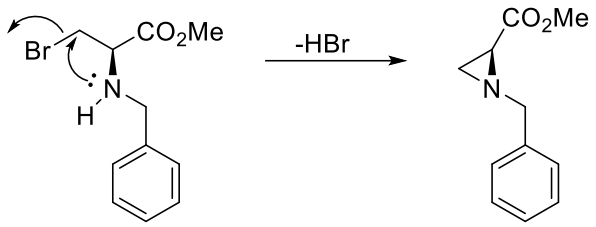

289 **290**

Scheme 3.30: Proposed formation of an unwanted aziridine derivative (**290**) from *N*-Bn-Ala(Br)-OMe (**289**)

Several bromination conditions were attempted to form *N*-Bn-Ala(Br)-OMe (**289**) from *N*-Bn-Ser-OMe (**286**) (**Table 3.3**).

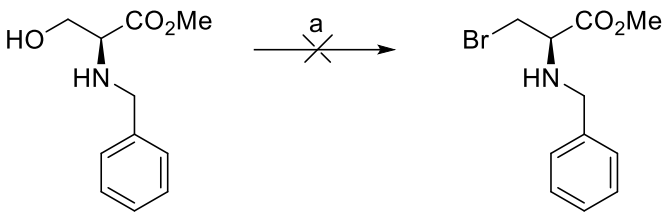

286 **289**

Entry	Conditions (a)	Yield[b]
1	NBS, PPh_3, THF, 0 °C, 20 h	nil
2	CBr_4, PPh_3, DCM, N_2, 6 h	nil
3	TCT, DMF, NaBr, DCM, rt	nil
4	Allyl bromide, CDI, ACN, reflux	**291* (52%)**
5	P_2O_5, KBr, ACN	nil
6	Xtalfluor-E, Et_4NBr, DCM, lutidine, 20 h	nil

Table 3.3: Various bromination conditions attempted unsuccessfully for the transformation of *N*-benzyl serine methyl ester into the corresponding bromoalanine derivative. All conditions (except **Entry 4**) resulted in a mixture of multiple unidentified products. b = presence (or lack thereof) of the desired product was determined by LCMS; *See **Scheme 3.31**.

The majority of the bromination conditions attempted were unsuccessful, resulting in a mixture of unidentifiable products. Whilst no evidence of aziridine formation was observed, it is probable that the nucleophilicity of the nitrogen was causing a significant problem.

The use of allyl bromide and CDI (**Table 3.3**, **Entry 4**) resulted in full conversion to an unknown product, which was recrystallised and subsequently revealed to be a cyclised derivative (**291**) (**Scheme 3.31**). This is likely to be due to the action of CDI (**292**), which is used as an amide coupling reagent. A proposed mechanism is given below in **Scheme 3.31.**

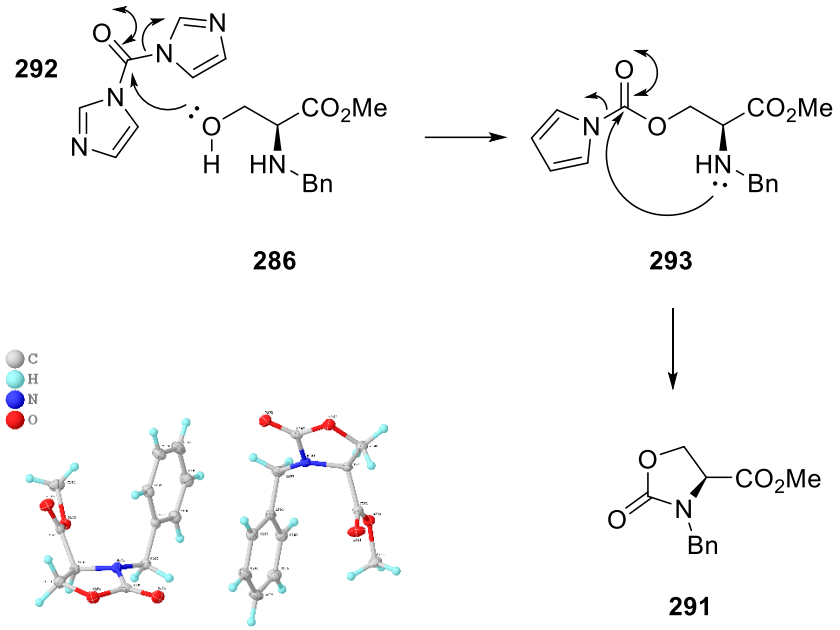

Scheme 3.31: Proposed mechanism for the formation of a cyclised carbamate (**291**) from the reaction of *N*-Bn-Ser-OMe (**286**) with CDI (**292**), along with the X-Ray molecular structure for said carbamate product (**291**). Molecular structure reported with a 50% thermal ellipsoid probability.

Two other routes to the desired product (**289**) were attempted (**Scheme 3.32**). First, Boc-Ala(Br)-OMe (**27**) was synthesised using a standard method. The Boc group was then removed, followed by attempted benzyl group protection. Unfortunately, the benzyl protection was unsuccessful, either due to aziridine formation or base-catalysed elimination. No evidence of the desired product (**289**) was observed by LCMS.

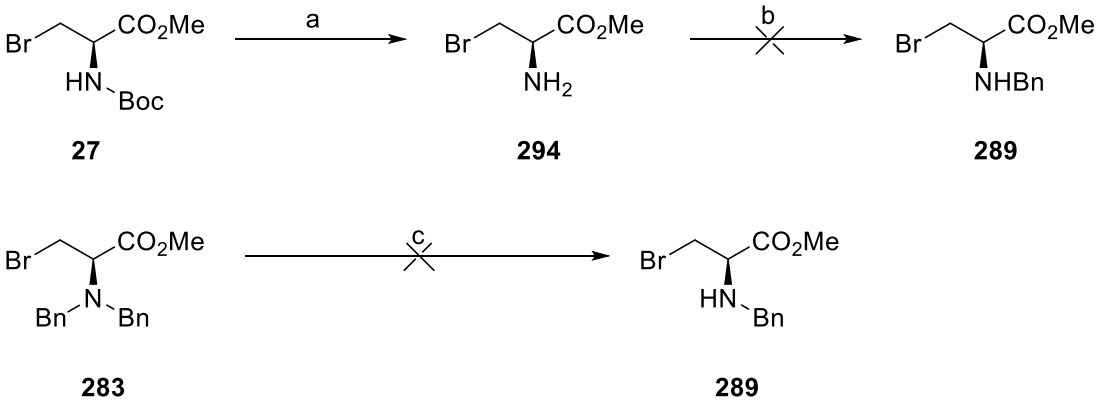

Scheme 3.32: Alternative routes to *N*-Bn-Ala(Br)-OMe (**289**) attempted; reagents and conditions: a) TFA, DCM, rt, 16 h, quant.; b) BnBr, K_2CO_3, MeCN, 20 h, rt; c) ammonium cerium (IV) nitrate, MeCN/H_2O (5:1), 2h, rt

A second route was attempted in which di-benzyl serine methyl ester (**287**) was brominated to produce *N*-$(Bn)_2$-Ala(Br)-OMe (**283**), followed by selective benzyl deprotection using

ammonium cerium (IV) nitrate. The use of this reagent for selective deprotection of one benzyl group on di-benzyl protected molecules was published in 2000 by Bull *et al.*[32] Whilst traces of the desired product (**289**) could be observed by LCMS, this method largely failed, resulting in a mixture of unidentified products.

Finally, Bn-Ala(Br)-OMe (**289**) was successfully synthesised by first making a doubly-protected (Boc, Bn) serine derivative (**295**) (**Scheme 3.33**). This was then brominated, followed by deprotection of the Boc group with TFA. The desired product (**289**) was afforded in a 10% overall yield.

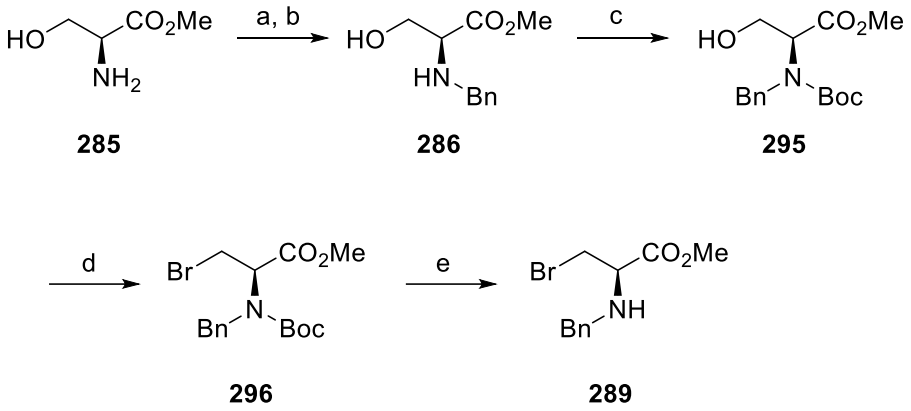

Scheme 3.33: Successful route for the synthesis of Bn-Ala(Br)-OMe (**289**); reagents and conditions: a) benzaldehyde, TEA, anhydrous MeOH, 1.5h, rt; b) $NaBH_4$, 0°C, 2 h, 33% across two steps; c) Boc_2O, TEA, THF, 16 h; d) NBS, PPh_3, THF, 0 °C, 20 h, 30% across two steps; e) TFA, DCM, 16 h, quant.

However, when the mono-benzyl bromoalanine substrate (**289**) was subjected to the Ni-catalysed electrochemical coupling conditions, the expected product was not formed. Instead, the benzyl group itself appeared to have coupled to the aryl bromide resulting in the formation of **297** (**Scheme 3.34**). The identity of this product was established by examination of LCMS data, alongside a comparison of the ^1H- and ^{19}F NMR spectra to published data.[33]

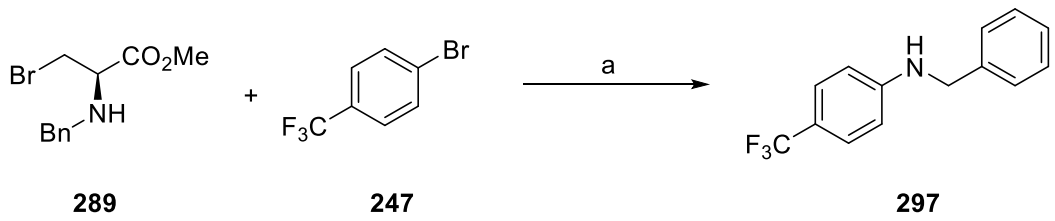

Scheme 3.34: Unwanted transamination of 4-bromobenzotrifluoride (**247**) to form *N*-benzyl-4-(trifluoromethyl)aniline (**297**); reagents and conditions: a) $[Ni(bpy)_3]Br_2$, DBU, $^nBu_4NBr$, DMA, 3 mL, 4 mA, 10 h, RVC (+) Ni foam (-), 54%.

This unexpected transformation was interesting, as the cleavage of the C-N bond is fairly difficult (C-N ΔHf_{298} = 770 kJ/mol) and amination of the aryl halide to form an *N*-arylated product is an example of the well-studied Buchwald-Hartwig reaction.[34] Electrochemical amination of aryl halides using secondary amines has been published previously (**Scheme 3.35**),[35] but these kinds of reactions do not usually involve the loss of an alkyl group from the amine starting materials.

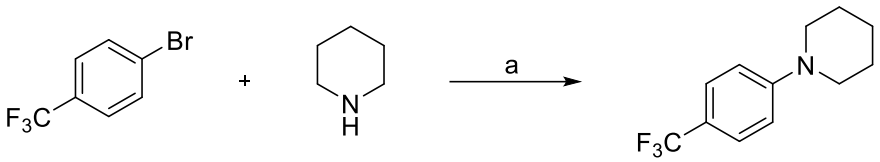

247 **298** **299**

Scheme 3.35: Electrochemical Buchwald-Hartwig-type amination of aryl halides by Li *et al.*;[35] Reagents and conditions: $NiBr_2$ ·glyme (10 mol%), dtbbpy (10 mol%), DMA (0.1 M), LiBr (4 equiv), RVC anode, Ni cathode, 4 mA, 0.2 mmol scale, RT, 4.5 h, 72%.

It was thought that alkene formation might be avoided if the bromo-alanine substrate was formed *in situ* in a similar manner to the work of Li *et al.* (see **Scheme 3.12**).[19] This procedure used an Appel reaction *in situ* to convert an alcohol to the active alkyl bromide, which could then participate in a Ni-catalysed coupling reaction. The authors note that when an alkyl bromide was used in place of the alcohol substrate, the alkene elimination product was overwhelmingly formed.

Therefore, it was thought that perhaps a serine derivative could be tosylated, and converted to a bromoalanine derivative *in situ* by reaction with the LiBr electrolyte. First, Boc-Ser(O-Ts)-OMe (**300**) was synthesised from Boc-Ser-OMe (**26**) using TsCl (**Scheme 3.36**).

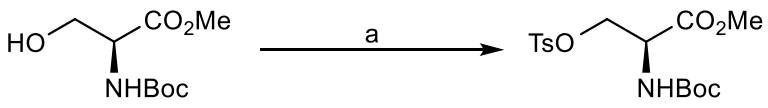

26 **300**

Scheme 3.36: Tosylation of Boc-Ser-OMe to form *N*-Boc-*O*-Ts-Ser-OMe (**300**); reagents and conditions: a) *p*-TsCl, pyridine, 0 °C, N_2, 8 h, then Et_2O added and stirred 14 h, 50%.

This compound (**300**) was then reacted under the same Ni-catalysed coupling conditions used in **Entry 7** (**Table 3.2**). The desired product peak was observed in the LCMS (*m/z* 248), along

with bromo-alanine (**27**) (*m/z* 282) and the usual alkene (**249**) (*m/z* 102). The use of the tosylate did not appear to be an effective strategy for avoiding alkene formation.

However, the transformation of tosylate to alkyl bromide is known to be dependent upon the solvent the reaction is performed in.[36] Cahiez *et al.* report that conversion of tosylates to alkyl bromides proceeds with a higher yield and lowered alkene formation in THF when compared to DMF. It was thought that the tosylate to bromide reaction may work more efficiently if the DMA solvent used was exchanged for a less-polar option.

As THF is fairly volatile and may evaporate over the course of a 10 h reaction, it was thought that dioxane might be a suitable alternative. Unfortunately, when this reaction was repeated using dioxane the resistance was too high, due to the inability of dioxane to dissolve the electrolyte (LiBr). Replacing LiBr with $^{t}Bu_4NBr$ did not improve the resistance, so this idea was abandoned.

Placing a tosyl group on the amine was also considered, as the nature of the amine protecting group has been shown to have the most significant impact on the reaction outcome thus far. Therefore, *N*-Ts-Ala(Br)-OMe (**302**) was synthesised in two steps from serine methyl ester hydrochloride (**285**) (**Scheme 3.37**).

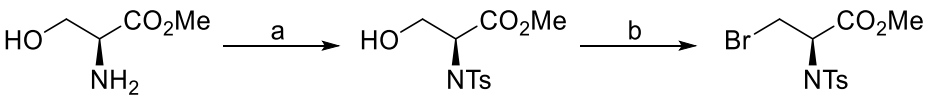

285 **301** **302**

Scheme 3.37: Installation of an *N*-tosyl protecting group on serine methyl ester, followed by Appel bromination; reagents and conditions: a) TsCl, Et_3N, DCM (anhyd.), Ar, 0 °C, 12 h, 85%; b) NBS, PPh_3, THF, 0 °C, 20 h, 41%.

When the *N*-tosyl substrate (**302**) was subjected to the Ni-catalysed coupling reaction, the desired product was not isolated, although traces were observed in the LCMS. Instead, the major product of the reaction appeared to be a β-alanine derivative (**303**) (**Scheme 3.38**). This was confirmed through a comparison of product ^{1}H- and COSY NMR spectra to existing data.[33]

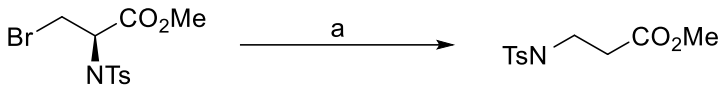

302 **303**

Scheme 3.38: Electrochemical Ni-catalysed conversion of an *N*-tosyl bromoalanine derivative (**302**) to a β-alanine derivative (**303**); reagents and conditions: a) 4-bromobenzotrifluoride, $NiCl_2$.glyme, dtbbpy, LiBr, DIPEA, 3 mA, 4 mL, 10 h, rt, Ar, C (+) Ni (-), undivided cell, 54%.

It is unclear what the exact mechanism of this transformation could be. The *N*-tosyl group may behave similarly to the *N*-benzyl group by permitting aziridine formation, which could subsequently undergo ring-opening hydroamination on reaction with cathodically generated H_2 gas (**Scheme 3.39**).

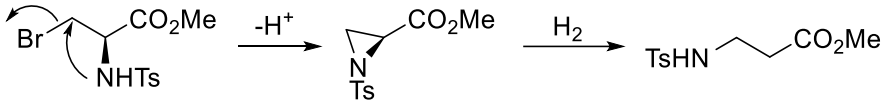

302 **304** **303**

Scheme 3.39: Possible mechanistic explanation for the isolation of a β-alanine derivative (**303**); initial aziridine formation followed by ring-opening with cathodically generated H_2.

Takeda *et al.* have reported isolation of the same β-alanine compound (**303**) from the serine-derived aziridine (**304**) when trying to perform Suzuki-Miyaura ring-opening arylation of aziridines,[37] which suggests that hydroamination is possible under similar conditions. Alternatively, the reaction may proceed through an alkene intermediate.

Given that the conversion of alkyl tosylates to alkyl bromides without incurring alkene formation is solvent-dependent, it was thought that running the Ni-catalysed coupling reaction of alkyl bromides in different solvents may have an impact on the product composition. **Table 3.4** displays the conditions attempted to explore this notion.

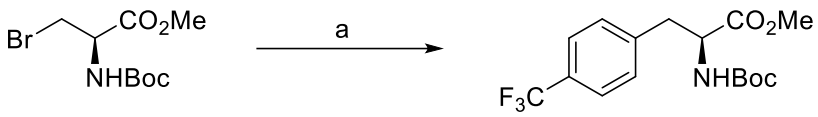

27 **248**

Entry	Conditions (deviation from a)
1	DMSO as solvent
2	DME (solvent) + $^{n}Bu_4NBr$ (electrolyte)
3	Dioxane (solvent) + $^{n}Bu_4NBr$ (electrolyte)
4	Dioxane/propylene carbonate (solvent) + LiFSI
5	DME (solvent) + 12-crown-4 (additive)

Table 3.4 Exploration of different reaction solvents for Ni-catalysed coupling. All entries resulted in formation of alkene **249** as the major product (determined by LCMS); reagents and conditions: a) 4-bromobenzotrifluoride, $NiCl_2$.glyme, dtbbpy, LiBr, DIPEA, 3 mA, 4 mL, 10 h, rt, Ar, C (+) Ni (-), undivided cell.

Non-polar solvents like dioxane and DME required alternative electrolytes or polar additives like propylene carbonate, as it was difficult to ensure electrolyte dissolution. However, none of these conditions had a significant impact on the reaction outcome.

It was assumed that the prevalent alkene formation was due to an E1cB mechanism, and thus dependent on the strength of the base present in the reaction mixture. Therefore, the Ni-catalysed coupling reaction was attempted with several different weak bases. **Table 3.5** displays the range of bases used and the subsequent reaction outcomes.

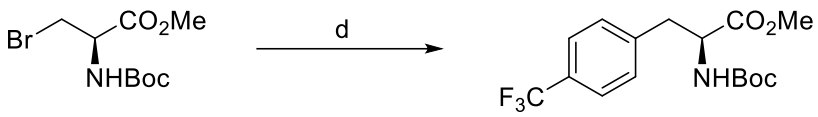

27 **248**

Entry	Base	pK_{aH}[a]	Outcome[c]
1	None	n/a	Starting material only
2	DIPEA	8.5	Alkene **249** + starting material + product (**248**)
3	DBU	13.9	Alkene **249** + starting material + product (**248**)
4	MeOH[b]	e	Starting material only
5	Na_2CO_3	e	See **Entry 1, Table 3.1** (**251, 252**)
6	K_2PO_4	e	See **Table 3.5**, entry 5 (**251, 252**)
7	2,4,6-collidine	7.5	Starting material + product (**248**) + bialkane **262**
8	Pyridine	3.4	Starting material + product (**248**) + bialkane **262**
9	2,6-di-^{t}Bu-pyridine	0.8	Starting material + product (**248**) + bialkane **262**
10	Imidazole	6.26	Alkene **249** + starting material + product (**248**) + bialkane **262**

Table 3.5: Bases attempted in the Ni-catalysed coupling reaction and the associated reaction outcomes; a = pK_{aH}(DMSO) values previously reported.[38–41] b = 20% v/v in DMA, electrogenerated MeO^-; c = The presence of substances in the product mixture was confirmed using TLC, LCMS, ^{1}H- and ^{19}F NMR; d) 4-bromobenzotrifluoride, $NiCl_2$.glyme, dtbbpy, LiBr, base, 3 mA, 4 mL, 10 h, rt, Ar, C (+) Ni (-), undivided cell; e = no data available.

These experiments showed a clear link between base strength and alkene generation. Stronger bases like DBU and DIPEA (**Table 3.5, Entries 2** and **3**) caused the alkene (**249**) to be produced as the major product, whilst weaker bases like those in the pyridine family (**Table 3.5, Entries 7, 8,** and **9**) did not permit alkene formation. Imidazole is a slightly stronger base than pyridine, but the use of this base still yielded alkene product.

It is possible to use a methanol additive to act as an electrogenerated base; [42] a proton can be abstracted at the cathode, generating an alkoxide ion. Unfortunately, when 20% MeOH was used as an additive (**Table 3.5, Entry 4**), the Ni-catalysed coupling reaction did not take place. The reaction also did not proceed when no base was used (**Table 3.5, Entry 1).**

Interestingly, when inorganic bases like Na_2CO_3 and K_2HPO_4 were used, the major products were bromo- and dibromo-substituted alkenes (**251, 252**) (**Table 3.5, Entries 5** and **6**). Both of these did not properly dissolve in the DMA solvent; the heterogeneity of the reaction mixture may have contributed to these products.

Despite the lack of alkene formation when using weaker bases like pyridine, the conversion to the product (**248**) was minimal (~ 6% by ^{1}H NMR). However, this may be due to competitive

biaryl (**253**) formation. The aryl bromide may be preferentially reacting with itself, leaving no aryl substrate left to couple with the comparatively less reactive alkyl bromide. This explains why bialkane (**262**) formation is observed.

To try and prevent biaryl formation, a reaction was run in which the aryl bromide was exchanged for an aryl chloride (**305**) (**Scheme 3.40**). Aryl chlorides are less reactive than aryl bromides, so the reactivities of the aryl and alkyl components should be more evenly matched. Pyridine was used as the base to establish whether the weakness of the base or the hyper-reactivity of the aryl bromide was the limiting factor for this reaction.

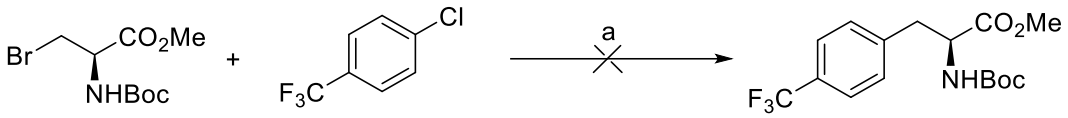

27 **305** **248**

Scheme 3.40: Attempted Ni-catalysed coupling of β-bromoalanine **27** and 4-chlorobenzotrifluoride (**305**): reagents and conditions: $[Ni(bpy)_3]Br_2$ (10 mol%), pyridine, $^nBu_4NBr$, DMA, rt, 4 mA, (+) RVC (-) Ni foam.

Unfortunately, only starting material and bialkane **262** were observed in the LCMS of the crude product mixture. TLC analysis suggested that biaryl **253** was the major product. This indicated that the lowered reactivity of the aryl chloride was not permitting efficient reaction between the aryl and alkyl components. Due to time restraints, no further work was undertaken in this area.

3.3.4 Other Ni-catalysed transformations

Electrochemically-assisted nickel catalysis has recently been used to couple aryl halides and thiols to generate *S*-arylated products. In 2019, the Mei group and the Wang group published similar procedures detailing the Ni-catalysed, electrochemical coupling of aryl halides with both alkyl and aryl thiols.[43,44]

An example of the *S*-arylation reaction is displayed below in **Scheme 3.41**.

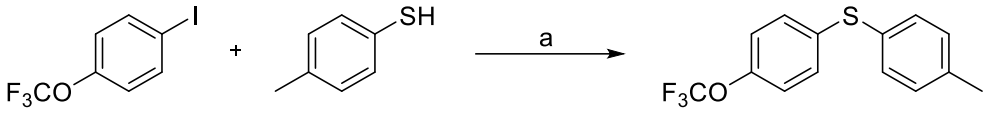

306 **307** **308**

Scheme 3.41: Electrochemical Ni-catalysed Ullmann-type thiolation of aryl iodides;[44] reagents and conditions: a) $NiCl_2$.glyme (10 mol%), dtbbpy (15 mol%), pyridine, DMA (4 mL), LiBr, undivided cell, rt, Ar, 12 h, 92%.

The conditions used in these types of reactions were very similar to our conditions developed for aryl/alkyl bromide coupling (See **Section 3.3.3**). By exchanging the alkyl bromide component for a thiol, it was thought that *S*-arylation of cysteine may be achieved. This would provide access to a range of novel *S*-arylated amino acid derivatives

The electrochemical Ni-catalysed *S*-arylation of Boc-Cys-OMe (**276**) was therefore attempted using the same conditions as for the aryl/alkyl bromide coupling (**Scheme 3.42**).

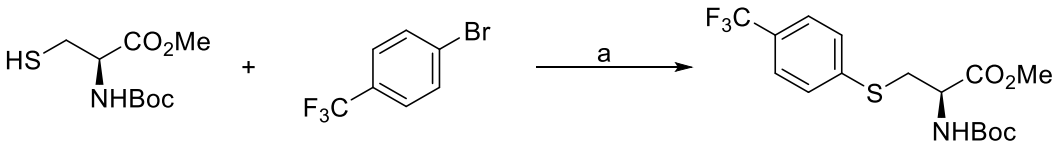

276 **247** **280**

Scheme 3.42: Electrochemical Ni-catalysed *S*-arylation of Boc-Cys-OMe (**276**); reagents and conditions: a) $NiCl_2$.glyme, dtbbpy, DIPEA, DMA, 4 mL, 3 mA, N_2, 10 h, C (+) Ni (-), undivided cell, 35%.

This reaction worked successfully, with **280** isolated in a yield of 35%. Unfortunately, work detailing the electrochemical *S*-arylation of cysteine-containing peptides was published in 2023 by Messaoudi and coworkers using similar conditions while we were developing our approach.[45]

The *S*-arylation reaction was also explored using di-cysteine as the substrate. Di-cysteine (**309**) was synthesised using hydrogen peroxide and catalytic NaI (**Scheme 3.43**).

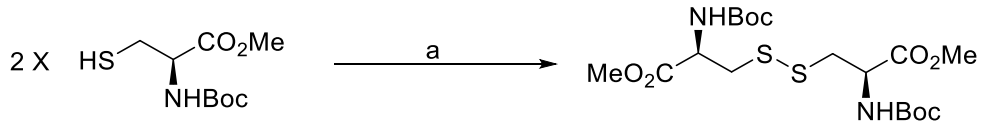

276 **309**

Scheme 3.43: Formation of di-cysteine **309** from two cysteine molecules; reagents and conditions: a) H_2O_2, NaI (cat.), EtOAc, 0.5 h, rt, quant.

It was found that the Ni-catalysed *S*-arylation reaction was also successful when using the cystine substrate (**309**) (**Scheme 3.44**). This could be due to the initial cathodic reduction of the disulfide to form Boc-Cys-OMe (**276**), which can then undergo *S*-arylation. Scission of disulfide bonds has been proven to take place under electrochemical conditions.[46]

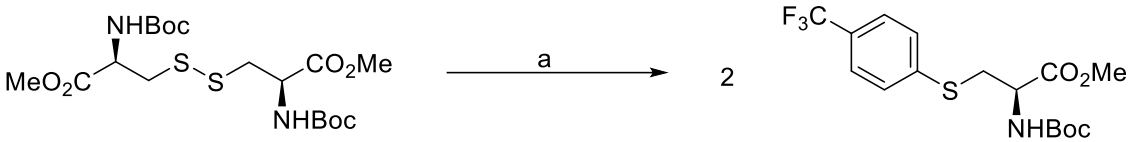

309 **280**

Scheme 3.44: Disulfide cleavage and subsequent Ni-catalysed *S*-arylation of cystine **309** under electrochemical conditions; reagents and conditions: $NiCl_2$.glyme, dtbbpy, DIPEA, DMA, 4 mL, 3 mA, N_2, 10 h, C (+) Ni (-), undivided cell, 31%.

An alternative explanation for this transformation is that the disulfide itself is an efficient coupling partner. In 2004, Taniguchi published a non-electrochemical procedure for the nickel-catalysed coupling of disulfides and aryl iodides (**Scheme 3.45**).[47] The author proposes that a Ni^0 species generated from the reduction of $NiBr_2$ by zinc is able to insert into the S-S bond. A similar event may be taking place in the reaction displayed in **Scheme 3.44**, except the reduction of Ni^{II} to Ni^0 instead takes place at the cathode.

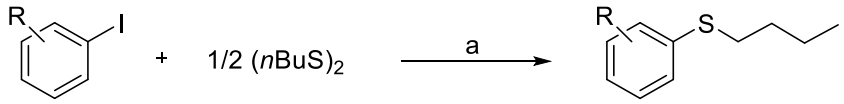

310

Scheme 3.45: Ni-catalysed reaction of disulfide compounds with aryl iodides using Zn as the reductant;[47] reagents and conditions: a) $NiBr_2$.bpy (10 mol%), Zn (2 equiv.), DMF, 110°C, 48 h.

Further investigation into this disulfide/aryl halide coupling is required, but it could potentially be a milder and 'greener' alternative to Taniguchi's reaction, which necessitates a high reaction temperature, a zinc reductant, and a long reaction time.

Given the success of the cysteine *S*-arylation reactions, it was thought that other amino acids may be suited to the Ni-catalysed arylation. *N*-arylation of lysine derivatives was therefore also explored using conditions developed by Kawamata *et al.* for aryl amination using amino acid esters (**Scheme 3.46**).[48]

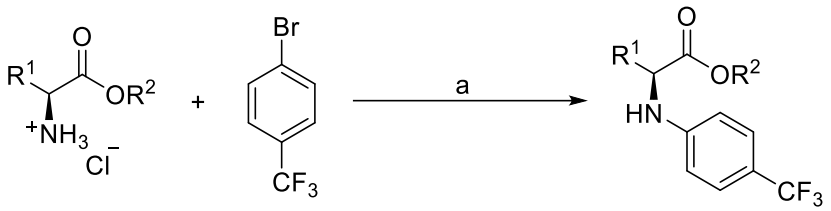

247

Scheme 3.46: Reductive amination of aryl bromides using amino acid esters developed by Kawamata *et al.*[48]; reagents and conditions: a) $[Ni(bpy)_3]Br_2$ (10 mol%), DBU, $^nBu_4NBr$, DMA, rt, 4 mA, (+) RVC (-) Ni foam, 47-70%.

Kawamata *et al.* performed the amination using the α-amine group on a range of amino acids. It was thought that the alternative use of the distal amine group on lysine derivatives may be useful for synthesising novel *N*-arylated lysine derivatives or in the context of peptide stapling. Therefore, a reaction was set up using *N*-Boc-Lys-OMe acetate salt (**311**) and 4-bromobenzotrifluoride (**312**) (**Scheme 3.47**).

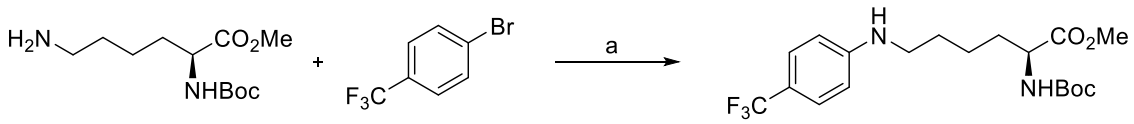

311 **247** **312**

Scheme 3.47: Electrochemical Ni-catalysed *N*-arylation of Boc-Lys-OMe (**311**) using 4-bromobenzotrifluoride (**247**); reagents and conditions: $[Ni(bpy)_3]Br_2$ (10 mol%), DBU, $^nBu_4NBr$, DMA, rt, 4 mA, (+) RVC (-) Ni foam.

The $[Ni(bpy)_3]Br_2$ catalyst was synthesised according to Kawamata *et al.* by the reaction of $NiBr_2.3H_2O$ and 3 equivalents of bipyridine in methanol, affording a pink crystalline solid. The Ni-catalysed arylation was successful, producing the desired *N*-arylated product (**312**). This was confirmed by analysis of the ^1H- and ^{19}F NMR spectra, along with LCMS data. However, this compound could not be fully characterised due to the presence of impurities.

The idea behind developing successful Ni-catalysed *N*-and *S*-arylation procedures was that cysteine and lysine residues in a larger peptide could be linked together using a 1,4-dibromoaryl moiety. To this end, the Kawamata *N*-arylation conditions were applied to Boc-Cys-OMe (**276**) (**Scheme 3.48**).

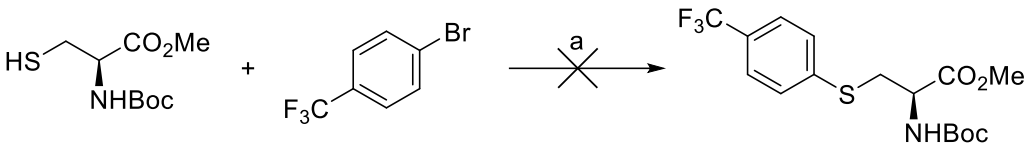

276 **247** **280**

Scheme 3.48: Electrochemical Ni-catalysed *S*-arylation of Boc-Cys-OMe (**276**); reagents and conditions: a) $[Ni(bpy)_3]Br_2$ (10 mol%), DBU, $^nBu_4NBr$, DMA, rt, 4 mA, (+) RVC (-) Ni foam.

Unfortunately, the reaction did not yield the desired *S*-arylation product. It was hoped that peptide stapling experiments may still be carried out using a model peptide with two lysine residues (**313**) (**Scheme 3.49**), but this was ultimately abandoned due to lack of time.

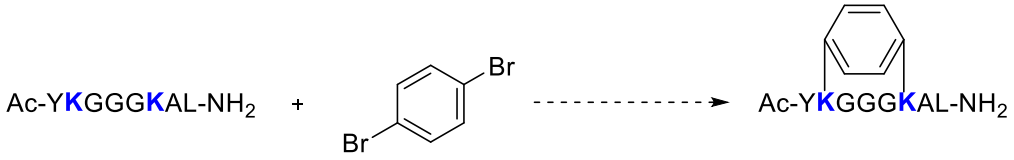

313 **314** **315**

Scheme 3.49: Proposed electrochemical peptide stapling using a dibromoaryl substrate (**314**) as a bridge between two lysine residues in a linear peptide.

3.4 Pd-catalysed acetoxylation of amino acid substrates

3.4.1 Previous work in the field of Pd-catalysed electrosynthesis

The integration of Pd-catalysis with electrochemistry has been a relatively recent development in organic synthesis, with one of the first instances of this type of reaction being published in 2007 by Amatore *et al.* (**Scheme 3.50**).[49]

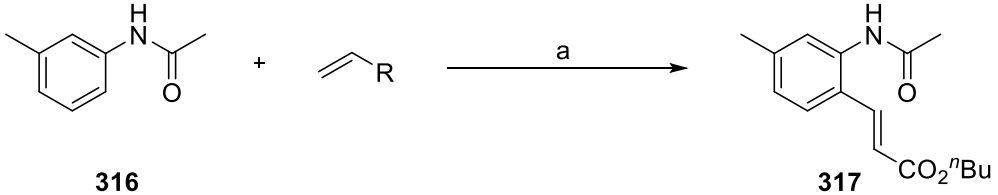

316 **317**

Scheme 3.50: Electrochemically-assisted Pd-catalysed Heck type reaction between arenes and alkenes;[49] reagents and conditions: a) $Pd(OAc)_2$ (10 mol%), benzoquinone (10 mol%), $^nBu_4NBF_4$ (0.3 M), AcOH, divided cell, C (+) Ni (-), 0.8V (vs. SCE), 78%.

The authors propose that initial activation of the aryl C-H bond is facilitated by weak coordination of the Pd^{II} centre to the amide oxygen and formation of a 6-membered palladacycle. This species may then react with the olefin *via* a carbopalladation mechanism. β-hydride elimination then furnishes the desired product.

Another example of a Pd-catalysed electrosynthetic procedure is shown in **Scheme 3.51**.[50] The Mei group successfully performed alkylation on a range of aryl substrates *via* reaction with alkyltrifluoroborate compounds, building on their earlier work involving methylation of ketoximes using organoboron reagents.[51] Interestingly, the reaction was successful using a simple undivided cell.

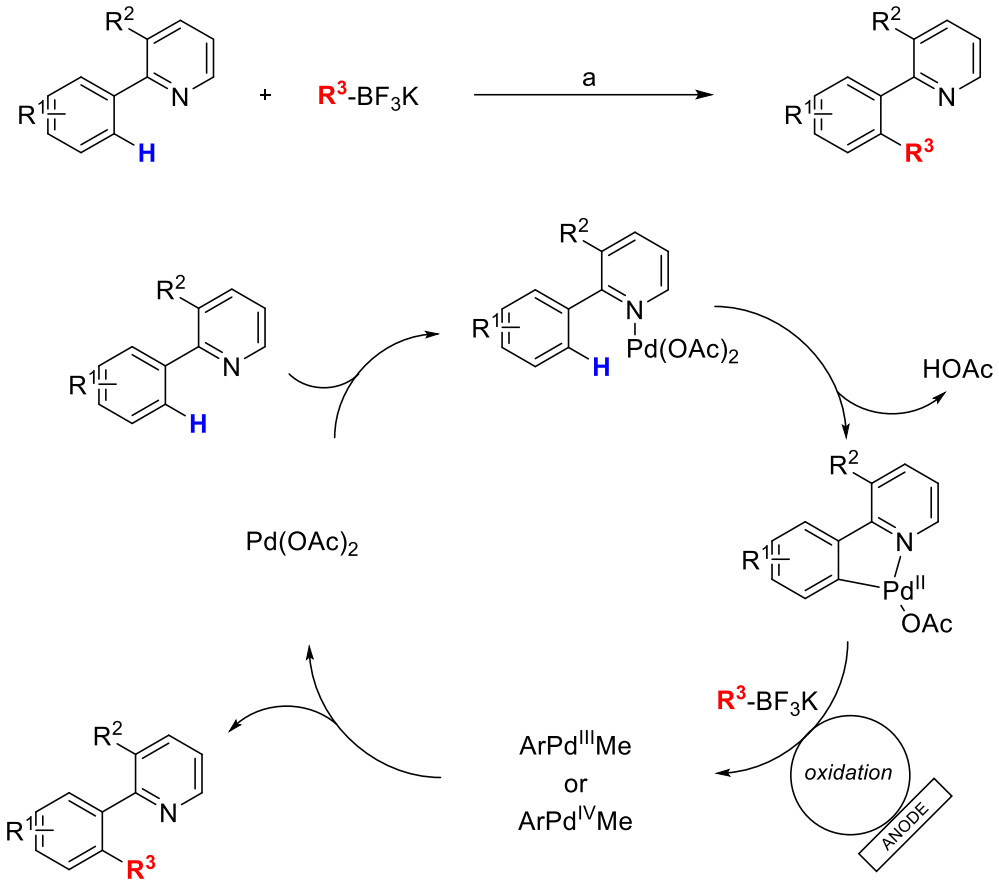

Scheme 3.51: Pd-catalaysed electrochemical alkylation of arenes using alkyltrifluoroborates;[50] reagents and conditions: a) $Pd(OAc)_2$ (10 mol%), TFE/AcOH/H_2O (4:4:1, 4.5 mL), undivided cell, Pt (+) Pt (-), 60 °C, 1.0 mA, 18−36 h, 20-74%. The mechanism proposed by Yang *et al.* is also provided.

In this reaction, the Pd centre is purported to coordinate to the nitrogen of the pyridyl moiety and insert itself into the CH bond, forming a five-membered palladacycle. The palladacycle may then be oxidised at the anode to form either a Pd^{III} or Pd^{IV} species, which subsequently

undergoes alkylation and reductive elimination to afford the desired product. One of the benefits of using electrochemistry to control the Pd catalytic cycle is that both Pd^{0}/Pd^{II} and $Pd^{II}/Pd^{III/IV}$ pathways can be accessed through careful selection of the applied potential.

Whilst there are a decent number of published precedents for Pd-catalysed electrochemical modification of sp^2 carbons, protocols for sp^3 modification are much scarcer. An example of successful Pd-catalysed electrochemical modification of sp^3 carbons in shown in **Scheme 3.52**. The Sanford group achieved Pd-catalysed electrochemical acetoxylation of a range of different substrates with both sp^2 and sp^3 carbon centres.[52]

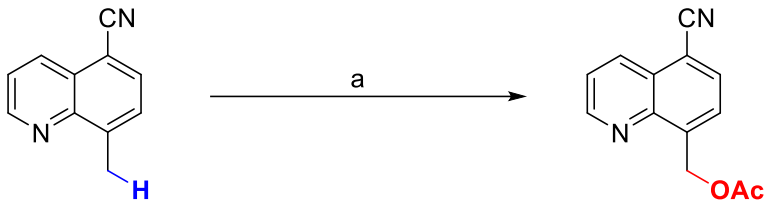

318 **319**

Scheme 3.52: Electrochemical acetoxylation of sp^3 carbons catalysed by palladium. A range of substrates were acetoxylated in this paper, using a range of directing groups. Acetoxylation was achieved using substrates with benzylic sp^3 carbons, unactivated sp^3 carbons, and sp^2 carbons;[52] reagents and conditions: a) $Pd(OAc)_2$ (10 mol%), benzoquinone (0.1 M), TMAOAc (0.5 M), AcOH/MeCN (1:4 v/v), 8 mA, 6 h, 75 °C, C (+) C (-), 75%.

The substrates investigated in this paper had a variety of different directing groups, including pyridyl, pyrazole, and oxime ether moieties. Acetoxylation was performed successfully at both activated and unactivated sp^3 carbon centres.

Due to the rarity of electrochemical Pd-catalysed C(sp^3)-H activation procedures, further exploration into this area is of interest. It was thought that proteinogenic amino acids, *e.g.* valine, might be suitable substrates for such reactions. An appropriate directing group may be appended onto either the amine or acid functionality, and Pd-catalysed electrochemical acetoxylation may be performed, resulting in synthesis of novel amino acids. Introduction of an acetoxy group to an sp^3 carbon centre on an otherwise unactivated aliphatic amino acid may also be used as a handle for further transformations. The rest of this chapter will describe efforts towards this goal.

3.4.2 Results and discussion

In 2017, Yang *et al.* published a procedure for Pd-catalysed electrochemical oxidation of unactivated sp^3 carbons (**Scheme 3.53**).[53]

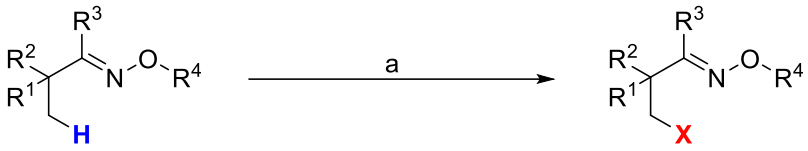

X = OAc, $OCOC_2H_5$, $OCOCF_3$, OTs, OMe, *etc.*

Scheme 3.53: Palladium-catalysed electrochemically-assisted oxidation of sp^3 carbons published by Yang *et al.*[53]; reagents and conditions: a) (when **X** = OAc) $Pd(OAc)_2$, NaOAc, AcOH, 70 °C, 1.5 mA, 12 h, Pt electrodes, divided cell, 18-92%.

The authors used an oxime as a directing group to manage the oxidation of the distal sp^3 centres. The proposed mechanism is shown below in **Scheme 3.54**. The oxime nitrogen is capable of coordinating with the Pd-centre, drawing the catalyst close to the C(sp^3)-H bond. Activation of this C-H bond is then able to take place, resulting in the formation of a five-membered palladacycle. The Pd^{II} species then undergoes anodic oxidation to Pd^{IV}, triggering reductive elimination.

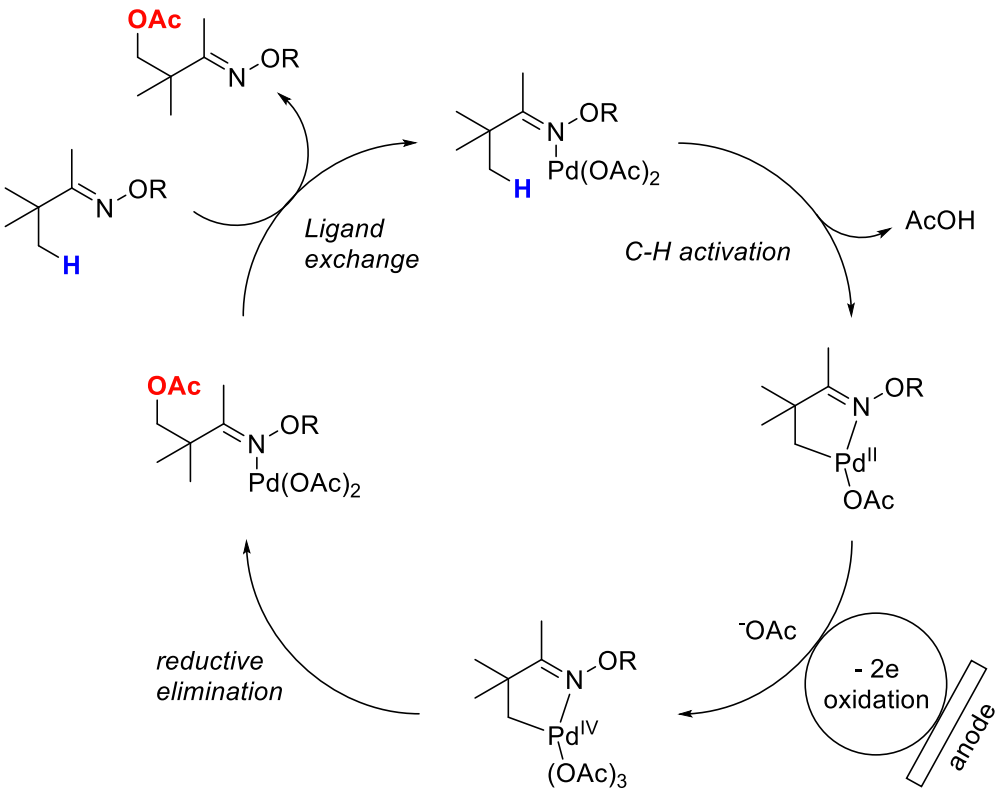

Scheme 3.54: Mechanism proposed by Yang *et al.*[53] for the Pd-catalysed anodic oxidation of oxime derivatives.

It was thought that perhaps a similar setup may be employed for the modification of remote unactivated sp^3 carbons on aliphatic amino acids such as valine and leucine. Initially the idea was to use the amino nitrogen as a handle for a directing group similar to the way in which Yang *et al.* used the oxime functionality. Many works involving C-H activation of distal bonds on aliphatic amino acids utilise a similar directing group strategy.[54] An illustration of this concept is shown in **Figure 3.11**.

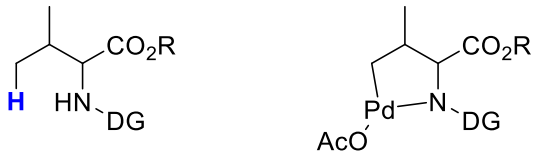

Figure 3.11: (L-R) Proposed valine substrate for Pd-catalysed electrochemical modification with directing group situated on the amino nitrogen; proposed structure for a five-membered palladacycle using this hypothetical substrate.

An oxime functionality cannot be installed into a valine derivative without losing the fundamental amino acid structure, so an alternative directing group was necessary. It was

thought that a directing group incorporating an imine moiety might be suitable. Imines have been known to act as directing groups for palladium catalysed reactions.[55]

Therefore, a valine derivative with an imine functionality was synthesised. First, benzophenone imine (**321**) was generated from benzophenone (**320**) using hexamethyldisilazane and catalytic TBAF. Benzophenone imine (**321**) was then reacted with valine methyl ester hydrochloride (**95**) to produce the desired valine imine derivative (**322**) (**Scheme 3.55**).

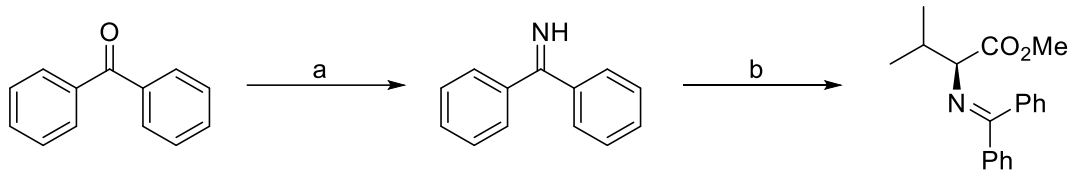

320 **321** **322**

Scheme 3.55: Transformation of benzophenone (**320**) to benzophenone imine (**321**) and subsequent reaction of the latter with valine methyl ester (**95**); reagents and conditions: a) Hexamethyldisilazane, TBAF (10 %), N_2, rt, 6 h, 89%; b) valine methyl ester hydrochloride, N_2, rt, 16 h, 71%.

An undivided cell cannot be used for most Pd-catalysed reactions as the active Pd catalyst will be reduced to Pd^0 (palladium black) at the cathode as soon as it is formed, thereby killing the catalyst.[52] A divided cell must therefore be used. An initial attempt to acetoxylate this substrate (**322**) using conditions similar to the protocol used by Yang *et al.* resulted in immediate deprotection of the imine protecting group upon reaction with the acetic acid used as solvent (**Scheme 3.56**), as determined by TLC.

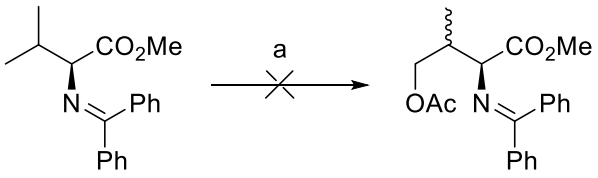

322 **323**

Scheme 3.56: Failed attempt to acetoxylate valine imine derivative **322**; Reagents and conditions: a) substrate (0.3 mmol), $Pd(OAc)_2$ (10 mol%), NaOAc (0.6 M), AcOH, 70 °C, 1.5 mA, 12 h

It was clear that benzophenone imine was not capable of acting as a directing group under these conditions. The use of acetic acid as the solvent appeared to be essential as a source of $^-$OAc anions; additionally, its high boiling point permits the elevated reaction temperature.

Therefore, alternative directing groups were explored. **Table 3.6** displays the substrates which were synthesised to this end.

Entry	Substrate
1	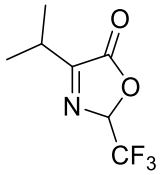 **324**
2	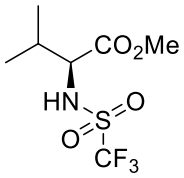 **325**
3	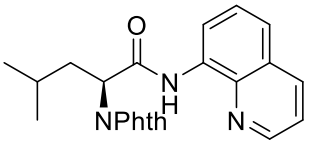 **326**

Table 3.6: Substrates synthesised when exploring different directing groups for Pd-catalysed electrochemical acetoxylation.

First, a cyclic valine derivative (**324**) was synthesised (**Table 3.6, Entry 1**) using trifluoroacetic anhydride (**Scheme 3.57**).

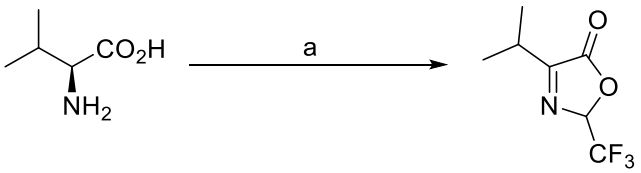

97 **324**

Scheme 3.57: Cyclisation of *L*-valine (**97**) to form compound **324**; reagents and conditions: a) neat TFAA, reflux, 80 °C for 30 mins then 120 °C for 30 mins, 59%

Whilst the cyclisation of valine destroys the stereochemistry, it was thought the introduction of a C=N bond may permit the amino nitrogen to coordinate loosely to the Pd centre, thus acting as a directing group. However, this group also failed to remain intact in the presence of acetic acid when it was trialled as a substrate using the conditions from **Scheme 3.56**. Post-reaction, the oxazolone **324** appeared to have reverted to valine (**97**), as determined by LCMS.

A triflyl-protected valine derivative (**325**) was also synthesised, as previous work has shown that weak σ-coordination between a triflamide nitrogen and a Pd-centre can facilitate distal C-H activation in amino acid derivatives.[56] The conditions used for synthesis of this substrate are shown below in **Scheme 3.58**.

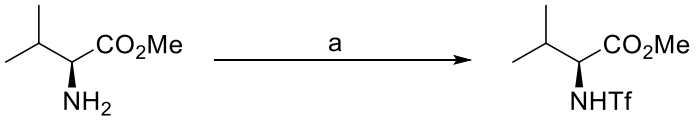

95 **325**

Scheme 3.58: Triflation of valine methyl ester hydrochloride (**95**) to form a triflyl-protected valine derivative (**325**); reagents and conditions: a) trifluoromethane sulfonic anhydride, Et_3N, anhydrous DCM, N_2, -78 °C then rt, 20 h, 81%.

When the triflamide substrate **325** was trialled using the Pd-catalysed acetoxylation conditions shown in **Scheme 3.56**, only starting material appeared to be present after the reaction (as observed by LCMS). Jia *et al.* have successfully achieved Pd-catalysed acetoxylation of triflamide derivatives under non-electrochemical conditions using 2,6-lutidine as a ligand;[57] however, a second attempt at electrochemical acetoxylation with additional lutidine as a ligand also failed to yield the desired product. Therefore, the triflamide substrate was rejected for future investigations.

Finally, a quinoline-substituted amino acid derivative was synthesised (**326**). This was obtained by initially installing a phthalimide protecting group on the amino functionality, followed by conversion to an acyl chloride (**329**) using $SOCl_2$ (**Scheme 3.59**). Acyl chloride **329** is then reacted with 8-aminoquinoline (**330**) to produce quinolinamide **326**.

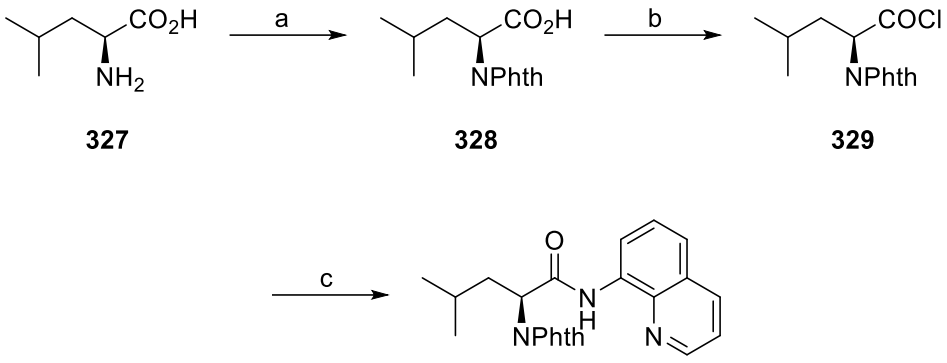

327 **328** **329**

326

Scheme 3.59: Synthesis of leucine-derived quinolinamide **326**; reagents and conditions: a) Phthalic anhydride, 170 °C, vacuum, 3 h, quant.; b) $SOCl_2$, toluene, reflux, 20 h; c) 8-aminoquinoline (**330**), Et_3N, anhydrous DCM, 0 °C, 20 h, 72% cross two steps.

The use of quinoline-derived directing groups in Pd-catalysed C-H activation of aliphatic amino acids has been well-studied.[58–60] Aminoquinolines are competent directing groups because they are bidentate and thus able to coordinate more effectively to metal centres. Leucine quinolinamide **326** was synthesised because the aminoquinoline directing group was expected to facilitate acetoxylation at the β-position instead of the γ-position (**Figure 3.12**). It was thought that a valine substrate might prohibit the reaction due to its tertiary β carbon, which may prove too sterically hindered for palladacycle formation.

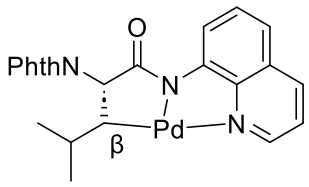

331

Figure 3.12: Proposed palladacycle configuration (**331**) using aminoquinoline leucine derivative **326**.

An initial attempt at the Pd-catalysed acetoxylation reaction was set up (**Scheme 3.60**) with added $Mn(OAc)_2$ as a promoter. This was because Corey *et al.* used this method when performing a similar reaction under non-electrochemical conditions.[59]

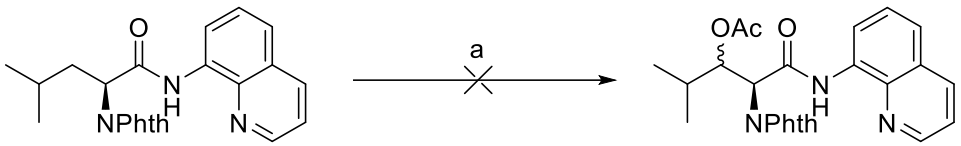

326 **332**

Scheme 3.60: Attempted acetoxylation of a leucine-derived substrate; reagents and conditions: a) $Pd(OAc)_2$ (20 mol%), $Mn(OAc)_2$ (1 equiv.), NaOAc, AcOH (4 mL), 1.5 mA, 12 h, rt

The LCMS analysis of the crude reaction mixture revealed that the starting material was the primary component, but a small amount of another compound with the correct mass ($(M+H)^+$ = 446 *m/z*) was also present. A ^{1}H NMR spectrum taken of the crude product mixture revealed that the starting material and acetoxylated product were present in a 7:3 ratio. Upon closer inspection, it appeared that the acetoxy group had not substituted onto the β-position (**332**), but instead had added to the quinoline ring (**333** or **334**). The ^{1}H NMR spectrum of the product featured resonances corresponding to 10 aliphatic protons, but only 5 resonances corresponding to aromatic protons (6 would be expected). The COSY spectrum indicated that acetoxylation had taken place at either the *ortho* or *para* position (**Figure 3.13**).

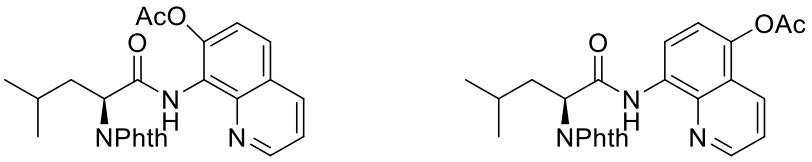

333 **334**

Figure 3.13: Possible structures for the acetoxylated quinoline product; (L-R) *ortho*-substituted (**333**), *para*-substituted (**334**).

Despite the lack of success in generating a β-acetoxylated product, several reaction conditions were attempted using this substrate (**Table 3.7**).

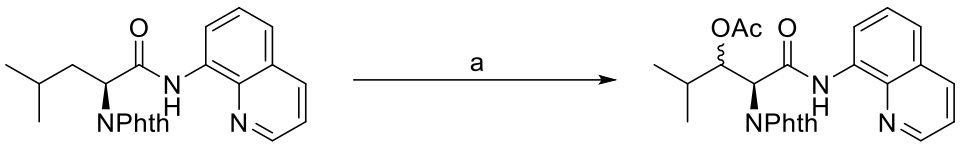

326 **332**

Entry	Deviation from (a)	Outcome[b]
1	At 80 °C instead of rt	Starting material
2	At 80 °C + benzoquinone (2 eq.)	Traces of two acetoxylated products
3	No $Mn(OAc)_2$, 80 °C	Trace of an acetoxylated product
4	Benzoquinone (0.1 M in cathodic chamber)	Traces of three acetoxylated products
5	Ac_2O (10 eq.) in AcOH/MeCN (1:4)	Traces of three acetoxylated products
6	TMAOAc instead of NaOAc, AcOH/MeCN (1:4), 8 mA	Traces of two acetoxylated products

Table 3.7: Various conditions attempted for the electrochemical acetoxylation of **326**; reagents and conditions: a) $Pd(OAc)_2$ (20 mol%), $Mn(OAc)_2$ (1 equiv.), NaOAc, AcOH (4 mL), 1.5 mA, 12 h, rt; b = As determined by LCMS of the crude product mixture.

None of the reaction conditions employed (**Table 3.7**) seemed to significantly influence the outcome of the reaction. The composition of the product mixture in each entry displayed in **Table 3.7** was assessed using TLC and LCMS. It was thought that heating the reaction to 80°C (**Table 3.7, Entries 1-3**) would be beneficial, as many Pd-catalysed acetoxylation protocols involve heating the reaction. However, this did not seem to make much of an impact.

The use of benzoquinone (BQ) as an additive has been employed by Shrestha *et al.*,[52] who used it as an electrochemically-recyclable oxidant. Whilst using a divided cell hypothetically means that the Pd-catalyst cannot be reduced by the cathode, it is possible that cathodically-generated species (*e.g.*, H_2) may be able to traverse the frit and reduce the catalyst to Pd^0. BQ is used in the cathodic chamber to prevent this process from happening. However, when this was used on the leucine-derived substrate (**Table 3.7, Entries 2-4**), it failed to elicit any significant change.

Despite the low current used in this reaction (1.5 mA), the voltage was often extremely high. This is probably due to the NaOAc electrolyte dissolving poorly in the solvent. An alternative

electrolyte with an acetate anion (tetramethylammonium acetate, TMAOAc) was trialled (**Table 3.7, Entry 6**), so that a higher current may be applied whilst preserving conductivity. TMAOAc has been used previously in electrochemical Pd-catalysed acetoxylation reactions.[61] Unfortunately the reaction conditions described in Entry 6 (**Table 3.7**) were unsuccessful.

Following this, a new substrate was synthesised. Fan and Ma published a protocol for the arylation and acetoxylation of amino acid derivatives utilising a bidentate 2-methoxyiminoacetyl (MIA) directing group.[62] Therefore, a valine derivative with a MIA directing group attached (**337**) was synthesised (**Scheme 3.61**).

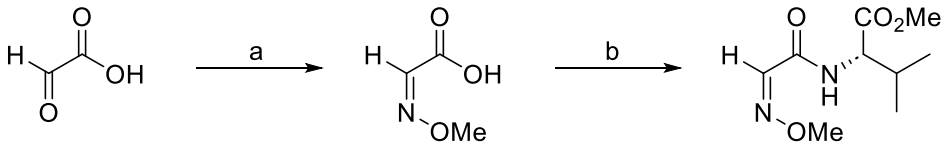

335 **336** **337**

Scheme 3.61: Synthesis of a MIA-valine derivative (**337**); reagents and conditions: a) methoxyamine hydrochloride, pyridine/MeOH (1:1), argon, rt, 1 h, 42%; b) valine methyl ester hydrochloride, isobutyl chloroformate, *N*-methylmorpholine, anhydrous THF, 0 °C, 20 h, 58%.

With the new MIA-valine substrate (**337**) in hand, a first attempt at Pd-catalysed electrochemical acetoxylation was made (**Table 3.8, Entry 1**). Whilst the majority of the product mixture consisted of starting material, traces of the desired γ-acetoxy product (**338**) were observed by both LCMS and ^{1}H NMR spectroscopy. This result was promising, as it indicated that the MIA directing group was stable under the acetoxylation conditions, and that the transformation was possible even at room temperature.

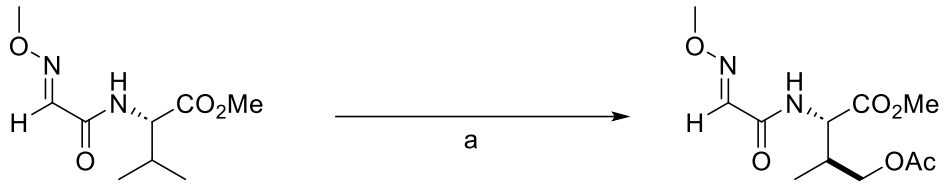

337 **338**

Entry	Deviation from (a)	Yield[c] /%
1	Room temperature	trace
2	None	23[b]
3	1.2 equiv. $Mn(OAc)_2$ added	40
4	TMAOAc instead of NaOAc	trace
5	Pt electrodes	2
6	$Pd(TFA)_2$	0
7	24 h	25[b]
8	10 equiv. Ac_2O added	5
9	70 °C	8
10	$NaNO_3$ (cat.) added	35
11	5,5'-dimethyl bipyridine (30 mol %) added	0
12	1.2 equiv. $MnBr_2.4H_2O$ added	0
13	MnO_2 (10 mol%) added	25

Table 3.8: The acetoxylation of a MIA-protected valine derivative (**338**) using Pd-catalysed electrochemistry; reagents and conditions: a) divided cell, graphite electrodes, 20 mol% $Pd(OAc)_2$, 0.6 M NaOAc in acetic acid (8 mL), 80 °C, 12 h, 1.5 mA; b = isolated yield of **338**; c = % conversion observed by ^{1}H NMR.

The same reaction was then run at 80 °C (**Table 3.8, Entry 2**), resulting in isolation of the desired product (**338**) in a yield of 23%. Given that the catalyst loading was 20 mol%, it was unclear whether catalyst renewal was in fact taking place. However, no Pd-black was observed post-reaction, indicating that the catalyst was still active. The product (**338**) appeared to be a single diastereomer (as observed by ^{1}H NMR), despite the creation of a second stereocentre at the β-carbon. This stereoselectivity is likely a feature of the MIA directing group, as Fan and Ma also observed this effect when performing γ-arylation of a valine-MIA derivative.[62]

The acetoxylation reaction was then run with additional $Mn(OAc)_2$ (1.2 eq.) in the hope that it would again act as an oxidation promoter similarly to the work published by Corey at al.[59] The

addition of the manganese salt did improve the conversion yield (as observed by ^{1}H NMR spectroscopy) (40%, **Table 3.8, Entry 3**). It is possible that the $Mn(OAc)_2$ is acting as a redox mediator; Mn^{II} is oxidised at the anode to Mn^{III}, which can in turn oxidise the Pd-substrate complex.

It was thought that a catalytic amount of an Mn^{II} salt may have the same effect; unfortunately, when 10 mol% of MnO_2 was added (25% ^{1}H NMR conversion, **Table 3.8, Entry 13**) the yield remained similar. The use of $MnBr_2.4H_2O$ (**Table 3.8, Entry 12**) yielded no discernible product (determined by LCMS).

When TMAOAc was used as the electrolyte instead of NaOAc, only traces of the desired product (**338**) were observed by LCMS (**Table 3.8, Entry 4**). This suggests that perhaps the nature of the cation plays a role in the success of the reaction.

Surprisingly, when the graphite electrodes were exchanged for platinum electrodes, the yield of the reaction (as observed by ^{1}H NMR) fell to 2% (**Table 3.8, Entry 5**). In the original work by Yang *et al.*[53], Pt electrodes were used throughout. Platinum is often the first choice for oxidation reactions due to its wide potential range and inertness. It is unusual for replacement of graphite electrodes with Pt electrodes to cause such a significant reduction in yield. However, the Pt electrodes used were Pt-plated copper and a green residue was observed post-reaction. It is possible that copper was interfering in the reaction.

An attempt to exchange the $Pd(OAc)_2$ catalyst for a $Pd(TFA)_2$ catalyst failed to yield any product (**Table 3.8, Entry 6**), as determined by TLC and LCMS. The $Pd(TFA)_2$ catalyst was selected because Yang *et al.*[53] found it to be the second-most efficient catalyst for electrochemical acetoxylation. It is possible that the absence of existing $^-$OAc ligands on the Pd centre disfavours the acetoxylation reaction.

To determine whether the acetoxylation reaction was just particularly sluggish, and would go to completion if a longer reaction time was used, a 24 h reaction was set up, **Table 3.8, Entry 7**). Unfortunately, this did not push the reaction to completion; only a 2% increase in the yield was observed. No Pd black was present after the reaction had taken place, suggesting the catalyst was still active. The results from this trial reaction suggest that either the electrochemical renewal of the active Pd catalyst is not taking place, or the model substrate (**337**) is simply not suited to this reaction.

A reaction with additional acetic anhydride was also run, to establish whether it would be a more effective source of $^-$OAc anions (**Table 3.8, Entry 8**). This addition appeared to hinder the reaction, giving rise to a conversion yield of only 5% (as measured by ^{1}H NMR spectroscopy).

The acetoxylation reaction was then attempted using a lower temperature of 70 °C (**Table 3.8, Entry 9**). This resulted in a yield reduction to 8% (conversion yield as observed by ^{1}H NMR spectroscopy).

Next, a reaction with a catalytic amount of $NaNO_3$ added (**Table 3.8, Entry 10**) was performed. $NaNO_3$ has been used previously as a redox co-catalyst in Pd-catalysed acetoxylations by Sanford *et al.*[63] The addition of sodium nitrate was also beneficial in our acetoxylation reaction, causing the isolated yield to increase to 35%.

A reaction was attempted using a bipyridine ligand to assess whether this would have any impact on the reaction outcome (**Table 3.8, Entry 11**). This modification prohibited any product formation. This is probably due to the ligand occupying too much space around the Pd centre, meaning that the substrate cannot form a palladacycle with it.

To determine whether the relatively low yields of the acetoxylation reaction were due to the unsuitability of the substrate, an analogous *tert*-leucine-MIA derivative (**339**) was synthesised using the same protocol as for the valine substrate (**Scheme 3.62**).

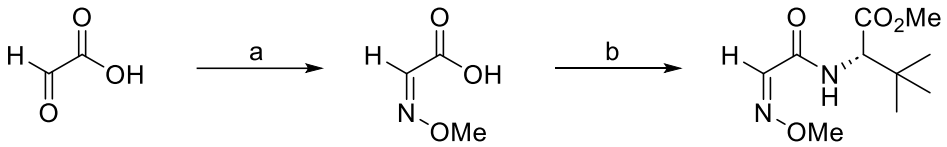

335 **336** **339**

Scheme 3.62: Synthesis of a MIA-*tert*-leucine derivative (**339**); reagents and conditions: a) methoxyamine hydrochloride, pyridine/MeOH (1:1), argon, rt, 1 h, 42%; b) *tert*-leucine methyl ester hydrochloride, isobutyl chloroformate, *N*-methylmorpholine, anhydrous THF, 0 °C, 20 h, 8%.

The additional methyl group at the β-position should reduce the dihedral angle between the β-substituents and facilitate more efficient palladacycle formation. However, when the acetoxylation reaction conditions from **Table 3.8, Entry 2** were applied to the *tert*-leucine substrate (**339**) (**Scheme 3.63**), a similar conversion yield (23%, determined using ^{1}H NMR spectroscopy) was achieved as for the valine substrate.

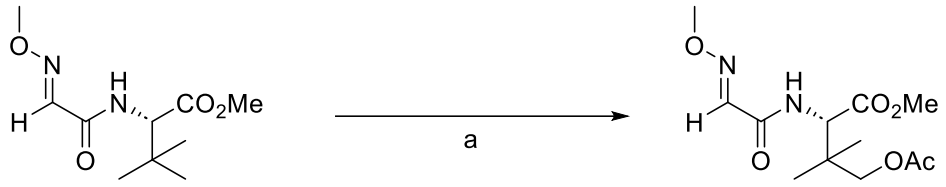

339 **340**

Figure 3.63: The acetoxylation of a MIA-protected *tert*-leucine derivative (**339**) using Pd-catalysed electrochemistry; reagents and conditions: a) divided cell, graphite electrodes, 20 mol% $Pd(OAc)_2$, 0.6 M NaOAc in acetic acid (8 mL), 80 °C, 12 h, 1.5 mA; 23% (^{1}H NMR conversion yield).

In Fan and Ma's work using the MIA auxiliary for arylation and acetoxylation, only two substrates were acetoxylated; MIA-isovaline (**341**), and MIA-(*O*-^{t}Bu)-threonine (**342**) (**Figure 3.14**). Whilst a MIA-valine derivative was synthesised, the authors did not use it for acetoxylation.[62] Therefore, it was decided that one of the two substrates in **Figure 3.14** should be synthesised and subjected to electrochemical acetoxylation. If the yield exceeded ~20%, the previous low yields could be attributed to unsuitable substrates.

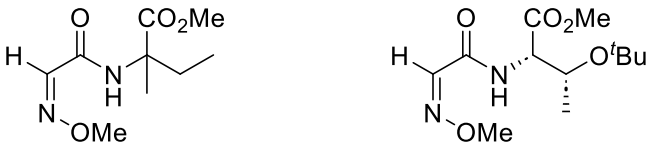

341 **342**

Figure 3.14: Successfully acetoxylated substrates, Fan and Ma;[62] (L-R) MIA-isovaline **341**, MIA-(*O*-^{t}Bu)-threonine **342**.

Therefore, the MIA-(*O*-^{t}Bu)-threonine derivative (**342**) was synthesised (**Scheme 3.64**).

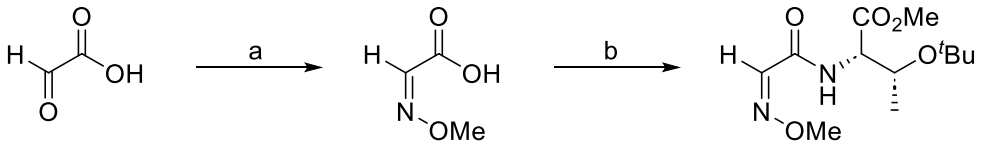

335 **336** **342**

Scheme 3.64: Synthesis of a MIA-(*O*-^{t}Bu)-threonine derivative (**342**); reagents and conditions: a) methoxyamine hydrochloride, pyridine/MeOH (1:1), argon, rt, 1 h, 42%; b) *O-tert*-Butyl threonine methyl ester hydrochloride, isobutyl chloroformate, *N*-methylmorpholine, anhydrous THF, 0 °C, 20 h, 52%.

However, due to issues which arose with the divided cell, the MIA-Thr-(*O*-^{t}Bu)-OMe substrate (**342**) was not subjected to the electrochemical acetoxylation conditions.

3.5 Chapter Summary

A method for Ni-catalysed electrochemical coupling of amino acid derived alkyl bromides and aryl bromides was developed, albeit with a low yield due to an unwanted elimination side-reaction (**Scheme 3.65**). The reaction was found to be most successful when a divided cell was used.

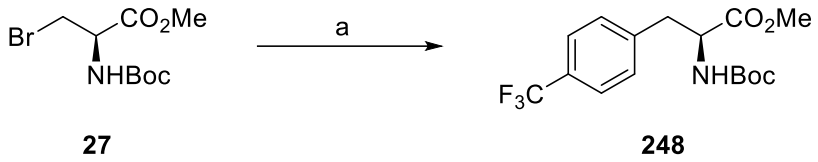

27 **248**

Scheme 3.65: Electrochemical cross-coupling of β-bromoalanine derivative **27** with 4-bromobenzotrifluoride (**247**) to form fluorinated phenylalanine derivative **248**; reagents and conditions: a) $NiCl_2$•dtbbpy (10 mol%), 4-bromobenzotrifluoride, LiBr, DIPEA, anhydrous DMA, 4 mL, Ar, 3 mA, C (+) Ni (-), rt, 10 h, divided cell, 25%.

S-Arylation of cysteine and cystine derivatives was also achieved under the same conditions (**Scheme 3.66**). A Ni-catalysed electrochemical *N*-arylation reaction with a lysine derivative (**311**) also showed promise (**Scheme 3.66**).

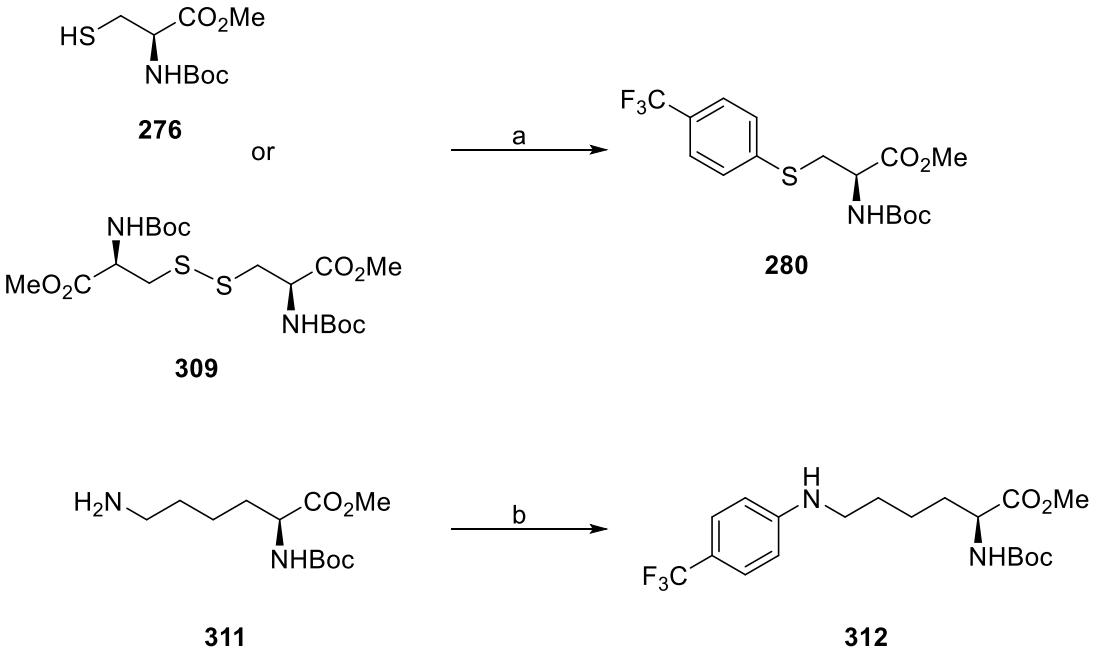

Scheme 3.66: Electrochemical Ni-catalysed *S*-arylation of Boc-Cys-OMe (**276**); reagents and conditions: a) $NiCl_2$.glyme, dtbbpy, DIPEA, DMA, 4 mL, 3 mA, N_2, 10 h, C (+) Ni (-), undivided cell, 35%; b) $[Ni(bpy)_3]Br_2$ (10 mol%), DBU, $^nBu_4NBr$, DMA, rt, 4 mA, (+) RVC (-) Ni foam.

In the second half of the chapter, Pd-catalysed electrochemical acetoxylation of valine derivatives was explored. A methoxyiminoacetic acid-derived directing group was found to be best for facilitating acetoxylation (**Scheme 3.67**).

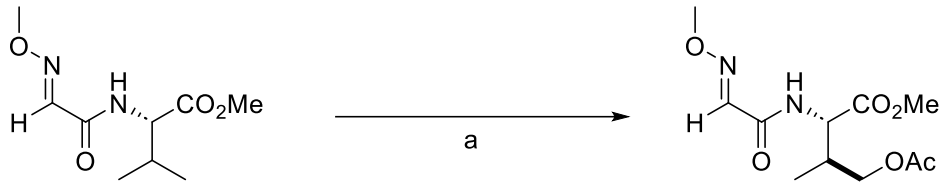

337 **338**

Scheme 3.67: Electrochemical Pd-catalysed acetoxylation of a valine derived substrate (**337**); reagents and conditions: a) divided cell, graphite electrodes, 20 mol% $Pd(OAc)_2$, $NaNO_3$, 0.6 M NaOAc in acetic acid (8 mL), 80 °C, 12 h, 1.5 mA, 35%.

3.6 References

1 W. D. G. Brittain and S. L. Cobb, *Org. Biomol. Chem.*, 2017, 16, 10–20.
2 C. Nájera and J. M. Sansano, *Chem. Rev.*, 2007, 107, 4584–4671.
3 L. Song, Z. Zhang, Z. Lv, J. Xu, M. Zhan, S. Tang, H. Li, N. Wang and L. Cai, *ACS Catal.*, 2023, **13**, 13569–13576.
4 R. Y. Zhu, K. Tanaka, G. C. Li, J. He, H. Y. Fu, S. H. Li and J. Q. Yu, *J. Am. Chem. Soc.*, 2015, **137**, 7067–7070.
5 M. A. Ashley, C. Yamauchi, J. C. K. Chu, S. Otsuka, H. Yorimitsu and T. Rovis, *Angew. Chem.*, 2019, **131**, 4042–4046.
6 C. Ma, P. Fang and T.-S. Mei, *ACS Catal.*, 2018, **8**, 7179–7189.
7 C. A. Malapit, M. B. Prater, J. R. Cabrera-Pardo, M. Li, T. D. Pham, T. P. McFadden, S. Blank and S. D. Minteer, *Chem. Rev.*, 2022, **122**, 3180–3218.
8 S. Changmai, S. Sultana and A. K. Saikia, *ChemistrySelect*, 2023, **8**, e202203530.
9 K.-J. Jiao, Y.-K. Xing, Q.-L. Yang, H. Qiu and T.-S. Mei, *Acc. Chem. Res.*, 2020, **53**, 300–310.
10 J. Lu, Y. Wang, T. McCallum and N. Fu, *iScience*, 2020, **23**, 101796.
11 V. P. Ananikov, *ACS Catal.*, 2015, 5, 1964–1971.
12 V. B. Phapale and D. J. Cárdenas, *Chem. Soc. Rev.*, 2009, **38**, 1598–1607.
13 R. Giovannini and P. Knochel, *J. Am. Chem. Soc*, 1998, **120**, 11186–11187.
14 S. Condon, D. Dupré, G. Falgayrac and J.-Y. Nédélec, *Eur. J. Org. Chem.*, 2002, **2002**, 105–111.
15 F. Lian, K. Xu, W. Meng, H. Zhang, Z. Tan and C. Zeng, *Chem. Commun.*, 2019, **55**, 14685–14688.
16 J. Luo, W. Wu, M. Hu and T. L. Liu, *ChemRxix*, 2020, DOI: 10.26434/chemrxiv.11813505.
17 X. Zhang, Z. Ye, Y. Li, Z. Zhao, W. Ma and F. Zhang, *Org. Lett.*, 2024, **26**, 6364–6369.
18 G. Laudadio, P. Neigenfind, R. Chebolu, V. D. Blasczak, S. J. Maddirala, M. D. Palkowitz, P. N. Bolduc, M. C. Nicastri, R. K. Puthukanoori, B. R. Paraselli and P. S. Baran, *Org. Lett.*, 2024, **26**, 2276–2281

19 Z. Li, W. Sun, X. Wang, L. Li, Y. Zhang and C. Li, *J. Am. Chem. Soc*, 2021, **143**, 3536– 3543.
20 T. M. Faraggi, C. Rouget-Virbel, J. A. Rincón, M. Barberis, C. Mateos, S. García-Cerrada, J. Agejas, O. de Frutos and D. W. C. MacMillan, *Org. Process Res. Dev.*, 2021, **25**, 1966–1973.
21 M. Gausmann, N. Kreidt and M. Christmann, *Org. Lett.*, 2023, **25**, 2228–2232.
22 C. Li, Y. Shi, Q. Chen, K. Zhang, and G. Yang, *J. Org. Chem.*, 2023, **88**, 4, 2306–2313
23 D. J. Weix, *Acc. Chem. Res.*, 2015, **48**, 1767–1775.
24 D. A. Everson, R. Shrestha and D. J. Weix, *J. Am. Chem. Soc*, 2010, **132**, 920–921.
25 R. Petakamsetty, R. P. Das and R. Ramapanicker, *Tetrahedron*, 2014, **70**, 9554–9563.
26 G. Occhialini, V. Palani, and A. E. Wendlandt, *J. Am. Chem. Soc.*, 2022, **144**, 145–152
27 J. Zhou and G. C. Fu, *J. Am. Chem. Soc*, 2003, **125**, 14726–14727.
28 H. Li, C. P. Breen, H. Seo, T. F. Jamison, Y. Q. Fang and M. M. Bio, *Org. Lett.*, 2018, **20**, 1338–1341.
29 J. Buchspies, D. J. Pyle, H. He and M. Szostak, *Molecules*, 2018, **23**, 3134.
30 X. Chang, Q. Zhang and C. Guo, *Org. Lett.*, 2019, **21**, 10–13.
31 R. Häner, B. Olano and D. Seebach, *Helv. Chim. Acta*, 1987, **70**, 1676–1693.
32 S. D. Bull, S. G. Davies, G. Fenton, A. W. Mulvaney, R. S. Prasad and A. D. Smith, *J. Chem. Soc. Perkin 1*, 2000, 3765–3774.
33 S. Furukawa, N. Morishima and K. Fujita, *Eur. J. Org. Chem.*, 2024, **27**, e202301105
34 P. A. Forero-Cortés and A. M. Haydl, *Org. Process Res. Dev.*, 2019, **23**, 1478–1483.
35 C. Li, Y. Kawamata, H. Nakamura, J. C. Vantourout, Z. Liu, Q. Hou, D. Bao, J. T. Starr, J. Chen, M. Yan and P. S. Baran, *Angew. Chem.*, 2017, **129**, 13268–13273.
36 G. Cahiez, O. Gager, A. Moyeux and T. Delacroix, *Adv. Synth. Catal.*, 2012, **354**, 1519–1528.
37 Y. Takeda, T. Matsuno, A. K. Sharma, W. M. C. Sameera and S. Minakata, *Chem. Eur. J.*, 2019, **25**, 10226–10231.
38 S. Tshepelevitsh, A. Kütt, M. Lõkov, I. Kaljurand, J. Saame, A. Heering, P. G. Plieger, R. Vianello and I. Leito, *Eur. J. Org. Chem.*, 2019, 2019, 6735–6748.
39 S. D. Lepore, A. Khoram, D. C. Bromfield, P. Cohn, V. Jairaj and M. A. Silvestri, *J. Org. Chem.*, 2005, **70**, 7443–7446.
40 K. Clarke and K. Rothwell, *J. Chem. Soc. (Resumed)*, 1960, 1885.
41 R. L. Benoit, M. Fréchette and D. Lefebvre, *Can. J. Chem.*, 1988, **66**, 1159–1162.
42 M. Klein and S. R. Waldvogel, *Angew. Chem. Int. Ed.*, 2022, **61**, e202204140.
43 D. Liu, H. Ma, P. Fang and T. Mei, *Angew. Chem.*, 2019, **131**, 5087–5091.
44 Y. Wang, L. Deng, X. Wang, Z. Wu, Y. Wang and Y. Pan, *ACS Catal.*, 2019, **9**, 1630– 1634.
45 L. Shen, O. Monasson, E. Peroni, F. Le Bideau and S. Messaoudi, *ChemRxix*, 2023, DOI:10.26434/chemrxiv-2023-zbnfd.
46 B. K. Malviya, E. C. Hansen, C. J. Kong, J. Imbrogno, J. Verghese, S. M. Guinness, C. A. Salazar, J. Desrosiers, C. O. Kappe and D. Cantillo, *Chem. Eur. J.*, 2023, **29**, e202302664
47 N. Taniguchi, *J. Org. Chem.*, 2004, **69**, 6904–6906.
48 Y. Kawamata, J. C. Vantourout, D. P. Hickey, P. Bai, L. Chen, Q. Hou, W. Qiao, K. Barman, M. A. Edwards, A. F. Garrido-Castro, J. N. deGruyter, H. Nakamura, K. Knouse, C. Qin, K. J. Clay, D. Bao, C. Li, J. T. Starr, C. Garcia-Irizarry, N. Sach, H. S. White, M. Neurock, S. D. Minteer and P. S. Baran, *J. Am. Chem. Soc*, 2019, **141**, 6392–6402.
49 C. Amatore, C. Cammoun and A. Jutand, *Adv. Synth. Catal.*, 2007, **349**, 292–296.

50 Q. L. Yang, C. Z. Li, L. W. Zhang, Y. Y. Li, X. Tong, X. Y. Wu and T. S. Mei, *Organometallics*, 2019, **38**, 1208–1212.
51 C. Ma, C. Q. Zhao, Y. Q. Li, L. P. Zhang, X. T. Xu, K. Zhang and T. S. Mei, *Chem. Commun.*, 2017, **53**, 12189–12192.
52 A. Shrestha, M. Lee, A. L. Dunn and M. S. Sanford, *Org. Lett.*, 2018, **20**, 204–207.
53 Q.-L. Yang, Y.-Q. Li, C. Ma, P. Fang, X.-J. Zhang and T.-S. Mei, *J. Am. Chem. Soc*, 2017, **139**, 3293–3298.
54 S. Sen, J. Das and D. Maiti, *Tetrahedron Chem.*, 2022, **1**, 100005.
55 S. St John-Campbell and J. A. Bull, *Org. Biomol. Chem.*, 2018, 16, 4582–4595.
56 K. S. L. Chan, M. Wasa, L. Chu, B. N. Laforteza, M. Miura and J.-Q. Yu, *Nat. Chem.*, 2014, **6**, 146–150.
57 W. Jia and M. Á. Fernández-Ibáñez, *Eur. J. Org. Chem.*, 2018, **2018**, 6088–6091.
58 O. Verho, M. Maetani, B. Melillo, J. Zoller and S. L. Schreiber, *Org. Lett.*, 2017, **19**, 4424–4427.
59 B. V. S. Reddy, L. R. Reddy and E. J. Corey, *Org. Lett.*, 2006, **8**, 3391–3394.
60 A. Dey, S. Pimparkar, A. Deb, S. Guin and D. Maiti, *Adv. Synth. Catal.*, 2017, **359**, 1301–1307.
61 Y.-Q. Li, Q.-L. Yang, P. Fang, T.-S. Mei and D. Zhang, *Org. Lett.*, 2017, **19**, 2905–2908.
62 M. Fan and D. Ma, *Angew. Chem. Int. Ed.*, 2013, **52**, 12152–12155.
63 K. J. Stowers, A. Kubota and M. S. Sanford, *Chem. Sci.*, 2012, **3**, 3192.

Chapter 4: Modification of amino acids *via* anodic oxidation reactions

4.1 Chapter Aims

The first section of this chapter will focus on electrochemical transformations of tyrosine and associated derivatives; in particular the electrochemical dimerisation of two tyrosine molecules to make dityrosines. The overall aim of this research was to apply oxidative homo-coupling techniques to tyrosine substrates to create a linkage between carbons on the phenol rings. Not only are dityrosines worthy targets in their own right, being able to create such linkages in larger peptides may be useful for cyclising or stapling peptides. The technique may also be expanded to allow cross-coupling of tyrosine derivatives with other phenols, facilitating synthesis of novel amino acids or tagging of tyrosine residues with phenolic labels.

The second section in this chapter will explore the Shono-type oxidation of proline derivatives mediated by Selectfluor. The aim of this section was to optimise the conversion of Boc-proline compounds to the corresponding 5-oxoproline derivatives whilst avoiding production of a 2-hydroxyl-5-oxoproline derivative. A secondary aim of this section was to investigate the influence of the protecting group on the amine nitrogen on the outcome of the reaction.

The third section of this chapter will discuss efforts to dimerise indole substrates after an unusual tricyclic indole dimer was isolated serendipitously. The aim of this section was to try and replicate this complex tricyclic structure with other indolic substrates, *e.g.*, tryptophan.

4.2 Tyrosine Modification Overview

4.2.1 Selective tyrosine tagging

Site-selective biorthogonal labelling of specific amino acid residues in a peptide chain can have many uses: as chemical probes for diagnostic purposes, as a modifier of chemical properties, or for exploring antibody-drug or peptide-drug conjugates.[1] Traditionally amino acid residues like lysine or cysteine[2] have been targeted for biorthogonal labelling because they will react readily with a number of reagents. Recently tyrosine has been explored as a target for bioconjugation due to its relatively low frequency in native peptides and its involvement in non-covalent interactions such as π-π stacking or hydrogen bonding (**Figure 4.1**).[3] Tyrosine is therefore an attractive target for site-selective bioconjugation because different tyrosine

residues in a native peptide will have different levels of accessibility and susceptibility towards modification.

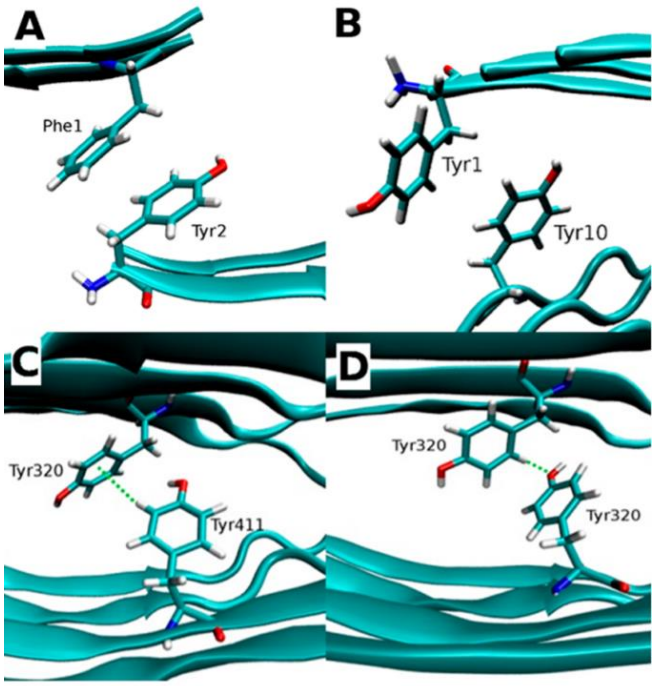

Figure 4.1: A depiction of various non-covalent interactions of tyrosine residues in amyloid peptides; A) π-π stacking, B) displaced π-π stacking, C) C-H/π interactions, D) C-H/O interactions.[4]

Tyrosine can also undergo a variety of chemical modifications, *i.e.*, nitration,[5] halogenation,[6] or oxidation,[7] making it a viable target for modification. Additionally, it is also capable of forming tyrosyl radicals upon oxidation. This is because the adjacent aromatic ring permits resonance of the radical, stabilising it (**Scheme 4.1**).

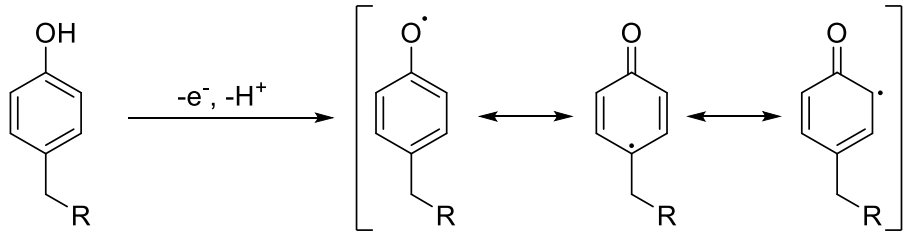

Scheme 4.1: Formation of a tyrosyl radical from a tyrosine residue and how the radical can participate in resonance across the aromatic ring, which enhances its stability. R = peptide chain.

The ability of tyrosine to readily form tyrosyl radicals means that electrochemical transformations are possible, which often take place *via* radical mechanisms. Many groups have used electro-organic reactions to modify tyrosine or tyrosine residues (see **Chapter 1**,

Section 1.4). Most of these reactions have utilised the hydroxyl group on tyrosine to create C-O bonds with relevant substrates. However, there have been fewer instances in which the phenolic structure of tyrosine has been exploited to create C-C bonds. This method would create a much stronger and resistant linkage, which is important in the context of peptide therapeutics. One known electrochemical method for creating C-C bonds from phenolic substrates is oxidative cross-coupling.

4.2.2 Electrochemical oxidative cross-coupling

Oxidative cross-coupling is a well-established technique for forming new C-C and C-heteroatom bonds. However, traditional oxidative cross-coupling often uses stoichiometric amounts of chemical oxidant and unwanted oxidation side reactions can frequently occur.[8] Recently, electrochemical oxidative-cross coupling has emerged as an efficient oxidant-free alternative which affords higher selectivity.[9]

Electrochemical oxidative cross-coupling involves anodic oxidative coupling of R_1-H and R_2-H (R = C or heteroatom) in conjunction with cathodic reduction of protons causing hydrogen evolution (**Scheme 4.2**).

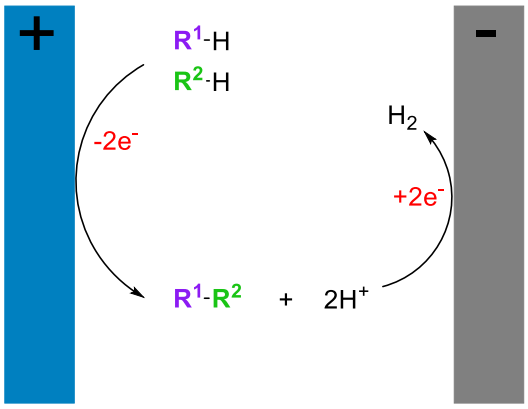

Scheme 4.2: General scheme for the electrochemical oxidative cross-coupling of R^1-H and R^2-H to form R^1-R^2 with cathodic hydrogen evolution.

Electrochemical coupling of molecules featuring sp^2 carbons, *e.g.*, phenols, arenes and alkenes has been of particular interest because traditional coupling of these groups using a chemical oxidant often requires installation of a leaving group (*i.e.*, Br, Cl) on one or both coupling partners. Electrochemical coupling can be performed without these leaving groups present, which facilitates substrate synthesis.

Homo- and hetero-coupling of phenols has been especially well-studied due to the prevalence of the 2,2'-biphenol scaffold in natural products and pharmaceuticals, and its use in ligand design.[10] **Scheme 4.3** shows an example of electrochemical coupling of two phenols to produce a biphenol product.[11]

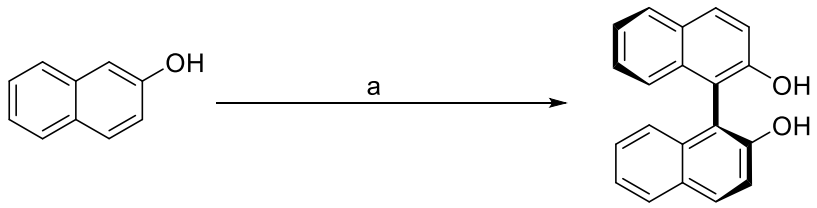

343 **344**

Scheme 4.3: An early example of anodic cross-coupling of phenols: 2-napthol (**343**) was reacted to form 1,1'-binapthol (**344**);[11] reagents and conditions: a) (+) (-) TEMPO-modified graphite felt, (–)-sparteine, $NaClO_4$, divided cell (Nafion 117), MeCN, Ar atmosphere, +0.60 V, 94%.

Electrochemical reactions involving phenol coupling often require careful crafting to ensure selectivity. A common problem encountered is the propensity for the products to undergo over-oxidation, due to their extended π-system. To avoid this problem, the oxidation potential of the product must be higher than the oxidation potentials of the reagents. Methods of mitigating the problem of over-oxidation include using fluorinated alcohols as solvents,[12] using partially-protected phenols as coupling partners,[13] or including additives in the reaction conditions.[14]

Another common issue faced by electrochemical phenol coupling reactions is undesired homo-coupling when the reagents are two different phenols. The general mechanism for the cross-coupling of phenols is shown in **Scheme 4.4.** Initially only one of the phenol coupling partners is oxidised to produce a phenoxyl radical. This is then subjected to nucleophilic attack by the second phenol. The product then undergoes a second oxidation step, resulting in rearomatization and the formation of the final 2,2'-biphenol product. Homo-coupling is a potential pitfall because both phenol substrates are capable of forming a phenoxyl radical, and both are capable of performing nucleophilic attack.

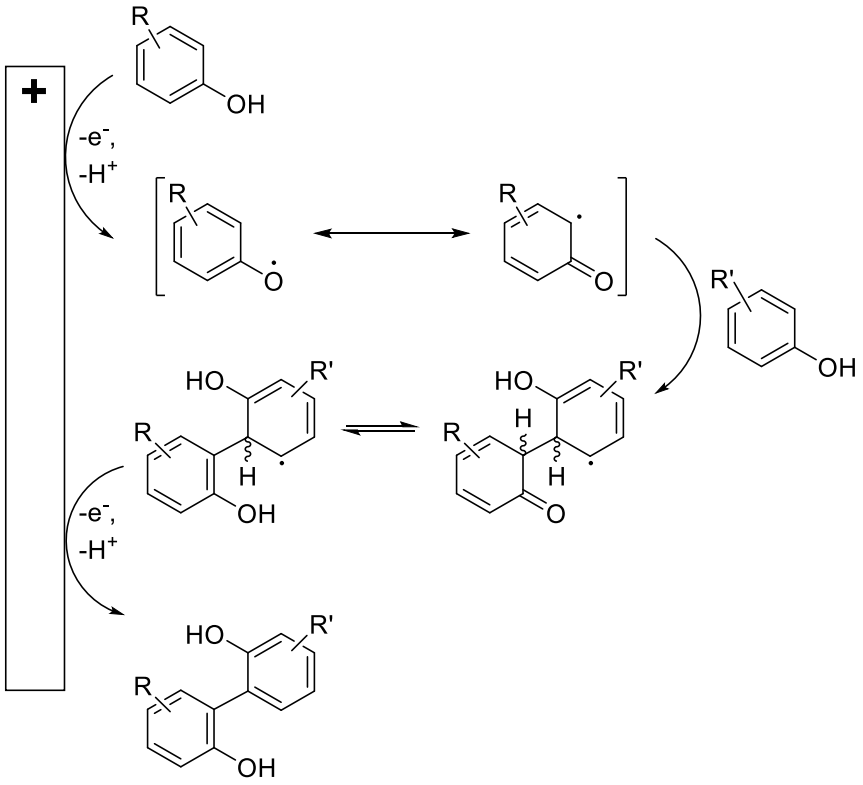

Scheme 4.4: General scheme for electrochemical anodic cross-coupling of phenols R-ArOH and R'-ArOH to produce an asymmetric 2,2'-biphenol product.

To avoid unwanted homo-coupling, the two coupling partners must therefore have different oxidation potentials, so that one is preferentially oxidised first. A difference in nucleophilicity will also help to prevent homo-coupling. Unfortunately, a low oxidation potential often coincides with a higher nucleophilicity due to higher electron density on the aryl ring. An example of a technique used to circumvent this problem is Waldvogel's application of *O*-silyl ethers as protecting groups on one of the coupling partners (**Scheme 4.5**).[13]

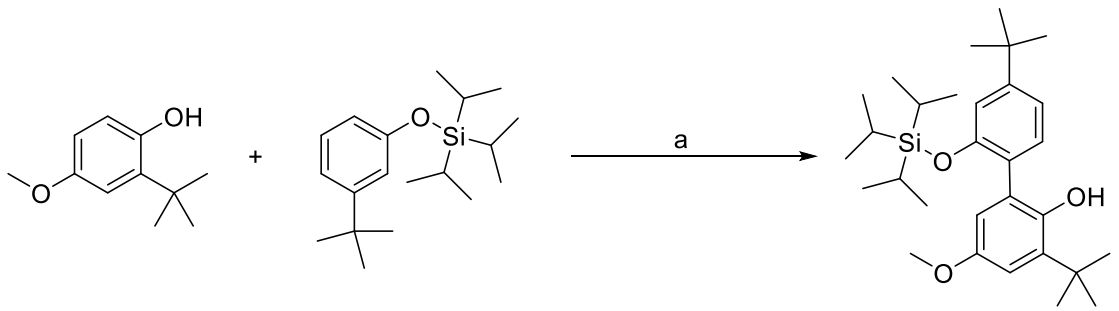

345 **346** **347**

Scheme 4.5: Electrochemical cross coupling of phenol **345** with phenolic silyl ether **346**;[13] reagents and conditions: a) (+) BDD (-) BDD, 0.09 M *N*-methyl-*N,N,N*-tributylammonium methylsulfate, HFIP/MeOH (0-18% v/v), 2.8 mA/cm^2, 50 °C, 2 F/mol, 92%.

The use of this method enables the selective oxidation of phenol **345** due to phenolic silyl ether **346**'s inability to form phenoxyl radicals. Because ether **346** is supplied in excess (3 equiv.), the phenoxyl radical formed from **345** is likely to undergo nucleophilic attack from **346**. Therefore, the asymmetric biphenol **347** is formed with no homo-coupling observed.

The partial protection of substrates as silyl ethers has the additional benefit of reducing overoxidation of the 2,2'-biphenol product. This is because the silyl group is large and bulky, causing a twist of the biaryl axis. This prevents the two aryl π-systems from conjugating to form an extended π-system, which reduces the likelihood that further oxidation will occur.

This section will discuss attempts to perform electrochemical oxidative cross-coupling reactions using tyrosine or tyrosine derivatives, taking advantage of the phenol moiety. One particular goal was the electrochemical synthesis of dityrosine (**348**) (**Figure 4.2**).

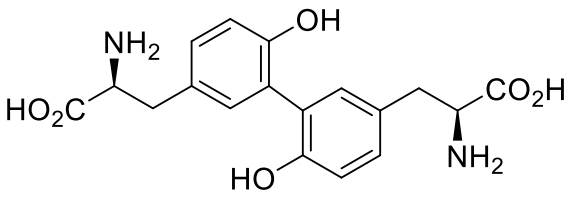

348

Figure 4.2: The structure of dityrosine (**348**), a common post-translational modification cross-linkage in natural proteins.

Dityrosine cross-linkages can form between tyrosyl residues as part of normal post-translational modification processes, or as a result of environmental stress on natural proteins.[15] Dityrosine linkages can also be clinical markers of neurodegenerative disease[16] or oxidative stress. The cross-linking of tyrosyl residues can have a significant impact on the properties of a peptide, often stabilising the structure of a peptide and improving its mechanical strength. Natural dityrosine linkages have been observed in elastomeric proteins such as resilin,[17] which is commonly found in insects. The stability conferred by dityrosine linkages has been exploited for the synthesis of peptide hydrogels, to improve their mechanical properties.[18] An additional feature of dityrosine cross-linkages is their fluorescent properties. Dityrosine (**348**) fluoresces at 400 nm and is therefore capable of acting as a probe for spectroscopic analysis.[19]

The synthesis of dityrosine (**348**) is therefore an interesting target for electrochemical oxidative coupling. This reaction could be potentially expanded to selectively induce dityrosine linkages in full peptides to modify their properties.

4.3 Tyrosine homocoupling under electrochemical conditions

The initial idea for the homo-coupling of two tyrosine molecules was to employ the method of partial protection with a silyl protecting group (**Scheme 4.5**). Despite this technique originally being used to avoid homo-coupling, Waldvogel *et al.* found that the protection of one coupling partner as a bulky silyl ether unexpectedly boosted the yield of the coupling reaction in other ways, *e.g.*, prevention of over-oxidation and reduction of nucleophilicity.[13]

Due to the nature of the coupling reaction, available protons on the amine and acid moieties of tyrosine need to be removed. The use of a phthalimide protecting group on the amine should neutralise its nucleophilicity and remove any protons that may interfere with the reaction. The acid can be protected using a simple methyl ester (**Scheme 4.6**).

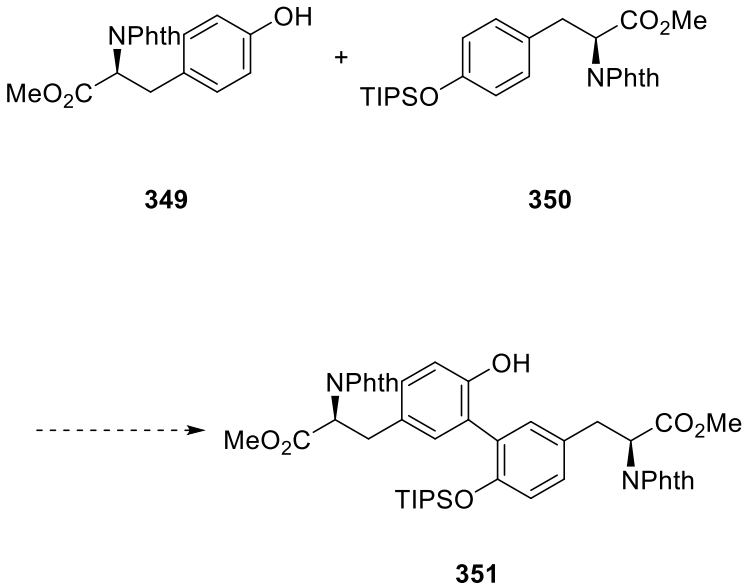

Scheme 4.6: Proposed scheme for synthesis of dityrosine derivative (**351**) *via* electrochemical cross-coupling of *N*-phthaloyl tyrosine methyl ester (**349**) and *N*-phthaloyl *O*-TIPS tyrosine methyl ester (**350**).

The first step in this synthesis was the reaction of commercially-available L-tyrosine methyl ester (**46**) with phthalic anhydride to form *N*-phthaloyl tyrosine methyl ester (**349**) (**Scheme 4.7**). A literature procedure was followed for this reaction,[20] and **349** was obtained in an excellent yield (77%).

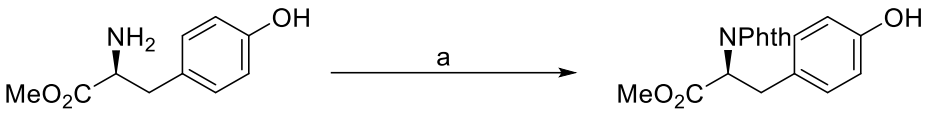

46 **349**

Scheme 4.7: Phthalimide protection of tyrosine methyl ester (**46**) using phthalic anhydride; reagents and conditions: a) phthalic anhydride (1.02 equiv.), toluene, reflux, 24 h, 77%.

Half of the material obtained was taken forward into the next reaction: the installation of a silyl ether to protect the hydroxyl moiety. The triisopropylsilyl (TIPS) protecting group was selected for this role as previous studies have revealed that a TIPS group results in higher yields and is less likely to be removed mid-reaction.[13] *N*-Phthaloyl tyrosine methyl ester (**349**) was therefore reacted with triisopropyl silyl chloride (TIPSCl) in the presence of imidazole (**Scheme 4.8**). This reaction worked well, achieving a 76% yield.

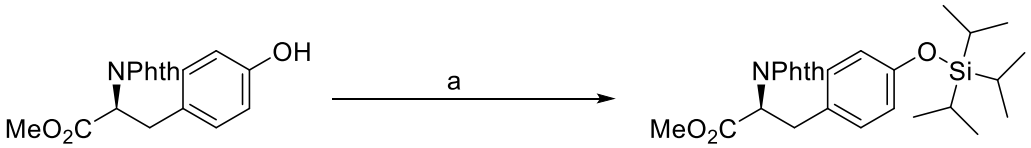

349 **350**

Scheme 4.8: The reaction of *N*-phthaloyl tyrosine methyl ester (**349**) to form a silyl ether (**350**); reagents and conditions: a) 1.2 equiv. TIPSCl, 2 equiv. imidazole, dry DCM, 24 h, r.t., 76%.

With the TIPS-protected substrate (**350**) in hand, the electrochemical coupling of tyrosine was first attempted using the conditions described by Waldvogel *et al.* for the cross-coupling of partially protected phenols (**Scheme 4.4**).[13] However, adjustments to the procedure were made due to lack of available materials. The original procedure calls for boron-doped diamond (BDD) electrodes and *N*-methyl-*N,N,N*-tributylammonium methylsulfate (MTBS) as the electrolyte. The BDD electrodes were substituted with platinum electrodes due to their lower cost. Previous studies have shown that whilst BDD anodes deliver a higher yield of product in cross-coupling reactions, platinum electrodes are still capable of performing the reaction (69% (BDD) vs. 57% (Pt)).[14] The MTBS electrolyte is not commercially available, so this was replaced by tetrabutylammonium bromide, commonly used as an electrolyte in electrochemical reactions. The amended reaction conditions are shown in **Scheme 4.9**.

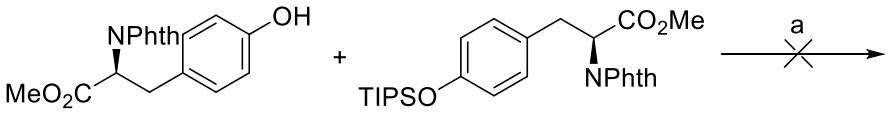

349 **350**

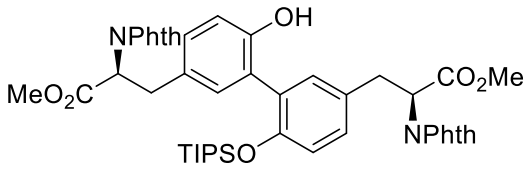

351

Scheme 4.9: Attempted electrochemical coupling of partially protected tyrosine; reagents and conditions: a) (+) Pt (-) Pt, 0.15 mmol tetrabutylammonium bromide, HFIP/MeOH (10% v/v), 2.8 mA/cm^2, 2 F/mol

The hexafluoroisopropanol (HFIP) solvent used in this reaction has been found to be an excellent solvent for cross-coupling reactions because it is capable of significantly stabilising the phenoxyl radicals produced.[21,22] This is due to the solvent preferentially participating in hydrogen bonding with phenoxyl radicals compared to the substrate. Additionally, HFIP is very electrochemically stable with a wide potential window; this prevents solvent degradation.[23]

The inclusion of a small amount of MeOH in the solvent mixture has also been found to boost yields and selectivity in electrochemical cross-coupling reactions.[14] This is thought to be due to methanol acting as a redox mediator (**Scheme 4.10**).

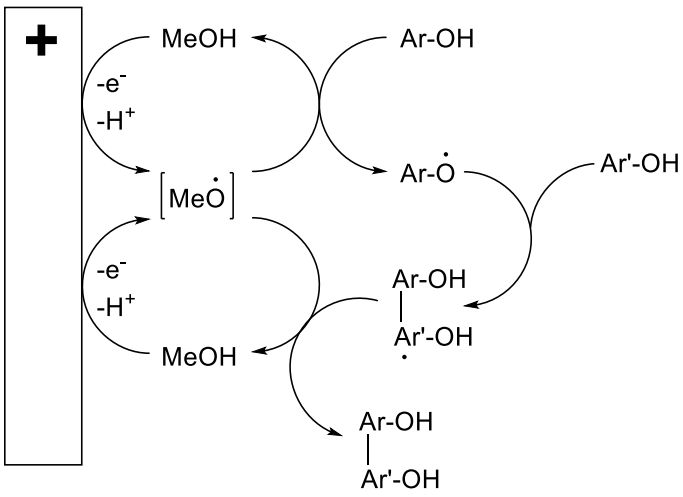

Scheme 4.10: Mechanism proposed by Waldvogel *et al.* to illustrate the role of methanol as an additive in electrochemical cross-coupling reactions.[14]

Unfortunately, the first attempt at the tyrosine coupling reaction using the reaction conditions in **Scheme 4.9** did not appear to have worked. There was no evidence of product formation found by either TLC or ^{1}H NMR spectroscopic analysis.

A possible explanation for this is that the aryl moiety on the tyrosine molecule (**349**) does not have enough electron density to undergo oxidation or to perform nucleophilic attack. Most of the 2,2'-biphenols synthesised under these conditions by the Waldvogel group were significantly more electron-rich than the tyrosine substrate (**349**) used in this experiment. Additionally, HFIP has a strong solvation effect on substrates;[24] substrates which are more soluble in HFIP experience a larger reduction in their nucleophilicity as a denser solvation sphere forms around them. Whilst this effect prevents over-oxidation in electron-rich substrates, it may have a more adverse impact on substrates with a lower electron density.

This reaction was attempted again, this time using reaction conditions intended for the coupling of phenols with electron withdrawing substituents (**Scheme 4.11**).[25] As these conditions were intended for phenols with electron-withdrawing substituents such as halide, carbonyl, and sulfonyl groups, they may work better for substrates such as tyrosine.

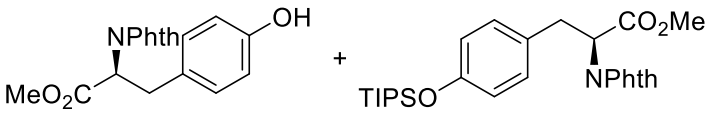

349 **350**

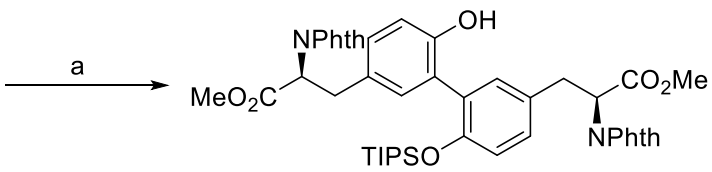

351

Scheme 4.11: Attempted electrochemical coupling of partially protected tyrosine; reagents and conditions: a) (+) graphite (-) graphite, DIPEA, HFIP, 5 mA/cm^2, 1.5 F/mol, TIPS-Tyr (**350**) in excess.

This reaction uses a solvent system of DIPEA/HFIP, which also doubles as the electrolyte. DIPEA can deprotonate HFIP, generating DIPEAH$^+$. The acid-base equilibrium between HFIP

and the conjugate acid of DIPEA ensures that the solution will have sufficient conductivity to allow a current to flow.[26]

On examination of the reaction mixture using TLC, no tyrosine (**349**) remained, however TIPS-tyrosine (**350**) was present. Removal of DIPEA followed by a second TLC revealed a potential product spot practically on the baseline. The product mixture was separated by column chromatography into fractions of TIPS-Tyr (**350**), a very small amount of *N*-phthaloyl tyrosine (**349**), and an impure fraction containing the baseline spot. ^{1}H NMR spectroscopic analysis of this third fraction suggested that this compound was very similar to *N*-phthaloyl tyrosine, except the aromatic peaks were shifted. It was thought that instead of a mixed TIPS-and-non-TIPS biphenol product (**351**), unprotected dityrosine (**352**) (**Figure 4.3**) had formed from the small amount of *N*-phthaloyl tyrosine (**349**) present in the reaction. Additionally, a peak at 649.8 *m/z* was observed in the ESI-LCMS spectrum, which corroborated this theory; the molecular mass of dityrosine (**352**) is 648.

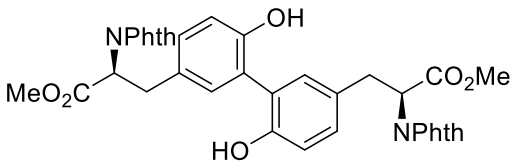

352

Figure 4.3: *N,N'*-diphthaloyl dityrosine (**352**), proposed product for the electrochemical coupling reaction described in **Scheme 4.11**.

It appeared that the TIPS protected tyrosine (**350**) was entirely unreactive during the cross-coupling reaction. This is due to the fact that the TIPS group not only prevents formation of a phenoxyl radical, but also increases the lipophilicity of the tyrosine molecule. Therefore, it will experience a greater solvation effect in HFIP, and will consequently have a reduced nucleophilicity. This means that the TIPS-tyrosine (**350**) is effectively prevented from being both the coupling partner to undergo oxidation, and the coupling partner that acts as a nucleophile. Whilst it may have been helpful in preventing over-oxidation, this does not seem to be a problem faced by tyrosine derivatives as they appear to be relatively electron-deficient and thus somewhat unreactive.

In order to confirm that *N,N'*-diphthaloyl dityrosine (**352**) had in fact been produced, a reaction was set up using the same conditions, but with *N*-phthaloyl tyrosine (**349**) as the sole substrate (**Scheme 4.12**).

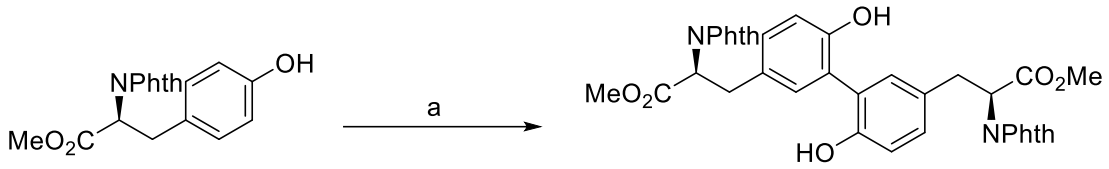

349 **352**

Scheme 4.12: The electrochemical homo-coupling of *N*-phthaloyl tyrosine (**349**) to produce *N,N'*-diphthaloyl dityrosine (**352**); reagents and conditions: a) (+) graphite (-) graphite, DIPEA, HFIP, 5 mA/cm^2, 1.5 F/mol, 20%.

This reaction worked, furnishing the desired product (**352**) in a 20% yield. The structure of the product was confirmed using mass spectrometry and ^{1}H NMR spectroscopy. As suspected from the previous reaction, the ^{1}H NMR spectrum of **352** (**Figure 4.4**) was identical to that of the starting material (**349**), except for the aromatic region. In the starting material (**349**), there are two doublets at 7.05 and 6.65 ppm, which account for the four aromatic protons on the phenol moiety. In the dityrosine product (**352**), there is a doublet at 6.99, J = 2.2, a doublet of doublets at 6.92, J = 8.3, J' = 2.2, and a doublet at 6.77, J = 8.2. This suggests that the proton at 6.92 ppm is coupled to both the proton at 6.77, and the proton at 6.99. A ^{1}H-COSY spectrum taken corroborates this; therefore, the proton at 6.99 is likely to be $\mathbf{H_a}$, the proton at 6.92 is likely to be $\mathbf{H_c}$, and the proton at 6.77 is likely to be $\mathbf{H_b}$ (**Figure 4.4**).

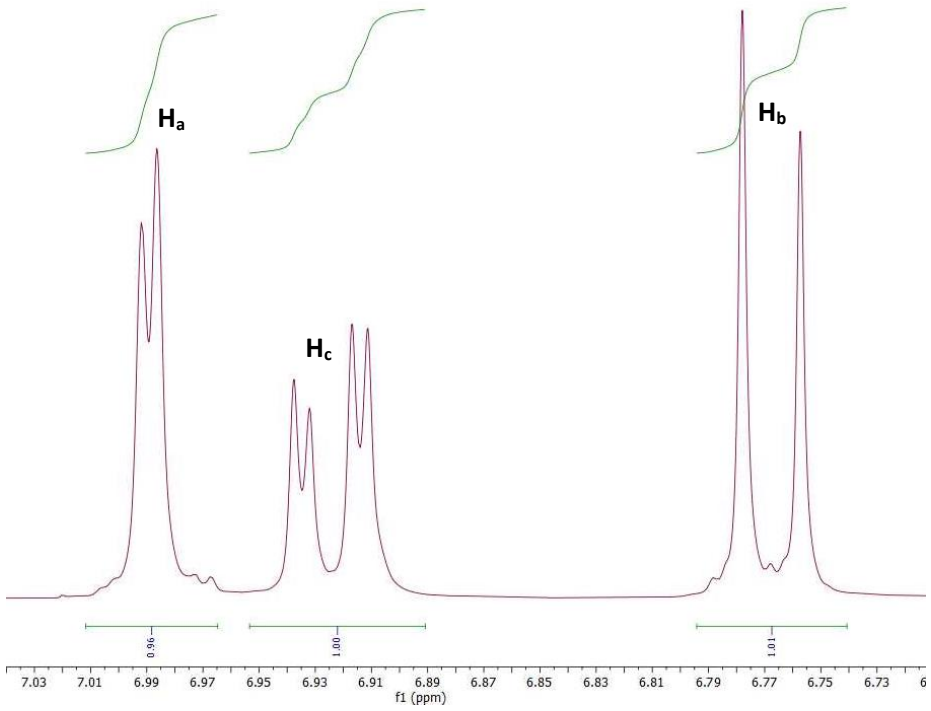

Figure 4.4: ^{1}H NMR spectrum (400 MHz, $CDCl_3$) of *N,N'*-diphthaloyl dityrosine (**352**) with the relevant aromatic protons labelled as $\mathbf{H_a}$, $\mathbf{H_b}$, and $\mathbf{H_c}$.

Due to the success of the dityrosine formation, the coupling reaction was then attempted using a tyrosine-containing dipeptide. Alanine was selected as the second amino acid for the dipeptide, as it does not feature any functional groups which may interfere with the electrochemical coupling reaction. A tyrosine-alanine derivative (**355**) was therefore synthesised using PyBOP (**Scheme 4.13**).

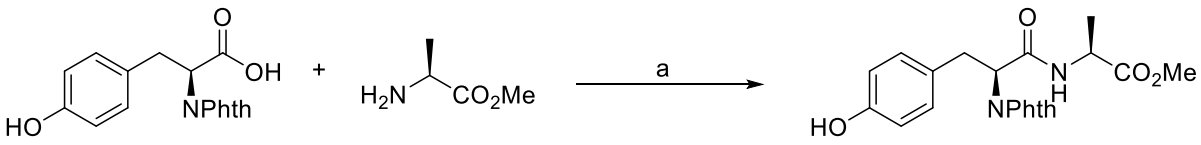

353 **354** **355**

Scheme 4.13: Dipeptide **355** formation from *N*-phthaloyltyrosine (**353**) and alanine methyl ester hydrochloride (**354**); reagents and conditions: a) DIPEA, PyBOP, anhyd. DCM, 20 h, RT, 71%.

The dipeptide (**355**) was then reacted under the same electrochemical coupling conditions used for tyrosine (**Scheme 4.14**).

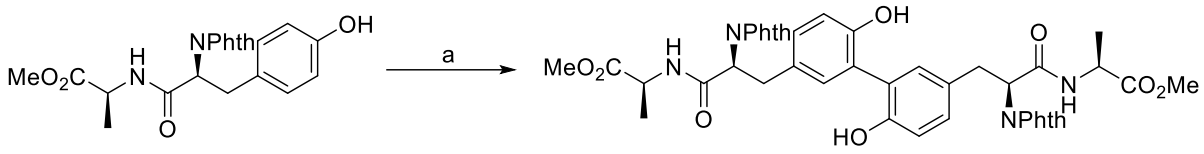

355 **356**

Scheme 4.14: Electrochemical oxidative homo-coupling of Tyr-Ala dipeptide **355**; reagents and conditions: a) (+) graphite (-) graphite, DIPEA, HFIP, 5 mA/cm^2, 1.5 F/mol, 18%.

The reaction was successful, producing the desired homo-coupled product **356** in a yield of 18%, comparable to that of dityrosine **352**. The identity of the product was confirmed using ^{1}H NMR and LCMS spectroscopic analysis.

Given the relative success of the homo-coupling reaction, the possibility of cross-coupling with tyrosine derivatives was then investigated. The ability to append different phenols onto tyrosine may be useful for synthesising unnatural amino acids. Therefore, a reaction was set up using *N*-phthaloyltyrosine methyl ester (**349**) and 4-hydroxybenzotrifluoride (**268**) (**Scheme 4.15**). 4-Hydroxybenzotrifluoride (**268**) was selected as the coupling partner because the fluorine atoms provide a ^{19}F handle for easier product identification *via* ^{19}F NMR, and the electron-withdrawing -CF_3 group may sufficiently reduce the reactivity of the phenol so that it does not participate in homo-coupling.

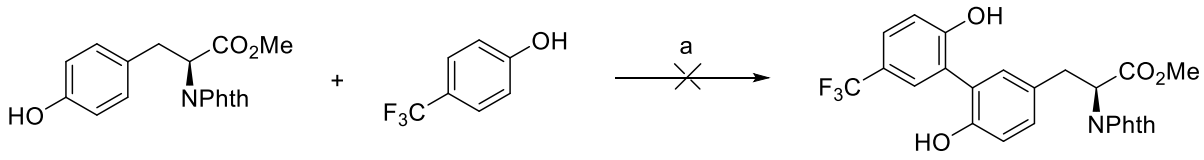

349 **268** **357**

Scheme 4.15: Attempted oxidative cross-coupling of *N*-phthaloyltyrosine methyl ester (**349**) and 4-hydroxybenzotrifluoride (**268**); reagents and conditions: a) (+) graphite (-) graphite, DIPEA, HFIP, 5 mA/cm^2, 1.5 F/mol

This reaction was found to be unsuccessful with none of the desired product (**357**) observed. Only one other fraction from this reaction was investigated, which appeared to be a fluoro-aryl compound. The ^{1}H NMR spectrum did not match that of 4-hydroxybenzotrifluoride (**268**). It was thought that the compound could be some kind of homo-coupled product. The ^{19}F NMR spectrum featured a doublet peak (δ = -71.9) at an unusually low frequency for an $(C)_{sp2}$-CF_3 moiety (usually ~-61-62 ppm), which could indicate a change in the fluorine environment (*e.g.* CF_3 to RCF_2). LCMS analysis of this product revealed that two compounds were in fact

present, both with very high masses ([M-H]$^-$ = 1199.3, 1211.2). The high masses indicate that perhaps larger polymeric compounds were formed (*e.g.*, **Figure 4.5**).

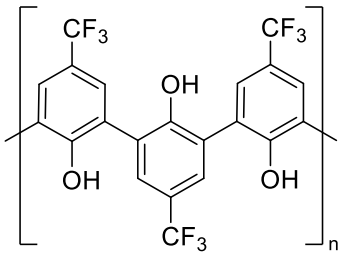

358

Figure 4.5: Possible structure for the major product of the reaction shown in **Scheme 4.15**.

This reaction indicates that the difference in reactivity between the tyrosine derivative (**349**) and the phenol coupling partner (**268**) is too great for effective coupling to take place. The 4-hydroxybenzotrifluoride (**268**) preferentially reacts with itself rather than with the tyrosine. In an attempt to prevent this, partial silyl ether protection was used to lower the reactivity of the phenol coupling partner, as described in earlier in the chapter. To this end, 4-methoxyphenol (**359**) was protected with a TIPS group (**Scheme 4.16**).

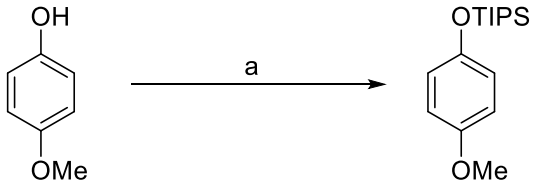

359 **360**

Scheme 4.16: TIPS protection of 4-methoxyphenol (**359**) using triisopropylsilyl chloride; reagents and conditions: a) TIPSCl, imidazole, DCM, 20 h, RT, 69%.

The TIPS-protected phenol (**360**) was then reacted with *N*-phthaloyltyrosine methyl ester (**349**) using the electrochemical oxidative coupling conditions shown (**Scheme 4.17**).

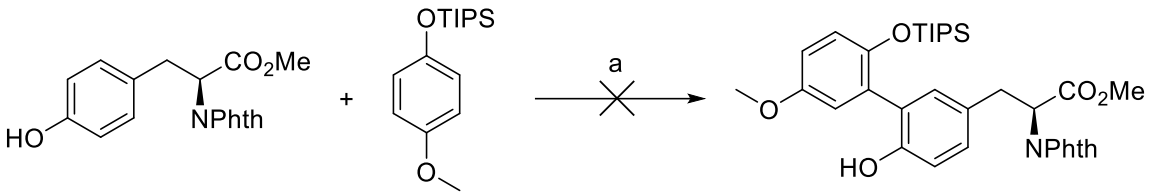

349 **360** **361**

Scheme 4.17: Attempted oxidative cross-coupling using TIPS-phenol **360** and *N*-phthaloyltyrosine methyl ester (**349**); reagents and conditions: a) (+) graphite (-) graphite, DIPEA, HFIP, 5 mA/cm^2, 1.5 F/mol

Whilst the mass of desired product from this reaction was observed by LCMS analysis (*m/z* = 604.6), the desired product **361** could not be isolated cleanly due to the presence of unwanted byproducts. Unreacted TIPS-phenol **360** was however recovered from the product mixture, which suggests that the addition of the TIPS group did indeed lower the reactivity of the phenol.

4.4 Shono-type oxidations of prolines under electrochemical conditions

After an unsuccessful attempt to fluorinate Boc-4-methylproline (**94**) using Selectfluor (see **Chapter 2**, **Section 2.3.2**), the fluorination reaction was attempted using Boc-Pro-OMe (**121**) as a substrate, using a range of conditions as shown in **Table 4.1**. Fluorination did not take place; instead, conversion of the starting material to a mixture of two pyroglutamic acid-derived products was observed. Traces of a fluorinated species were seen in the ^{19}F NMR spectrum of the crude product mixture.

Pyroglutamic derivative **120** was identified by comparison of the ^{1}H NMR spectrum to existing spectroscopic data,[27] and confirmed by LCMS (*m/z* = 144.1). Product **362** has not been synthesised previously, but a comparison of the ^{1}H NMR spectra of products **120** and **362** revealed that **362** possessed a very similar structure to **120**, but had no α-H. This suggested that a substituent had been placed at the α-carbon. The LCMS spectrum of **362** had a peak with *m/z* = 160.2, which indicated a hydroxyl substituent. A similar hydroxyl substitution was also seen when synthesising fluorinated enones (See **Chapter 2**, **Section 2.3.3**). The source of the oxygen substituents is unclear, given the exclusion of water and air from the reaction.

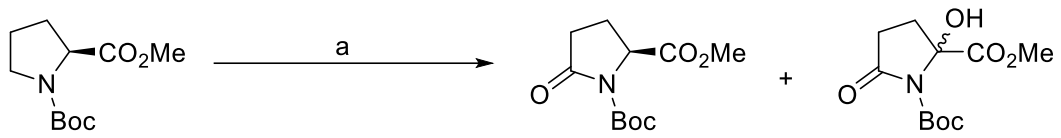

121 **120** **362**

Entry	Deviation from (a)	% 120[b]	% 362[b]
1	None	50	50
2	No current	0	0
3	No Selectfluor	0	0
4	Wet solvent, air	66	33
5	10% H_2O, air	86	14
6	10% H_2O, air, 1.5 equiv. Selectfluor	93	7
7	Dry MeCN, air, 1.5 equiv. Selectfluor	77	23

Table 4.1: The transformation of *N*-Boc proline methyl ester (**121**) into a mixture of pyroglutamic acid derivatives (**120, 362**) and various conditions attempted, alongside the proportion of **120** and **362** in each of the product mixtures; reagents and conditions: a) undivided cell, Selectfluor (3 equiv.), dry MeCN, $NaNO_3$ (cat.), 3 mA, 3 F/mol, inert atmosphere, RVC electrodes; b = proportion determined by ^{1}H NMR of crude product mixture.

A number of variations on the oxidation conditions were trialled in an attempt to push the reaction towards a single product. Both Selectfluor and the electric current were found to be essential to the success of the reaction (**Table 4.1**, **Entries 2 and 3**).

The inclusion of water and oxygen in the reaction appeared to favour the generation of product **120** (**Table 4.1, Entries 4-6**). This result was somewhat unexpected, as the hydroxyl substituent on product **362** might suggest that it would instead be favoured. Given the fluorine signals observed in the ^{19}F NMR spectrum, it is possible that an unstable 2-fluoroproline (**363**) is initially formed, which is rapidly hydrolysed during work-up (**Scheme 4.18**). The use of inert conditions would favour production of the fluorinated intermediate **363**.

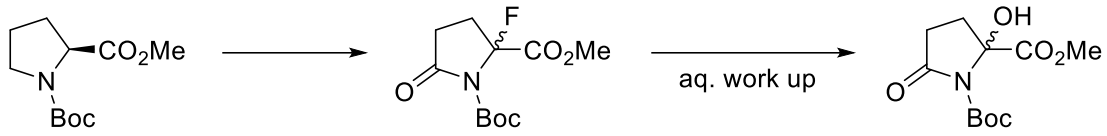

121 **363** **362**

Scheme 4.18: Possible route towards α-hydroxylated product **362** *via* initial fluorination at the α-carbon.

Reports of isolable 2-fluoroprolines are rare, due to their tendency to hydrolyse or eliminate to produce pyrrolines. In 2016, Ulbrich *et al.* managed to isolate a 2-fluoro-3-chloroproline derivative (**365**), alongside the corresponding chlorohydrin **366** (**Scheme 4.19**).[28] The adjacent electron-withdrawing 3-chloro substituent was used in a successful attempt to stabilise the α(C-F) bond. Compound **365** was reportedly then stable for a few days.

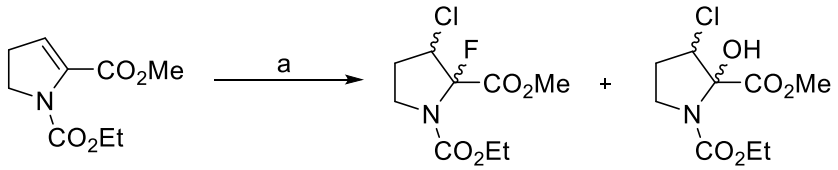

364 **365** **366**

Scheme 4.19: Chlorofluorination of protected pyrroline **364** to generate an α-fluoro-β-chloroproline derivative (**365**);[28] reagents and conditions: a) NCS, py.9HF, DCM, rt, 3 days, 20%.

The formation of the ketone functionality by substitution of oxygen onto C-5 is most likely due to a Selectfluor-assisted Shono-type oxidation. The Shono oxidation is a well-known electrochemical transformation,[29] which transforms amides and carbamates into *N*-acyliminium ions, which can then be captured by various nucleophiles (**Scheme 4.20**).

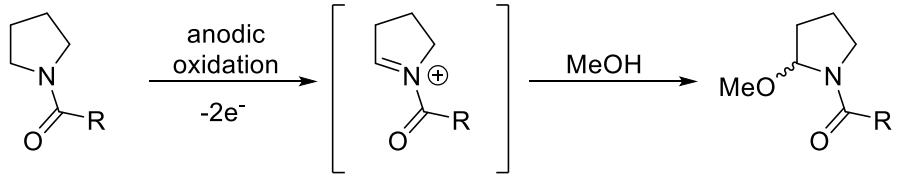

Scheme 4.20: An example of a Shono oxidation. The amide or carbonate is oxidised at the anode to form an *N*-acyliminium ion, which can then be captured by a nucleophile.

In the transformation displayed in **Scheme 4.1**, it is likely that Boc-Pro-OMe (**121**) is undergoing a Shono oxidation to generate an *N*-acyliminium ion, which can react with oxygen

in the air or hydroxyl ions from water. This species can be further oxidised to pyroglutamic acid derivative **120**. The proposed mechanism is shown below in **Scheme 4.21**.

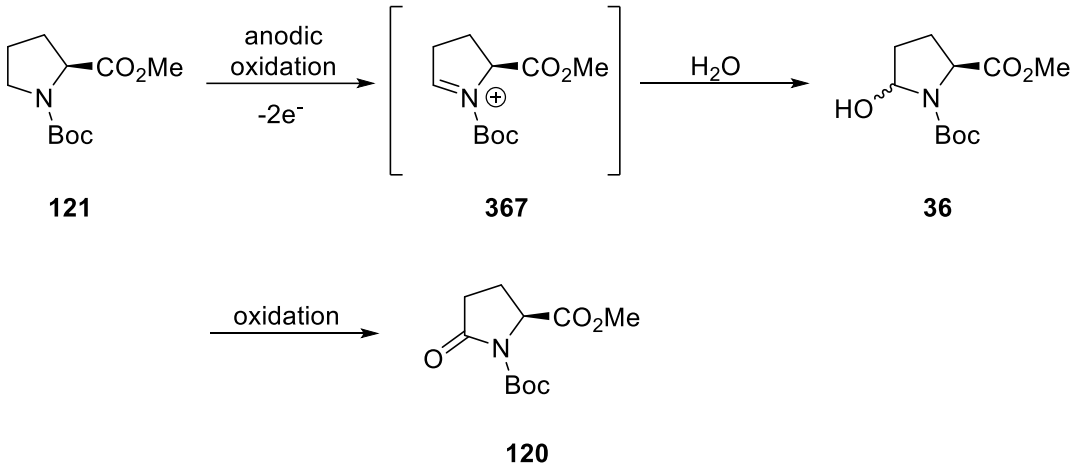

Scheme 4.21: Proposed mechanism for the formation of pyroglutamic acid derivative **120** from Boc-Pro-OMe (**121**) *via* an *N*-acyliminium ion (**367**). It is probable that Selectfluor may be involved in one or both of the oxidation steps as a mediator or oxidant.

Ticconi *et al.* reported isolation of the same compound (**120**) when investigating amino acid oxidations mediated by the phthalimide *N*-oxyl radical (PINO).[30] This group also isolated 5-hydroxyl derivatives from the same reaction, which lends support to the idea that the 5-hydroxyl derivative **368** is an intermediate in oxoproline formation (**Scheme 4.22**).

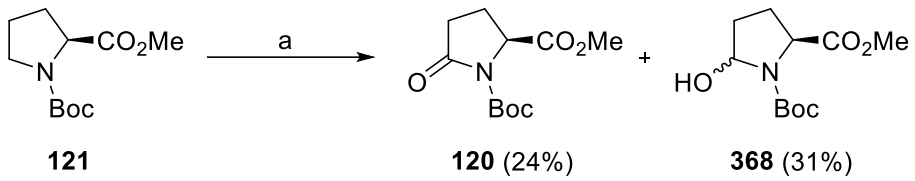

Scheme 4.22: PINO-mediated oxidation of Boc-Pro-OMe (**121**) to form a mixture of oxidation products (**368** = mixture of diastereomers);[30] Reagents and conditions: a) $Co(OAc)_2$ (0.5 mol%), NHPI (5 mol%), MeCN, rt, 24 h, oxygen atmosphere.

The anodic oxidation of cyclic carbamates like proline derivative **121** is not a new reaction. There have been few reports of electrochemical oxidations of carbamates to form carbamate lactams. The Stahl group reported a ketoABNO-mediated electrochemical oxidation of carbamates (**Scheme 4.23**).[31]

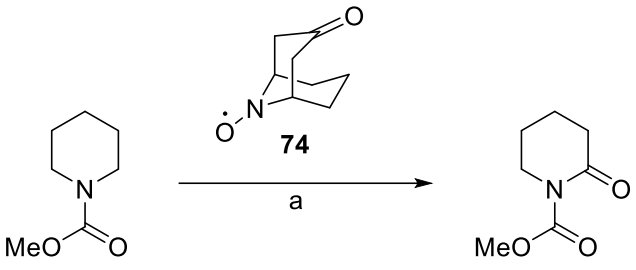

369 370

Scheme 4.23: Electrochemical ketoABNO-mediated oxidation of cyclic carbamates;[31] reagents and conditions: a) ketoABNO (**74**) or $PhCO_2ABNO$ (60 mol%), H_2O (50 equiv.), MeCN, $NaClO_4$ (0.1 M), rt, RVC (+) Pt (-), undivided cell, 86%.

It is likely that our oxidation protocol (**Table 4.1, Entry 6**) works similarly to the one published by Stahl and coworkers. The Stahl procedure is mediated by ketoABNO (**74**) (or the analogous $PhCO_2ABNO$), which behaves as a redox mediator, and facilitates the anodic oxidation. Given that Selectfluor is also a redox mediator, it is probable that it plays the same role in our reaction. Hence, the absence of Selectfluor in the reaction mixture prohibited product generation (**Table 4.1, Entry 3**). The benefit of using Selectfluor as a redox mediator is that no additional electrolyte is required, which cuts down on unnecessary chemical waste.

Whilst there have been no procedures published for electrochemical Selectfluor-mediated carbamate oxidation, a similar non-electrochemical procedure was published in 2023 by Chang *et al.*[32] The authors used Selectfluor or NFSI in conjunction with catalytic copper to effect oxidation of proline derivatives (**Scheme 4.24**). These were then reacted with Lewis acids and nucleophiles to generate a range of 5-substituted prolines.

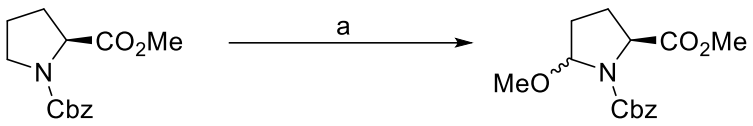

371 372

Scheme 4.24: Cu-catalysed Selectfluor-mediated oxidation of proline residues published by Chang *et al.*;[32] reagents and conditions: a) CuCN(10 mol%), MeOH, H_2O, NFSI/Selectfluor (2 equiv.), MeCN, 2-8 h.

There is a possibility that the α-hydroxylation observed with the formation of product **362** (See **Table 4.1**) could be due to a second Shono-type oxidation event, rather than as a result of fluorination. However, there are very few reports of Shono-oxidation of the more highly substituted site (*i.e.*, the α-C in proline). Libendi *et al.* have achieved selective α-methoxylation

of cyclic amines, but a cyano- protecting group was required to stabilise the desired *N*-acyliminium ion (**Scheme 4.25**).[33]

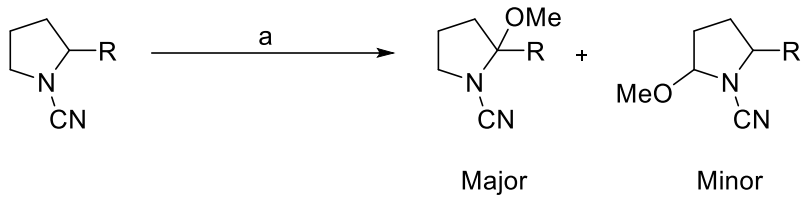

Scheme 4.25: Regioselective electrochemical α-methoxylation of cyclic amines;[33] reagents and conditions: a) Et_4NBF_4, MeOH, -50 °C, 2.5 F/mol, graphite electrodes, various ratios/yields.

It is therefore unlikely that the α-hydroxylation is due to Shono-oxidation instead of initial fluorination. To establish whether other protecting groups would also facilitate this kind of oxidation, an *N*-acetyl proline derivative (**373**) was synthesised, along with a Pro-Gly dipeptide (**374**) (**Scheme 4.26**).

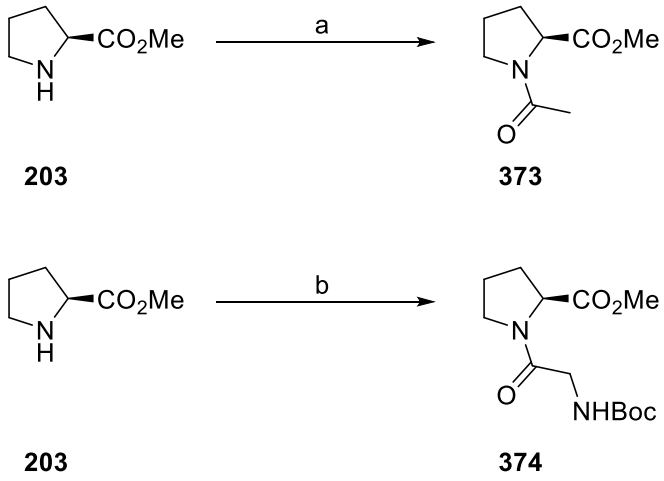

Scheme 4.26: Installation of an acetyl group to form *N*-acetyl proline methyl ester (**373**) (top), and synthesis of Boc-Gly-Pro-OMe (**374**) (below); reagents and conditions: a) Ac_2O, Et_3N, DMAP, DCM, N_2, RT, 2.5 h, 82%; b) Boc-Gly-OH, Et_3N, HOBt, EDC.HCl, DCM, 20 h, 0 °C, 87%.

Both the *N*-acetyl proline **373** and the proline-glycine **374** were subjected to the oxidation conditions from **Table 4.1, Entry 6**. The two substrates both yielded the desired 5-oxoproline products (**375** and **376**), confirming that the nature of the protecting group does not matter, so long as it is a carbamate or an amide (**Scheme 4.27**). **376** was not isolated but its presence was confirmed using ^{1}H NMR and LCMS analysis of the crude product mixture.

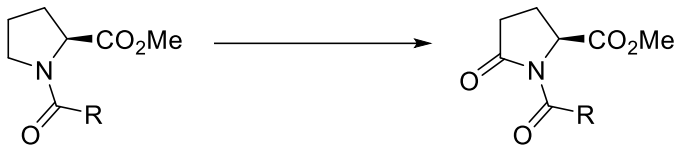

373 (R = Me)
374 (R = CH_2NHBoc

375 (R = Me)
376 (R = CH_2NHBoc

Scheme 4.27: Selectfluor-mediated electrochemical Shono-type oxidation of *N*-Ac-Pro-OMe (**373**) and Pro-Gly dipeptide (**374**) (R = Me, -CH_2NHBoc) to form the corresponding 5-oxoprolines (**375** and **376**); reagents and conditions: a) undivided cell, Selectfluor (1.5 equiv.), H_2O/MeCN (1:4), 3 mA, 3 F/mol, RVC electrodes, **375** (57%).

Interestingly, when the electrodes were switched from RVC to graphite and the reaction conditions from Entry 6 (**Table 4.1**) were applied to Boc-Pro-OMe (**121**), no reaction took place (**Scheme 4.28**).

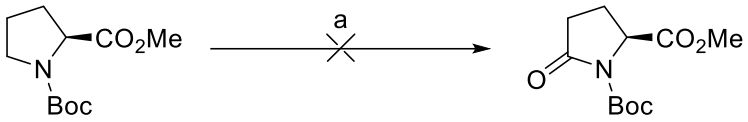

121 **120**

Scheme 4.28: Unsuccessful attempt at oxidation of Boc-Pro-OMe (**121**) using graphite electrodes instead of RVC; reagents and conditions: a) undivided cell, Selectfluor (1.5 equiv.), H_2O/MeCN (1:4), 3 mA, 3 F/mol, graphite electrodes.

This could perhaps be due to RVC electrodes being more efficient at performing oxidation of Selectfluor. However, a total lack of product was deemed to be unusual. When the same reaction was performed with graphite electrodes under inert conditions, a completely different product mixture was obtained, along with distinct fluorine multiplets in the ^{19}F NMR spectrum (**Figure 4.6**).

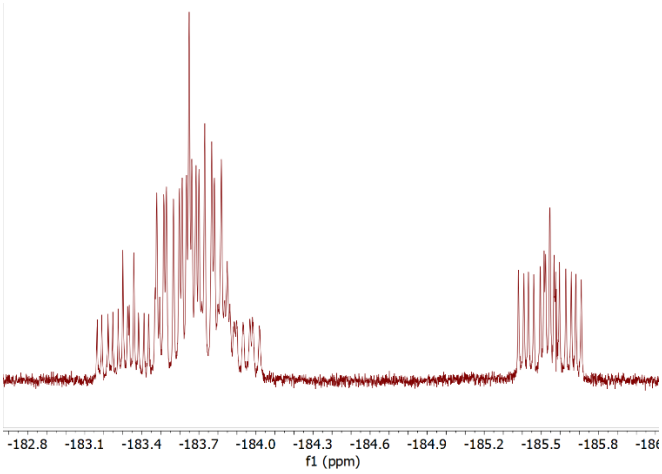

Figure 4.6: ^{19}F NMR spectrum (376 MHz, $CDCl_3$) of the crude product mixture generated when Boc-Pro-OMe (**121**) was reacted under the conditions shown in **Scheme 4.28**, except with an inert atmosphere.

The LCMS spectrum of the major product generated when Boc-Pro-OMe (121) was reacted with Selectfluor (conditions shown in **Scheme 4.28**, except with an inert atmosphere) had a peak with *m/z* values of 146.1 and 164.1. If the M^+ is 146, this indicates that the product structure is either a hydroxyl-substituted product (*e.g.* **377**), or perhaps a fluorine-substituted product with a double bond (*e.g.* **378**) (**Figure 4.7**). Whilst the ^{19}F NMR spectrum does have complex multiplets in the correct ppm range for a C(sp^3)-F bond, it is possible that this might be caused by a minor additional product. If the M^+ is 164, the product could be a fluorinated hydroxyproline derivative (**379**) (**Figure 4.7**). However, the most likely structure is a hydroxyproline derivative (**377**).

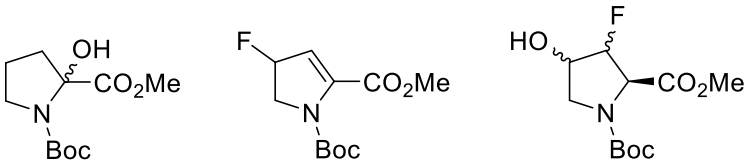

377 **378** **379**

MW: 245 MW: 245 MW: 263

Figure 4.7: Possible structures for the unknown product; (L-R) Boc-2-hydroxyproline methyl ester (**377**), a fluoroproline with a double bond (**378**), fluorohydrin **379**.

Comparison of the ^1H NMR spectrum of the product with spectral data for 3-, 4-, and 5-hydroxyprolines published in the literature confirmed that the product was none of these.[34–36] Therefore, the only possible option would be the 2-substituted hydroxyproline (**377**) (**Figure 4.7**). However, the proton signals in the ^1H NMR spectrum of the product do not support this

theory (**Figure 4.8**). The three peaks at ~5.6, ~4.9, and ~4.5 ppm are fairly high for aliphatic protons that aren't situated on the α-position. Additionally, examination of the COSY spectrum revealed that none of these three protons are correlated with each other, but the two at 4.9 and 4.5 ppm are correlated with the two at 2.6 and 2.3 ppm. Also, there should be 6 proton peaks instead of 5. The product appears to exist as a mixture of at least two stereoisomers.

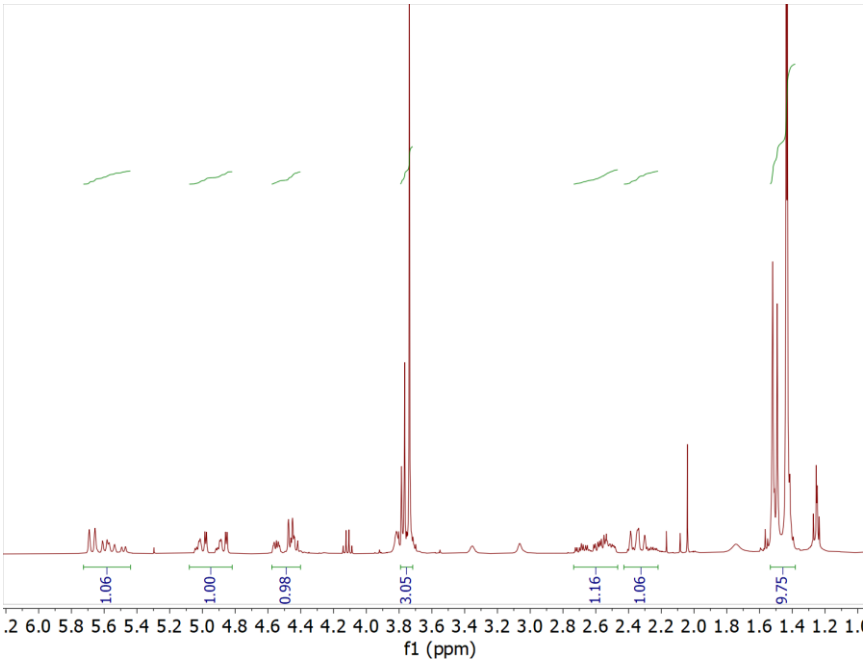

Figure 4.8: ^{1}H NMR spectrum (400 MHz, $CDCl_3$) for the unknown product produced from the reaction of Boc-Pro-OMe (**121**) with Selectfluor under electrochemical conditions (conditions shown in **Scheme 4.28**, except with an inert atmosphere).

The unknown product is therefore unlikely to be 2-hydroxyproline **377**. The presence of five proton peaks suggests that the unknown product is more likely to be fluorohydrin **379** rather than fluoroalkene **378**. However, due to a lack of available data, this unknown product ultimately could not be identified.

4.5 Indole dimerization using electrochemical conditions

When attempting to trifluoromethylate 3-methylindole (**165**), an unusual tricyclic dimer (**166**) was instead formed (see **Chapter 2**, **Section 2.4.2**) (**Scheme 4.29**).

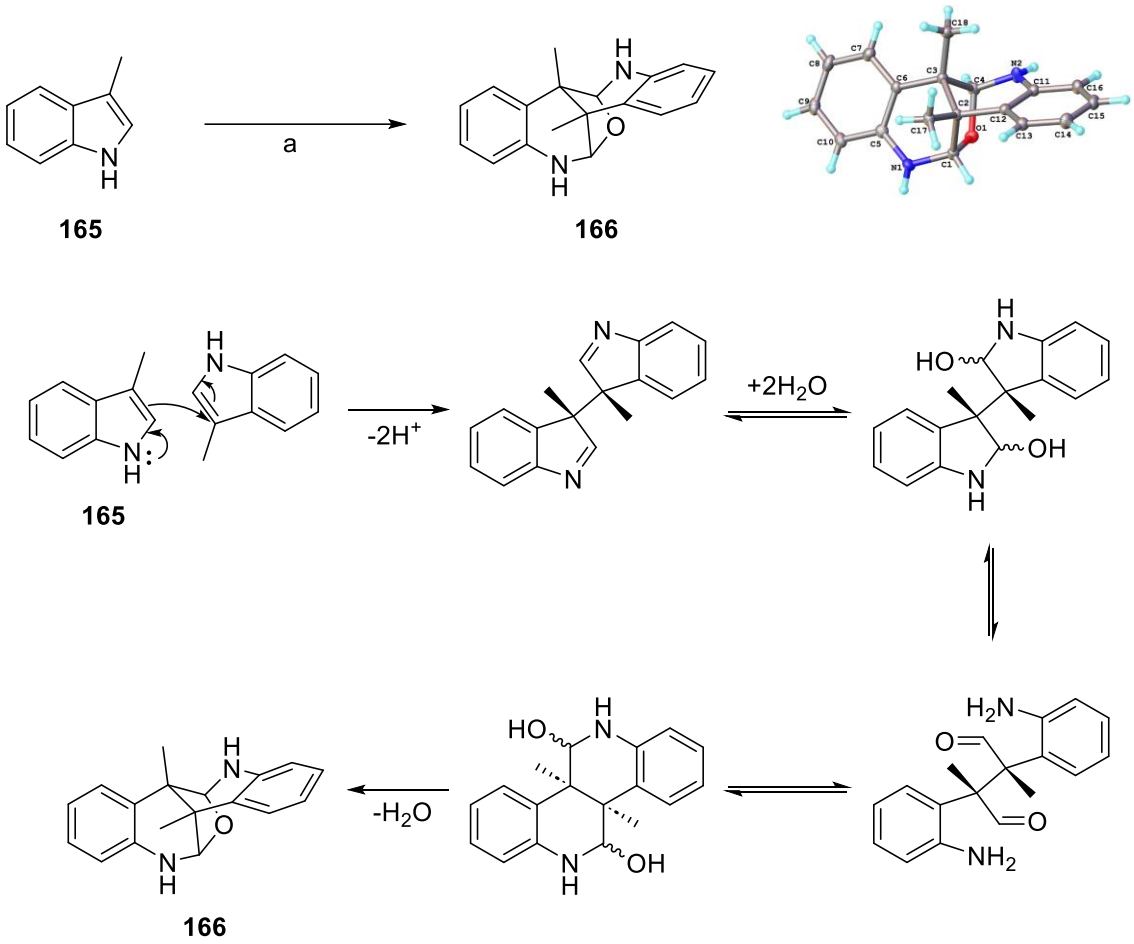

Scheme 4.29: Conversion of 3-methyl indole (**165**) to polycyclic dimer (**166**), the structure of which was confirmed by X-Ray crystallography; reagents and conditions: a) sodium triflinate, 0.2M Bu_4NPF_6, DMSO, 5 mA, 3 F/mol, graphite electrodes. Molecular structure also displayed, reported with a 50% thermal ellipsoid probability. Proposed mechanism also provided (Ling *et al.*[37])

As mentioned, this structure has been previously reported by Ling *et al.* in 2002.[37] Ling *et al.* also suggest a mechanism for its formation (**Scheme 4.29**). Prior to this paper, the structure of **166** had been previously misreported (**Figure 4.9**).

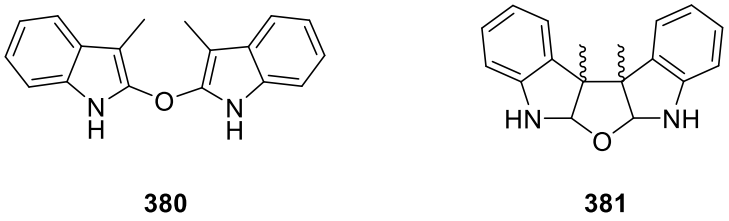

Figure 4.9: Previous structures (**380** and **381**) which were incorrectly attributed to the dimeric indole **166**.

Ling *et al.* suggest that **166** has in fact been formed from 3-methylindole (**165**) as a result of oxidation by $FeCl_3$,[38] copper methoxide,[39] pulse radiolysis,[40] and anodic oxidation.[41]

It was thought that perhaps other indole compounds may be capable of forming such dimeric structures under oxidative conditions. Generation of a highly complex and rigid structure in a single step may prove beneficial for construction of novel bioactive compounds. Therefore, the electrochemical conditions displayed in **Scheme 4.29** (excluding sodium triflinate) were applied to a number of other indoles. The results of these investigations are summarised in **Table 4.2**.

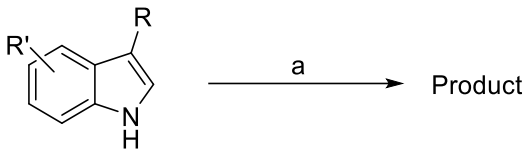

Entry	Substrate	Product	Yield (%)[b]
1	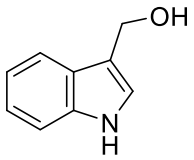 **212**	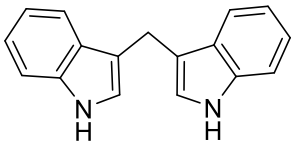 **382**	22
2	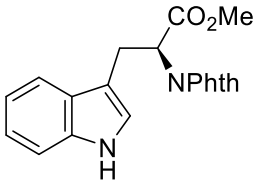 **162**	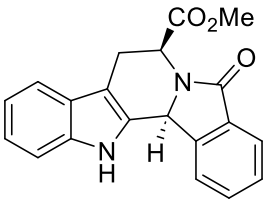 **383**	8
3[c]	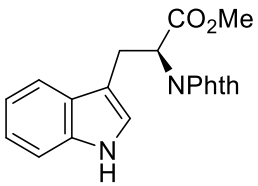 **162**	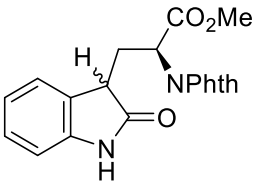 **384**	33

4	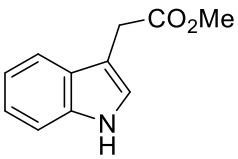 **195**	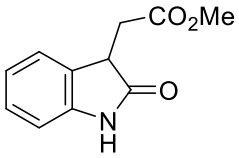 **385**	11
6	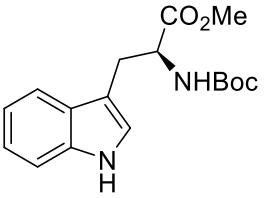 **164**	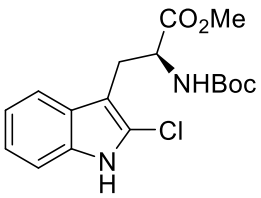 **175**	trace
7	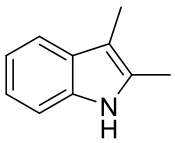 **386**	Multiple unidentified products	n/a
8	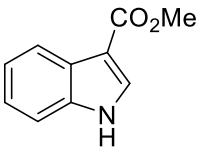 **169**	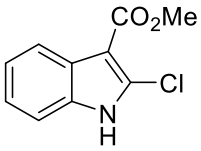 **170**	3
9	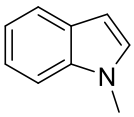 **210**	Starting material + minor unidentified products	n/a

Table 4.2: Indoles used as substrates for electrochemical oxidation, their resultant products, and corresponding yields; a) 0.2M Bu_4NPF_6, DMSO, 5 mA, 3 F/mol, graphite electrodes; b = isolated yield; c = $MnBr_2$ (10 mol%) added to reaction mixture.

The production of the known natural product diindolylmethane (DIM) (**382**) was observed from the attempted dimerization of indole-3-carbinol (**212**) (**Table 4.2, Entry 1**). This transformation occurs within the human body, but the electrochemical transformation of indole-3-carbinol (**212**) into DIM (**382**) has not been reported before. However, electrochemical syntheses of diindolylmethanes from alcohols and indoles without a C-3 substituent have been known since the 1990s.[42] An example of such a procedure published by Li *et al.* is shown below in **Scheme 4.30**.[43]

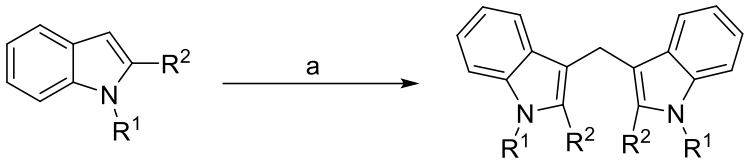

Scheme 4.30: The electrochemical reaction of indoles with methanol to produce diindolylmethanes;[43] reagents and conditions: a) C (+) Pt (-), 20 mA, MeOH (10 e.), Et_4NBF_4 (1 eq.), NHPI (10 mol%), H_2O (8.0 mL), air, rt, 4 h.

The mechanism proposed by Li *et al.* for the transformation shown in **Scheme 4.30** involves generation of a carbinol intermediate (**388**); a tautomer of indole-3-carbinol (**212**) (**Scheme 4.31**). It is therefore plausible that formation of DIM (**382**) from indole-3-carbinol (**212**) could follow a similar mechanistic route to the one shown in **Scheme 4.31**.

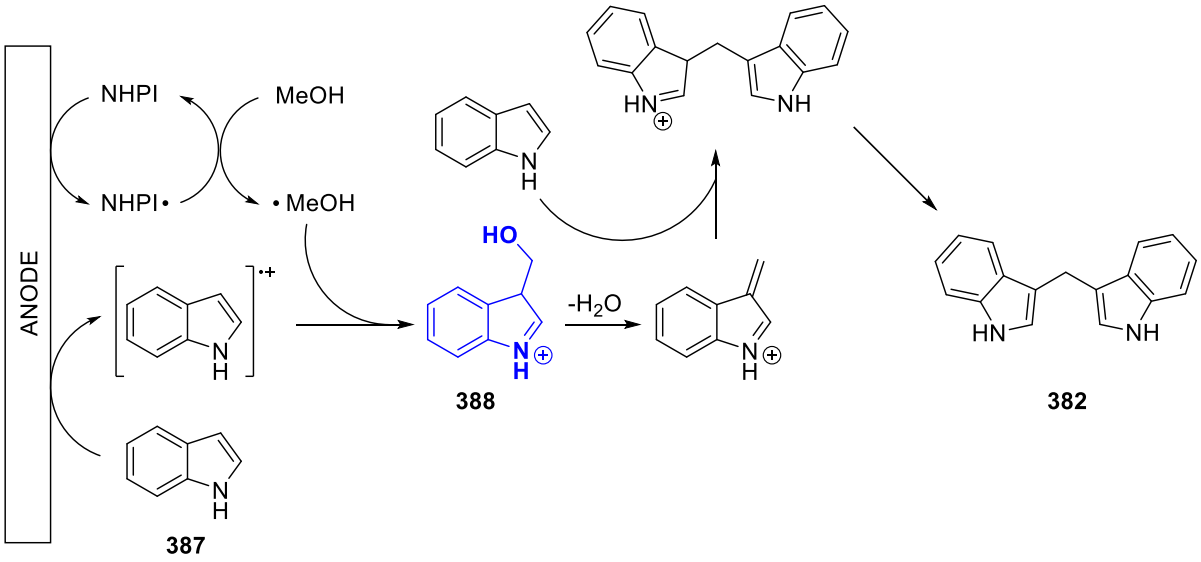

Scheme 4.31: Mechanism proposed by Li *et al.* for the coupling of indoles and alcohols to form diindolylmethanes.[43]

The next substrate with which dimerization was attempted was phthalimide-protected tryptophan (**162**). This substrate was trialled because it was thought that a tryptophan dimer similar to **166** would be an interesting motif which could be incorporated into peptides. However, an attempt to dimerise phthalimide-protected tryptophan **162** resulted instead in the isolation of a compound with an unusual fused structure ((*S,S*)-**383**) (**Table 4.2, Entry 2**). This compound was identified by comparison of the ^{1}H NMR spectrum to published data,[44] and confirmed by LCMS (*m/z* 333.4).

A diastereomer of this compound ((*R,S*)-**383**) has been made previously[45] by reaction of *N*-Phth-Trp-OMe (**162**) with trifluoromethylsulfonic acid (TfOH) to form hydroxylactam **389**. This was then immediately followed by reduction of the hydroxyl group using Hantzsch ester **390** in conjunction with a phosphoric acid catalyst (**391**) to deliver enantiopure (*R,S*)-**383** (**Scheme 4.32**).

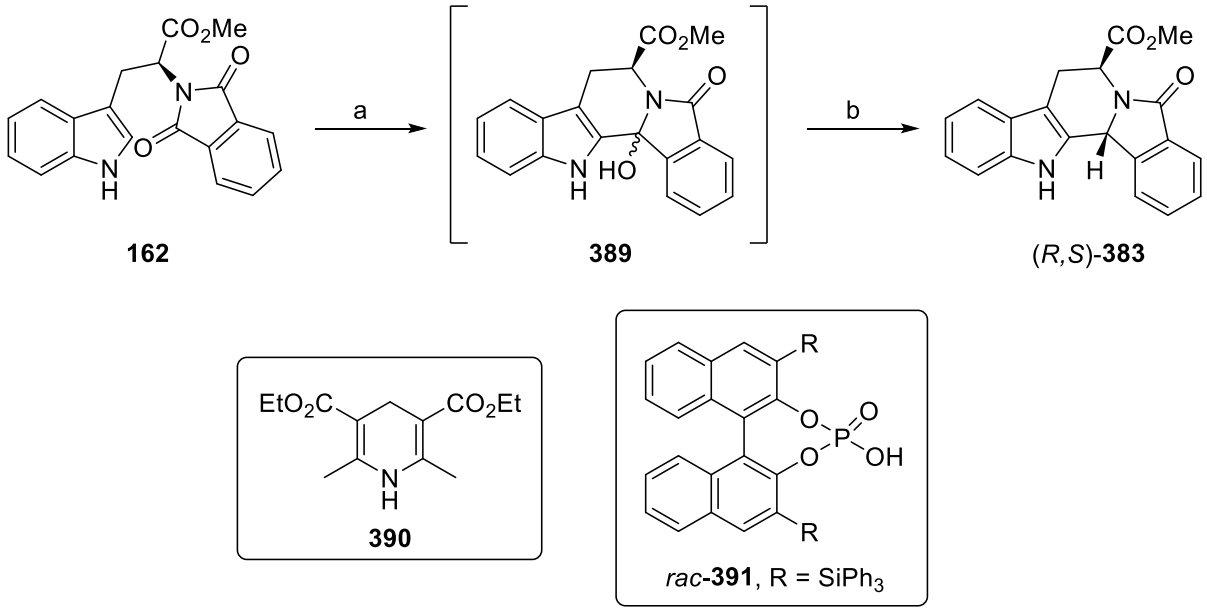

Scheme 4.32: Synthetic route towards (*R,S*)-**383** reported by Yin *et al.*[45] involving cyclisation of *N*-Phth-Trp-OMe (**162**) to form hydroxylactam **389**, followed by reduction using Hantzsch ester **390** as the hydride source; reagents and conditions: a) TfOH, DCM, 0 °C to rt, 30 mins, used without purification; b) Hantzsch ester **390**, *(rac)*-**391** (10 mol%), toluene, 60 °C, 75% over two steps.

It is probable that the transformation of *N*-Phth-Trp-OMe (**162**) that we observed (**Table 4.2, Entry 2**) follows a similar pathway to Yin *et al.* (**Scheme 4.32**). However, it is unclear how the cyclisation and subsequent reduction takes place under the electrochemical conditions described in **Scheme 4.29**. Additionally, our conditions formed the opposite diastereomer in an apparently enantioselective manner.

A second reaction of *N*-Phth-Trp-OMe (**162**) with additional $MnBr_2$ (10 mol%) included in the reaction mixture did not result in formation of fused product (*S,S*)-**383**. Instead, an oxindole (**384**) was formed (**Table 4.2, Entry 3**). An oxindole product (**385**) was also isolated from the reaction of methylindole-3-acetate (**195**) (**Table 4.2, Entry 4**). These products likely resulted from the reactions being carried out under air and in a wet solvent. A report published in 2023 detailed the formation of oxindoles from indoles under electrochemical conditions (**Scheme 4.33**).[46]

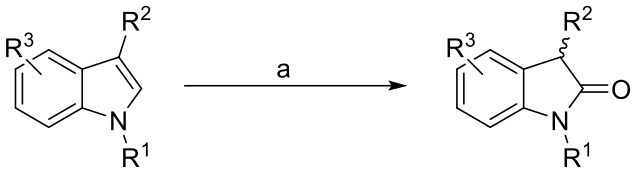

Scheme 4.33: Electrochemical oxidation of indoles to form oxindoles; work by Arteaga Giraldo *et al.*;[46] reagents and conditions: a) KBr (1 eq.), MeCN/H_2O (5:1), GC (+) GC (-), undivided cell, 2.5 mA, 2 F/mol.

It is probable that the oxindoles observed during our own investigations arise due to a similar mechanism. However, in this paper, the authors purport that this transformation occurs *via* a bromo-substituted intermediate generated from the reaction between the indole substrate and KBr (**Scheme 4.34**).

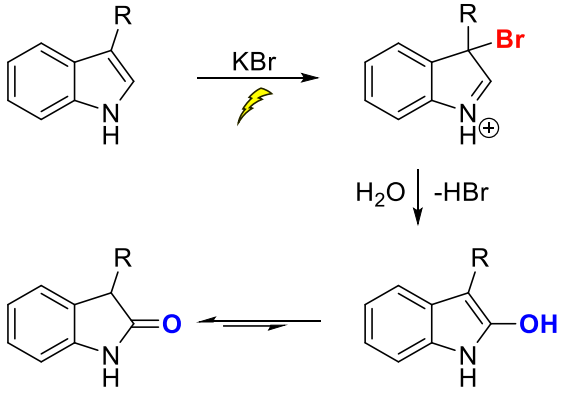

Scheme 4.34: Mechanism proposed by Arteaga Giraldo *et al.*[46] for bromide-mediated electrochemical oxindole synthesis.

Given that there was no source of bromide ions in our reaction, it is unlikely that oxindole formation occurred *via* the above mechanism. However, Giraldo *et al.*[46] do not discuss whether or not the bromide source is essential for product formation.

When *N*-methylindole (**210**) was used as the substrate for electrochemical dimerisation, the majority of the product mixture comprised of the starting material (determined by TLC and LCMS analysis) (**Table 4.2, Entry 9**). Small amounts of minor products were formed but none could be identified, and there was no evidence of the desired tricyclic dimer in the LCMS spectrum.

Contrary to the reaction of the *N*-Phth-Trp-OMe substrate (**162**), anodic oxidation of Boc-Trp-OMe (**164**) did not appear to result in formation of an oxindole. Instead, traces of the 2-chlorotryptophan product (**175**) (See **Chapter 2, Section 2.5.2**) were observed in the ^{1}H NMR spectrum of the crude product mixture (**Table 4.2, Entry 6**). At the time of reaction this product

was not identified, but was recognised to be chlorotryptophan **175** when **175** was properly synthesised at a later date (See **Chapter 2**).

Anodic oxidation of 2,3-dimethylindole (**386**) resulted in formation of a number of products (**Table 4.2, Entry 7**). Two fractions were isolated. Fraction 1 appeared to consist of mostly starting material, with an additional product (*m/z* = 289). This mass suggests that the product is some sort of dimer (starting material M_r = 145). The dimer could only be linked through the indolic benzene ring (*e.g.*, **392**) to achieve this mass, which is unlikely (**Figure 4.10**). However, the ^{1}H NMR spectrum of Fraction 1 corroborates this theory, with peaks for six aromatic protons.

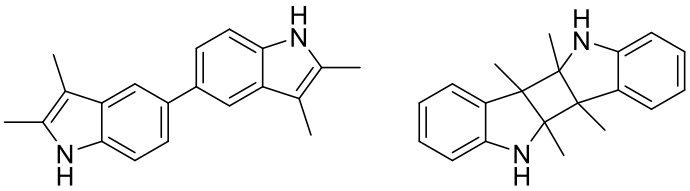

392 **393**

Figure 4.10: Possible structures for the unknown products from the anodic oxidation of 2,3-dimethylindole; (L-R) dimer linked through benzene ring (**392**) (Fraction 1), dimer linked through C-3 and C-4 (**393**) (Fraction 2).

The product in Fraction 2 had a similar mass (*m/z* = 291) to the product in Fraction 1, which again suggests the presence of a dimer. However, the dimer is most likely linked at positions 2 and 3 instead of on the benzene ring (*e.g.*, **393**) (**Figure 4.10**). This structure is suggested as a possibility because it fits the LCMS data.

When methylindole-3-carboxylate (**169**) was used as the substrate, a very small amount of the corresponding 2-chloro derivative (**170**) was isolated (**Table 4.2, Entry 8**). This was found to be due to trace amounts of DCM present in the reaction mixture (see **Chapter 2**, **Section 2.5.2**).

Whilst only a handful of indoles were tested, the tricyclic dimer structure appeared elusive; it is possible that this product is just a unique quirk of the 3-methylindole substrate (**165**).

4.6 Unexpected Reactions of Iodoindoles

When preparing substrates for electrochemical chlorination (See **Chapter 2**, **Section 2.5.2**), a 5-iodoindole derivative (**188**) was synthesised by reacting an indole with NIS in neat TFA (**Scheme 4.35**).

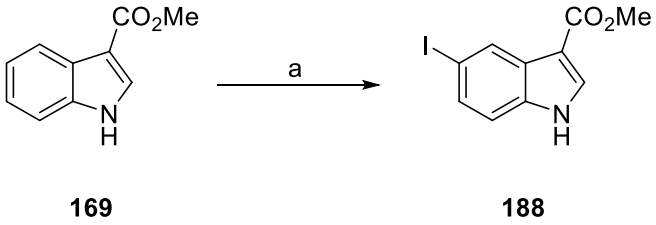

169 **188**

Scheme 4.35: Iodination of methyl-3-indole carboxylate (**169**) to produce 5-iodo derivative **188**; reagents and conditions: a) NIS, TFA (neat), 1 h, rt, 28%.

This reaction successfully afforded the desired product in a 28% yield. Both the 6-iodo and 7-iodo (**395**) products were also observed in the product mixture (determined by comparisons of the ^{1}H NMR spectrum of the crude product mixture to published data),[47] though these were not isolated. At a later date the reaction was repeated using slightly altered conditions ($CHCl_3$ solvent instead of neat TFA), which gave rise to a different product (**394**). This product was identified using X-ray crystallography, revealing that the iodine had substituted onto the 6-position, and an ethoxy substituent of unknown origin had been placed at the 2-position (**Scheme 4.36**). TLC analysis of the crude reaction mixture indicated only starting material and 6-iodo-2-ethoxy **394** were present, along with traces of mono-iodinated compounds (assessed by LCMS).

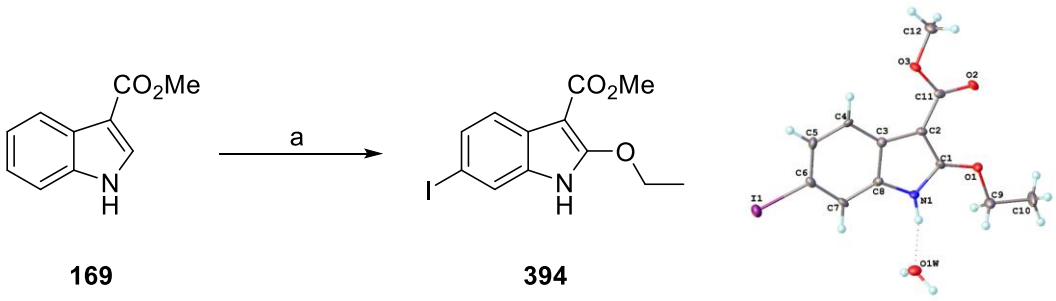

169 **394**

Scheme 4.36: Unexpected transformation of methyl-3-indole carboxylate (**169**) into the corresponding 6-iodo-2-ethoxy derivative (**394**); reagents and conditions: a) TFA (2 equiv.), NIS, $CHCl_3$, 4 h, rt, 20%. The molecular structure of **394** is also displayed, and is reported with a 50% thermal ellipsoid probability.

It was initially unclear where the ethoxy substituent had arisen from. Inspection of the chloroform used in the reaction revealed that it contained 0.75 % ethanol as a stabiliser, which was presumed to be the cause of the ethoxy substitution. To verify whether this was the case, a reaction was run instead using $CDCl_3$, which did not contain any ethanol as a stabiliser. This reaction did not produce an ethoxy-substituted product, confirming that the trace ethanol in the non-deuterated chloroform was causing the issue. Instead, the 7-iodo derivative (**395**) was isolated as the major product (**Scheme 4.37**). The 5-iodo (**188**) and 6-iodo products were also observed (confirmed by ^{1}H NMR spectroscopic analysis).

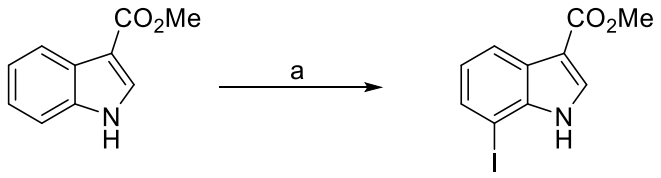

169 **395**

Scheme 4.37: Iodination of methyl-3-indole carboxylate (**169**) at the 7-position in deuterated chloroform; Reagents and conditions: a) NIS, TFA (2 equiv.), $CDCl_3$, 4h, rt, 21%.

To investigate whether the yield of the reaction shown in **Scheme 4.36** could be improved, a trial using additional ethanol (10% EtOH in $CHCl_3$) was run. This did not make a significant difference to the yield of **394** (conversion of 20% assessed by ^{1}H NMR). Only the starting material and ethoxy product (**394**) were observed in the ^{1}H NMR spectrum of the crude reaction mixture.

It is interesting to note that only the 6-iodo-2-ethoxy compound **394** was isolated from the reaction shown in **Scheme 4.36**. Given the propensity of the indole substrate to undergo iodination at multiple positions (C-5, C-6, and C-7), observation of 5- or 7-iodo-2-ethoxy products (**396, 397**) may be expected (**Figure 4.11**). However, examination of LCMS and ^{1}H NMR spectroscopic data of the crude product mixture did not indicate the presence of either of these compounds. It is possible that the ethoxy substituent adds to the molecule first, activating the 6-position only for iodination (**Scheme 4.38**).

396 **397**

Figure 4.11: Structures of the expected products from the reaction shown in **Scheme 4.36**. No evidence of the 5-iodo-2-ethoxy product (**396**) and the 7-iodo-2-ethoxy product (**397**) was observed.

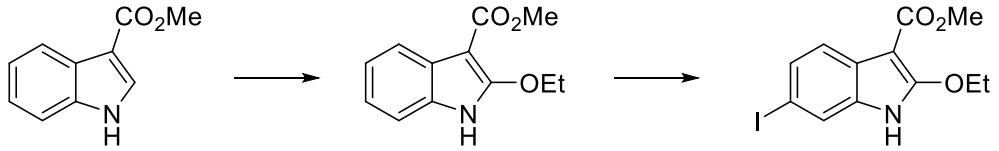

169 **398** **394**

Scheme 4.38: Plausible route for formation of 6-iodo-2-ethoxy product **394** from methyl-3-indole carboxylate (**169**) *via* a 2-ethoxy intermediate (**398**).

4.7 Chapter summary

A dityrosine compound (**352**) was successfully synthesised via electrochemical oxidative coupling (**Scheme 4.39**).

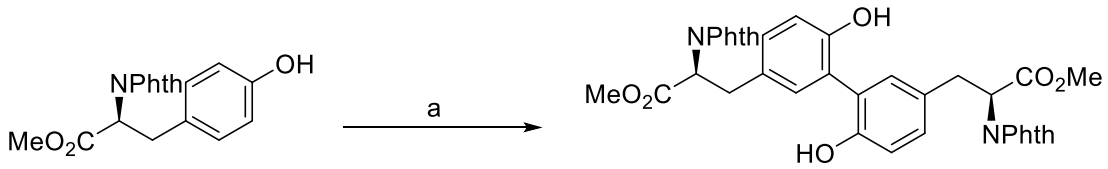

349 **352**

Scheme 4.39: The electrochemical homo-coupling of *N*-phthaloyl tyrosine (**349**) to produce *N,N'*-diphthaloyl dityrosine (**352**); reagents and conditions: a) (+) graphite (-) graphite, DIPEA, HFIP, 5 mA/cm^2, 1.5 F/mol, 20%.

To establish whether the coupling conditions would remain effective for larger tyrosine-containing substrates, a Tyr-Ala dipeptide was successfully coupled to itself without a diminished yield (See **Section 4.3, Scheme 4.14**).

Selectfluor-mediated Shono-type oxidation of proline-derived substrates was explored (**Scheme 4.40**).

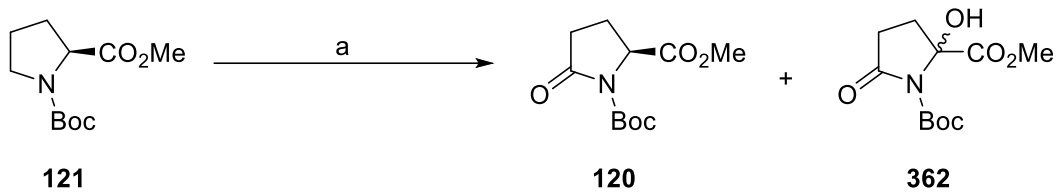

121 **120** **362**

Scheme 4.40: Shono-type oxidation of proline mediated by Selectfluor, forming a mixture of 5-oxoproline derivatives (**120, 362**); reagents and conditions: a) various; see **Table 4.1.**

An α-hydroxylated byproduct (**362**) was postulated to occur *via* an α-fluorinated intermediate (**363**), which are notoriously unstable. It was found that the oxidation takes place when the proline nitrogen is protected with a Boc or acetyl group, or as an amide in a Pro-Gly dipeptide (See **Section 4.4, Scheme 4.27**).

An intriguing tricyclic dimer was isolated from the attempted electrochemical trifluoromethylation of 3-methylindole (**Scheme 4.41**).

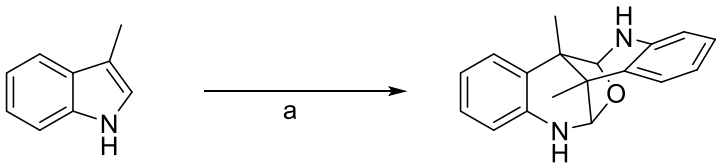

165 **166**

Scheme 4.41: Conversion of 3-methyl indole (**165**) to polycyclic dimer **166**; reagents and conditions: a) 0.2M Bu_4NPF_6, DMSO, 5 mA, 3 F/mol, graphite electrodes.

Due to the novelty of this complex structure, a number of other indolic substrates were reacted under electrochemical conditions in an attempt to replicate this scaffold (See **Section 4.5, Table 4.2**). All of the indole substrates trialled failed to generate the desired tricyclic dimer, but several substrates underwent an alternative transformation. A couple of substrates (**162, 195**) (including a tryptophan derivative) were converted to oxindoles (**384, 385**). Indole-3-carbinol (**212**) reacted to form diindolylmethane (DIM) (**382**).

An unexpected 6-iodo-2-ethoxy product (**394**) was isolated when attempting to iodinate methyl-3-indole carboxylate (**169**) (**Scheme 4.42**).

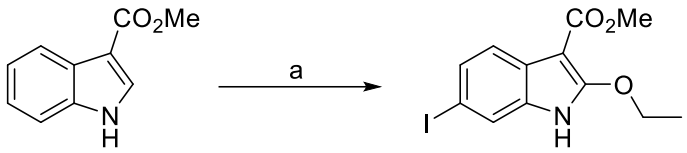

169 **394**

Scheme 4.42: Unexpected transformation of methyl-3-indole carboxylate (**169**) into the corresponding 6-iodo-2-ethoxy derivative (**394**); reagents and conditions: a) TFA (2 equiv.), NIS, $CHCl_3$, 4 h, rt, 20%.

This was assumed to occur due to the presence of minor amounts (0.75%) of EtOH added to the reaction solvent as a stabiliser. Only the 6-iodo derivative (**394**) was isolated, despite the lack of selectivity normally exhibited by iodination reactions.

4.8 References

1 O. Boutureira and G. J. L. Bernardes, *Chem. Rev.*, 2015, **115**, 2174–2195.
2 C. Canovas, P.-S. Bellaye, M. Moreau, A. Romieu, F. Denat and V. Goncalves, *Org. Biomol. Chem.*, 2018, **16**, 8831–8836.
3 D. Alvarez Dorta, D. Deniaud, M. Mével and S. G. Gouin, *Chem. Eur. J.*, 2020, **26**, 14257–14269.
4 I. M. Stanković, D. M. Božinovski, E. N. Brothers, M. R. Belić, M. B. Hall and S. D. Zarić, *Cryst. Growth Des.*, 2017, **17**, 6353–6362.
5 D. Matters, H. J. Cooper, L. McDonnell, J. Iniesta, J. Heptinstall, P. Derrick, D. Walton and I. Peterson, *Anal. Biochem.*, 2006, **356**, 171–181.
6 F. Sanger and E. O. P. Thompson, *Biochim. Biophys. Acta*, 1963, **71**, 468–471.
7 T. Michon, M. Chenu, N. Kellershon, M. Desmadril and J. Guéguen, *Biochemistry*, 1997, **36**, 8504–8513.
8 C. S. Yeung and V. M. Dong, *Chem. Rev.*, 2011, **111**, 1215–1292.
9 S. Tang, Y. Liu and A. Lei, *Chem.*, 2018, **4**, 27–45.
10 J. L. Röckl, D. Pollok, R. Franke and S. R. Waldvogel, *Acc. Chem. Res.*, 2020, **53**, 45–61.
11 T. Osa, Y. Kashiwagi, Y. Yanagisawa and J. M. Bobbitt, *J. Chem. Soc., Chem. Commun.*, 1994, 2535–2537.
12 J. L. Röckl, M. Dörr and S. R. Waldvogel, *ChemElectroChem*, 2020, **7**, 3686–3694.
13 A. Wiebe, D. Schollmeyer, K. M. Dyballa, R. Franke and S. R. Waldvogel, *Angew. Chem.*, 2016, **128**, 11979–11983.
14 A. Kirste, B. Elsler, G. Schnakenburg and S. R. Waldvogel, *J. Am. Chem. Soc*, 2012, **134**, 3571–3576.
15 J. M. Souza, B. I. Giasson, Q. Chen, V. M.-Y. Lee and H. Ischiropoulos, *J. Biol. Chem.*, 2000, **275**, 18344–18349.
16 Y. K. Al-Hilaly, T. L. Williams, M. Stewart-Parker, L. Ford, E. Skaria, M. Cole, W. G. Bucher, K. L. Morris, A. A. Sada, J. R. Thorpe and L. C. Serpell, *Acta Neuropathol. Commun.*, 2013, **1**, 83.
17 B. P. Partlow, M. B. Applegate, F. G. Omenetto and D. L. Kaplan, *ACS Biomater. Sci. Eng.*, 2016, **2**, 2108–2121.

18 Y. Ding, Y. Li, M. Qin, Y. Cao and W. Wang, *Langmuir*, 2013, **29**, 13299–13306.
19 D. A. Malencik and S. R. Anderson, *Amino Acids*, 2003, **25**, 233–247.
20 A. C. Sather, H. G. Lee, V. Y. De La Rosa, Y. Yang, P. Müller and S. L. Buchwald, *J. Am. Chem. Soc.*, 2015, **137**, 13433–13438.
21 L. Eberson, M. P. Hartshorn and O. Persson, *J. Chem. Soc., Perkin Transactions 2*, 1995, **2**, 1735.
22 M. Lucarini, V. Mugnaini, G. F. Pedulli and M. Guerra, *J. Am. Chem. Soc*, 2003, **125**, 8318–8329.
23 J. M. Ramos-Villaseñor, E. Rodríguez-Cárdenas, C. E. Barrera Díaz and B. A. Frontana-Uribe, *J. Electrochem. Soc.*, 2020, 167, 155509.
24 B. Elsler, A. Wiebe, D. Schollmeyer, K. M. Dyballa, R. Franke and S. R. Waldvogel, *Chemistry – A European Journal*, 2015, 21, 12321–12325.
25 J. L. Röckl, D. Schollmeyer, R. Franke and S. R. Waldvogel, *Angewandte Chemie*, 2020, 132, 323–327.
26 Y. Imada, Y. Okada and K. Chiba, *ChemElectroChem*, 2020, 7, 1619–1622.
27 Z. Sun, Z. Shang, N. Forelli, K. H. L. Po, S. Chen, S. F. Brady and X. Li, *Angewandte Chemie International Edition*, 2020, 59, 19868–19872.
28 D. Ulbrich, C. G. Daniliuc and G. Haufe, *J. Fluor. Chem.*, 2016, 188, 65–75.
29 A. M. Jones and C. E. Banks, *Beilstein-Institut Zur Forderung der Chemischen Wissenschaften*, 2014, preprint, DOI: 10.3762/bjoc.10.323.
30 B. Ticconi, M. Mazzonna, O. Lanzalunga and A. Lapi, *Tetrahedron*, 2019, 75, 3579–3585.
31 F. Wang, M. Rafiee and S. S. Stahl, *Angewandte Chemie*, 2018, 130, 6796–6800.
32 Z. Chang, S. Wang, J. Huang, G. Chen, Z. Tang, R. Wang and D. Zhao, *Sci Adv*, DOI:10.1126/sciadv.adj3090.
33 S. S. Libendi, Y. Demizu, Y. Matsumura and O. Onomura, *Tetrahedron*, 2008, 64, 3935–3942.
34 M.-C. Li, Y.-J. Liu, K.-C. Hsu, T.-H. Lin, C.-W. Lin, J.-C. Horng and S.-K. Wang, *Bioorg Chem*, 2022, 119, 105491.
35 V. K. Aggarwal, C. J. Astle, H. Iding, B. Wirz and M. Rogers-Evans, *Tetrahedron Lett.*, 2005, 46, 945–947.
36 C. K. Prier, M. M. C. Lo, H. Li and N. Yasuda, *Adv Synth Catal*, 2019, 361, 5140–5143.
37 K.-Q. Ling, T. Ren, J. D. Protasiewicz and L. M. Sayre, *Tetrahedron Lett.*, 2002, 43, 6903–6905.
38 H. von Dobeneck and W. Lehnerer, *Chem Ber*, 1957, 90, 161–171.
39 J. Tsuji, H. Kezuka, H. Takayanagi and K. Yamamoto, *Bull Chem Soc Jpn*, 1981, 54, 2369–2373.
40 X. Shen, J. Lind, T. E. Eriksen and G. Merényi, *J. Chem. Soc., Perkin Trans. 2*, 1989, 555–562.
41 A. Berlin, A. Canavesi, G. Schiavon, S. Zecchin and G. Zotti, *Tetrahedron*, 1996, 52, 7947–7960.
42 K. Suda and T. Takanami, *Chem Lett*, 1994, 23, 1915–1916.
43 B. Li, H. Qin, K. Yan, J. Ma, J. Yang and J. Wen, *Organic Chemistry Frontiers*, 2022, 9, 6861–6868.
44 P. B. Wakchaure, V. G. Puranik and N. P. Argade, *Tetrahedron Asymmetry*, 2009, 20, 220–224.
45 Q. Yin, S. G. Wang and S. L. You, *Org. Lett.*, 2013, 15, 2688–2691.
46 J. J. Arteaga Giraldo, A. C. Lindsay, R. C.-Y. Seo, P. A. Kilmartin and J. Sperry, *Org. Biomol. Chem.*, 2023, 21, 5609–5615.
47 M. Somei, A. Tanimoto, H. Orita, F. Yamada and T. Ohta, *Heterocycles*, 2001, 54, 425.

Chapter 5: Conclusions and Future Work

5.1 Conclusions and Future Work - Chapter 2

An initial foray into electrochemical fluorination of amino acid derivatives using the method of Baran *et al.* revealed that fluorination could be achieved with valine and leucine (replicated from previously published conditions[1]), but other fluorination of amino acids with tertiary carbons were less successful (**Section 2.3.2**). The attempted fluorination of an isoleucine derivative (**93**) resulted in non-selective fluorine substitution at two sites, the beta and gamma carbons, generating a mixture of four fluorinated diastereomers (**99a-99b**). Fluorination of a 4-methylproline derivative (**94**) also proved to be unsuccessful, producing an unidentified byproduct.

The compatibility of various amine-protecting groups with the fluorination protocol was also investigated, in an attempt to find alternatives to the phthalimide group used by the Baran group (**Section 2.3.2**). A Boc protecting group was found to permit the electrochemical fluorination of valine to proceed in a 34% yield. Whilst this is a low yield, a Boc group is much more convenient for general use, particularly in the context of peptide synthesis. In addition, when assessing the protecting group compatibility, it was initially assumed that the nitrogen would have to be doubly protected, *i.e.*, with both protons removed. The success of the Boc group disproved this notion. Therefore, future work may entail the synthesis of several valine derivatives with other single protecting groups, *e.g.*, Fmoc, Ts, Bn (mono), allyl, Bz, etc. These could be subjected to electrochemical fluorination and assessed on their success.

Electrochemical fluorination of proline-derived hemioxalates was also attempted (**Section 2.3.3**). This was largely unsuccessful, in part due to the tendency of proline to undergo alternative transformations under electrochemical conditions. When a benzyl group is used to protect the amine, conversion to a pyrrole (**126**) is observed. When an amide or carbamate group is used as a protecting group, the proline is oxidised to form the corresponding 5-oxoproline (**120**).

During this investigation, a number of fluorinated unsaturated lactams (**Scheme 5.1**) were isolated from the reactions of *N*-benzyl-2-methylpyrrole carboxylate (**126**) and 2-methylpyrrole carboxylate (**136**) with Selectfluor. These compounds were isolated in low yields, but may be of interest due to their unusual fluorinated structures (**Scheme 5.1**).

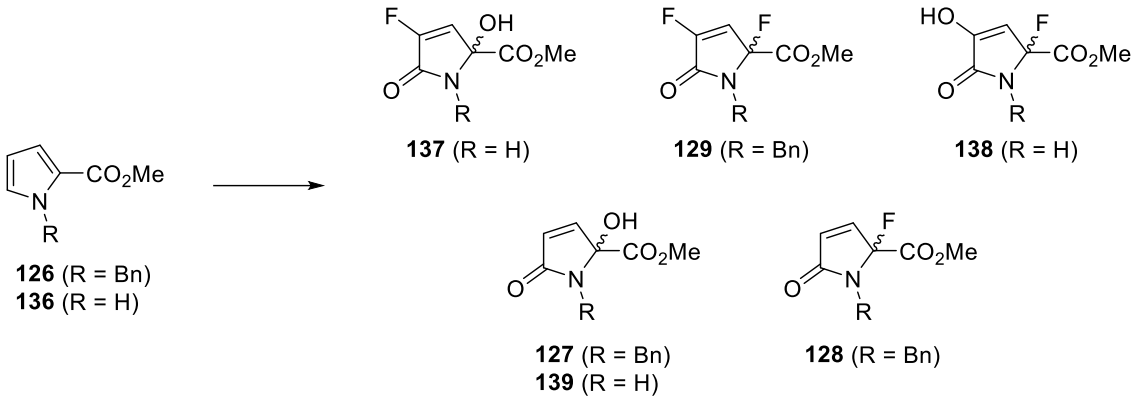

Scheme 5.1: Fluorination of proline-derived pyrroles (**126** and **136**) using Selectfluor, resulting in generation of several fluorinated enones (**128, 129, 137, 138**); reagents and conditions: various, see **Section 2.3.3.**

Future work could involve optimising these fluorination reactions to obtain better yields and selectivity. Additionally, the possibility of removing the methyl ester protecting group to permit further reactions could be explored. If the fluorinated lactams can tolerate amide coupling reactions, they may be able to be built into larger peptides as a proline mimic.

Electrochemical trifluoromethylation of tryptophan derivatives was also briefly investigated (**Section 2.4.2**). Trifluoromethylation of Phth-Trp-OMe (**162**) was achieved in a yield of 35%; further optimisation is required to boost this yield.

An electrochemical chlorination procedure using DCM as the chlorine source was developed, and the method was applied to a range of aromatic and heteroaromatic molecules (**Section 2.5.2, Table 2.8**). The yields of chlorination were variable, but the reaction was more successful with electron-rich substrates. Gratifyingly, a tryptophan substrate (**164**) was successfully chlorinated in a 55% yield. Future work in this area may include further mechanistic experiments (*e.g.* CV) to try and establish a mechanism for the chlorination reaction. In particular, the possible role of DMSO in the reaction needs to be investigated, as during optimisation of the method it was found that exchanging the DMSO solvent for MeCN does not permit reaction to take place (**Table 2.7, Entry 6**). A reaction could be run with a smaller proportion of DMSO present (*e.g.*, 1 : 1 : 8 DCM/DMSO/MeCN) to assess the impact on the reaction outcome.

5.2 Conclusions and Future Work - Chapter 3

A method for electrochemical Ni-catalysed coupling of amino acid-derived alkyl bromides and aryl bromides was developed (**Section 3.3.5**). However, the issues of excessive generation

of unwanted alkene byproducts, and preferential formation of biaryl were not fully resolved, resulting in low yields of the desired phenylalanine-derived product (**Table 3.1**). The priority for any future work in this area should be solving the biaryl formation problem. The use of a pyridine base appears to prevent alkene formation, but the alkyl bromide/aryl bromide reaction is not rapid enough to compete with biaryl formation. The use of a dibenzyl protecting group should be revisited (See **Table 3.2**), as the reaction with this substrate successfully generated the desired product and there was leftover aryl bromide post-reaction.

Alternatively, the reaction of 4-bromoproline (**259**) with aryl bromides could be re-examined. This reaction successfully afforded the desired product (**263**) without any discernible elimination to form an alkene, so it could therefore be optimised independently (**Scheme 5.2**). This would provide access to a range of novel arylated proline derivatives.

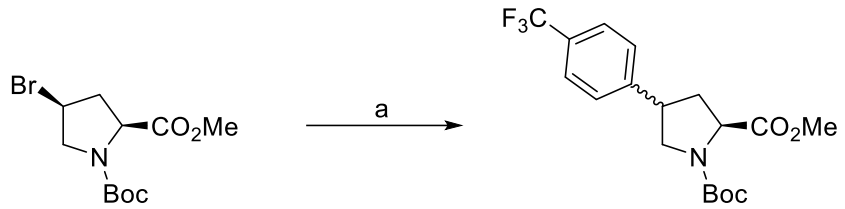

Scheme 5.2: Electrochemical Ni-catalysed coupling of 4-bromoproline **259** with 4-bromobenzotrifluoride (**247**) to form arylated proline derivative **263**; reagents and conditions: a) $NiCl_2$•dtbbpy (10 mol%), LiBr, DIPEA, anhydrous DMA, 4 mL, Ar, 3 mA, C (+) Ni (-), rt, 10 h, 36% (^{1}H NMR conversion yield).

During this investigation, the reaction of *N*-Bn-Ala(Br)-OMe (**289**) with 4-bromobenzotrifluoride (**247**) resulted in the formation of *N*-benzylaniline derivative **297**. This transformation requires further investigation to establish how the C-N bond breaks in such a way. To probe this mechanism, an *N*-benzylalanine derivative (**399**) could be synthesised and subjected to the Ni-catalysed coupling conditions (**Scheme 5.3**). This would indicate the role of the bromine substituent in the original reaction, which may proceed *via* an alkene or aziridine intermediate.

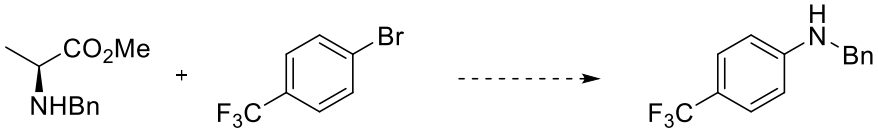

399 **247** **297**

Scheme 5.3: Proposed Ni-catalysed electrochemical reaction of *N*-Bn-Ala-OMe (**399**) with 4-bromobenzotrifluoride (**247**).

Electrochemical Ni-catalysed reactions between cysteine-derived substrates and aryl bromides were also investigated (**Section 3.3.4**). *S*-Arylation was achieved with both cysteine (**Scheme 3.42**) and dicysteine substrates (**Scheme 3.44**). During this process, an electrochemical method for *S*-arylation of cysteine using similar conditions to ours was published.[2] However, *S*-arylation of disulfide substrates, *e.g.*, dicysteine, remains underexplored. There is therefore opportunity for future work in this area. The method could potentially be optimised using a model substrate, then applied to a range of disulfide compounds (**Scheme 5.4**).

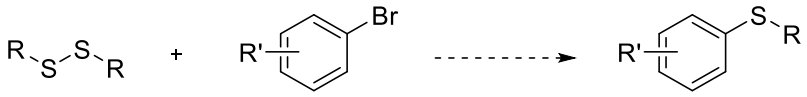

Scheme 5.4: Proposed synthetic protocol development for the generation of aryl sulfides from disulfides.

Electrochemical *N*-arylation of lysine derivatives was also explored briefly (**Scheme 3.47**). Future work would first involve optimising this reaction, and then performing the reaction with a range of aryl bromides to generate novel *N*-arylated lysine derivatives. As mentioned in **Chapter 3, Section 3.3.4**, this reaction could also be used to staple or cyclise larger peptides containing two lysine derivatives using a dibromoaryl linker. Future work may involve investigating this possibility.

A method for Pd-catalysed acetoxylation of valine-derived substrates was developed, using a methoxyiminoacetic acid directing group (**Section 3.4.2**) (**Scheme 5.5**).

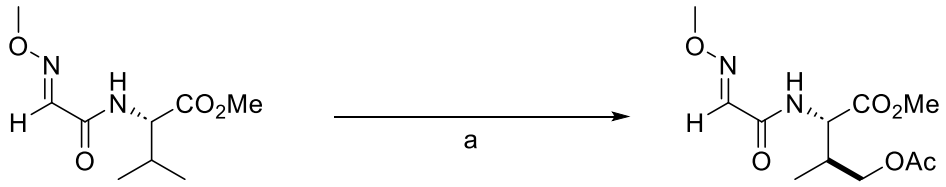

337 **338**

Scheme 5.5: Electrochemical Pd-catalysed acetoxylation of a valine derived substrate (**337**) with an MIA directing group; reagents and conditions: divided cell, graphite electrodes, 20 mol% $Pd(OAc)_2$, cat. $NaNO_3$, 0.6 M NaOAc in acetic acid (8 mL), 80 °C, 12 h, 1.5 mA, 35% (conversion by ^1H NMR).

While the reaction successfully produced the desired product (**338**), it was unclear whether catalyst renewal was taking place or not. A MIA-Thr(O^tBu)-OMe substrate (**342**) was

synthesised to assess whether the valine substrate was simply low-yielding. However, the malfunctioning of the divided cell prevented the acetoxylation of this substrate from being run. Future work should include attempting acetoxylation of this substrate (**342**). If the reaction is a success (*i.e.*, a yield significantly higher than 20%), this indicates that the acetoxylation method is sound, but the valine derivative is a poor model substrate.

Additionally, the possibility of performing Pd-catalysed arylation instead of acetoxylation should be explored (**Scheme 5.6**). The MIA directing group is known to be effective at promoting arylation as well as acetoxylation;[3] it would be interesting to investigate whether this could take place under electrochemical control.

337

Scheme 5.6: Proposed electrochemical arylation of MIA-Val-OMe (**337**) using a haloarene (X = Br, I) to generate novel amino acid derivatives.

5.3 Conclusions and Future Work - Chapter 4

A method for oxidative homocoupling of tyrosine derivatives was developed, resulting in the synthesis of a dityrosine derivative (**352**) in a 20% yield (**Section 4.3, Scheme 4.12**). The method was also successful with a tyrosine-containing dipeptide, without a significant yield reduction (**Scheme 4.14**). Future work may involve attempting to cyclise a larger peptide with a tyrosine residue on each end (**Scheme 5.7**). As this transformation would be intramolecular, an increase in the yield might be expected.

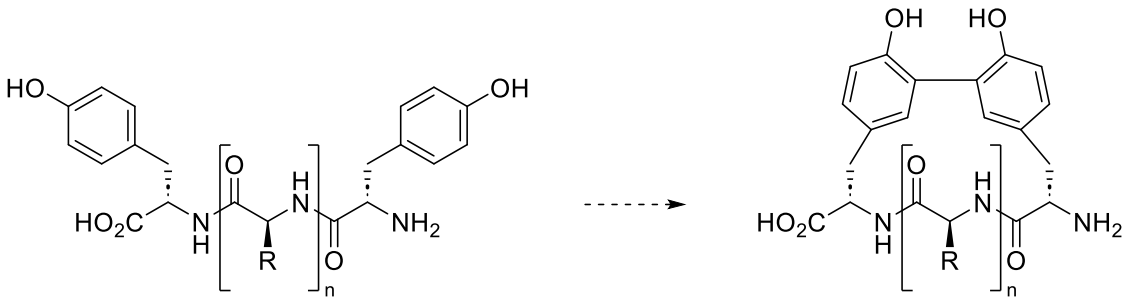

Scheme 5.7: Proposed cyclisation of a peptide containing two tyrosine residues using electrochemical oxidative homo-coupling. R = amino acid side chains

Attempts at electrochemical oxidative cross-coupling of tyrosine derivatives with other phenols were also made but to no avail. However, this is still a valid avenue of investigation. Cross-coupling of tyrosines with other phenols would provide access to novel amino acids (**Scheme 5.8**). Further experimentation with the method is required to achieve this goal.

Scheme 5.8: Proposed oxidative-cross coupling of tyrosine with other phenols to generate novel amino acids.

The Shono-type oxidation of proline derivatives to form the corresponding 5-oxoprolines was also explored (**Section 4.4**) (**Scheme 5.9**).

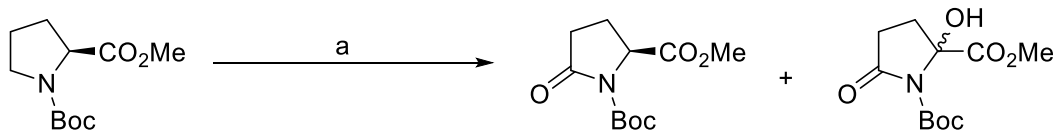

121 **120** **362**

Scheme 5.9: Electrochemical Shono-type oxidation of Boc-Pro-OMe (**121**) to form oxoprolines **120** and **362**; reagents and conditions: a) various, see **Section 4.4**

A number of experiments were performed to manipulate the composition of the product mixture seen in **Scheme 5.9**. Future work could involve investigating ways to favour the minor 2-hydroxy-5-oxoproline product **362** instead of the major 5-oxoproline **120**. Additionally, the hypothesis that the minor product (**362**) forms *via* a fluorinated intermediate could be

investigated by taking samples at various points during the reaction and analysing by ^{19}F spectroscopy.

Electrochemical Selectfluor-mediated Shono-type reactions have not been previously published, so the scope of this reaction could be expanded beyond proline-derived substrates in the future. The protocol could be applied to a variety of cyclic carbamates to illustrate general applicability (**Scheme 5.10**).

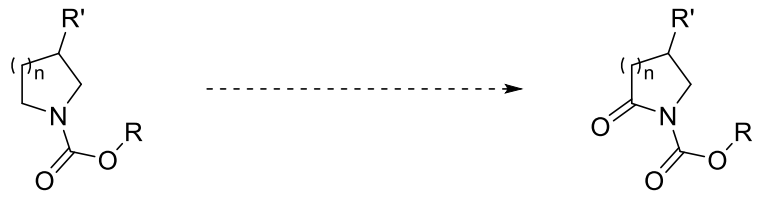

Scheme 5.10: Proposed electrochemical oxidation of other cyclic carbamates.

Shono reactions often use an alternative nucleophile to trap the anodically-generated *N*-acyliminium ion. This possibility could be explored using the Selectfluor-mediated conditions described in **Section 4.4**. An example of how the inclusion of methanol may permit trapping of the *N*-acyliminium ion is displayed in **Scheme 5.11**.

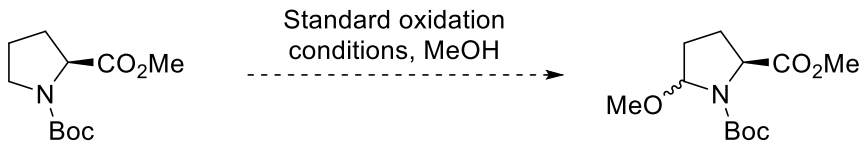

121 **400**

Scheme 5.11: Proposed electrochemical methoxylation of Boc-Pro-OMe (**121**).

Due to the accidental synthesis of tricyclic dimer **166** from 3-methylindole (**165**) (**Scheme 5.12**), a range of other indoles were reacted under the same conditions in an attempt to replicate the intriguing dimer structure (**Section 4.5**).

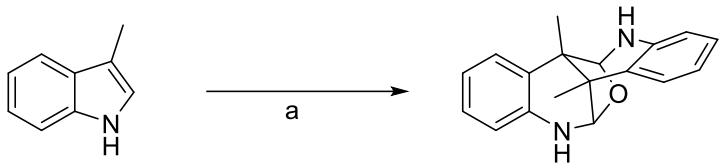

165 **166**

Scheme 5.12: Conversion of 3-methyl indole (**165**) to polycyclic dimer (**166**); reagents and conditions: a) sodium triflinate, 0.2M Bu_4NPF_6, DMSO, 5 mA, 3 F/mol, graphite electrodes.

None of the indoles investigated (**Table 4.2**) successfully formed the desired dimer, although a number of indolic compounds underwent alternative transformations. Future work in this area might include expanding the range of indoles tested, as the original indole substrates were few in number. In addition, further investigation into the transformation of *N*-Phth-Trp-OMe (**162**) to form fused compound **383** might be warranted. It is unclear exactly how this transformation takes place under the electrochemical conditions used, or why a single diastereomer is formed.

An unexpected 2-ethoxy-6-iodo tryptophan product (**394**) was isolated during an attempt to synthesise 5-iodoindole **188** (**Section 4.6**) (**Figure 5.1**). This was determined to be due to the presence of 0.75% ethanol present in the reaction solvent ($CHCl_3$). To determine whether the iodination or the substitution of the ethoxy group takes place first, a reaction could be run without NIS and with additional EtOH.

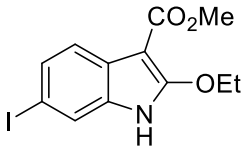

394

Figure 5.1: 6-iodo-2-ethoxy product **394** isolated from the reaction of methyl-3-indole carboxylate (**169**) with NIS.

In summary, the application of electro-organic synthesis techniques to a range of amino acid-derived substrates was explored. As a result, several unnatural amino acids were synthesised. Much of the work presented in this thesis has evolved into electrosynthetic methodology development in a number of different areas, including fluorination, chlorination, Ni-catalysis,

acetoxylation, and oxidation. As such, the transformations discussed have scope beyond amino acid and peptide substrates.

5.4 References

1 Y. Takahira, M. Chen, Y. Kawamata, P. Mykhailiuk, H. Nakamura, B. K. Peters, S. H. Reisberg, C. Li, L. Chen, T. Hoshikawa, T. Shibuguchi and P. S. Baran, *Synlett*, 2019, **30**, 1178–1182.

2 L. Shen, O. Monasson, E. Peroni, F. Le Bideau and S. Messaoudi, *ChemRxix*, 2023, DOI:10.26434/chemrxiv-2023-zbnfd.

3 M. Fan and D. Ma, *Angew. Chem. Int. Ed.*, 2013, **52**, 12152–12155.

Chapter 6: Experimental

6.1 General experimental

All NMR spectra were recorded using a Bruker Avance III spectrometer: ^{1}H-, ^{13}C-, and ^{19}F-NMR were recorded at 400 MHz, 101 MHz, and 376 MHz, respectively. Chemical shifts (δ) are reported in ppm relative to residual solvent peaks ($CHCl_3$ δ = ^{1}H 7.26 ppm, ^{13}C 77.0 ppm), and coupling constants are reported in Hertz (Hz). Mass spectra were collected using ESI-LC in MeCN using a Waters TQD mass spectrometer with a Acquity UPLC BEH C18 1.7 µm (2.1 mm x 50 mm). ESI-LC was collected using water containing formic acid (0.1% v/v) and MeCN mixture in a 95:5 to 5:95 gradient over 5 min. IR spectra was collected using a FTIR Perkin Elmer Spectrum Two: UATR Two spectrometer with 1 cm^{-1} resolution (neat compound). CHN data was not reported as per the norm within the peptide science field, as many compounds are hygroscopic/contain counterions, which limits the accuracy of the data.

Thin layer chromatography (TLC) was carried out using silica coated plates backed with Polygram™ polyester sheets sourced from Fisher Scientific. The TLC plates were visualised with a UV lamp (λ = 254 nm), followed by staining with potassium permanganate solution where necessary. Column chromatography was carried out using silica gel with pore size 60 Å, 230-400 mesh particle size, and 40-63 µm particle size. Both manual column chromatography and automated column chromatography (Combiflash NextGen 100) were used.

All starting materials and reagents were purchased from commercial sources (Merck, Fluorochem, Fisher Scientific, Apollo Scientific, TCI) and used as received unless stated otherwise. Anhydrous solvents were purchased from Fisher Scientific and stored over molecular sieves under an inert atmosphere. For all experiments a thorough COSHH risk assessment was produced, and standard health and safety protocols were adhered to throughout. Correct PPE was used whilst in the laboratory/when handling chemicals, and procedures for safe handling and disposal of chemicals were followed.

Electrochemical reactions were carried out using an IKA ElectraSyn 2.0 electrochemistry kit, featuring an undivided cell (ElectraSyn vial) and galvanostatic set-up. Electrodes were purchased from IKA with approximate dimensions of 7 × 1.5 × 55 mm. All electrochemical reactions were conducted under nitrogen unless otherwise noted. **Figure 6.1** illustrates the undivided and divided cell setups.

Figure 6.1: The undivided cell set up features a 10 mL glass vial with a stirrer bar, into which is placed the reaction mixture. Two electrodes are installed in the Electrasyn cap, which is then screwed onto the reaction vial. This unit is then connected to the Electrasyn and the reaction can start. The divided cell setup uses the IKA Pro-Divide, which features two PTFE chambers separated by a glass frit (pore size 10-16 µm). The reaction mixture is placed inside each of the chambers (3-7 mL) and electrodes are installed. This unit can then be connected to the Electrasyn and the reaction can start.

6.2 Experimental for compounds from Chapter 2

6.2.1 General procedure for synthesis of phthalimide methyl esters

The amino acid substrate (1 equiv.) and phthalic anhydride (**96**) (1 equiv.) were heated together at 170 °C for 3 h under reduced pressure. The mixture was then allowed to cool to room temperature, yielding the desired phthalimide-protected amino acid in a quantitative yield. This was then dissolved in MeOH (50 mL) and cooled to 0 °C. Thionyl chloride (2.5 equiv.) was added dropwise and the solution was allowed to warm to room temperature whilst stirring overnight. The solvent was removed under reduced pressure. The crude product mixture was purified using silica gel chromatography to afford the phthalimide methyl ester.

6.2.2 General procedure for electrochemical fluorination

The protected amino acid (0.3 mmol, 1 equiv.) was dissolved in anhydrous MeCN (5 ml), to which Selectfluor (0.320 g, 0.9 mmol, 3 equiv.) and sodium nitrate (5.10 mg, 0.06 mmol, 0.2 equiv.) were added. The solution was placed in an undivided cell (ElectraSyn 2.0 vial) equipped with two reticulated vitreous carbon (RVC) electrodes and a stirrer bar. The reaction mixture was degassed by bubbling nitrogen through the solution for 0.5 h. A current of 3 mA

was then applied with alternating polarity every two minutes and a total charge of 3 F/mol. The reaction mixture was poured into sat. $NaHCO_3$ and extracted with DCM (20 mL), then washed with brine (20 mL). The organic fraction was dried over $MgSO_4$, filtered, then concentrated under reduced pressure. The crude product mixture was purified using silica gel chromatography where necessary. For a more detailed discussion of how the conditions for electrochemical reactions were chosen, see **Chapter 2**.

6.2.3 General procedure for electrochemical chlorination

The substrate (0.3 mmol) was dissolved in 4mL of a 10% v/v DCM mixture in DMSO containing Bu_4NBF_4 (148 mg, 0.45 mmol, 0.11 M). The solution was placed in an undivided cell (ElectraSyn 2.0 vial) equipped with two graphite electrodes and a stirrer bar under air. A 5 mA current was applied for 10 h with a total charge of 6 F/mol delivered (or 3 F/mol). The electrodes were rinsed with DCM and the reaction mixture was poured onto water (20 mL), then extracted with further DCM (20 mL). The mixture was washed once again with water, then with brine. The organic fraction was dried using $MgSO_4$, filtered, then concentrated under reduced pressure. The crude product mixture was then purified using column chromatography.

6.2.4 *L*-*N*-Phthaloyl valine methyl ester (91)

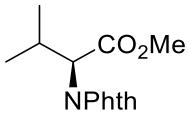

91

The title compound was obtained by performing **General Procedure Section 6.2.1** using *L*-valine (**97**) (1.00 g, 8.55 mmol, 1 equiv.) and phthalic anhydride (**96**) (1.26 g, 8.55 mmol, 1 equiv.). This yielded the desired *L*-*N*-phthaloyl valine (**98**) (2.12 g) as a glassy colourless solid. This was then reacted without purification with thionyl chloride (2.56 g, 1.56 mL, 21.5 mmol, 2.5 equiv.), and the crude product mixture was purified using silica gel chromatography (5:1 Hexane: EtOAc) affording **91** as a colourless oil (1.62 g, 6.28 mmol, 72%).

^{1}H NMR (400 MHz, $CDCl_3$) δ 7.83 (2H, m, ArH), 7.75 (2H, m, ArH), 4.60 (1H, d, *J* = 8.5, α-H), 3.71 (3H, s, CO_2CH_3), 2.79 (1H, m, β-H), 1.21 (3H, d, *J* = 7.0, -CH_3), 0.89 (3H, d, *J* = 6.5, -CH_3).

^{13}C NMR (101 MHz, $CDCl_3$) δ 169.1, 167.6, 134.5, 131.6, 123.7, 57.3, 52.3, 28.3, 20.8, 19.2.

ESI-MS (LCMS): found *m/z* [M+H]+ 262.6

Spectroscopic data match those previously published.[1]

6.2.5 *L*-*N*-Phthaloyl leucine methyl ester (92)

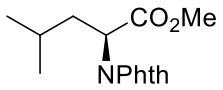

92

The title compound was afforded following **General Procedure Section 6.2.1** using *L*-leucine (**327**) (1.00 g, 7.60 mmol, 1 equiv.) and phthalic anhydride (**96**) (1.13 g, 7.60 mmol, 1 equiv.) to afford pure *L*-*N*-phthaloyl leucine (**328**) (1.99 g). This was then reacted without purification with thionyl chloride (2.27 g, 1.38 mL, 19.0 mmol, 2.5 equiv.), and the crude product mixture was purified using silica gel chromatography (5:1 hexane: EtOAc), yielding **92** as a colourless oil (1.65 g, 6.00 mmol, 79%).

^{1}H NMR (400 MHz, $CDCl_3$) δ 7.87 (2H, m, Ar-H), 7.75 (2H, m, Ar-H), 4.97 (1H, dd, *J* = 12.0, 4.5, α-H), 3.73 (3H, s, CO_2CH_3), 2.36 (1H, ddd, *J* = 14.0, 11.5, 4.0, -CH_2), 1.97 (1H, ddd, *J* = 14.0, 10.0, 4.0, -CH_2), 1.49 (1H, m, $(CH_3)_2$C**H**), 0.97 (3H, d, *J* = 6.5, -CH_3), 0.94 (3H, d, *J* = 6.5, -CH_3).

^{13}C NMR (101 MHz, $CDCl_3$) δ 170.3, 167.8, 134.2, 131.8, 123.6, 52.8, 50.6, 37.3, 25.1, 23.2, 21.0.

ESI-MS (LCMS): found *m/z* [M+H]+ 276.6

Spectroscopic data match those previously published.[2]

6.2.6 *L*-*N*-Phthaloyl isoleucine methyl ester (93)

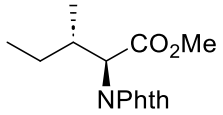

93

General Procedure 6.2.1 was performed using *L*-isoleucine (0.996 g, 7.60 mmol, 1 equiv.)

and phthalic anhydride (**96**) (1.11 g, 7.60 mmol, 1 equiv.) to afford pure *L*-*N*-phthaloyl isoleucine as a pale yellow glassy solid (1.98 g). This was reacted with thionyl chloride (2.26 g, 1.38 mL, 19.0 mmol, 2.5 equiv.), then purified using silica gel chromatography (30% EtOAc/hexane) to furnish **93** as a pale-yellow oil (1.610 g, 5.85 mmol, 77%).

^{1}H NMR (400 MHz, $CDCl_3$) δ 7.88 (2H, m, Ar-H), 7.77 (2H, m, Ar-H), 4.67 (1H, d, *J* = 8.0, α-H), 3.73 (3H, s, -CO_2CH_3), 2.56 (1H, m, β-H), 1.52 (1H, m, -$CH_2C\mathbf{H_3}$), 1.13 (3H, d, *J* = 7.0, -$CHC\mathbf{H_3}$), 1.06 (1H, m, -$C\mathbf{H_2}CH_3$), 0.89 (3H, t, *J* = 7.5, $CH_2C\mathbf{H_3}$).

^{13}C NMR (101 MHz, $CDCl_3$) δ 169.4, 167.8, 134.2, 131.7, 123.6, 57.0, 52.4, 34.5, 25.7, 16.8, 11.0.

ESI-MS (LCMS): found *m/z* $[M+H]^+$ 276.7

Spectroscopic data match those previously published.[3]

6.2.7 *L*-*N*-(Boc)$_2$ valine methyl ester (104)

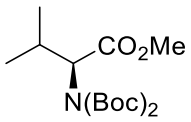

104

L-*N*-Boc valine methyl ester (**108**) (500 mg, 2.20 mmol, 1 equiv.) was dissolved in dry THF (3 mL) and added to a flask under nitrogen at -78 °C. A further 5 mL of dry THF was added, after which KHMDS (402 mg, 0.5 M in toluene solution, 4.00 mL, 2.00 mmol, 0.93 equiv.) was added slowly over a period of 5 minutes. The solution was stirred for 0.5 h before Boc_2O (1030 mg, 4.30 mmol, 2 equiv.) in THF (2 mL) was added. The reaction was allowed to warm to room temperature and left to stir for 17 h. The reaction mixture was then poured into sat. aq. NH_4Cl (20 mL) and extracted with EtOAc (25 mL). The combined organic fractions were washed with $NaHCO_3$ (20 mL), and then brine (20 mL). The organic solution was dried using $MgSO_4$, filtered, then the solvent was removed under reduced pressure. Silica gel chromatography (20% hexane/EtOAc) was used to isolate the product, affording **104** as a colourless oil (151 mg, 0.590 mmol, 27%).

^{1}H NMR (400 MHz, $CDCl_3$) δ 4.48, (1H, d, *J* = 9.5, α-H), 3.66 (3H, s, -CO_2CH_3), 2.44 (1H, m, β-H), 1.46 (18H, s, $(Boc)_2$), 1.10 (3H, d, *J* = 6.5, -CH_3), 0.84 (3H, d, *J* = 7.0, -CH_3).

^{13}C NMR (101 MHz, $CDCl_3$) δ 170.8, 152.1, 82.5, 63.1, 51.7, 31.5, 28.7, 27.8, 22.6, 22.1, 18.7, 14.1.

ESI-MS (LCMS): found *m/z* $[2M+Na]^+$ 686.0

Spectroscopic data match those previously published.[4]

6.2.8 *L-N,N*-Dibenzyl valine methyl ester (105)

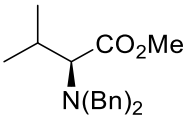

105

L-Valine methyl ester (**95**) (0.996 g, 7.60 mmol, 1 equiv.) and K_2CO_3 (3.32 g, 24.0 mmol, 3.15 equiv.) were dissolved in EtOH (50 mL). Benzyl bromide (3.92 g, 2.73 mL, 22.9 mmol, 3 equiv.) was added dropwise and the reaction mixture was heated at reflux for 3 h. The mixture was filtered, and the residue was washed with EtOAc (25 mL). The filtrate was concentrated under reduced pressure then redissolved in EtOAc (20 mL) before being washed with water (20 mL), aq. $NaHCO_3$ (20 mL), and brine (20 mL). The product was purified using silica gel chromatography (10% EtOAc/hexane), affording **105** as a colourless liquid (1.080 g, 3.50 mmol, 46%).

^{1}H NMR (400 MHz, $CDCl_3$) δ 7.25-7.47 (10H, m, Ar-H), 4.03 (2H, d, *J* = 13.5, Ar-CH_2), 3.81 (3H, s, CO_2CH_3), 3.32 (2H, d, *J* = 15.0, Ar-CH_2), 2.91 (1H, d, *J* = 11.0, α-H), 2.19 (1H, m, β-H), 1.06 (3H, d, *J* = 6.5, -CH_3), 0.82 (3H, d, *J* = 6.5, CH_3).

^{13}C NMR (101 MHz, $CDCl_3$) δ 172.5, 139.6, 138.6, 128.8, 128.4, 128.2, 127.7, 127.5, 127.0, 72.8, 68.2, 54.7, 50.7, 27.2, 20.0, 19.6.

ESI-MS (LCMS): found *m/z* $[M+H]^+$ 312.6

Spectroscopic data match those previously published.[5]

6.2.9 1 *L-N*-Phthaloyl-3-fluorovaline methyl ester (89)

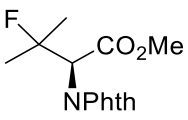

89

General Procedure Section 6.2.2 was followed using *L*-*N*-phthaloyl valine methyl ester (**91**) as the substrate (78 mg, 0.3 mmol), and the desired product (**89**) was obtained as a pale-yellow oil (57 mg, 0.2 mmol, 71%).

^{1}H NMR (400 MHz, $CDCl_3$) δ 7.86 (2H, m, Ar-H), 7.79 (2H, m, Ar-H), 5.00 (1H, d, *J* = 10.5, α-H), 3.74 (3H, s, -CO_2CH_3), 1.71 (3H, d, *J* = 23.0, -CH_3), 1.59 (3H, d, *J* = 23.0, -CH_3).

^{13}C NMR (101 MHz, $CDCl_3$) δ 167.5, 166.7 (d, *J* = 10.0), 134.3, 131.7, 123.7, 95.3 (d, *J* = 171.5), 57.7 (d, *J* = 26.0), 52.6, 26.3 (d, *J* = 23.0), 23.77 (d, *J* = 23.0)

^{19}F NMR (376 MHz, $CDCl_3$) δ -136.6 (m)

ESI-MS (LCMS): found *m/z* $[M+H]^+$ 280.4

Spectroscopic data match those previously published.[6]

6.2.10 *L*-*N*-Phthaloyl-4-fluoroleucine methyl ester (90)

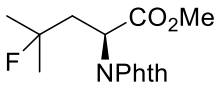

90

General Procedure Section 6.2.2 was followed using *L*-*N*-phthaloyl leucine methyl ester (**92**) as the substrate (83 mg, 0.300 mmol). The crude product mixture was purified using silica gel chromatography (20% EtOAc/hexane). The desired product (**90**) was obtained as a colourless oil (40 mg, 0.135 mmol, 45%).

^{1}H NMR (400 MHz, $CDCl_3$) δ 7.87 (2H, m, Ar-H), 7.75 (2H, m, Ar-H), 5.17 (1H, dd, *J* = 11.5, 2.5, α-H), 3.73 (3H, s, CO_2CH_3), 2.80 (1H, m, -CH_2), 2.50 (1H, ddd, *J* = 29.0, 15.5, 3.0, -CH_2), 1.46 (3H, d, *J* = 21.0, -CH_3), 1.37 (3H, d, *J* = 21.0, -CH_3).

^{13}C NMR (101 MHz, $CDCl_3$) δ 169.8, 167.6, 134.2, 131.9, 123.6, 94.3 (d, *J* = 165.5), 53.2, 48.3, 38.6 (d, *J* = 21.0), 27.9 (d, *J* = 24.0), 25.5 (d, *J* = 25.5)

^{19}F NMR (376 MHz, $CDCl_3$) δ -143.4 (m)

ESI-MS (LCMS): found *m/z* $[M+H]^+$ 294.5

Spectroscopic data match those previously published.[6]

6.2.11 *L-N*-(Boc)-3-fluorovaline methyl ester (113)

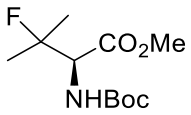

113

General Procedure Section 6.2.2 was followed using *L-N,N'*-$(Boc)_2$ valine methyl ester (**104**) as the substrate (91 mg, 0.3 mmol) and the crude product was purified using silica gel chromatography (10% EtOAc/hexane) to afford the product (**113**) (23 mg, 0.1 mmol, 34%).

^{1}H NMR (400 MHz, $CDCl_3$) δ 5.32 (1H, br d, *J* = 6.0, N-H), 4.35 (1H, dd, *J* = 13.5, 6.0, α-H), 3.76 (3H, s, CO_2CH_3), 1.43 (9H, s, Boc), 1.44 (3H, m, -CH_3), 1.40 (3H, m, -CH_3).

^{13}C NMR (101 MHz, $CDCl_3$) δ 170.2, 155.4, 95.2 (d, *J* = 121.0), 82.0, 80.3, 52.3, 28.2, 26.9, 24.3 (d, *J* = 10.0).

^{19}F NMR (376 MHz, $CDCl_3$) δ -149.0 (m)

ESI-MS (LCMS): found *m/z* $[M+H]^+$ 250.5

Spectroscopic data match those previously published.[7]

6.2.12 2-(((3*R*,5*S*)-1-(tert-butoxycarbonyl)-5-(methoxycarbonyl)pyrrolidin-3-yl)oxy)-2-oxoacetic acid (118)

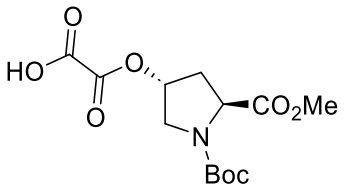

118

Boc-Hyp-OMe (**117**) (0.505 g, 2.04 mmol, 1 equiv.) was dissolved in anhydrous diethyl ether (20 mL) and placed under an argon atmosphere. The solution was cooled to 0 °C and set to stir before oxalyl chloride (0.35 mL, 4.08 mmol, 2 equiv.) was added dropwise. The reaction

mixture was allowed to cool to room temperature and left to stir overnight. The reaction was cooled to 0 °C and quenched by the dropwise addition of water (20 mL). The resulting mixture was stirred for 1 h at room temperature. The aqueous layer was removed and extracted with Et_2O (3 × 20 mL). The combined organics were dried with $MgSO_4$, filtered, and the solvent was removed under reduced pressure. The desired product (**118**) was isolated as a colourless oil (0.543 g, 1.71 mmol, 84%).

^{1}H NMR (400 MHz, $CDCl_3$) δ 5.42 (1H, s, CH), 4.49 (0.4H, t, *J* = 8.0, CH), 4.43 (0.6H, t, *J* = 8.0, CH), 3.84-3.76 (2H, m, CH_2), 3.75 (3H, s, CO_2Me), 2.53 (1H, m, CH_2), 2.30 (1H, m, CH_2), 1.45 and 1.41 (9H, s, Boc)

^{13}C NMR (101 MHz, $CDCl_3$) δ* 172.9, 172.8, 158.1, 158.0, 157.9, 157.9, 154.3, 154.0, 81.5, 81.2, 75.3, 74.7, 57.8, 57.4, 52.6, 52.4, 51.8, 51.7, 36.2, 35.3, 28.3, 28.2.

ESI-MS (LCMS): found *m/z* $[M+H\text{-}Boc]^+$ 218.2

*peak doubling observed due to rotamers.

Spectroscopic data match those previously published.[8]

6.2.13 (*S*)-1-tert-Butoxycarbonyl-5-methoxycarbonyl-pyrrolidin-2-one (120)

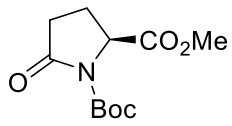

120

L-Boc-Pro-OMe (**121**) (75 mg, 0.3 mmol, 1 equiv.) was dissolved in H_2O/MeCN (1:9, 5 mL) in an ElectraSyn vial along with Selectfluor (0.165 g, 0.45 mmol, 1.5 equiv.) and $NaNO_3$ (5.1 mg, 0.06 mmol, 0.2 equiv.). RVC electrodes were placed in the solution and a 5 mA current was passed through the reaction for 3 F/mol. The reaction mixture was poured onto aq. $NaHCO_3$ (20 mL) and extracted with DCM before being washed with brine. The solution was dried, and the solvent was removed *in vacuo* to yield the product **120** (53 mg, 0.2 mmol, 66%)

^{1}H NMR (400 MHz, $CDCl_3$) δ 4.59 (1H, dd, *J* = 6.5, 2.0, α-H), 3.75 (3H, s, -OMe), 2.58 (1H, m, -CH_2), 2.46 (1H, m, -CH_2), 2.30 (1H, m, -CH_2), 2.01 (1H, m, -CH_2), 1.46 (9H, s, -Boc)

^{13}C NMR (101 MHz, $CDCl_3$) δ 173.2, 171.8, 149.3, 83.6, 58.8, 52.5, 31.1, 27.9, 21.5.

ESI-MS (LCMS): found *m/z* $[M+H\text{-}Boc]^+$ 144.1

Spectroscopic data match those previously published.[9]

6.2.14 *N*-Bn-Pro-OMe (130)

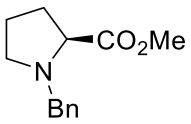

130

Proline methyl ester hydrochloride (**203**) (0.498 g, 3.03 mmol, 1 equiv.) was dissolved in anhydrous DCM (5 mL) and Et_3N (1.05 mL, 7.58 mmol, 2.5 equiv.) was added, followed by dropwise addition of benzyl bromide (0.36 mL, 3.03 mmol, 1 equiv.). The reaction mixture was stirred for 2 h at room temperature, then was diluted with sat. aq. Na_2CO_3 solution (20 mL) and extracted with EtOAc (3 × 20 mL). The combined organics were washed with brine, dried, then filtered, followed by removal of the solvent *in vacuo*. The crude product was purified by silica gel chromatography (10% EtOAc in hexane), yielding the desired product (**130**) as a colourless oil (0.577 g, 2.64 mmol, 87%).

^{1}H NMR (400 MHz, $CDCl_3$) δ 7.23-7.50 (5H, m, Ar-H), 3.78 (1H, d, *J* = 13.0, Ar-CH_2), 3.52 (3H, s, CO_2Me), 3.46 (1H, d, *J* = 13.0, Ar-CH_2), 3.14 (1H, dd, *J* = 9.0, 6.0, α-H), 2.94 (1H, m, CH_2), 2.28 (1H, q, *J* = 9.0, CH_2), 2.08-1.96 (1H, m, CH_2), 1.89-1.74 (2H, m, CH_2), 1.69-1.60 (1H, m, CH_2)

^{13}C NMR (101 MHz, $CDCl_3$) δ 174.5, 138.3, 129.2, 128.2, 127.1, 65.2, 58.7, 53.2, 51.6, 29.3, 23.0.

ESI-MS (LCMS): found *m/z* $[M+H]^+$ 220.2

Spectroscopic data match those previously published.[10]

6.2.15 *N*-Bn-Hyp-OMe (123)

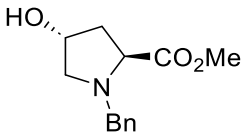

123

trans-4-Hydroxyproline methyl ester hydrochloride (**122**) (1.003 g, 5.5 mmol, 1 equiv.) was dissolved in toluene and DIPEA (2.4 mL, 13.8 mmol, 2.5 equiv.) was added. The mixture was

cooled to 0 °C and benzyl bromide (0.72 mL, 6.1 mmol, 1.1 equiv.) was added dropwise. The reaction mixture was heated to reflux for 6h, after which sat. aq. $NaHCO_3$ (20 mL) was added. The crude product was extracted with EtOAc (2 × 20 mL). The combined organic fractions were dried with $MgSO_4$ and filtered, before the solvent was removed under reduced pressure. The title compound (**123**) was obtained by purification of the crude product mixture using silica gel chromatography (EtOAc/Hexane 0→100%) as a pale yellow oil (0.760 g, 3.2 mmol, 58%)

^{1}H NMR (400 MHz, $CDCl_3$) δ 7.26-7.16 (5H, m, Ar-H), 4.39 (1H, m, -C**H**OH), 3.83 (1H, d, *J* = 13.0, Bn-CH_2), 3.60 (1H, d, *J* = 13.0, Bn-CH_2), 3.59 (3H, s, -CO_2Me), 3.55 (1H, t, *J* = 8.0, α-H), 3.27 (1H, dd, *J* = 10.0, *J'* = 5.5, -CH_2), 2.41 (1H, dd, *J* = 10.0, *J'* = 4.0, -CH_2), 2.19 (1H, m, -CH_2), 2.02 (1H, m, -CH_2), 1.88 (1H, br s, -OH)

^{13}C NMR (101 MHz, $CDCl_3$) δ 174.0, 138.0, 129.1, 128.3, 127.3, 70.3, 63.6, 61.1, 58.2, 51.8, 39.6.

ESI-MS (LCMS): found *m/z* $[M+H]^+$ 236.2

Spectroscopic data match those previously published.[9]

6.2.16 2-(((3R,5S)-1-(benzyl)-5-(methoxycarbonyl)pyrrolidin-3-yl)oxy)-2-oxoacetic acid (124)

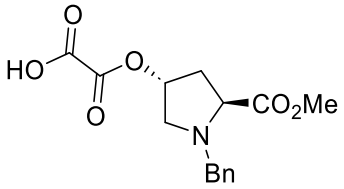

124

Bn-Hyp-OMe (**123**) (200 mg, 0.85 mmol, 1 equiv.) was dissolved in anhydrous diethyl ether (20 mL) and placed under an argon atmosphere. The solution was cooled to 0°C and set to stir before oxalyl chloride (0.15 mL, 1.7 mmol, 2 equiv.) was added dropwise. The reaction mixture was allowed to cool to room temperature and left to stir overnight. The reaction was cooled to 0 °C and quenched by the dropwise addition of water (20 mL). The resulting mixture was stirred for 1 h at room temperature. The aqueous layer was removed and extracted with Et_2O (3 × 20 mL). The combined organics were dried with $MgSO_4$, filtered, and the solvent was removed under reduced pressure. The desired product (**124**) was isolated as a pale yellow oil (134 mg, 0.44 mmol, 51%).

^{1}H NMR (400 MHz, $CDCl_3$) δ 7.26-7.11 (5H, m, Ar-H), 4.33 (1H, m, CH), 3.81 (1H, d, *J* = 13.0, Bn-CH_2), 3.59 (1H, d, *J* = 13.0, Bn-CH_2), 3.55 (3H, s, CO_2Me), 3.53-3.49 (1H, m, CH), 3.24 (1H, dd, *J* = 10.0, 5.5, CH_2), 2.39 (1H, dd, *J* = 10.0, 4.0, CH_2), 2.13 (1H, m, CH_2), 2.03 - 1.92 (1H, m, CH_2).

^{13}C NMR (101 MHz, $CDCl_3$) δ 175.4, 173.9, 173.2, 137.5, 129.3, 128.3, 127.4, 69.8, 63.8, 61.2, 58.5, 51.9, 39.4.

ESI-MS (LCMS): found *m/z* $[M+H-COCOOH]^+$ 236.2

6.2.17 Oxalate dimer 125

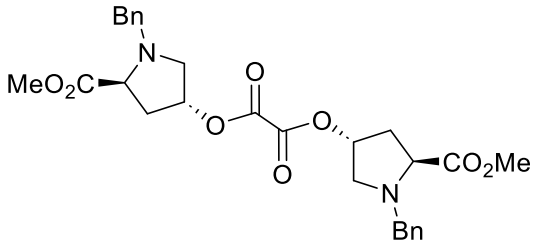

125

Bn-Hyp-OMe (**123**) (335 mg, 1.42 mmol, 2.2 equiv.) was dissolved in diethyl ether/pyridine (anhydrous, 1:1, 20 mL) under an argon atmosphere. The solution was cooled to 0 °C and oxalyl chloride (0.05 mL, 0.64 mmol, 1 equiv.) was added dropwise. The solution was then refluxed for three hours. After cooling to room temperature, the solution was washed with HCl (1 M, 20 mL), H_2O (20 mL), and aq. $NaHCO_3$ (20 mL). The organic fraction was dried with $MgSO_4$ and filtered, followed by removal of the solvent. The crude product mixture was purified by silica gel column chromatography (EtOAc/hexane 0→100%), affording the desired compound (**125**) as a yellow oil (224 mg, 0.43 mmol, 62%)

^{1}H NMR (400 MHz, $CDCl_3$) δ 7.34 (8H, s, Ar-H), 7.28 (2H, m, Ar-H), 5.37 (2H, m, CH), 3.93 (2H, d, *J* = 13.0, Bn-CH_2), 3.72 (2H, d, *J* = 13.0, Bn-CH_2), 3.71 (6H, s, CO_2Me), 3.65 (2H, m, CH), 3.49 (2H, dd, *J* = 11.0, 6.5, CH_2), 2.68 (2H, dd, *J* = 11.0, 3.5, CH_2), 2.46 (2H, dt, *J* = 14.0, 7.5, CH_2), 2.31 (2H, ddd, *J* = 14.0, 7.5, 3.5, CH_2).

^{13}C NMR (101 MHz, $CDCl_3$) δ 173.1, 157.2, 137.5, 129.0, 128.4, 127.4, 75.9, 63.6, 57.8, 57.7, 52.0, 36.1.

ESI-MS (LCMS): found *m/z* $[M+H]^+$ 525.7

ESI-MS (HRMS): found *m/z* $[M+H]^+$ 525.2230

IR V_{max} (solid) / cm^{-1} (ATR) 1722 (C=O), 1614 (C=O), 1456 (C=C), 1210 (C-O-C)

6.2.18 Methyl 1-benzyl-1H-pyrrole-2-carboxylate (126)

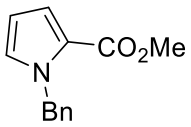

126

Bn-Hyp-OMe (**123**) (70 mg, 0.3 mmol, 1 equiv.), Selectfluor (160 mg, 0.6 mmol, 2 equiv), and K_2PO_4 (73 mg, 0.6 mmol, 2 equiv.) were placed in an ElectraSyn vial and dissolved in MeCN/H_2O (4:1). Graphite electrodes were placed in the solution, and the mixture was degassed by bubbling N_2 through the solution for 15 mins. A 5 mA current was applied for a total charge of 2 F/mol. Et_2O (20 mL) was added, and the solution was washed with water then brine. The organic fraction was dried with $MgSO_4$, then filtered. The solvent was removed *in vacuo* and the crude product was purified with silica gel chromatography (EtOAc/hexane, 0→100%), affording the title compound (**126**) as a colourless oil (47 mg, 0.22 mmol, 74%)

^{1}H NMR (400 MHz, $CDCl_3$) δ 7.27-7.15 (H, m, Bn Ar-H), 7.03 (2H, m, Bn Ar-H), 6.93 (1H, dd, *J* = 4.0, 2.0, Py Ar-H), 6.82 (1H, dd, *J* = 2.5, 2.0, Py Ar-H), 6.12 (1H, dd, *J* = 4.0, 2.5, Py Ar-H) 5.50 (2H, s, -CH_2-), 3.70 (3H, s, CO_2Me).

^{13}C NMR (101 MHz, $CDCl_3$) δ 161.5, 138.3, 129.1, 128.6, 127.4, 126.9, 122.0, 118.4, 108.5, 52.1, 51.1.

ESI-MS (LCMS): found *m/z* $[M+H]^+$ 216.2

Spectroscopic data match those previously published.[11]

6.2.19 Enones 129, 128, and 127

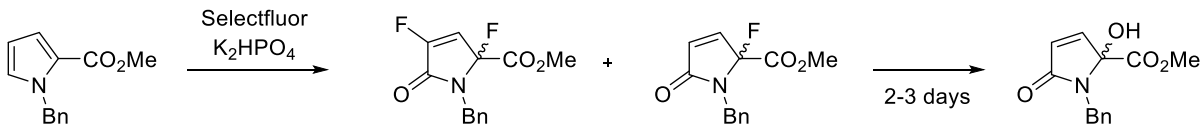

126 **129** **128** **127**

Bn-pyrrole-OMe (**126**) (70 mg, 0.3 mmol, 1 equiv.), Selectfluor (160 mg, 0.6 mmol, 2 equiv), and K_2PO_4 (73 mg, 0.6 mmol, 2 equiv.) were placed in an ElectraSyn vial and dissolved in

MeCN/H_2O (4:1). Graphite electrodes were placed in the solution, and the mixture was degassed by bubbling N_2 through the solution for 15 mins. A 5 mA current was applied for a total charge of 2 F/mol. Et_2O (20 mL) was added, and the solution was washed with water then brine. The organic fraction was dried with $MgSO_4$, then filtered. The solvent was removed in vacuo and the crude product was purified with preparative thin layer chromatography (EtOAc/hexane, 30%), resulting in isolation of **129** as a purple solid and **128** as a white solid. Conversion of **128** to **127** took place within ~2-3 days, affording the latter as a colourless crystalline solid.

129

^{1}H NMR (599 MHz, $CDCl_3$) δ 7.35 – 7.27 (5H, m, Ar-H), 6.25 (1H, t, *J* = 1.5, β-H), 4.80 (1H, d, *J* = 15.5, -NCH_2-), 4.41 (1H, d, *J* = 15.5, -NCH_2-), 3.39 (3H, s, CO_2Me).

^{13}C NMR (151 MHz, $CDCl_3$) δ 162.9 (d), 154.4 (d), 134.9, 128.6, 128.5, 128.0, 113.2 (dd, *J* = 19.5, 7.5), 96.8 (d), 53.3, 43.6.

^{19}F NMR (376 MHz, $CDCl_3$) δ -130.5 (t, J = 2.0), -142.8.

ESI-MS (LCMS): found *m/z* $[M+H]^+$ 268.1

ESI-MS (HMRS): found *m/z* $[M+H]^+$ 268.0796

128

^{1}H NMR (599 MHz, $CDCl_3$) δ 7.30 – 7.27 (5H, m, Ar-H), 6.96 (1H, dd, *J* = 6.0, 1.0, -HC=CH-), 6.40 (1H, d, *J* = 6.0, -HC=CH-), 4.79 (1H, d, *J* = 15.0, -NCH_2-), 4.39 (1H, d, *J* = 15.5, -NCH_2-), 3.37 (3H, s, CO_2Me).

^{13}C NMR (101 MHz, $CDCl_3$) δ 169.6 (d, *J* = 3.0), 164.9 (d, *J* = 41.0), 141.6 (d, *J* = 17.5), 135.8, 130.2 (d, *J* = 3.5), 128.5, 128.4, 127.7, 100.6 (d, *J* = 215.0), 53.1, 43.0.

^{19}F NMR (376 MHz, $CDCl_3$) δ -141.1.

ESI-MS (LCMS): found *m/z* $[M+H]^+$ 250.0

ESI-MS (HRMS): found *m/z* $[M+H]^+$ 250.0889

127

^{1}H NMR (400 MHz, $CDCl_3$) δ 7.30-7.20 (5H, m, Ar-H), 6.78 (1H, d, *J* = 6.0, CH=CH), 6.32 (1H, d, *J* = 6.0, CH=CH), 4.87 (1H, d, *J* = 15.0, Bn-CH_2), 4.14 (1H, d, *J* = 15.0, Bn-CH_2), 3.19 (3H, s, CO_2Me)

^{13}C NMR (101 MHz, $CDCl_3$) δ 170.5, 170.0, 144.7, 136.1, 129.3, 128.9, 128.3, 127.6, 88.1, 53.6, 41.9

ESI-MS (LCMS): found *m/z* $[M+H]^+$ 248.1

IR V_{max}/ cm^{-1} (ATR): 3174 (C-OH), 1737 (C=O), 1668 (alkene C=C), 1454 (aromatic C=C).

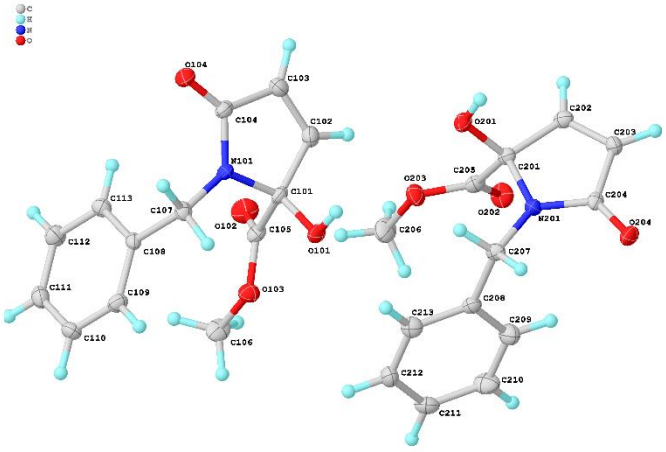

Figure 6.1: X-ray crystal structure for **127**. Crystal structure reported with a 50% thermal ellipsoid probability.

6.2.20 Ethyl oxalate 132

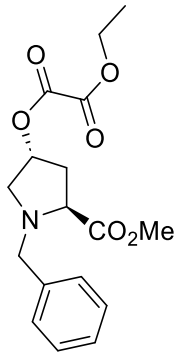

132

Bn-Hyp-OMe (**123**) (0.387 g, 1.65 mmol, 1 equiv.) was dissolved in anhydrous DCM (20 mL), and Et_3N (0.27 mL, 2.0 mmol, 1.2 equiv.) and DMAP (28 mg, 0.165 mmol, 0.1 equiv.) were added. The solution was cooled to 0 °C and ethyl chloroxoacetate (0.22 mL, 2.0 mmol, 1.2 equiv.) was added dropwise. The mixture was then stirred for 1 h before it was quenched with sat. aq. NH_4Cl. The product was extracted using DCM and the combined organic fractions were dried ($MgSO_4$), filtered, and concentrated. The desired compound (**132**) was obtained

as a yellow oil (0.326 g, 0.98 mmol, 59%) following purification with silica gel chromatography (EtOAc/hexane 0→100%).

^{1}H NMR (400 MHz, $CDCl_3$) δ 7.34-7.23 (5H, m, Ar-H), 5.38 (1H, m, α-H), 4.36 (2H, q, *J* = 7.0, -C**H₂**CH_3), 3.93 (1H, d, *J* = 13.0, Ar-C**H₂**-), 3.71 (1H, d, *J* = 13.0, Ar-C**H₂**-), 3.69 (3H, s, -CO_2Me), 3.67 – 3.62 (1H, m, CH), 3.49 (1H, dd, *J* = 11.0, 6.0, CH_2), 2.69 (1H, dd, *J* = 11.0, 3.5, CH_2), 2.46 (1H, m, CH_2), 2.31 (1H, ddd, *J* = 14.0, 7.5, 3.0, CH_2) 1.39 (3H, t, *J* = 7.0, -CH_2C**H₃**).

^{13}C NMR (101 MHz, $CDCl_3$) δ 173.1, 157.6, 157.5, 137.6, 129.0, 128.4, 127.4, 75.8, 63.7, 63.3, 57.8, 57.7, 51.9, 36.1, 13.9.

LCMS $[M+H]^+$ = 336.3

IR V_{max}/ cm^{-1} (ATR): 1630 (C=O), 1456 (C=C aromatic), 1212 (C-O-C).

6.2.21 Caesium oxalate 133

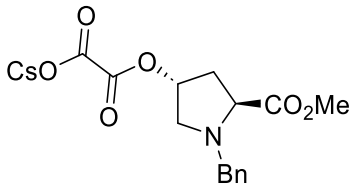

133

Ethyl oxalate **132** (213 mg, 0.6 mmol, 1 equiv.) was dissolved in THF and CsOH solution (0.6 mL, 1 M, 0.6 mmol, 1equiv.) was added dropwise. The reaction mixture was stirred for 5 mins at an ambient temperature, before the mixture was concentrated *in vacuo*. The desired product (**133**) was obtained without purification as a white solid.

6.2.22 *N*-Bn-Hyp(*O*-tetrafluoropyridyl)-OMe (134)

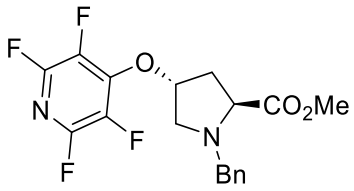

134

Bn-Hyp-OMe (**123**) (1.514 g, 6.4 mmol, 1 equiv.) and K_2CO_3 (0.845 g, 6.4 mmol, 1 equiv.) were dissolved in MeCN (20 mL) and stirred for 30 mins. Pentafluoropyridine (2.7 mL, 25.8 mmol, 4 equiv.) was then added dropwise. The mixture was then stirred for 20 h, followed by filtration and solvent removal. The crude mixture was purified using silica gel chromatography (EtOAc/hexane, 0→100%), furnishing the desired product (**134**) as a yellow oil (1.113 g, 0.29 mmol, 45%).

^{1}H NMR (400 MHz, $CDCl_3$) δ 7.42 – 7.23 (5H, m, ArH), 5.39 (1H, triplet of pentets, *J* = 4.5, 2.5, α-H), 3.98 (1H, d, *J* = 13.0, Bn-CH_2), 3.81 – 3.74 (2H, m, Bn-CH_2 and proline CH), 3.72 (3H, s, CO_2Me), 3.52 (1H, dd, *J* = 11.5, 5.5, CH), 2.89 – 2.84 (1H, m, CH), 2.47 (2H, dd, *J* = 7.5, 4.5, β-CH_2).

^{13}C NMR (101 MHz, $CDCl_3$) δ 173.0, 145.7 – 145.2 (m), 143.2 – 142.9 (m), 137.4, 136.5 – 135.8 (m), 133.6 (m), 128.9, 128.4, 127.5, 83.0 (t, *J* = 4.0), 63.6, 58.5, 57.9, 52.0, 37.3.

^{19}F NMR (376 MHz, $CDCl_3$) δ -89.1 – -89.7 (m), -157.6 – -157.8 (m), -157.9 – -158.1 (m).

ESI-MS (LCMS): found *m/z* $[M+H]^+$ 385.3

IR V_{max}/ cm^{-1} (ATR): 1735 (C=O), 1469 (C=C), 1090 (C-F)

6.2.23 4-Chloro-2-methylpyrrole carboxylate (135)

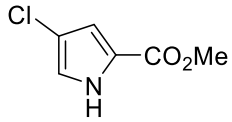

135

L-trans-Hydroxyproline methyl ester hydrochloride (**122**) (40 mg, 0.21 mmol, 1 equiv.), Selectfluor (172 mg, 0 mmol, 2 equiv), and K_2PO_4 (83 mg, 0 mmol, 2 equiv.) were placed in an ElectraSyn vial and dissolved in MeCN/H_2O (4:1). Graphite electrodes were placed in the solution, and the mixture was degassed by bubbling N_2 through the solution for 15 mins. A 5 mA current was applied for a total charge of 2 F/mol. Et_2O (20 mL) was added, and the solution was washed with water then brine. The organic fraction was dried with $MgSO_4$, then filtered. The solvent was removed *in vacuo* and the crude product was purified with silica gel chromatography (Et_3N/MeOH/DCM, 1:5:94), affording the title compound (**135**) as a colourless crystalline solid (20 mg, 0.12 mmol, 57%).

^{1}H NMR (400 MHz, $CDCl_3$) δ 8.99 (1H, br s, NH), 6.83 (1H, dd, *J* = 3.0, 1.5, ArH), 6.75 (1H, dd, *J* = 4.5, 1.5, ArH), 3.79 (3H, s, CO_2Me).

ESI-MS (LCMS): found *m/z* $[M+H]^+$ = 159.1, 160.2

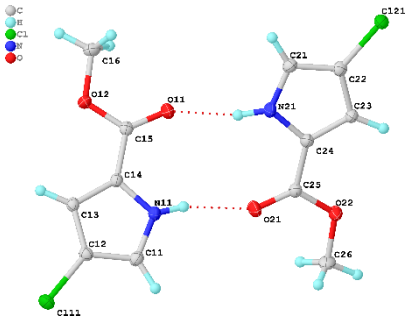

Figure 6.2: X-Ray molecular structure for **135**. Molecular structure reported with a 50% thermal ellipsoid probability.

Spectroscopic data match those previously published.[12]

6.2.24 Enones 137, 138 and 139

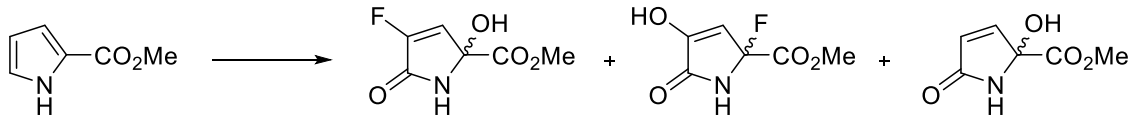

136 **137** **138** **139**

Methyl-2-pyrrole carboxylate (**136**) (241 mg, 1.9 mmol, 1 equiv.), Selectfluor (1.92 g, mmol, 2 equiv), and K_2PO_4 (438 mg, mmol, 2 equiv.) were dissolved in MeCN/H_2O (4:1) and stirred for 20 h. Et_2O (20 mL) was added, and the solution was washed with water then brine. The organic fraction was dried with $MgSO_4$, then filtered. The solvent was removed *in vacuo* and the crude product was purified with silica gel chromatography (EtOAc/hexane, 0→100%), furnishing the product **137** as a white solid (25 mg, 0.14 mmol, 7%), **138** as a yellow oil (12 mg, 0.07 mmol, 4%), and **139** as a colourless oil (36 mg, 0.23 mmol, 12%).

137

^{1}H NMR (400 MHz, $CDCl_3$) δ 7.15 (1H, s, NH), 6.08 (1H, q, *J* = 2.0, =CHR), 3.97 (3H, s, CO_2Me).

^{13}C NMR (151 MHz, $CDCl_3$) δ 165.8 (t, *J* = 30.0), 159.3, 140.4 (t, *J* = 10.5), 112.5 (t, *J* = 251.5), 107.2 (t, *J* = 23.5), 53.5.

^{19}F NMR (376 MHz, $CDCl_3$) δ -113.2 (dd, *J* = 3.0, 2.0)

ESI-MS (LCMS): found *m/z* $[M-H]^-$ 176.2

ESI-MS (HRMS): found *m/z* $[M-H]^-$ 176.0146

IR V_{max} / cm^{-1} (ATR): 3257 (OH), 1731 (C=O), 1637 (alkene C=C) 1257 (C-O-C) 1066 (C-F).

138

^{1}H NMR (400 MHz, $CDCl_3$) δ 7.26 (1H, s, OH), 6.28 (1H, t, *J* = 1.5, CH), 4.96 (1H, s, NH), 3.87 (3H, s, CO_2Me).

^{13}C NMR (151 MHz, $CDCl_3$) δ 169.2 (d, *J* = 3.0), 164.3 (d, *J* = 32.0), 153.6 (d, *J* = 286.5), 118.0 (d, *J* = 5.0), 82.5 (d, *J* = 9.5), 54.2.

^{19}F NMR (376 MHz, $CDCl_3$) δ -135.5 (t, *J* = 2.0).

ESI-MS (LCMS): found $[M+H]^+$ 175.9

ESI-MS (HRMS): found $[M+H]^+$ 176.0362

139

^{1}H NMR (599 MHz, $CDCl_3$) δ 6.93 (1H, dd, *J* = 5.5, 1.5, CH), 6.58 (1H, br s, OH), 6.17 (1H, dd, *J* = 5.5, 1.5, CH), 4.42 (1H, br s, NH), 3.84 (3H, s, CO_2Me).

^{13}C NMR (151 MHz, $CDCl_3$) δ 172.3, 170.0, 146.9, 128.6, 86.9, 54.0.

ESI-MS (LCMS): found $[M+H]^+$ = 157.9

ESI-MS (HRMS): found $[M+H]^+$ = 158.0453

IR V_{max} / cm^{-1} (ATR): 3257 (OH), 1701 (C=O), 1422 (C=C),

6.2.25 *N*-Phth-*L*-Trp-OMe (162)

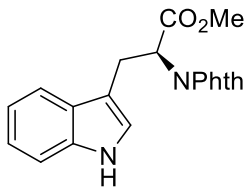

162

L-Tryptophan (**25**) (1.059 g, 4.9 mmol, 1 equiv.) was dissolved in MeOH (20 mL) and cooled to 0 °C. Thionyl chloride (0.93 mL, 13 mmol, 2.5 equiv.) was added. The desired methyl ester (**161**) was isolated in quantitative yield. *L*-Tryptophan methyl ester (**161**) (1.030 g, 4.7 mmol, 1 equiv.) and phthalic anhydride (**96**) (0.750 g, 5.1 mmol, 1.1 equiv.) were dissolved in toluene (25 mL). Et_3N (0.7 mL, 5.1 mmol, 1.1 equiv.) was added, and the reaction mixture was heated at reflux for 12 h whilst stirring. The solvent was removed *in vacuo* and the crude mixture was

purified by column chromatography (20-40% EtOAc in hexane). The desired product (**162**) was obtained as a yellow oil (1.102 g, 3.1 mmol, 67%).

^{1}H NMR (400 MHz, $CDCl_3$) δ 8.03 (1H, s, N-H), 7.77 (2H, m, Phth), 7.67 (2H, m, Phth), 7.62 (1H, d, *J* = 8.0, ArH), 7.28 (1H, dt, *J* = 8.0, 1.0, ArH), 7.14 (1H, ddd, *J* = 7.5, 7.0, 1.0, ArH), 7.07 (1H, ddd, *J* = 7.5, 7.0, 1.0, ArH), 7.02 (1H, d, *J* = 2.5, ArH), 5.30 (1H, dd, *J* = 9.0, 6.5, α-H), 3.82 (3H, s, CO_2Me), 3.79-3.75 (2H, m, β-CH_2).

ESI-MS (LCMS): found *m/z* $[M+H]^+$ 349.6

Spectroscopic data match those previously published.[13]

6.2.26 *S*-(Trifluoromethyl)thianthrenium triflate (149)

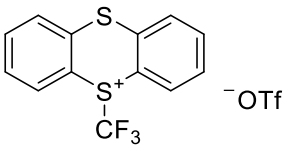

149

Thianthrene (**159**) (1.009 g, 4.6 mmol, 1 equiv.) was dissolved in DCM (20 mL), and the solution was stirred. Triflic anhydride (0.85 mL, 5.1 mmol, 1.1 equiv.) was added dropwise, a condenser was placed on the flask, and the mixture was heated to 35 °C for 22 h. Aq. $NaHCO_3$ (sat., 30 mL) was added, and the aqueous layer was removed. The solvent was removed from the organic fraction to give the desired salt (**149**) as an orange solid (1.134 g, 2.7 mmol, 57%).

^{1}H NMR (400 MHz, $CDCl_3$) δ 8.60 (2H, dd, *J* = 8.0, 1.5, Ar-H), 7.92 (2H, ddd, *J* = 8.0, 7.0, 1.5, Ar-H), 7.85 (2H, dd, *J* = 8.0, 1.5, Ar-H), 7.79 (2H, ddd, *J* = 8.0, 7.0, 1.5, Ar-H)

^{13}C NMR (101 MHz, $CDCl_3$) δ 137.0, 136.7, 136.7, 130.4, 129.5, 120.5 (m), 108.8.*

^{19}F NMR (376 MHz, $CDCl_3$) δ -51.1 (s), -78.4 (s)

ESI-MS (LCMS): found *m/z* $[M\text{-}OTf^-]^+$ 285.5

Spectroscopic data match those previously published.[14]

* Peak for (CF_3) in triflate anion not observed.

6.2.27 *N*-Phth-Trp(2-trifluoromethyl)-OMe (163)

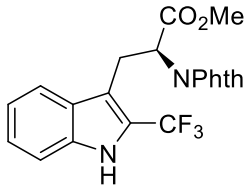

163

N-Phth-Trp-OMe (**162**) (109 mg, 0.31 mmol, 1 equiv.) and sodium triflinate (80 mg, 0.52 mmol, 1.7 equiv.) were dissolved in DMSO (4 mL) alongside Bu_4NPF_6 (348 mg, 0.9 mmol, 3 equiv.). The solution was placed inside an ElectraSyn vial with graphite electrodes and a 5 mA current was passed through the solution. In total, 3 F/mol of charge were delivered. The mixture was diluted with DCM and washed with H_2O (3 × 20 mL), followed by brine (20 mL). The crude product mixture was purified by silica gel chromatography (10% EtOAc in hexane), and the 2-trifluoromethyl product (**163**) was isolated (46 mg, 0.12 mmol, 35%).

^{1}H NMR (400 MHz, $CDCl_3$) δ 7.74 (2H, m, Phth), 7.65 (2H, m, Phth), 7.58 (1H, d, *J* = 8.0, Ar-H), 7.30 (1H, d, *J* = 8.0, Ar-H), 7.20 (1H, t, *J* = 7.5, Ar-H), 7.02 (1H, ddd, *J* = 8.5, 7.0, 1.0, Ar-H), 5.20 (1H, dd, *J* = 11.5, 4.0, α-H), 3.91 (1H, m, β-CH_2), 3.82 (3H, s, CO_2Me), 3.78 (1H, m, β-CH_2).

^{13}C NMR (101 MHz, $CDCl_3$) δ 169.2, 167.4, 127.2, 124.8, 123.4, 122.9 (q, *J* = 37.0), 120.8, 119.6, 113.1 (d, *J* = 2.5), 111.9, 53.0, 52.7, 31.0, 23.7.

^{19}F NMR (376 MHz, $CDCl_3$) δ -58.4 (s)

ESI-MS (LCMS): found *m/z* $[M+H]^+$ 417.6

Spectroscopic data match those previously published.[15]

6.2.28 *N*-Boc-Trp(2-trifluoromethyl)-OMe (224)

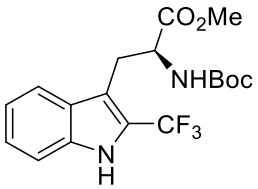

224

The **General Procedure Section 6.2.27** was followed using *N*-Boc-Trp-OMe (**164**) (95 mg, 0.3 mmol, 1 equiv.). The crude product mixture was purified using silica gel chromatography

(10-15% EtOAc in hexane), producing the desired 2-trifluoromethyl derivative (**224**) (27 mg, 0.069 mmol, 23%).

^{1}H NMR (400 MHz, $CDCl_3$) δ 8.46 (1H, br s, N-H), 7.72 (1H, d, *J* = 8.0, Ar-H), 7.41 (1H, d, *J* = 8.0, Ar-H), 7.34 (1H, t, *J* = 7.0, Ar-H), 7.22 (1H, t, *J* = 7.0, Ar-H), 5.15 (1H, d, *J* = 8.0, N-H), 4.68 (1H, m, α-H), 3.67 (3H, s, CO_2Me), 3.39 (2H, qd, *J* = 14.0, *J'* = 6.5, β-CH_2), 1.40 (9H, s, Boc)

^{13}C NMR (101 MHz, $CDCl_3$) δ 172.3, 154.9, 135.2, 127.5, 125.1, 121.0, 120.4, 112.6, 111.8, 79.9, 53.8, 52.4, 28.2, 27.5.*

^{19}F NMR (376 MHz, $CDCl_3$) δ -58.0 (s)

ESI-MS (LCMS): found *m/z* $[M+H]^+$ 287.5

Spectroscopic data match those previously published.[16]

*Peaks for (CF_3) and (indole-**C**-CF_3) not observed.

6.2.29 3-(((*tert*-Butyldimethylsilyl)oxy)methyl)-1H-indole (211)

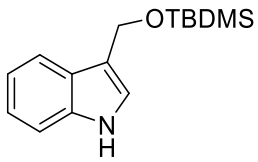

211

Indole-3-carbinol (**212**) (0.470 g, 3.3 mmol, 1 equiv.) and imidazole (0.541 g, 7.9 mmol, 2.4 equiv.) were dissolved in DMF (5 mL). TBDMSCl (0.963 g, 6.4 mmol, 1.9 equiv.) was then added and the reaction was stirred at room temperature for 30 mins. H_2O (20 mL) was added, and the mixture was extracted with EtOAc. The organic fraction was washed with brine then dried and filtered. The solvent was removed *in vacuo* and the desired product (**211**) was isolated as a yellow oil (0.560 g, 2.2 mmol, 67%).

^{1}H NMR (400 MHz, $CDCl_3$) δ 8.10 (1H, s, N-H), 7.69 (1H, d, *J* = 7.5, Ar-H), 7.37, (1H, d, *J* = 8.0, Ar-H), 7.22 (1H, ddd, *J* = 8.0, 7.0, 1.0, Ar-H), 7.17-7.12 (2H, m, Ar-H), 4.97 (2H, d, *J* = 1.0, CH_2), 0.96 (9H, s, ^{t}Bu), 0.14 (6H, s, -Si(CH_3)$_2$)

^{13}C NMR (101 MHz, $CDCl_3$) δ 136.6, 126.6, 122.4, 122.0, 119.4, 119.3, 111.2, 58.3, 26.1, 25.7, 18.6, -5.1.

ESI-MS (LCMS): found *m/z* $[M+H]^+$ 263.4

Spectroscopic data match those previously published.[17]

6.2.30 Synthesis of Brevianamide F (206)

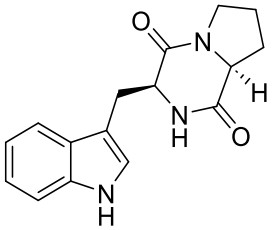

206

L-Proline methyl ester hydrochloride (**203**) (0.265 g, 1.6 mmol, 1 equiv.) was dissolved in DCM (20 mL) and the reaction was cooled to 0 °C. Triethylamine (0.75 mL, 5.3 mmol, 3.5 equiv.) was added dropwise, followed by HOBt (0.344 g, 2.3 mmol, 1.5 equiv.) and Boc-Trp(Boc)-OH (**202**) (0.912 g, 2.3 mmol, 1.5 equiv.). The reaction mixture was stirred for 10 mins, after which EDC•HCl (0.442 g, 2.3 mmol, 1.5 equiv.) was added. The reaction was allowed to warm to room temperature and left to stir overnight. After completion, HCl solution (1 M, 20 mL) was added to quench the reaction, and the aqueous layer was extracted using DCM (2 × 20 mL). The organic fractions were combined, dried, and filtered, followed by removal of the solvent *in vacuo*. The crude product mixture was then purified using column chromatography (10-20% EtOAc in hexane) affording Boc-Trp(Boc)-Pro-OMe (**204**) as a yellow oil.

Boc-Trp(Boc)-Pro-OMe (**204**) was dissolved in DCM (20 mL) and an excess of TFA (2.75 mL) was added. The reaction mixture was stirred at room temperature for 1 h, then the solvent and excess TFA was removed *in vacuo*. The crude product was dissolved directly in methanol, and the solution was cooled to 0 °C. Ammonium hydroxide (0.9 mL of a 5 M aqueous NH_4OH solution) was added dropwise, after which the reaction mixture was stirred at room temperature overnight. The solution was concentrated *in vacuo* then dissolved in DCM. The product solution was washed with H_2O (3 × 20 mL), and then the aqueous layer was back-extracted with further DCM (20 mL). The organic fractions were combined, dried ($MgSO_4$), and filtered, followed by solvent removal. The crude product was redissolved in a minimum amount of DCM and cooled to 0 °C, causing precipitation of a white solid. The solid was collected by filtration and the precipitation was repeated twice more to yield the desired product (**206**) as a white solid (126 mg, 0.44 mmol, 28%).

^{1}H NMR (400 MHz, $CDCl_3$) δ 7.61 (1H, d, *J* = 8.0, Ar-H), 7.43 (1H, d, *J* = 8.0, Ar-H), 7.27 (1H, m, Ar-H), 7.17 (1H, ddd, *J* = 7.5, 7.0, 1.0, Ar-H), 7.14 (1H, d, *J* = 2.0, Ar-H), 5.74 (1H, s, N-H),

4.40 (1H, d, *J* = 11.0, Trp-α-H), 4.10 (1H, t, *J* = 8.0, Pro-α-H), 3.79 (1H, ddd, *J* = 15.0, 4.0, 1.0, Trp-CH_2), 3.72-3.58 (2H, m, Pro-CH_2), 2.99 (1H, dd, *J* = 15.0, 11.0, Trp-CH_2), 2.35 (1H, m, Pro-CH_2), 2.04 (2H, m, Pro-CH_2), 1.94 (1H, m, Pro-CH_2).

^{13}C NMR (101 MHz, $CDCl_3$) δ 169.4, 165.6, 136.7, 126.7, 123.4, 122.8, 120.0, 118.5, 111.6, 109.9, 59.3, 54.6, 45.5, 28.3, 26.9, 22.6.

ESI-MS (LCMS): found *m/z* $[M+H]^+$ 284.6

Spectroscopic data match those previously published.[18]

6.2.31 *N*-Acetylindole-3-acetic acid methyl ester (173)

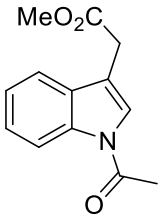

173

Methyl indole-3-acetate (**195**) (0.305 g, 1.6 mmol, 1 equiv.) was dissolved in DMF (10 mL). Acetic anhydride (0.75 mL, 0.81 g, 7.9 mmol, 5 equiv.) was added dropwise, followed by potassium carbonate (1.108 g, 8.0 mmol, 5 equiv.). The mixture was then stirred for 2 h at reflux, after which the reaction was quenched by addition of aq. sat. $NaHCO_3$ (30 mL). The product was extracted thrice using EtOAc (3 × 20 mL), and washed with water (20 mL) then brine (20 mL). The organic fraction was dried using $MgSO_4$, filtered, then the solvent was removed. The crude product mixture was purified by silica gel chromatography using an eluent of 1:5 EtOAc/hexane, affording the desired product (**173**) as a golden oil (0.248 g, 1.1 mmol, 67%).

^{1}H NMR (400 MHz, $CDCl_3$) δ 8.44 (1H, d, *J* = 7.5, Ar-H), 7.52 (1H, d, *J* = 7.5, Ar-H), 7.42 (1H, s, Ar-H), 7.37 (1H, td, *J* = 7.5, 1.5, Ar-H), 7.30 (1H, td, *J* = 7.5, 1.0, Ar-H), 3.74 (3H, s, CO_2CH_3), 3.72 (2H, d, *J* = 1.0, -CH_2-), 2.58 (3H, s, $COCH_3$).

^{13}C NMR (101 MHz, $CDCl_3$) δ 171.3, 168.5, 135.7, 130.1, 125.5, 123.9, 123.7, 118.9, 116.7, 114.9, 52.2, 30.7, 23.9.

ESI-MS (LCMS): found *m/z* $[M+H]^+$ 232.5

Spectroscopic data match those previously published.[19]

6.2.32 5-Iodo-1H-indole-3-carboxylic acid methyl ester (188)

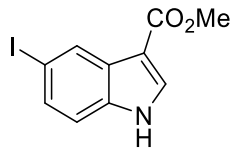

188

Methyl indole-3-carboxylate (**169**) (0.249 g, 1.4 mmol, 1 equiv.) was dissolved in TFA (2 mL), and *N*-iodo succinamide (0.362 g, 1.6 mmol, 1.1.equiv.) was added. The solution was stirred for 1 h, after which the TFA was removed under reduced pressure. The resulting solid was redissolved in EtOAc and washed with sodium thiosulfate solution (30 mL, 1M). The organic fraction was dried with $MgSO_4$, filtered, and the solvent was removed. The crude product mixture was purified by silica gel chromatography (1:4 EtOAc/hexane) and the desired product (**188**) was obtained as a pale pink solid (0.120 g, 0.4 mmol, 28%).

^{1}H NMR (400 MHz, DMSO) δ 8.37 (1H, d, *J* = 1.5, ArH), 8.07 (1H, d, *J* = 3.0, ArH), 7.47 (1H, dd, *J* = 8.5, 1.5, ArH), 7.34 (1H, d, *J* = 8.5, ArH), 3.81 (3H, s, CO_2Me).

^{13}C NMR (101 MHz, DMSO) δ 164.9, 136.0, 133.6, 130.9, 129.3, 128.6, 115.2, 106.3, 86.1, 51.2.

ESI-MS (LCMS): found *m/z* $[M+H]^+$ 302.2

Spectroscopic data match those previously published.[20]

6.2.33 *N*-Boc-Trp(*N'*-Ac)-OMe (176)

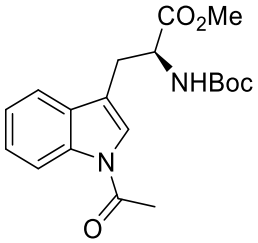

176

L-Boc-Trp-OMe (**164**) (0.299 g, 1.0 mmol, 1 equiv.) was dissolved in dry DCM and placed under an inert atmosphere. TBAHS (37 mg, 0.01 mmol, 0.1 equiv.) was added alongside freshly ground NaOH (0.198 g, 5.0 mmol, 5 equiv.). The reaction was cooled to 0 °C and stirred for 10 mins, after which AcCl (0.21 mL, 3.0 mmol, 3 equiv.) was added dropwise. The

reaction was allowed to warm to room temperature and left to stir overnight. The reaction was quenched with H_2O (30 mL). The aqueous layer was washed with EtOAc (2 × 20 mL) and then the combined organic fractions were washed with brine. The organic fraction was then dried and filtered, and the solvent was removed in vacuo. The crude product mixture was then purified using column chromatography (10-30% EtOAc in hexane) to yield the desired product (**176**) (0.254 g, 0.7 mmol, 75%).

^{1}H NMR (400 MHz, CDCl3) δ 7.49 (1H, d, *J* = 7.5, Ar-H), 7.35 (1H, t, *J* = 7.5, Ar-H), 7.28 (2H, m, Ar-H), 5.26 (1H, d, *J* = 8.0, Ar-H), 4.70 (1H, m, α-H), 3.70 (3H, s, CO_2Me), 3.21 (2H, m, -CH2-), 2.58 (3H, s, Ac), 1.44 (9H, s, Boc).

^{13}C NMR (101 MHz, $CDCl_3$) δ 172.4, 168.4, 155.2, 135.7, 130.6, 125.4, 123.6, 123.4, 118.8, 117.2, 116.6, 80.1, 53.4, 52.5, 28.3, 28.0, 24.0.

ESI-MS (LCMS): found *m/z* [M+H-Boc]+ 263.4

Spectroscopic data match those previously published.[21]

6.2.34 2-Chloro-1H-indole-3-carboxylic acid methyl ester (170)

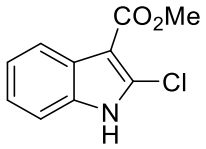

170

Methyl indole-3-carboxylate (**169**) (58 mg, 0.3 mmol) was reacted using **General Procedure 6.2.3**. The crude product was purified using silica gel chromatography (15% EtOAc in hexane) to furnish the desired product (**170**) as a crystalline white solid, (48 mg, 0.21 mmol, 69%).

^{1}H NMR (400 MHz, $CDCl_3$) δ 8.68 (1H, br s, N-H), 8.11-8.15 (1H, m, Ar-H), 7.32-7.36 (1H, m, Ar-H), 7.27-7.31 (2H, m, Ar-H), 3.99 (3H, s, CO_2CH_3).

^{13}C NMR (101 MHz, $CDCl_3$) δ 133.7, 130.2, 126.2, 123.6, 122.4, 121.5, 110.6, 104.5, 51.3, 31.0.

ESI-MS (LCMS): found *m/z* $[M+H]^+$ 210.0, 212.0

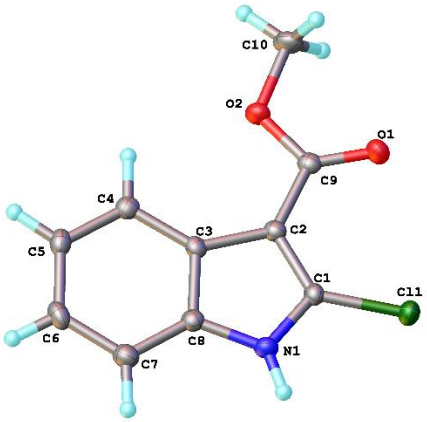

Figure 6.3: X-Ray molecular structure for **170**. Molecular structure reported with a 50% thermal ellipsoid probability.

Spectroscopic data match those previously published.[22]

6.2.35 *N*-Boc-2-Chloro-*L*-tryptophan methyl ester (175)

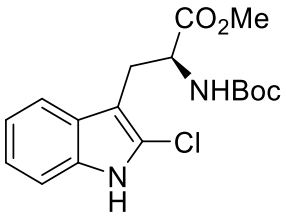

175

General Procedure Section 6.2.3 was followed using *N*-Boc-L-tryptophan methyl ester (**164**) (95 mg, 0.3 mmol) as a substrate and a total charge of 3 F/mol. The crude reaction mixture was purified using silica gel chromatography (15% EtOAc in hexane) to give the desired product (**175**) as a white solid (58 mg, 0.17 mmol, 55%).

^{1}H NMR (400 MHz, $CDCl_3$) δ 8.14 (1H, s, N-H), 7.49 (1H, d, *J* = 8.0, Ar-H), 7.27 (1H, d, *J* = 8.5, Ar-H), 7.12-7.21 (2H, dt, *J* = 22.0, 7.5), 5.16 (1H, br d, *J* = 8.0, N-H), 4.66 (1H, m, α-H), 3.71 (3H, s, CO_2CH_3), 3.21-3.34 (2H, qd, *J* = 16.5, 8.0, β-CH_2), 1.44 (9H, s, Boc).

^{13}C NMR (101 MHz, $CDCl_3$) δ 172.6, 155.1, 134.4, 127.8, 122.4, 122.2, 120.3, 118.3, 110.5, 106.5, 79.9, 53.7, 52.5, 28.4, 27.1.

ESI-MS (LCMS): found *m/z* $[M+H\text{-}Boc]^+$ 253.4

ESI-MS (HRMS): found *m/z* $[M+H\text{-}Boc]^+$ 253.0741

IR V_{max} / cm^{-1} (ATR): 3363 (N-H), 1735 (C=O), 1680 (C=O), 743 (C-Cl)

6.2.36 *N*-Boc-*N'*-Acetyl-2-chloro-*L*-tryptophan methyl ester (177)

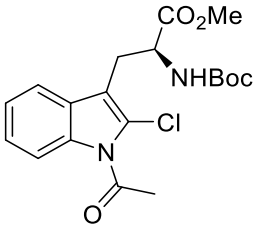

177

General Procedure Section 6.2.3 was followed using *N*-Boc-*N'*-acetyl-*L*-tryptophan methyl ester (**176**) (95 mg, 0.27 mmol) as a substrate. The crude reaction mixture was purified using silica gel chromatography (20% EtOAc in hexane) to give the desired product (**177**) as a white solid (40 mg, 0.1 mmol, 38%).

^{1}H NMR (400 MHz, $CDCl_3$) δ 8.35 (1H, d, *J* = 8.0, Ar-H), 7.49 (1H, d, *J* = 8.0, Ar-H), 7.38-7.30 (2H, m, Ar-H), 5.19 (1H, d, *J* = 8.5, N-H), 4.67 (1H, q, *J* = 7.5, α-H), 3.70 (3H, s, CO_2Me), 3.33-3.19 (2H, qd, *J* = 20.5, 6.5, CH_2), 2.83 (3H, s, N-Ac), 1.42 (9H, s, Boc)

^{13}C NMR (101 MHz, $CDCl_3$) δ 172.1, 169.5, 154.9, 135.8, 128.3, 125.6, 124.0, 121.7, 118.1, 116.3, 115.8, 80.0, 52.9, 52.6, 28.3, 27.8, 27.7.

ESI-MS (LCMS): *m/z* $[M+H\text{-}Boc]^+$ 295.0

ESI-MS (HRMS): *m/z* $[M+H\text{-}Boc]^+$ 295.0852

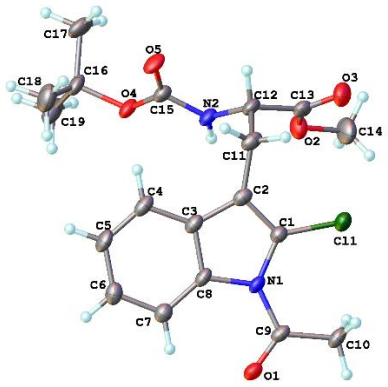

Figure 6.4: X-Ray molecular structure for **177**. Molecular structure reported with a 50% thermal ellipsoid probability.

6.2.37 2-Chloro-3-methylindole (178)

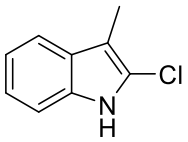

178

3-Methylindole (**165**) (39 mg, 0.3 mmol) was reacted electrochemically following **General Procedure 6.2.3**. The crude product mixture was purified using silica gel chromatography with an eluent of 10% v/v EtOAC/hexane, affording the product (**178**) as a brown solid (4 mg, 0.02 mmol, 8%).

^{1}H NMR (400 MHz, $CDCl_3$) δ 7.92 (1H, s, N-H), 7.49 (1H, d, *J* = 7.5, Ar-H), 7.28 (1H, m, Ar-H), 7.20 (1H, td, *J* = 8.0, 1.5, Ar-H), 7.15 (1H, td, *J* = 7.5, 1.5), 2.28 (3H, s, CH_3).

^{13}C NMR (101 MHz, $CDCl_3$) δ 134.4, 128.3, 122.2, 120.0, 118.3, 110.3, 108.0, 8.3.

ESI-MS (LCMS): found *m/z* $[M-H]^-$ 164.1, 166.9

Spectroscopic data match those previously published.[23]

6.2.38 2,4,6-Trimethoxychlorobenzene (179)

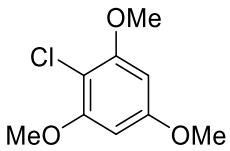

179

General Procedure Section 6.2.3 was followed using 1,3,5-trimethoxybenzene (**151**) (63 mg, 0.38 mmol) as a substrate. The resulting crude mixture was purified by silica gel chromatography (1:9 EtOAc/hexane) to furnish the desired product (**179**) (23 mg, 0.12 mmol, 31%).

^{1}H NMR (400 MHz, $CDCl_3$) δ 6.21 (2H, s, Ar-H), 3.90 (6H, s, $-OCH_3$), 3.83 (3H, s, $-OCH_3$).

^{13}C NMR (101 MHz, $CDCl_3$) δ 159.4, 156.5, 102.7, 91.6, 56.3, 55.6.

ESI-MS (LCMS): found *m/z* $[M+H]^+$ 203.9

Spectroscopic data match those previously published.[24]

6.2.39 2-Chloro-indole-3-carboxaldehyde (172)

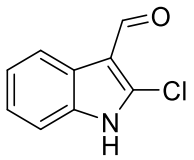

172

Indole-3-carboxaldehyde (**171**) (77 mg, 0.6 mmol) was reacted using **General Procedure Section 6.2.3**, and the crude product mixture was purified using an eluent of 1:4 EtOAc/hexane. The desired product (**172**) was isolated as a brown solid (12 mg, 0.07 mmol, 11%).

^{1}H NMR (400 MHz, DMSO) δ 10.00 (1H, s, C(O)H), 8.09 – 8.04 (1H, m, Ar-H), 7.48 – 7.39 (1H, m, Ar-H), 7.33 – 7.21 (2H, m, Ar-H).

^{13}C NMR (101 MHz, DMSO) δ 183.8, 135.3, 135.1, 124.8, 124.3, 123.3, 120.4, 112.4, 112.2.

ESI-MS (LCMS): found *m/z* $[M+H]^+$ 180.7

Spectroscopic data match those previously published.[25]

6.2.40 *N*-Acetyl-2-chloroindole-3-acetic acid methyl ester (174)

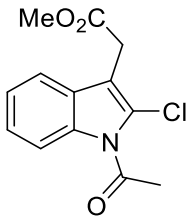

174

N-Acetylindole-3-acetic acid methyl ester (**173**) (73 mg, 0.3 mmol) was reacted according to **General Procedure Section 6.2.3**. The crude reaction mixture was purified using silica gel chromatography (1:9 EtOAc/hexane), furnishing the desired product as a white solid (**174**) (16 mg, 0.06 mmol, 19%).

^{1}H NMR (400 MHz, $CDCl_3$) δ 8.38 (1H, d, *J* = 8, Ar-H), 7.48 (1H, d, *J* = 3.5, Ar-H), 7.30-7.40 (2H, m, Ar-H), 3.79 (2H, s, -CH_2-), 3.74 (3H, s, CO_2CH_3), 2.85 (3H, s, $COCH_3$).

^{13}C NMR (101 MHz, $CDCl_3$) δ 170.4, 169.5, 135.8, 127.8, 125.6, 124.1, 121.8, 118.1, 116.5, 113.9, 52.4, 30.2, 27.7.

ESI-MS (LCMS): found *m/z* $[M+H\text{-Acetyl}]^+$ 224.3, 226.0

ESI-MS (HRMS): found *m/z* $[M+H\text{-Acetyl}]^+$ 224.0486, 226.0465

IR V_{max} / cm^{-1} (ATR): 1697 (C=O), 1471 (aromatic C=C), 1155 (C-O-C), 752 (C-Cl).

6.2.41 2-Chloroimidazo[1,2-*a*]pyridine (183)

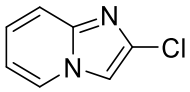

183

Imidazo[1,2-*a*]pyridine (**182**) (35 mg, 0.03 mL, 0.3 mmol) was subjected to electrochemical chlorination using **General Procedure Section 6.2.3**. The desired product (**183**) was isolated as a green solid using silica gel chromatography (2:3 EtOAc/hexane) (38 mg, 0.25 mmol, 84%).

^{1}H NMR (400 MHz, $CDCl_3$) δ 8.07 (1H, dt, *J* = 7.0, 1.0, Ar-H), 7.61 (1H, dt, *J* = 9.0, 1.0, Ar-H), 7.56 (1H, s, Ar-H), 7.22 (1H, ddd, *J* = 9.0, 6.5, 1.0, Ar-H), 6.93 (1H, td, *J* = 7.0, 1.0, Ar-H).

^{13}C NMR (101 MHz, $CDCl_3$) δ 130.2, 124.4, 122.6, 118.1, 113.0.

ESI-MS (LCMS): found *m/z* $[M+H]^+$ 153.1, 155.1

Spectroscopic data match those previously published.[26]

6.2.42 *N*-(2,6-Dichloro-4-hydroxyphenyl)acetamide (181)

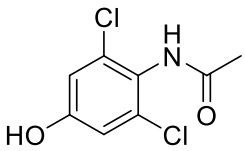

181

4-Acetamidophenol (**180**) (45 mg, 0.3 mmol) was chlorinated according to **General Procedure Section 6.2.3**. The crude product mixture was purified using silica gel

chromatography (1:1 EtOAc/hexane), and the dichlorinated product (**181**) was obtained as a brown oil (27 mg, 0.12 mmol, 41%).

^{1}H NMR (400 MHz, CD_3CN) δ 7.54 (2H, s, Ar-H), 2.05 (3H, s, CH_3).

^{13}C NMR (101 MHz, CD_3CN) δ 168.7, 144.7, 132.5, 121.3, 119.5, 23.2.

ESI-MS (LCMS): found *m/z* $[M+H]^+$ 220.1, 222.1, 224.1

Spectroscopic data match those previously published.[27]

6.2.43 5-Iodo-methyl 2-oxoindoline-3-carboxylate (189)

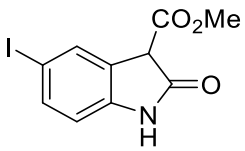

189

5-iodo-1H-indole-3-carboxylic acid methyl ester (**188**) (71 mg, 0.24 mmol) was subjected to **General Procedure Section 6.2.3**. The crude product mixture was purified using silica gel chromatography (1:5 EtOAc/hexane), affording the oxindole product (**189**) as a white solid (18 mg, 0.06 mmol, 24%).

^{1}H NMR (400 MHz, $CDCl_3$) δ 8.66 (1H, s, N-H), 7.46 (1H, dd, *J* = 8.0, 1.5, Ar-H), 7.34 (1H, d, *J* = 1.5, Ar-H), 7.04 (1H, d, *J* = 8.0, Ar-H), 4.96 (1H, s, C**H**CO_2Me), 3.70 (3H, s, -CO_2CH_3)

ESI-MS (LCMS): found *m/z* $[M+H]^+$ 316.3

ESI-MS (HRMS): found *m/z* $[M+H]^+$ 315.9463

IR V_{max} / cm^{-1} (ATR): 1732 (C=O), 1440 (aromatic C=C), 1257 (C-O-C), 1066 (C-O-C)

6.2.44 *p*-Methoxybenzoic acid (191)

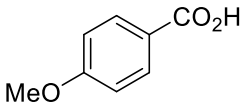

191

Ethyl 4-methoxybenzoylacetate (**190**) (67 mg, 0.058 mL, 0.3 mmol) was reacted according to **General Procedure Section 6.2.3**. The crude product mixture was subjected to silica gel

chromatography (1:9 EtOAc/hexane), and the product (**191**) was isolated as a white solid (19 mg, 0.1 mmol, 41%).

^{1}H NMR (400 MHz, CD_3CN) δ 7.98 (2H, m, Ar-H), 7.01 (2H, m, Ar-H), 3.87 (3H, s, -OCH_3)

^{13}C NMR (101 MHz, CD_3CN) δ 166.8, 163.6, 131.7, 122.2, 113.8, 55.3.

ESI-MS (LCMS): found *m/z* $[M+H]^+$ 153.3

Spectroscopic data match those previously published.[28]

6.2.45 3-Chloro-2-methylpyrrole carboxylate (187)

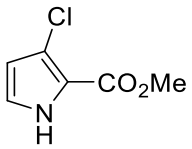

187

2-Methylpyrrole carboxylate (**136**) (38 mg, 0.3 mmol) was reacted according to **General Procedure Section 6.2.3**. The crude product mixture was purified using silica gel chromatography (EtOAc/hexane, 0→100%). The title compound (**187**) was obtained as a white solid (22 mg, 0.12 mmol, 45%).

^{1}H NMR (400 MHz, $CDCl_3$) δ 6.84 (1H, dd, *J* = 4.0, 3.0, Ar-H), 6.11 (1H, dd, *J* = 4.0, 3.0, Ar-H), 3.86 (3H, s, CO_2Me).

^{13}C NMR (101 MHz, $CDCl_3$) δ 160.8, 121.7, 120.4, 116.4, 108.9, 51.7.

ESI-MS (LCMS): found $[M+H]^+$ 160.0

Spectroscopic data match those previously published.[29]

6.3 Experimental for compounds from Chapter 3

6.3.1 General procedure A for bromination of amino acid alcohols

The amino acid substrate (1 equiv.) and PPh_3 (1.3 equiv.) were dissolved in THF and cooled to 0 °C. NBS (1.3 equiv.) was added portionwise and the reaction was allowed to reach ambient temperature whilst stirring overnight. The solvent was removed *in vacuo*, followed by

addition of Et_2O. The solution was filtered, and the solvent was again removed. The crude product was purified by silica gel chromatography (EtOAc/hexane, 0-100%).

6.3.2 General procedure B for bromination of amino acid alcohols

The amino acid substrate (1 equiv.) was dissolved in anhydrous DCM, placed under an inert atmosphere, and cooled to 0 °C. CBr_4 (1.5 equiv.) was then added slowly. In a separate RBF, PPh_3 (1.2 equiv.) was dissolved in anhydrous DCM under an inert atmosphere. The PPh_3 solution was then added dropwise to the reaction mixture. The mixture was stirred at 0 °C for 1 h, then at an ambient temperature for 6 h. Et_2O was added, and the resulting slurry was filtered. The solvent was removed *in vacuo*, followed by a second addition of Et_2O and subsequent filtration/rotary evaporation. The crude product was purified using silica gel chromatography (EtOAc/hexane, 0-100%).

6.3.3 General procedure A for Ni-catalysed coupling

Solution A: $NiCl_2$.glyme (9.9 mg, 0.045 mmol, 0.3 equiv.) and dtbbpy (20.8 mg, 0.068 mmol, 0.45 equiv.) ([Ni]:Ligand = 1:1.5) were placed in an RBF under an inert atmosphere and anhydrous DMA (6 mL) was added. The mixture was stirred until green and homogenous (~1 hour).

Solution B: LiBr (119 mg, 1.37 mmol) was placed in an RBF under an inert atmosphere, and anhydrous DMA (6 mL) was added. The mixture was stirred until dissolved.

The substrate (1 equiv.) and 4-bromobenzotrifluoride (**247**) (1.5 equiv.) were added to an ElectraSyn vial with a graphite anode and nickel foam cathode and placed under an inert atmosphere. Solution A (2 mL) and Solution B (2 mL) were added to the vial and the mixture was degassed for 20 mins using a stream of argon. DIPEA (4 equiv.) was then added to the mixture and a 3 mA current was applied for 10 h at room temperature. The product mixture was diluted with DCM and washed with aq. $NaHCO_3$ then brine. The organic layer was dried with $MgSO_4$ and filtered, followed by solvent removal *in vacuo*. The crude product was purified using silica gel chromatography.

Divided cell modification: the bromoalanine substrate (1 equiv.) and 4-bromobenzotrifluoride (**247**) (1.5 equiv.) added to the cathodic chamber with Solution A (2 mL) and Solution B (2 mL). To the anodic chamber was added Solution B (4 mL) and DIPEA (4 equiv.). The reaction then follows the same procedure as for the undivided cell.

6.3.4 General procedure B for Ni-catalysed coupling

In an ElectraSyn vial equipped with a stir bar, RVC anode, and Ni foam cathode were placed the alkyl bromide substrate (1 equiv.), $[Ni(bpy)_3]Br_2$ (0.1 equiv.), and $^nBu_4NBr$ (193 mg, 0.6 mmol). The reaction vessel was placed under an inert atmosphere and DMA (4 mL) was added to the vial. The mixture was degassed using a stream of argon for 20 mins, after which DBU (3 equiv.) and 4-bromobenzotrifluoride (**247**) (2 equiv.) were added. A current of 4 mA was applied to the reaction mixture for 3-10 h. Once complete, the crude product mixture was diluted with DCM and washed with sat. aq. NH_4Cl. The organic fraction was dried ($MgSO_4$), filtered, and concentrated under reduced pressure. The desired product was isolated after purification using silica gel chromatography (EtOAc/hexane 0→100%).

6.3.5 General procedure for Boc group deprotection

The Boc-protected substrate (1 equiv.) was dissolved in DCM (20 mL) and an excess of TFA was added (5-10 equiv.). The solution was stirred for 4-20 h, after which the solvent was removed *in vacuo*. The product mixture was washed several times with Et_2O to remove excess TFA, furnishing the desired product without purification.

6.3.6 General Procedure for synthesis of MIA-amino acids

2-Methoxyiminoacetic acid (1 equiv.) was dissolved in dry THF. To this was added *N*-methyl morpholine (2.5 equiv.), and the solution was cooled to 0 °C and placed under argon. Isobutyl chloroformate (1 equiv.) was then added dropwise, and the reaction was stirred for 1h. Amino acid methyl ester hydrochloride (1 equiv.) was then added, after which the reaction was allowed to warm to room temperature and was left to stir overnight. The solvent was removed *in vacuo* and H_2O (20 mL) was added, followed by extraction with EtOAc (25 mL). The organic fraction was washed with brine before drying with $MgSO_4$, filtering, and solvent removal. The crude product was purified using column chromatography (silica gel, EtOAc:hexane 1:3).

6.3.7 Boc-Ala-(Br)-OMe (27)

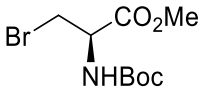

27

The title compound was synthesised using **General procedure for bromination A** (**Section 6.3.1**). Boc-Ser-OMe (**26**) (2.024 g, 9.2 mmol, 1 equiv.) was reacted with PPh_3 (3.139 g, 11.8 mmol, 1.3 equiv.) and NBS (2.110 g, 11.8 mmol, 1.3 equiv.) to afford the desired compound (**27**) as a white solid (1.646 g, 5.8 mmol, 63%).

^{1}H NMR (400 MHz, $CDCl_3$) δ 5.45 – 5.39 (1H, m, α-H), 4.74 (1H, dt, *J* = 7.5, 3.5, -CH_2-), 3.79 (3H, s, CO_2Me), 3.70 (1H, dd, *J* = 10.5, 3.5, -CH_2-), 1.44 (9H, s, Boc).

^{13}C NMR (101 MHz, $CDCl_3$) δ 169.7, 155.0, 80.5, 53.9, 53.0, 34.1, 28.3.

ESI-MS (LCMS): found *m/z* $[M+H\text{-}Boc]^+$ 182.0, 184.0

Spectroscopic data match those previously published.[30]

6.3.8 Methyl *N*-Boc-α,β-didehydroalaninate (249)

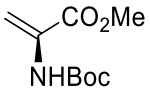

249

The title compound (**249**) was obtained as a side product in the reaction of Boc-Ala(Br)-OMe (**27**) (43 mg, 0.15 mmol, 1 equiv.) according to the **General procedure for Ni-catalysed coupling A** (**Section 6.3.3**), as a colourless oil (22 mg, 0.11 mmol, 72%).

^{1}H NMR (400 MHz, $CDCl_3$) δ 7.01 (1H, br s, NH), 6.15 (1H, br s, =CH_2), 5.72 (1H, d, *J* = 1.5, =CH_2), 3.83 (3H, s, CO_2Me), 1.48 (9H, s, Boc).

^{13}C NMR (101 MHz, $CDCl_3$) δ 164.5, 152.6, 131.3, 105.2, 80.2, 52.9, 28.2.

ESI-MS (LCMS): found *m/z* $[M+H\text{-}Boc]^+$ 102.1

Spectroscopic data match those previously published.[31]

6.3.9 *N*-Boc-β,β-dibromodehydroalanine methyl ester (252)

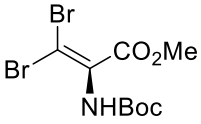

252

The title compound (**252**) was obtained as a side product in the reaction of Boc-Ala(Br)-OMe (**27**) (41 mg, 0.15 mmol, 1 equiv.) according to the **General procedure for Ni-catalysed**

coupling A (**Section 6.3.3**) using Na_2CO_3 (40 mg, 0.4 mmol, 2 equiv.) in place of DIPEA, as a colourless crystalline solid (19 mg, 0.05 mmol, 36%).

^{1}H NMR (400 MHz, $CDCl_3$) δ 3.88 (3H, s, CO_2Me), 1.46 (9H, s, Boc).

^{13}C NMR (101 MHz, $CDCl_3$) δ 162.57, 150.9, 132.8, 121.5, 82.7, 53.0, 28.0.

ESI-MS (LCMS): found *m/z* $[M+H\text{-}Boc]^+$ 258.0, 260.0, 262.0

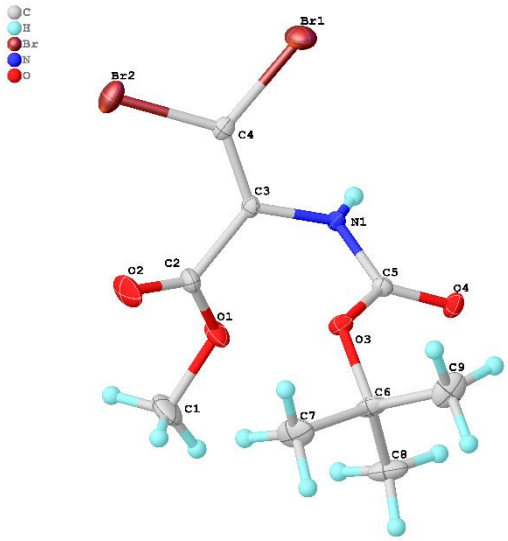

Figure 6.5: Molecular structure for **252**. Molecular structure reported with 50% thermal ellipsoid probability.

Spectroscopic data match those previously published.[32]

6.3.10 *N*-Boc-(4-trifluoromethyl)phenylalanine methyl ester (248)

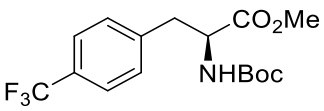

248

The title compound (**248**) was obtained from the reaction of Boc-Ala(Br)-OMe (**27**) (86 mg, 0.3 mmol, 1 equiv.) with 4-bromobenzotrifluoride (**247**) (0.06 mL, 0.45 mmol, 1.5 equiv.) according to the **General procedure for Ni-catalysed coupling A** (**Section 6.3.3**) using the divided cell modification, as a pale yellow oil (26 mg, 0.08 mmol, 25%).

^{1}H NMR (400 MHz, $CDCl_3$) δ 7.55 (2H, d, *J* = 8.0, Ar-H), 7.25 (2H, d, *J* = 8.0, Ar-H), 5.00 (1H, br d, *J* = 8.5, NH), 4.62 (1H, d, *J* = 7.5, α-H), 3.73 (3H, s, CO_2Me), 3.25 – 3.03 (2H, m, -CH_2-) 1.41 (9H, s, Boc).

^{13}C NMR (101 MHz, $CDCl_3$) δ 171.9, 155.0, 140.3, 129.7, 129.4 (m), 125.4 (m), 122.8 (m), 80.2, 54.2, 52.4, 38.3, 28.3.

^{19}F NMR (376 MHz, $CDCl_3$) δ 63.5 (s)

ESI-MS (LCMS): found *m/z* $[M+H\text{-}Boc]^+$ 248.2

Spectroscopic data match those previously published.[33]

6.3.11 Boc-Thr(Br)-OMe (258)

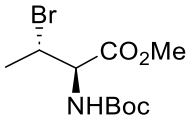

258

The title compound (**258**) was obtained from the reaction of *N*-Boc-Thr-OMe (**255**)(1.011 g, 4.3 mmol, 1 equiv.) with PPh_3 (1.486 g, 5.6 mmol, 1.3 equiv.) and NBS (0.998 g, 5.6 mmol, 1.3 equiv.) using **General procedure for bromination A** (**Section 6.3.1**) as a colourless oil (0.886 g, 3.0 mmol, 69%).

^{1}H NMR (400 MHz, $CDCl_3$) δ 5.44 (1H, d, *J* = 9.0, NH), 4.53 (1H, dd, *J* = 9.0, 3.5, α-H), 4.33 (1H, qd, *J* = 7.0, 3.5, β-H), 3.79 (3H, s, CO_2Me), 1.78 (3H, d, *J* = 7.0 Hz, C**H$_3$**CBr), 1.44 (9H, s, Boc)

^{13}C NMR (101 MHz, $CDCl_3$) δ 169.4, 154.9, 80.4, 59.4, 52.6, 49.6, 28.3, 22.8.

ESI-MS (LCMS): found *m/z* $[M+H\text{-}Boc]^+$ 196.1, 198.0

Spectroscopic data match those previously published.[34]

6.3.12 *N*-Boc-4-bromoproline methyl ester (259)

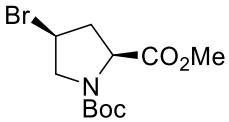

259

The title compound (**259**) was obtained from the reaction of *N*-Boc-Hyp-OMe (**117**) (507 mg, 2.04 mmol, 1 equiv.) with PPh_3 (644 mg, 2.45 mmol, 1.2 equiv.) and CBr_4 (1.019 g, 3.06 mmol,

1.5 equiv.) using **General procedure for bromination B** (**Section 6.3.2**) as a colourless oil (451 mg, 1.4 mmol, 71%).

^{1}H NMR (400 MHz, $CDCl_3$) 4.42 – 4.26 (2H, m, α-H and CH), 4.15-4.00 (1H, m, CH_2), 3.78 (3H, s, CO_2Me), 3.72 (1H, m, CH_2), 2.84 (1H, m, CH_2), 2.50-2.38 (1H, m, CH_2), 1.45 (9H, d (rotameric), Boc).

^{13}C NMR (101 MHz, $CDCl_3$)* δ 172.2, 172.0, 153.7, 153.1, 80.7, 80.7, 58.3, 57.9, 55.6, 55.1, 52.5, 52.3, 42.1, 41.2, 41.0, 40.0, 28.4, 28.2.

*Peaks doubled due to presence of rotamers.

ESI-MS (LCMS): found *m/z* $[M+H\text{-}Boc]^+$ 208.1, 210.0

Spectroscopic data match those previously published.[35]

6.3.13 *N*-Boc-Ala(I)-OMe (260)

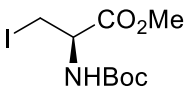

260

PPh_3 (1.214 g, 4.6 mmol, 1 equiv.), imidazole (0.309 g, 4.6 mmol, 1 equiv.), and I_2 (1.200 g, 4.6 mmol, 1 equiv.) were added successively to a solution of Boc-Ser-OMe (**26**) (1.007 g, 4.6 mmol, 1 equiv.) in DCM (20 mL). The reaction mixture was stirred at room temperature overnight, then the solvent was removed *in vacuo* and the crude product was purified using silica gel chromatography (EtOAc/hexane, 0-100%). The desired product (**260**) was isolated as a yellow oil (1.134 g, 3.5 mmol, 75%).

^{1}H NMR (400 MHz, $CDCl_3$) δ 5.35 (1H, br d, *J* = 7.5, NH), 4.52 (1H, dt, *J* = 7.5, 4.0, α-H), 3.80 (3H, s, CO_2Me), 3.62 – 3.53 (2H, m, -CH_2), 1.46 (9H, s, Boc).

^{13}C NMR (101 MHz, $CDCl_3$) δ 170.1, 154.9, 80.5, 53.7, 53.0, 28.3, 7.8.

ESI-MS (LCMS): found *m/z* $[M+H\text{-}Boc]^+$ 230.0

Spectroscopic data match those previously published.[36]

6.3.14 *N*-Boc-(*O*-Tetrafluoropyridyl)serine methyl ester (269)

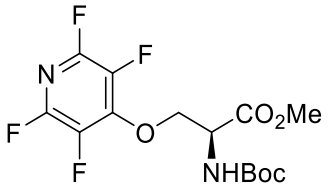

269

Boc-Ser-OMe (**26**) (0.582 g, 2.3 mmol, 1 equiv.) was dissolved in MeCN and K_2CO_3 (338 mg, 2.3 mmol, 1 equiv.) was added. To this mixture pentafluoropyridine (1.0 mL, 9.1 mmol, 4 equiv.) was added dropwise. The reaction mixture was stirred at ambient temperature overnight, then filtered. The solvent was removed by evaporation and the crude product was purified using silica gel chromatography (EtOAc/hexane, 0→100%), affording the title compound (**269**) as a white solid (0.498 g, 1.2 mmol, 51%).

^{1}H NMR (400 MHz, $CDCl_3$) δ 5.49 (1H, d, *J* = 8.0, NH), 4.82 (2H, q, *J* = 12.0, CH_2), 4.70 (1H, d, *J* = 9.0, α-H), 3.85 (3H, s, CO_2Me), 1.48 (9H, s, Boc).

^{13}C NMR (101 MHz, $CDCl_3$) δ 169.3, 155.1, 146.7, 145.7 – 144.8 (m), 143.2 – 142.1 (m), 137.3 – 135.7 (m), 134.2 – 133.2 (m), 74.4 (t, *J* = 4.5), 54.0, 53.0, 28.2.

^{19}F NMR (376 MHz, $CDCl_3$) δ -89.7 – -89.9 (m), -158.1 – -158.4 (m).

ESI-MS (LCMS): found *m/z* $[M+H\text{-}Boc]^+$ 269.3

Spectroscopic data match those previously published.[37]

6.3.15 *O*-(Tetrafluoropyridyl)serine methyl ester (272)

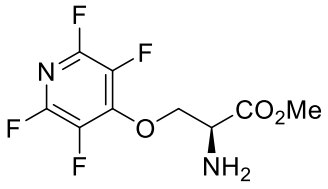

272

Boc-Ser(*O*-TFP)-OMe (**269**) (300 mg, 0.82 mmol, 1 equiv.) was deprotected according to the **General Procedure for Boc deprotection (Section 6.3.5)**, furnishing the desired product (**272**) as a white solid in a quantitative yield.

^{1}H NMR (400 MHz, MeOD) δ 5.04 – 4.97 (2H, m, CH_2), 4.68 (1H, t, *J* = 3.5, α-H), 3.92 (3H, s, CO_2Me).

^{13}C NMR (101 MHz, MeOD) δ 166.4, 146.3 – 145.5 (m), 145.3 – 145.0 (m), 142.9 – 142.6 (m), 136.9 – 136.3 (m), 135.0 – 132.7 (m), 71.3 (t, *J* = 4.5), 52.8, 52.8.

^{19}F NMR (376 MHz, MeOD) δ -92.9 – -93.2 (m), -159.7 – -159.9 (m).

ESI-MS (LCMS): found *m/z* $[M+H]^+$ 269.2

IR V_{max} / cm^{-1} (ATR): 1745 (C=O), 1472 (CH_2), 1441 (aromatic C=C), 1197 (C-F), 1095 (C-O-C).

6.3.16 *N*-Boc-(*S*-tetrafluoropyridyl)cysteine methyl ester (277)

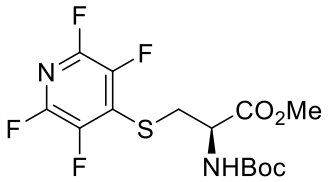

277

Boc-Cys-OMe (**276**) (1.095 g, 4.3 mmol, 1 equiv.) and Et_3N (1.2 mL, 8.5 mmol, 2 equiv.) were dissolved in anhydrous THF (20 mL), placed under an inert atmosphere, and cooled to 0 °C. Pentafluoropyridine (0.51 mL, 4.7 mmol, 1.1 equiv.) was added dropwise, and the mixture was stirred for 20 mins at rt. The reaction mixture was concentrated, and DCM (20 mL) was added. The solution was washed with brine and the aqueous layer was extracted with DCM (3 × 20 mL). The combined organic fractions were dried using $MgSO_4$, filtered, then concentrated *in vacuo*. The crude product was purified using silica gel chromatography (EtOAc/hexane 0→100%), affording the title compound (**277**) as a white solid (1.28 g, 3.3 mmol, 78%).

^{1}H NMR (400 MHz, $CDCl_3$) δ 5.31 (1H, d, *J* = 7.5, NH), 4.63 (1H, m, α-H), 3.83 - 3.74 (1H, m, -SCH_2-), 3.76 (3H, s, CO_2Me), 3.47 (1H, dd, *J* = 14.0, *J'* = 5.5, -SCH_2-), 1.41 (9H, s, Boc).

^{13}C NMR (101 MHz, $CDCl_3$) δ 170.0, 154.7, 144.8 – 144.4 (ddd, *J* = 3.0, 13.0, 17.0), 143.0 – 142.7 (m), 142.3 – 142.0 (ddd, *J* = 3.0, 13.0, 17.0), 140.4 – 140.1 (m), 130.0 (t, *J* = 17.0), 80.7, 53.9, 52.9, 35.5 (t, *J* = 4.0), 28.1.

^{19}F NMR (376 MHz, $CDCl_3$) δ -90.7 – -90.9 (m), -136.3 – -136.5 (m).

ESI-MS (LCMS): found *m/z* $[M+H-Boc]^+$ 285.2

Spectroscopic data match those previously published.[38]

6.3.17 Sulfone 279 and Sulfoxide 278

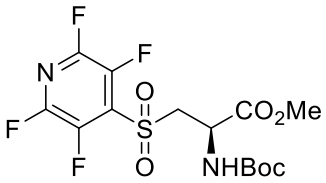

279

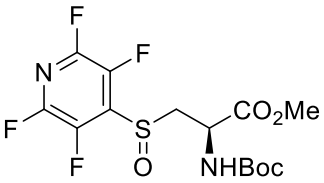

278

Boc-Cys(*S*-TFP)-OMe (**277**) (0.601 g, 1.6 mmol, 1 equiv.), ammonium heptamolybdate tetrahydrate (10.3 mg, 0.008 mmol, 0.005 equiv.), EtOH (2 mL), and 30% aqueous H_2O_2 solution (0.64 mL, 6.4 mmol, 4 equiv.) were added successively to a 5 mL tube. The tube was sealed with a screw cap and the mixture was stirred for 3 h at 70 °C. Alternatively, the mixture could be stirred in an RBF for 3 days at rt. After completion, the reaction mixture was diluted with H_2O (10 mL) and extracted with DCM (3 × 10 mL). The combined organic fractions were dried with $MgSO_4$, then filtered and concentrated *in vacuo*. The crude product mixture was purified using silica gel chromatography, furnishing the title compounds as crystalline white solids (**278**, 178 mg, 0.4 mmol, 27%), (**279**, 225 mg, 0.6 mmol, 36%).

279

^{1}H NMR (599 MHz, $CDCl_3$) δ 5.50 (1H, s, NH), 4.62 (1H, m, α-H), 4.16 (1H, m, -CH_2-), 4.06 (1H, m, -CH_2-), 3.81 (3H, s, -CO_2Me), 1.30 (9H, s, Boc)

^{13}C NMR (151 MHz, $CDCl_3$) δ 168.7, 154.8, 144.84 (m), 143.2 (m), 139.9 (m), 138.1 (m), 131.7 (t, *J* = 12.5), 81.5, 57.6, 53.5, 50.1, 27.9

^{19}F NMR (376 MHz, $CDCl_3$) δ -85.5 – -86.0 (m), -137.0 – -137.4 (m).

ESI-MS (LCMS): found *m/z* $[M+H\text{-}Boc]^+$ 317.2

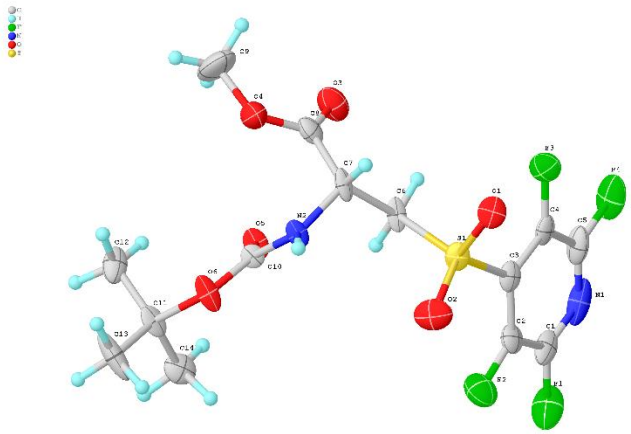

Figure 6.6: X-Ray molecular structure for **279**. Molecular structure reported with a 50% thermal ellipsoid probability.

278

^{1}H NMR (599 MHz, $CDCl_3$) δ 5.58 (1H, m, NH), 4.69 (1H, m, α-H), 3.97 (1H, m, β-H), 3.85 – 3.76 (4H, m, CO_2Me and β-H), 1.39 (9H, s, Boc).

^{13}C NMR (151 MHz, $CDCl_3$) δ 169.8 (d, *J* = 19.5), 155.0 (d, *J* = 9.5), 144.3 (m), 142.6 (m), 140.2 (m), 138.4 (m), 136.2 (m), 81.2, 55.0 (d, *J* = 11.0), 53.3 (d, *J* = 11.0), 49.3 (d, *J* = 10.0), 28.0 (d, *J* = 1.5).*

^{19}F NMR (376 MHz, $CDCl_3$) δ -87.3 (tt, *J* = 28.0, 11.0), -140.7 (dddd, *J* = 66.5, 30.5, 20.5, 7.0).

ESI-MS (LCMS): found *m/z* $[M+H\text{-}Boc]^+$ 301.1

*doubling of peaks observed due to the chirality of the sulfur atom.

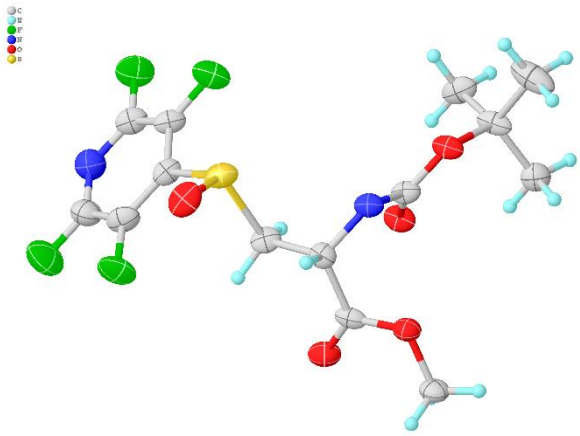

Figure 6.7: X-Ray molecular structure for **278**. Molecular structure reported with a 50% thermal ellipsoid probability.

6.3.18 Fmoc-Ala(Br)-OMe (281)

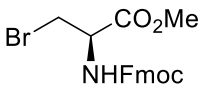

281

The title compound (**281**) was obtained following reaction of Fmoc-Ser-OMe (355 mg, 1.0 mmol) with PPh_3 (349 mg, 1.3 mmol) and NBS (255 mg, 1.4 mmol) according to **General procedure A for bromination of amino acid alcohols (Section 6.3.1)** as a white solid (281 mg, 0.7 mmol, 67%).

^{1}H NMR (400 MHz, $CDCl_3$) δ 7.80 (2H, d, *J* = 7.5, ArH), 7.64 (2H, d, *J* = 7.5, ArH), 7.44 (2H, t, *J* = 7.5, ArH), 7.37 (2H, d, *J* = 7.5, ArH), 5.75 (1H, d, *J* = 8.0, NH), 4.88 – 4.82 (1H, m, α-H), 4.45 (2H, d, *J* = 7.5, Fmoc CH_2), 4.28 (1H, t, *J* = 7.5, Fmoc CH), 3.86 (2H, s, CO_2Me), 3.83 – 3.75 (1H, m, β-CH_2).

^{13}C NMR (101 MHz, $CDCl_3$) δ 169.4, 155.5, 143.8, 143.6, 141.3, 127.8, 127.1, 125.1, 120.1, 67.4, 54.4, 53.2, 47.1, 33.7.

ESI-MS (LCMS): found *m/z* $[M+H]^+$ 404.2, 406.2

Spectroscopic data match those previously published.[39]

6.3.19 Methyl *N*-Fmoc-α,β-didehydroalaninate (284)

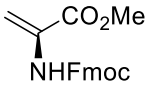

284

The title compound (**284**) was obtained as a side product in the reaction of Fmoc-Ala(Br)-OMe (**281**) (95 mg, 0.24 mmol, 1 equiv.) according to the **General procedure for Ni-catalysed coupling A** (**6.3.3**), as a brown solid (46 mg, 0.15 mmol, 61%).

^{1}H NMR (400 MHz, $CDCl_3$) δ 7.78 (2H, dt, *J* = 7.5, 1.0, ArH), 7.61 (2H, dq, *J* = 7.5, 1.0, ArH), 7.42 (2H, tdd, *J* = 7.5, 1.0, 1.0, ArH), 7.33 (2H, td, *J* = 7.5, 1.0, ArH), 6.25 (1H, s, R=CH_2), 5.81 (1H, d, *J* = 1.5, R=CH_2), 4.47 (2H, d, *J* = 7.0, Fmoc-CH_2), 4.26 (1H, t, *J* = 7.0, Fmoc-CH), 3.86 (3H, s, CO_2Me).

^{13}C NMR (101 MHz, $CDCl_3$) δ 164.3, 153.2, 143.7, 141.4, 131.0, 127.9, 127.2, 125.0, 120.1, 106.3, 67.2, 53.0, 47.0.

ESI-MS (LCMS): found *m/z* $[M+H]^+$ 324.3

Spectroscopic data match those previously published.[40]

6.3.20 Trt-Ala(Br)-OMe (282)

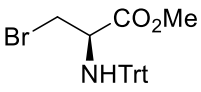

282

The title compound (**282**) was obtained following reaction of Trt-Ser-OMe (504 mg, 1.38 mmol, 1 equiv.) with PPh_3 (443 mg, 1.66 mmol) and CBr_4 (682 mg, 2.08 mmol) according to **General procedure B for bromination of amino acid alcohols (6.3.2)** as a white solid (248 mg, 0.6 mmol, 41%).

^{1}H NMR (400 MHz, $CDCl_3$) δ 7.63 – 7.55 (5H, m, Ar-H), 7.40 – 7.31 (7H, m, Ar-H), 7.29 – 7.22 (3H, m, Ar-H), 3.76 (1H, ddd, *J* = 10.0, 7.0, 3.5, α-H), 3.64 (1H, dd, *J* = 10.0, 3.5, -CH_2-), 3.46 (1H, dd, *J* = 10.0, 7.0, -CH_2-), 3.37 (3H, s, CO_2Me), 3.00 (1H, d, *J* = 10.0, NH).

^{13}C NMR (101 MHz, $CDCl_3$) δ 172.7, 145.6, 128.7, 128.1, 126.7, 71.2, 56.9, 52.1, 35.4.

ESI-MS (LCMS): found *m/z* $[M\text{-}Trt]^-$ 179.1, 181.0

IR V_{max} / cm^{-1} (ATR): 1698 (C=O), 1489 (C=C), 1205 (C-O-C), 695 (C-Br).

6.3.21 *N,N'*-Dibenzyl serine methyl ester (287)

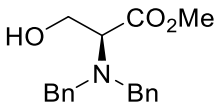

287

Serine methyl ester hydrochloride (**285**) (999 mg, 6.5 mmol, 1 equiv.) was dissolved in MeCN (20 mL) and K_2CO_3 (4.467 g, 32.3 mmol, 5 equiv.) was added. The solution was cooled to 0 °C and benzyl bromide (1.92 mL, 16.1 mmol, 2.5 equiv.) was added dropwise. The reaction was stirred overnight, then filtered. The resulting solution was concentrated *in vacuo* and the desired product (**287**) was obtained as a colourless oil after purification using silica gel chromatography (EtOAc/hexane 0→100%) (1.542 g, 5.2 mmol, 80%).

^{1}H NMR (400 MHz, $CDCl_3$) δ 7.36 – 7.21 (10H, m, ArH), 3.92 (2H, d, *J* = 13.5, -NCH_2), 3.80 (3H, s, CO_2Me), 3.76 (2H, br d, *J* = 8.0, β-CH_2), 3.68 (2H, d, *J* = 13.5, -NCH_2), 3.57 (1H, dd, *J* = 8.0, 6.5, α-H).

^{13}C NMR (101 MHz, $CDCl_3$) δ 171.9, 138.8, 129.1, 128.6, 127.5, 61.9, 59.6, 54.9, 51.5.

ESI-MS (LCMS): found *m/z* $[M+H]^+$ 300.3, 301.3

Spectroscopic data match those previously published.[41]

6.3.22 *N,N'*-Dibenzyl-β-bromoalanine methyl ester (283)

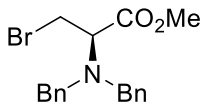

283

The title compound (**283**) was obtained as a colourless oil following reaction of *N*(Bn)$_2$-Ser-OMe (**287**) (400 mg, 1.34 mmol) with PPh_3 (456 mg, 1.74 mmol) and NBS (315 mg, 1.74 mmol) according to **General procedure A for bromination of amino acid alcohols (6.3.1)**. (165 mg, 0.5 mmol, 34%).

^{1}H NMR (400 MHz, $CDCl_3$) δ 7.31 (4H, m, ArH), 7.23 (4H, m, ArH), 7.15 (2H, m, ArH), 3.79 (2H, d, *J* = 14.0, Ar-C**H$_2$**), 3.71 (3H, s, CO_2Me), 3.62-3.55 (2H, m, -CH_2-Br), 3.46 (2H, d, *J* = 14.0, Ar-CH_2), 3.38 (1H, dd, *J* = 9.0, 5.5, -CH_2C**H**-).

^{13}C NMR (101 MHz, $CDCl_3$) δ 170.5, 138.7, 129.0, 128.4, 127.4, 62.8, 55.0, 51.7, 29.9.

ESI-MS (LCMS): found *m/z* $[M+H]^+$ 362.2, 364.0

Spectroscopic data match those previously published.[42]

6.3.23 Bn-Ser-OMe (286)

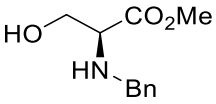

286

Serine methyl ester hydrochloride (**285**) (0.993 g, 6.4 mmol, 1.2 equiv.) was dissolved in anhydrous MeOH (15 mL), cooled to 0 °C and placed under an inert atmosphere. Et_3N (2.22 mL, 16 mmol, 3 equiv.) and benzaldehyde (0.54 mL, 5.3 mmol, 1 equiv.) were added dropwise. The mixture was allowed to warm to rt and stirred for 6 h. $NaBH_4$ (222 mg, 5.8 mmol, 1.1 equiv.) was then added in portions before the reaction mixture was left to stir overnight. H_2O (20 mL) was added to quench the reaction before the mixture was filtered through a pad of celite. The solution was diluted with EtOAc (20 mL) then washed with brine. The organic fraction was dried using $MgSO_4$, filtered, then concentrated. The crude product was then purified using silica gel chromatography (EtOAc/hexane 0→100%), furnishing the desired compound (**286**) as a colourless oil (441 mg, 2.1 mmol, 33%).

^{1}H NMR (400 MHz, $CDCl_3$) δ 7.39 – 7.22 (5H, m, ArH), 3.88 (1H, d, *J* = 13.0, $ArCH_2$-), 3.78 (1H, dd, *J* = 11.0, 4.5, α-H), 3.74 (1H, d, *J* = 13.0, $ArCH_2$-), 3.74 (3H, s, CO_2Me), 3.62 (1H, dd, *J* = 11.0, 6.5, β-CH_2), 3.44 (1H, dd, *J* = 6.5, 4.5, β-CH_2).

^{13}C NMR (101 MHz, $CDCl_3$) 173.5, 139.2, 128.54, 128.4, 127.4, 62.6, 61.9, 52.2, 52.1.

ESI-MS (LCMS): found *m/z* $[M+H]^+$ 210.2

Spectroscopic data match those previously published.[43]

6.3.24 3-Benzyl-2-oxo-oxazolidine-4-carboxylic acid methyl ester (291)

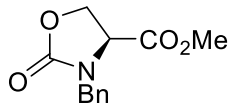

291

Bn-Ser-OMe (**286**) (0.567 g, 2.7 mmol, 1 equiv.) and CDI (0.437 g, 2.7 mmol, 1 equiv.) were dissolved in anhydrous MeCN. Allyl bromide (1.17 mL, 13.6 mmol, 5 equiv.) was added, and the mixture was stirred at rt for 0.5 h. The reaction mixture was then refluxed for a further 1.5 h. Once cooled, diethyl ether (20 mL) and H_2O (20 mL) were added. The organic fraction was then washed with aq. HCl (1 M, 20 mL), sat. Na_2CO_3 (20 mL), and H_2O (20 mL) successively, before it was dried using $MgSO_4$ and filtered. The solution was concentrated *in vacuo* and purified using silica gel chromatography (EtOAc/hexane 0→100%), affording the title compound (**291**) as a colourless crystalline solid (330 mg, 1.4 mmol, 52%).

^{1}H NMR (400 MHz, $CDCl_3$) δ 7.36 – 7.19 (5H, m, Ar-H), 4.80 (1H, d, *J* = 15.0, Bn-CH_2-), 4.38 – 4.26 (2H, m, α-H + β-CH_2), 4.21 (1H, d, *J* = 15.0, Bn-CH_2-), 4.09 (1H, dd, *J* = 9.5, 5.0, β-CH_2), 3.68 (3H, s, CO_2Me).

^{13}C NMR (101 MHz, $CDCl_3$) δ 169.9, 157.7, 135.1, 128.9, 128.4, 128.2, 64.4, 55.9, 52.8, 47.2.

ESI-MS (LCMS): found *m/z* $[M+H]^+$ 236.2

IR V_{max} / cm^{-1} (ATR): 1735.5 (C=O), 1409.2 (C-H), 1244.0 (C-O-C).

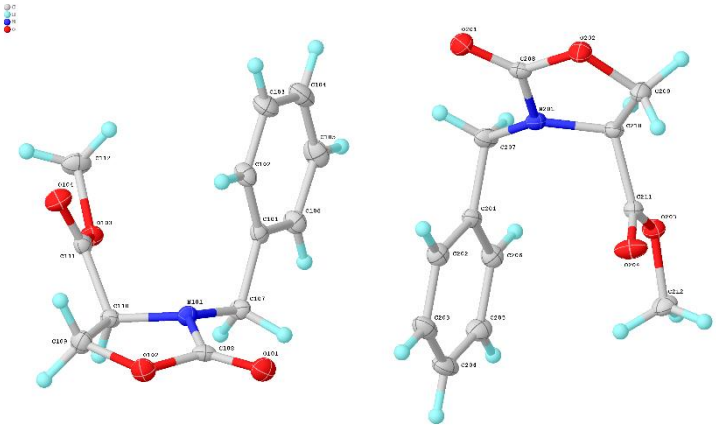

Figure 6.8: X-Ray molecular structure for **291**. Molecular structure reported with a 50% thermal ellipsoid probability.

6.3.25 β-Bromoalanine methyl ester (294)

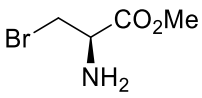

294

Boc-Ala(Br)-OMe (**27**) (302 mg, 1.1 mmol, 1 equiv.) was deprotected according to the **General Procedure for Boc deprotection (Section 6.3.5)**, furnishing the desired product (**294**) as a yellow solid in a quantitative yield.

^{1}H NMR (400 MHz, MeOD) δ 4.79 (1H, dd, *J* = 4.5, 3.5, α-H), 4.07 – 3.93 (2H, m, CH_2), 3.90 (3H, s, CO_2Me), 3.84 – 3.78 (2H, m, NH_2).

^{13}C NMR (101 MHz, MeOD) δ 166.8, 53.4, 53.0, 28.8.

ESI-MS (LCMS): found *m/z* $[M+H]^+$ 181.8, 183.8

Spectroscopic data match those previously published.[44]

6.3.26 *N*-Boc-*N'*-Bn-Ala(Br)-OMe (296)

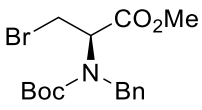

296

To a solution of Bn-Ser-OMe (**286**) (0.722 g, 3.5 mmol, 1 equiv.) in THF (20 mL) under an argon atmosphere was added Et_3N (0.48 mL, 3.5 mmol, 1 equiv.). Boc_2O (0.830 g, 3.8 mmol, 1.1 equiv.) was then added, and the reaction mixture was stirred for 16 h. HCl (1 M, 10 mL) was used to quench the reaction, before extraction with Et_2O (3 × 20 mL). The combined organic fractions were washed with brine, then dried ($MgSO_4$), filtered, and concentrated under reduced pressure to yield *N*-Boc-*N'*-Bn-Ser-OMe (**295**) (0.447 g). *N*-Boc-*N'*-Bn-Ser-OMe (**295**) was then reacted without purification with PPh_3 (0.491 g, 1.9 mmol, 1.3 equiv.) and NBS (0.332 g, 1.9 mmol, 1.3 equiv.) according to the **General procedure for bromination of amino acid alcohols A**, affording the title compound (**296**) as a colourless oil (381 mg, 1.0 mmol, 30% across two steps).

^{1}H NMR (400 MHz, $CDCl_3$) δ 7.42 – 7.23 (5H, m, ArH), 4.89 – 4.63 (1H, m, $BnCH_2$), 4.51 – 4.40 (1H, m, $BnCH_2$ (1H) and β-CH_2 (0.6H)), 4.19 – 4.09 (0.6H, m, β-CH_2), 3.91 (2H, dd, *J* = 10.5, 5.5, α-H), 3.83 (0.4H, m, β-CH_2), 3.64 (3.4H, s, CO_2Me (3H) and β-CH_2 (0.4H)), 1.51 – 1.43 (9H, m, Boc).

ESI-MS (LCMS): found *m/z* $[M+H\text{-Boc}]^+$ 271.9, 273.9

ESI-MS (HRMS): found *m/z* $[M+H\text{-Boc}]^+$ 272.0299, 274.0283

6.3.27 Bn-Ala(Br)-OMe (289)

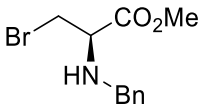

289

N-Boc-*N'*-Bn-Ala(Br)-OMe (**296**) (0.381 g, 1.0 mmol, 1 equiv.) was dissolved in DCM and an excess of TFA (0.25 mL) was added dropwise, furnishing the title compound (**289**) as a white crystalline solid in a quantitative yield.

^{1}H NMR (400 MHz, CD_3CN) δ 7.55 (2H, m, ArH), 7.49 – 7.46 (1H, m, ArH), 7.43 – 7.39 (3H, m, ArH), 4.43 (1H, td, *J* = 4.0, 1.5, NH), 4.29 (2H, s, Bn-CH_2), 4.12 (2H, ddd, *J* = 12.0, 4.0, 1.5, -CH_2-), 3.91 (1H, ddd, *J* = 12.0, 3.5, 1.5, α-H), 3.80 (3H, d, *J* = 1.5, CO_2Me).

ESI-MS (LCMS): found *m/z* $[M+H]^+$ 272.1, 274.1

ESI-MS (HRMS): found *m/z* $[M+H]^+$ 272.0292, 274.0296

6.3.28 *N*-(4-Trifluoromethylbenzyl)aniline (297)

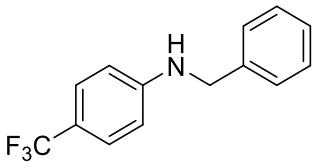

297

The title compound (**297**) was obtained as the major product of the reaction between *N*-Bn-Ala(Br)-OMe (**289**) (67 mg, 0.25 mmol, 1 equiv.) and 4-bromobenzotrifluoride (**247**) (0.07 mL, 0.5 mmol, 2 equiv.) according to the **General procedure B for Ni-catalysed coupling (Section 6.3.4)**. The product was obtained as a colourless oil (34 mg, 0.14 mmol, 54%)

^{1}H NMR (700 MHz, $CDCl_3$) δ 7.58 – 7.26 (7H, m, Ar-H), 6.65 (2H, d, *J* = 8.0, Ar-H), 4.58 – 4.17 (3H, m, NH and Bn-CH_2).

^{13}C NMR (176 MHz, $CDCl_3$) δ 150.5, 138.5, 128.8, 127.5, 127.4, 126.9, 124.2, 119.1 (q, *J* = 33.5). 112.0, 47.8.

^{19}F NMR (376 MHz, $CDCl_3$) δ -61.0.

ESI-MS (LCMS): found *m/z* $[M+H]^+$ 252.2

Spectroscopic data match those previously published.[45]

6.3.29 Boc-Ser(OTs)-OMe (300)

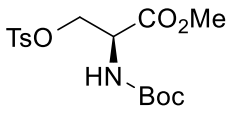

300

Boc-Ser-OMe (**26**) (0.689 g, 3.1 mmol, 1 equiv.) was dissolved in anhydrous pyridine (10 mL) under an inert atmosphere and cooled to 0 °C. *p*-Toluenesulfonyl chloride (2.901 g, 15.7 mmol, 5 equiv.) was added, and the mixture was stirred at 0 °C for 6 h. Et_2O (10 mL) was added to the solution and the resulting white slurry was stirred for a further 14 h. The solution was washed with H_2O, 10% aq. $KHSO_4$, sat. aq. $NaHCO_3$, and brine. The organic fraction was dried with $MgSO_4$, filtered, concentrated *in vacuo*, then purified by silica gel chromatography (EtOAc/hexane 0→100%). The title compound (**300**) was afforded as a colourless oil (0.591 g, 1.6 mmol, 50%).

^{1}H NMR (400 MHz, $CDCl_3$) δ 7.78 (2H, d, *J* = 8.5, Ar-H), 7.37 (1H, d, *J* = 8.0, Ar-H), 5.32 (1H, d, *J* = 8.0, NH), 4.52 (1H, dt, *J* = 8.5, 3.0, α-H), 4.41 (1H, dd, *J* = 10.0, 3.0, -CH_2), 4.30 (1H, dd, *J* = 10.0, 3.0, -CH_2), 3.71 (3H, s, CO_2Me), 2.47 (3H, s, Ar-CH_3), 1.43 (9H, s, Boc).

^{13}C NMR (101 MHz, $CDCl_3$) δ 169.0, 155.0, 145.2, 132.4, 130.0, 128.0, 80.5, 69.5, 53.0, 52.9, 28.2, 21.7.

ESI-MS (LCMS): found *m/z* $[M\text{-Boc}+H]^+$ 274.1

Spectroscopic data match those previously published.[46]

6.3.30 Ts-Ser-OMe (301)

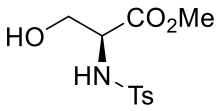

301

Serine methyl ester hydrochloride (**285**) (1.007 g, 6.45 mmol, 1 equiv.) was dissolved in anhydrous DCM (20 mL) under an argon atmosphere and cooled to 0 °C. Et_3N (1.8 mL, 12.9 mmol, 2 equiv.) was added, followed by the dropwise addition of a solution of *p*-toluenesulfonyl chloride (1.225 g, 6.45 mmol, 1 equiv.) in DCM (5 mL). The reaction mixture was stirred at an ambient temperature for 12 h, then filtered. The filtrate was concentrated under reduced pressure, then dissolved in EtOAc. The solution was washed with aq. $NaHCO_3$, aq. citric acid (10%), and H_2O. The organic fraction was dried ($MgSO_4$), filtered, and concentrated *in vacuo*. The crude product was purified by recrystallisation (EtOAc/hexane 1:1), yielding a white crystalline solid (**301**) (1.508 g, 5.5 mmol, 85%).

^{1}H NMR (400 MHz, $CDCl_3$) δ 7.77 (2H, d, *J* = 8.5, ArH), 7.33 (2H, d, *J* = 8.0, ArH), 5.67 (1H, d, *J* = 7.5, NH), 4.01 (1H, dt, *J* = 7.5, 4.0, α-H), 3.91 (2H, d, *J* = 4.0, β-CH_2), 3.64 (3H, s, CO_2Me), 2.45 (3H, s, Ar-Me), 2.39 (1H, br s, OH).

^{13}C NMR (176 MHz, $CDCl_3$) δ 170.1, 144.0, 136.4, 129.8, 127.2, 63.7, 57.6, 53.0, 21.6.

ESI-MS (LCMS): found *m/z* $[M+H]^+$ 274.1

Spectroscopic data match those previously published.[47]

6.3.31 Ts-Ala(Br)-OMe (302)

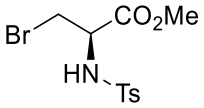

302

The title compound (**302**) was obtained from the reaction of Ts-Ser-OMe (**301**) (285 mg, 1.0 mmol, 1 equiv.) with NBS (248 mg, 1.4 mmol, 1.3 equiv.) and PPh_3 (363 mg, 1.4 mmol, 1.3 equiv.) using the **General procedure for bromination of amino acid alcohols A (Section 6.3.1)**, as a colourless oil (143 mg, 0.4 mmol, 41%).

^{1}H NMR (599 MHz, $CDCl_3$) δ 7.74 (2H, d, *J* = 8.5, Ar-H), 7.30 (1H, d, *J* = 8.0, Ar-H), 5.58 (1H, d, *J* = 8.0, NH), 4.38 (1H, dt, *J* = 8.1, 3.5, CH), 3.71 (1H, dd, *J* = 10.5, 3.5, CH_2), 3.65 (3H, s, CO_2Me), 3.57 (1H, dd, *J* = 10.5, 4.0, CH_2), 2.42 (3H, s, Ar-Me).

^{13}C NMR (151 MHz, $CDCl_3$) δ 168.7, 144.0, 136.8, 129.8, 127.1, 55.8, 53.2, 33.9, 21.6.

ESI-MS (LCMS): found *m/z* $[M+H]^+$ 336.1, 338.1

Spectroscopic data match those previously published.[48]

6.3.32 Methyl 3-((4-methylphenyl)sulfonamido)propanoate (303)

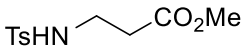

303

The title compound (**303**) was isolated as the major product after Ts-Ala(Br)-OMe (**302**) (53 mg, 0.15 mmol, 1 equiv.) was used as the substrate with the **General procedure for Ni-catalysed coupling A (Section 6.3.3)**. The product was obtained as a colourless oil (15 mg, 0.06 mmol, 38%).

^{1}H NMR (400 MHz, $CDCl_3$) δ 7.74 (2H, d, *J* = 8.5, Ar-H), 7.31 (2H, d, *J* = 8.0, Ar-H), 5.14 (1H, br t, *J* = 6.5, NH), 3.66 (3H, s, CO_2Me), 3.22 – 3.15 (2H, q, *J* = 4.0, -NHC**H$_2$**-), 2.56 – 2.51 (2H, t, *J* = 8.0, -C**H$_2$**CO_2Me), 2.43 (3H, s, Ar-CH_3).

^{13}C NMR (101 MHz, $CDCl_3$) δ 172.5, 143.5, 137.0, 129.8, 127.0, 52.0, 38.7, 33.8, 21.5.

ESI-MS (LCMS): found *m/z* $[M+H]^+$ 258.1

Spectroscopic data match those previously published.[49]

6.3.33 Boc-Cys(4-trifluoromethylphenyl)-OMe (280)

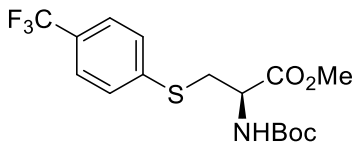

280

The title compound (**280**) was obtained after reaction of Boc-Cys-OMe (**276**) (35 mg, 0.15 mmol, 1 equiv.) with 4-bromobenzotrifluoride (**247**) (0.03 mL, 0.22 mmol, 1.5 equiv.) according to the **General Procedure for Ni-catalysed coupling A (Section 6.3.3).** The product was obtained as a yellow oil (20 mg, 0.05 mmol, 35%)

^{1}H NMR (400 MHz, $CDCl_3$) δ 7.52 (2H d, *J* = 8.0, Ar-H), 7.46 (2H, d, *J* = 8.0, Ar-H), 5.31 (1H d, *J* = 8.0, NH), 4.75 – 4.47 (1H, m, α-H), 3.62 (3H, s, CO_2Me), 3.55 – 3.31 (2H, m, β-CH_2), 1.40 (9H, s, Boc).

^{13}C NMR (101 MHz, $CDCl_3$) δ 170.7, 154.9, 140.5, 129.4, 128.5 (m), 125.8 (m), 125.4, 80.3, 53.4, 52.6, 36.0, 28.2.

^{19}F NMR (376 MHz, $CDCl_3$) δ -62.6.

ESI-MS (LCMS): found *m/z* $[M+H\text{-}Boc]^+$ 280.2

Spectroscopic data match those previously published.[50]

6.3.34 Dimethyl 3,3'-disulfanediyl (2*R*,2'*R*)-bis(2-((tert-butoxycarbonyl)amino)-propanoate) (309)

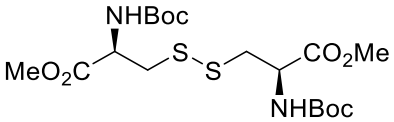

309

Boc-Cys-OMe (**276**) (1.017 g, 4.26 mmol, 1 equiv.) was dissolved in EtOAc and cooled to 0 °C. NaI (67 mg, 0.426 mmol, 0.1 equiv.) and H_2O_2 (30% in H_2O, 0.48 mL, 4.26 mmol, 1 equiv.) were added. The mixture was stirred at room temperature for 30 mins, after which sat. aq.

$Na_2S_2O_3$ (10 mL) was added, and the product was extracted with with EtOAc (3 × 20 mL). The combined organic fractions were washed with brine, dried ($MgSO_4$), filtered, and concentrated under reduced pressure to furnish the desired product **309** as a white solid in a quantitative yield.

^{1}H NMR (400 MHz, $CDCl_3$) δ 5.40 (2H, br s, NH), 4.61 (2H, br s, α-H), 3.78 (6H, s, CO_2Me), 3.18 (4H, d, *J* = 5.0, -CH_2S-), 1.47 (18H, s, Boc)

^{13}C NMR (101 MHz, $CDCl_3$) δ 171.2, 155.0, 80.3, 52.8, 52.7, 41.3, 28.3.

ESI-MS (LCMS): found *m/z* $[M- 2(Boc) + H]^+$ 269.2

Spectroscopic data match those previously published.[51]

6.3.35 $[Ni(bpy)_3]Br_2$ [52]

Bipyridine (2.504 g, 16 mmol, 3 equiv.) was dissolved in MeOH (4 mL), and a solution of $NiBr_2.3H_2O$ (1.448 g, 5.33 mmol, 1 equiv.) in MeOH (4 mL) was added, resulting in an immediate colour change (green → pink). Once the reaction cooled to room temperature, the reaction mixture was concentrated under reduced pressure, and acetone (~5 mL) and MeOH (~1 mL) were added. The resulting pink crystalline solid precipitate was isolated by Buchner filtration and required no further purification.

6.3.36 Methyl-*N*-(diphenylmethylene)-*L*-valinate (322)

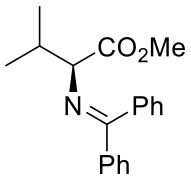

322

A flask was charged with benzophenone (**320**) (1.004 g, 5.5 mmol, 1equiv.) under N_2 and HMDS (2.3 mL, 11 mmol, 2 equiv.) was added, followed by TBAF (0.55 mL, 1M in THF, 0.55 mmol, 0.1 equiv). The mixture was stirred at room temperature for 6h. The crude reaction mixture was concentrated under high vacuum then purified using column chromatography (10% Et_3N in hexane) to produce benzophenone imine (**321**) (0.893 g, 4.9 mmol, 89%), which was used immediately. *L*-Valine methyl ester hydrochloride (**95**) (0.515 g, 3.9 mmol, 1 equiv.) and benzophenone imine (0.893 g, 4.9 mmol, 1.3 equiv.) were dissolved in DCM (20 mL) and

placed under an inert atmosphere. The reaction was stirred for 16 h then poured onto sat. aq. $NaHCO_3$ and extracted with further DCM (10 mL). The organic fraction was washed with brine before being dried with $MgSO_4$. The mixture was filtered, and the solvent was removed *in vacuo*. The crude product was purified by column chromatography (0-5% EtOAc in hexane) to give the desired imine (**322**) (0.823 g, 2.8 mmol, 71%)

^{1}H NMR (400 MHz, CDCl3) δ 7.68 (2H, m, Ar-H), 7.46 (2H, m, Ar-H), 7.41 (1H, m, Ar-H), 7.36 (2H, m, Ar-H), 7.17 (2H, m, Ar-H), 3.88 (1H, d, *J* = 6.0, α-H), 3.74 (3H, s, CO_2Me), 2.39 (1H, m, β-H), 1.01 (3H, d, *J* = 7.0, -$(CH_3)_2$), 0.90 (3H, d, *J* = 7.0, -$(CH_3)_2$)

ESI-MS (LCMS): found *m/z* $[M+H]^+$ 296.4

Spectroscopic data match those previously published.[53]

6.3.37 2-trifluoromethyl-4-isopropyl-oxazolin-5-one (324)

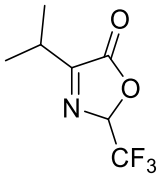

324

Trifluoroacetic anhydride (1 mL, 6.7 mmol, 2.6 equiv.) was cooled to 0 °C. *L*-valine (**97**) (0.303 g, 2.6 mmol, 1 equiv.) was added portionwise. The solution was stirred for 5 mins before it was heated at reflux for 2 h. The solvent was removed to afford the desired product (**324**) as a yellow oil (298 mg, 1.5 mmol, 59%).

^{1}H NMR (400 MHz, $CDCl_3$) δ 6.11 (1H, qd, *J* = 4.0, 2.0, C**H**-CF_3), 3.09 (1H, quintet of doublets, *J* = 7.0, 2.0, C**H**-$(CH_3)_2$), 1.36 (6H, dd, *J* = 7.0, 3.0, -CH_3)

^{19}F NMR (376 MHz, $CDCl_3$) δ -75.7 (s)

ESI-MS (LCMS): found *m/z* $[M-H]^-$ 194.2

Spectroscopic data match those previously published.[54]

6.3.38 *(S)-N*-Trifluoromethanesulfonylvaline methyl ester (325)

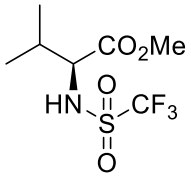

325

L-Valine methyl ester hydrochloride (**95**) (0.301 g, 1.8 mmol, 1 equiv.) was dissolved in dry DCM (25 mL) and placed under an argon atmosphere. Triethylamine (0.50 mL, 3.6 mmol, 2 equiv.) was added dropwise with stirring. The reaction mixture was cooled to -78 °C and trifluoromethanesulfonic anhydride (0.30 mL dissolved in 3 mL dry DCM, 1.8 mmol, 1 equiv.) was added dropwise. The reaction mixture was allowed to warm to room temperature and left to stir overnight. The solvent was removed *in vacuo* to yield the desired product (**325**) as a yellow oil (383 mg, 1.5 mmol, 81%)

^{1}H NMR (400 MHz, $CDCl_3$) δ 5.69 (1H, br s, N-H), 4.09 (1H, br s, α-H), 3.83 (3H, s, CO_2Me), 2.23 (1H, m, β-H), 1.06 (3H, d, *J* = 7.0, -CH_3), 0.95 (3H, d, *J* = 7.0, -CH_3)

^{13}C NMR (101 MHz, $CDCl_3$) δ 171.0, 119.9 (m), 62.4, 52.9, 31.6, 18.8, 17.1.

^{19}F NMR (376 MHz, $CDCl_3$) δ -77.1 (s)

ESI-MS (LCMS): found *m/z* $[M-H]^-$ 262.4

Spectroscopic data match those previously published.[55]

6.3.39 *N*-Phthaloylleucine-*N'*-quinolin-8-yl amide (326)

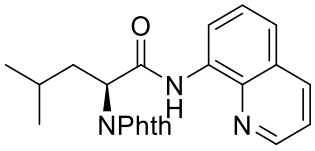

326

N-Phth-Leu-OH (**328**) (1.310 g, 5.0 mmol, 1 equiv.) was dissolved in toluene. Thionyl chloride (1.08 mL, 15.1 mmol, 3 equiv.) was added dropwise and the reaction was heated at reflux for 3h. The solvent was then removed *in vacuo* to give the corresponding acid chloride (**329**) as a yellow oil. This was dissolved in a minimum amount of dry DCM and used immediately. 8-aminoquinoline (**330**) (0.716 g, 5.0 mmol, 1 equiv.) was dissolved in dry DCM and placed under argon. Triethylamine (0.83 mL, 6.0 mmol, 1.2 equiv.) was added dropwise and the reaction mixture was cooled to 0 °C. The fresh *N*-Phth-Leu-OCl (**329**) (3.8 mmol in DCM) was

then added dropwise. The solution was left to stir at room temperature overnight, after which H_2O (30 mL) was added and the mixture was extracted with DCM (2 × 20 mL). The organic fractions were combined, then washed with sat. aq. $NaHCO_3$ and brine before being dried and filtered. The solvent was removed *in vacuo* and the crude product mixture was purified using column chromatography (20-30% EtOAc in hexane) to give the desired product (**326**) as a yellow solid (1.399 g, 72%, 3.6 mmol).

^{1}H NMR (400 MHz, $CDCl_3$) δ 8.73 (2H, m, Ar-H), 8.16 (1H, dd, *J* = 8.5, 1.5, Ar-H), 7.94 (2H, m, Phth-H), 7.78 (2H, m, Phth-H), 7.54 (1H, d, *J* = 1.5, Ar-H), 7.52 (1H, s, Ar-H), 7.45 (1H, dd, *J* = 8.5, 4.0, Ar-H), 5.25 (1H, dd, *J* = 11.5, 5.0, α-H), 2.68 (1H, m, β-CH_2), 2.14 (1H, m, β-CH_2), 1.65 (1H, m, γ-H), 1.07 (6H, dd, *J* = 10.5, 6.5, (-CH_3)$_2$)

^{13}C NMR (101 MHz, $CDCl_3$) δ 168.2, 167.4, 148.4, 147.5, 136.3, 136.0, 134.2, 133.9, 131.9, 127.9, 127.4, 127.3, 123.6, 121.9, 121.6, 121.4, 116.7, 53.6, 37.4, 31.0, 25.6, 23.3, 21.3.

ESI-MS (LCMS): found *m/z* $[M+H]^+$ 388.9

Spectroscopic data match those previously published.[56]

6.3.40 2-Methoxyiminoacetic acid (336)

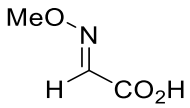

336

Glyoxylic acid monohydrate (**335**) (1.460 g, 16.3 mmol, 1 equiv.) was dissolved in a 1:1 pyridine:MeOH mixture (10 mL) and the reaction was placed under argon. Methoxyamine hydrochloride (1.441 g, 17.4 mmol, 1.1 equiv.) was added and the reaction was stirred at room temperature for 1 h. After completion, the reaction was quenched with sat. aq. NH_4Cl solution (20 mL) and extracted thrice with EtOAc (3 × 20 mL). The combined organics were dried and filtered before the solvent was removed, followed by purification by column chromatography (silica gel, 10% MeOH in EtOAc) to yield the title compound (**336**) as a colourless oil. (861 mg, 6.8 mmol, 42%)

^{1}H NMR (400 MHz, $CDCl_3$) δ 14.67 (1H, br s, CO_2H), 7.45 (1H, s, N=CH), 3.93 (3H, s, OMe)

^{13}C NMR (101 MHz, $CDCl_3$) δ 165.5, 141.3, 63.1

ESI-MS (LCMS): found *m/z* $[M+H]^+$ 104.1

Spectroscopic data match those previously published.[57]

6.3.41 MIA-Val-OMe (337)

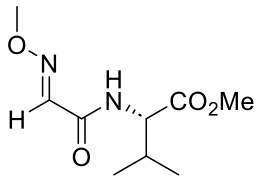

337

The **General Procedure for synthesis of MIA-amino acids (Section 6.3.6)** was followed, using 2-methoxyiminoacetic acid (**336**) (0.505 g, 4.9 mmol, 1 equiv.), *N*-methyl morpholine (1.5 mL, 12.1 mmol, 2.5 equiv.), Isobutyl chloroformate (0.63 mL, 4.9 mmol, 1 equiv.) and *L*-valine methyl ester hydrochloride (**95**) (0.974 g, 5 mmol, 1 equiv.). The title compound (**337**) was afforded as a yellow oil (613 mg, 2.8 mmol, 58%).

^{1}H NMR (400 MHz, $CDCl_3$) δ 7.42 (1H, s, N=C-H), 6.98 (1H, br d, *J* = 8.0, N-H), 4.63 (1H, dd, *J* = 9.0, 5.0, α-H), 4.03 (3H, s, N-O-CH_3), 3.78 (3H, s, CO_2Me), 2.24 (1H, m, β-H), 0.98 (6H, dd, *J* = 10.0, 7.0, $(-CH_3)_2$)

^{13}C NMR (101 MHz, $CDCl_3$) δ 172.1, 161.5, 142.5, 63.2, 56.8, 52.3, 31.5, 19.0, 17.9.

ESI-MS (LCMS): found *m/z* $[M+H]^+$ 217.5

Spectroscopic data match those previously published.[57]

6.3.42 MIA-Val(OAc)-OMe (338)

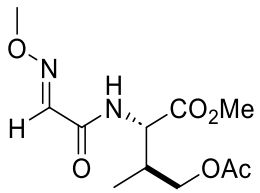

338

N-MIA-Val-OMe (**337**) (67 mg, 0.3 mmol, 1 equiv.) and $Pd(OAc)_2$ (13 mg, 0.06 mmol, 0.2 equiv.) were dissolved in a 0.6 M solution of NaOAc in acetic acid (4 mL) and placed in the anodic chamber of a divided cell. A further 4 mL of the electrolyte solution was placed in the cathodic chamber. The cell was furnished with graphite electrodes and heated to 80 °C. A 1.5 h current was applied for 12 h (2.21 F/mol). Once cool, ethyl acetate (20 mL) was added to the reaction mixture and the solution was washed with H_2O (25 mL) then brine (25 mL). The organic fraction was dried and filtered before the solvent was removed *in vacuo*. The crude

product mixture was purified by column chromatography (20-40% EtOAc in hexane) and the desired product (**338**) was isolated as a colourless oil (19 mg, 0.07 mmol, 23%).

^{1}H NMR (400 MHz, $CDCl_3$) δ 7.43 (1H, s, N=C-H), 7.18 (1H, d, *J* = 9.0, N-H), 4.81 (1H, dd, *J* = 9.0, 5.0, α-H), 4.14 – 3.94 (5H, m, -N-OMe and γ-CH_2), 3.79 (3H, s, CO_2Me), 2.55 (1H, m, β-H), 2.11 (3H, s, OAc), 1.04 (d, 3H, *J* = 7.0, -CH_3).

^{13}C NMR (101 MHz, $CDCl_3$) δ 171.5, 170.7, 161.7, 142.4, 65.4, 63.2, 53.9, 52.5, 35.4, 29.7, 20.8, 13.9.

ESI-MS (LCMS): found *m/z* $[M+H]^+$ 275.3

ESI-MS (HRMS): found *m/z* $[M+H]^+$ 275.1276

6.3.43 MIA-*tert*-leucine methyl ester (339)

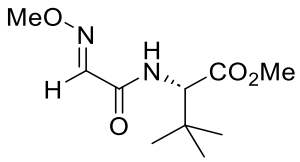

339

The **General Procedure for synthesis of MIA-amino acids (Section 6.3.6)** was followed, using 2-methoxyiminoacetic acid (**336**) (0.677 g, 6.6 mmol, 1 equiv), *N*-ethylmorpholine (2.07 mL, 16.4 mmol, 2.5 equiv.), isobutyl chloroformate (0.85 mL, 6.6 mmol, 1 equiv.), and *tert*-leucine methyl ester hydrochloride (1.429 g, 7.9 mmol, 1.2 equiv.). The crude product was purified using silica gel chromatography (5% EtOAc in hexane), yielding a pale yellow oil (**339**) (120 mg, 0.5 mmol, 8%).

^{1}H NMR (400 MHz, $CDCl_3$) δ 6.97 (1H, br d, *J* = 9.5, NH), 4.45 (1H, d, *J* = 9.5, α-H), 3.94 (3H, s, CO_2Me), 3.67 (3H, s, N-OMe), 0.93 (9H, s, -$(CH_3)_3$)

^{13}C NMR (101 MHz, $CDCl_3$) δ 171.6, 161.3, 142.4, 63.1, 59.6, 51.9, 35.0, 26.5

ESI-MS (LCMS): found *m/z* $[M+H]^+$ 231.4

ESI-MS (HRMS): found *m/z* $[M+H]^+$ 231.1353

IR V_{max} / cm^{-1}(ATR): 2966 (NH), 1737 (C=O), 1522 (C=O), 1217 (C-O-C).

6.3.44 MIA-Thr-(O-tBu)-OMe (342)

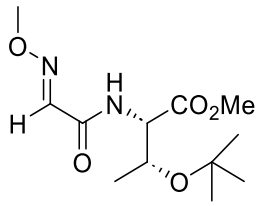

342

The title compound (**342**) was obtained from the reaction of (*O*-tBu)-threonine methyl ester hydrochloride (1.311 g, 5.8 mmol, 1.2 equiv.) with 2-methoxyiminoacetic acid (**336**) (0.546 g, 4.9 mmol, 1 equiv.), *N*-ethylmorpholine (1.53 mL, 12.1 mmol, 2.5 equiv.), and isobutyl chloroformate (0.63 mL, 4.9 mmol, 1 equiv.) following the **General Procedure for synthesis of MIA-amino acids (Section 6.3.6)**. (755 mg, 2.5 mmol, 52%)

^{1}H NMR (400 MHz, $CDCl_3$) δ 7.44 (1H, s, C**H**=NOMe), 7.20 (1H, br d, *J* = 9.5, N**H**), 4.57 (1H, dd, *J* = 9.5, 2.0, -NHC**H**), 4.27 (1H, qd, *J* = 6.5, 2.0, - C**H**(OtBu)CH_3), 4.03 (3H, s, CO_2Me), 3.74 (3H, s, -NOMe), 1.21 (3H, d, *J* = 6.5, -CH(OtBu)C**H$_3$**), 1.16 (9H, s, -O^{t}Bu).

^{13}C NMR (101 MHz, $CDCl_3$) 171.0, 162.1, 142.4, 74.2, 67.5, 63.2, 57.6, 52.3, 28.3, 21.0.

ESI-MS (LCMS): found *m/z* $[M+H]^+$ 275.3

Spectroscopic data match those previously published.[57]

6.4 Experimental for compounds from Chapter 4

6.4.1 General procedure for electrochemical coupling of tyrosine derivatives

The substrate (2 equiv.) was dissolved in hexafluoroisopropanol (HFIP) (5 mL) and DIPEA was added (1.7 equiv.). The solution was added to an ElectraSyn vial equipped with graphite electrodes and a stirrer bar under air. A 5 mA current was applied with a total charge of 1.15 F/mol. The solvent was removed under reduced pressure and the crude material was redissolved in DCM (25 mL) and washed with 1 M HCl (20 mL) and water (20 mL). The organic fraction was dried ($MgSO_4$), filtered, and the solvent was removed *in vacuo.* The crude products were then purified using silica gel chromatography.

6.4.2 General procedure for oxidation of indole substrates

Indole (1 equiv.) and Bu_4NPF_6 (3 equiv.) were dissolved in DMSO (4 mL). Graphite electrodes were placed in the reaction mixture. A 5 mA current was applied to the reaction with a total charge delivered of 3 F/mol. The solution was extracted with DCM and washed with H_2O (3 × 20 mL) and brine (20 mL), before the organic fraction was dried with $MgSO_4$ and filtered. The solvent was removed *in vacuo* and the crude product was purified using column chromatography.

6.4.3 *N*-Phthaloyltyrosine methyl ester (349)

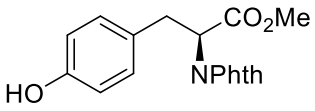

349

L-Tyrosine methyl ester (**46**) (1.00 g, 5.10 mmol, 1 equiv.) and phthalic anhydride (**96**) (0.774 g, 5.20 mmol, 1.02 equiv.) were dissolved in toluene (30 mL) and heated at reflux overnight. The solvent was removed under reduced pressure and the crude mixture was purified using silica gel chromatography (30% EtOAc/hexane) to afford the desired product (**349**) as a glassy colourless solid (1.29 g, 3.98 mmol, 77%).

^{1}H NMR (400 MHz, $CDCl_3$) δ 7.80 (2H, m, Phth-H), 7.71 (2H, m, Phth-H), 7.03 (2H, d, *J* = 8.5, Ar-H), 6.65 (2H, d, *J* = 8.5, Ar-H), 5.23 (1H, s (br), OH), 5.12 (1H, dd, *J* = 11.0, 5.5, α-H), 3.80 (3H, s, CO_2CH_3), 3.51 (2H, m, -CH_2).

^{13}C NMR (101 MHz, $CDCl_3$) δ 169.4, 167.5, 154.3, 134.2, 131.6, 130.1, 128.8, 123.5, 115.5, 53.4, 52.9, 33.8.

ESI-MS (LCMS): found *m/z* $[M+H]^+$ 325.6

Spectroscopic data match those previously published.[58]

6.4.4 *N*-Phthaloyl-*O*-(triisopropylsilyl)-tyrosine methyl ester (350)

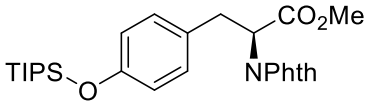

350

L-*N*-Phthaloyl tyrosine methyl ester (**349**) (0.500 g, 1.50 mmol, 1 equiv.) and imidazole (0.209 g, 3.10 mmol, 2 equiv.) were dissolved in dry DCM (30 mL). TIPSCl (0.355 g, 0.4 mL, 1.80

mmol, 1.2 equiv.) was added dropwise. The reaction mixture was allowed to stir overnight. The solution was filtered, and the filtrate was washed with water (20 mL), NaOH (20 mL, 10% w/w), then water again (20 mL). The organic fraction was dried ($MgSO_4$), filtered, and concentrated under reduced pressure. The crude product was purified using silica gel chromatography (30% EtOAc/hexane), furnishing the desired product (**350**) as a colourless oil (0.597 g, 1.16 mmol, 77%)

^{1}H NMR (400 MHz, $CDCl_3$) δ 7.78 (2H, m, Phth-H), 7.70 (2H, m, Phth-H), 7.00 (2H, d, *J* = 8.5, Ar-H), 6.69 (2H, d, *J* = 8.5, Ar-H), 5.13 (1H, dd, *J* = 11.5, 5.5, α-H), 3.80 (3H, s, CO_2CH_3), 3.49 (2H, m, -CH_2), 1.14 (3H, m, -SiC**H**$(CH_3)_2$), 1.00 (18H, dd, *J* = 7.5, 3.5, -SiCH(C**H$_3$**)$_2$)

^{13}C NMR (101 MHz, $CDCl_3$) δ 207.0, 169.4, 167.4, 154.8, 134.0, 131.6, 129.8, 128.9, 123.4, 120.1, 53.0 (d, *J* = 50.5), 33.9, 31.0, 17.8, 12.4.

ESI-MS (LCMS): found *m/z* $[M+H]^+$ 482.9

ESI-MS (HRMS): found *m/z* $[M+H]^+$ 482.2358

IR V_{max} / cm^{-1}(ATR): 1714 (C=O), 1509 (C=O), 1465 (C=C), 1386 (CH_3 bend).

6.4.5 *N,N'*-Diphthaloyldityrosine (352)

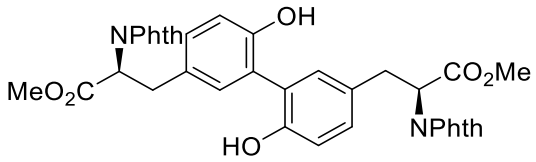

352

L-*N*-Phthaloyl tyrosine methyl ester (**349**) (162 mg, 0.500 mmol, 2 equiv.) and DIPEA were reacted according to the **General procedure for electrochemical coupling of tyrosine derivatives (Section 6.4.1)**. The crude product was purified by silica gel chromatography (30% EtOAc/hexane) to afford the title compound (**352**) as a yellow oil (31.0 mg, 0.0510 mmol, 20%).

^{1}H NMR (400 MHz, $CDCl_3$) δ 7.79 (4H, m, Phth-H), 7.72 (4H, m, Phth-H), 6.97 (2H, d, *J* = 2.5, Ar-H), 6.92 (2H, dd, *J* = 8.0, 2.5, Ar-H), 6.76 (2H, d, *J* = 8.0, Ar-H), 5.10 (2H, dd, *J* = 12.0, 4.5, α-H), 3.80 (6H, s, CO_2CH_3), 3.51 (2H, dd, *J* = 14.0, 5.0, -CH_2), 3.34 (2H, dd, *J* = 13.5, 11.5, -CH_2)

^{13}C NMR (101 MHz, $CDCl_3$) δ 169.1, 167.5, 152.5, 134.3, 131.4, 131.1, 130.5, 128.9, 123.7, 123.2, 116.9, 53.6, 52.9, 34.1.

ESI-MS (LCMS): found *m/z* $[M+H]^+$ 649.8

ESI-MS (HRMS): found *m/z* $[M+H]^+$ 649.1806.

6.4.6 Synthesis of *N*-Phth-Tyr-Ala-OMe (355)

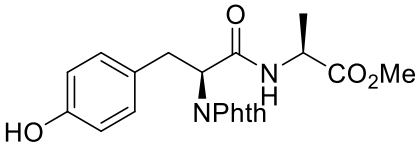

355

N-Phth-Tyr-OH (**353**) (0.510 g, 1.6 mmol, 1 equiv.) was dissolved in dry DCM alongside *L*-alanine methyl ester hydrochloride (**354**) (0.230 g, 1.6 mmol, 1 equiv.). DIPEA (0.31 mL, 1.8 mmol, 1.1 equiv.) was added, followed by PyBOP (0.920 g, 1.8 mmol, 1.1 equiv.). The reaction mixture was stirred overnight at room temperature. The solution was washed with 1 M aq. HCl solution, followed by brine. The organic fraction was dried and filtered before the solvent was removed. The crude mixture was purified using column chromatography (40% EtOAc in hexane) to give the desired dipeptide (**355**) (461, 1.4 mmol, 71%).

^{1}H NMR (400 MHz, $CDCl_3$) δ 7.67 (2H, m, Phth), 7.60 (2H, m, Phth), 6.92 (2H, d, *J* = 8.0, Ar-H), 6.61 (2H, d, *J* = 8.0, Ar-H), 5.10 (1H, m, Tyr-α-H), 4.55 (1H, m, Ala-α-H), 3.57 (3H, s, CO_2Me), 3.42 (2H, m, Tyr-β-CH_2), 1.31 (3H, d, *J* = 7.0, Ala-CH_3)

ESI-MS (LCMS): found *m/z* $[M+H]^+$ 397.7

ESI-MS (HRMS): found *m/z* $[M+H]^+$ 397.1404

IR V_{max} / cm^{-1}(ATR): 2903 (OH), 1701 (C=O), 1514 (C=C aromatic), 1389 (CH_3).

6.3.7 Ala-Tyr dimer 356

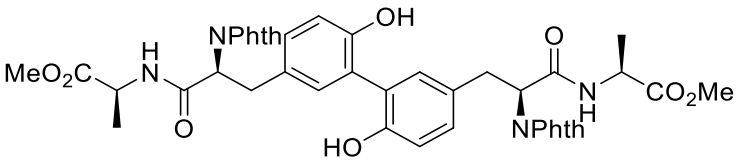

356

N-Phth-Tyr-Ala-OMe (**355**) (181 mg, 0.46 mmol, 2 equiv.) and DIPEA (0.15 mL, 0.87 mmol, 1.9 equiv.) were reacted according to the **General procedure for electrochemical coupling of tyrosine derivatives (Section 6.4.1)**. The resulting product mixture was purified by column

chromatography (30% EtOAc/hexane) and the desired product (**356**) was isolated as a yellow solid (32 mg, 0.08 mmol,18%).

^{1}H NMR (400 MHz, $CDCl_3$) δ 7.80 (4H, m, Phth), 7.73 (4H, m, Phth), 6.96 (2H, m, Ar-H), 6.88 (2H, m, Ar-H), 6.77 (2H, m, Ar-H), 5.12 (2H, m, Tyr-α-H), 4.61 (2H, Ala-α-H), 3.63 (6H, s, CO_2Me), 3.54 – 3.31 (4H, m, Tyr β-CH_2), 1.39 (d, 6H, *J* = 7.0, Ala β-CH_3).

^{13}C NMR (101 MHz, $CDCl_3$) δ 173.4, 168.1, 168.0, 152.5, 134.5, 134.4, 131.4, 131.3, 130.3, 128.9, 123.7, 117.2, 55.8, 52.6, 48.4, 34.0, 18.2.

ESI-MS (LCMS): found *m/z* $[M+H]^+$ 792.0

ESI MS (HRMS): found *m/z* $[M+H]^+$ 791.2586

IR V_{max} / cm^{-1}(ATR): 3270 (OH), 1708 (C=O), 1649 (C=O), 1535 (C=C), 1381 (CH_3 bend)

6.3.8 4-(Triisopropylsiloxy)methoxybenzene (360)

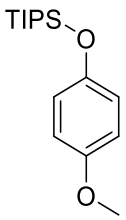

360

4-Methoxyphenol (**359**) (0.494 g, 4.0 mmol, 1 equiv.) was dissolved in dry DCM (30 mL) alongside imidazole (0.557 g, 8.2 mmol, 2 equiv.). TIPSCl (1.03 mL, 4.8 mmol, 1.2 equiv.) was added dropwise and the reaction mixture was stirred at room temperature overnight. The reaction mixture was washed with water (20 mL), NaOH solution (20 mL, 10% w/w), and water again (20 mL). The organic fraction was dried with $MgSO_4$ and filtered before the solvent was removed *in vacuo*. The crude mixture was purified using column chromatography (20% EtOAc in hexane) to yield the desired product (**360**) (0.770 g, 2.7 mmol, 69%).

^{1}H NMR (400 MHz, CDCl3) δ 6.80 (4H, m, Ar-H), 3.78 (3H, s, -OMe), 1.25 (3H, m, SiC**H**$(CH_3)_2$), 1.14-1.09 (18H, m, SiCH(C**H**$_3)_2$)

^{13}C NMR (101 MHz, $CDCl_3$) δ 153.9, 149.8, 120.4, 114.4, 55.6, 18.0, 12.6

ESI-MS (LCMS): found *m/z* $[M+H]^+$ 281.4

Spectroscopic data match those previously published.[59]

6.4.9 *N*-Acetyl proline methyl ester (373)

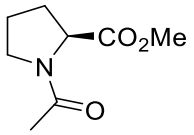

373

L-Proline methyl ester hydrochloride (**203**) (1.004 g, 6.1 mmol, 1 equiv.) and DMAP (0.191 g, 1.5 mmol, 0.25 equiv.) were dissolved in DCM (20 mL), and the flask was placed under an inert atmosphere. Et_3N (3.4 mL, 24.2 mmol, 4 equiv.) and Ac_2O (1.2 mL, 12.1 mmol, 2 equiv.) were added sequentially, and the mixture was stirred for 2.5 h. The solution was diluted with DCM (10 mL) then washed with aq. Na_2CO_3 (20 mL) and aq. citric acid (10%, 20 mL). The organic fraction was dried ($MgSO_4$), filtered, and then concentrated under reduced pressure. The crude product was purified using silica gel chromatography (1:9 AcOH/EtOH) to yield the title compound (**373**) as a colourless oil (0.853 g, 5.0 mmol, 82%, mixture of rotamers).

^{1}H NMR (400 MHz, MeOD)* δ 4.66 (0.2H, dd, *J* = 8.5, 2.5, α-H), 4.43 (0.8H, dd, *J* = 8.5, 4.0, α-H), 3.80 (0.6H, s, CO_2Me), 3.74 (2.4H, s, CO_2Me), 3.70 – 3.61 (1.6H, m, -CH_2-), 3.58 – 3.48 (0.4H, m, -CH_2-), 2.43 – 2.15 (1.3H, m, -CH_2-), 2.12 (2.3H, s, -COMe), 2.09 – 1.84 (3.4H, m, -COMe and -CH_2-).

^{13}C NMR (101 MHz, MeOD)* δ 173.2, 172.9, 171.1, 170.8, 60.2, 58.7, 52.1, 51.6, 46.2, 30.8, 29.2, 24.4, 22.4, 21.0.

ESI-MS (LCMS): found *m/z* $[M+H]^+$ 172.2

Spectroscopic data match those previously published.[60]

*doubling or splitting of peaks observed due to the presence of rotamers.

6.4.10 *N*-Boc-Gly-Pro-OMe (374)

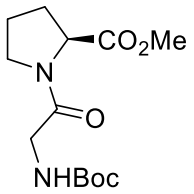

374

Proline methyl ester hydrochloride (**203**) (346 mg, 2.0 mmol, 1.1 equiv.) was dissolved in DCM (20 mL) and the solution was cooled to 0 °C. Et_3N (0.64 mL, 4.6 mmol, 2.5 equiv.), HOBt (318 mg, 2.0 mmol, 1.1 equiv.), and Boc-Gly-OH (326 mg, 1.9 mmol, 1 equiv.) were then added to

the solution. After 10 mins, EDC.HCl (427 mg, 2.2 mmol, 1.2 equiv.) was then added and the solution was allowed to cool to room temperature. After 20 h, the reaction mixture was quenched by addition of HCl (1M, 20 mL) and the aqueous layer was extracted with DCM (20 mL). The organic fractions were dried ($MgSO_4$), filtered, and concentrated. The crude product was purified using silica gel chromatography (5% MeOH in DCM), affording the title compound (**374**) as a yellow oil (462 mg, 1.6 mmol, 87%).

^{1}H NMR (400 MHz, $CDCl_3$) δ 5.38 (1H, br s, NH), 4.39 (0.85H, dd, *J* = 8.5, 3.5, α-H), 4.32 (0.15H, dd, *J* = 8.5, 2.5, α-H), 3.96 – 3.72 (2H, m, CH_2), 3.65 (0.45H, s, CO_2Me), 3.61 (2.65H, s, CO_2Me), 3.54 – 3.44 (1H, m, CH_2), 3.37 (1H, dt, *J* = 9.5, 7.0, CH_2), 2.22 – 1.82 (4H, m, CH_2), 1.32 (9H, s, Boc).

^{13}C NMR (101 MHz, $CDCl_3$) δ 172.3, 167.4, 155.8, 79.5, 58.8, 52.2, 45.8, 42.9, 28.9, 28.2, 24.6.

ESI-MS (LCMS): found *m/z* $[M+H]^+$ 287.4

Spectroscopic data match those previously published.[60]

6.4.11 *N*-Acetyl-5-oxoproline methyl ester (375)

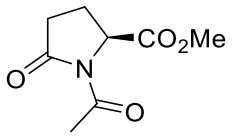

373

N-Ac-Pro-OMe (**373**) (53 mg, 0.3 mmol, 1 equiv.) was dissolved in H_2O/MeCN (1:9, 5 mL) in an ElectraSyn vial along with Selectfluor (0.169 g, 0.45 mmol, 1.5 equiv.). RVC electrodes were placed in the solution and a 5 mA current was passed through the reaction for 3 F/mol. The reaction mixture was poured onto aq. $NaHCO_3$ (20 mL) and extracted with DCM (20 mL) before being washed with brine (20 mL). The solution was dried, and the solvent was removed *in vacuo.* Purification of the crude product mixture (silica gel, hexane/EtOAc) afforded the product **375** as a colourless oil (31 mg, 0.2 mmol, 54%).

^{1}H NMR (400 MHz, $CDCl_3$) δ 4.77 (1H, dd, *J* = 9.5, 2.5, α-H), 3.77 (3H, s, CO_2Me), 2.73 (1H, ddd, *J* = 18.0, 10.5, 9.5, CH_2), 2.58 (1H, td, *J* = 9.0, 3.5, CH_2), 2.53 (3H, s, COMe), 2.33 (1H, ddt, *J* = 13.5, 10.5, 9.5 Hz, CH_2), 2.13 – 2.05 (1H, m, CH_2).

^{13}C NMR (101 MHz, $CDCl_3$) δ 174.4, 171.6, 171.1, 57.7, 52.7, 31.8, 24.6, 21.3.

ESI-MS (LCMS): found *m/z* $[M+H]^+$ 186.1

Spectroscopic data match those previously published.[61]

6.4.12 Tricyclic dimer 166

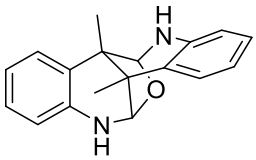

166

3-Methylindole (**165**) (80 mg, 0.6 mmol, 1 equiv.) and Bu_4NPF_6 (348 mg, 0.9 mmol, 3 equiv.) were reacted according to the **General procedure for oxidation of indole substrates (Section 6.4.2)**. Silica gel chromatography (20-40% EtOAc/hexane) of the crude product mixture afforded the title compound **166** as a pale crystalline solid (124 mg, 0.4 mmol, 73%)

^{1}H NMR (400 MHz, $CDCl_3$) δ 7.31 (2H, dd, *J* = 7.5, 1.0, Ar-H), 7.14 (2H, td, *J* = 7.5, 1.0, Ar-H), 6.86 (2H, td, *J* = 7.5, 1.0, Ar-H), 6.59 (2H, dd, *J* = 8.0, 1.0, Ar-H), 5.01 (2H, d, *J* = 4.0, NH-C**H**-OR), 4.93 (2H, br d, N-H), 1.36 (6H, s, CH_3)

^{13}C NMR (101 MHz, $CDCl_3$) δ 141.6, 128.8, 128.0, 126.5, 119.6, 96.7, 43.6, 13.2

ESI-MS (LCMS): found *m/z* $[M+H]^+$ 279.7

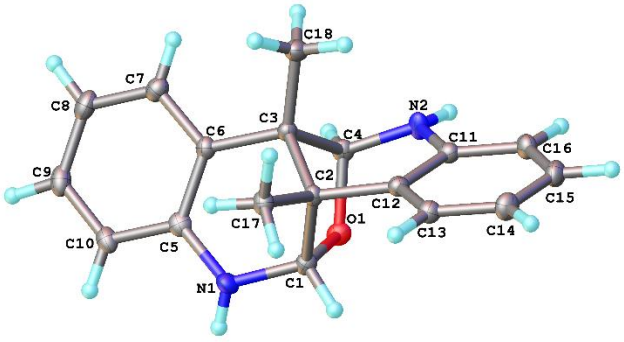

Figure 6.9: X-Ray molecular structure for **166**. Molecular structure reported with a 50% thermal ellipsoid probability.

Spectroscopic data match those previously published.[62]

6.4.13 Diindolylmethane (DIM) (382)

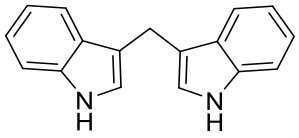

382

Indole-3-carbinol (**212**) (44 mg, 0.3 mmol, 1 equiv.) was reacted according to the **General procedure for oxidation of indole substrates (Section 6.4.2)**. The crude product mixture was purified using column chromatography (10-40% EtOAc in hexane) and the dimeric product (**382**) was isolated as a pale brown solid (9 mg, 0.07 mmol, 22%).

^{1}H NMR (400 MHz, $CDCl_3$) δ 7.95 (2H, br s, N-H), 7.65 (2H, d, *J* = 8.0, Ar-H), 7.39 (2H, d, *J* = 8.0, Ar-H), 7.21 (2H, ddd, *J* = 8.5, 7.0, 1.0, Ar-H), 7.12 (2H, ddd, *J* = 8.5, 7.0, 1.0, Ar-H), 6.98 (2H, m, Ar-H), 4.28 (2H, d, CH_2)

ESI-MS (LCMS): found *m/z* $[M+H]^+$ 247.5

Spectroscopic data match those previously published.[63]

6.4.14 Methyl 2-(2-oxo-3-indolinyl)acetate (385)

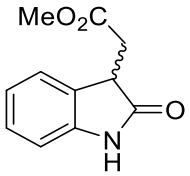

385

The **General procedure for oxidation of indole substrates (Section 6.4.2)** was followed using methyl indole-3-acetate (**195**) (59 mg, 0.3 mmol, 1 equiv), and the crude product mixture was purified by column chromatography (20-30% EtOAc in hexane) to yield the oxindole **385** (7 mg, 0.03 mmol, 11%)

^{1}H NMR (400 MHz, $CDCl_3$) δ 7.66 (1H, br d, *J* = 17.5, NH), 7.27 – 7.23 (1H, m, ArH), 7.04 (1H, td, *J* = 7.5, 1.0, ArH), 6.90 (1H, dd, *J* = 8.0, 1.0, ArH), 3.84 (1H, dd, *J* = 8.0, 4.5, CH), 3.72 (3H, s, CO_2Me), 3.11 (1H, dd, *J* = 17.0, 4.5, CH_2), 2.87 (1H, dd, *J* = 17.0, 8.0, CH_2).

ESI-MS (LCMS): found *m/z* $[M+H]^+$ 206.5

Spectroscopic data match those previously published.[64]

6.4.15 Oxindole 384

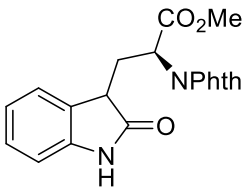

384

The **General procedure for oxidation of indole substrates (Section 6.4.2)** was followed using N-Phth-Trp-OMe (**162**) (109 mg, 0.3 mmol, 1 equiv.) with the addition of $MnBr_2$ (9 mg, 0.03 mmol, 0.1 equiv.), generating the product (**384**) as a solid mixture of diastereomers (38 mg, 0.1 mmol, 33%).

^{1}H NMR (400 MHz, $CDCl_3$)* δ 8.97 (0.36H, br s, NH), 8.73 (0.64H, s, NH), 7.80 – 7.76 (0.7H, m, Phth), 7.70 – 7.64 (2.6H, m, Phth), 7.56 – 7.52 (0.7H, m, Phth), 7.30 – 7.25 (0.6H, m, ArH), 7.20 – 7.05 (1H, m, ArH), 6.92 – 6.85 (0.4H, m, ArH), 6.80 (0.7H, tt, *J* = 7.5, 1.0, ArH), 6.67 – 6.58 (1.3H, m, ArH), 5.14 (0.64H, dd, *J* = 11.0, 4.5, α-H), 4.99 (0.36H, dd, *J* = 11.5, 3.0, α-H), 3.75 (1.9H, s, CO_2Me), 3.72 (1.1H, s, CO_2Me), 3.63 – 3.54 (1H, m, indole CH), 3.27 (0.4H, ddd, *J* = 15.0, 11.5, 3.5, CH_2), 3.12 – 2.86 (1.6H, m, CH_2).

^{13}C NMR (101 MHz, $CDCl_3$)* δ 179.4, 178.8, 169.5, 169.2, 167.3, 167.2, 141.9, 141.2, 134.0, 133.9, 131.8, 131.6, 128.6, 127.9, 127.6, 127.5, 123.9, 123.6, 123.5, 123.2, 122.7, 122.1, 110.4, 110.0, 53.0, 49.1, 48.8, 43.4 , 43.1, 28.6, 28.0.

*doubling of peaks observed due to the presence of diastereomers

ESI-MS (LCMS): found *m/z* $[M+H]^+$ 365.4

ESI-MS (HRMS): found *m/z* $[M+H]^+$ 365.1144

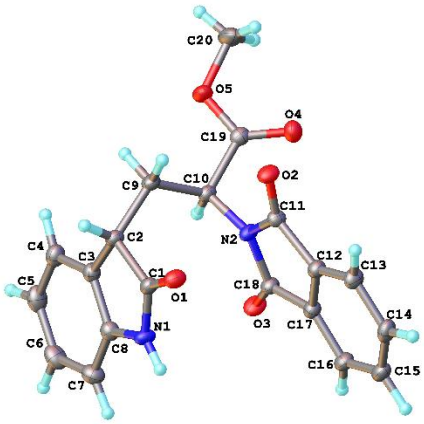

Figure 6.10: X-ray molecular structure for **384**. The molecule has an (*S,S*)-configuration, although this may not represent the bulk of the sample. Molecular structure reported with a 50% thermal ellipsoid probability.

6.4.16 (6-Iodo-2-ethoxy)methyl-3-indole carboxylate (394)

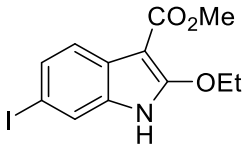

394

Methyl-3-indole carboxylate (**169**) (305 mg, 1.71 mmol, 1 equiv.) and NIS (0.381 g, 1.71 mmol, 1 equiv.) were dissolved in $CHCl_3$ (10 mL, 0.75% EtOH added as stabiliser). TFA (0.26 mL, 3.43 mmol, 2 equiv.) was added dropwise and the solution was stirred for 4 h. The mixture was then diluted with EtOAc (20 mL), and washed with aq. $Na_2S_2O_3$ (20 mL, 1 M). The organic fraction was dried ($MgSO_4$), filtered, and concentrated *in vacuo*, after which the crude product was purified using silica gel chromatography (EtOAc/hexane 1:4) to afford the title compound (**394**) as a white crystalline solid (118 mg, 0.3 mmol, 20%).

^{1}H NMR (400 MHz, $CDCl_3$) δ 9.37 (1H, br s, NH), 7.73 (1H, d, *J* = 8.5, Ar-H), 7.56 (1H, d, *J* = 1.5, Ar-H), 7.46 (1H, dd, *J* = 8.5, 1.5, Ar-H), 4.36 (2H, q, *J* = 7.0, -OC**H$_2$**CH_3), 3.92 (3H, s, CO_2Me), 1.31 (3H, t, *J* = 7.0, -OCH_2C**H$_3$**).

^{13}C NMR (101 MHz, $CDCl_3$) δ 165.2, 156.5, 131.0, 130.9, 125.6, 122.6, 119.4, 111.6, 89.7, 84.6, 69.5, 51.0, 15.0.

ESI-MS (LCMS): found *m/z* $[M+H]^+$ = 346.1

IR V_{max} / cm^{-1} (ATR): 3194 (NH), 1655 (C=O), 1210 (C-O-C), 532 (C-I)

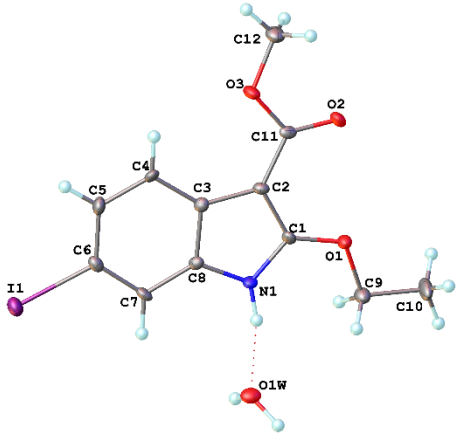

Figure 6.11: X-Ray molecular structure for **394**. Molecular structure reported with a 50% thermal ellipsoid probability.

6.4.17 (7-Iodo)methyl-3-indole carboxylate (395)

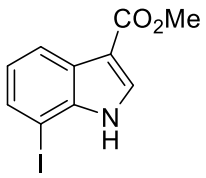

395

Methyl-3-indole carboxylate (**169**) (101 mg, 0.6 mmol, 1 equiv.) and NIS (0.132 g, 0.6 mmol, 1 equiv.) were dissolved in deuterated $CHCl_3$ (3 mL). TFA (0.09 mL, 1.2 mmol, 2 equiv.) was added dropwise and the solution was stirred for 4 h. The mixture was then diluted with EtOAc (20 mL), and washed with aq. $Na_2S_2O_3$ (20 mL, 1 M). The organic fraction was dried ($MgSO_4$), filtered, and concentrated *in vacuo*, after which the crude product was purified using silica gel chromatography (EtOAc/hexane 1:9) to afford the title compound (**395**) as a pink crystalline solid (36 mg, 0.1 mmol, 21%)

^{1}H NMR (400 MHz, $(CD_3)_2CO$) δ 8.17 (1H, dt, *J* = 8.0, 1.0, Ar-H), 8.10 – 8.07 (1H, m, Ar-H), 7.67 (1H, dd, *J* = 7.5, 1.0, Ar-H), 7.05 (1H, t, *J* = 8.0, Ar-H), 3.87 (3H, s, CO_2Me).

^{13}C NMR (151 MHz, $(CD_3)_2CO$) δ 164.6, 138.5, 132.1, 131.8, 126.6, 123.1, 121.2, 109.0, 76.1, 50.3.

ESI-MS (LCMS): found *m/z* $[M+H]^+$ 302.1

Spectroscopic data match those previously published.[65]

6.5 References

1 D. M. Shendage, R. Fröhlich and G. Haufe, *Org. Lett.*, 2004, **6**, 3675–3678.
2 S. Mukherjee, B. Maji, A. Tlahuext-Aca and F. Glorius, *J. Am. Chem. Soc*, 2016, **138**, 16200–16203.
3 C. J. Easton, A. J. Edwards, S. B. McNabb, M. C. Merrett, J. L. O'Connell, G. W. Simpson, J. S. Simpson and A. C. Willis, *Org. Biomol. Chem.*, 2003, **1**, 2492–2498.
4 J. Zheng, B. Yin, W. Huang, X. Li, H. Yao, Z. Liu, J. Zhang and S. Jiang, *Tetrahedron Lett*, 2009, **50**, 5094–5097.
5 N. Matsuda, K. Hirano, T. Satoh and M. Miura, *Angew. Chem. Int. Ed.*, 2012, **51**, 11827–11831.
6 H. Egami, S. Masuda, Y. Kawato and Y. Hamashima, *Org. Lett.*, 2018, **20**, 1367–1370.
7 J. Groves, X. Huang, W. Liu, and J. Hooker, US Patent, WO2015134467A1, 2015.
8 X. Zhang and D. W. C. MacMillan, *J. Am. Chem. Soc*, 2016, **138**, 13862–13865.

9 Y. Tian, J. Jin, C. Wang, W. Lv, X. Li, X. Che, Y. Gong, Y. Li, Q. Li, J. Hou, P. G. Wang and J. Shen, *Bioorg Med Chem Lett*, 2016, **26**, 2434–2437.
10 V. Vinayagam, T. V. Hajay Kumar, R. Nune, S. K. Karre and S. K. Sadhukhan, *J Org Chem*, 2023, **88**, 2122–2131.
11 S. Liu and C. C. Tzschucke, *Eur. J. Org. Chem.*, 2016, **2016**, 3509–3513.
12 F. D. Polyak, A. V. Eremeev, M. P. Gavars, A. P. Gaukhman and I. B. Mazheika, *Chem Heterocycl Compd (N Y)*, 1988, **24**, 733–735.
13 N. Alqahtani, S. K. Porwal, E. D. James, D. M. Bis, J. A. Karty, A. L. Lane and R. Viswanathan, *Org. Biomol. Chem.*, 2015, **13**, 7177–7192.
14 H. Jia, A. P. Häring, F. Berger, L. Zhang and T. Ritter, *J. Am. Chem. Soc*, 2021, **143**, 7623–7628.
15 I. Guerrero and A. Correa, *Org. Lett.*, 2020, **22**, 1754–1759.
16 Y. Cheng, X. Yuan, J. Ma and S. Yu, *Chem. Eur. J.*, 2015, **21**, 8355–8359.
17 J. Cramer, A. Lakkaichi, B. Aliu, R. P. Jakob, S. Klein, I. Cattaneo, X. Jiang, S. Rabbani, O. Schwardt, G. Zimmer, M. Ciancaglini, T. Abreu Mota, T. Maier and B. Ernst, *J. Am. Chem. Soc*, 2021, **143**, 17465–17478.
18 H. Song, J. Song, L. Yan, W. He, P. Wang, Y. Xu, H. Wei and W. Xie, *Tetrahedron Lett*, 2021, **85**, 153486.
19 A. Unzue, H. Zhao, G. Lolli, J. Dong, J. Zhu, M. Zechner, A. Dolbois, A. Caflisch and C. Nevado, *J. Med. Chem.*, 2016, **59**, 3087–3097.
20 D. Tejedor, R. Diana-Rivero and F. García-Tellado, *Molecules*, 2020, **25**, 5595.
21 A. Coste, M. Toumi, K. Wright, V. Razafimahaléo, F. Couty, J. Marrot and G. Evano, *Org. Lett.*, 2008, **10**, 3841–3844.
22 D. Zaienne, S. Willems, S. Schierle, J. Heering and D. Merk, *J. Med. Chem.*, 2021, **64**, 15126–15140.
23 S. Tang, J.-H. Li, Y.-X. Xie and N.-X. Wang, *Synthesis (Stuttg)*, 2007, **2007**, 1535–1541.
24 Z. Fu, Z. Li, Y. Song, R. Yang, Y. Liu and H. Cai, *J. Org. Chem.*, 2016, **81**, 2794–2803.
25 F. Ling, D. Cheng, T. Liu, L. Liu, Y. Li, J. Li and W. Zhong, *Green Chem*, 2021, **23**, 4107–4113.
26 S. Kumar, N. Sharma, I. K. Maurya, A. K. K. Bhasin, N. Wangoo, P. Brandão, V. Félix, K. K. Bhasin and R. K. Sharma, *Eur J. Med. Chem.*, 2016, **123**, 916–924.
27 Y. Liang, F. Lin, Y. Adeli, R. Jin and N. Jiao, *Angew. Chem.*, 2019, **131**, 4614–4618.
28 D. Schröder, M. Buděšínský and J. Roithová, *J. Am. Chem. Soc*, 2012, **134**, 15897–15905.
29 Z. Fang, P.-C. Liao, Y.-L. Yang, F.-L. Yang, Y.-L. Chen, Y. Lam, K.-F. Hua and S.-H. Wu, *J. Med. Chem.*, 2010, **53**, 7967–7978.
30 O. A. Battenberg, M. B. Nodwell and S. A. Sieber, *J. Org. Chem.*, 2011, **76**, 6075–6087.
31 M. Gausmann, N. Kreidt and M. Christmann, *Org. Lett.*, 2023, **25**, 2228–2232.
32 A. S. Abreu, N. O. Silva, P. M. T. Ferreira and M.-J. R. P. Queiroz, *Tetrahedron Lett.*, 2003, **44**, 3377–3379.
33 T. M. Faraggi, C. Rouget-Virbel, J. A. Rincón, M. Barberis, C. Mateos, S. García-Cerrada, J. Agejas, O. de Frutos and D. W. C. MacMillan, *Org Process Res Dev*, 2021, **25**, 1966–1973.
34 A. Dumas, D. Li, S. Pinet, D. Corona-Becerril and S. Hanessian, *Can J Chem*, 2021, **99**, 603–613.
35 A. S. Odoh, C. Keeler and B. Kim, *Org. Lett.*, 2024, **26**, 4013–4017.
36 M. Molkenthin, W. M. Nau and B. J. Nachtsheim, *Chem European J*, 2021, **27**, 16488–16497.

37 A. S. Hudson, A. Hoose, C. R. Coxon, G. Sandford and S. L. Cobb, *Tetrahedron Lett.*, 2013, **54**, 4865–4867.
38 P. Miao, M. Zhang, Z. Ni, Q. Chen and Z. Sun, *J. Org. Chem.*, 2024, **89**, 1543–1551.
39 P. García-Reynaga, A. K. Carrillo and M. S. VanNieuwenhze, *Org. Lett.*, 2012, **14**, 1030–1033.
40 P. Palamini, E. M. D. Allouche and J. Waser, *Org. Lett.*, 2023, **25**, 6791–6795.
41 C. Couturier, J. Blanchet, T. Schlama and J. Zhu, *Org. Lett.*, 2006, **8**, 2183–2186.
42 S. Tang, Z. H. Xu, T. Liu, S. W. Wang, J. Yu, J. Liu, Y. Hong, S. L. Chen, J. He and J. H. Li, *Angew. Chem. Int. Ed.*, 2021, **60**, 21360–21367.
43 C. J. J. Hall, W. R. F. Goundry and T. J. Donohoe, *Angew. Chem. Int. Ed.*, 2021, **60**, 6981–6985.
44 V. Kraehmer and D. Rehder, *Dalton Trans*, 2012, **41**, 5225–5234.
45 S. Furukawa, N. Morishima and K. Fujita, *Eur. J. Org. Chem.*, 2024, **27**, e202301105
46 Z. Z. Han, T. Dong, X. X. Ming, F. Kuang and C. P. Zhang, *ChemMedChem*, 2021, **16**, 3177–3180.
47 A. Z. Halimehjani and B. Breit, *Chemical Commun*, 2023, **59**, 4376–4379.
48 N. J. Church, D. W. Young, C. H. A Nh, H. B. H A Ho and N. H. O Ho, *J. Chem. Soc., Perkin Trans 1*, 1998, 1475-1482.
49 J. Ren, F. Du, M. Jia, Z. Hu, Z. Chen and C. Zhang, *Angew. Chem. Int. Ed.*, 2021, **60**, 24171–24178.
50 Y. Du, R. M. Pearson, C. Lim, S. M. Sartor, M. D. Ryan, H. Yang, N. H. Damrauer and G. M. Miyake, *Chem. Eur. J.l*, 2017, **23**, 10962–10968.
51 B. Rønne Kristensen and C. M. Pedersen, *Eur. J. Org. Chem.*, 2023, **26**, e202300213.
52 C. Li, Y. Kawamata, H. Nakamura, J. C. Vantourout, Z. Liu, Q. Hou, D. Bao, J. T. Starr, J. Chen, M. Yan and P. S. Baran, *Angew. Chem.*, 2017, **129**, 13268–13273.
53 D. Okumatsu, K. Kawanaka, S. Kainuma, K. Kiyokawa and S. Minakata, *Chem. Eur. J.*, 2023, **29**, e202203722.
54 M. Latrache, C. Lefebvre, M. Abe and N. Hoffmann, *J. Org. Chem.*, 2023, **88**, 16435–16455.
55 W. Jia and M. Á. Fernández-Ibáñez, *Eur. J. Org. Chem.*, 2018, **2018**, 6088–6091.
56 L. D. Tran and O. Daugulis, *Angew. Chem. Int. Ed.*, 2012, **51**, 5188–5191.
57 M. Fan and D. Ma, *Angew. Chem. Int. Ed.*, 2013, **52**, 12152– 12155.
58 X. S. Zhang, Z. W. Li and Z. J. Shi, *Org. Chem. Front.*, 2014, **1**, 44–49.
59 C. Chauvier, T. Godou and T. Cantat, *Chem. Commun.*, 2017, **53**, 11697–11700.
60 E. Morisset, A. Chardon, J. Rouden and J. Blanchet, *Eur. J. Org. Chem.*, 2020, **2020**, 388–392.
61 V. Denniel, P. Bauchat, D. Danion and R. Danion-Bougot, *Tetrahedron Lett.*, 1996, **37**, 5111–5114.
62 K.-Q. Ling, T. Ren, J. D. Protasiewicz and L. M. Sayre, *Tetrahedron Lett.*, 2002, **43**, 6903–6905.
63 G. Guo, Y. Ye, X. Bao, Y. Yuan and C. Huo, *Adv Synth Catal*, 2023, **365**, 3540–3545.
64 S. V. Shelar and N. P. Argade, *Org. Biomol. Chem.*, 2019, **17**, 6671–6677.
65 M. Somei, A. Tanimoto, H. Orita, F. Yamada and T. Ohta, *Heterocycles*, 2001, **54**, 425.

Appendix

A.1 General X-Ray Crystallography

For acquiring X-ray crystallography data, a single crystal was taken from the sample and analysed at 120.0 K. The data was collected using a Bruker D8 Venture, and the radiation source was Mo Kα (λ = 0.71073). The structure was solved by direct method and refined by full-matrix least squares on F2 using Olex2. Sample analysis and refinement was carried out by Dr Dmitry Yufit and Dr Toby Blundell, Durham University.

A.2 Crystal structure determination of 127

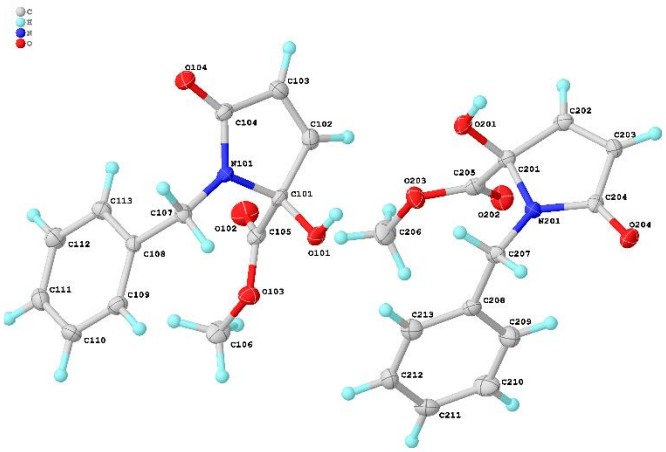

Figure A.1: X-ray molecular structure for **127**. Molecular structure reported with a 50% thermal ellipsoid probability.

Crystal data and structure refinement for 127	
Identification code	23srv154
Empirical formula	$C_{13}H_{13}NO_4$
Formula weight	247.24
Temperature/K	120.00
Crystal system	orthorhombic
Space group	$P2_12_12_1$
a/Å	8.7980(8)
b/Å	9.8241(9)
c/Å	26.590(2)
α/°	90
β/°	90
γ/°	90
Volume/Å^3	2298.2(4)
Z	8
ρ_{calc}g/cm^3	1.429
μ/mm^{-1}	0.107
F(000)	1040.0
Crystal size/mm^3	0.356 × 0.061 × 0.04
Radiation	Mo Kα (λ = 0.71073)
2Θ range for data collection/°	4.42 to 56.602
Index ranges	-11 ≤ h ≤ 11, -13 ≤ k ≤ 13, -35 ≤ l ≤ 35
Reflections collected	47028
Independent reflections	5717 [R_{int} = 0.1287, R_{sigma} = 0.0822]
Data/restraints/parameters	5717/0/332
Goodness-of-fit on F^2	1.026
Final R indexes [I>=2σ (I)]	R_1 = 0.0701, wR_2 = 0.1712
Final R indexes [all data]	R_1 = 0.1124, wR_2 = 0.2011
Largest diff. peak/hole / e Å^{-3}	0.68/-0.37
Flack parameter	-0.7(10)

Table A.1: Crystal data and structure refinement for **127**.

A.3 Crystal structure determination of 4-chloro-2-methylpyrrole carboxylate (135)

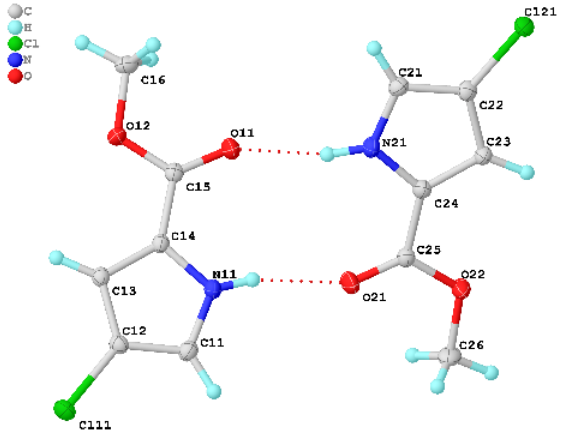

Figure A.2: X-Ray molecular structure for **135**. Molecular structure reported with a 50% thermal ellipsoid probability.

Crystal data and structure refinement for 135	
Identification code	23srv189
Empirical formula	$C_6H_6ClNO_2$
Formula weight	159.57
Temperature/K	120.00
Crystal system	monoclinic
Space group	$P2_1/n$
a/Å	10.5400(3)
b/Å	7.3196(2)
c/Å	18.3009(4)
α/°	90
β/°	101.4540(10)
γ/°	90
Volume/Å^3	1383.77(6)
Z	8
ρ_{calc}g/cm^3	1.532
μ/mm^{-1}	0.483
F(000)	656.0
Crystal size/mm^3	0.119 × 0.076 × 0.068
Radiation	Mo Kα (λ = 0.71073)
2Θ range for data collection/°	4.14 to 63.614
Index ranges	-15 ≤ h ≤ 15, -10 ≤ k ≤ 10, -27 ≤ l ≤ 27
Reflections collected	44947
Independent reflections	4715 [R_{int} = 0.0664, R_{sigma} = 0.0360]
Data/restraints/parameters	4715/0/191
Goodness-of-fit on F^2	1.195
Final R indexes [I>=2σ (I)]	R_1 = 0.0581, wR_2 = 0.1142
Final R indexes [all data]	R_1 = 0.0716, wR_2 = 0.1191
Largest diff. peak/hole / e Å^{-3}	0.45/-0.56

Table A.2: Crystal data and structure refinement for **135**.

A.4 Crystal structure determination of 2-chloro-1H-indole-3-carboxylic acid methyl ester (170)

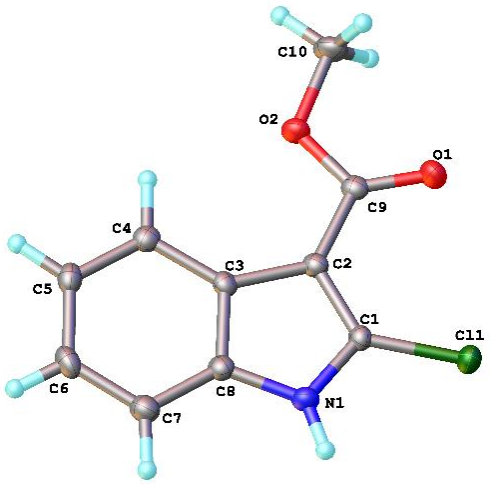

Figure A.3: X-Ray molecular structure for **170**. Molecular structure reported with a 50% thermal ellipsoid probability.

Crystal data and structure refinement for 170	
Identification code	21srv397
Empirical formula	$C_{10}H_8ClNO_2$
Formula weight	209.62
Temperature/K	120.0
Crystal system	monoclinic
Space group	Cc
a/Å	6.8706(2)
b/Å	16.9272(4)
c/Å	16.2469(4)
α/°	90
β/°	100.4785(10)
γ/°	90
Volume/Å^3	1858.00(8)
Z	8
ρ_{calc}g/cm^3	1.499
μ/mm^{-1}	0.380
F(000)	864.0
Crystal size/mm^3	0.23 × 0.06 × 0.01
Radiation	Mo Kα (λ = 0.71073)
2Θ range for data collection/°	4.812 to 60
Index ranges	-9 ≤ h ≤ 9, -23 ≤ k ≤ 23, -22 ≤ l ≤ 22
Reflections collected	33037
Independent reflections	5398 [R_{int} = 0.0482, R_{sigma} = 0.0350]
Data/restraints/parameters	5398/2/317
Goodness-of-fit on F^2	1.032
Final R indexes [I>=2σ (I)]	R_1 = 0.0350, wR_2 = 0.0765
Final R indexes [all data]	R_1 = 0.0382, wR_2 = 0.0782
Largest diff. peak/hole / e Å^{-3}	0.25/-0.20
Flack parameter	0.00(3)

Table A.3: Crystal data and structure refinement for **170**.

A.5 Crystal structure determination of N-Boc-N'-acetyl-2-chloro-L-tryptophan methyl ester (177)

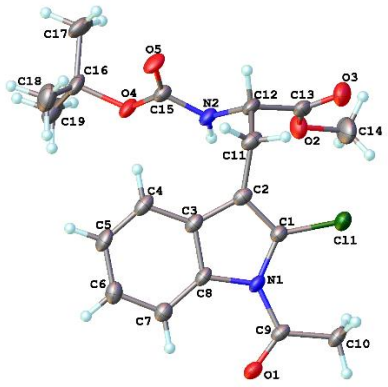

Figure A.4: X-Ray molecular structure for **177**. Molecular structure reported with a 50% thermal ellipsoid probability.

Crystal data and structure refinement for **177**.	
Identification code	22srv079
Empirical formula	$C_{19}H_{23}ClN_2O_5$
Formula weight	394.84
Temperature/K	120.00
Crystal system	orthorhombic
Space group	$P2_12_12_1$
a/Å	6.7091(5)
b/Å	11.7142(9)
c/Å	24.3043(19)
α/°	90
β/°	90
γ/°	90
Volume/Å^3	1910.1(3)
Z	4
ρ_{calc}g/cm^3	1.373
μ/mm^{-1}	0.233
F(000)	832.0
Crystal size/mm^3	0.33 × 0.05 × 0.01
Radiation	Mo Kα (λ = 0.71073)
2Θ range for data collection/°	3.86 to 51.976
Index ranges	-8 ≤ h ≤ 8, -14 ≤ k ≤ 14, -29 ≤ l ≤ 29
Reflections collected	18357
Independent reflections	3754 [R_{int} = 0.0592, R_{sigma} = 0.0508]
Data/restraints/parameters	3754/0/249
Goodness-of-fit on F^2	1.038
Final R indexes [I>=2σ (I)]	R_1 = 0.0481, wR_2 = 0.1092
Final R indexes [all data]	R_1 = 0.0629, wR_2 = 0.1170
Largest diff. peak/hole / e Å^{-3}	1.08/-0.25
Flack parameter	-0.01(5)

Table A.4: Crystal data and structure refinement for **177**

A.6 Crystal structure determination of N-Boc-β,β-dibromodehydroalanine methyl ester (252)

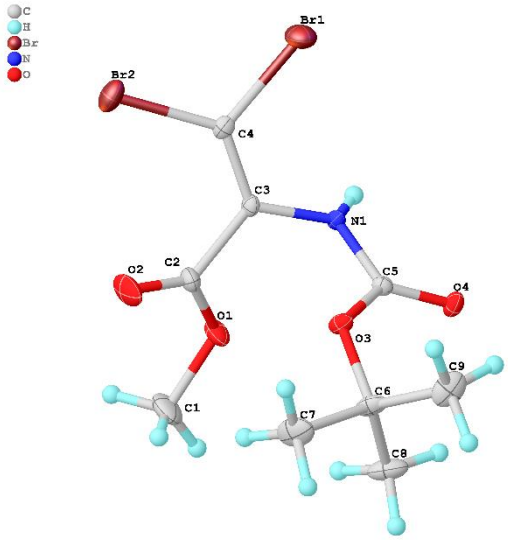

Figure A.5: Molecular structure for **252**. Molecular structure reported with 50% thermal ellipsoid probability.

Crystal data and structure refinement for 252.	
Identification code	23srv297
Empirical formula	$C_9H_{13}Br_2NO_4$
Formula weight	359.02
Temperature/K	120.00
Crystal system	triclinic
Space group	P-1
a/Å	7.5762(3)
b/Å	9.2485(4)
c/Å	10.2592(4)
α/°	75.573(2)
β/°	83.907(2)
γ/°	67.532(2)
Volume/Å^3	643.29(5)
Z	2
ρ_{calc}g/cm^3	1.854
μ/mm^{-1}	6.299
F(000)	352.0
Crystal size/mm^3	0.106 × 0.089 × 0.031
Radiation	Mo Kα (λ = 0.71073)
2Θ range for data collection/°	4.1 to 66.332
Index ranges	-11 ≤ h ≤ 11, -14 ≤ k ≤ 14, -15 ≤ l ≤ 15
Reflections collected	28373
Independent reflections	4924 [R_{int} = 0.0404, R_{sigma} = 0.0308]
Data/restraints/parameters	4924/0/153
Goodness-of-fit on F^2	1.064
Final R indexes [I>=2σ (I)]	R_1 = 0.0345, wR_2 = 0.0835
Final R indexes [all data]	R_1 = 0.0459, wR_2 = 0.0875
Largest diff. peak/hole / e Å^{-3}	1.65/-0.72

Table A.5: Crystal data and structure refinement for **252**

A.7 Crystal structure determination of sulfoxide 278

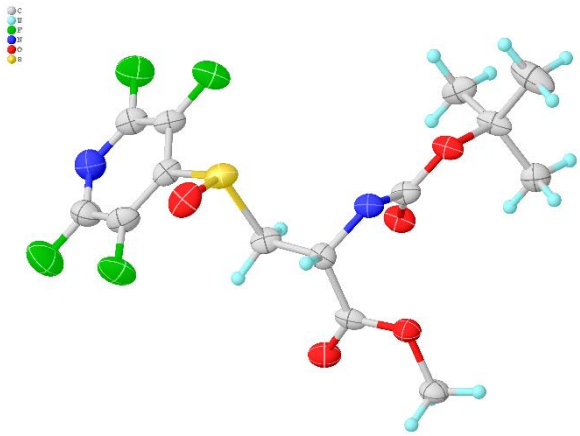

Figure A.6: X-Ray molecular structure for **278**. Molecular structure reported with a 50% thermal ellipsoid probability.

Crystal data and structure refinement for 278.	
Identification code	23srv305
Empirical formula	$C_{14}H_{15}F_4N_2O_5S$
Formula weight	399.34
Temperature/K	120.00
Crystal system	monoclinic
Space group	$P2_1$
a/Å	12.0535(11)
b/Å	5.1597(4)
c/Å	14.8337(12)
α/°	90
β/°	110.447(4)
γ/°	90
Volume/Å^3	864.42(13)
Z	2
ρ_{calc}g/cm^3	1.534
μ/mm^{-1}	0.257
F(000)	410.0
Crystal size/mm^3	0.171 × 0.044 × 0.026
Radiation	Mo Kα (λ = 0.71073)
2Θ range for data collection/°	3.77 to 55.986
Index ranges	-15 ≤ h ≤ 15, -6 ≤ k ≤ 6, -19 ≤ l ≤ 19
Reflections collected	41965
Independent reflections	4168 [R_{int} = 0.1627, R_{sigma} = 0.1082]
Data/restraints/parameters	4168/1/239
Goodness-of-fit on F^2	1.017
Final R indexes [I>=2σ (I)]	R_1 = 0.0732, wR_2 = 0.1563
Final R indexes [all data]	R_1 = 0.1298, wR_2 = 0.1839
Largest diff. peak/hole / e Å^{-3}	0.56/-0.38
Flack parameter	0.07(11)

Table A.6: Crystal data and structure refinement for **278**

A.8 Crystal structure determination of sulfone 279

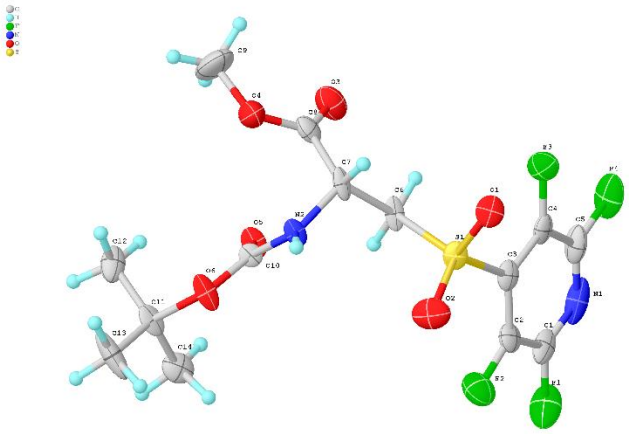

Figure 6.7: X-Ray molecular structure for **279**. Molecular structure reported with a 50% thermal ellipsoid probability.

Crystal data and structure refinement for 279	
Identification code	23srv304
Empirical formula	$C_{15.5}H_{19}F_4N_2O_{6.5}S$
Formula weight	445.39
Temperature/K	120.00
Crystal system	monoclinic
Space group	$P2_1$
a/Å	15.0237(18)
b/Å	5.0441(6)
c/Å	15.8281(19)
α/°	90
β/°	115.235(4)
γ/°	90
Volume/Å^3	1085.0(2)
Z	2
ρ_{calc}g/cm^3	1.363
μ/mm^{-1}	0.217
F(000)	460.0
Crystal size/mm^3	0.388 × 0.056 × 0.034
Radiation	Mo Kα (λ = 0.71073)
2Θ range for data collection/°	5.43 to 54.99
Index ranges	-19 ≤ h ≤ 19, -6 ≤ k ≤ 6, -20 ≤ l ≤ 20
Reflections collected	18900
Independent reflections	4979 [R_{int} = 0.0854, R_{sigma} = 0.0939]
Data/restraints/parameters	4979/360/248
Goodness-of-fit on F^2	1.028
Final R indexes [I>=2σ (I)]	R_1 = 0.0692, wR_2 = 0.1494
Final R indexes [all data]	R_1 = 0.0941, wR_2 = 0.1596
Largest diff. peak/hole / e Å^{-3}	0.35/-0.31
Flack parameter	0.03(9)

Table A.7: Crystal data and structure refinement for **279**.

A.9 Crystal structure determination of 3-Benzyl-2-oxo-oxazolidine-4-carboxylic acid methyl ester (291)

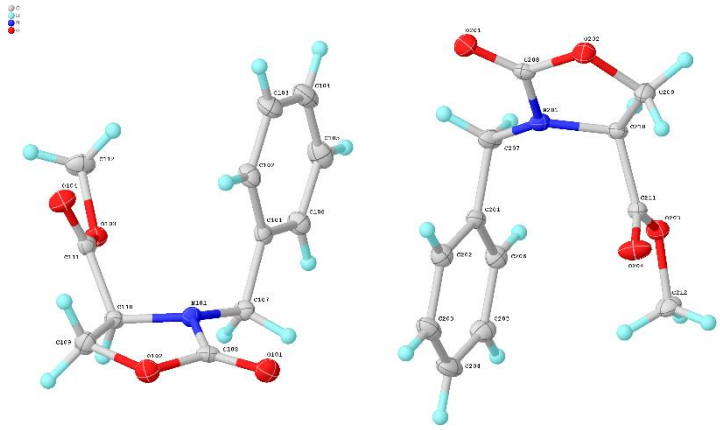

Figure A.8: X-Ray molecular structure for **291**. Molecular structure reported with a 50% thermal ellipsoid probability.

Crystal data and structure refinement for 291	
Identification code	24srv023
Empirical formula	$C_{12}H_{13}NO_4$
Formula weight	235.23
Temperature/K	120.00
Crystal system	monoclinic
Space group	$P2_1$
a/Å	13.6162(5)
b/Å	5.7386(2)
c/Å	14.3659(5)
α/°	90
β/°	100.5380(10)
γ/°	90
Volume/Å^3	1103.59(7)
Z	4
ρ_{calc}g/cm^3	1.416
μ/mm^{-1}	0.107
F(000)	496.0
Crystal size/mm^3	0.226 × 0.114 × 0.1
Radiation	Mo Kα (λ = 0.71073)
2Θ range for data collection/°	4.56 to 61.272
Index ranges	-19 ≤ h ≤ 19, -8 ≤ k ≤ 8, -20 ≤ l ≤ 20
Reflections collected	41180
Independent reflections	6767 [R_{int} = 0.0401, R_{sigma} = 0.0280]
Data/restraints/parameters	6767/1/309
Goodness-of-fit on F^2	1.085
Final R indexes [I>=2σ (I)]	R_1 = 0.0401, wR_2 = 0.0920
Final R indexes [all data]	R_1 = 0.0425, wR_2 = 0.0931
Largest diff. peak/hole / e Å^{-3}	0.31/-0.21
Flack parameter	0.2(3)

Table A.8: Crystal data and structure refinement for **291**.

A.10 Crystal structure determination of dimer 166

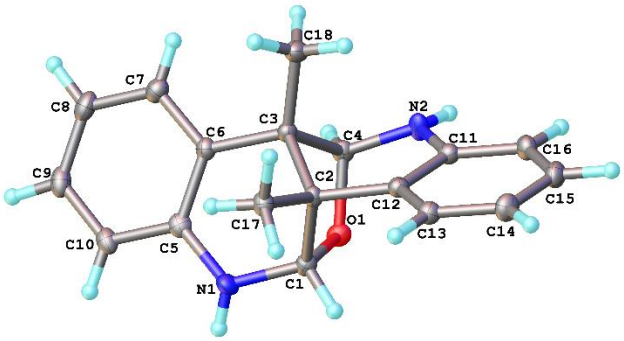

Figure A.9: X-Ray molecular structure for **166**. Molecular structure reported with a 50% thermal ellipsoid probability.

Crystal data and structure refinement for 166	
Identification code	21srv357
Empirical formula	$C_{18}H_{18}N_2O$
Formula weight	278.34
Temperature/K	120.0
Crystal system	orthorhombic
Space group	$Pna2_1$
a/Å	8.8753(3)
b/Å	20.3343(6)
c/Å	7.4709(2)
α/°	90
β/°	90
γ/°	90
Volume/Å^3	1348.30(7)
Z	4
ρ_{calc}g/cm^3	1.371
μ/mm^{-1}	0.086
F(000)	592.0
Crystal size/mm^3	0.37 × 0.08 × 0.02
Radiation	Mo Kα (λ = 0.71073)
2Θ range for data collection/°	4.006 to 59.986
Index ranges	-12 ≤ h ≤ 12, -28 ≤ k ≤ 28, -10 ≤ l ≤ 10
Reflections collected	24594
Independent reflections	3947 [R_{int} = 0.0774, R_{sigma} = 0.0548]
Data/restraints/parameters	3947/1/263
Goodness-of-fit on F^2	1.076
Final R indexes [I>=2σ (I)]	R_1 = 0.0493, wR_2 = 0.1144
Final R indexes [all data]	R_1 = 0.0544, wR_2 = 0.1172
Largest diff. peak/hole / e Å^{-3}	0.30/-0.24
Flack parameter	-0.1(7)

Table A.9: Crystal data and structure refinement for **166**.

A.11 Crystal structure determination of oxindole 384

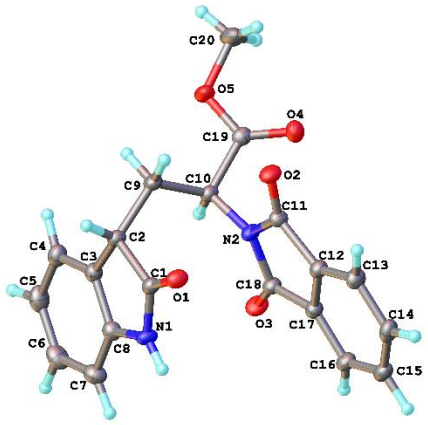

Figure A.10: X-ray molecular structure for **384**. Molecular structure reported with a 50% thermal ellipsoid probability.

Crystal data and structure refinement for 384	
Identification code	21srv398
Empirical formula	$C_{20}H_{16}N_2O_5$
Formula weight	364.35
Temperature/K	120.0
Crystal system	orthorhombic
Space group	$P2_12_12_1$
a/Å	7.9950(3)
b/Å	12.9171(4)
c/Å	16.6867(6)
α/°	90
β/°	90
γ/°	90
Volume/Å^3	1723.27(10)
Z	4
ρ_{calc}g/cm^3	1.404
μ/mm^{-1}	0.853
F(000)	760.0
Crystal size/mm^3	0.24 × 0.04 × 0.03
Radiation	Mo Kα (λ = 1.54178)
2Θ range for data collection/°	8.656 to 144.936
Index ranges	-9 ≤ h ≤ 9, -15 ≤ k ≤ 15, -20 ≤ l ≤ 20
Reflections collected	14319
Independent reflections	3387 [R_{int} = 0.0643, R_{sigma} = 0.0536]
Data/restraints/parameters	3387/0/308
Goodness-of-fit on F^2	1.049
Final R indexes [I>=2σ (I)]	R_1 = 0.0371, wR_2 = 0.0913
Final R indexes [all data]	R_1 = 0.0397, wR_2 = 0.0939
Largest diff. peak/hole / e Å^{-3}	0.23/-0.20
Flack parameter	-0.26(15)

Table A.10: Crystal data and structure refinement for **384**.

A.12 Crystal structure determination of 394

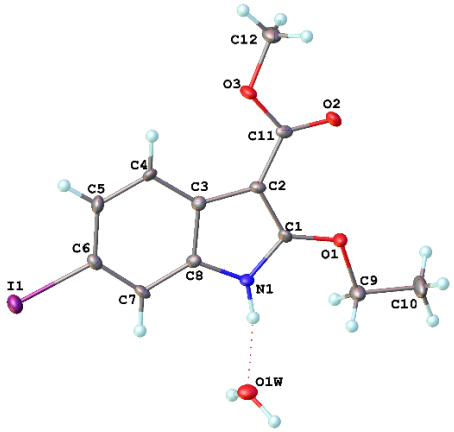

Figure A.11: X-Ray molecular structure for **394**. Molecular structure reported with a 50% thermal ellipsoid probability.

Crystal data and structure refinement for 394	
Identification code	22srv210
Empirical formula	$C_{12}H_{14}INO_4$
Formula weight	363.14
Temperature/K	120.00
Crystal system	orthorhombic
Space group	$Pna2_1$
a/Å	14.1730(5)
b/Å	21.6804(8)
c/Å	4.3047(2)
α/°	90
β/°	90
γ/°	90
Volume/Å^3	1322.73(9)
Z	4
ρ_{calc}g/cm^3	1.824
μ/mm^{-1}	2.427
F(000)	712.0
Crystal size/mm^3	0.17 × 0.02 × 0.01
Radiation	Mo Kα (λ = 0.71073)
2Θ range for data collection/°	4.73 to 59.966
Index ranges	-19 ≤ h ≤ 19, -30 ≤ k ≤ 30, -6 ≤ l ≤ 6
Reflections collected	29593
Independent reflections	3840 [R_{int} = 0.0669, R_{sigma} = 0.0406]
Data/restraints/parameters	3840/4/178
Goodness-of-fit on F^2	1.123
Final R indexes [I>=2σ (I)]	R_1 = 0.0376, wR_2 = 0.0821
Final R indexes [all data]	R_1 = 0.0397, wR_2 = 0.0831
Largest diff. peak/hole / e Å^{-3}	1.21/-1.80
Flack parameter	-0.01(2)

Table A.11: Crystal data and structure refinement for **394**.

A.13 Crystal structure determination of 186

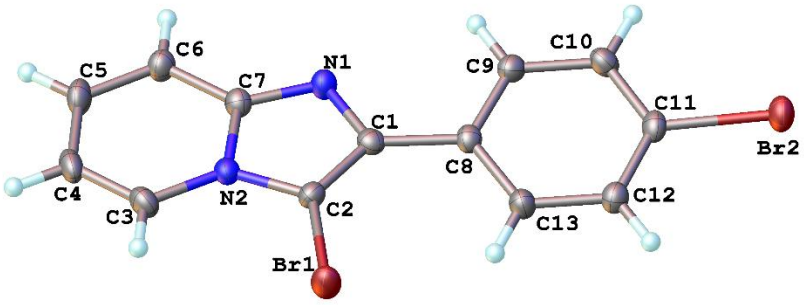

Figure A.12: Molecular structure of **186**. Molecular structure reported with a 50% thermal ellipsoid probability.

Crystal data and structure refinement for 186	
Identification code	22srv150
Empirical formula	$C_{13}H_8Br_2N_2$
Formula weight	352.03
Temperature/K	120.00
Crystal system	triclinic
Space group	P-1
a/Å	7.3478(4)
b/Å	8.1495(5)
c/Å	11.0011(7)
α/°	78.228(2)
β/°	72.594(2)
γ/°	68.920(2)
Volume/Å^3	583.08(6)
Z	2
ρ_{calc}g/cm^3	2.005
μ/mm^{-1}	6.927
F(000)	340.0
Crystal size/mm^3	0.24 × 0.01 × 0.005
Radiation	Mo Kα (λ = 0.71073)
2Θ range for data collection/°	3.902 to 59.988
Index ranges	-10 ≤ h ≤ 10, -11 ≤ k ≤ 11, -15 ≤ l ≤ 15
Reflections collected	14927
Independent reflections	3404 [R_{int} = 0.0505, R_{sigma} = 0.0453]
Data/restraints/parameters	3404/0/154
Goodness-of-fit on F^2	1.087
Final R indexes [I>=2σ (I)]	R_1 = 0.0353, wR_2 = 0.0643
Final R indexes [all data]	R_1 = 0.0525, wR_2 = 0.0684
Largest diff. peak/hole / e Å^{-3}	0.56/-0.62

Table A.12: Crystal data and structure refinement for **186**.